NASA/CR—2006-214400 GE99–030–N

Development of a Liner Design Methodology and Relevant Results of Acoustic Suppression in the Farfield for Mixer-Ejector Nozzles

M. Salikuddin
General Electric Aircraft Engines, Cincinnati, Ohio

September 2006

NASA STI Program . . . in Profile

Since its founding, NASA has been dedicated to the advancement of aeronautics and space science. The NASA Scientific and Technical Information (STI) program plays a key part in helping NASA maintain this important role.

The NASA STI Program operates under the auspices of the Agency Chief Information Officer. It collects, organizes, provides for archiving, and disseminates NASA's STI. The NASA STI program provides access to the NASA Aeronautics and Space Database and its public interface, the NASA Technical Reports Server, thus providing one of the largest collections of aeronautical and space science STI in the world. Results are published in both non-NASA channels and by NASA in the NASA STI Report Series, which includes the following report types:

- TECHNICAL PUBLICATION. Reports of completed research or a major significant phase of research that present the results of NASA programs and include extensive data or theoretical analysis. Includes compilations of significant scientific and technical data and information deemed to be of continuing reference value. NASA counterpart of peer-reviewed formal professional papers but has less stringent limitations on manuscript length and extent of graphic presentations.

- TECHNICAL MEMORANDUM. Scientific and technical findings that are preliminary or of specialized interest, e.g., quick release reports, working papers, and bibliographies that contain minimal annotation. Does not contain extensive analysis.

- CONTRACTOR REPORT. Scientific and technical findings by NASA-sponsored contractors and grantees.

- CONFERENCE PUBLICATION. Collected papers from scientific and technical conferences, symposia, seminars, or other meetings sponsored or cosponsored by NASA.

- SPECIAL PUBLICATION. Scientific, technical, or historical information from NASA programs, projects, and missions, often concerned with subjects having substantial public interest.

- TECHNICAL TRANSLATION. English-language translations of foreign scientific and technical material pertinent to NASA's mission.

Specialized services also include creating custom thesauri, building customized databases, organizing and publishing research results.

For more information about the NASA STI program, see the following:

- Access the NASA STI program home page at *http://www.sti.nasa.gov*

- E-mail your question via the Internet to *help@sti.nasa.gov*

- Fax your question to the NASA STI Help Desk at 301–621–0134

- Telephone the NASA STI Help Desk at 301–621–0390

- Write to:
  NASA STI Help Desk
  NASA Center for AeroSpace Information
  7121 Standard Drive
  Hanover, MD 21076–1320

NASA/CR—2006-214400 GE99–030–N

Development of a Liner Design Methodology and Relevant Results of Acoustic Suppression in the Farfield for Mixer-Ejector Nozzles

M. Salikuddin
General Electric Aircraft Engines, Cincinnati, Ohio

Prepared under Contract NAS3–26617 and NAS3–27235

National Aeronautics and
Space Administration

Glenn Research Center
Cleveland, Ohio 44135

September 2006

Document History

This research was originally published internally as GE99–030–N in December 1999.

This work was sponsored by the Fundamental Aeronautics Program at the NASA Glenn Research Center.

Level of Review: This material has been technically reviewed by expert reviewer(s).

Available from

NASA Center for Aerospace Information
7121 Standard Drive
Hanover, MD 21076–1320

National Technical Information Service
5285 Port Royal Road
Springfield, VA 22161

Available electronically at http://gltrs.grc.nasa.gov

FOREWORD

This report is prepared by GE Aircraft Engines, Cincinnati, Ohio for NASA-Glenn Research Center (previously known as Lewis Research Center), Cleveland, Ohio under HSR Program, Contract NAS3-27235. Mr. Gene Krejsa was the Project Manager for NASA-Glenn Research Center initially and Dr. James Bridges took over his responsibility at a later date. Mr. Fred Krause was the Project Manager for GEAE. GEAE Program Manager was Dr. R. K. Majjigi.

The author is thankful to Mr. D. Cicon and Mr. Fred Stern of P&W for their advice and contribution in the selection of liner configurations. Special recognition and thanks to Mr. G. T. Szczepkowski and Mr. R. S. Coffin for their contributions in the farfield noise prediction code development.

CONTENTS

	Topics	Page
	FOREWORD	iii
1.0	INTRODUCTION	1
2.0	ACOUSTIC LINER DESIGNS FOR MIXER-EJECTOR NOZZLES	3
3.0	NORMAL IMPEDANCE	11
	3.1 Existing Prediction Method	11
	3.1.1 SDOF Type Liners with Perforated Facesheet	11
	3.1.2 SDOF Type Liners with Woven wiremesh (Linear Facesheet)	12
	3.1.3 Bulk Only	13
	3.1.4 Bulk with Perforated Facesheet	14
	3.1.5 Bulk with Woven wiremesh (Linear Facesheet)	15
	3.2 Using Measured Ambient Normal Impedance	25
	3.3 Using Measured Ambient Normal Impedance and Measured Relative In-situ Impedance due to Flow & Temperature	30
	3.4 Current Prediction Method	34
4.0	ACOUSTIC SUPPRESSION PREDICTION DUE TO EJECTOR TREATMENT	39
	4.1 Modal Analysis Technique	39
	4.2 Semi-Empirical Models for Acoustically Treated mixer-Ejector Suppressors	39
5.0	PREDICTION OF FARFIELD NOISE INCLUDING EPNdB USING PREDICTED ACOUSTIC SUPPRESSION SPECTRUM	49
	5.1 Extracted Noise Components for Farfield Prediction	49
	5.2 Construction of Frequency Factors for PWL and SPL Prediction	49
	5.3 Prediction of Farfield Noise for Different Liner Designs	61

	Topics	Page
5.4	Validation of the Use of Frequency Factor for Different Liner Designs	70
6.0	OPTIMUM LINER DESIGNS AND SENSITIVITY STUDIES	79
6.1	Liner Depth (D)	79
6.2	Bulk Resistivity	79
6.3	Facesheet Porosity	89
6.4	Facesheet Thickness	106
6.5	Facesheet Hole Diameter	117
6.6	Sensitivity Studies	128
7.0	LINER DESIGN AND FARFIELD NOISE PREDICTION	141
7.1	Normal Impedance and Acoustic Suppression for Ideal Liner	141
7.2	Full-Scale Mixer-Ejector	141
7.3	LSM Mixer-Ejector	147
7.4	1/7-Scale Mixer-Ejector	154
7.5	Comparison of 1/7-Scale, LSM, and Full-Scale Liner Characteristics	158
7.6	Advantages of EPNL Prediction Process	164
8.0	CONCLUDING REMARKS	175
APPENDIX A	EPNLPROCESS – LINER DESIGN METHODOLOGY COMPUTER CODE	177
A.1	Definition of Input Parameters	178
A.2	Procedure to Predict Liner Performance and Effectiveness	182
A.3	Data Contained in HWREFINT='HWREFINT.dat'	183
A.4	Data Contained in TRTREFINT='TRTREFINT.dat'	184
A.5	Data Contained in TRTREFEXT='TRTREFEXT.dat'	185

	Topics	Page
	A.6 Sample Input File for the Program to Evaluate Frequency Factor γ(f) Spectrum (ITEST=0)	186
	A.7 Data Contained in Output File 'REFILSCOEFF.dat'	188
	A.8 Data Contained in Output File 'TRTOUTPUTtest0.out'	189
	A.9 Sample Input File for the Program to Evaluate Acoustic Characteristics of Treated Ejector of an Arbitrary Liner Design (ITEST=1)	193
	A.10 Data Contained in Output File 'TRTOUTPUTtest1.out'	195
APPENDIX B	LINER SUPPRESSION IN EPNdB FOR FULL-SCALE MIXER-EJECTOR AT APPROACH CONDITIONS	199
APPENDIX C	ACOUSTIC SUPPRESSION DUE TO SDOF TYPE LINER DESIGNS FOR LSM MIXER-EJECTOR NOZZLES	211
	C.1 Introduction	211
	C.2 Optimization of SDOF Type Liner Design	215
APPENDIX D	LSM BUILD-1 MIXER-EJECTOR TEST RESULTS AND COMPARISON WITH PREDICTION	233
	D.1 Total, External, and Internal Noise Components	233
	D.2 Comparison between Measured and Predicted EPNL	241
	D.3 Effect of Incremental Treatment on Noise Suppression	241
APPENDIX E	LINER DESIGN AND FARFIELD NOISE PREDICTION FOR PROPOSED LSM BUILD-2 (LSM-2) MIXER-EJECTOR	259
	E.1 Optimization of Facesheet Parameters	259
	E.2 Acoustic Suppression Characteristics of LSM-2 Liner Designs with Different T-Foam Bulk Absorbers	268
	REFERENCES	277

1.0 INTRODUCTION

Acoustic liner is an essential element for the ejector to suppress internal noise for HSCT application. Thus, a liner technology program is laid out to develop a liner design methodology, which is aimed at designing, developing, and demonstrating promising acoustic liner concepts for small as well as large scale mixer-ejector models.

The overall approach to arrive at the liner design methodology under CPC program is based on the liner optimization model, which is solely based on the laboratory tests of liner samples, data correlation, and some amount of analytical modeling. Mixer-ejector internal noise, utilized in the correlation process, is extracted as a component source using semi-empirical noise prediction model SMEM (i.e., Stone Mixer Ejector Model) from the measured acoustic farfield data for various mixer-ejector models. These efforts to develop correlation for impedance and acoustic suppression predictions for bulk absorber and SDOF type liners are described in a number of reports (Ref. 1-4).

The liner design methodology involves the prediction of farfield noise, including EPNL, for a treated mixer-ejector in terms of various noise components (i.e., internal, external, and total). The EPNL computation for a liner design requires prediction models for normal impedance, acoustic suppression in the ejector, and external noise component for the mixer-ejector. The normal impedance is predicted by a number of ways, namely, using the existing prediction models, the correlation developed under current liner technology program, and measured data acquired in the current liner technology program. Acoustic suppression predictions are obtained either by a modal analysis method or by currently developed suppression/ impedance correlation. Stone's noise prediction method (Ref. 5) is utilized to compute external noise component (i.e., premerged and merged together) and thus the internal noise component is extracted using mixer-ejector test data.

The introductory process of liner design and various parameters for the liners are described in section 2. Normal impedance and acoustic suppression prediction methods are described in sections 3 and 4. The procedure for farfield noise estimation using predicted acoustic suppression for different liner designs is described in section 5. Optimization of liner design for minimum EPNL with respect to liner parameters is carried out and the results are presented in section 6. Based on the availability of liner materials (i.e., bulk and facesheet) and the manufacturing constraints realistic liners are designed. The acoustic characteristics of these liners and their impact on farfield noise are evaluated and compared with optimum liners for different scale ejectors in section 7. Concluding remarks are made in section 8.

The liner design methodology, including the input output examples for the computer code, is briefly described in appendix A. Acoustic characteristics of various liner designs at approach condition is described in appendix B. SDOF type liner designs for LSM scale mixer-ejector is presented in appendix C. Test results of LSM build-1 and their comparisons with predictions are presented in appendix D. Liner optimization and designs for the proposed LSM build-2 mixer-ejector are described in appendix E. Finally, the relevant references are listed in the last section.

2.0 ACOUSTIC LINER DESIGNS FOR MIXER-EJECTOR NOZZLES

Design of acoustic liners for ejector treatment is carried out for 1/7-scale, LSM (i.e., 0.565-scale), and full-scale mixer-ejectors. Side and end views of a typical 1/7-scale mixer-ejector are shown in Figure 1. The flaps and sidewalls of the ejector are treated with acoustic panels (also called as treatment trays) of different sizes to cover the entire ejector surface. The acoustic treatment trays for flaps and sidewalls of a 1/7-scale ejector are schematically shown in Figure 2. The surface area of each treatment tray is about 3"x1.5" or 2.5"x1.5". For full-scale ejector 12"x12" size treatment trays are planned to be used. For each scale an optimized liner configuration is established. Most designs are performed for bulk absorber type liners. Some effort is made towards designing SDOF type liners, especially for LSM mixer-ejector application. A typical bulk absorber liner is shown in figure 3.

Liner design methodology includes the physical design of a liner, prediction of its normal impedance at the flow and acoustic environment at which it will be used, prediction of acoustic suppression inside the ejector, and the prediction of acoustic field, including EPNdB, in the farfield due to the treatment.

The physical liners may either be bulk absorber or SDOF type with a specific depth D. For bulk absorber type liner the construction includes a bulk material with a facesheet. In this the variables include the bulk properties (i.e., its resistivity or density) and facesheet properties (for perforates: porosity σ, thickness t, and hole diameter d, for linear: resistivity). For SDOF type liner the facesheet properties are the only variables. Utilizing these properties, including the liner depth, the normal impedance is predicted accounting for the flow Mach number M, temperature T, and acoustic environment (OASPL) effects. This could be achieved by utilizing existing prediction methods, the currently developed prediction methods, or construction of normal impedance utilizing experimental data acquired under the current program. The objective is to design a liner to achieve optimum impedance, which in terns gives the maximum acoustic suppression. **The optimum specific resistance R and reactance X range between 1.5 to 2 and -0.5 to 0.0, respectively, are chosen for the liner designs for maximum acoustic suppression on the basis of past experience.** Since the current prediction models are developed recently, the liner designs described in this report utilize the existing impedance prediction methods and the current test results.

Utilizing the normal impedance, flow and temperature conditions, and the geometry of the ejector the acoustic suppression spectrum can be predicted. This can be achieved either by utilizing a modal analysis method or a semi-empirical correlation. The semi-empirical

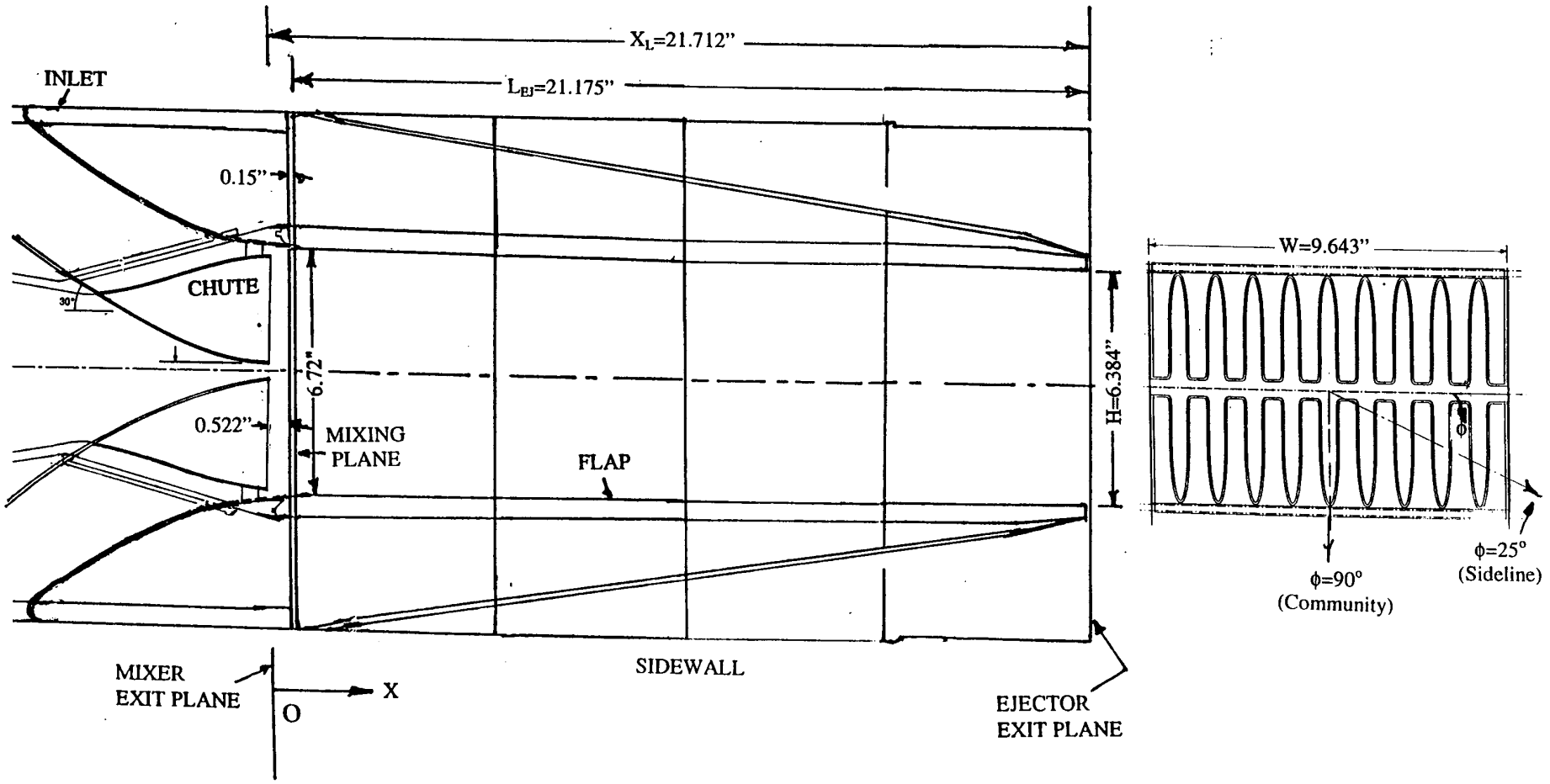

Figure 1. Side and end views of an aero type 20-cold & 18-hot chute Gen 2.5 mixer ejector nozzle (8cMixer); SAR=2.9, Penetration=92.5%, CER=1.05, MAR=0.95.

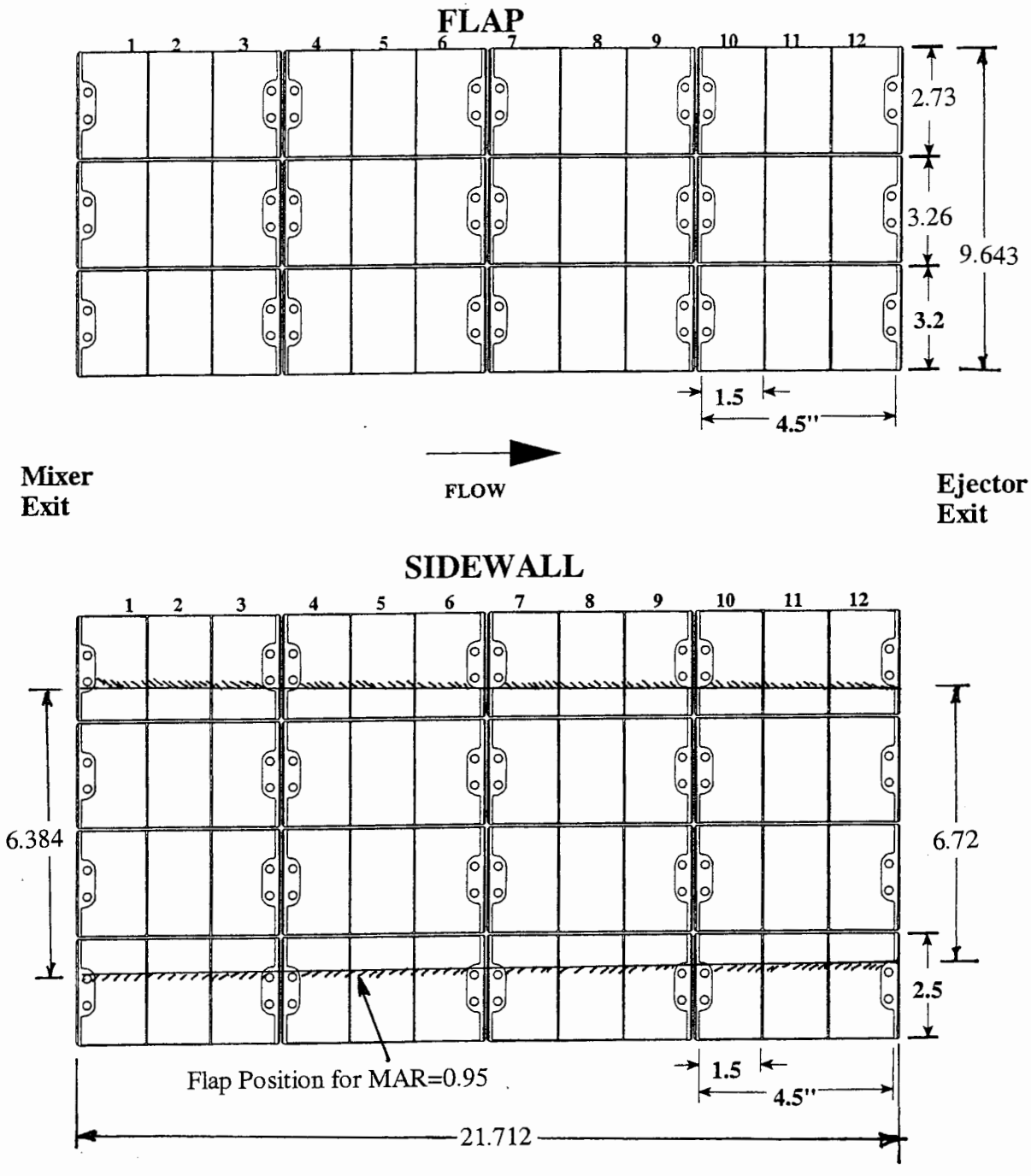

Figure 2. Schematic of acoustic treatment trays for the 21.7" (160" full-scale) flaps and sidewalls for Gen 2.5 mixer-ejector nozzles (all dimensions are in inches).

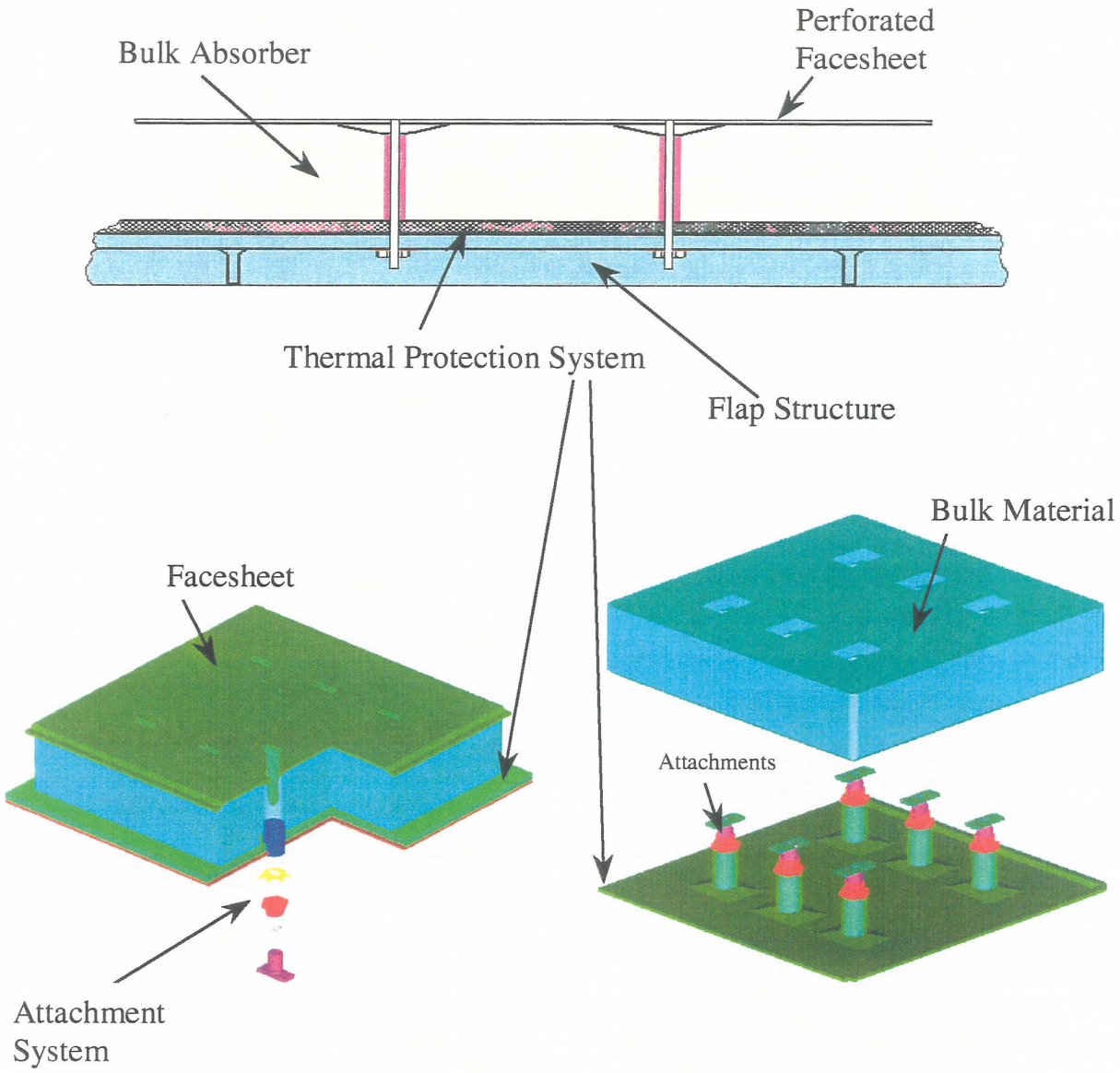

Figure 3. A typical bulk absorber liner for HSCT application.

method is currently developed utilizing the liner technology test data and mixer-ejector test data. Again, since the correlation is developed recently the results presented in this report are based on modal analysis acoustic suppression prediction.

The farfield acoustic (including EPNL) computation for a liner design involves prediction of internal noise component in the ejector and its radiation to the farfield. In this process, measured farfield acoustic data for mixer-ejectors are utilized. The predicted acoustic suppression inside an ejector is significantly different compared to the actual internal component of measured ΔPWL, especially at lower frequencies. Therefore, a frequency dependent correction factor, calculated from the predicted acoustic suppression and ΔPWL for a test case, is utilized to minimize the prediction uncertainties.

Figure 4 illustrates the process of farfield noise estimation due to acoustically treated ejector. The physical properties of the liner design and the flow and acoustic environment on the treatment surface of the mixer-ejector (M, T, and OASPL), as shown in Figure 4(a) are used to estimate the normal impedance of the treatment. This is schematically illustrated in Figure 4(b) along with the optimum impedance. The acoustic suppression internal to the ejector due to the treatment is then evaluated utilizing the normal impedance, the mean flow parameters (M_x and T_x), and the physical dimension of the treated ejector. This acoustic suppression thus derived is shown in Figure 4(c). The acoustic suppression reduces the internal noise in the ejector and the reduced noise is radiated to the farfield. Farfield noise is a function of the polar angle θ and the azimuthal angle φ. Figure 4(d) schematically illustrates the radiated internal noise for treated as well as the hardwall ejector configurations. The external noise is assumed to be the same for both ejector configurations and is also shown in Figure 4(d). The internal noise difference between the hardwall and treated configurations (shown as shaded area) is the effect of treatment at this location (φ and θ). This internal noise reduction is the **performance of the liner.** The actual noise field is the sum of internal and the external noise components as shown in Figure 4(e). The noise reduction due to the liner, shown by shaded area in this figure, is the **effectiveness of the liner**.

It is important to realize the difference between the liner performance and liner effectiveness. While the liner performance depends only on the liner design, ejector dimension, and flow and acoustic environments in the ejector, the liner effectiveness depends on these parameters and on the external noise components. With a best performing liner the effectiveness can be poor if the external noise is relatively higher compared to the internal component.

PWL, PNL, and EPNL are constructed utilizing the spectral sound pressure levels at various locations for internal, external, and total noise components. The optimum impedance maximizes acoustic suppression in terms of ΔSPL and ΔPWL. In other words the minimum SPL and PWL are achieved when the liner impedance lies within the optimum levels. However, EPNL minimization is less critical, since the EPNL involves annoyance factors

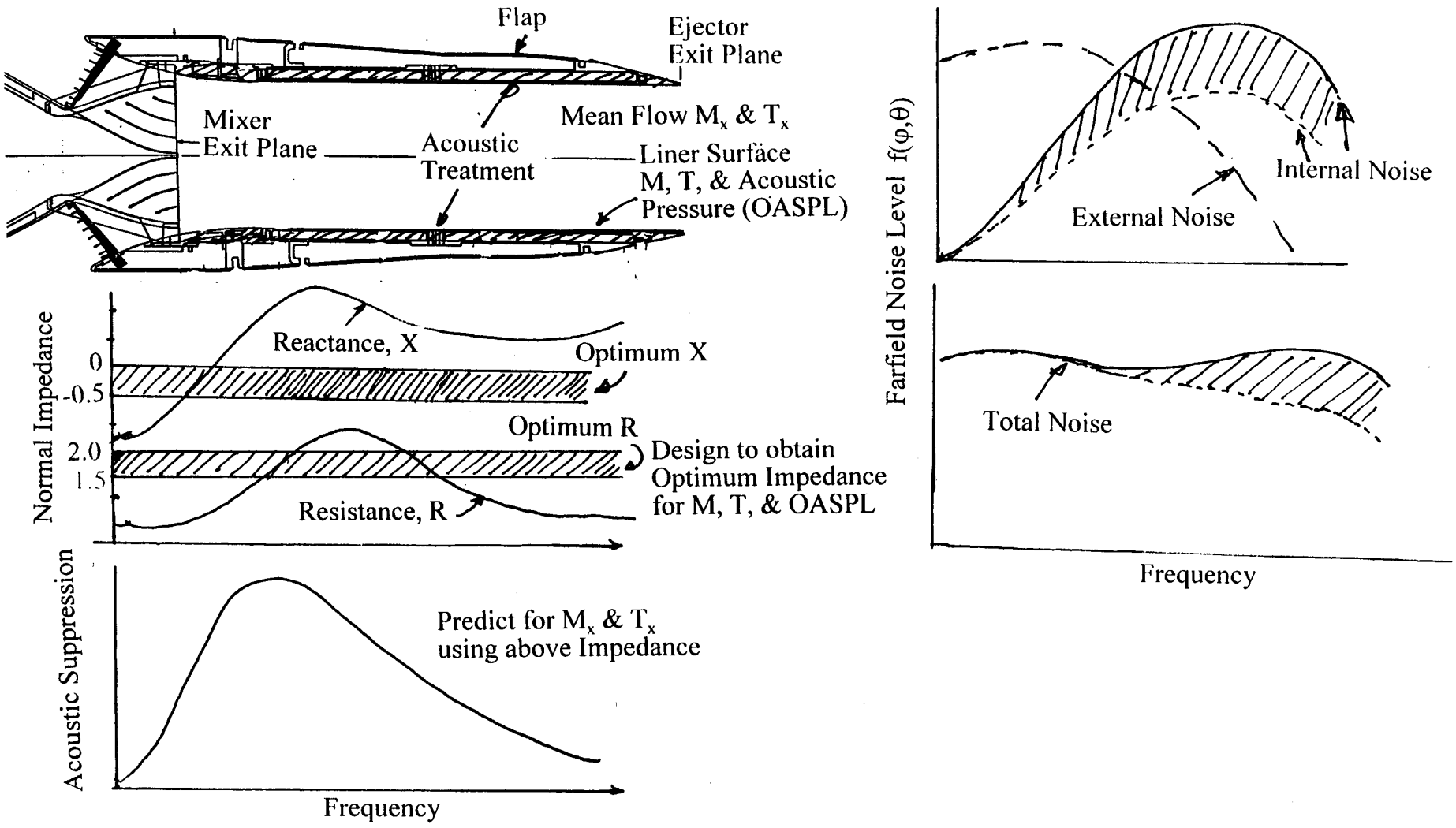

Figure 4. Process to evaluate acoustic liner impact on the farfield noise for treated mixer-ejector nozzles.

dependant on frequencies. If a liner design achieves optimum impedance at frequencies critical to EPNL it may not be necessary to achieve optimum impedance at frequencies of very low annoyance values.

Acoustic suppression or sound power insertion loss and farfield noise estimates for optimum as well as the realistic liners are made. The acoustic suppression is predicted by using a modal analysis computer code for rectangular duct treated on two opposing sides. The remaining two surfaces are considered to be untreated. Hence, an equivalent treatment length is calculated for the treated ejector, assuming that, the entire treatment is on the two opposing flap surfaces. The equivalent length is utilized in acoustic suppression prediction.

Based on the measured and CFD data for DSM models for a typical takeoff condition (i.e., NPR=3.43, T8=1551°R) the liner designs are carried out for a grazing flow Mach number of M=0.8, liner static temperature of T=500°F, and a static pressure of 13.24 psi. The cutback conditions (i.e., NPR=2.48, T8=1291°R) are relatively less severe compared to takeoff and the corresponding grazing flow Mach number and static temperature are 0.72 and 360°F, respectively. The boundary layer displacement thickness for the full-scale ejector is assumed to be 0.20". The approximate displacement thicknesses used for LSM and 1/7-scale ejectors are 0.11" and 0.05", respectively. Based on the internal dynamic pressure data for Gen 2 mixer-ejector nozzles (Ref. 6) the dynamic pressure levels for different scale ejectors are established.

The nozzle parameters, critical frequencies, and various liner design parameters with respect to the corresponding scale factors for the three cases, considered in the current effort, are listed below:

	Full Scale	**LSM**	**1/7-Scale**
Nozzle Parameters:			
A8 - Square Inches	1225.7	391	22.6
Linear Scale Factor	1.0	0.565	0.136
Average Sidewall Height - Inches	48.69	27.47	6.56
Flap Width - Inches	71.17	40.20	9.643
A_T/A_m	7.4	7.4	8.0
A_{Teff}/A_m	6.7	6.7	6.5
Equivalent Treatment Length - Inches	166.81	94.25	21.48
Liner Parameters:			
Peak Noy Frequency - Hz.	3150	5600	22300
Maximum Frequency - Hz.	10000	17900	70700
OASPL , dB- Takeoff	180.0	177.5	171.5
OASPL , dB- Cutback	174.5	171.0	166.0
Displacement Thickness, δ^* - Inches	0.20	0.11	0.05

Utilizing the above temperature, pressure, grazing flow, and dynamic pressure conditions for takeoff and using the set boundary layer displacement thicknesses for different scale liners, the bulk resistivity, liner depth, and facesheet properties are varied to arrive at optimum liner designs, such that the desired impedance values are attained at critical frequencies, especially at and around the peak Noy frequencies. The optimization process is further validated and improved on the basis of minimum EPNL and is described in section 6.

While, the liner design is based on a typical takeoff condition, the acoustic suppression spectra for the same liners are computed for the takeoff as well as at cutback (i.e., NPR=2.48, T8=1291°R) conditions utilizing the ejector flow and geometrical properties. The normal impedance spectra at cutback are predicted for the liner with the appropriate grazing flow and dynamic pressure conditions. Based on the measured and CFD data for DSM models for the takeoff condition (i.e., NPR=3.43, T8=1551°R) the average estimated mean flow Mach number (M_x) and static temperature (T_x) are 0.85 and 530°F, respectively. For cutback case the estimated average mean flow Mach number (M_x) and static temperature (T_x) are 0.73 and 400°F, respectively. The acoustic characteristics and farfield noise predicted for different liner designs for three different scales are described in section 7.

3.0 NORMAL IMPEDANCE

Normal impedance of the treatment is essential to predict the acoustic suppression capability of the mixer-ejector system. This is evaluated by four different methods for the current application and is briefly described in this section.

3.1 Existing Prediction Method: Several prediction methods are available in the literature to evaluate normal impedance for acoustic liners accounting for flow, temperature, and acoustic environment. One of the methods used at GE Aircraft Engines is utilized for the development of liner design methodology. Following expressions are used to predict normal impedance Z_i ($Z_i = R + iX$, R and X being the resistance and reactance) of various liner designs:

3.1.1 - SDOF Type Liners with Perforated Facesheet

$$R = \left(R_{gf} + adc + bdc(v_{rms})\right)$$

$$X = \left(k_i(xmc) - \cot(k_i l)\right)$$

$$|z_i| = \sqrt{\left(R_{gf} + adc + bdc(v_{rms})\right)^2 + \left(k_i(xmc) - \cot(k_i l)\right)^2}$$

where

$$adc = \left(\frac{32(vmu)(t)}{\rho c \sigma (c_d) d^2}\right)$$

$$bdc = \left(\frac{1}{2c(\sigma c_d)^2}\right)$$

$$vmu = (.00001488)\left(\frac{T^{1.5}}{T + 120}\right)$$

$$v_{rms} = \sqrt{\sum_i \left(\frac{.0002(10^{\frac{SPL_i}{20}})}{\rho c |z_i|}\right)^2}$$

$$k_i = \frac{2\pi f_i}{c}$$

$$xmc = \frac{t + \alpha d}{\sigma}$$

$$\alpha = .85\frac{\left(1 - .7\sqrt{\sigma}\right)}{\left(1 + 305(mach)^3\right)}$$

$mach$ = Grazing flow Mach number

$$R_{gf} = \frac{mach}{\sigma\left(2 + 1.256\frac{\delta^*}{d}\right)}$$

δ^* = Boundary Layer Displacement Thickness, inch

C_d = Discharge Coefficient

D = Facesheet Hole Diameter, inch

t = Facesheet Thickness, inch

σ = Facesheet Porosity

ρ = Density of Air, gm/cm^3

c = Speed of Sound, ft/sec

T = Absolute Temperature, Kelvin

SPL = Sound Pressure Level at each frequency, dB

f_i = Frequency, Hz

l = Liner Depth, inch

3.1.2 - SDOF type Liners with Woven Wiremesh (Linear Facesheet)

$$R = (adc + bdc(v_i))$$

$$X = \left(\frac{Xm}{\rho c} - \cot(k_i l)\right)$$

$$|z_i| = \sqrt{(adc + bdc(v_i))^2 + \left(\frac{Xm}{\rho c} - \cot(k_i l)\right)^2}$$

where

$$adc = \left(\frac{R_{100}}{\rho c}\right)\left(\frac{1.5 - .2NLF}{.5 + .8NLF}\right)$$

$$bdc = \left(\frac{R_{100}}{100\rho c}\right)\left(\frac{NLF - 1}{.5 + .8NLF}\right)$$

$$v_i = \frac{.0002(10^{\frac{SPL_i}{20}})}{\rho c|z_i|}$$

$$k_i = \frac{2\pi f_i}{c}$$

Xm = Mass Reaction

R_{100} = DC flow resistance of the facesheet at a through flow velocity of 100 cm/sec.

NLF = Nonlinear factor = R_{150}/R_{20}

3.1.3 – Bulk Only

$$R = ((r_i)(re\coth_i) - (x_i)(im\coth_i))$$

$$X = ((x_i)(re\coth_i) + (r_i)(im\coth_i))$$

$$|z_i| = \sqrt{((r_i)(re\coth_i) - (x_i)(im\coth_i))^2 + ((x_i)(re\coth_i) + (r_i)(im\coth_i))^2}$$

where

$$r_i = 1 + .05854\left(\frac{f_i\rho}{(rstv)}\right)^{-.75}$$

$$re\coth_i = \frac{\left(\sinh\left[l\left(.19478k_i\left(\frac{f_i\rho}{(rstv)}\right)^{-.59}\right)\right]\right)\left(\cosh\left[l\left(.19478k_i\left(\frac{f_i\rho}{(rstv)}\right)^{-.59}\right)\right]\right)}{\left(\cos\left[lk_i\left(1+.09746\left(\frac{f_i\rho}{(rstv)}\right)^{-.7}\right)\right]\right)^2\left(\sinh\left[l\left(.19478k_i\left(\frac{f_i\rho}{(rstv)}\right)^{-.59}\right)\right]\right)^2 + \left(\sin\left[lk_i\left(1+.09746\left(\frac{f_i\rho}{(rstv)}\right)^{-.7}\right)\right]\right)^2\left(\cosh\left[l\left(.19478k_i\left(\frac{f_i\rho}{(rstv)}\right)^{-.59}\right)\right]\right)^2}$$

$$x_i = -.0877\left(\frac{f_i\rho}{(rstv)}\right)^{-.73}$$

$$im\coth_i = \frac{-\left(\sin\left[lk_i\left(1+.09746\left(\frac{f_i\rho}{(rstv)}\right)^{-.7}\right)\right]\right)\left(\cos\left[lk_i\left(1+.09746\left(\frac{f_i\rho}{(rstv)}\right)^{-.7}\right)\right]\right)}{\left(\cos\left[lk_i\left(1+.09746\left(\frac{f_i\rho}{(rstv)}\right)^{-.7}\right)\right]\right)^2\left(\sinh\left[l\left(.19478k_i\left(\frac{f_i\rho}{(rstv)}\right)^{-.59}\right)\right]\right)^2 + \left(\sin\left[lk_i\left(1+.09746\left(\frac{f_i\rho}{(rstv)}\right)^{-.7}\right)\right]\right)^2\left(\cosh\left[l\left(.19478k_i\left(\frac{f_i\rho}{(rstv)}\right)^{-.59}\right)\right]\right)^2}$$

$$k_i = \frac{2\pi f_i}{c}$$

rstv=Bulk Resistivity, Rayls/cm

3.1.4 – Bulk with Perforated Facesheet

$$R = \left(R_{gf} + adc + bdc(v_{rms}) + (r_i)(re\coth_i) - (x_i)(im\coth_i)\right)$$

$$X = \left(k_i(xmc) + (x_i)(re\coth_i) + (r_i)(im\coth_i)\right)$$

$$|z_i| = \sqrt{\left(R_{gf} + adc + bdc(v_{rms}) + (r_i)(re\coth_i) - (x_i)(im\coth_i)\right)^2 + \left(k_i(xmc) + (x_i)(re\coth_i) + (r_i)(im\coth_i)\right)^2}$$

where

$$adc = \left(\frac{32(vmu)(t)}{\rho c \sigma (c_d) d^2}\right) \text{ and } bdc = \left(\frac{1}{2c(\sigma c_d)^2}\right)$$

$$vmu = (.00001488)\left(\frac{T^{1.5}}{T+120}\right), \quad v_{rms} = \sqrt{\sum_i \left(\frac{.0002(10^{\frac{SPL_i}{20}})}{\rho c |z_i|}\right)^2}, \quad \text{and} \quad r_i = 1 + .05854\left(\frac{f_i\rho}{(rstv)}\right)^{-.75}$$

$$re\coth_i = \frac{\left(\sinh\left[l\left(.19478k_i\left(\frac{f_i\rho}{(rstv)}\right)^{-.59}\right)\right]\right)\left(\cosh\left[l\left(.19478k_i\left(\frac{f_i\rho}{(rstv)}\right)^{-.59}\right)\right]\right)}{\left(\cos\left[lk_i\left(1 + .09746\left(\frac{f_i\rho}{(rstv)}\right)^{-.7}\right)\right]\right)^2\left(\sinh\left[l\left(.19478k_i\left(\frac{f_i\rho}{(rstv)}\right)^{-.59}\right)\right]\right)^2 + \left(\sin\left[lk_i\left(1 + .09746\left(\frac{f_i\rho}{(rstv)}\right)^{-.7}\right)\right]\right)^2\left(\cosh\left[l\left(.19478k_i\left(\frac{f_i\rho}{(rstv)}\right)^{-.59}\right)\right]\right)^2}$$

$$x_i = -.0877\left(\frac{f_i\rho}{(rstv)}\right)^{-.73}$$

$$im\coth_i = \frac{-\left(\sin\left[lk_i\left(1 + .09746\left(\frac{f_i\rho}{(rstv)}\right)^{-.7}\right)\right]\right)\left(\cos\left[lk_i\left(1 + .09746\left(\frac{f_i\rho}{(rstv)}\right)^{-.7}\right)\right]\right)}{\left(\cos\left[lk_i\left(1 + .09746\left(\frac{f_i\rho}{(rstv)}\right)^{-.7}\right)\right]\right)^2\left(\sinh\left[l\left(.19478k_i\left(\frac{f_i\rho}{(rstv)}\right)^{-.59}\right)\right]\right)^2 + \left(\sin\left[lk_i\left(1 + .09746\left(\frac{f_i\rho}{(rstv)}\right)^{-.7}\right)\right]\right)^2\left(\cosh\left[l\left(.19478k_i\left(\frac{f_i\rho}{(rstv)}\right)^{-.59}\right)\right]\right)^2}$$

$$k_i = \frac{2\pi f_i}{c}, xmc = \frac{t + \alpha d}{\sigma} \quad \text{and} \quad \alpha = .85\frac{\left(1 - .7\sqrt{\sigma}\right)}{\left(1 + 305(mach)^3\right)}$$

3.1.5. Bulk with Woven Wiremesh (Linear Facesheet)

$$R = \left(adc + bdc(v_i) + (r_i)(re\coth_i) - (x_i)(im\coth_i)\right) \quad \text{and} \quad X = \left((Xm/(\rho c)) + (x_i)(re\coth_i) + (r_i)(im\coth_i)\right)$$

$$|z_i| = \sqrt{\left(adc + bdc(v_i) + (r_i)(re\coth_i) - (x_i)(im\coth_i)\right)^2 + \left((Xm/(\rho c)) + (x_i)(re\coth_i) + (r_i)(im\coth_i)\right)^2}$$

where

$$adc = \left(\frac{R_{100}}{\rho c}\right)\left(\frac{1.5 - .2NLF}{.5 + .8NLF}\right) \quad \text{and} \quad bdc = \left(\frac{R_{100}}{100\rho c}\right)\left(\frac{NLF - 1}{.5 + .8NLF}\right)$$

$$v_i = \frac{.0002(10^{\frac{SPL_i}{20}})}{\rho c|z_i|} \quad \text{and} \quad r_i = 1 + .05854\left(\frac{f_i\rho}{(rstv)}\right)^{-.75}$$

$$re\coth_i = \frac{\left(\sinh\left[l\left(.19478k_i\left(\frac{f_i\rho}{(rstv)}\right)^{-.59}\right)\right]\right)\left(\cosh\left[l\left(.19478k_i\left(\frac{f_i\rho}{(rstv)}\right)^{-.59}\right)\right]\right)}{\left(\cos\left[lk_i\left(1 + .09746\left(\frac{f_i\rho}{(rstv)}\right)^{-.7}\right)\right]\right)^2\left(\sinh\left[l\left(.19478k_i\left(\frac{f_i\rho}{(rstv)}\right)^{-.59}\right)\right]\right)^2 + \left(\sin\left[lk_i\left(1 + .09746\left(\frac{f_i\rho}{(rstv)}\right)^{-.7}\right)\right]\right)^2\left(\cosh\left[l\left(.19478k_i\left(\frac{f_i\rho}{(rstv)}\right)^{-.59}\right)\right]\right)^2}$$

$$x_i = -.0877\left(\frac{f_i\rho}{(rstv)}\right)^{-.73}$$

$$im\coth_i = \frac{-\left(\sin\left[lk_i\left(1 + .09746\left(\frac{f_i\rho}{(rstv)}\right)^{-.7}\right)\right]\right)\left(\cos\left[lk_i\left(1 + .09746\left(\frac{f_i\rho}{(rstv)}\right)^{-.7}\right)\right]\right)}{\left(\cos\left[lk_i\left(1 + .09746\left(\frac{f_i\rho}{(rstv)}\right)^{-.7}\right)\right]\right)^2\left(\sinh\left[l\left(.19478k_i\left(\frac{f_i\rho}{(rstv)}\right)^{-.59}\right)\right]\right)^2 + \left(\sin\left[lk_i\left(1 + .09746\left(\frac{f_i\rho}{(rstv)}\right)^{-.7}\right)\right]\right)^2\left(\cosh\left[l\left(.19478k_i\left(\frac{f_i\rho}{(rstv)}\right)^{-.59}\right)\right]\right)^2}$$

A normal impedance prediction code is developed utilizing the above expressions for bulk absorber and SDOF type liner designs. The measured DC flow resistances of bulks and woven wiremesh type facesheets and facesheet properties of perforates are used in predicting the normal impedance for various bulk samples with and without facesheets. Normal impedance expressions for facesheets are based on reference 6. The prediction of bulk impedance is based on Delany & Bazley method (Ref. 7) and it assumes linear addition of reactance and resistance of the bulk and facesheet in the calculation of the combined values for the liner.

Normal impedance of several bulk absorber and SDOF type liner designs is predicted and compared with the measured data. Following measured data at ambient condition are used for normal impedance prediction;

Material Description	**Sample Depth Inches**	**A Rayls/cm**	**B Rayls. sec/cm^2**	**R100 Rayls/cm**
Silicon Carbide - 100 ppi	0.4	5.5	0.0320	8.70
Silicon Carbide - 200 ppi	0.4	23.0	0.1475	37.75
Felt Metal - 5% Dense	0.4	40.0	0.0800	48.00
T-Foam - 12 lb/cft	0.5	11.8	0.1040	22.20
T-Foam - 12 lb/cft	1.3	21.9	0.1213	34.10
T-Foam - 12 lb/cft	2.0	24.3	0.1352	37.80

It should be noted that the samples of 0.4" and 0.5" deep correspond to 1/7-scale liners and the other two depths of T-Foam samples, namely 1.3" and 2.0", correspond to LSM and full scale liners, respectively. The same samples are also tested with and without perforated facesheets to evaluate their normal impedance spectra. Two perforated sheets (0.025"-thick and 0.045" hole diameter) with 21% and 37% porosities, were used in the impedance measurement tests.

Since Delany & Bazley method does not account for the bulk nonlinearity, the prediction for each bulk absorber case is made using A (A is the linear part of resistivity) as well as the resistivity at 100 cm/sec, R_{100} (i.e., R_{100}=A+100B, B being the nonlinear coefficient) values. Typical comparisons of data with predictions, especially for bulk absorbers pertinent to HSCT application, are shown in Figures 5 through 11.

Figure 5, for 100 ppi 0.4"-deep Silicon Carbide (SiC), shows good agreement between data and prediction for bulk with and without facesheets. For resistance predictions with 'A' value seems to be closer to the measured data. Predicted reactance is not influenced by bulk resistivity. At higher frequencies, while the reactance is slightly under predicted for bulk only configuration, the trend is reversed for bulk with 21% porous facesheet. If the predicted

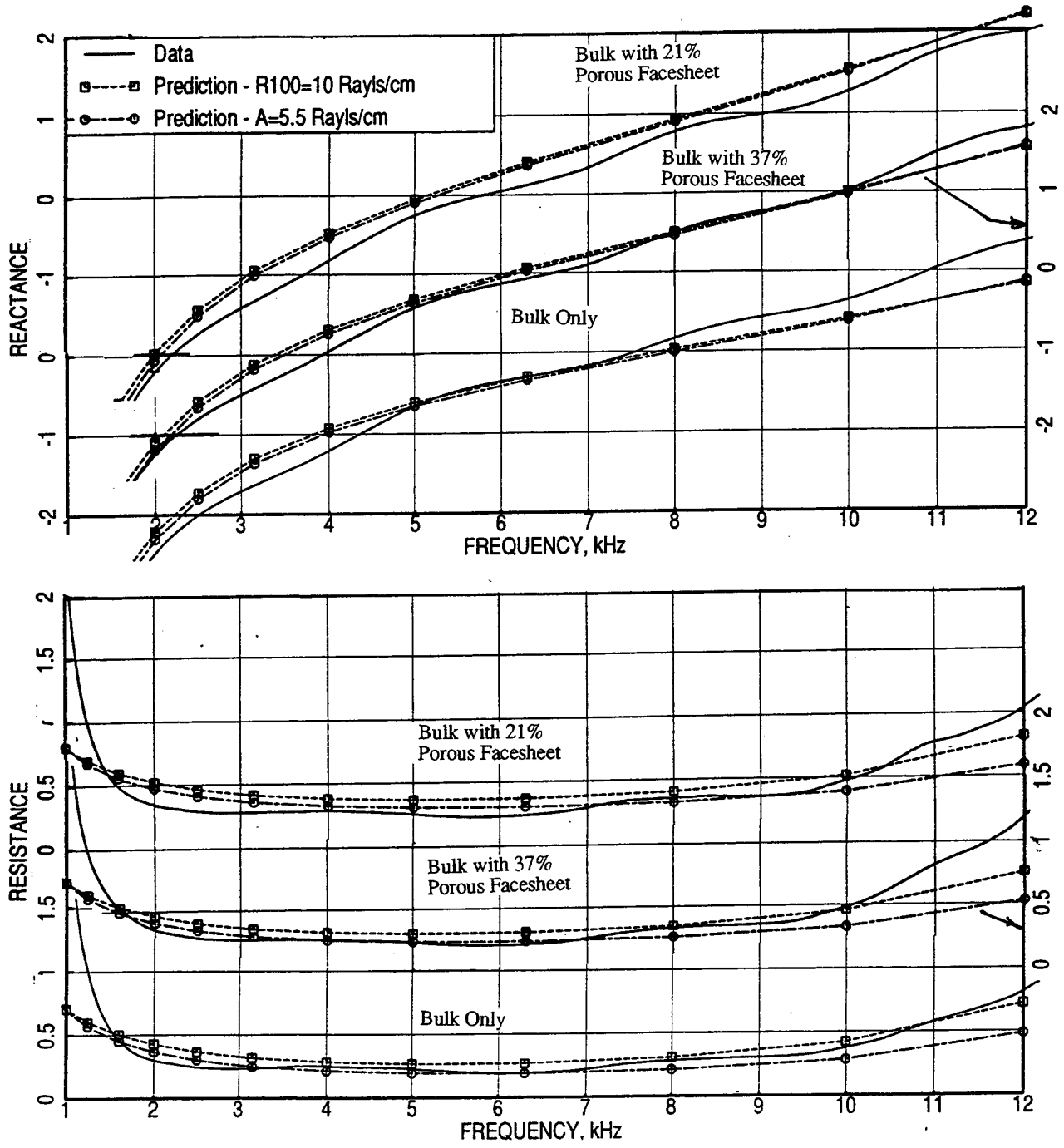

Figure 5. Comparison of measured and predicted normal impedance for a 0.4"-deep 100 ppi Silicon carbide bulk sample with and without facesheet, facesheet thickness and hole diameters are 0.025" and 0.045", excitation OASPL=150 dB.

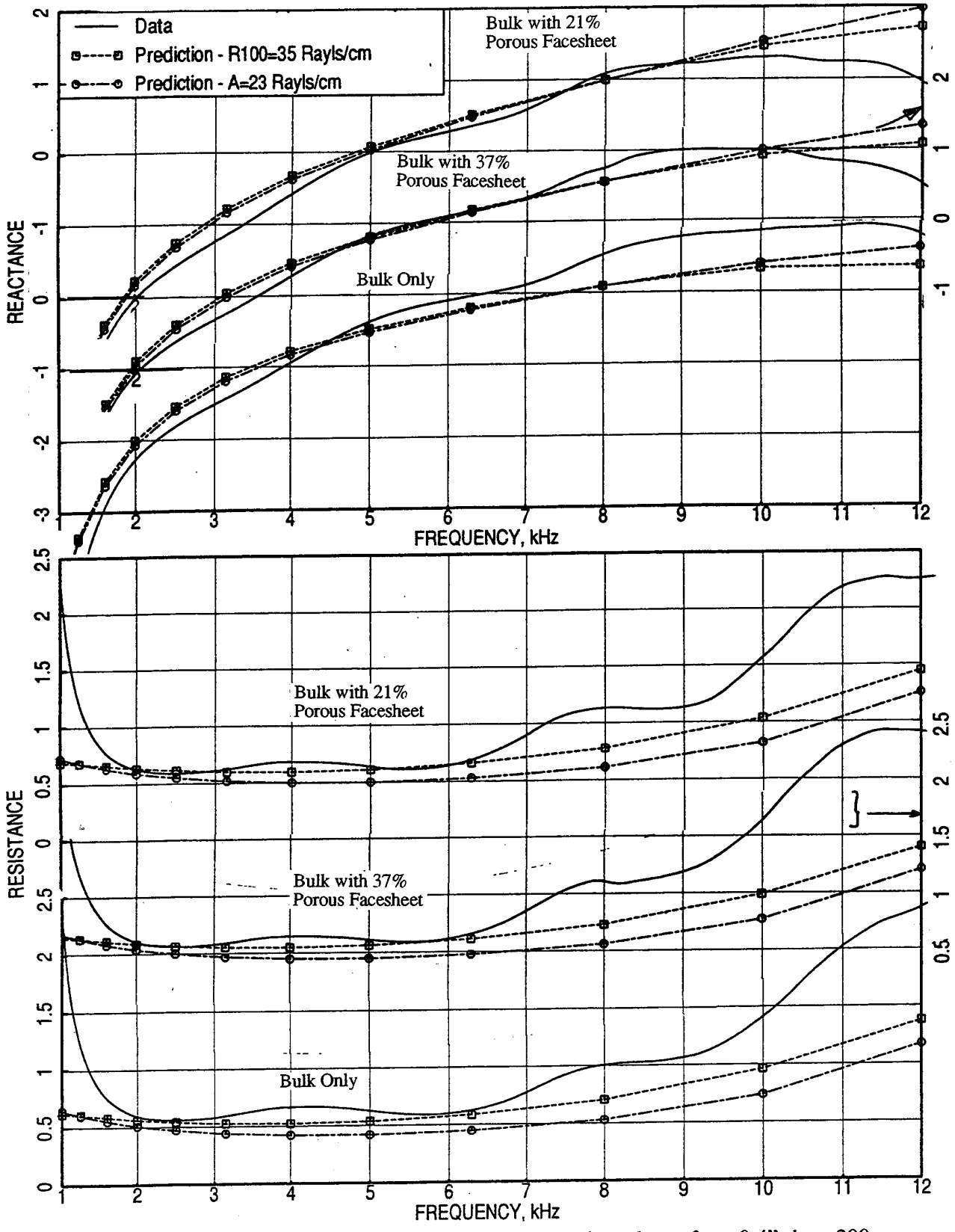

Figure 6. Comparison of measured and predicted normal impedance for a 0.4"-deep 200 ppi Silicon carbide bulk sample with and without facesheet, facesheet thickness and hole diameters are 0.025" and 0.045", excitation OASPL=150 dB.

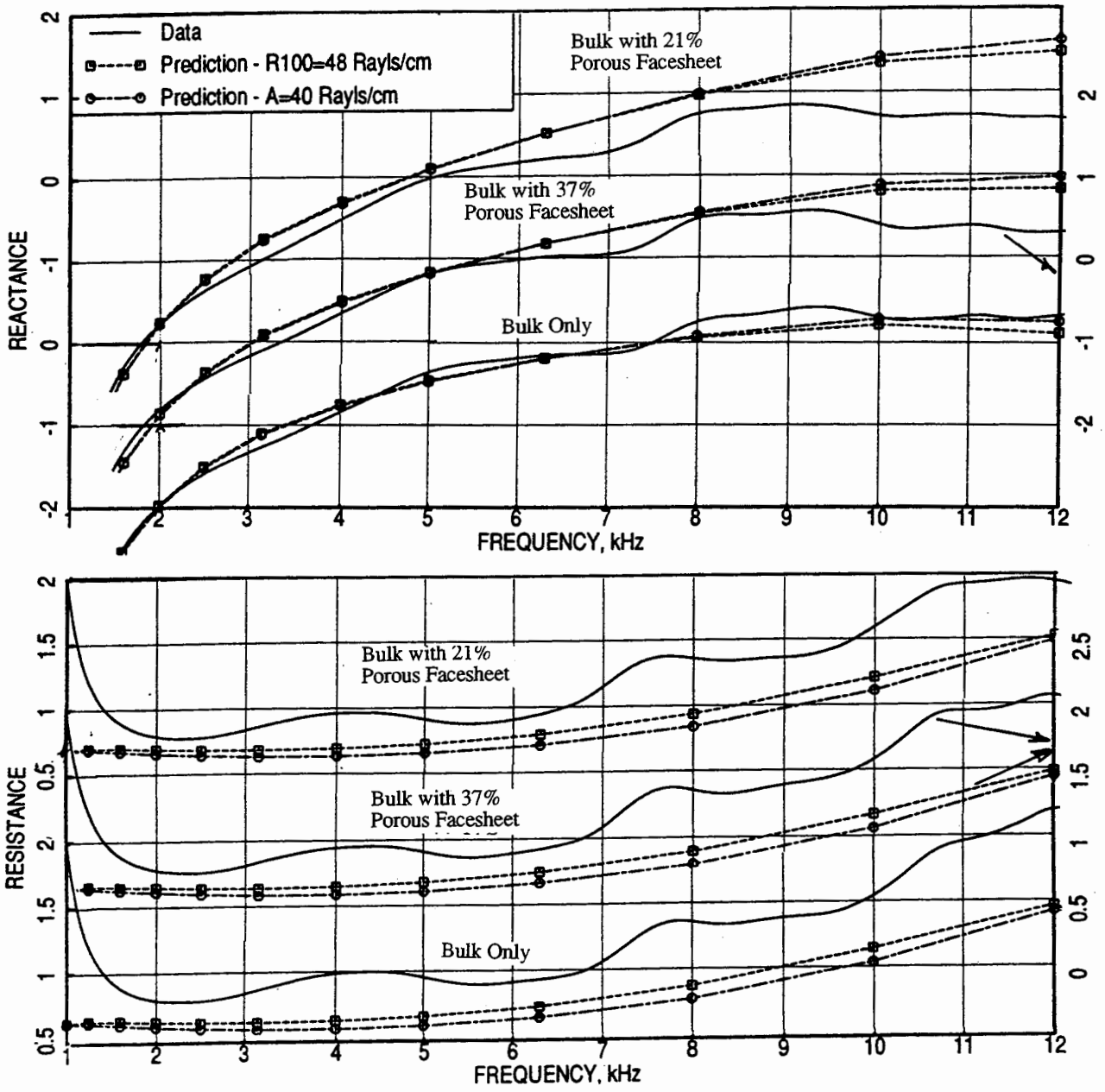

Figure 7. Comparison of measured and predicted normal impedance for a 0.4"-deep 5% dense Feltmetal bulk sample with and without facesheet, facesheet thickness and hole diameters are 0.025" and 0.045", excitation OASPL=150 dB.

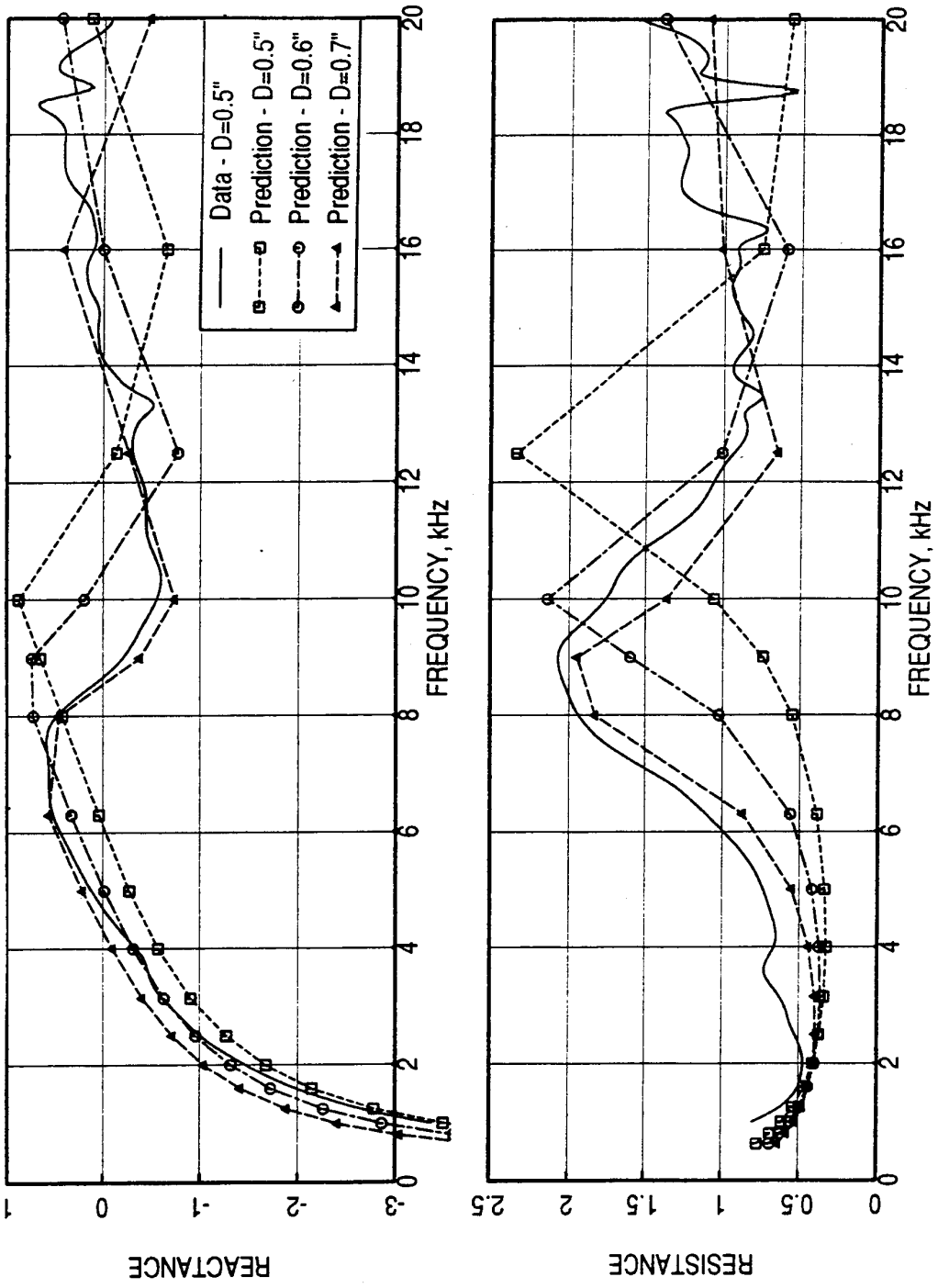

Figure 8. Comparison of measured and predicted (using A=11.8 Rayls/cm) normal impedance for a 0.5"-deep 12 lb/cft T-Foam bulk sample, excitation OASPL=150 dB.

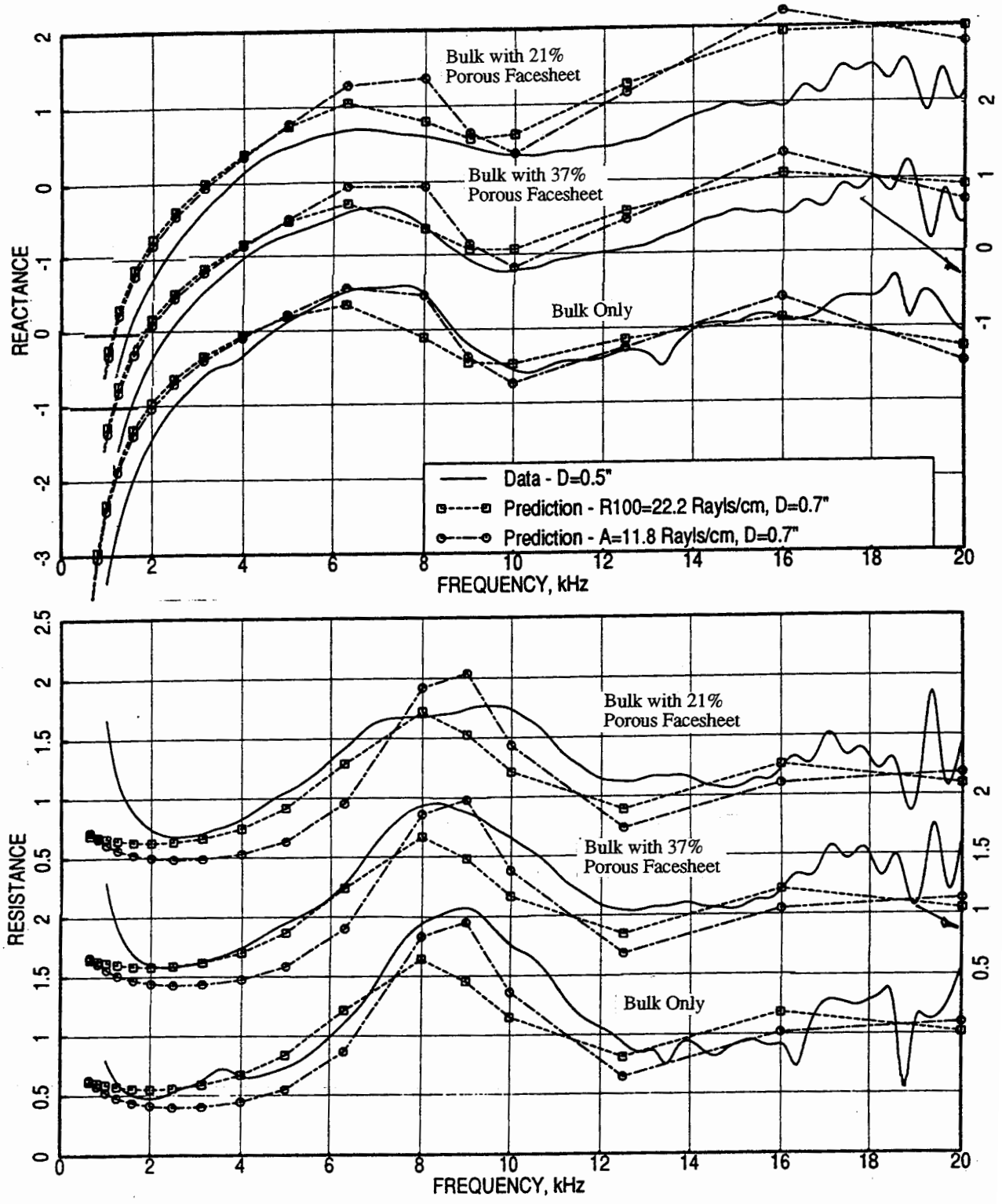

Figure 9. Comparison of measured and predicted normal impedance for a 0.5"-deep 12 lb/cft T-Foam bulk sample with and without facesheet, facesheet thickness and hole diameters are 0.025" and 0.045", excitation OASPL=150 dB.

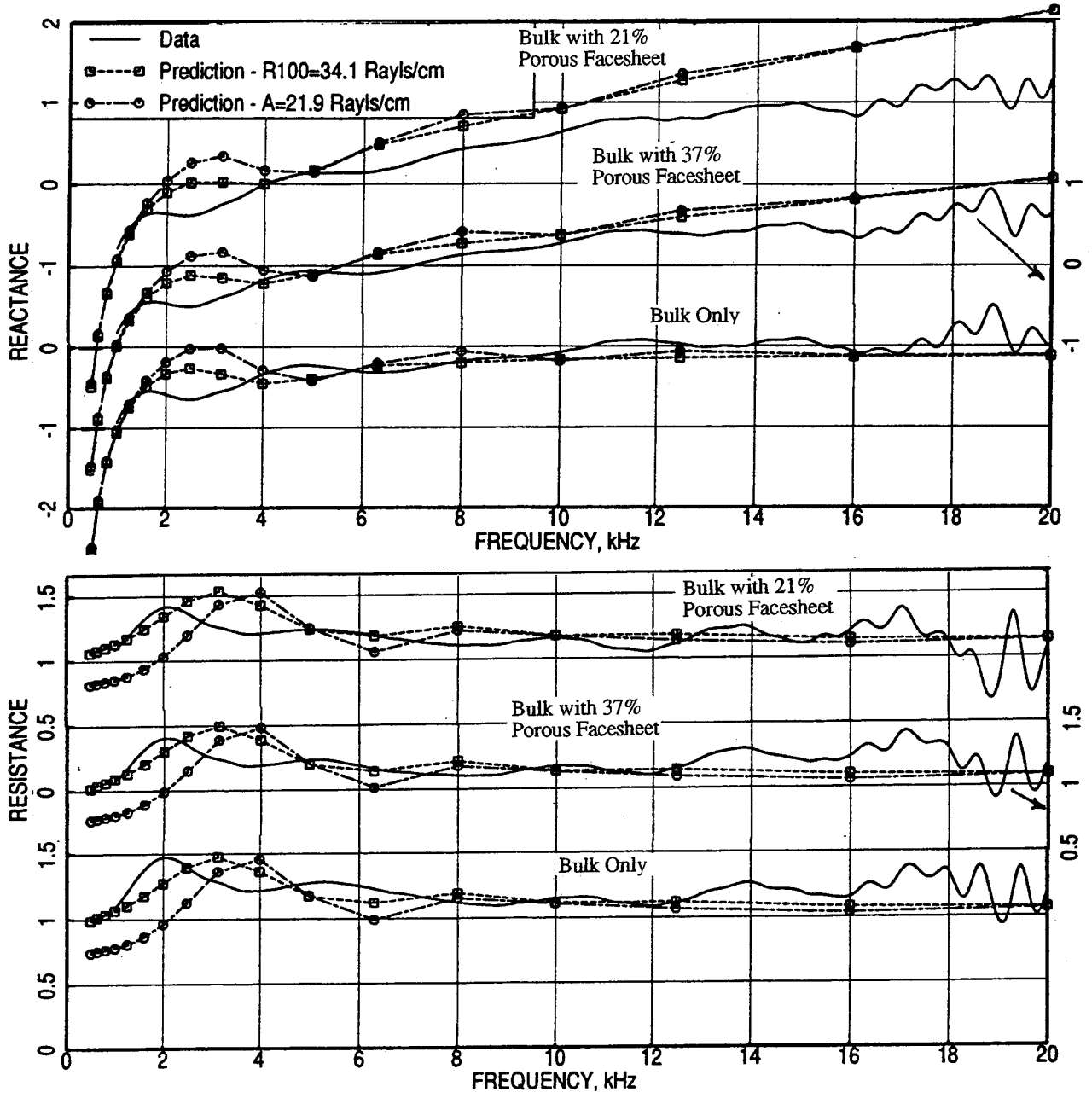

Figure 10. Comparison of measured and predicted normal impedance for a 1.3"-deep 12 lb/cft T-Foam bulk sample with and without facesheet, facesheet thickness and hole diameters are 0.025" and 0.045", excitation OASPL=150 dB.

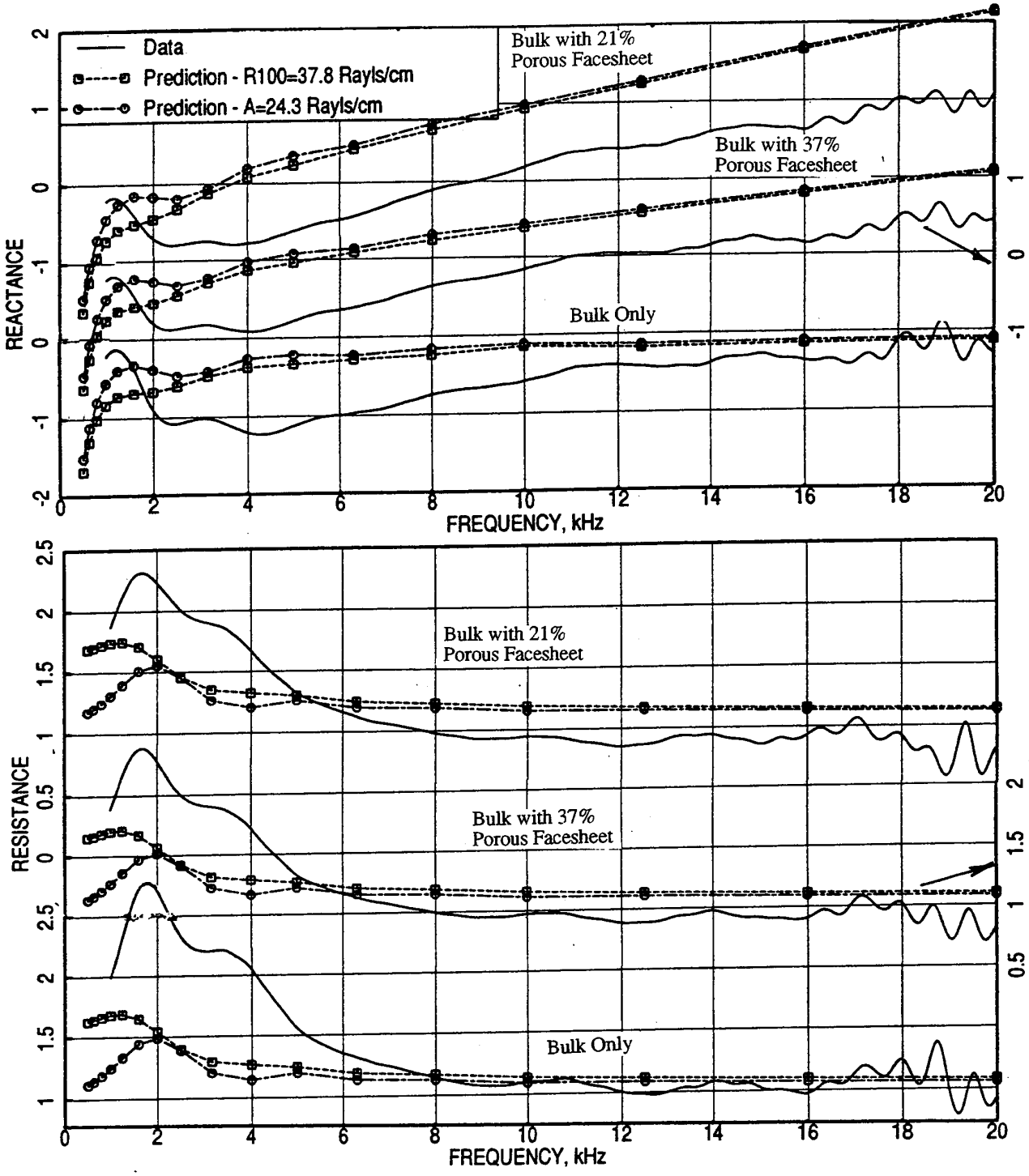

Figure 11. Comparison of measured and predicted normal impedance for a 2.0"-deep 12 lb/cft T-Foam bulk sample with and without facesheet, facesheet thickness and hole diameters are 0.025" and 0.045", excitation OASPL=150 dB.

reactance is matched with the data for bulk only configuration and the same predicted reactance shift is applied to the other two bulk with facesheet cases, the predicted reactance will be slightly higher compared to data at higher frequencies. This difference will be higher for a facesheet with lower porosity. This indicates that the linear addition of bulk and facesheet reactance does not reflect the reality. Similar results for 0.4" deep 200 ppi Silicon carbide and Feltmetal bulk samples are shown in Figures 7 and 8, respectively. For 200 ppi Silicon carbide the agreement between data and prediction is good for entire frequency range for reactance and at lower frequencies up to 7 kHz for resistance. At higher frequencies the predicted resistance levels are lower compared to measured data. Bulk resistivity R_{100} gives a better prediction of resistance than 'A' value. For felt metal, while the reactance comparison is similar to 200-ppi Silicon carbide case, the predicted resistance is lower compared to data for entire frequency range. The resistance agreement between data and prediction seems to be better for lower resistive bulk and gradually deviates with increasing resistivity. The reactance agreement is better for bulk alone and bulk with facesheet of higher porosity.

Measured normal impedance for a 0.5" deep 12 lbf T-foam sample is compared with predicted results in Figure 8. Predicted impedance for a 0.7" deep sample compares well with the measured data. The characteristics of T-foam are quite different from the bulk materials utilized in developing the prediction code. The relation between speed of sound and the T-foam resistivity could be different compared to other bulk materials. Comparison of measured impedance for the 0.5" T-Foam samples (i.e., with and without facesheet) with 0.7" deep sample prediction is shown in Figure 9. Considering the differences in SiC and T-Foam materials (fiber thickness, weave, etc.) the agreement between data and prediction is reasonably good.

Measured and predicted impedance spectrum for 12 lbf T-Foam samples of 1.3" and 2.0" deep are shown in Figures 10 and 11, respectively. The influence of cavity depth on impedance is considerably reduced with increased bulk depth. For 1.3" deep samples the agreement between data and prediction is good for resistance. For bulk only configuration the reactance agreement is very good. For bulk with facesheets the reactance agreement deteriorates with increasing frequency and with decreasing facesheet porosity. For 2.0" deep sample the resistance agreement between data and prediction is poor at lower frequencies. Reactance is overpredicted at most frequencies.

In general, the agreement between the data and prediction is acceptable for the materials considered such that, the prediction code can be used to design the liners for different scale

mixer-ejectors. However, better prediction for HSCT liner designs is being developed utilizing the more relevant test data under the liner technology program.

3.2 Using Measured Ambient Normal Impedance: A large number of normal impedance measurements are made for various bulk and SDOF type liner designs at ambient conditions for the development of normal impedance prediction methods (Ref. 3). Attempt is made to utilize the measured data to derive the normal impedance of various liner designs accounting for flow, temperature, and acoustic environment effects. The prediction method described in section 3.1 is utilized in this process to evaluate the relative impedance due to flow, temperature, and acoustic environment. The relative impedance spectra are added to the measured ambient data to obtain the final results. The prediction method is used to predict the normal impedance at ambient condition at which the measurement is made for a liner design. Normal impedance is also predicted at the desired flow, temperature T_{des}, and acoustic conditions for the same liner design. Multiplying the following temperature factor normalizes the frequency for the desired prediction;

$\sqrt{(T_{amb}/T_{des})}$, T_{amb} being the ambient temperature.

Thus the relative impedance is derived and is added to the measured impedance with respect to normalized frequency. Figures 12 and 13 show typical constructed normal impedance along with the measured and predicted results with respect to actual frequency for a full scale liner design. It should be noted that the measured data is available in narrowband up to 20 kHz. and the predicted and constructed data are obtained in 1/3-octabe band up to 10 kHz. Figure 12 shows the impedance results for a 100-ppi 2"-deep bulk absorber with a perforated facesheet for takeoff and cutback conditions. The predicted resistance at the desired temperature agrees well with the constructed values. The predicted reactance seems to be higher compared to the constructed values, especially at higher frequencies. Similar results at cutback conditions are shown in Figure 13 for 2"-deep T-Foam bulk absorbers of different bulk densities. While the agreement between predicted and constructed data is reasonable for 8 lbf T-Foam, it is not so for 12 lbf T-Foam. For this case the constructed impedance levels are significantly off from the prediction.

Similar results for LSM scale liner designs are shown in Figures 14 and 15. Figure 14 shows the impedance plots for 1.2"-deep 100 ppi SiC bulk absorbers with facesheets of different porosity for takeoff conditions. Reasonable agreement is observed between constructed and predicted results. Predicted resistance levels are slightly lower and reactance levels are slightly higher compared to the constructed data. Figure 15 shows the similar results for two

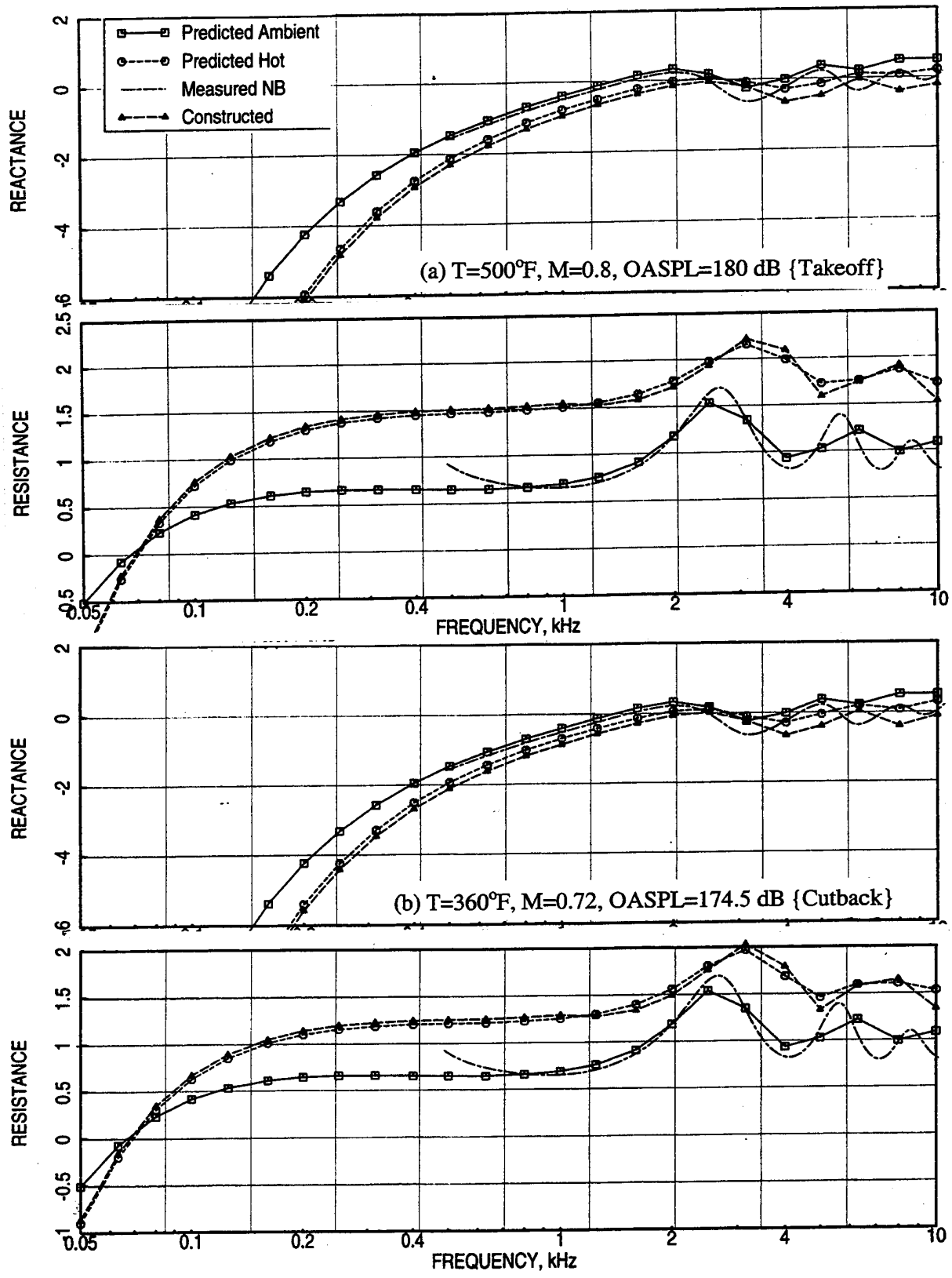

Figure 12. Construction of normal impedance spectra for a full-scale 2..0"-deep 100 ppi Silicon Carbide liner with a 40% porous facesheet (t=d=0.04").

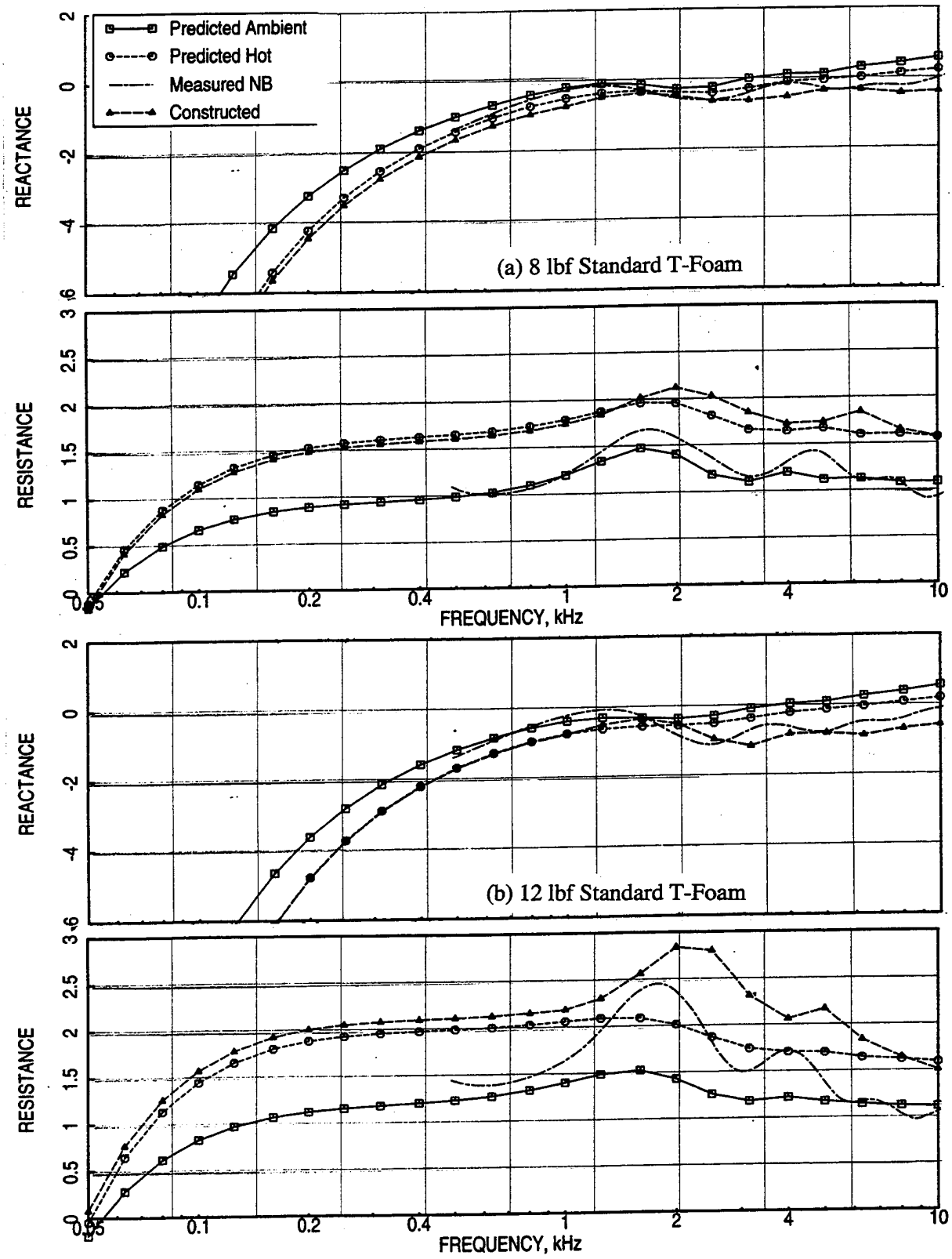

Figure 13. Construction of normal impedance spectra for full-scale 2..0"-deep T-Foam liners with a 40% porous facesheet (t=d=0.04") for cutback conditions (T=360°F, M=0.72, OASPL=174.5 dB).

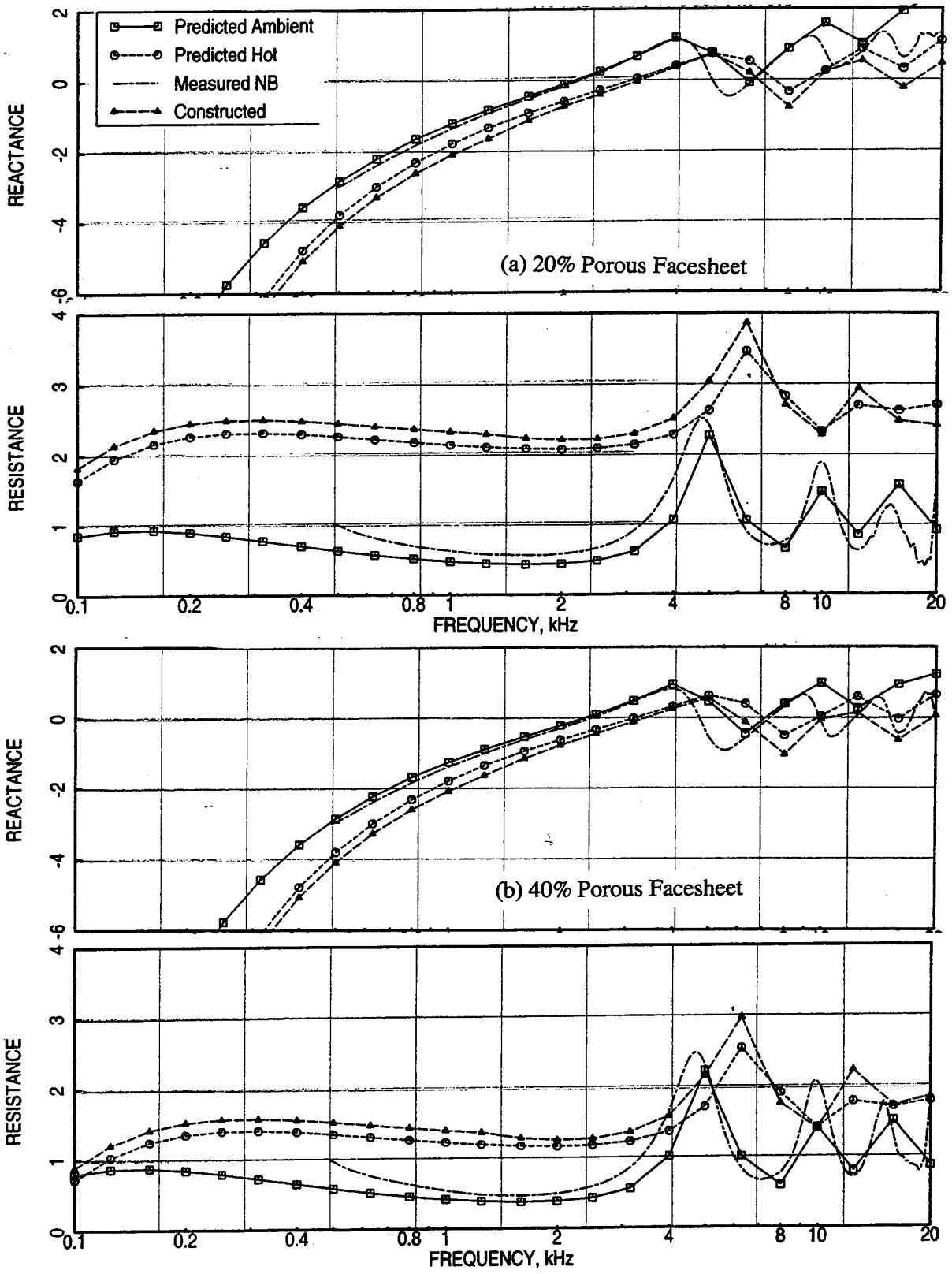

Figure 14. Construction of normal impedance spectra for LSM size 1.2"-deep 100 ppi Silicon Carbide liners with facesheets of different porosities (t=d=0.04") for takeoff conditions (T=500°F, M=0.8, OASPL=180 dB).

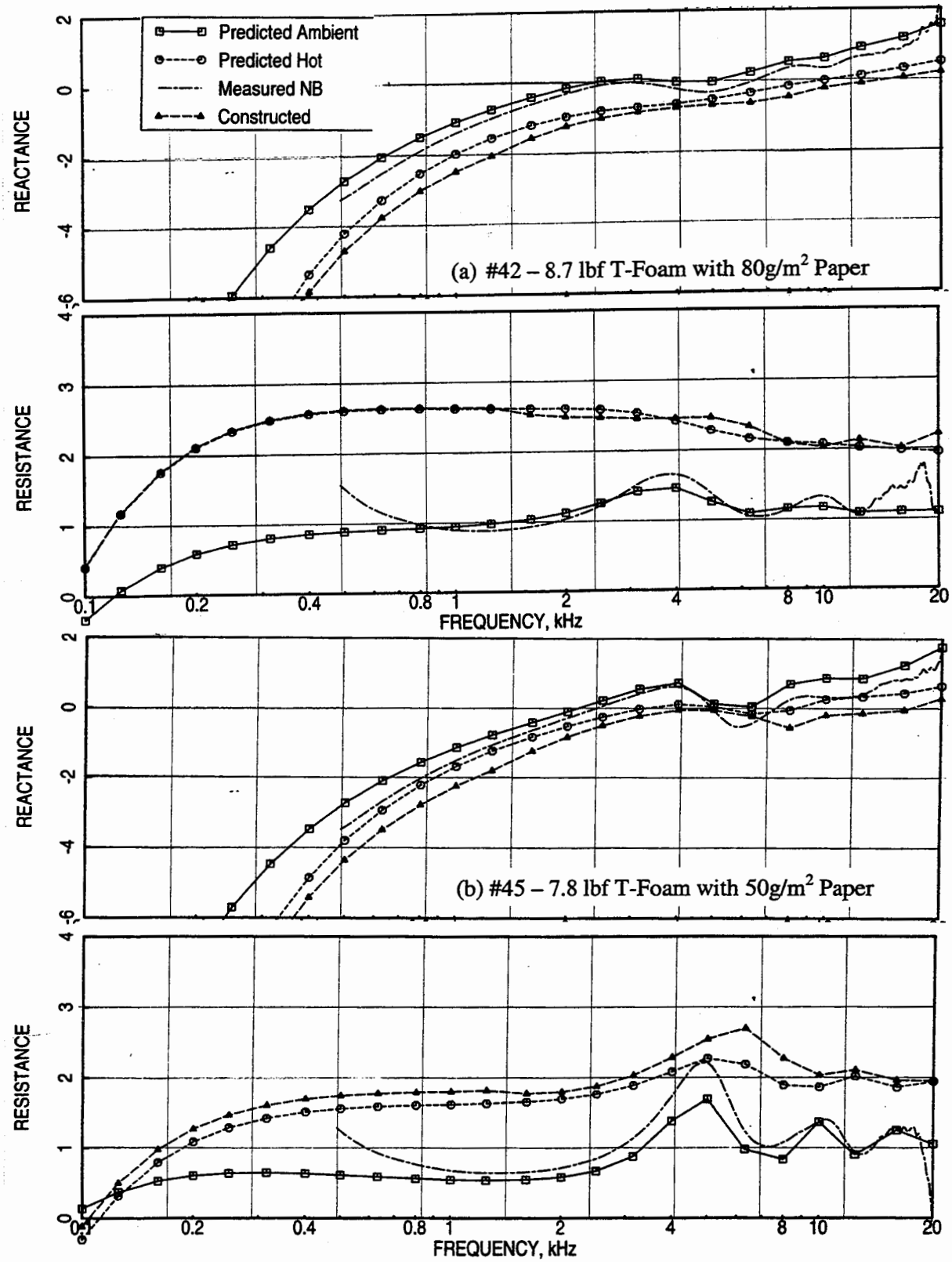

Figure 15. Construction of normal impedance spectra for LSM size 1.2"-deep T-Foam liners with three layers of woven paper construction and with 37% porous facesheets (t=0.04", d=0.054") for takeoff conditions (T=500°F, M=0.8, OASPL=180 dB).

different T-Foam bulk absorbers with 3 layers of paper construction (Ref 3). While the agreement between predicted and constructed impedance levels are reasonably good for T-Foam with papers of 80 g/m2 the agreement is not so good for the T-Foam liner with papers of 50 g/m2.

Finally, similar results for a 1/7-scale liner design are shown in Figure 16 for takeoff and cutback conditions. For 1/7-scale the normal impedance is required up to 80 kHz for acoustic suppression evaluation. Since the measured data is only available up to 20 kHz the predicted data at the desired condition is utilized above 20 kHz. The predicted data is shifted to match the constructed levels at 20 kHz. and used above 20 kHz. This process is again performed with respect to normalized frequency. The results shown in Figure 16 are for a 0.5"-deep 100 ppi SiC bulk absorber with a 37% porous perforated facesheet. Agreement between predicted and constructed data is very well for reactance and is reasonably good for resistance.

3.3 Using Measured Ambient Normal Impedance and Measured Relative In-situ Impedance due to Flow & Temperature: In addition to normal impedance measurements at ambient condition a number of tests are conducted in a flow duct facility to evaluate the effect of grazing flow Mach number and temperature of heated flows on normal impedance for bulk absorber and SDOF type liners (Ref. 3). These data can be directly used to derive normal impedance of a liner design in desired flow and temperature conditions. The evaluated relative impedance using the measurements is available at a number of set Mach numbers and temperature conditions. To utilize the data at any other condition not the same as measured conditions it is necessary to interpolated/extrapolated the data. Again, the data is limited to 20 kHz. Data above this frequency would require a prediction model. The predicted results can, then be shifted to match with the constructed data at 20 kHz (similar to what is described in section 3.2).

Figure 17 shows the effect of grazing flow Mach number on the normal impedance for 0.5"-deep bulk absorbers with perforated facesheet. The data at M=0.0 is the normal impedance measured at ambient condition. The relative impedance evaluated from in-situ impedance measurements (Ref. 3) are then added to the ambient data to account for the grazing flow effects. Figure 18 shows the effect of grazing flow temperature at M=0.55 for the same bulk absorber liners. Again, the adders to the ambient data are the relative impedance due to M=0.55 and relative impedance due to temperature difference relative to the ambient. This process is performed with respect to normalized frequency.

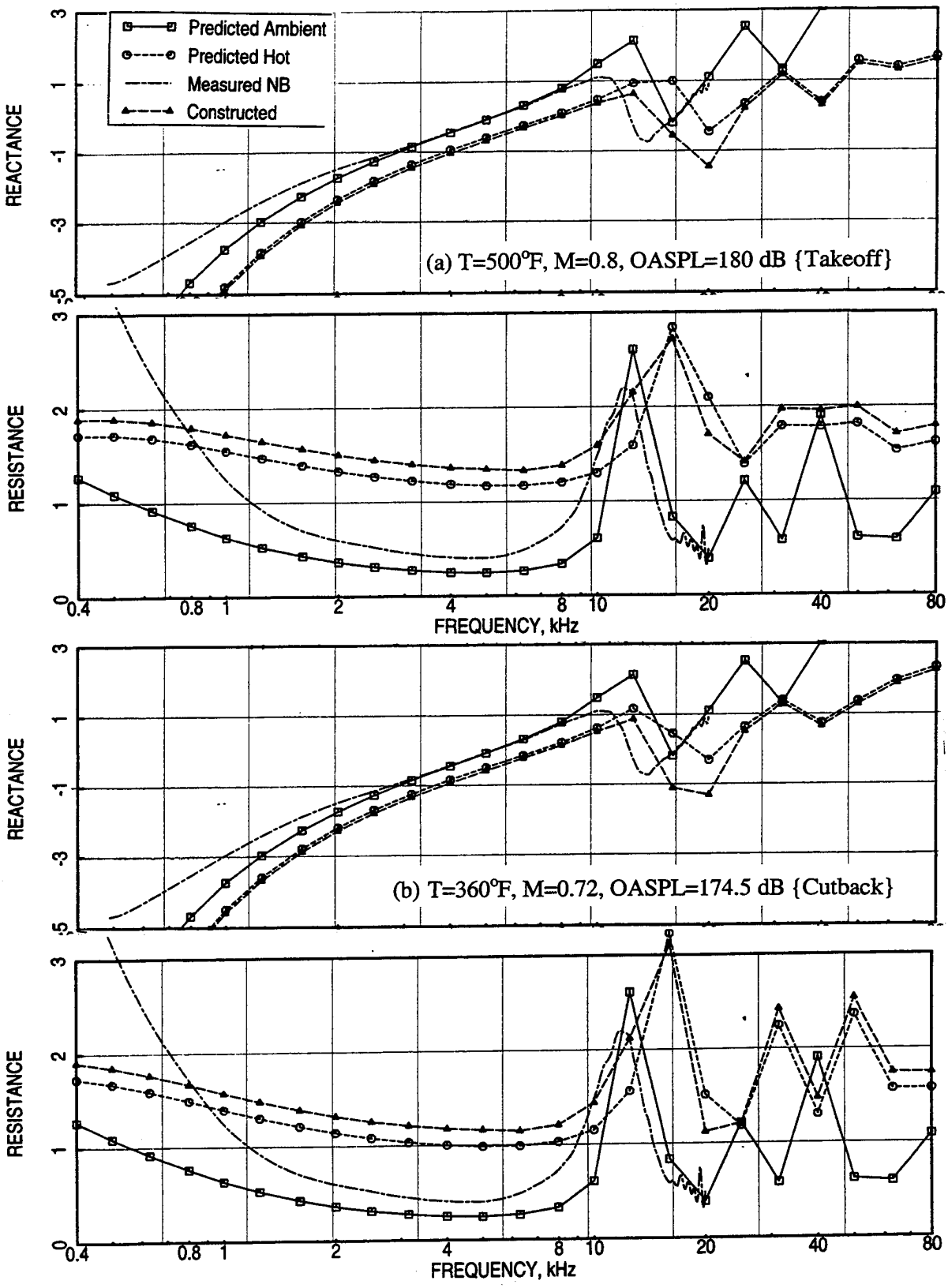

Figure 16. Construction of normal impedance spectra for a 1/7-scale 0.5"-deep 100 ppi Silicon Carbide liner with a 37% porous facesheet (t=0.025", d=0.045").

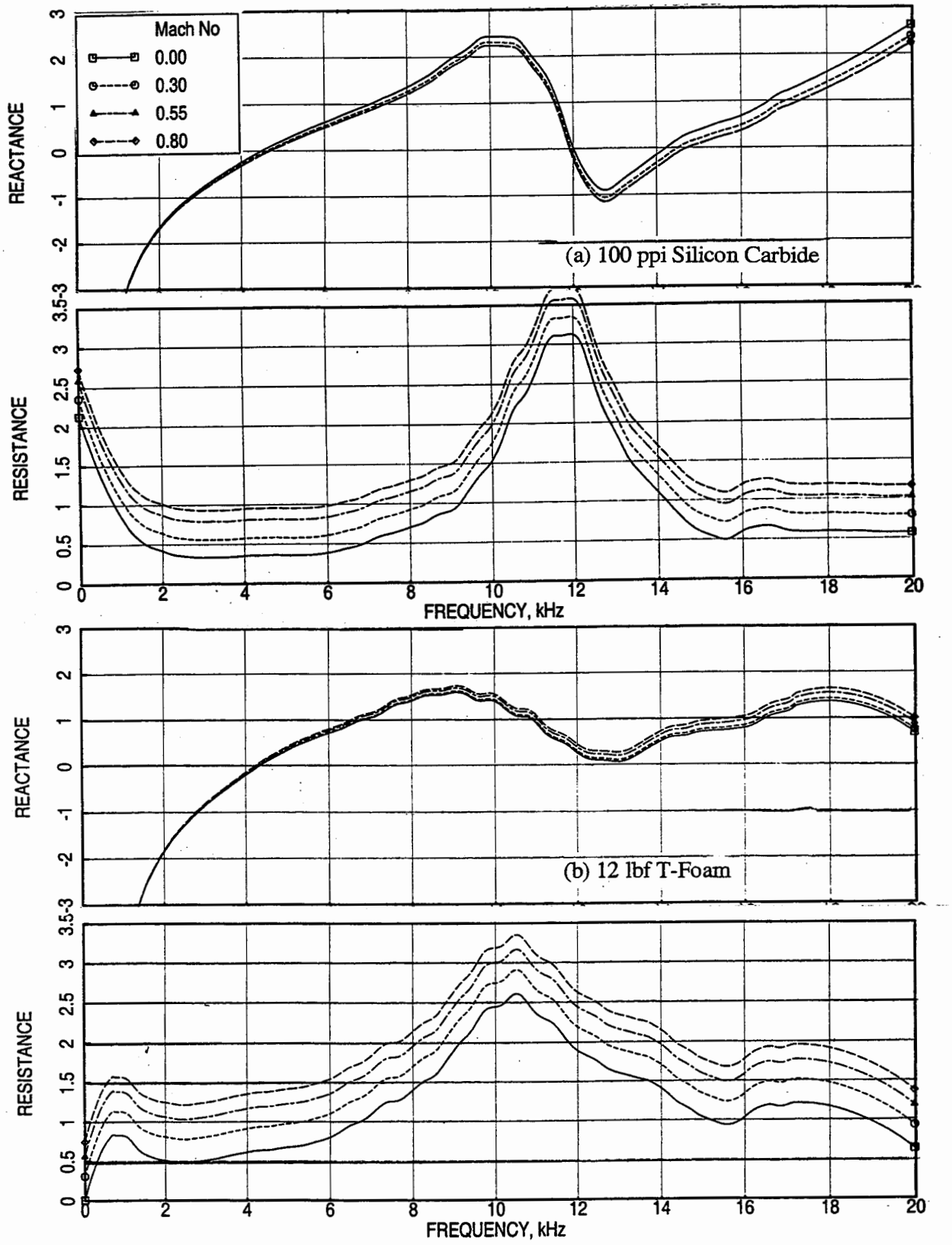

Figure 17. Effect of grazing flow Mach number (M) on normal impedance for 0.5"-deep (a) 100 ppi Silicon Carbide and (b) 12 lbf T-Foam panels with 20% porous 0.025"-thick facesheet with 0.04" diameter holes.

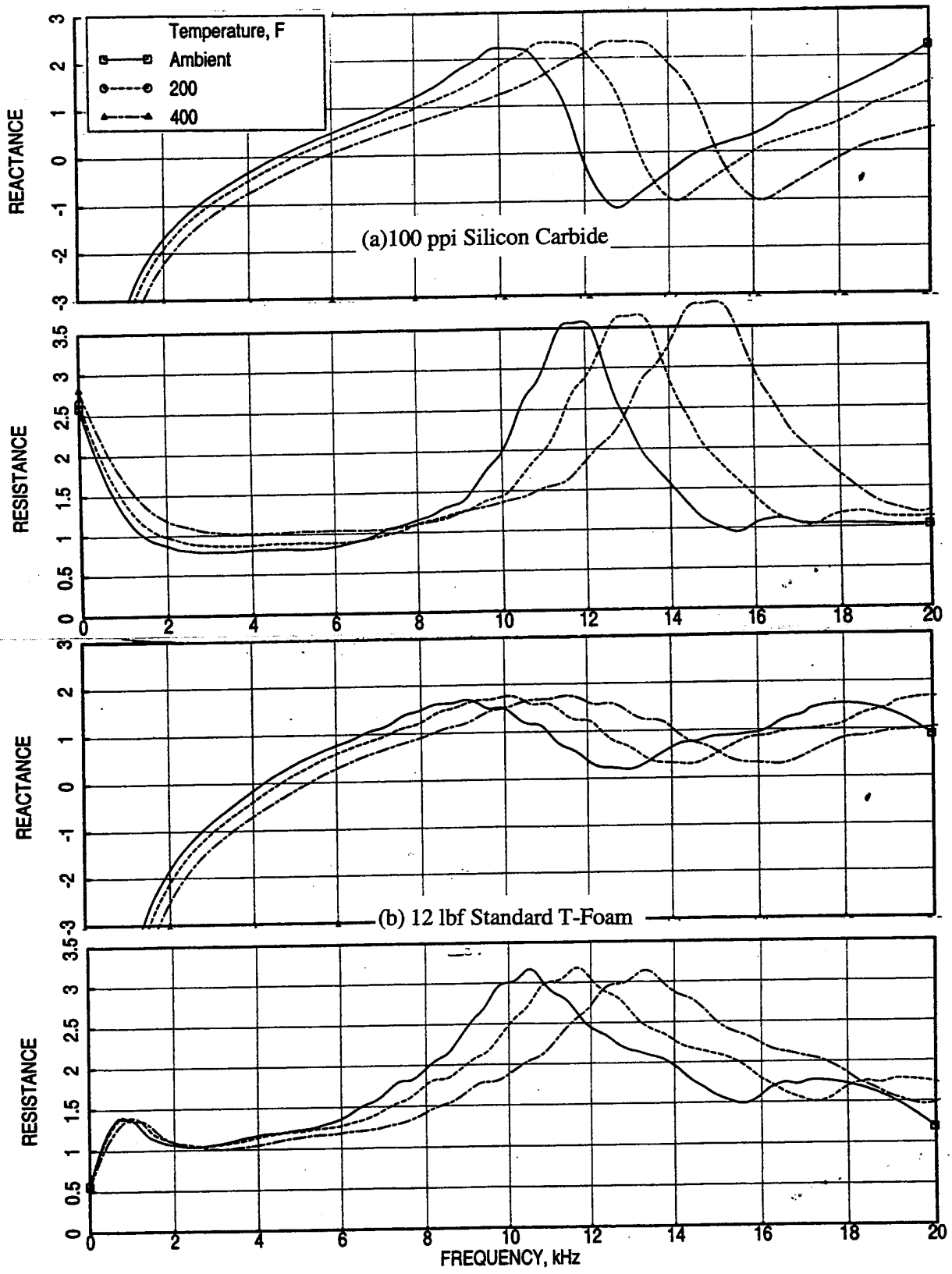

Figure 18. Effect of grazing flow temperature (T) on normal impedance for 0.5"-deep bulk absorber panels with 20% porous 0.025"-thick facesheet with 0.04" diameter holes at M=0.55.

3.4 Current Prediction Method: The current normal impedance prediction methods for various liner designs are developed using the measured ambient normal impedance and measured in-situ impedance at different grazing flow Mach numbers and temperatures. In addition, measured boundary layer parameters (i.e., displacement thickness) and DC flow resistance data for various panels are utilized in the development of these prediction methods. Correlated expressions, relevant results, and the physical description of the development work are presented in a separate report (Ref. 4).

Comparisons of normal impedance are made between the existing prediction (Prediction – Old), the current prediction (Prediction – New), and the evaluated data, described in section 3.3 (Measured) in Figures 19 through 21. Figure 19 shows the impedance comparisons for 0.5"-deep 100 ppi SiC and 12 lbf T-Foam absorbers with perforated facesheet at ambient condition without any grazing flow. Agreement between data and current prediction seems to be better compared to the old prediction. Similar conclusion can be drawn from the results of Figure 20, which are for the same absorbers of Figure 19 but with a grazing flow Mach number of 0.8. Similar comparisons at a heated condition of 400°F at a grazing flow Mach number of 0.8 are shown in Figure 21. While, the agreement between new prediction with data is reasonably good for 100 ppi SiC, the agreement is not so good for the 12 lbf T-Foam absorber. In general, the predicted normal resistance at and around the ant-resonance frequency is much higher compared to the measured data. At this stage it may not be possible to improve the prediction method due to the program closeout. However, it is essential to improve the prediction methods in future when the HSCT program will continue.

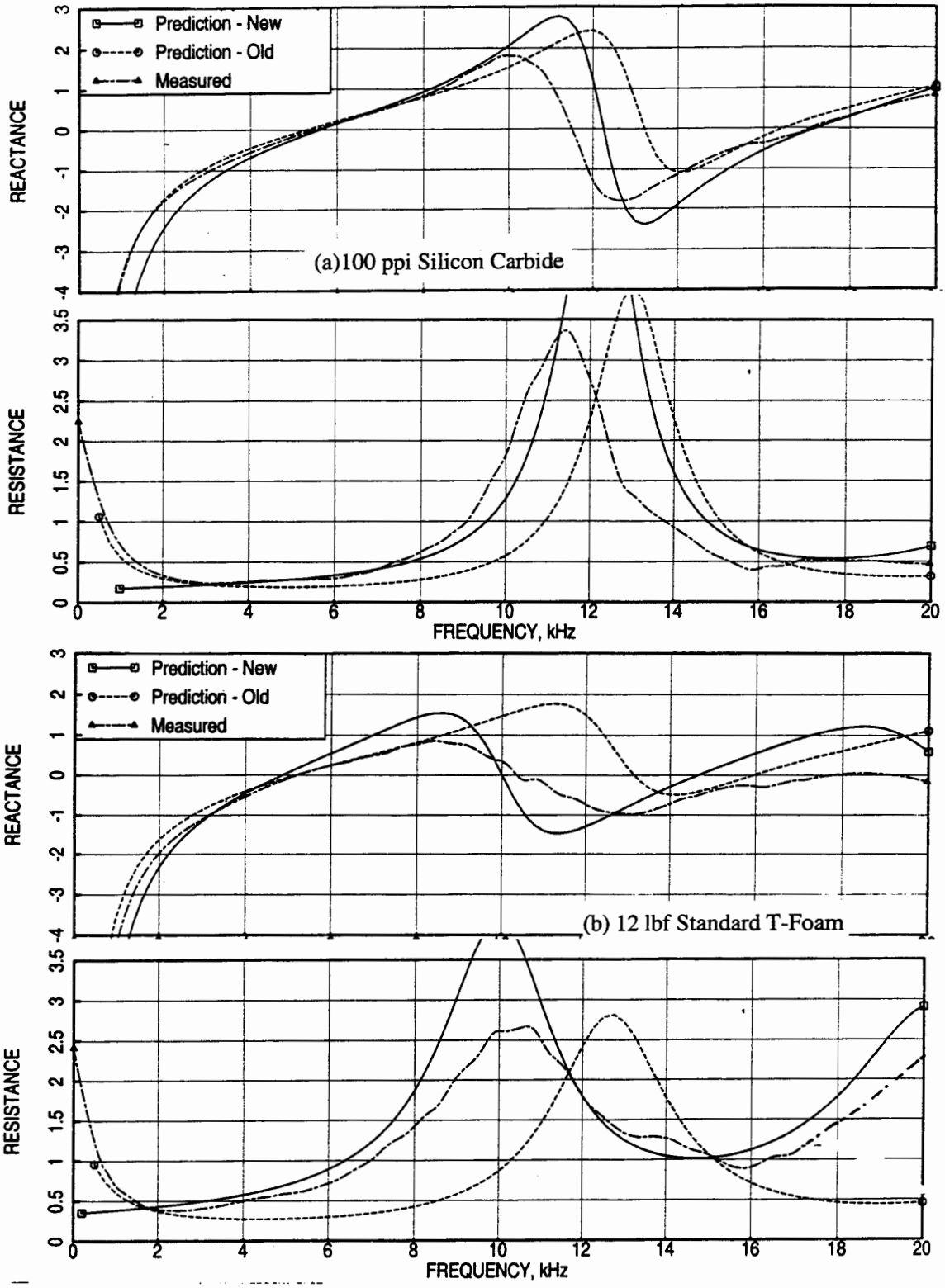

Figure 19. Comparison of normal impedance spectra between data and predictions for 0.5"-deep bulk absorber liners with 40% porous facesheet (t=0.025", d=0.04") at ambient condition, M=0, OASPL=154 dB.

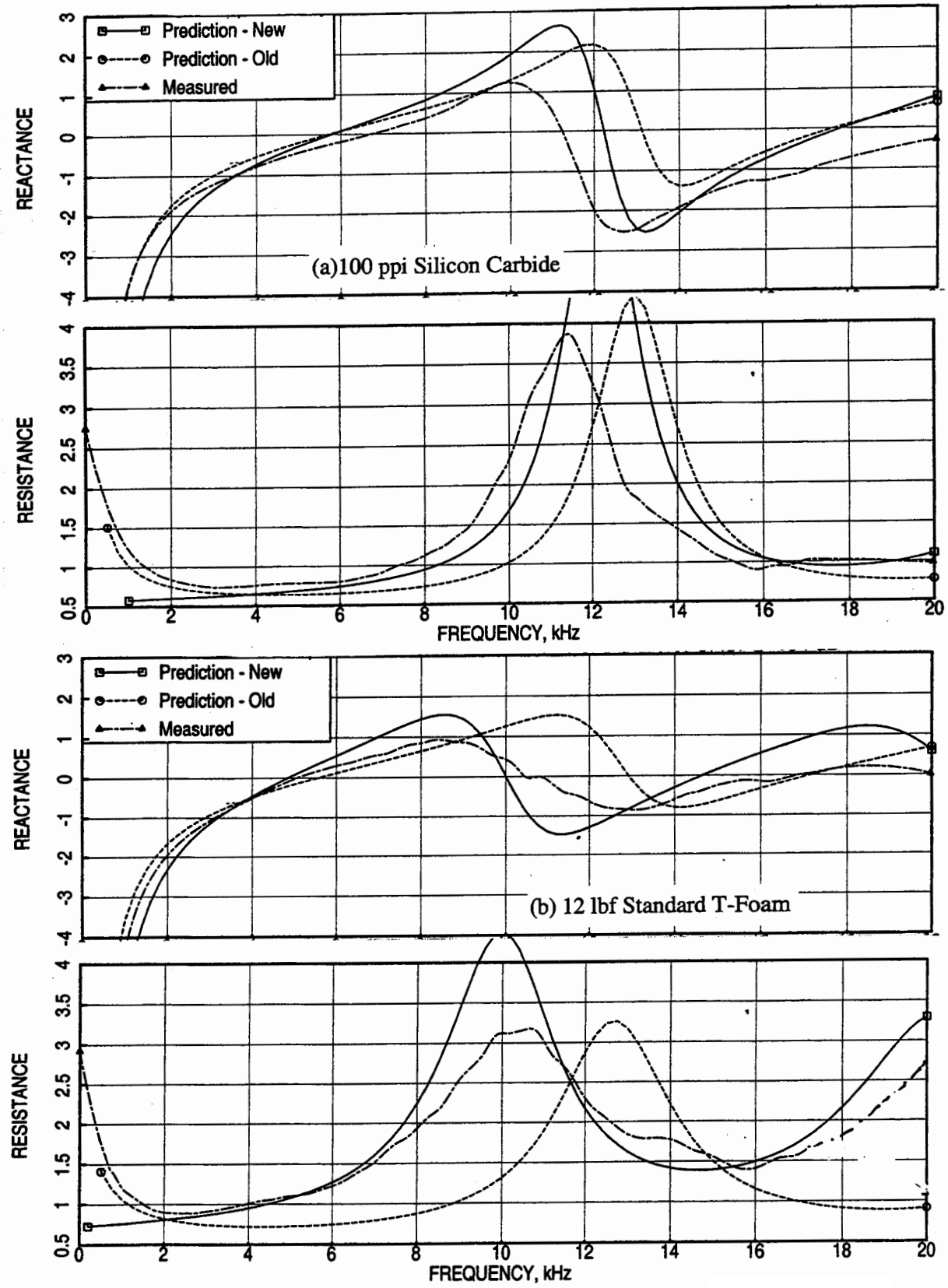

Figure 20. Comparison of normal impedance spectra between data and predictions for 0.5"-deep bulk absorber liners with 40% porous facesheet (t=0.025", d=0.04") at ambient temperature, M=0.8, OASPL=154 dB.

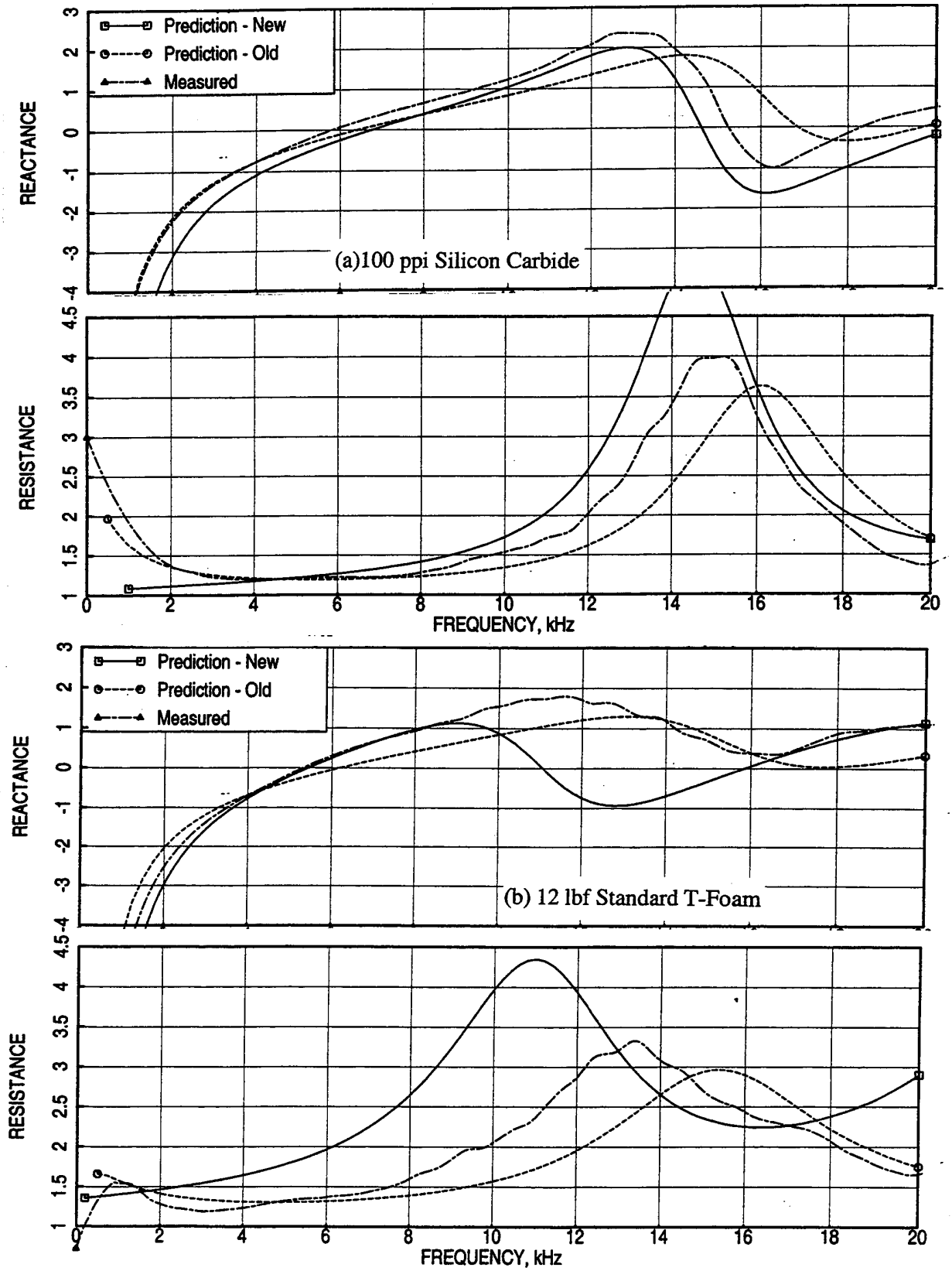

Figure 21. Comparison of normal impedance spectra between data and predictions for 0.5"-deep bulk absorber liners with 20% porous facesheet (t=0.025", d=0.04"), T=400°F, M=0.8, OASPL=154 dB.

4.0 ACOUSTIC SUPPRESSION PREDICTION DUE TO EJECTOR TREATMENT

Acoustic suppression internal to a treated ejector can be evaluated either by modal analysis technique or by semi-empirical methods based on measured data. For the current program both these methods are available for HSCT application. Uniform flow and temperature conditions are assumed in both these methods. Normal impedance spectra for the treatment are the main input for acoustic suppression evaluation. In addition, the ejector geometry, flow conditions, and the boundary layer displacement thickness on the ejector surface are required as inputs.

4.1 Modal Analysis Technique: A rectangular duct modal analysis computer program is adapted to evaluate the acoustic suppression performance of treated ejectors. The analytical method is simplified to duct modal analysis with the assumption of equal modal energy distribution. The physical background of this method is described in Reference 1. Currently, the acoustic suppression due to the first 50 transverse modes along the two treated flaps (with hard sidewalls) is accounted for. Acoustic suppression due to successive modes, up to 10 transverse modes, for three treated mixer-ejector models (i.e., full-scale, LSM, and 1/7-scale) at takeoff and cutback conditions are shown in Figures 22 through 24. Similar results covering 50 transverse modes at an interval of 5 modes are shown in Figures 25 through 27. Based on the model size and flow conditions different number of modes are being cut-on at different frequencies. The first 10 modes cover most acoustic suppression up to the peak levels. The first 50 modes, as considered in the current analysis, cover the acoustic suppression for frequencies up to about 5, 10, and 40 kHz for full-scale, LSM, and 1/7-scale size ejectors. Apparently, several more modes (of the order of 110 to 120) are to be included in the analysis to cover the acoustic suppression for the entire frequency range of interest. The contribution from these additional modes may not change the peak suppression level and its frequency, but expected to increase the acoustic suppression at higher frequencies.

4.2 Semi-Empirical Models for Acoustically Treated Mixer-Ejector Suppressors: Measured farfield data for a number of mixer-ejector tests are used in the development of semi-empirical models to predict acoustic suppression inside treated ejectors. A mode cut-off ratio is applied in this approach. Normal impedance used in this computation is predicted from various correlation schemes for bulk absorber liners. Normal impedance prediction schemes are developed using the laboratory test data acquired under the current program (Refs. 1 and 3). The development process for normal impedance and acoustic suppression evaluation, performed by Dr. E. J. Rice, is described in Reference 4. Figure 28 shows comparisons between the predicted acoustic suppression with measured ΔPWL data for a

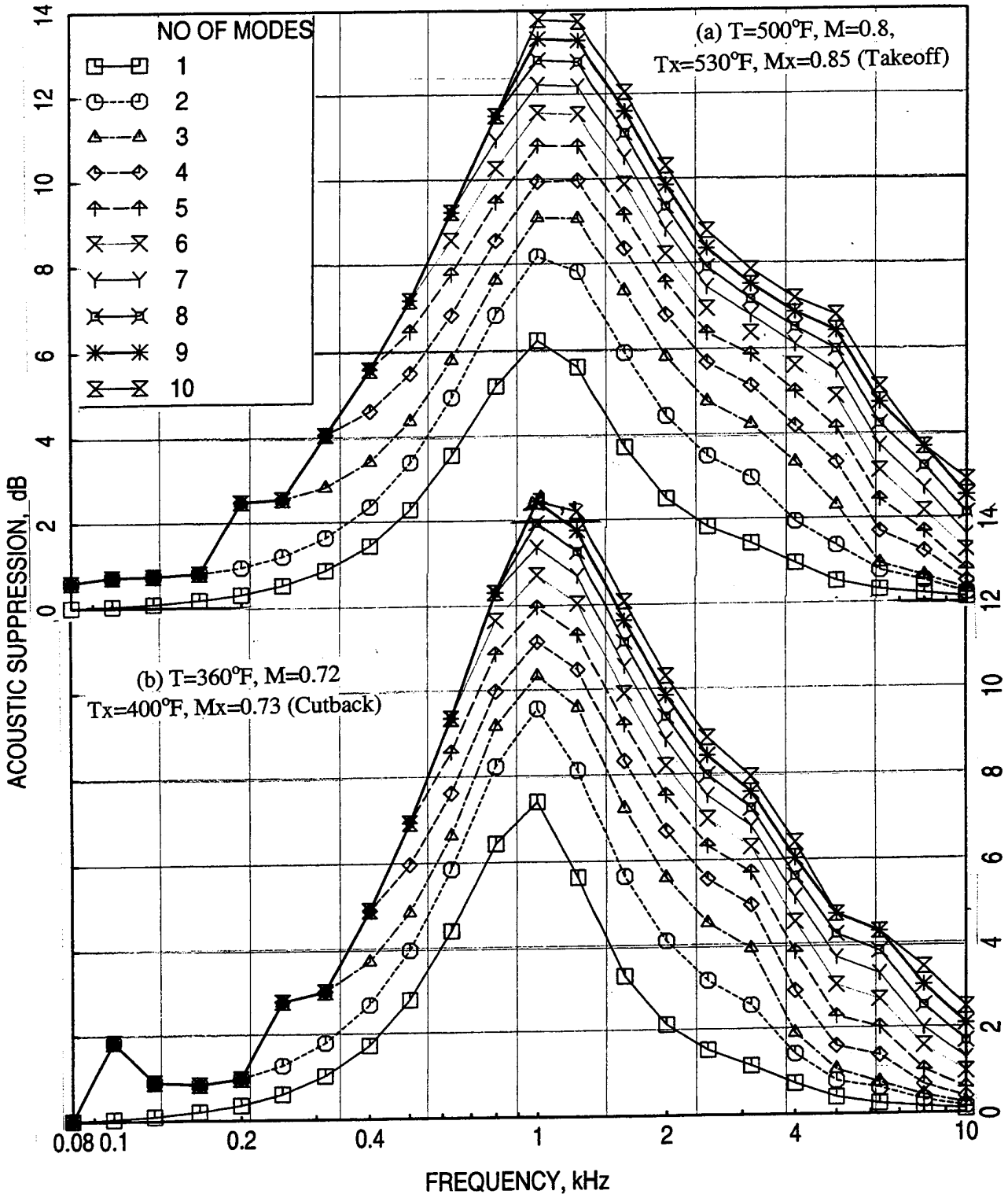

Figure 22. Contribution of first 10 transverse modes on predicted acoustic suppression spectra for a full-scale mixer-ejector liner design, D=2", R=10 Rayls/cm, S=40%, t=0.04", d=0.04", OASPL=180 dB.

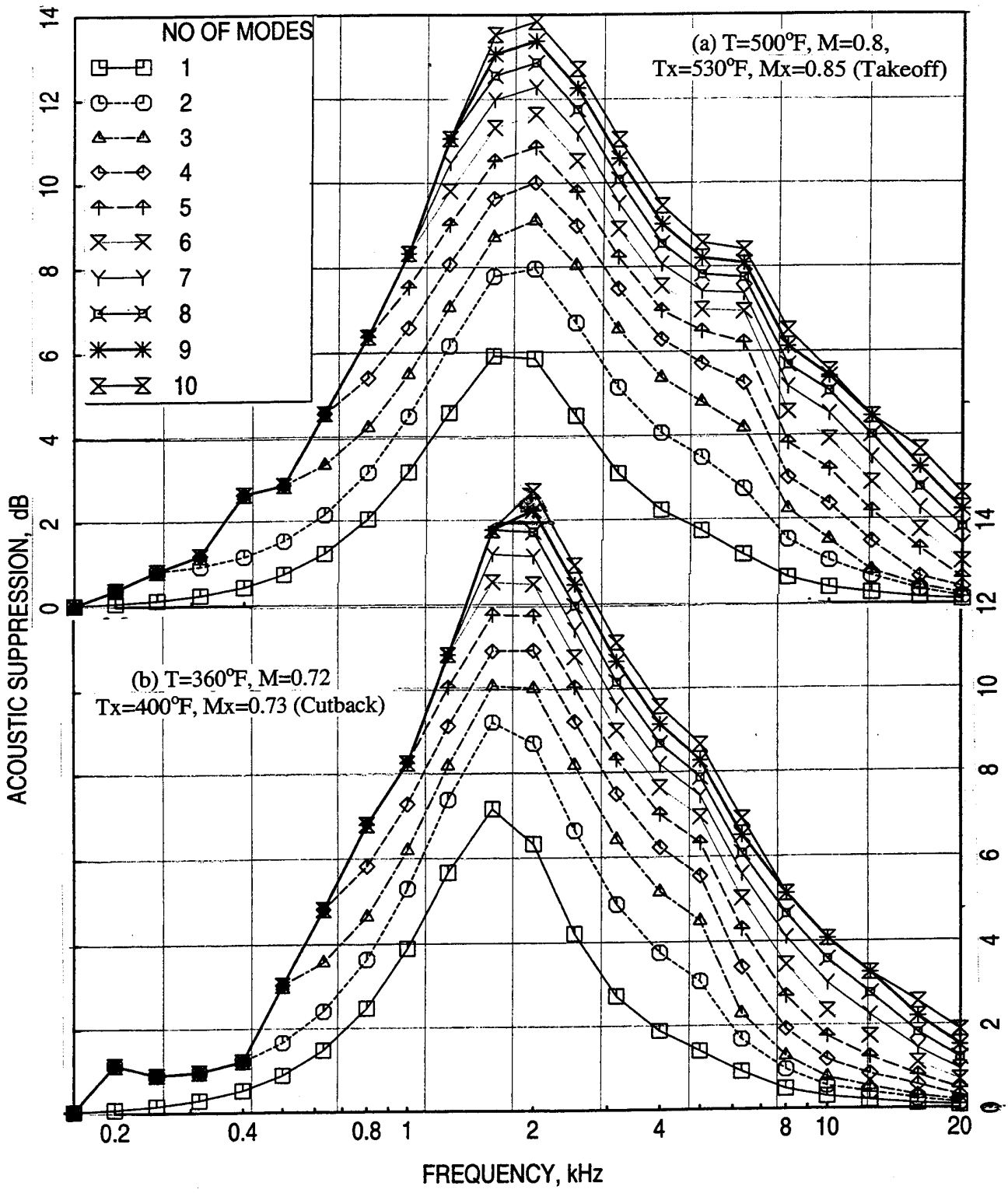

Figure 23. Contribution of first 10 transverse modes on predicted acoustic suppression spectra for an LSM mixer-ejector liner design, D=1.2", R=20 Rayls/cm, S=40%, t=0.02", d=0.025", OASPL=177 dB.

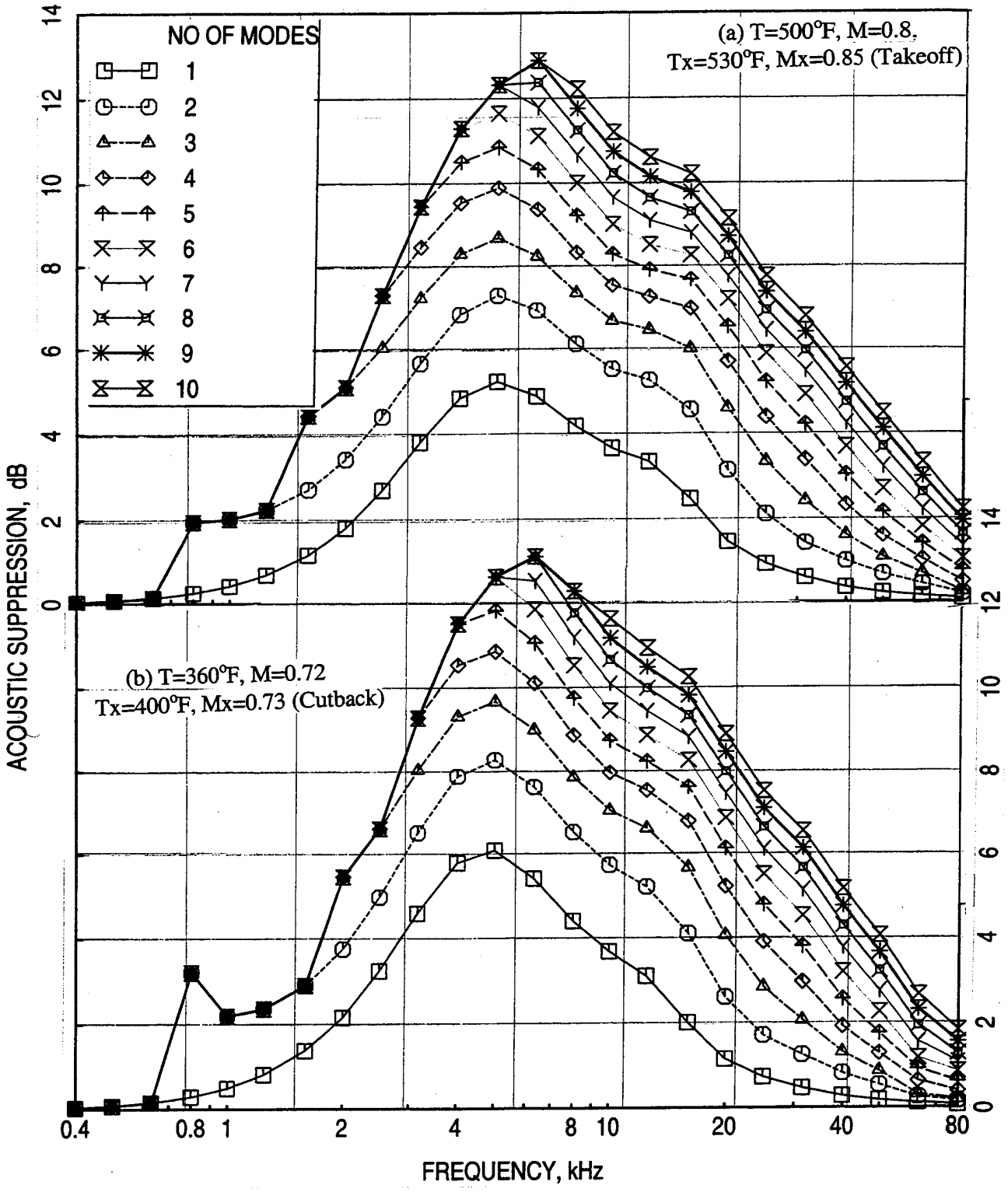

Figure 24. Contribution of first 10 transverse modes on predicted acoustic suppression spectra for a 1/7-scale mixer-ejector liner design, D=0.485", R=60 Rayls/cm, S=45%, t=0.015", d=0.02", OASPL=171 dB.

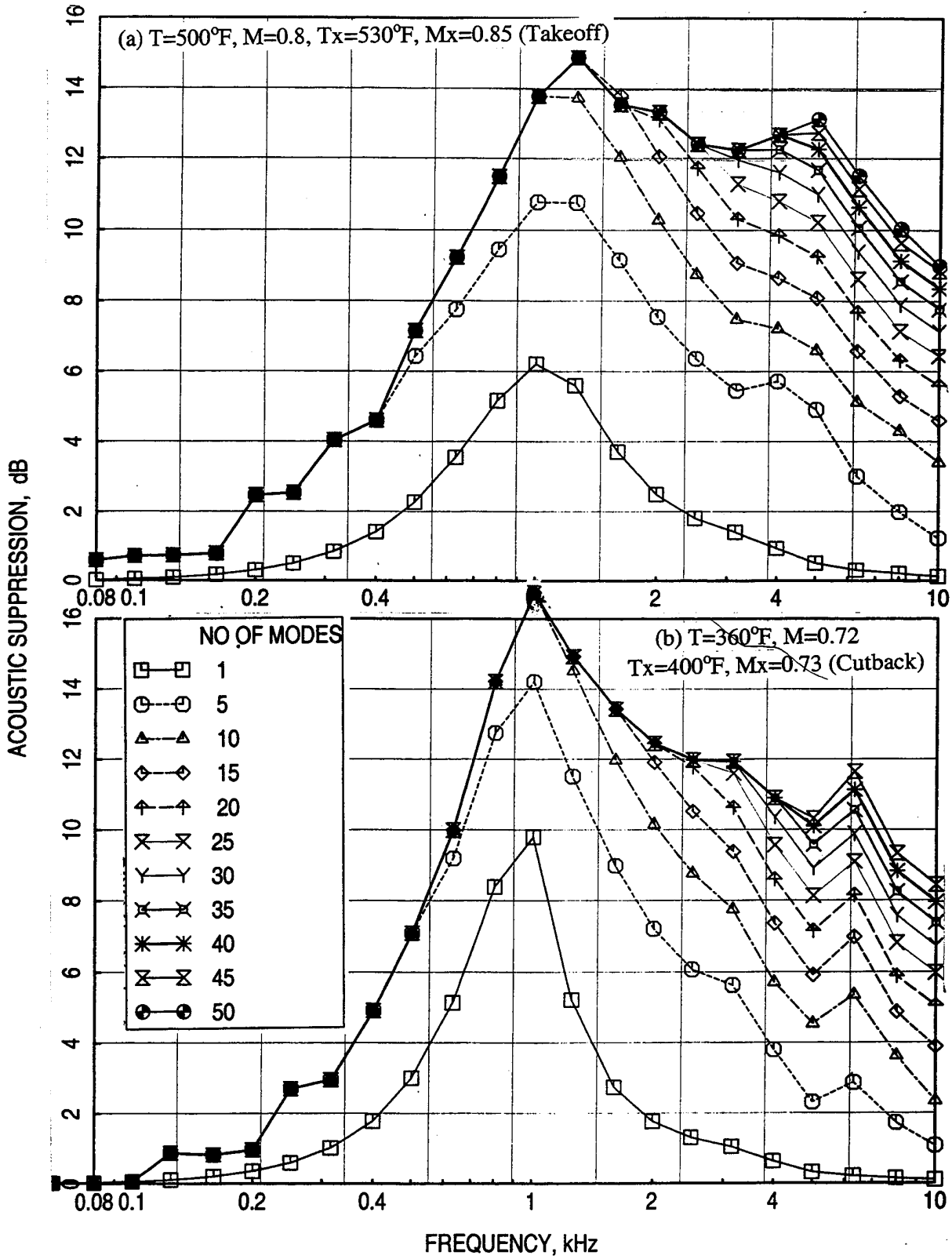

Figure 25. Contribution of first 50 transverse modes on predicted acoustic suppression spectra for a full-scale mixer-ejector liner design, D=2", R=10 Rayls/cm, S=40%, t=0.04", d=0.04", OASPL=180 dB.

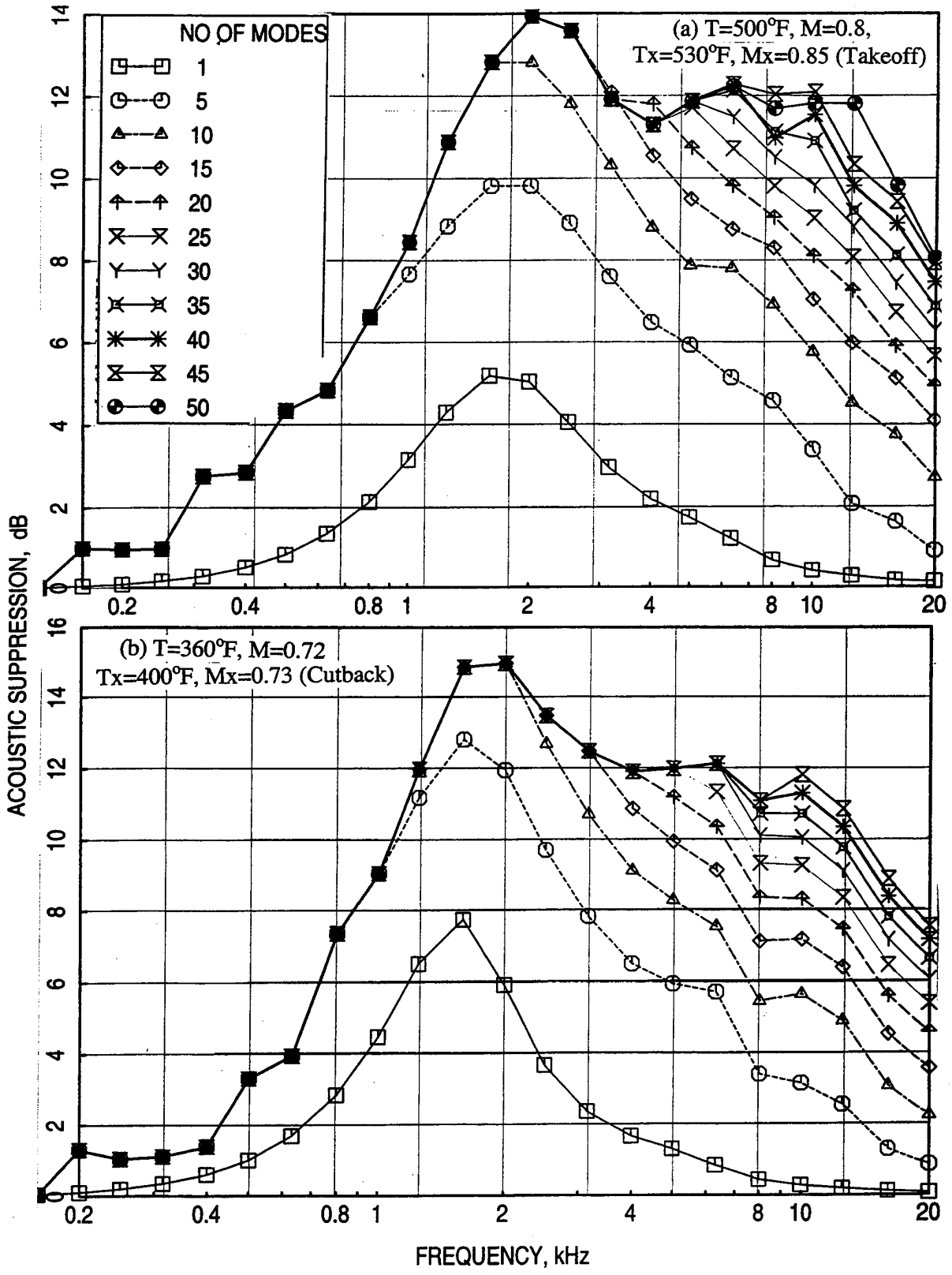

Figure 26. Contribution of first 50 transverse modes on predicted acoustic suppression spectra for an LSM mixer-ejector liner design, D=1.2", R=20 Rayls/cm, S=37%, t=0.04", d=0.054", OASPL=177 dB.

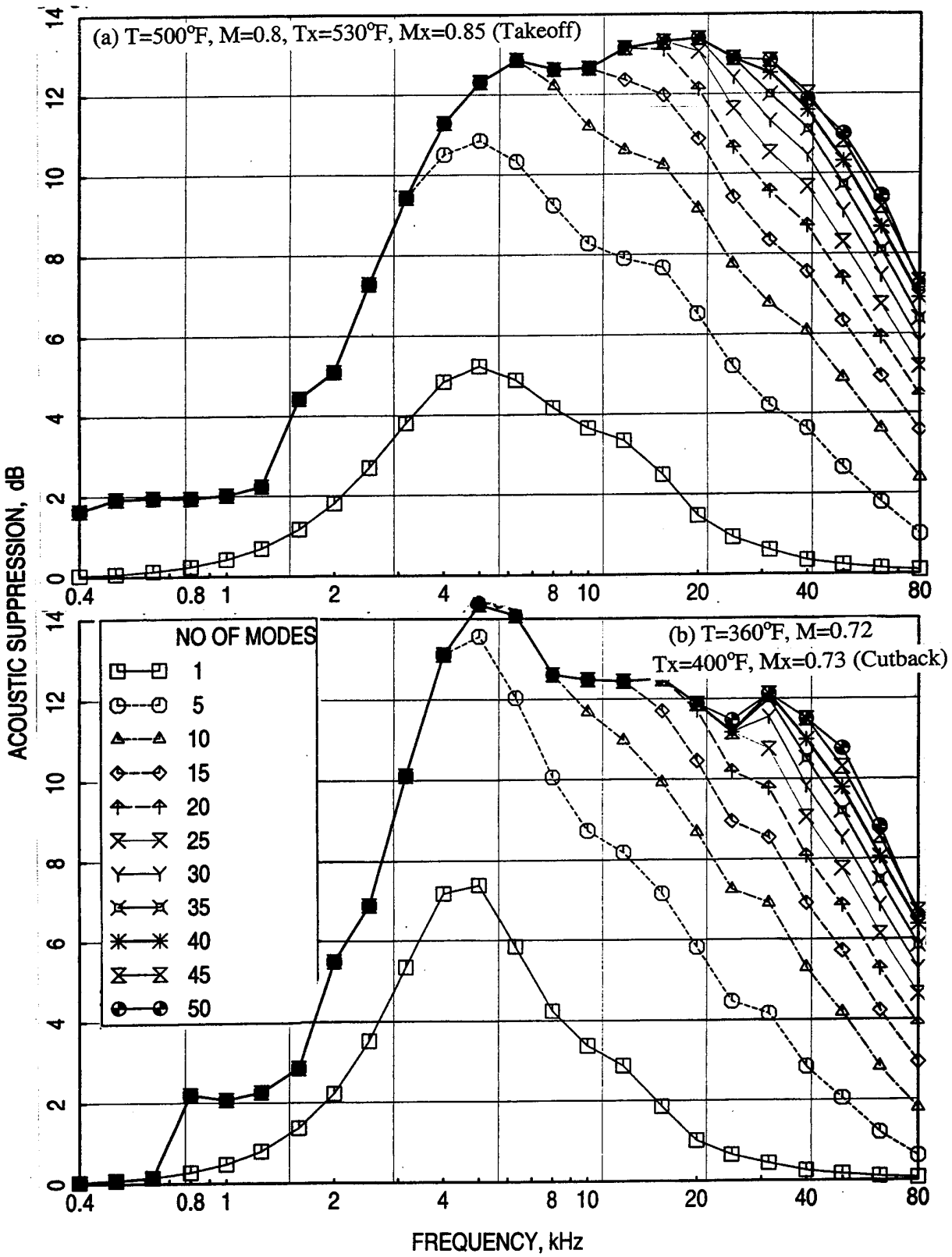

Figure 27. Contribution of first 50 transverse modes on predicted acoustic suppression spectra for a 1/7-scale mixer-ejector liner design, D=0.485", R=60 Rayls/cm, S=45%, t=0.015", d=0.02", OASPL=171 dB.

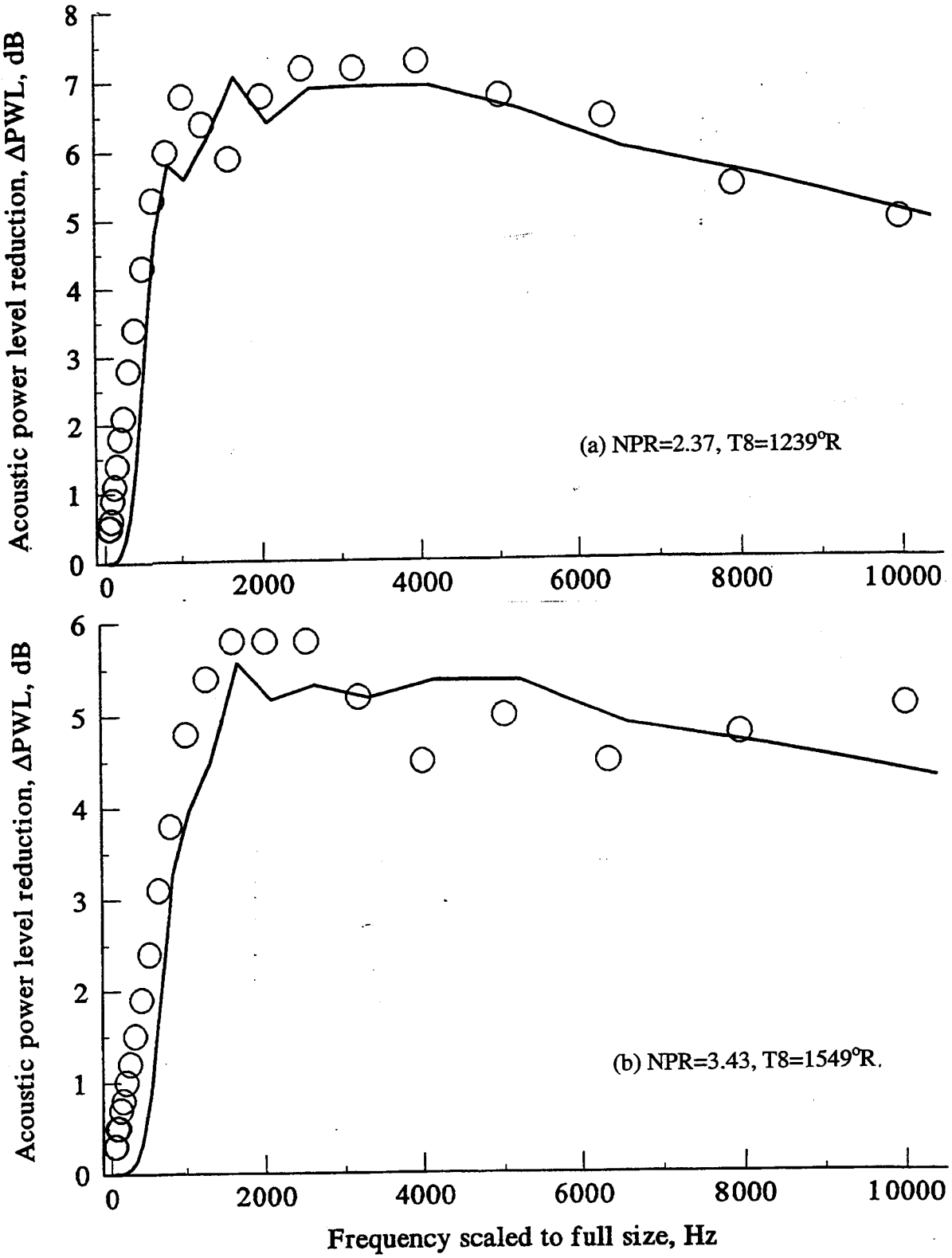

Figure 28. Comparison of measured ΔPWL with predicted acoustic suppression for a 1/7-scale mixer-ejector treated with 100 ppi 0.5"-deep Silicon Carbide liner with a 37% porous facesheet (t=0.025", d=0.045").

fully treated 1/7-scale mixer-ejector (see Figures 1 and 2) at two different aerothermodynamic conditions. The data is presented with respect to full-scale frequency. The agreement between the data and prediction is reasonably good. For lower pressure ratio condition the agreement between data and prediction is much better compared to the similar comparison for higher pressure ratio case. The discrepancies between data and prediction at NPR=3.43 could be due to the inaccuracy in the normal resistance prediction as shown in Figure 21(a). These discrepancies in impedance and acoustic suppression need to be minimized by improving the prediction models.

The liner design methodology currently utilizes the modal analysis method for acoustic suppression prediction. The currently developed method by Rice under the HSCT program is not utilized in liner design development due to the program closeout. However, a code based on the current method is available for acoustic suppression prediction.

5.0 PREDICTION OF FARFIELD NOISE INCLUDING EPNDB USING PREDICTED ACOUSTIC SUPPRESSION SPECTRUM

The objective is to predict farfield noise including EPNdB for different ejector treatment not being tested for farfield noise measurements, so that, a more effective treatment design can be achieved. The first step towards this objective is to develop a correlation between the internal noise component in the farfield with the acoustic suppression or insertion loss (predicted or measured) due to treatment in the ejector. Extraction of internal noise component from measured farfield data for mixer-ejector systems are described in Reference 3. The measured farfield data for NRA model with mixer 8, tested in Cell 41 of GEAE, are utilized in the current analysis. The flaps and sidewalls for the treated and hardwall configurations were 21.7" long (i.e., 160" for full scale). Half-inch deep 100-ppi Silicon Carbide bulk absorber was used for the liner. Measured bulk resistivity was 8.45 Rayls/cm. A 37% porous 0.025"-thick (t) perforated facesheet with hole diameter d=0.045" was used in this liner. The analysis is carried out for takeoff (NPR=3.43, T8=1551°R, V_j=2359 ft/sec) and cutback (NPR=2.37, T8=1238°R, V_j=1813 ft/sec) conditions.

5.1 Extracted Noise Components for Farfield Prediction: The extracted internal component of SPL and PWL spectra and OASPL and PNL directivities at takeoff conditions for the treated configuration are compared in Figures 29 through 31 with those for the hardwall data. Similar comparisons for external noise components are shown in Figures 32 and 33. To summarize the results derived from the extraction process the internal and the external components, and the total SPL and PWL spectra and OASPL and PNL directivities for hardwall and treated configurations are compared in Figures 34 through 36. Similar exercise is performed for cutback condition for hardwall and fully treated configurations. The extracted data for takeoff and cutback conditions are utilized to develop the farfield noise prediction for different liner designs.

5.2 Construction of Frequency Factors for PWL and SPL Prediction: The extracted internal component of PWL for takeoff and cutback conditions are used to compute the measured acoustic suppression ΔPWL due to acoustic treatment, which is the difference of PWL between hardwall and treated configurations. For the same conditions the acoustic suppression spectra are also predicted (as described in section 4.0) utilizing the predicted or measured normal impedance of the liner used in the mixer-ejector. The insertion loss spectrum should be the same as the internal component of ΔPWL at each condition, if the insertion loss prediction is accurate and if the ΔPWL computation accounts for azimuthal variation due to non-axisymmetry of the ejector and the internal noise component extraction

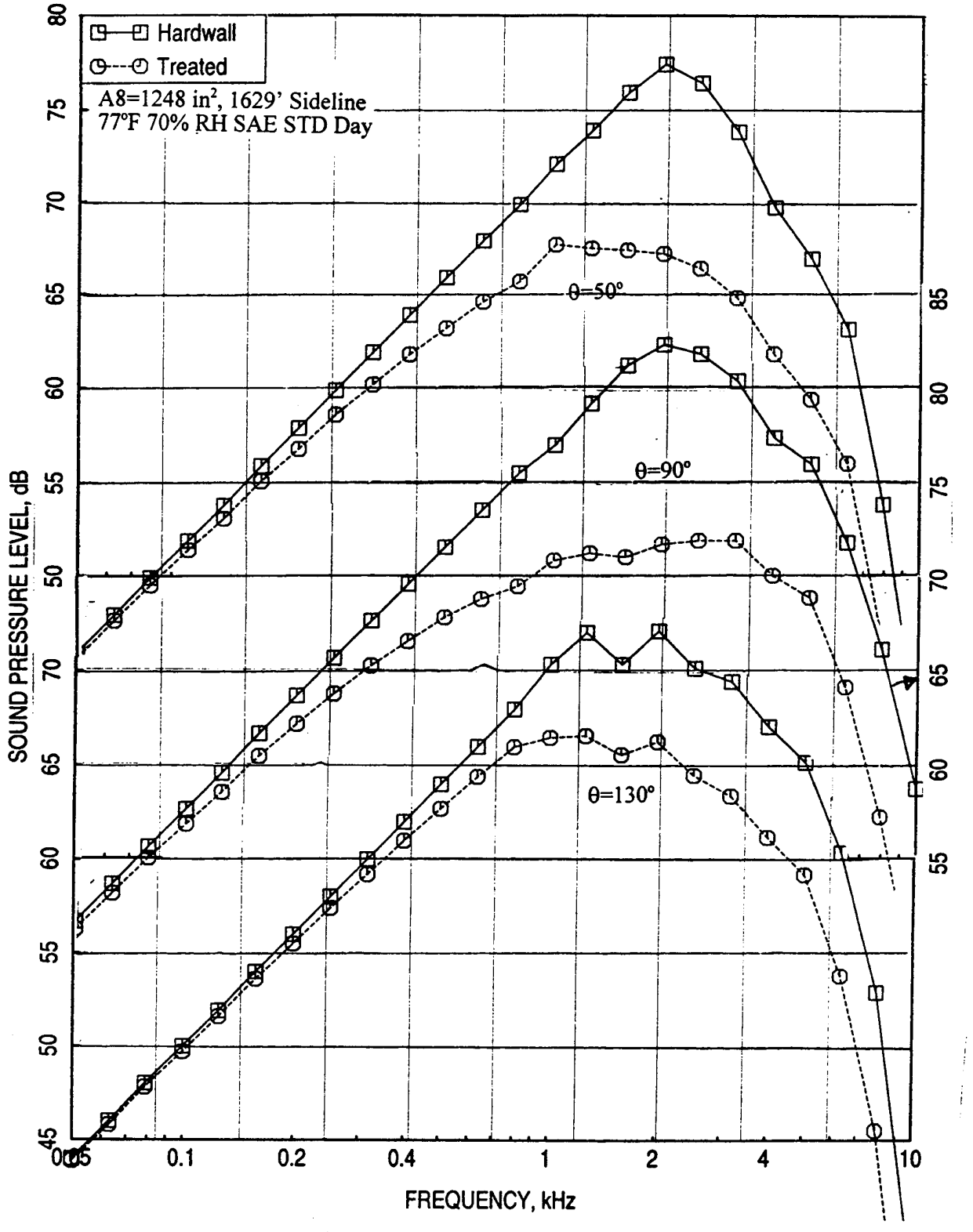

Figure 29. Comparison of extracted internal components of SPL spectrum at various polar angles θ between fully treated and hardwalled 22.12" long ejector for NRA model with mixer 8; NPR=3.43, T8=1551°R, V_j=2359 ft/sec, M=0.32 {takeoff}.

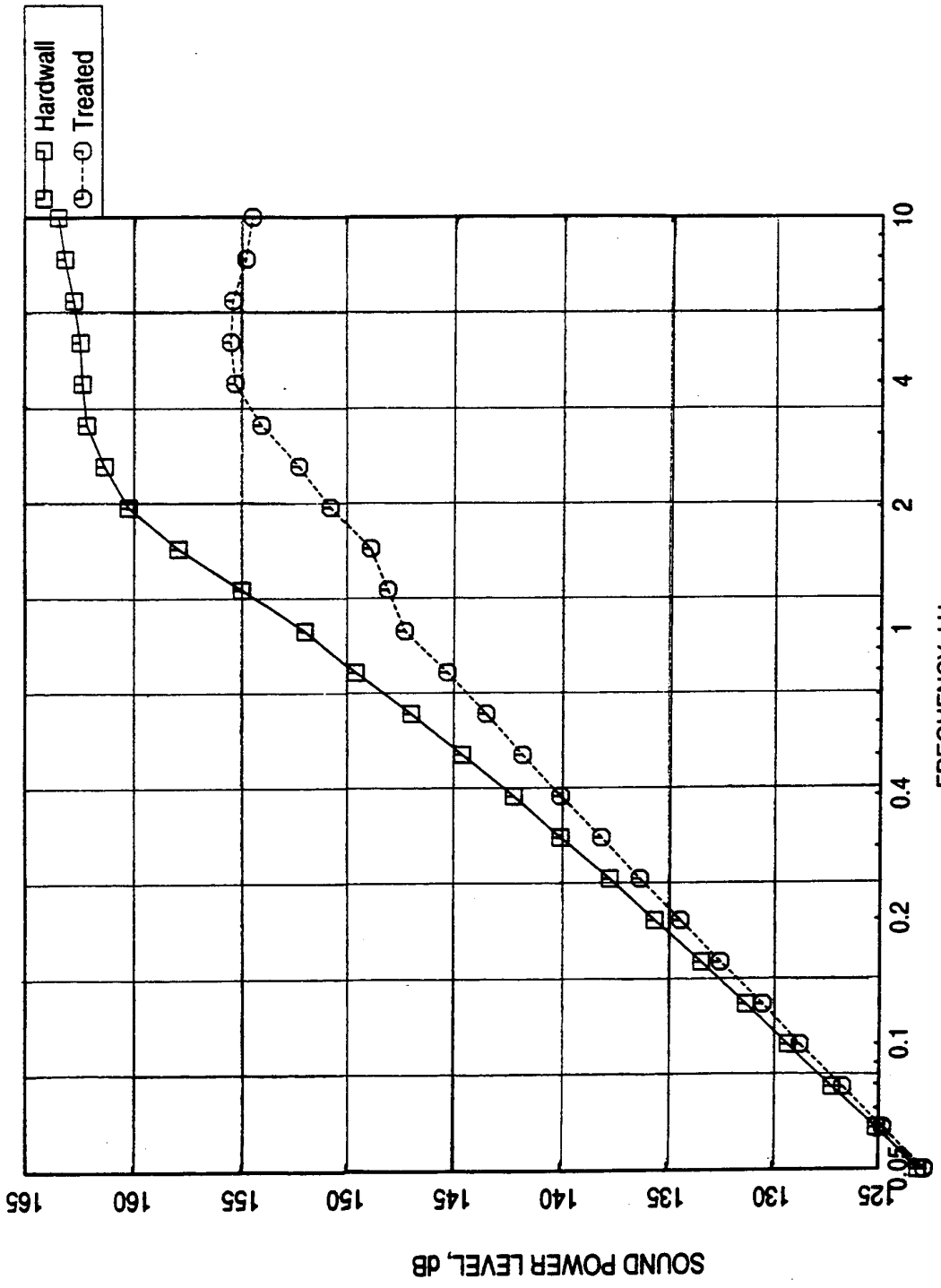

Figure 30. Comparison of internal components of PWL spectrum between fully treated and hardwalled 22.12" long ejector for NRA model with mixer 8; NPR=3.43, T8=1551°R, V_j=2359 ft/sec, M=0.32 {takeoff}.

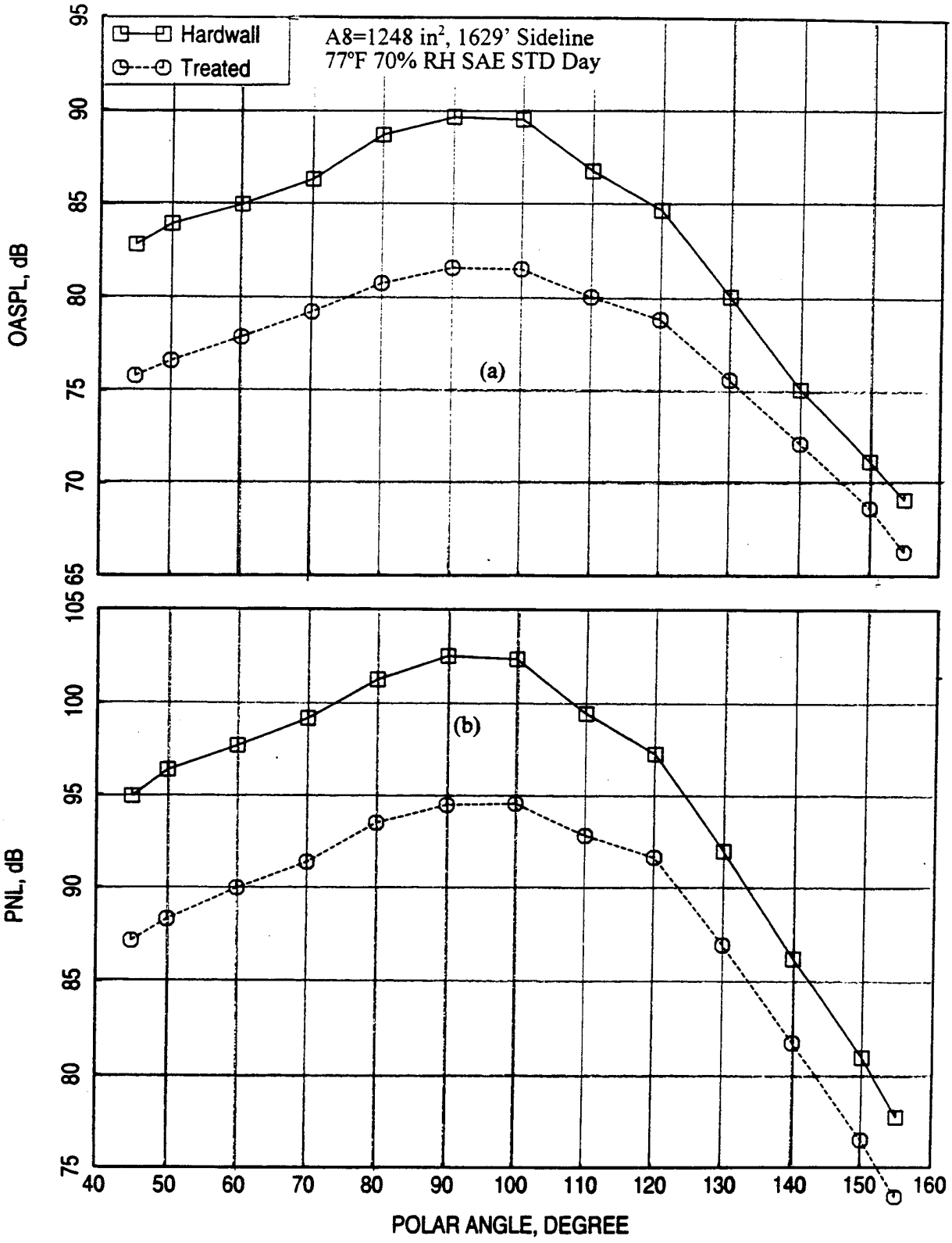

Figure 31. Comparison of internal components of (a) OASPL and (b) PNL directivities between fully treated and hardwalled 22.12" long ejector for NRA model with mixer 8; NPR=3.43, T8=1551°R, V_j=2359 ft/sec, M=0.32 {takeoff}.

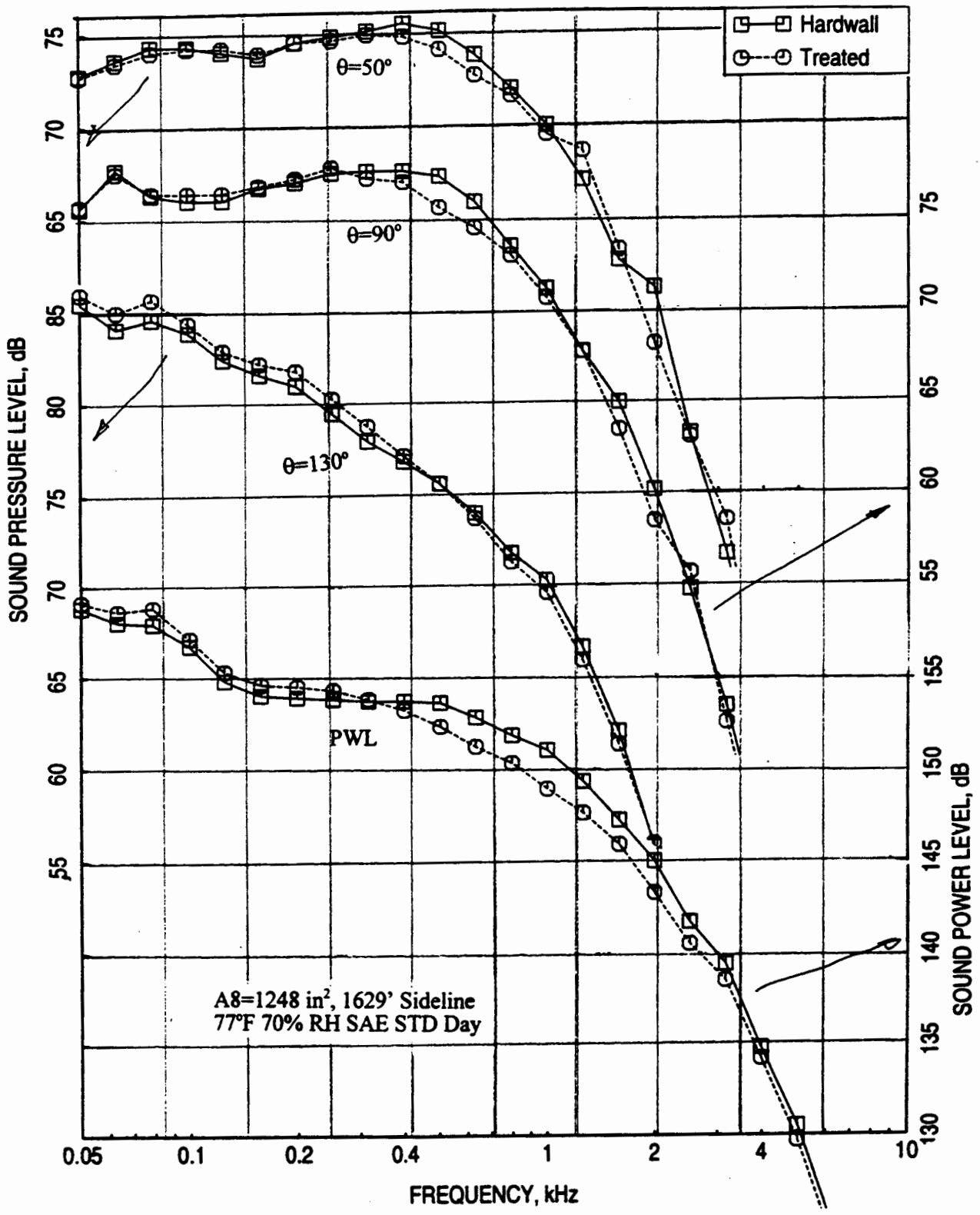

Figure 32. Comparison of external components of SPL spectrum at various polar angles θ and PWL spectrum between fully treated and hardwalled 22.12" long ejector for NRA model with mixer 8; NPR=3.43, T8=1551°R, V_j=2359 ft/sec, M=0.32 {takeoff}.

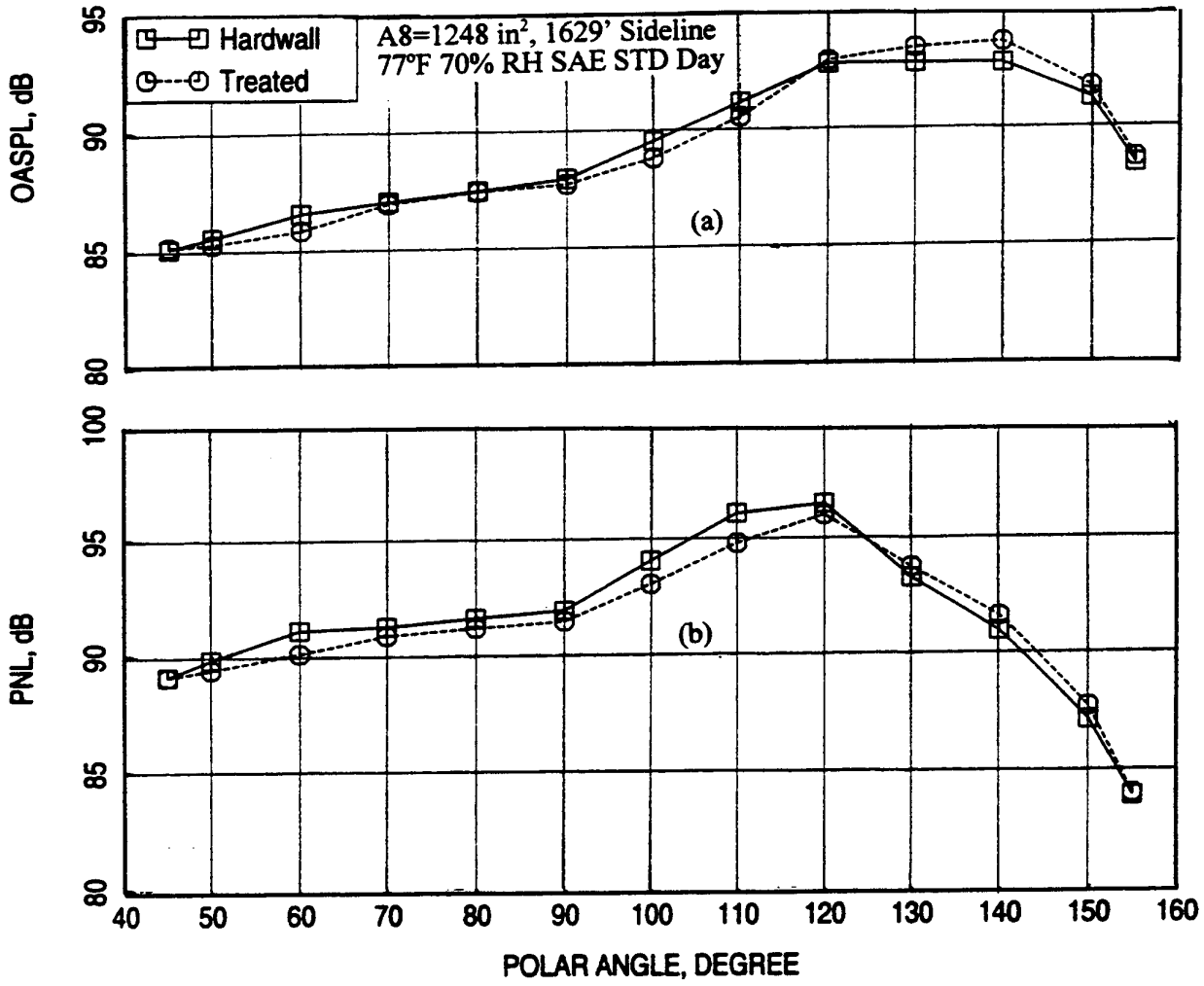

Figure 33.: Comparison of external components of (a) OASPL and (b) PNL directivities between fully treated and hardwalled 22.12" long ejector for NRA model with mixer 8; NPR=3.43, T8=1551°R, V_j=2359, M=0.32 ft/sec {takeoff}.

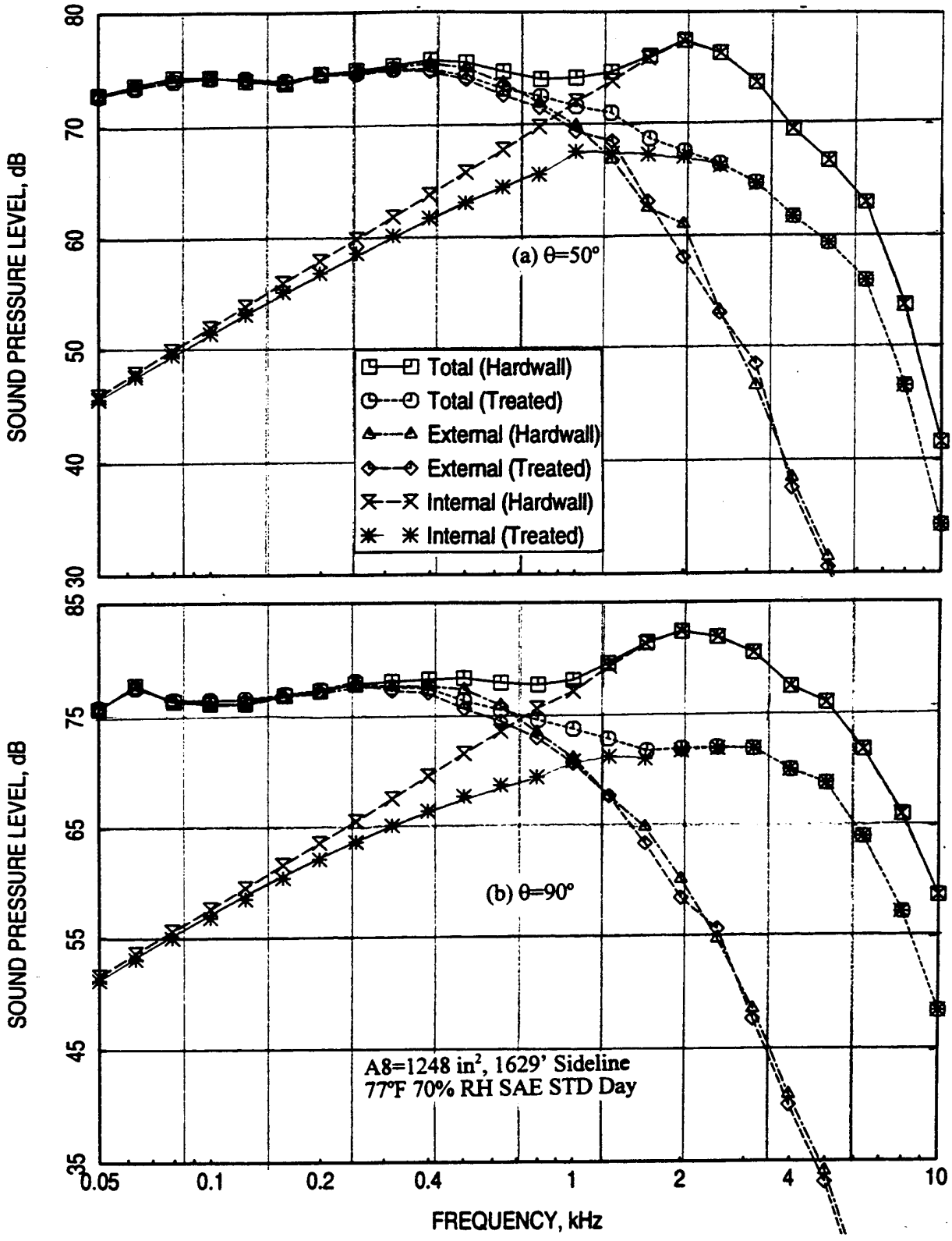

Figure 34. Measured SPL spectra compared with the modified predicted external components (i.e., merged and premerged) and extracted internal components for hardwalled and fully treated 22.12" long ejector for NRA model with mixer 8; NPR=3.43, T8=1551°R, V_j=2359 ft/sec, M=0.32 {takeoff}.

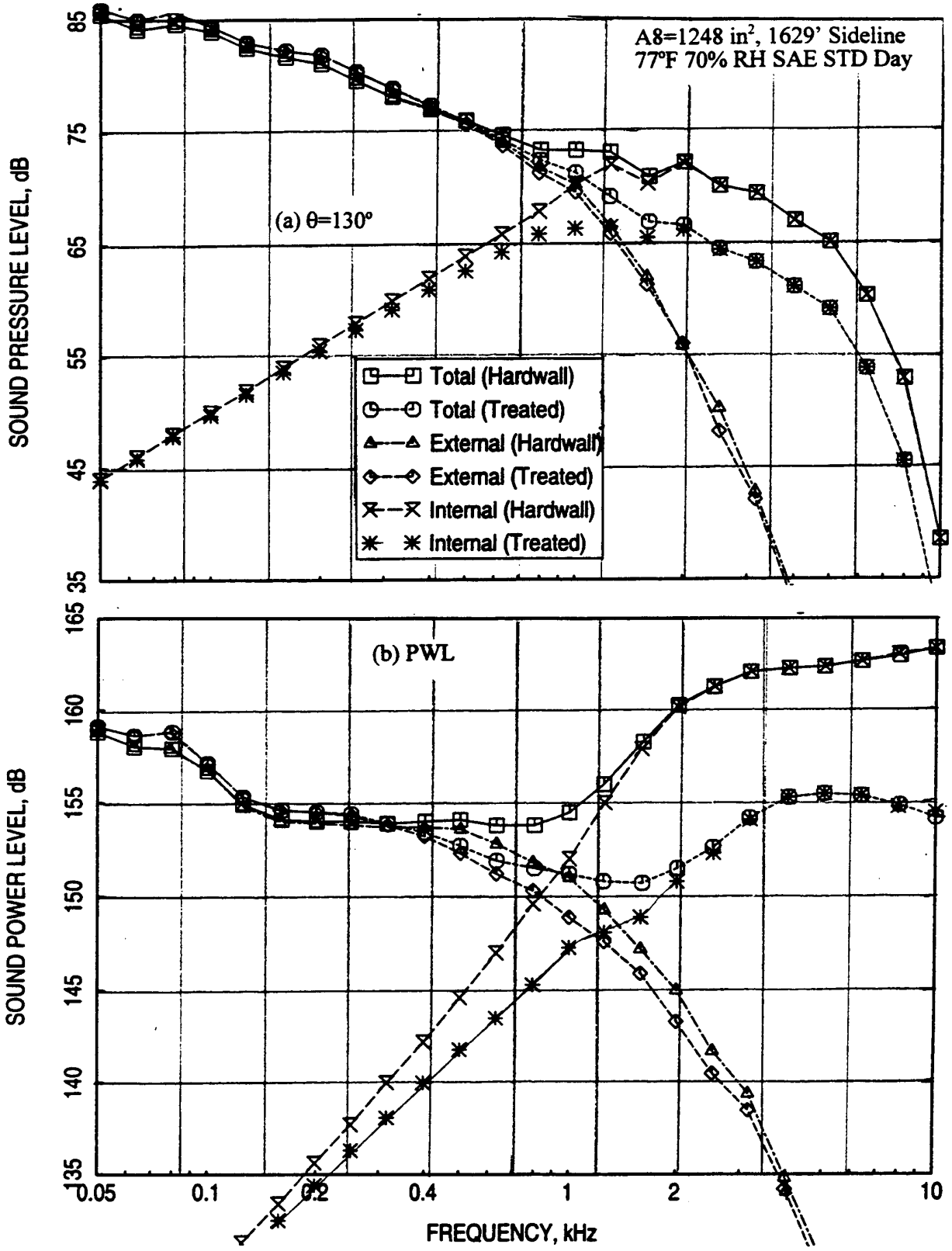

Figure 35. Measured SPL and PWL spectra compared with the modified predicted external components (i.e., merged and premerged) and extracted internal components for hardwalled and fully treated 22.12" long ejector for NRA model with mixer 8; NPR=3.43, T8=1551°R, V_j=2359 ft/sec, M=0.32 {takeoff}.

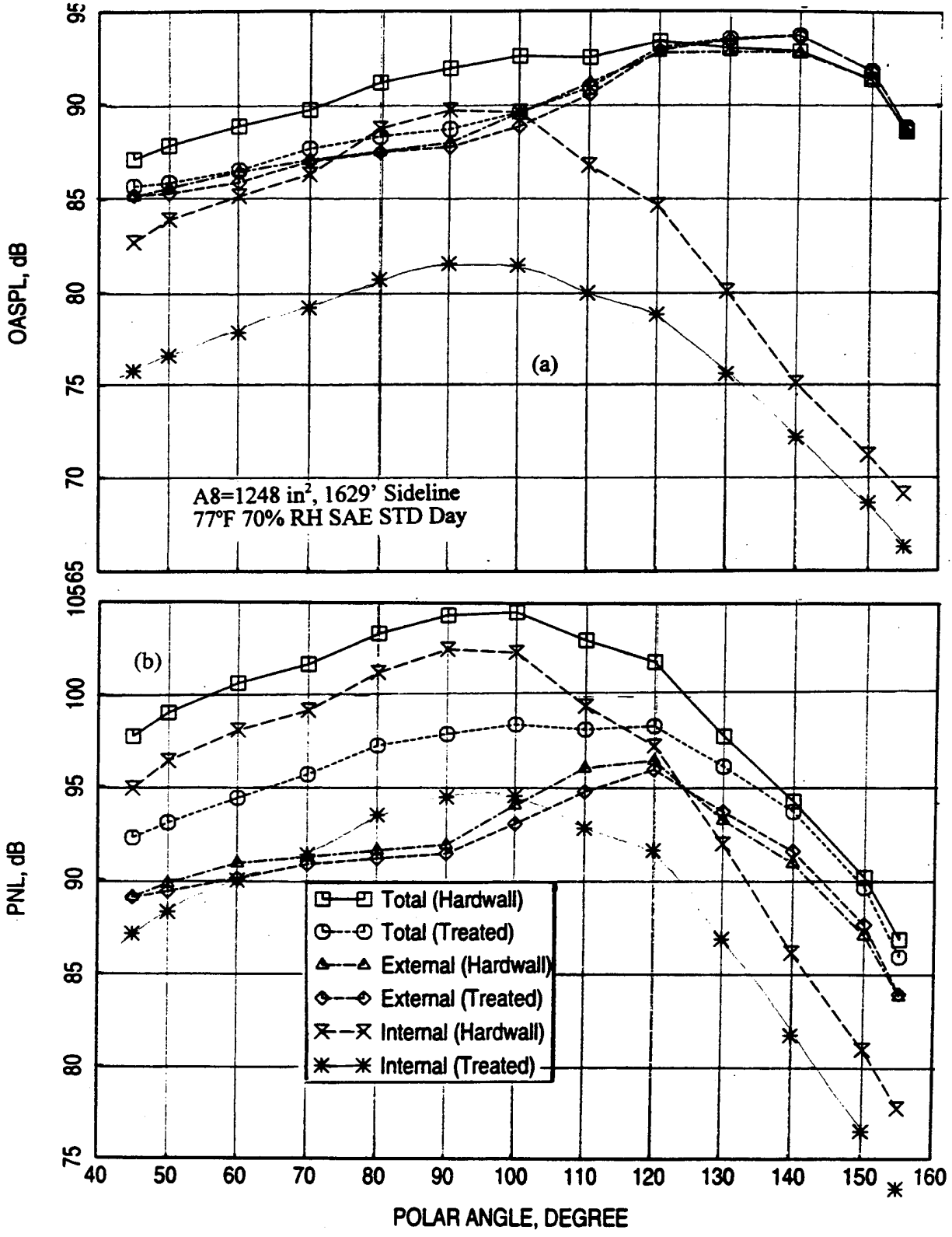

Figure 36. Measured OASPL and PNL directivities compared with the modified predicted external components (i.e., merged and premerged) and extracted internal components for hardwalled and fully treated 22.12" long ejector for NRA model with mixer 8; NPR=3.43, T8=1551°R, V_j=2359 ft/sec, M=0.32. {takeoff}.

used for PWL calculation is accurate. However, significant difference exists between insertion loss and ΔPWL spectra. To minimize the uncertainties associated with insertion loss prediction, internal noise extraction process, and azimuthal variation of farfield noise, a frequency dependent factor γ(f), termed as **acoustic suppression transfer factor**, is developed to equalize the predicted insertion loss ILo(f) at each frequency with the internal component of ΔPWLo(f) extracted from measured data.

$$\gamma(f) = 10^{\{(\Delta PWLo(f)/10)-(ILo(f)/10)\}} \qquad (1)$$

Figure 37(a) shows the predicted insertion loss and the corresponding extracted internal component of ΔPWL spectra for the takeoff condition. A modified version of insertion loss, by smoothing high frequency data, is also shown in this figure. As expected significant difference is observed between the insertion loss and ΔPWL spectra. The correlated acoustic suppression transfer factor γ(f), thus derived, is shown in Figure 37(b). The acoustic suppression transfer factors for modified insertion loss data are shown in Figure 38 for takeoff and cutback conditions. The transfer factor γ(f) seems to be dependent on the ejector flow conditions. Thus, it is essential to derive γ(f) for each condition for liner performance prediction.

Then, for the same condition, the frequency dependent γ(f) is utilized to calculate the internal component of ΔPWL(f) from the predicted acoustic suppression IL(f) for different liner designs.

$$\Delta PWL(f) = 10 \log \{\gamma(f)\} + IL(f) \qquad (2)$$

The internal component of PWL for treated configuration is calculated as follows;

$$PWL_{Treated}(f) = PWL_{Hard}(f) - \Delta PWL(f) \qquad (3)$$

The internal component of PWL for hardwall configuration is termed as PWL_{Hard}. The next step is to develop a procedure to calculate internal component of SPL spectra at various polar angles θ utilizing the internal component of PWL spectrum. Assuming that the internal component of SPL at a frequency will change by a factor δ(f) compared to the test case, the internal component of PWL(f) for a treated configuration can be expressed as follows;

$$PWL(f) = 10 \log [\Sigma\Sigma(\delta(f)p_o^2(f))\,\Delta A] = PWLo(f) + 10 \log(\delta(f)) \qquad (4)$$

Thus, $$\delta(f) = 10^{[\{PWL(f) - PWLo(f)\}/10]} \qquad (5)$$

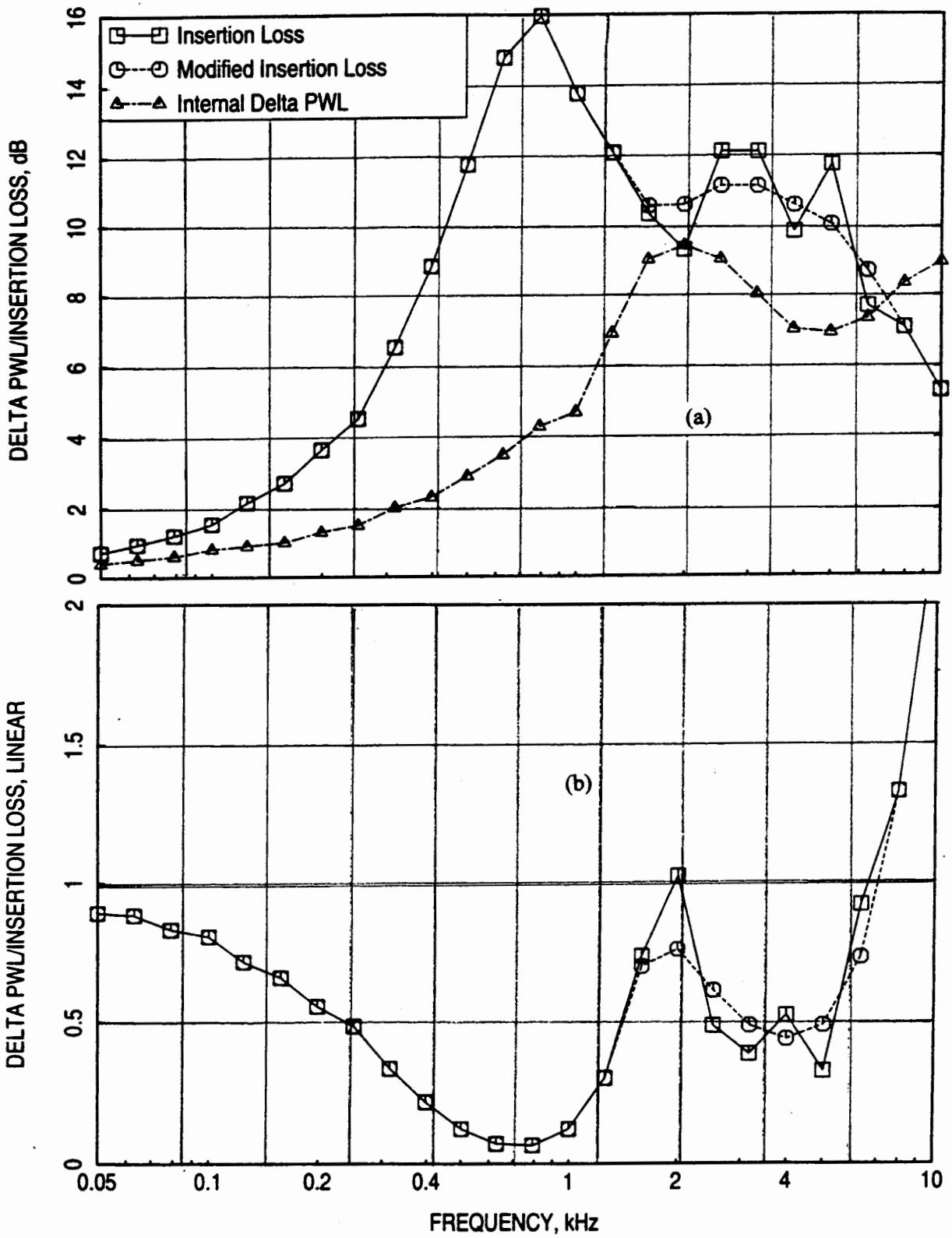

Figure 37. (a) Comparison of predicted acoustic suppression (Tx=530°F, Mx=0.85) and internal component of ΔPWL spectra and (b) γ(f) spectrum for fully treated 22.12" long ejector for NRA model with mixer 8; NPR=3.43, T8=1551°R, V_j=2359 ft/sec, M=0.32 {takeoff}.

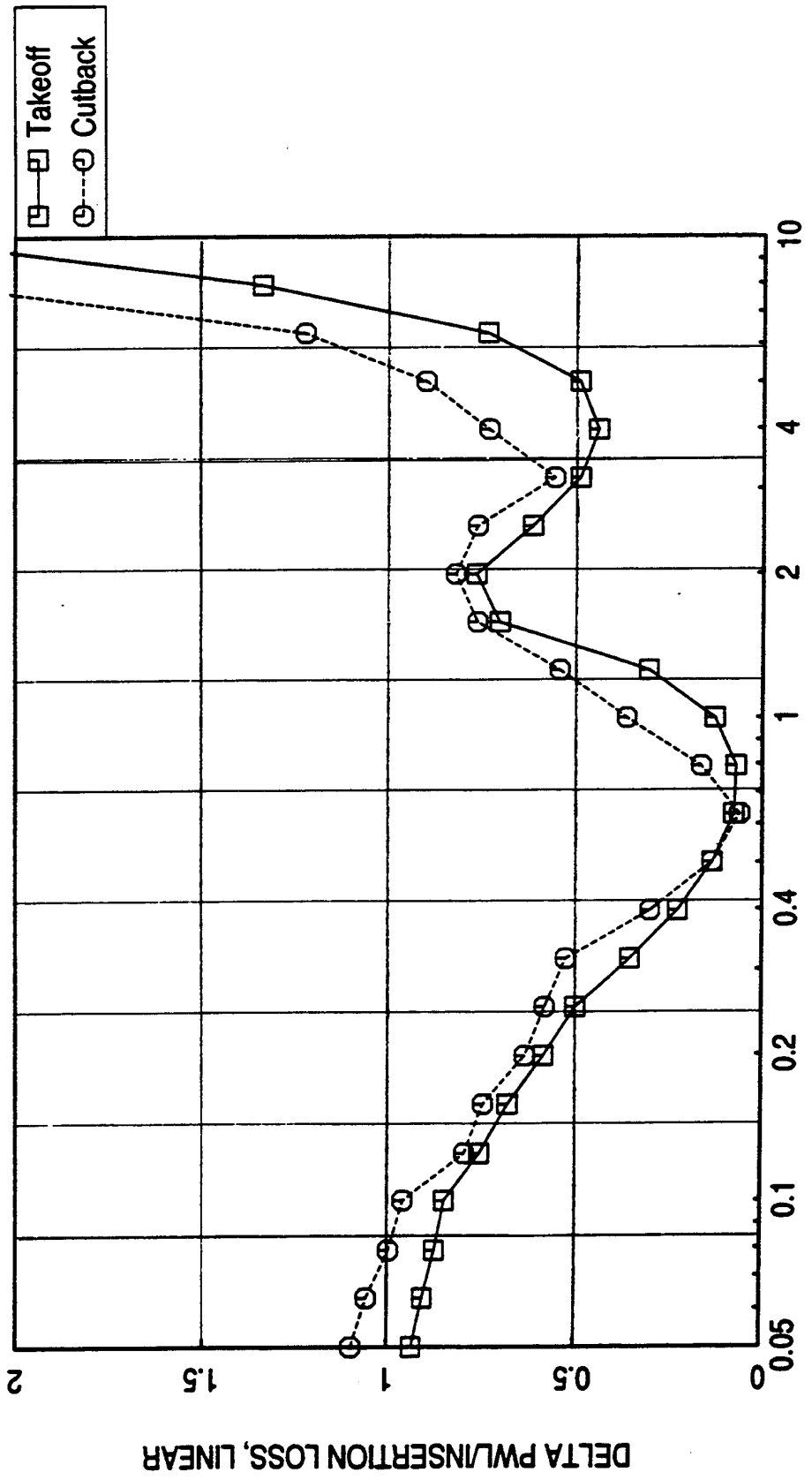

Figure 38. Correlation factor γ(f) spectra for fully treated 22.12" long ejector for NRA model with mixer 8 at takeoff (NPR=3.43, T8=1551°R, V_j=2359 ft/sec) and cutback (NPR=2.37, T8=1238°R, V_j=1813 ft/sec) conditions; M=0.32.

where; $p_o^2(f)$ = Internal component of SPL at f in linear scale for the test case

PWLo(f) = Internal component of PWL at f in dB for the test case

ΔA = Elemental area for integration

The internal component of SPL is thus derived using the corresponding test case value (i.e., SPLo(f)) as follows;

$$SPL(f) = SPLo(f) + 10 \log(\delta(f)) \qquad (6)$$

5.3 Prediction of Farfield Noise for Different Liner designs: For the same 1/7-scale mixer-ejector farfield noise is predicted utilizing the procedure outlined above for three different liner designs, including the one used for the test case (Design #1). The other two new designs, termed as Design #2 and Optimum are assumed to have bulk of resistivity 40 Rayls/cm. The facesheets are different for these two designs. The predicted normal impedance for all three designs is shown in Figure 39. Clearly, the two new designs are different with respect to their normal impedance compared to Design #1.

Figure 40 shows the predicted insertion loss spectra and the corresponding internal component of ΔPWL spectra derived using equation (2) for three different liner designs. Design #1 in this figure is the same as the test case used in the derivation of $\gamma(f)$ for takeoff. Figure 41(a) shows the internal component of PWL spectra for hardwall and the three treated configurations at takeoff, derived using Equation (3). The SPL factor $\delta(f)$ for the three liner designs are evaluated using equation (5) and are plotted in Figure 41(b). As expected, the factor becomes unity for Design #1, since it is the test case.

The internal component of SPL spectra at several polar angles θ and OASPL and PNL directivities for the three treated and the hardwall configurations are shown in Figures 42 and 43. PNL directivities are used to compute the internal component of EPNL and are listed in Figure 43. The external component of farfield noise is assumed to be the same for all treated configurations for the same aerothermodynamic condition. Thus, the total farfield noise is constructed using the external (see Figure 32) and respective internal components of SPL spectra. These spectra are used to compute PWL, OASPL, PNL, and EPNL. Figures 44 through 46 show the total SPL spectra at several polar angles, PWL spectra, and OASPL and PNL directivities for hardwall and the three treated configurations for takeoff. Computed EPNL are listed in Figure 45. Similar exercise is performed for cutback condition. The method described here is also applied to LSM and full-scale liner designs and the farfield results are obtained.

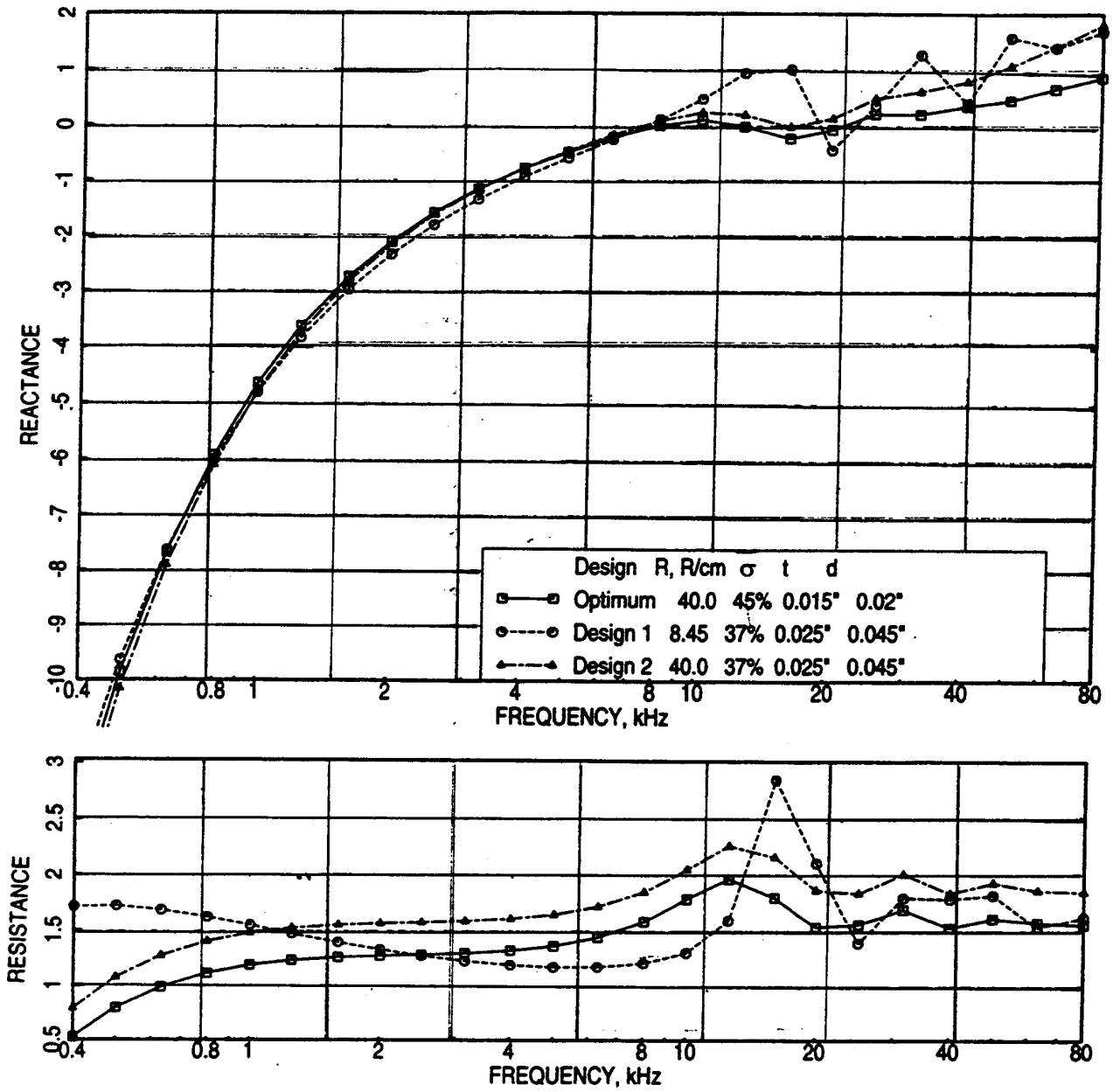

Figure 39. Comparison of predicted normal impedance spectra between optimum and two realistic liner designs for 1/7-scale mixer-ejector, D=0.485", T=500°F, M=0.8, OASPL=171 dB.

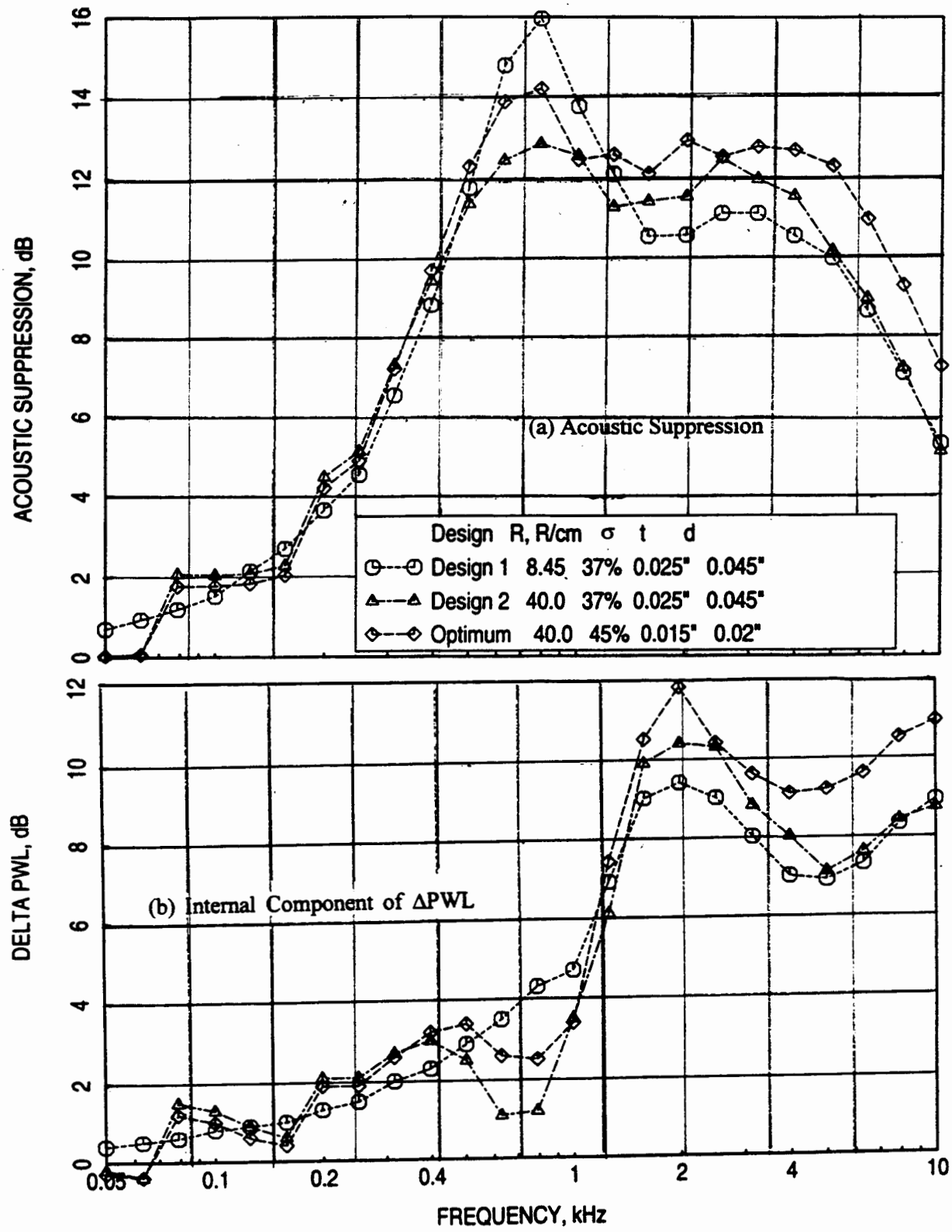

Figure 40. (a) Predicted acoustic suppression (Tx=530°F, Mx=0.85) and (b) internal component of ΔPWL spectra for 22.12" long ejector fully treated with three different liners for NRA model with mixer 8; NPR=3.43, T8=1551°R, V_j=2359 ft/sec, M=0.32 {takeoff}.

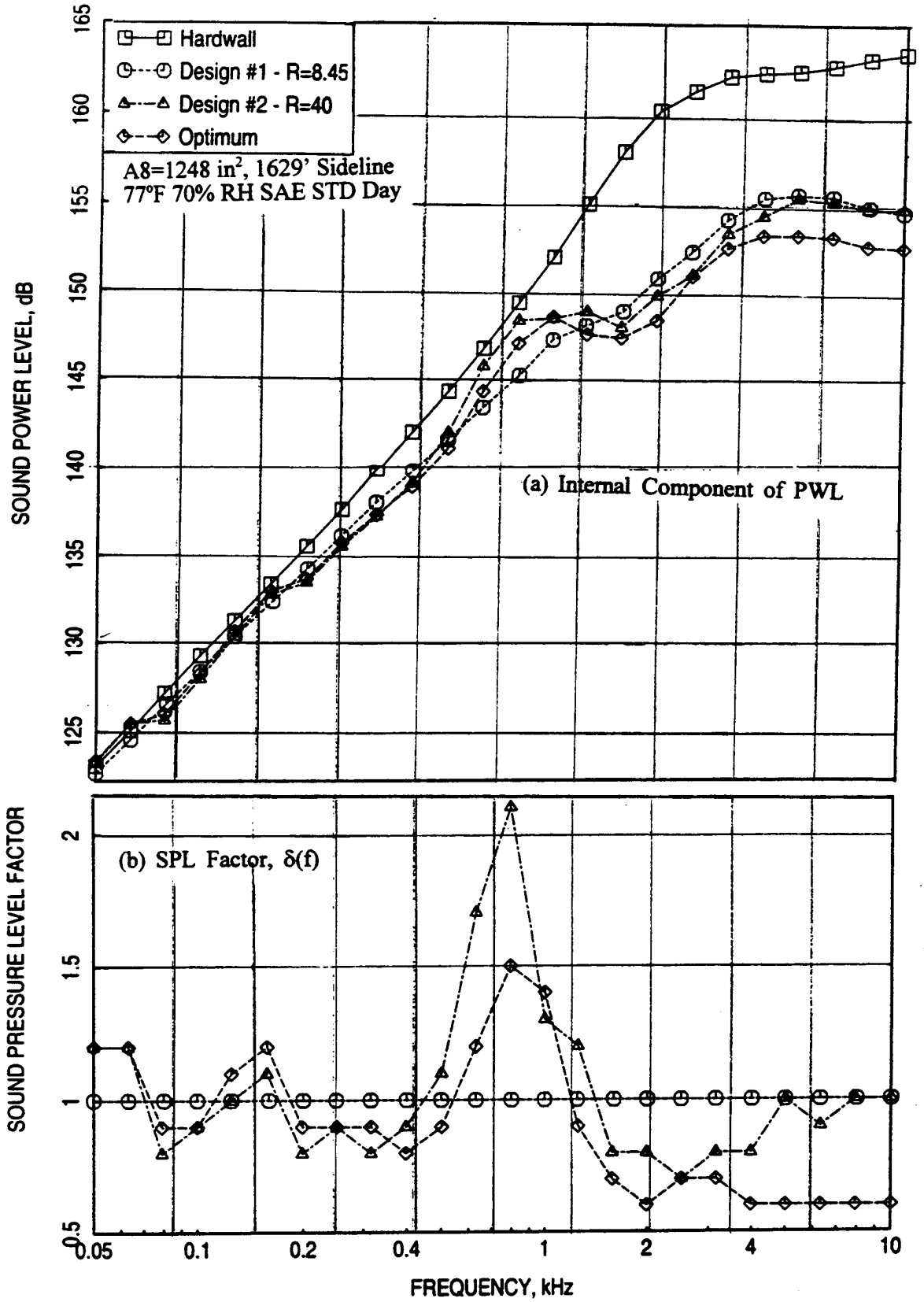

Figure 41. (a) Internal component of PWL spectra for hardwalled and three fully treated and (b) SPL factor δ(f) spectra for three fully treated 22.12" long ejector for NRA model with mixer 8; NPR=3.43, T8=1551°R, V_j=2359 ft/sec, M=0.32 {takeoff}.

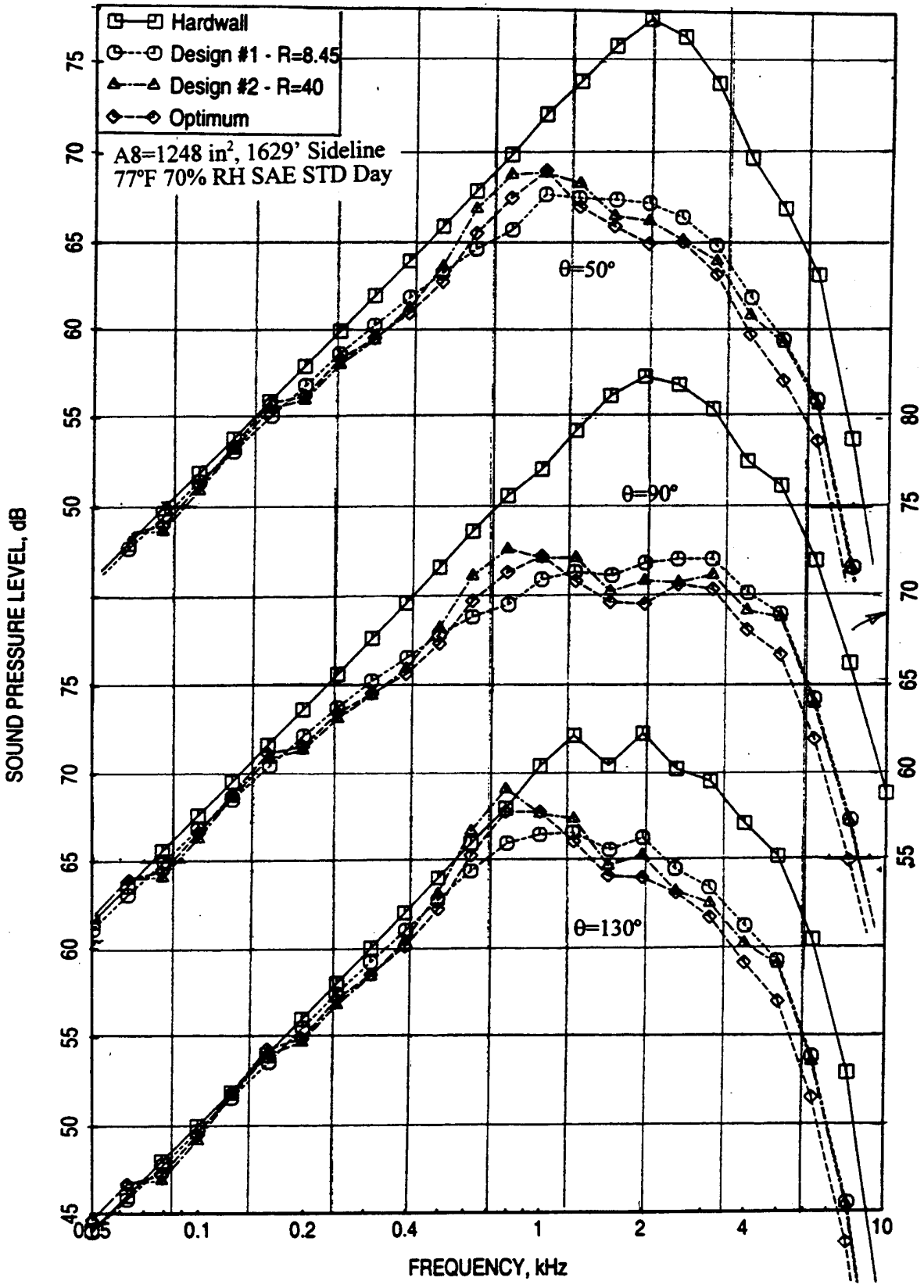

Figure 42. Internal component of SPL spectra at various polar angles θ for hardwalled and three fully treated 22.12" long ejector for NRA model with mixer 8; NPR=3.43, T8=1551°R, V_j=2359 ft/sec, M=0.32 {takeoff}.

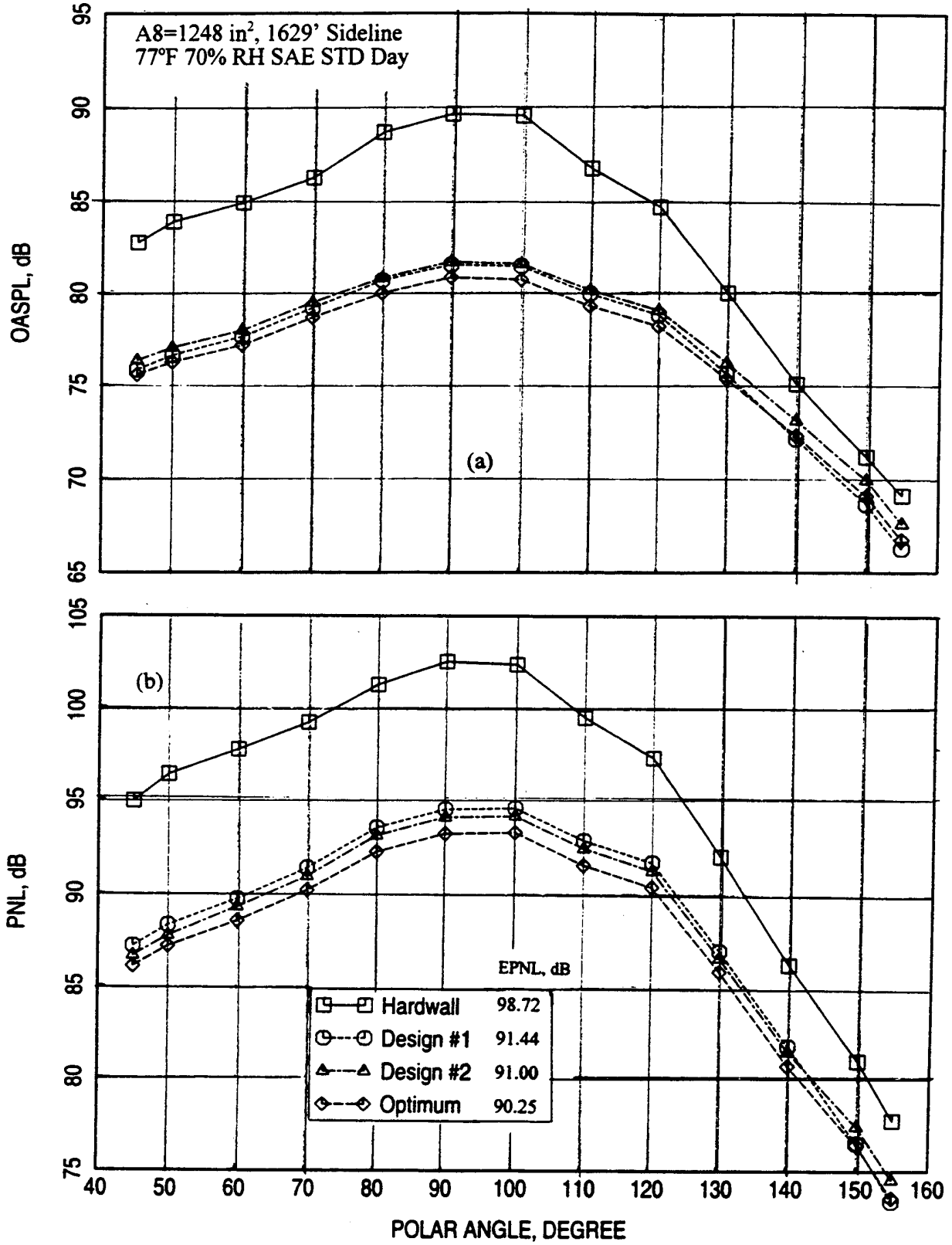

Figure 43. Internal component of (a) OASPL and (b) PNL directivities for hardwalled and three fully treated 22.12" long ejector for NRA model with mixer 8; NPR=3.43, T8=1551°R, V_j=2359 ft/sec, M=0.32 {takeoff}.

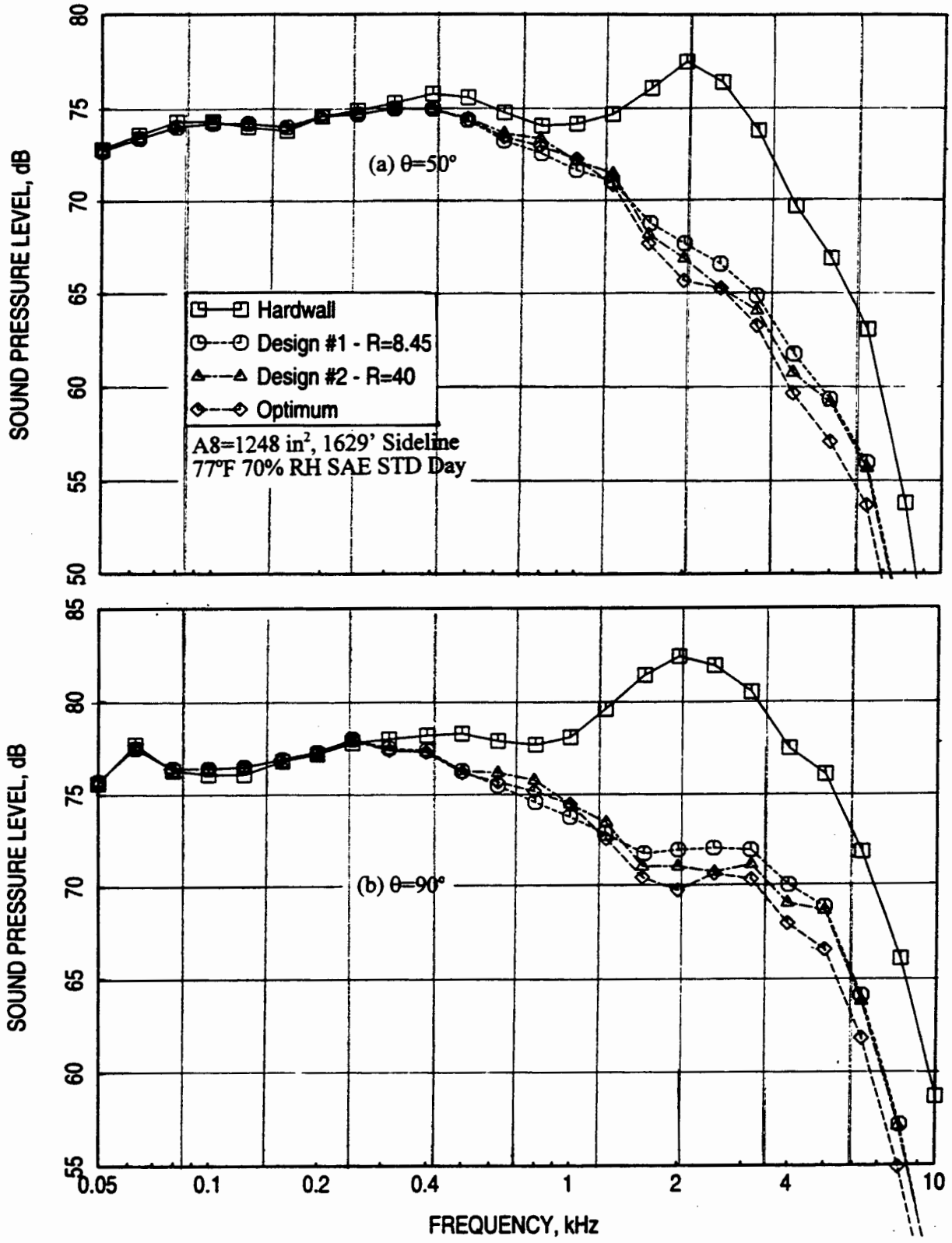

Figure 44. Total SPL spectra at various polar angles θ for hardwalled and three fully treated 22.12" long ejector for NRA model with mixer 8; NPR=3.43, T8=1551°R, V_j=2359 ft/sec, M=0.32 {takeoff}.

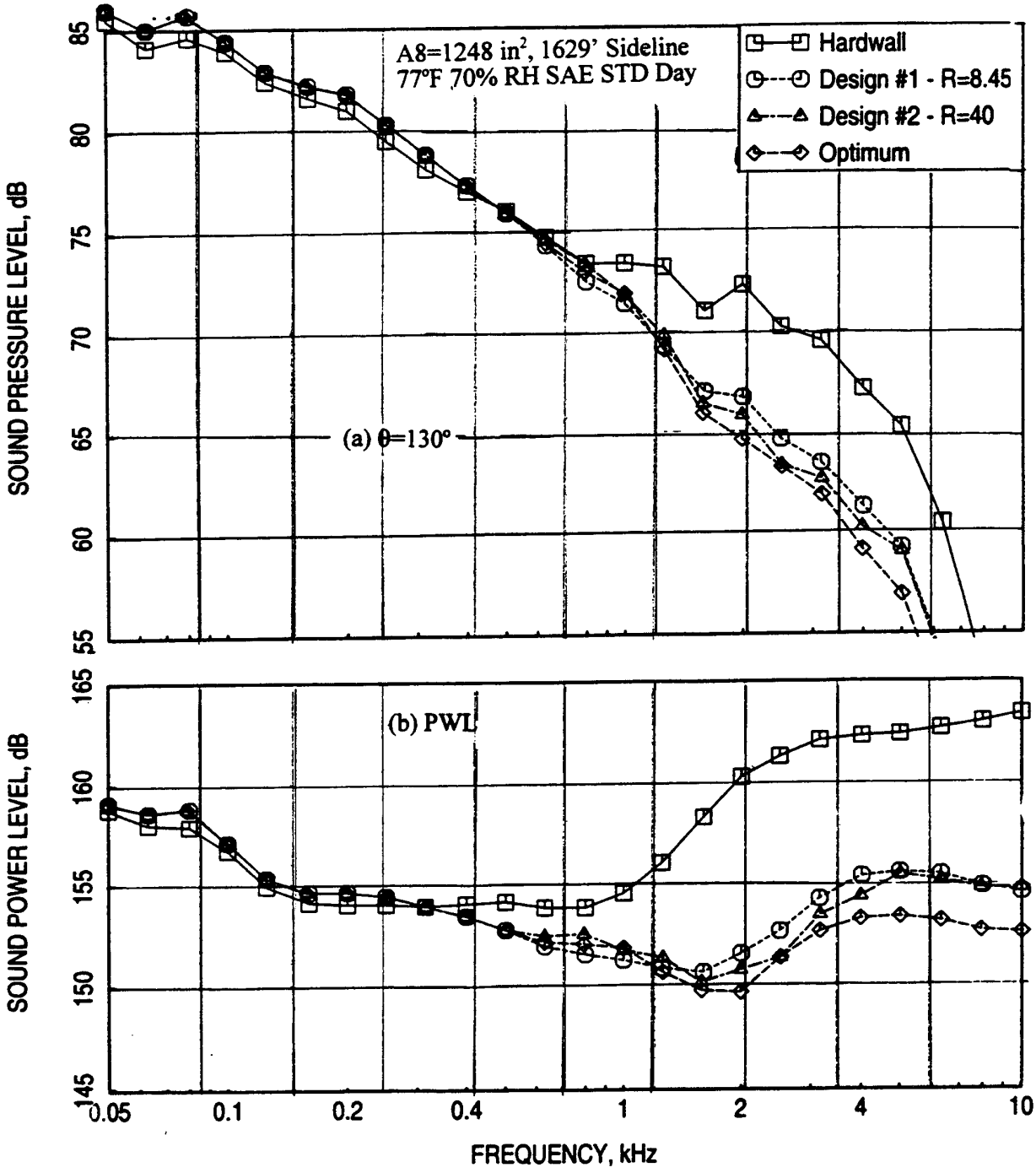

Figure 45. Total SPL spectra at θ=130° and PWL spectra for hardwalled and three fully treated 22.12" long ejector for NRA model with mixer 8; NPR=3.43, T8=1551°R, V_j=2359 ft/sec, M=0.32 {takeoff}.

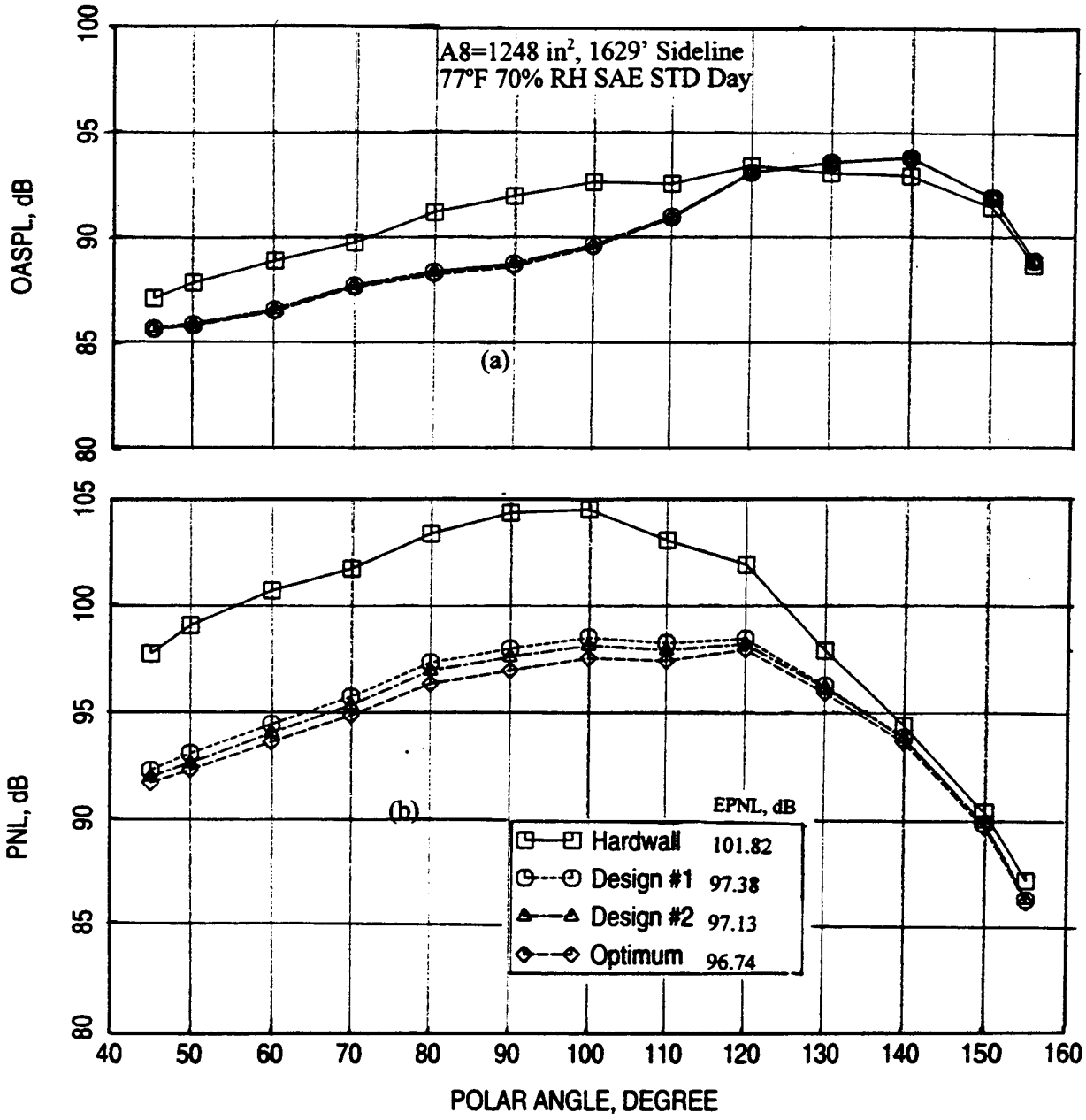

Figure 46. Total (a) OASPL and (b) PNL directivities for hardwalled and three fully treated 22.12" long ejector for NRA model with mixer 8; NPR=3.43, T8=1551°R, V_j=2359 ft/sec, M=0.32 {takeoff}.

5.4 Validation of the Use of Frequency Factor for Different Liner Designs: The farfield noise prediction for different liner designs are made with the assumption that the frequency factors $\gamma(f)$ and $\delta(f)$ are the same for each case. This is verified by utilizing the P&W's Gen 1 mixer-ejector test data. GEN 1 mixer-ejector, shown in Figure 47, with different liner designs are tested at NASA Glenn anechoic freejet facility (i.e., NATR). Internal noise component from the measured farfield acoustic data is extracted for this mixer-ejector with different liners and at different aerothermodynamic conditions. Based on the hardwall and the treated configurations the ΔPWL of internal noise component is derived. Figure 48 shows the ΔPWL spectra for two categories of bulk absorbers with varying resistivity at a typical takeoff condition (i.e., NPR=3.43, T8=1551°R) with flight simulation Mach number of 0.3. Clearly, the effect of treatment variation is observed in these results.

The DC flow resistance for these bulk absorbers, measured at GEAE at room temperature, is used to predict the normal impedance at the takeoff condition (i.e., NPR=3.43, T8=1551°R). The grazing flow Mach number and wall temperature are assumed to be 0.6 and 500°F, respectively. The following table lists the measured DC flow resistance at ambient temperature and their predicted values at 500°F for various bulk absorbers:

Bulk Material	Resistivity Rayls/cm a Room Temperature	Resistivity Rayls/c at 500°F
100 ppi SiC	9.88	15.17
200 ppi SiC	24.26	37.27
400 ppi SiC	53.18	81.67
HTP 3.3	50.50	68.48
HTP 4.6	59.84	91.89
HTP 4.86	92.30	141.74

Figure 49 shows the predicted normal impedance spectra at the takeoff condition for the above listed bulk materials with a 37% porous perforated facesheet of thickness 0.025" and with 0.07" diameter holes. The corresponding acoustic suppression spectra are predicted using the modal analysis method for a two-sided treated rectangular ejector with uniform flow Mach number of 0.631 and temperature of 928°R (see Figure 50), which are the mixed flow conditions in the ejector.

The internal component of ΔPWL based on the measured data and the corresponding predicted acoustic suppression spectra for 100ppi SiC foam liner are shown in Figure 51. Even though the peak acoustic suppression is higher compared to measured ΔPWL, the peak frequencies are close. In general, except for the last two frequency bands, the spectral shape

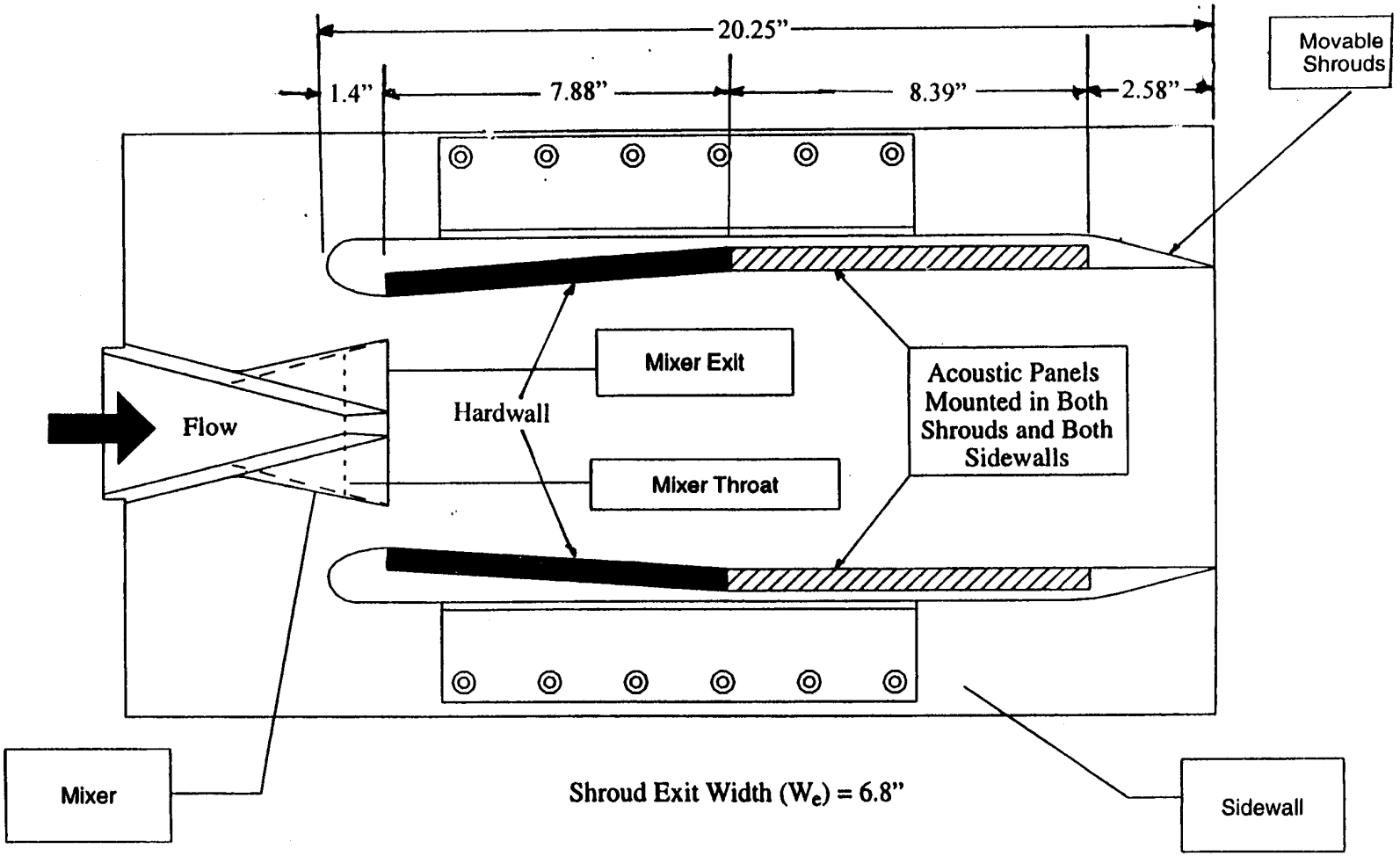

Figure 47. Acoustic treatment for P&W vortical mixer-ejector nozzle for NATR tests, SAR=4.9, MAR=0.97

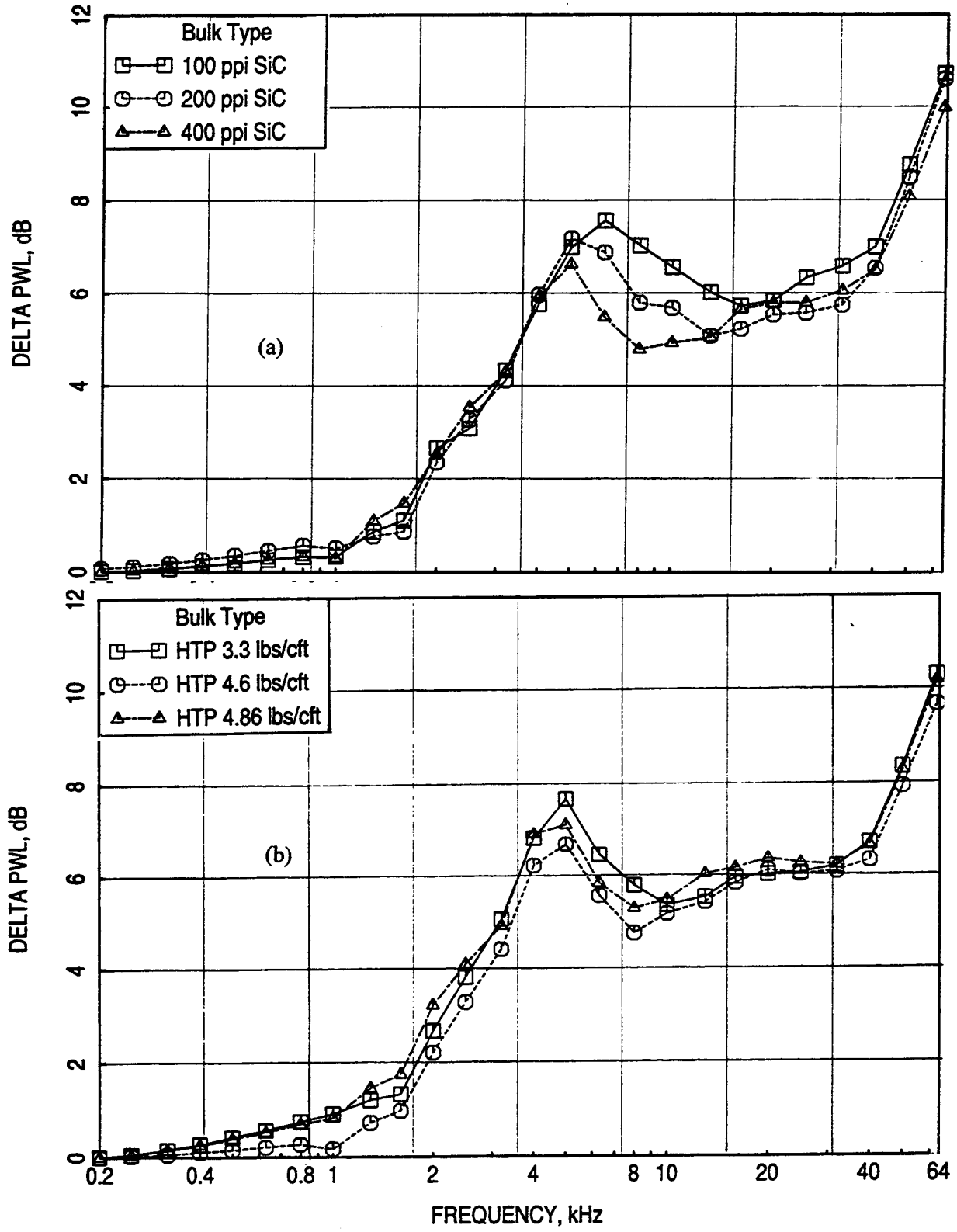

Figure 48. Internal component of ΔPWL spectra for Gen 1 mixer-ejector with (a) SiC and (b) HTP bulk absorber liners with 37% porous facesshhet (t=0.025" and d=0.07"); NPR=3.43, T8=1551°R, V_j=2359 ft/sec, M=0.3.

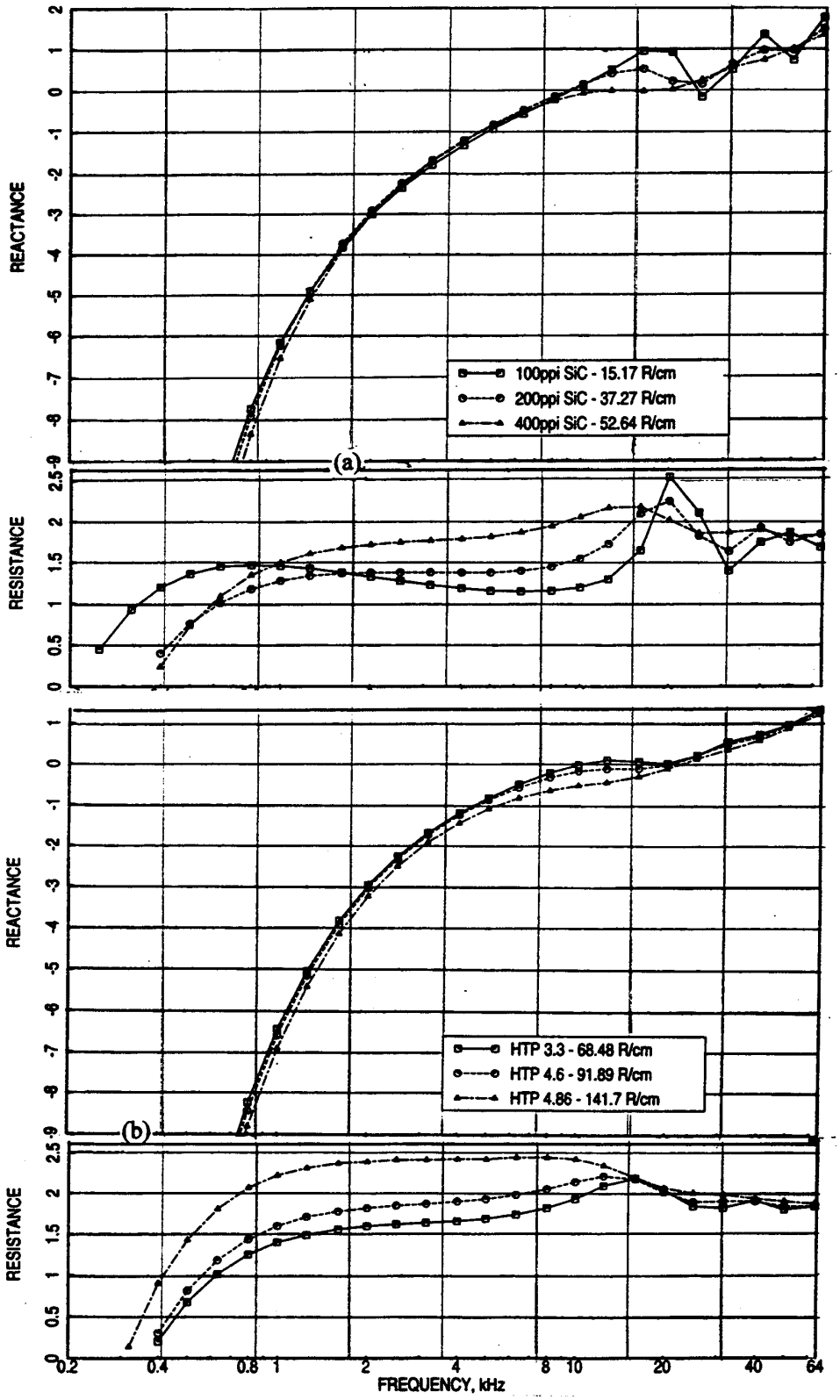

Figure 49. Predicted normal impedance with grazing flow Mach number of 0.6 and static temperature of 500°F for (a) SiC and (b) HTP bulk absorber liners with 37% porous facesshhet (t=0.025" and d=0.07").

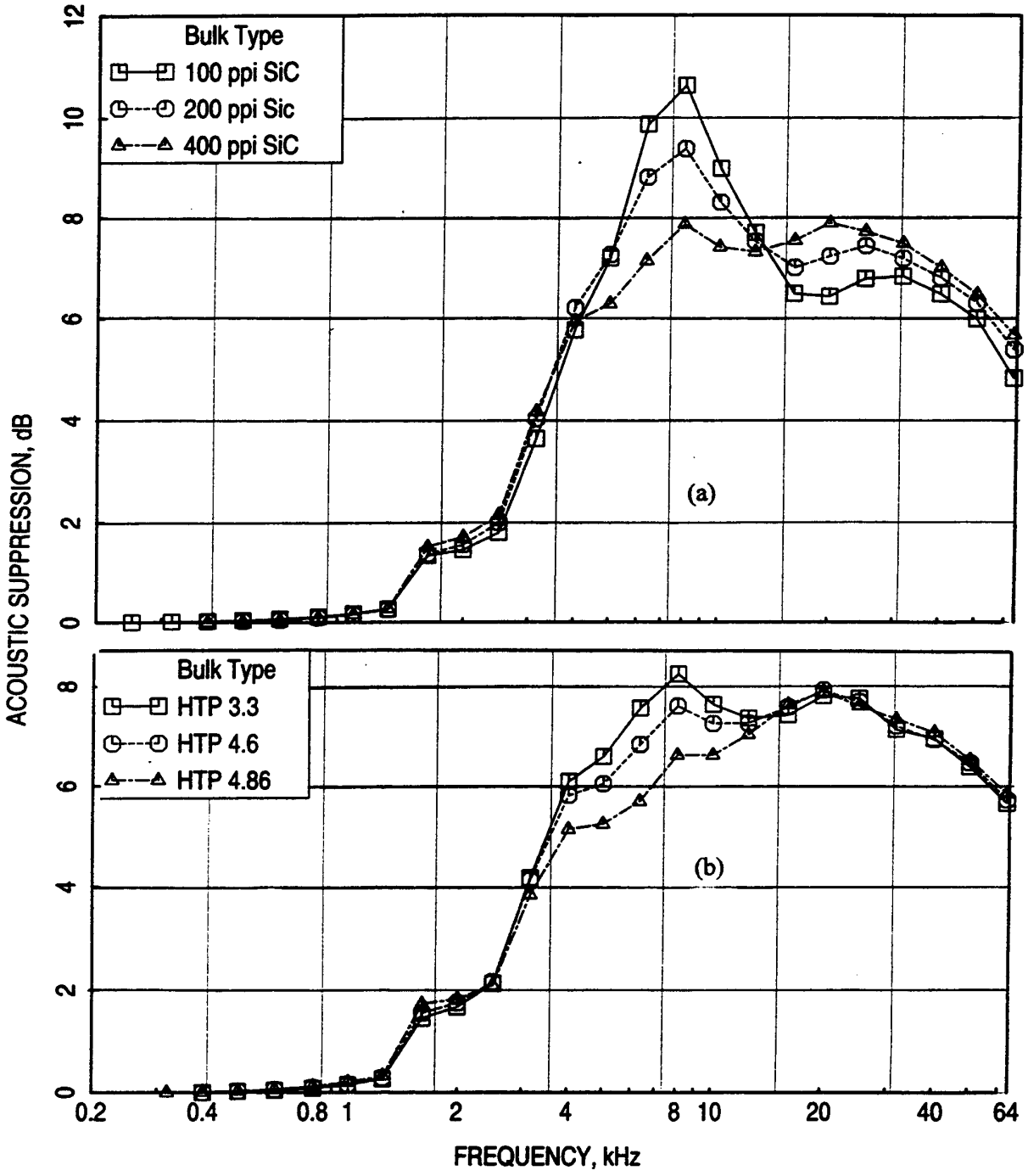

Figure 50. Predicted acoustic suppression with mixed flow Mach number of 0.63 and temperature of 928°R , for Gen 1 mixer-ejector with (a) SiC and (b) HTP bulk absorber liners with 37% porous facesshhet (t=0.025" and d=0.07"); NPR=3.43, T8=1551°R, V_j=2359 ft/sec, M=0.32.

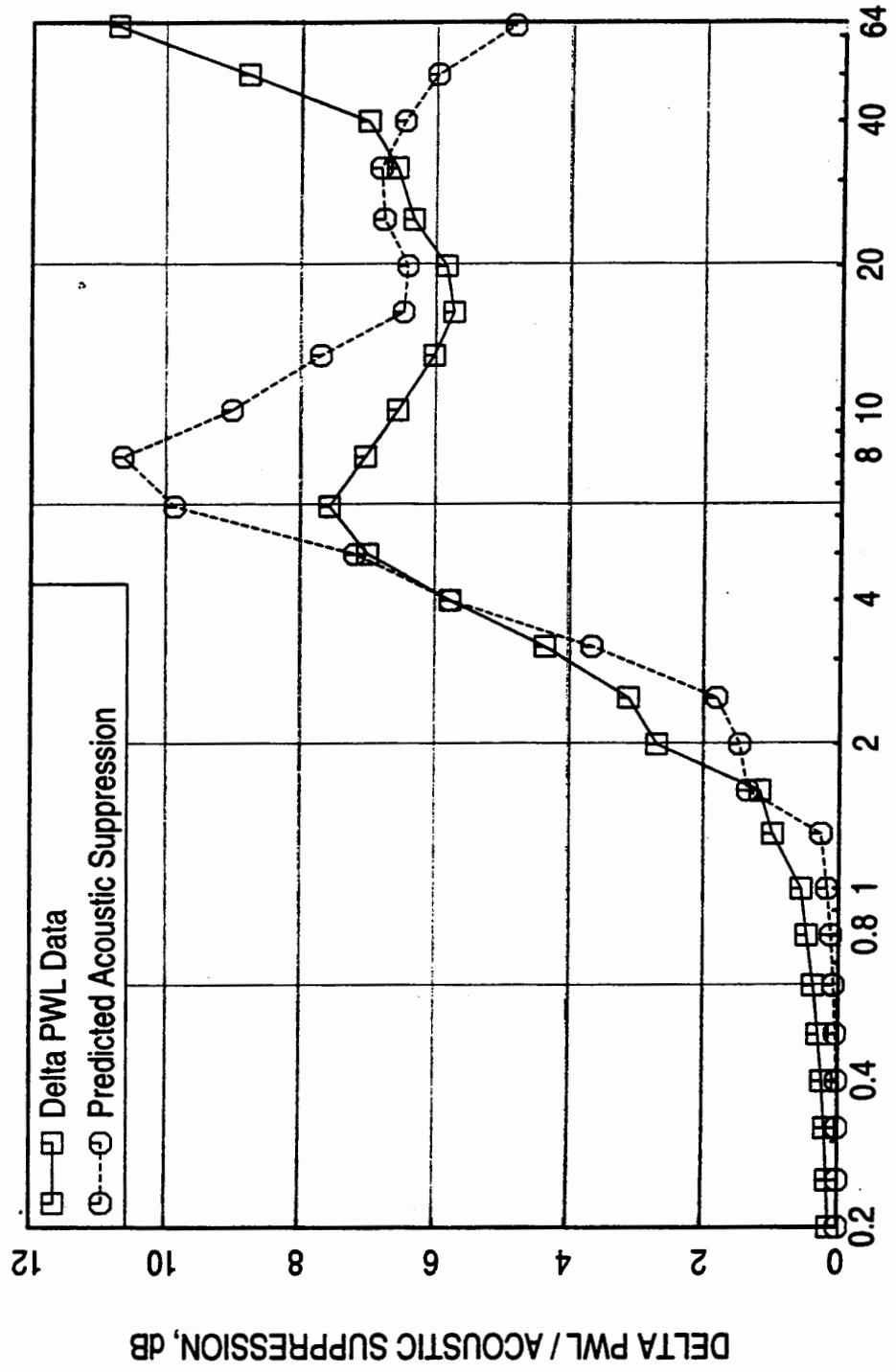

Figure 51. Internal component of ΔPWL and predicted acoustic suppression spectra for Gen 1 mixer-ejector with 100 ppi SiC bulk absorber liner with 37% porous facesshhet (t=0.025" and d=0.07"); NPR=3.43, T8=1551°R, V_j=2359 ft/sec, M=0.3.

of ΔPWL is similar to that of the acoustic suppression. It should be noted that the beginning half of the ejector, closer to the mixer exit, was not treated.

The measured ΔPWL and the predicted acoustic suppression for the 100 ppi SiC liner, plotted in Figure 51, are used to compute a frequency dependent correction factor. This factor is used to compute the ΔPWL and thus the internal component of PWL for other bulk absorber liner configurations. The data and the predicted PWL for various liner configurations are shown in Figure 52. The agreement between the prediction and data is reasonably well.

Thus, the use of the correction factor seems to be reasonable for different liner designs for the same mixer-ejector at a given ejector flow condition. However, the validity of its use for different mixer-ejector geometry and for different scale mixer-ejectors is not known. The correction factor for a 1/7-scale mixer-ejector described earlier in this section is compared with the correction factor of the 1/10-scale Gen 1 mixer-ejector in Figure 53. Significant difference between the two correction factor spectra is observed. These differences can not be attributed to the difference in the mixer-ejector scale factor, since extreme design differences exist between the two models.

At this stage, utilizing the normal impedance, acoustic suppression, and farfield noise prediction methods, a liner design methodology is developed. A computer code to predict the noise components in the farfield with the design inputs (physical and measured acoustic properties of the liner components) is developed. The details of the liner design methodology computer code are described in the appendix A.

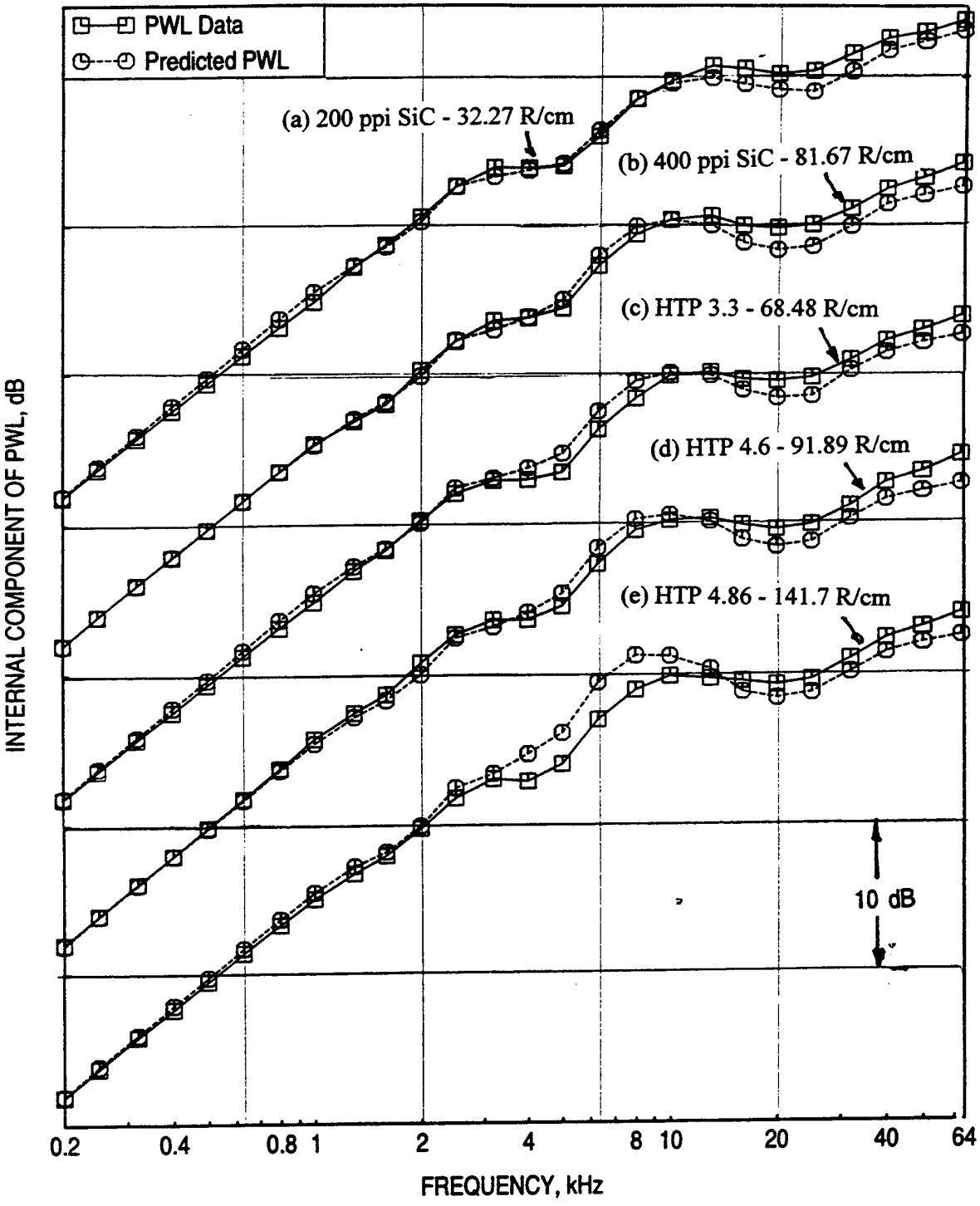

Figure 52. Comparison of internal component of PWL for Gen 1 mixer-ejector between data and prediction for various bulk absorber liners with 37% porous facesshhet (t=0.025" and d=0.07"); NPR=3.43, T8=1551°R, V_j=2359 ft/sec, M=0.3.

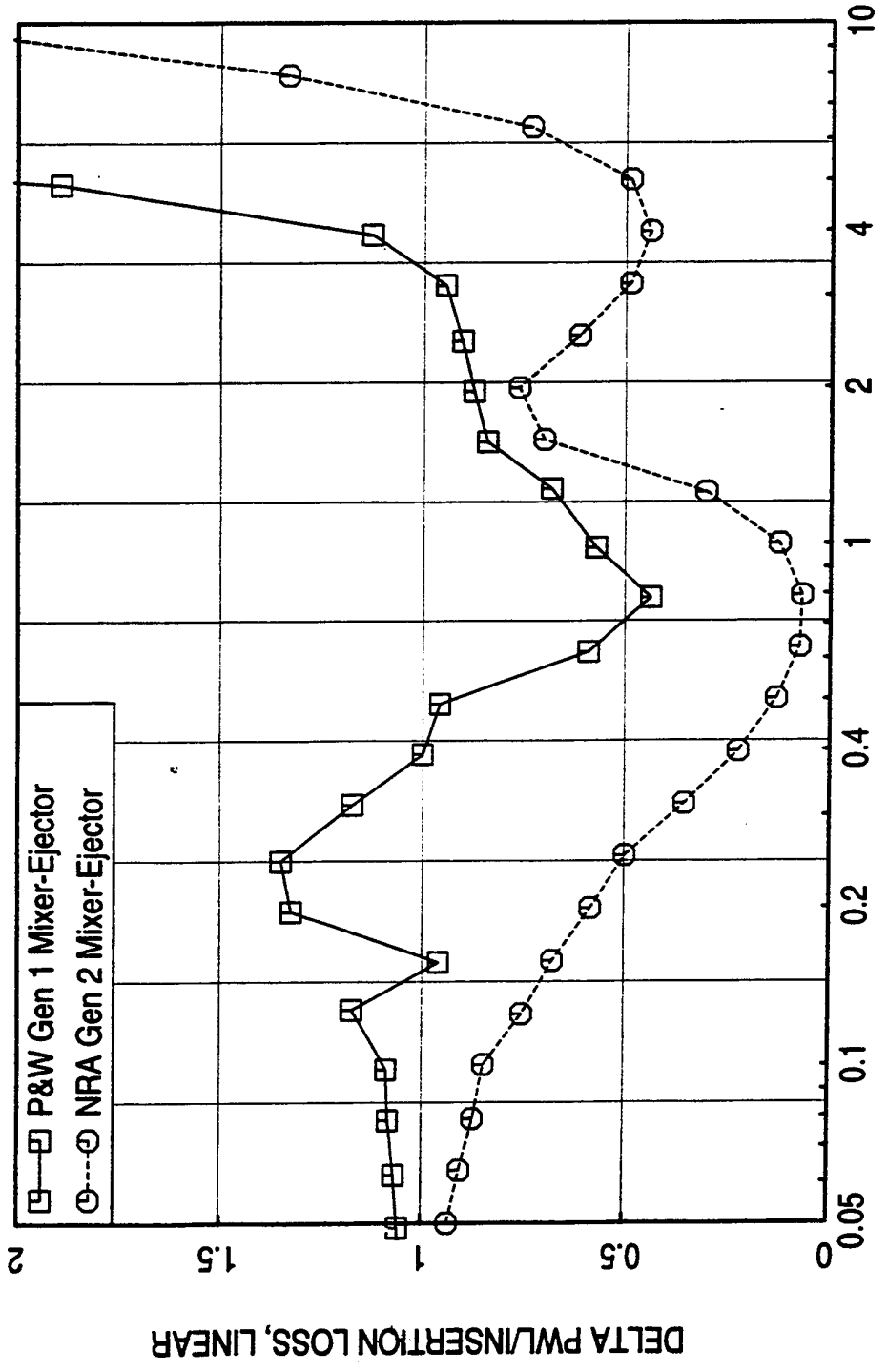

Figure 53. Comparison of correction factor spectra between 8-lobed Gen 1 and 20-lobed Gen 2 mixer-ejectors; NPR=3.43, T8=1551°R, V_j=2359 ft/sec.

6.0 OPTIMUM LINER DESIGNS AND SENSITIVITY STUDIES

The liner optimization process based on the optimum impedance and corresponding acoustic suppression was presented in a coordination memo GE96-143N (Ref. 8). Various physical (liner depth and facesheet geometry) and acoustic characteristics (DC flow resistance) are optimized in this study. Figure 54 summarizes the variation of bulk resistivity, liner depth, and facesheet properties with respect to linear scale factor for optimum liner designs. Similar optimization process is repeated in this section with respect to achieving a minimum EPNdB using the process described in section 5.0. This process would establish whether the optimum parameters on optimum impedance basis remain the same when optimized with respect to minimum EPNL. In this exercise the physical and acoustic properties for each design are varied and the corresponding EPNL are calculated. In addition, the sensitivity of the design with respect to EPNL is studied for flow and acoustic environment of the ejector. In this study grazing flow Mach number M and temperature T, mean flow Mach number Mx, temperature Tx, boundary layer displacement thickness δ^*, and OASPL are considered.

6.1 Liner Depth (D): Figure 55 shows the normal impedance and acoustic suppression spectra for full scale liner designs with different liner depths for a fixed bulk resistivity (10 Rayls/cm) and for the same facesheet. The acoustic suppression increases at lower frequencies with increasing liner depth without impacting on high frequency results. However, for liner depths above 2", the acoustic suppression at mid frequency range seems to be decreasing with increasing D. Figure 56 shows the PNL directivities for each of the liner depths. Both total and internal components indicate EPNL reduction with increasing D up to about D=2.67". Slight EPNL increase is observed for higher liner depths.

Similar results for LSM and 1/7-scale liners are shown in Figures 57 through 60. The variation of acoustic properties with respect to the liner depth is similar to those observed for full-scale designs. The predicted EPNL for each scale is plotted with respect to liner depth in Figure 61. While the slopes of EPNL with respect to liner depth are drastically different, they seem to collapse better when plotted as ratio of liner depth and linear scale factor. At higher liner depths the EPNL variation is insignificant. The optimum liner depths, thus evaluated, 2.0", 1.2", and 0.485", for full scale, LSM, and 1/7-scale, respectively, are again the same as those obtained earlier. It should be noted that the liner depth for 1/7-scale is much higher compared to 0.27" on the basis of its linear scale factor.

6.2 Bulk Resistivity: Keeping the optimum liner depths and facesheet properties the same, bulk resistivity is varied for each of the three mixer-ejector cases. Figure 62 shows predicted

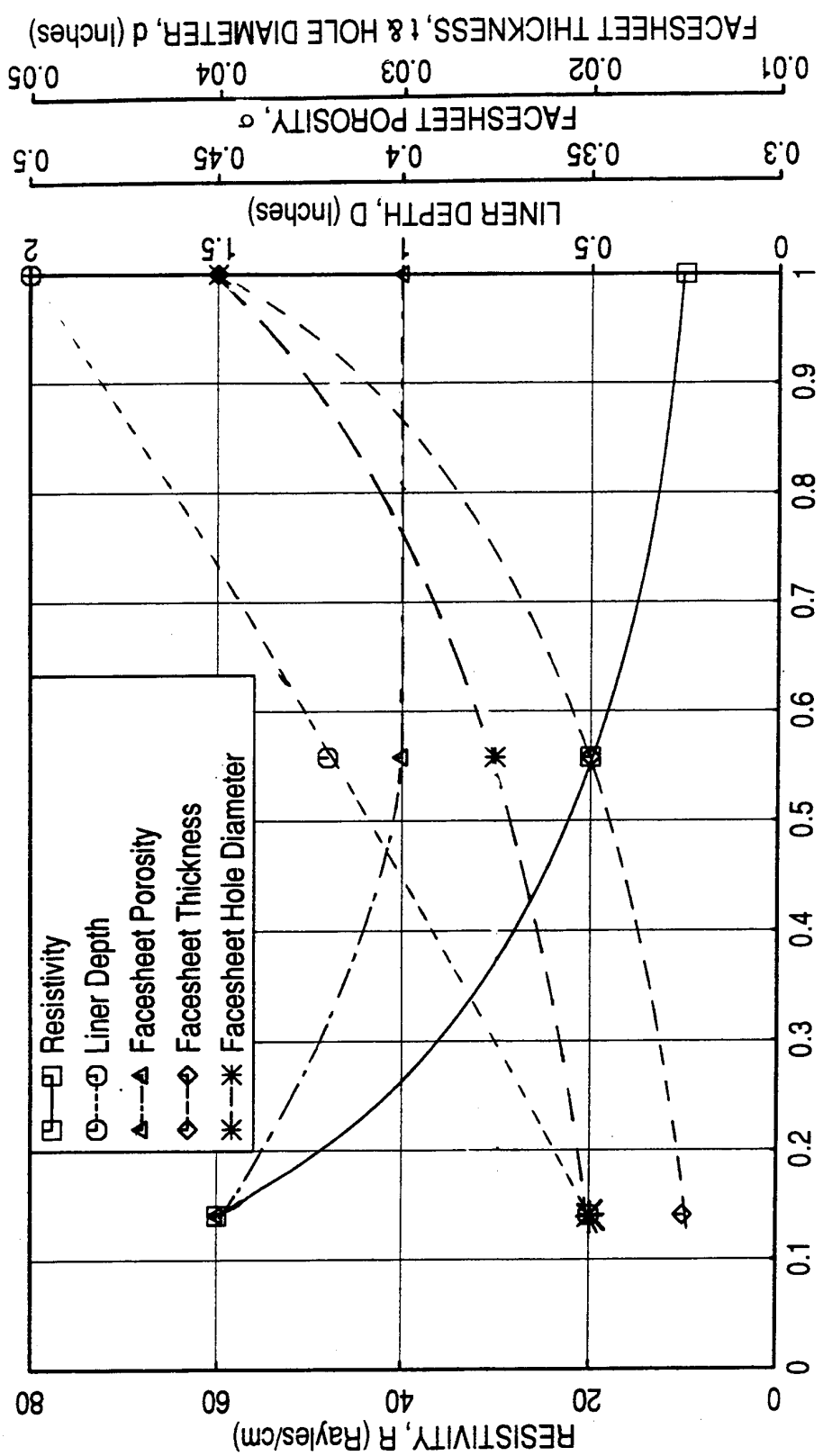

Figure 54. Variation of bulk resistivity, liner depth, and facesheet properties with respect to mixer-ejector linear scale factor for optimum liner designs, static temperature=500°F, grazing flow Mach number=0.8.

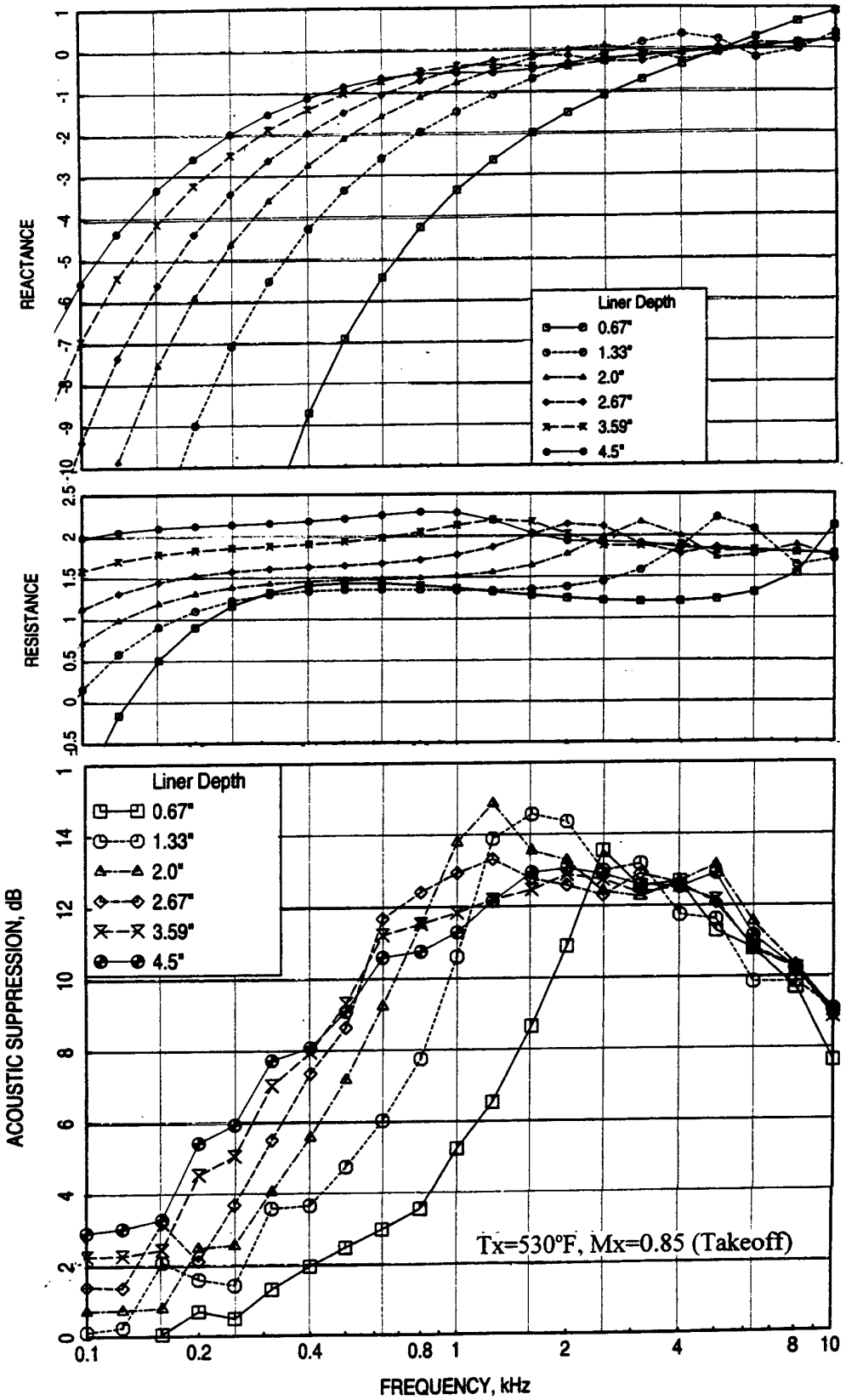

Figure 55. Effect of liner depth (D) on predicted normal impedance and acoustic suppression spectra for a full scale mixer-ejector liner design, S=40%, t=0.04", d=0.04", R=10 Rayls/cm, T=500°F, M=0.8, OASPL=180 dB (takeoff).

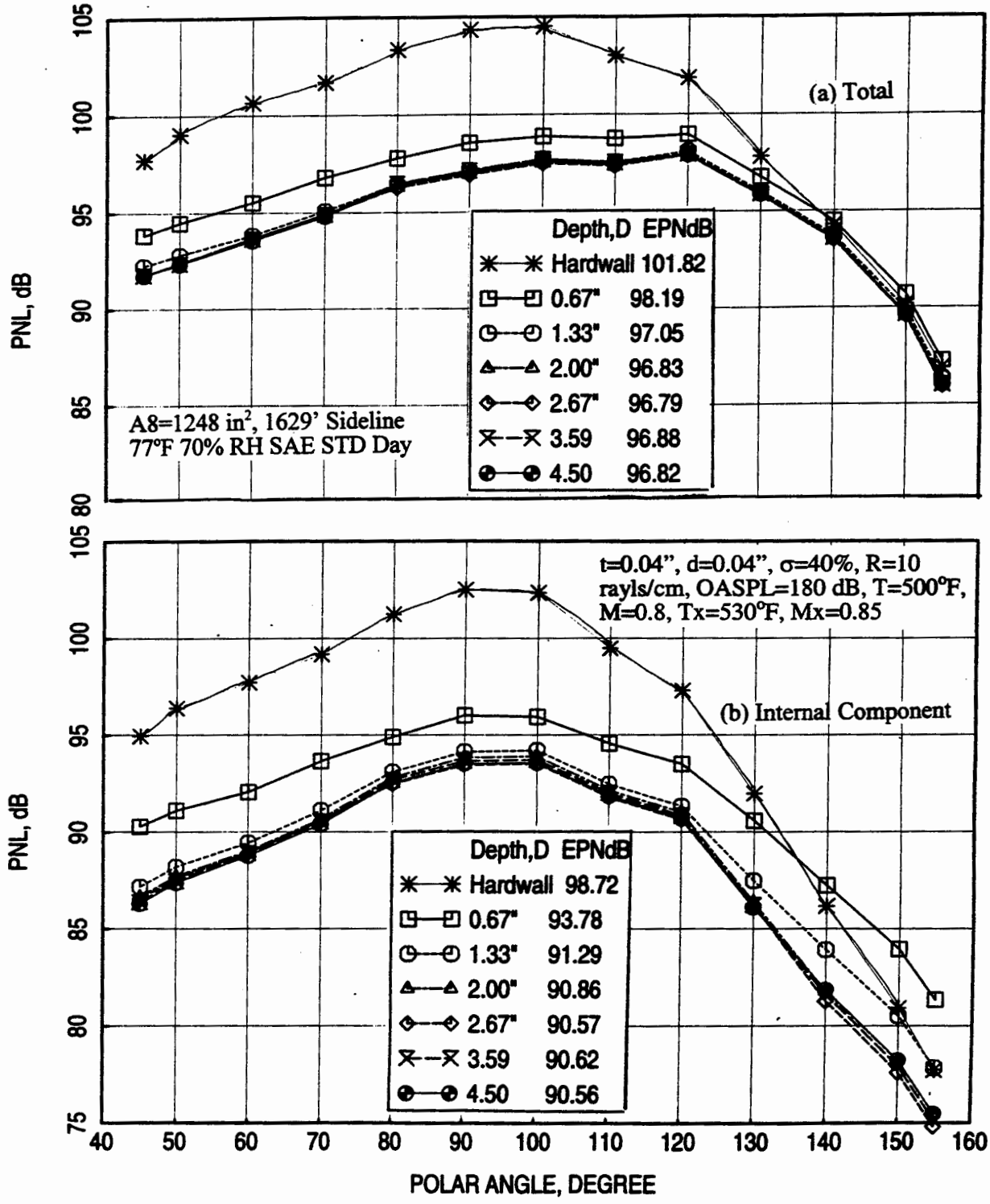

Figure 56. Effect of liner depth (D) on predicted (a) total and (b) internal component of PNL directivities for a full scale mixer-ejector liner design, NPR=3.43, T8=1551°R, V_j=2359 ft/sec, M=0.32 {takeoff}.

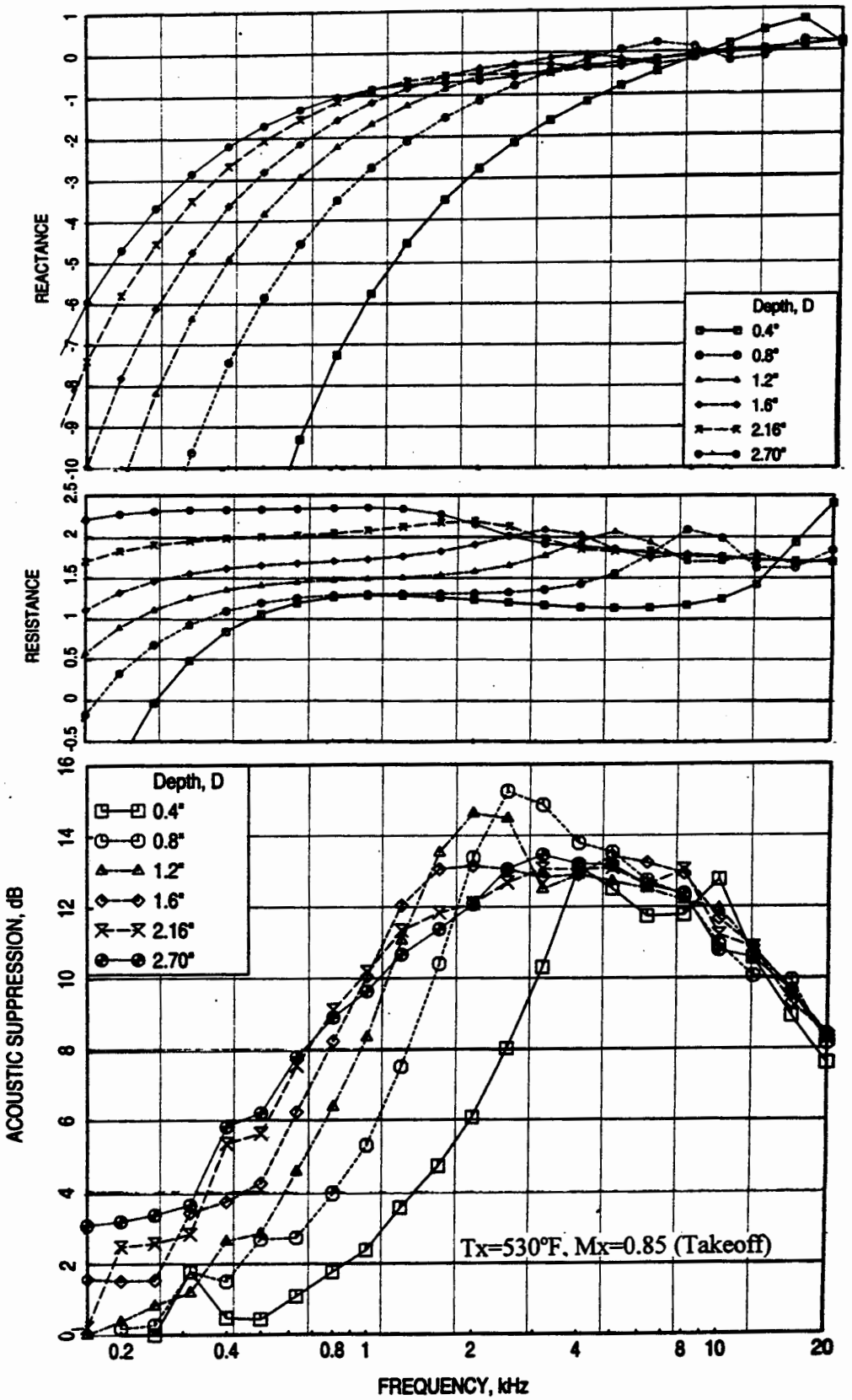

Figure 57. Effect of liner depth (D) on predicted normal impedance and acoustic suppression spectra for an LSM mixer-ejector liner design, S=40%, t=0.02", d=0.025", R=20 Rayls/cm, T=500°F, M=0.8, OASPL=177.5 dB (takeoff)..

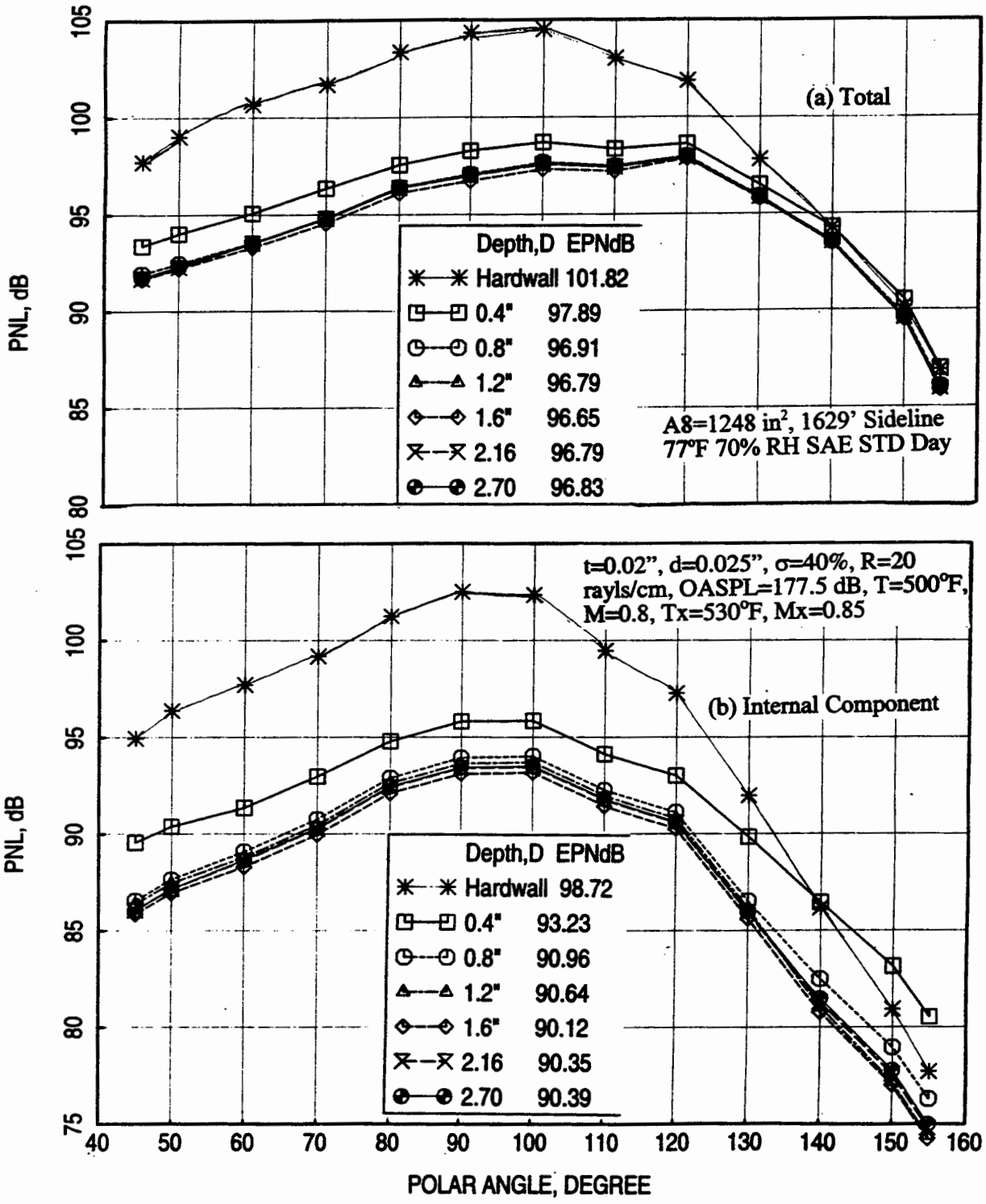

Figure 58. Effect of liner depth (D) on predicted (a) total and (b) internal component of PNL directivities for an LSM mixer-ejector liner design, NPR=3.43, T8=1551°R, V_j=2359 ft/sec, M=0.32 {takeoff}.

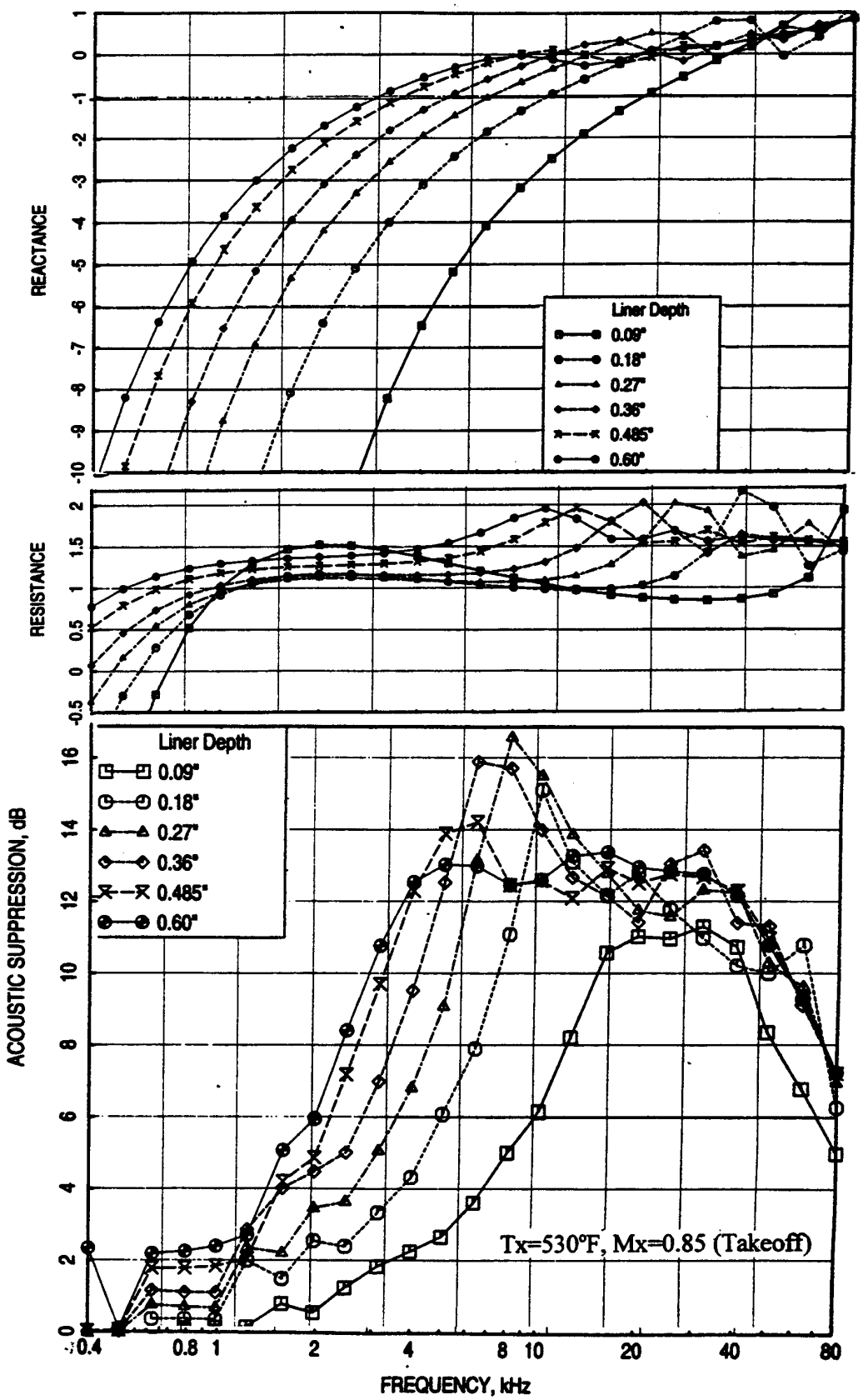

Figure 59. Effect of liner depth (D) on predicted normal impedance and acoustic suppression spectra for a liner design for NRA model with mixer 8, S=45%, t=0.02", d=0.015", R=40 Rayls/cm, T=500°F, M=0.8, OASPL=171.5 dB (takeoff).

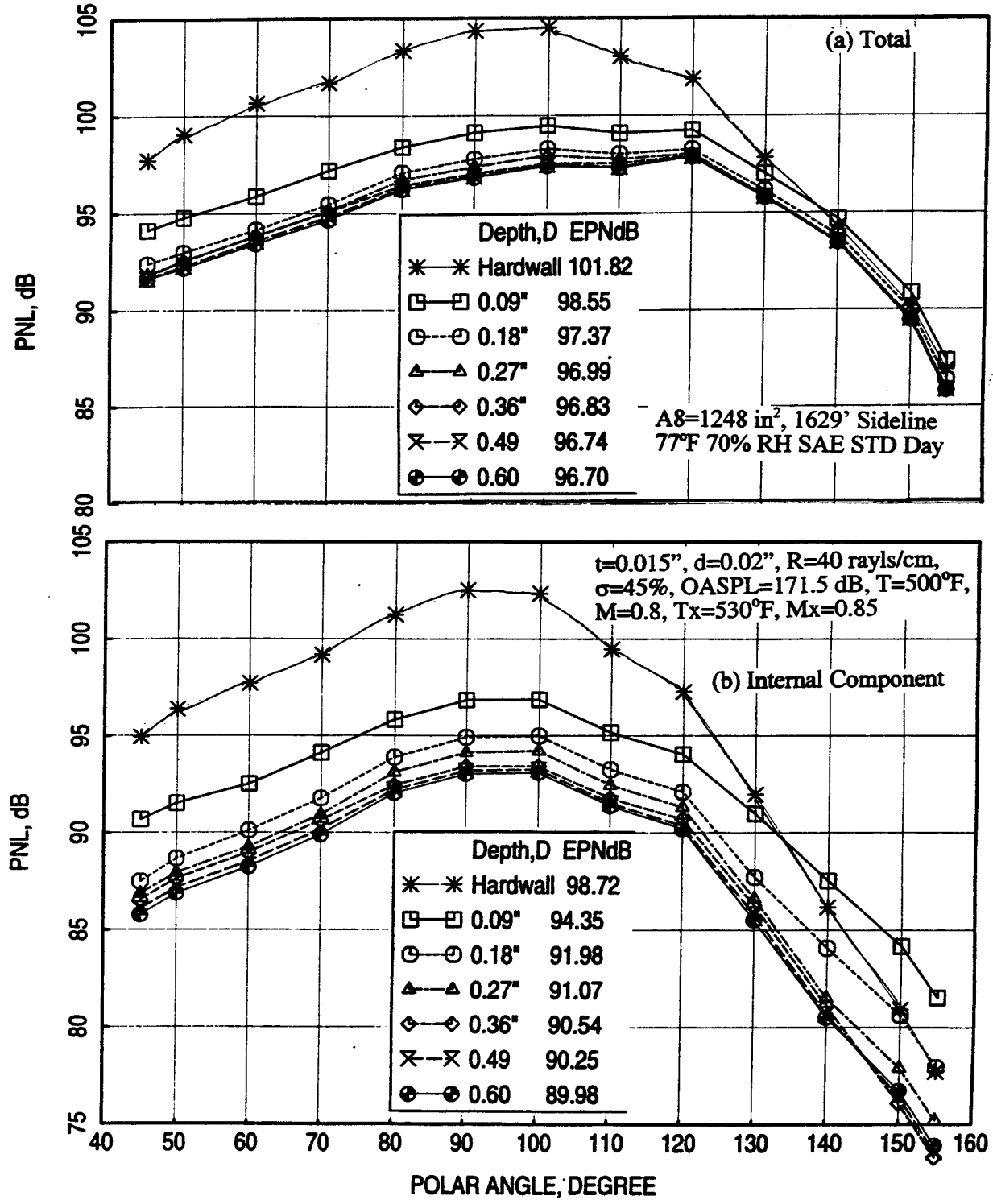

Figure 60. Effect of liner depth (D) on predicted (a) total and (b) internal component of PNL directivities for a liner design for NRA model with mixer 8, NPR=3.43, T8=1551°R, V_j=2359 ft/sec, M=0.32 {takeoff}.

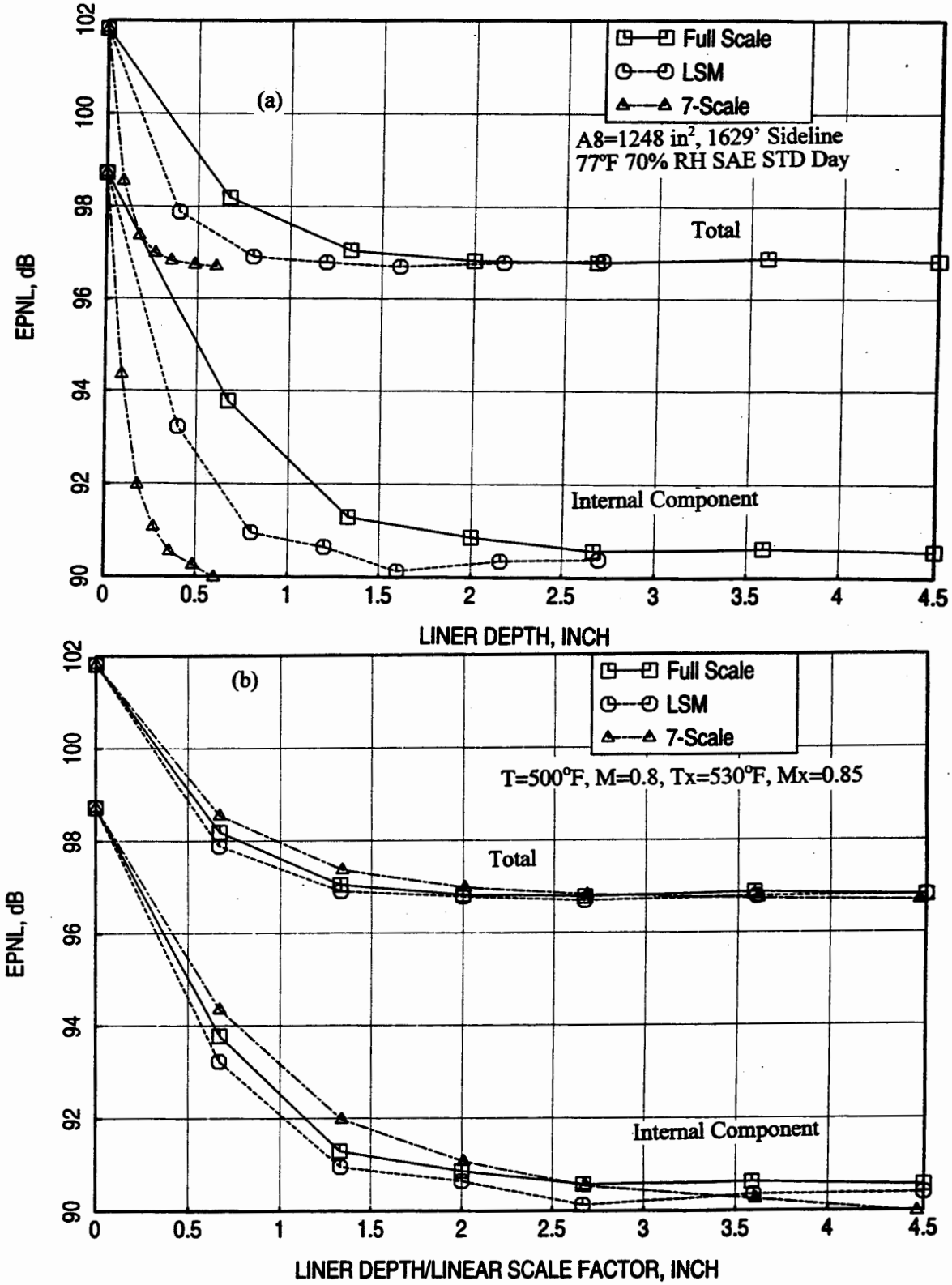

Figure 61. Effect of liner depth (D) on predicted total and internal component of EPNL for three different scale mixer-ejector liner designs, NPR=3.43, T8=1551°R, V_j=2359 ft/sec, M=0.32 {takeoff}.

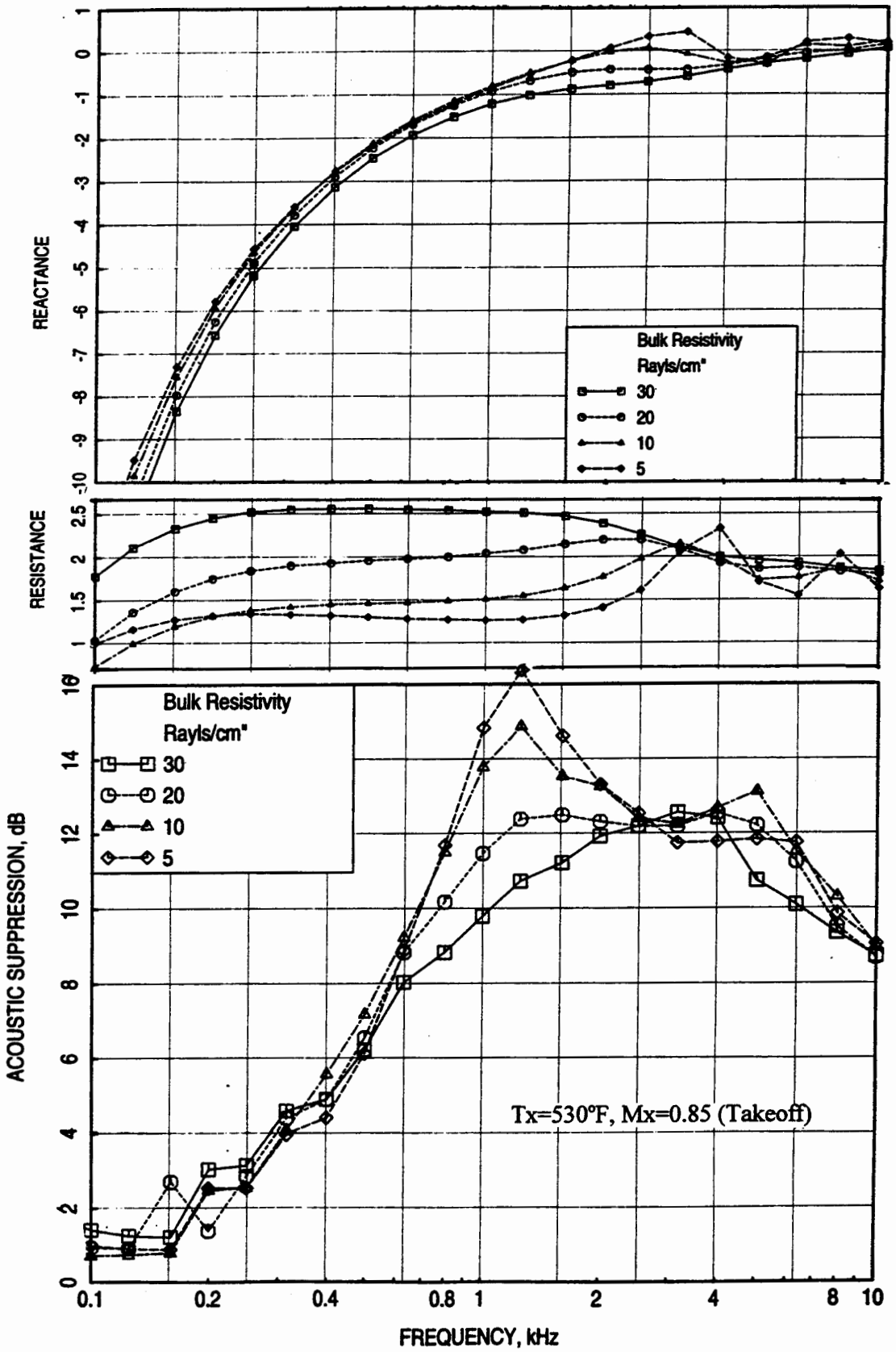

Figure 62. Effect of bulk resistivity on predicted normal impedance and acoustic suppression spectra for a full scale mixer-ejector liner design, D=2.0", S=40%, t=0.04", d=0.04", T=500°F, M=0.8, OASPL=180 dB (takeoff).

normal impedance and acoustic suppression for a full-scale mixer-ejector liner with different bulk resistivity. The acoustic suppression increases at mid frequency range with decreasing bulk resistivity. However, the EPNL, based on the predicted PNL directivities (see Figure 63), decreases with decreasing bulk resistivity and the trends gets reversed at very low value of bulk resistivity. Similar results for LSM and 1/7-scale designs are shown in Figures 64 through 67. Finally, the EPNL is plotted with respect to bulk resistivity as well as with respect to the product of bulk resistivity and linear scale factors for all three mixer-ejector designs in Figure 68. Clearly, the minimum EPNL for different scale designs appears at different bulk resistivity. The optimum resistivity increases with decreasing linear scale factor. For total EPNL the scale factor proportionality of bulk resistivity is reasonably good. A finer variation can result in a more accurate optimum bulk resistivity. However, the optimum resistivities are kept the same (i.e., 10, 20, and 60 Rayls/cm for full scale, LSM, and 1/7-scale designs) as before (Ref. 8), since their impact on EPNL is relatively small if varied by a small amount.

6.3 Facesheet Porosity: Keeping the optimum liner depths, bulk resistivity, and facesheet thickness and hole diameter the same, the facesheet porosity is varied for each of the three mixer-ejector cases. Figure 69 shows predicted normal impedance and acoustic suppression for a full-scale mixer-ejector liner with different facesheet porosity. The acoustic suppression increases at mid and high frequency ranges with increasing facesheet porosity. Also, the EPNL, based on the predicted PNL directivities (see Figure 70), decreases with increasing facesheet porosity. Similar results for a thicker facesheet (t=0.1") with larger hole diameter (d=0.1") are also evaluated and presented in Figures 71 and 72. The acoustic characteristics are similar to what is observed for thinner facesheets with smaller hole diameter. The EPNL for these two sets of facesheets is plotted with respect to facesheet porosity in Figure 73. EPNL for both the sets of facesheets decreases with increasing porosity. However, the levels for the thicker facesheets are higher compared to the thinner facesheets. This is due to the increased mass reactance of the thicker facesheets at higher frequencies.

Similar results for LSM and 1/7-scale designs are shown in Figures 74 through 77. Again, the EPNL decreases monotonically with increasing facesheet porosity for mixer-ejectors of all three scales. Finally, the EPNL is plotted with respect to facesheet porosity for all three mixer-ejector designs in Figure 78. Clearly, the minimum EPNL for all three scale designs monotonically decreases with increasing facesheet porosity. The rate of EPNL decrease reduces at higher porosities. With this trend there is no scaling requirements to set the optimum porosity. A very high value of facesheet porosity is desirable for each case.

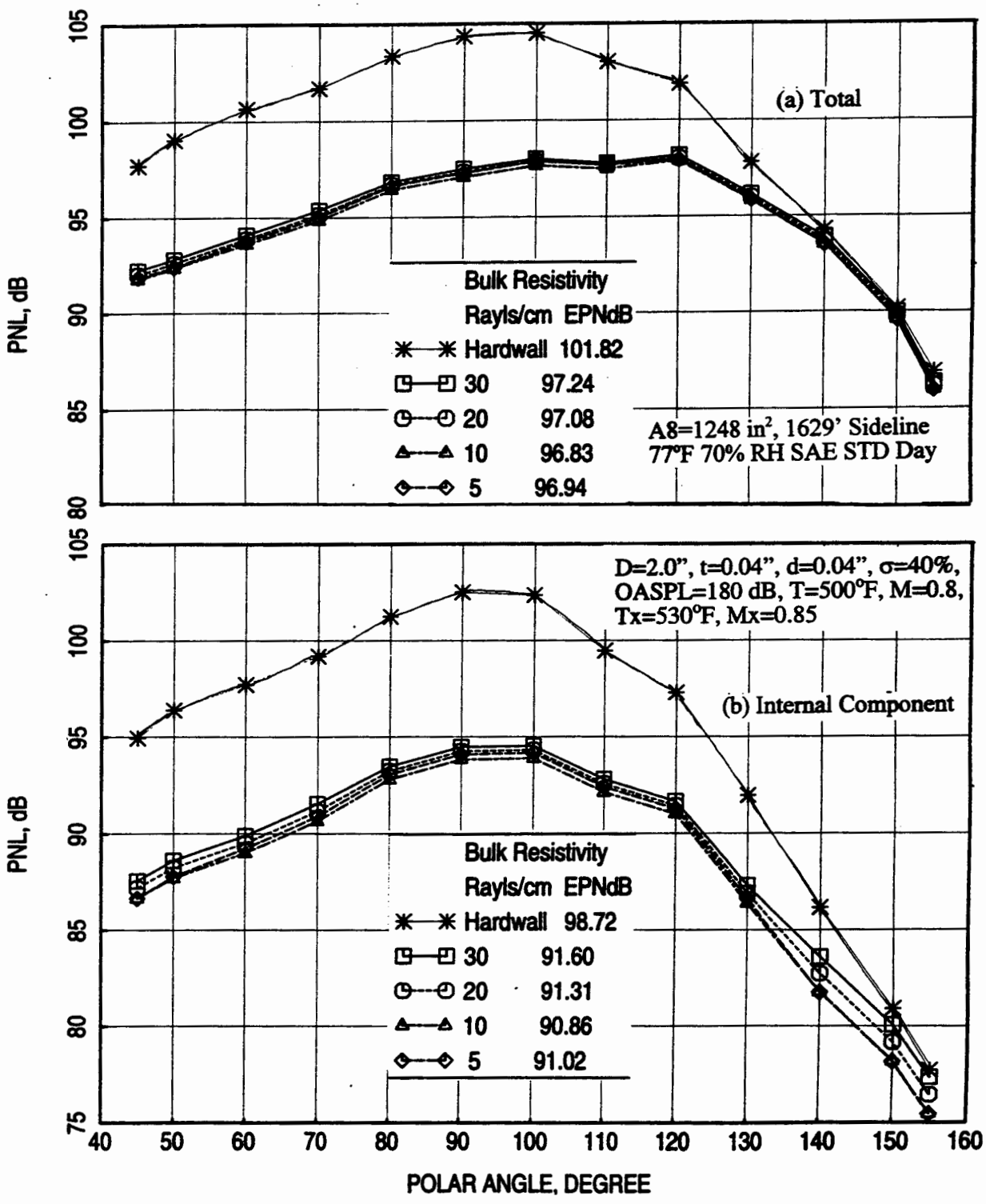

Figure 63. Effect of bulk resistivity on predicted (a) total and (b) internal component of PNL directivities for a full scale mixer-ejector liner design, NPR=3.43, T8=1551°R, V_j=2359 ft/sec, M=0.32 {takeoff}.

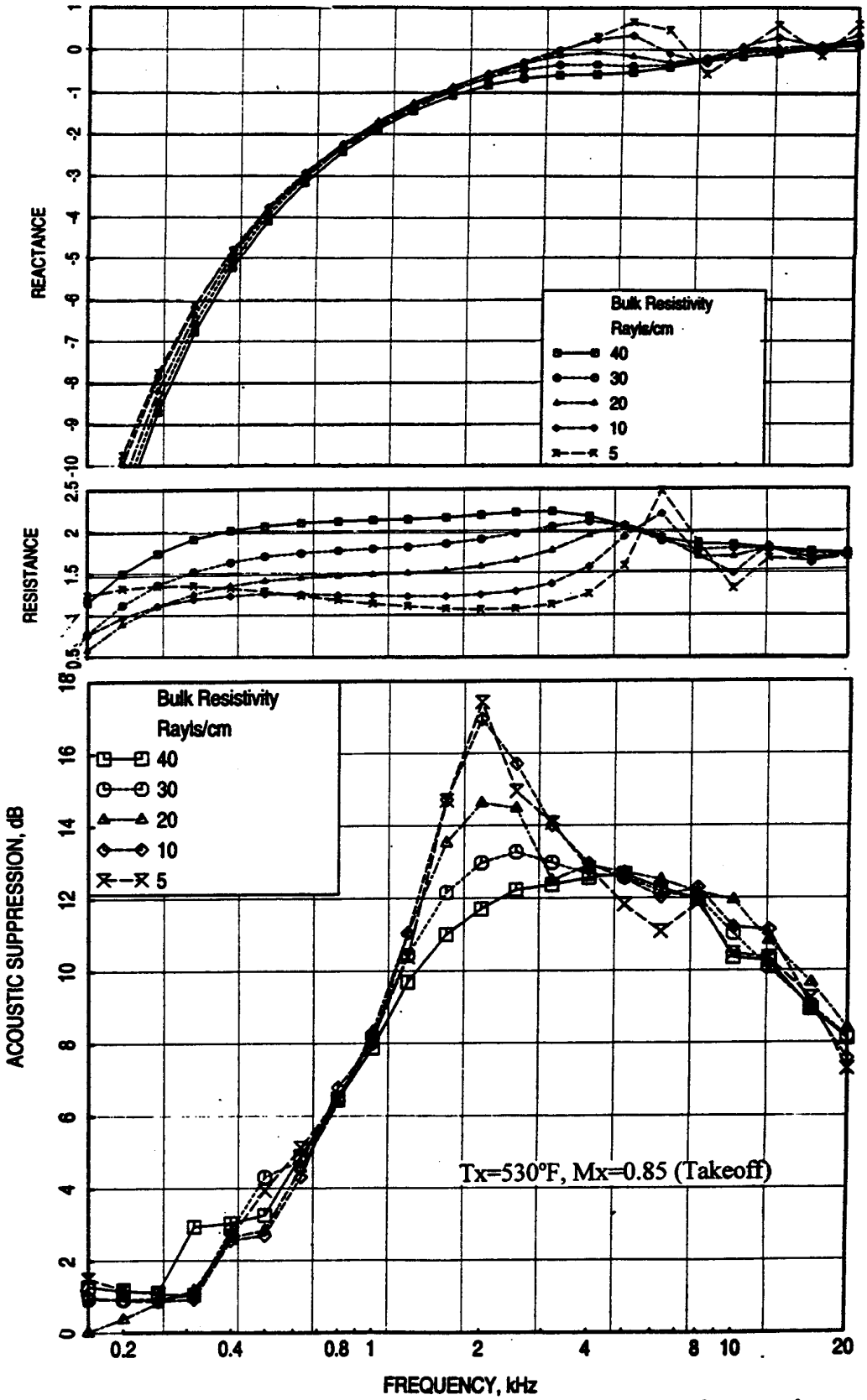

Figure 64. Effect of bulk resistivity on predicted normal impedance and acoustic suppression spectra for an LSM mixer-ejector liner design, D=1.2", S=40%, t=0.02", d=0.025", T=500°F, M=0.8, OASPL=177.5 dB (takeoff)..

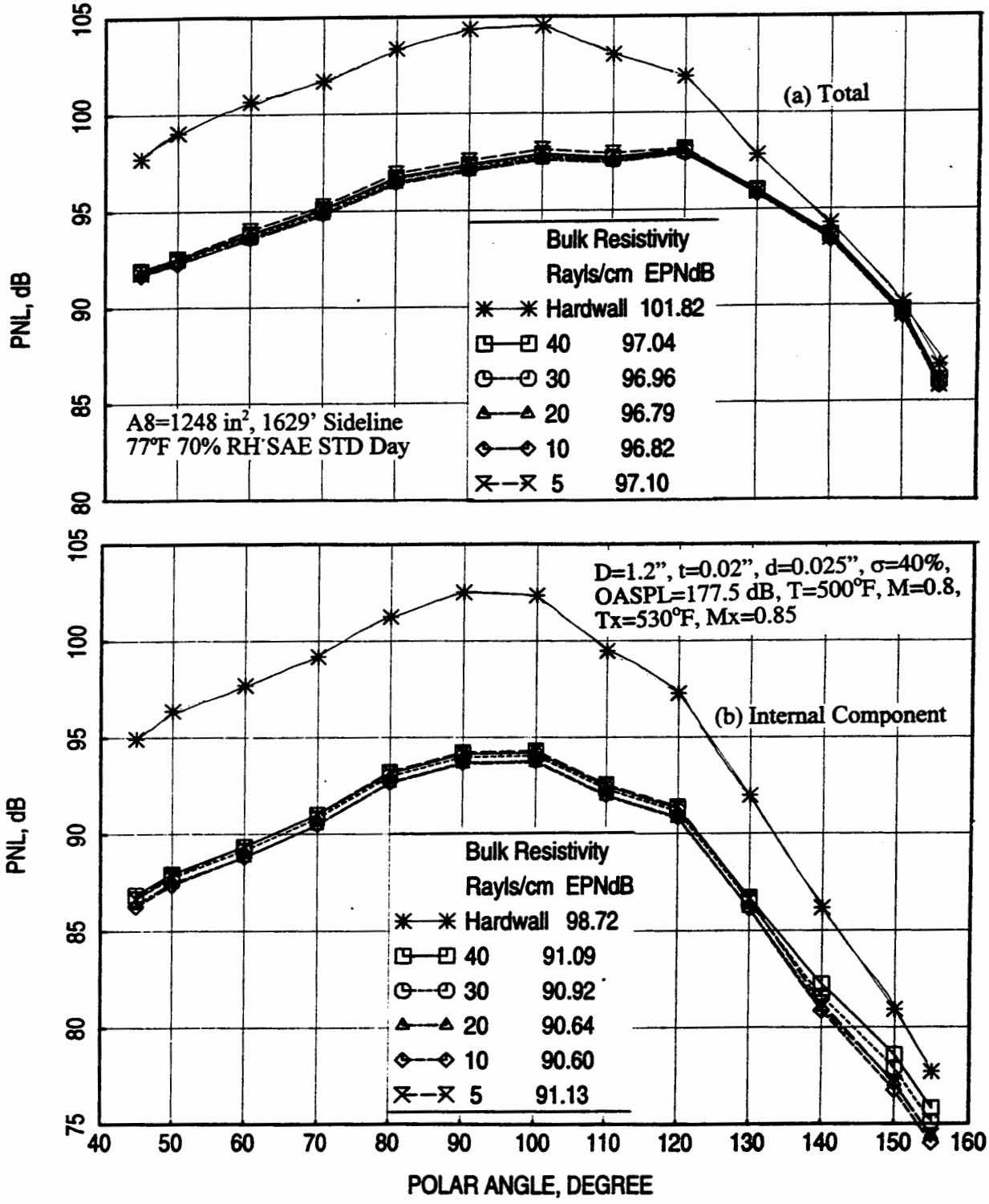

Figure 65. Effect of bulk resistivity on predicted (a) total and (b) internal component of PNL directivities for an LSM mixer-ejector liner design, NPR=3.43, T8=1551°R, V_j=2359 ft/sec, M=0.32 {takeoff}.

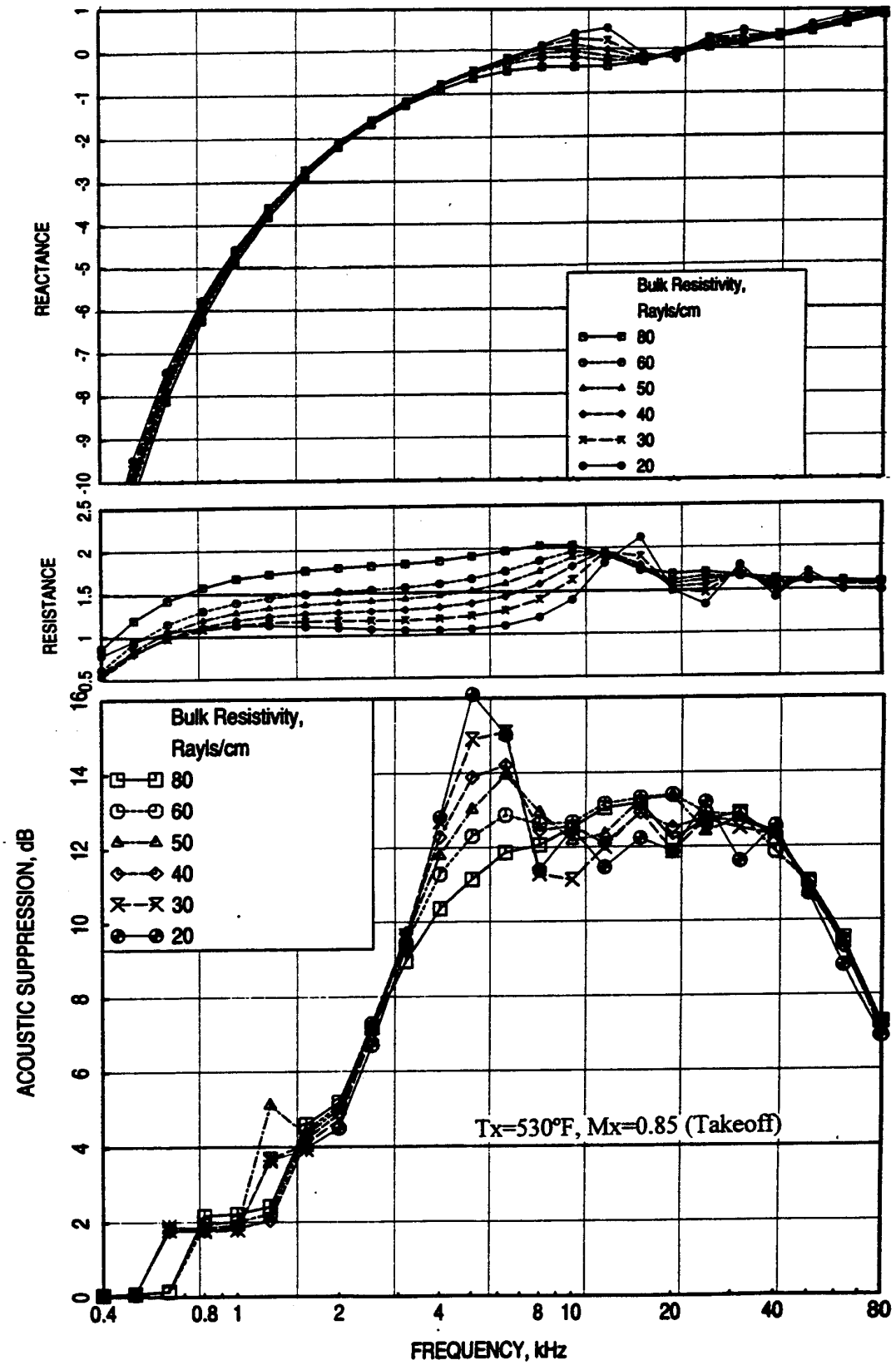

Figure 66., Effect of bulk resistivity on predicted normal impedance and acoustic suppression spectra for a liner design for NRA model with mixer 8, D=0.485", S=45%, t=0.015", d=0.02", T=500°F, M=0.8, OASPL=171.5 dB (takeoff).

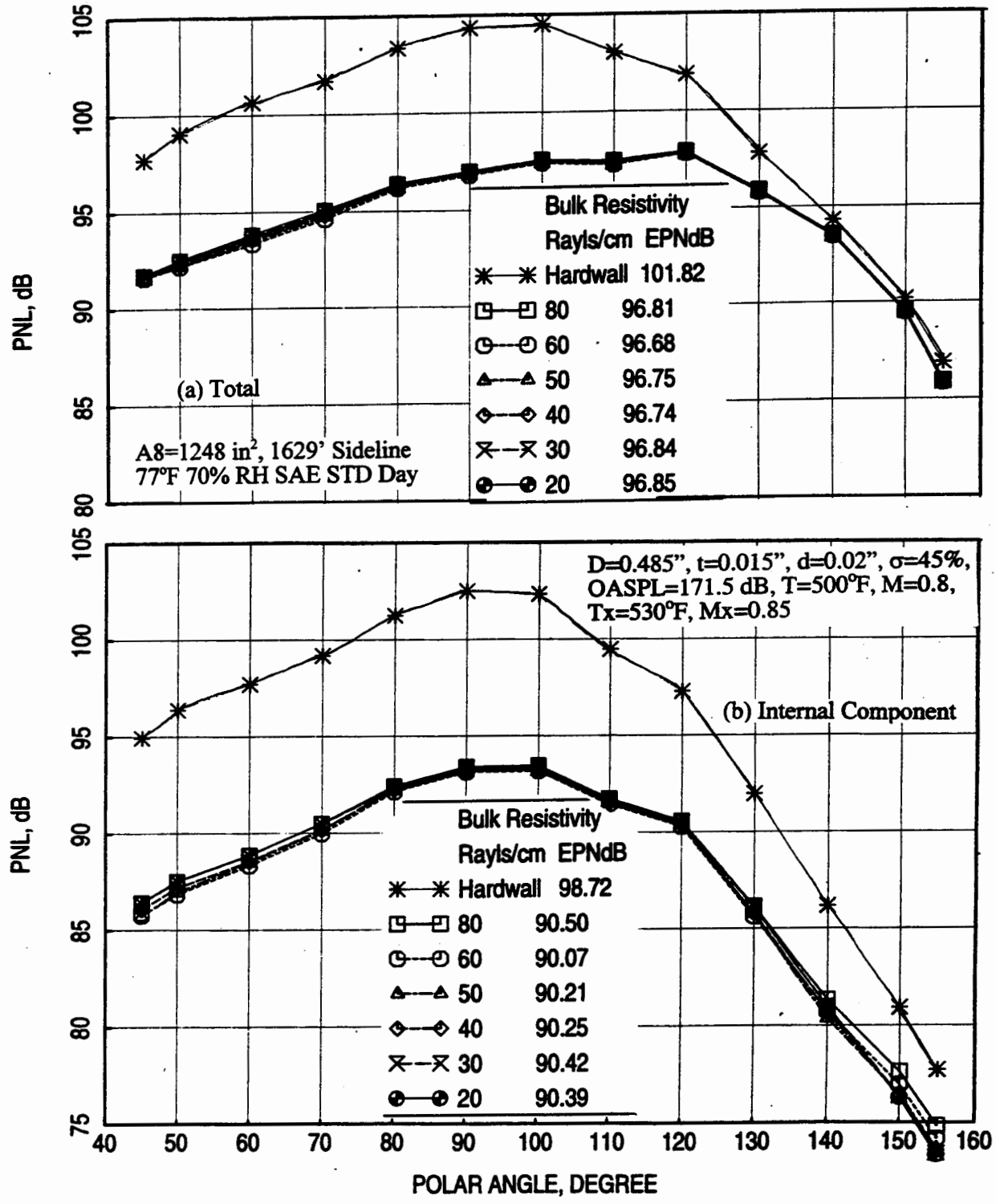

Figure 67. Effect of bulk resistivity on predicted (a) total and (b) internal component of PNL directivities for a liner design for NRA model with mixer 8, NPR=3.43, T8=1551°R, V_j=2359 ft/sec, M=0.32 {takeoff}.

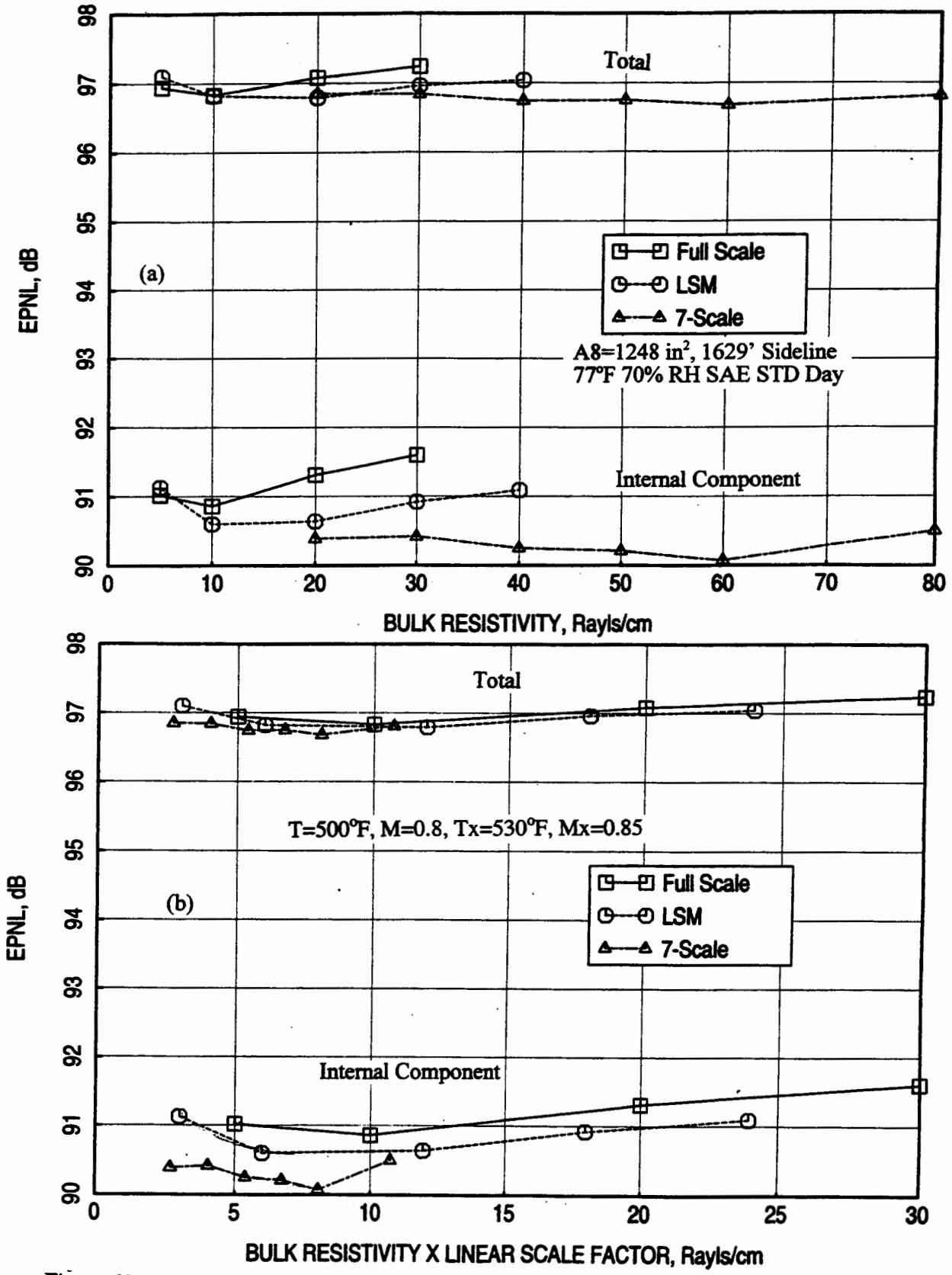

Figure 68. Effect of bulk resistivity on predicted total and internal component of EPNL for three different scale mixer-ejector liner designs, NPR=3.43, T8=1551°R, V_j=2359 ft/sec, M=0.32 {takeoff}.

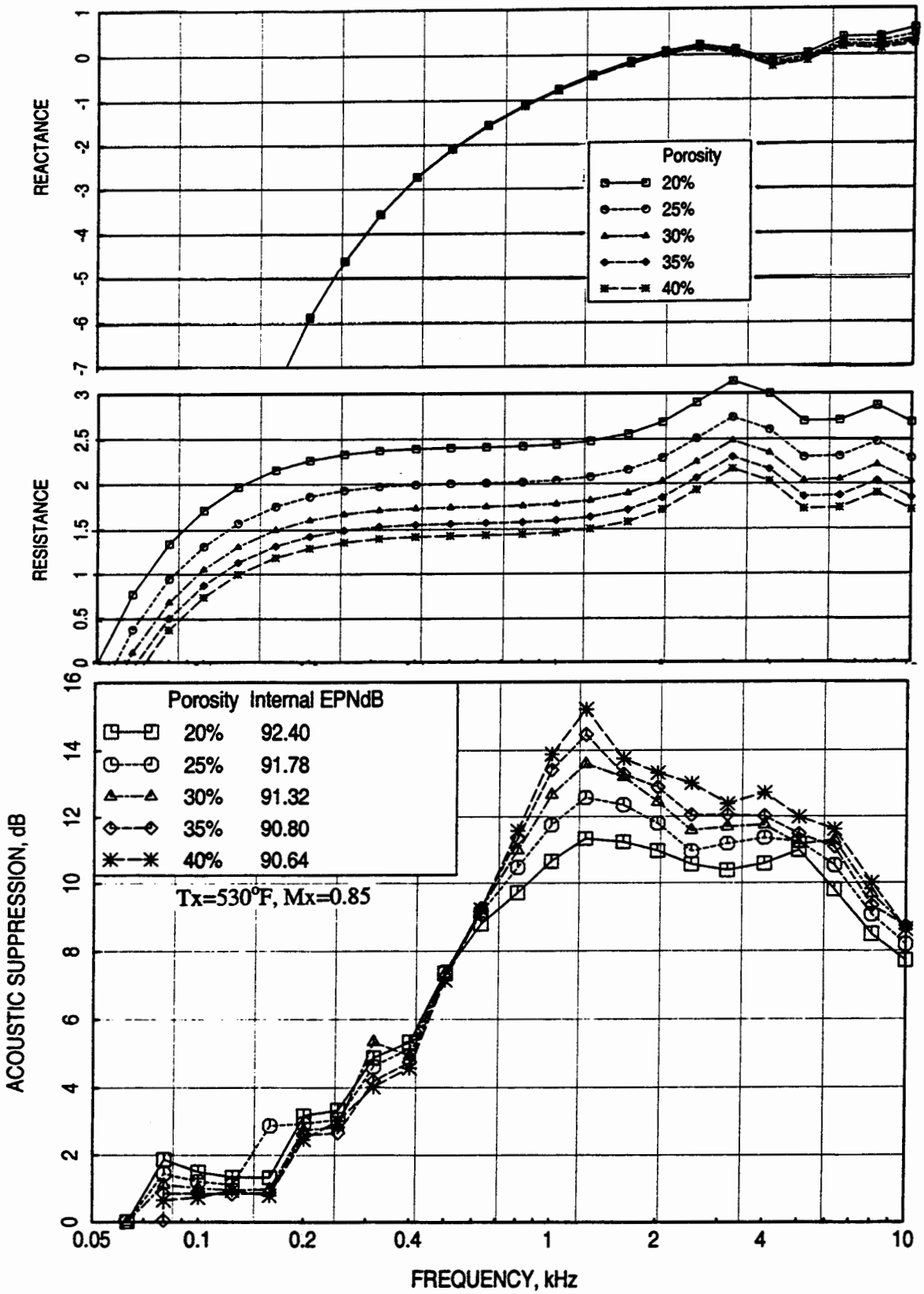

Figure 69. Effect of facesheet porosity (σ) on predicted normal impedance and acoustic suppression spectra for a full-scale mixer-ejector liner design, D=2.0", t=0.04", d=0.04", R=9 Rayls/cm, T=500°F, M=0.8, OASPL=180 dB (takeoff).

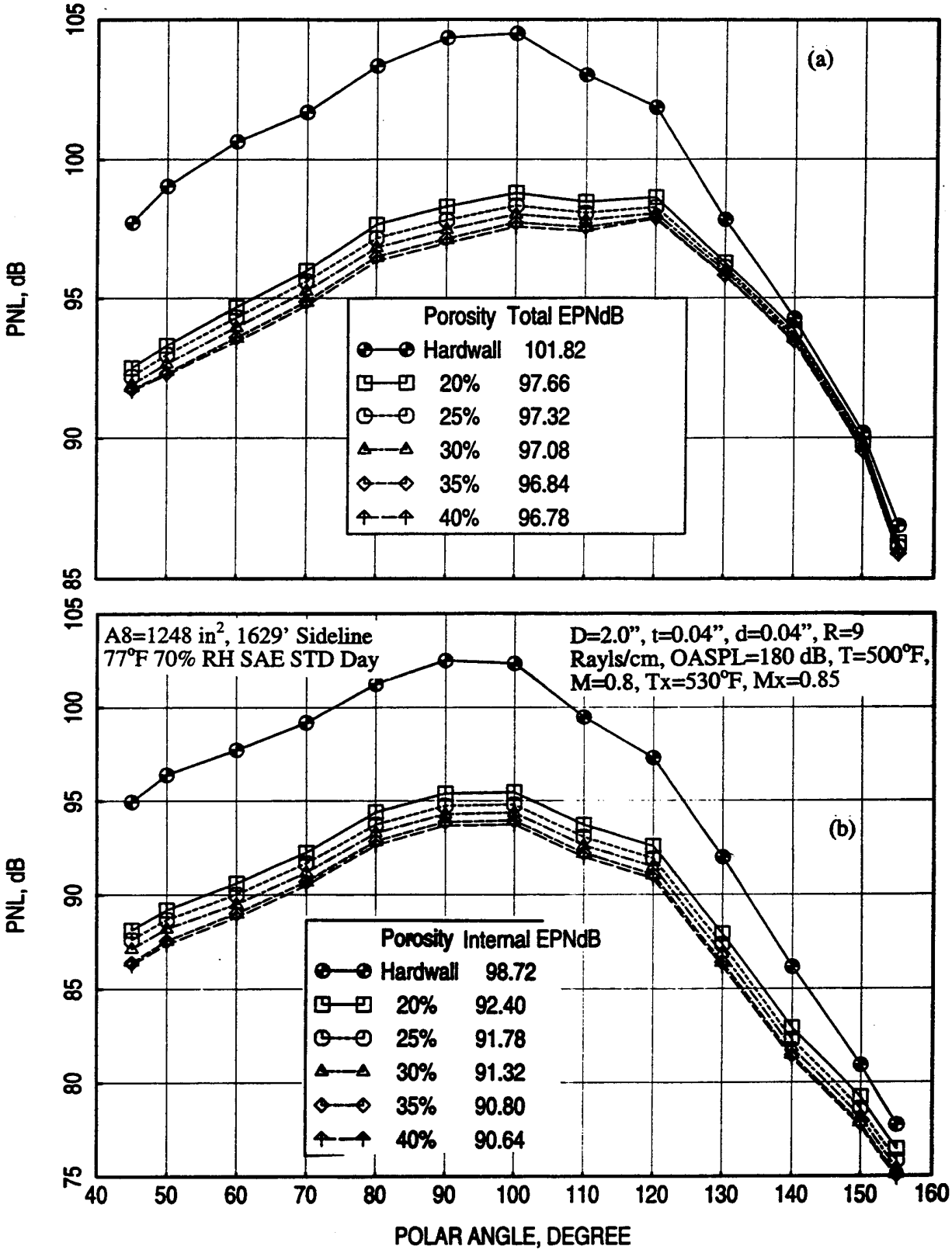

Figure 70. Effect of facesheet porosity (σ) on predicted (a) total and (b) internal component of PNL directivities for a full-scale mixer-ejector liner design, NPR=3.43, T8=1551°R, V_j=2359 ft/sec, M=0.32 {takeoff}.

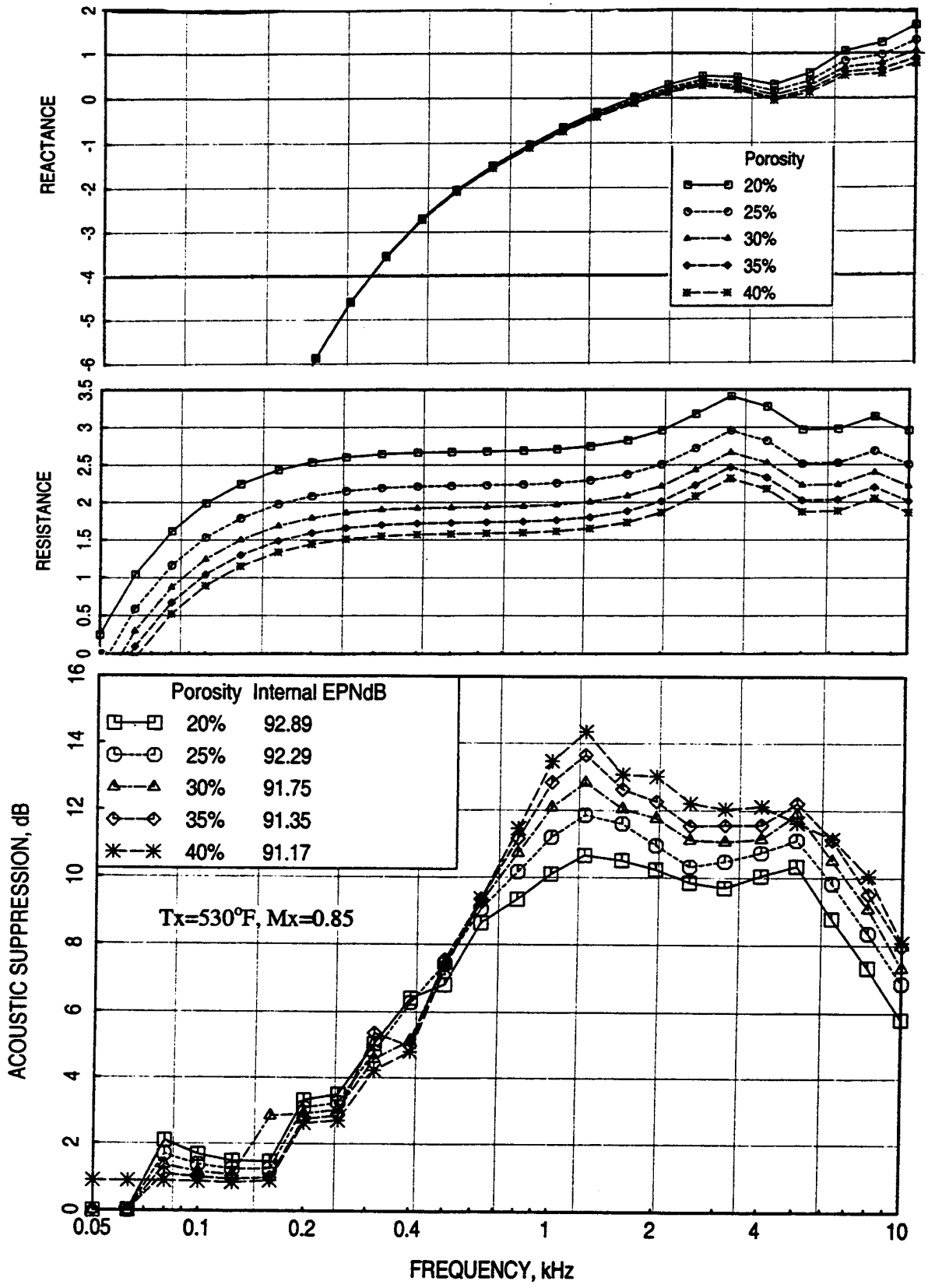

Figure 71. Effect of facesheet porosity (σ) on predicted normal impedance and acoustic suppression spectra for a full-scale mixer-ejector liner design, D=2.0", t=0.10", d=0.10", R=9 Rayls/cm, T=500°F, M=0.8, OASPL=180 dB (takeoff).

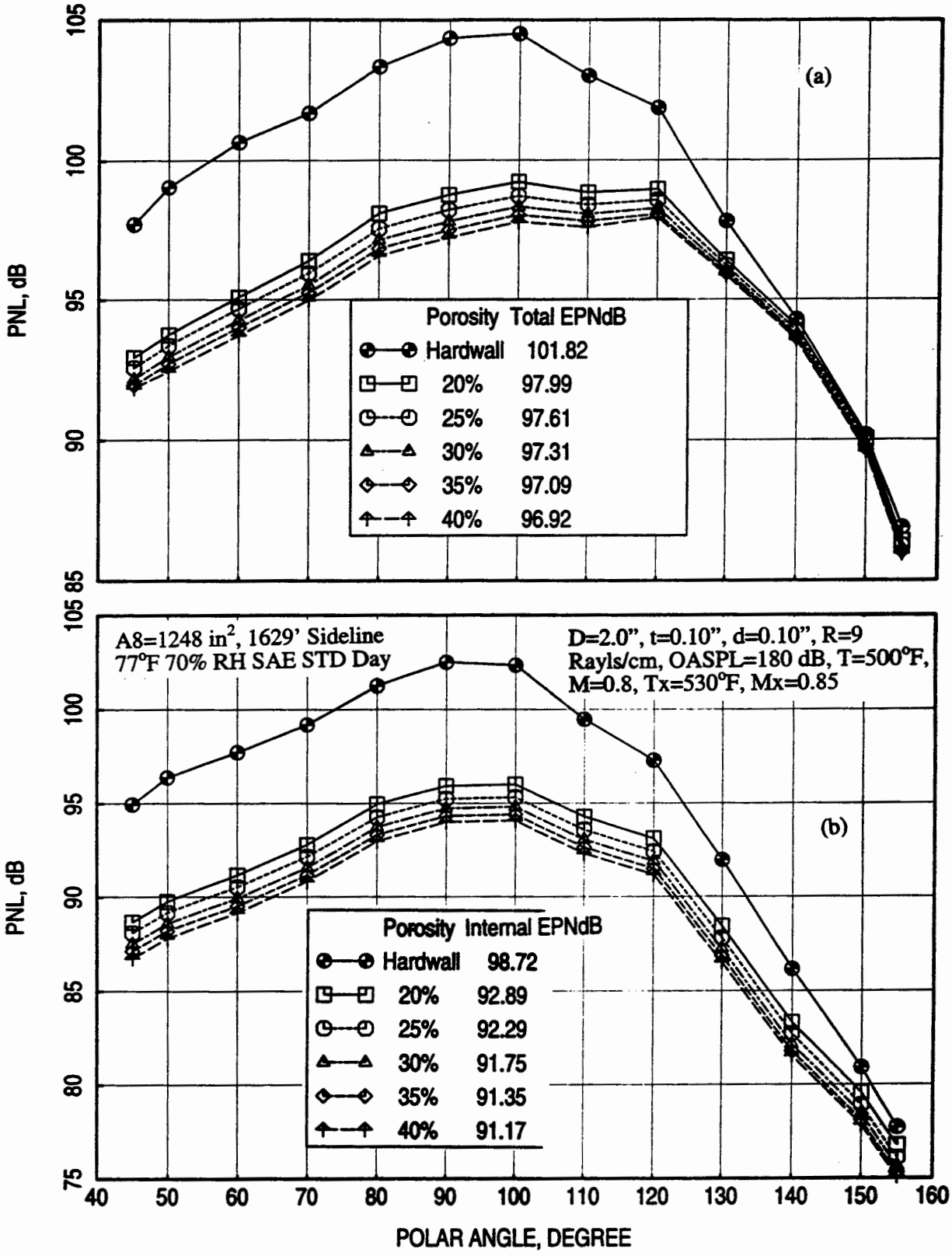

Figure 72. Effect of facesheet porosity (σ) on predicted (a) total and (b) internal component of PNL directivities for a full-scale mixer-ejector liner design, NPR=3.43, T8=1551°R, V_j=2359 ft/sec, M=0.32 {takeoff}.

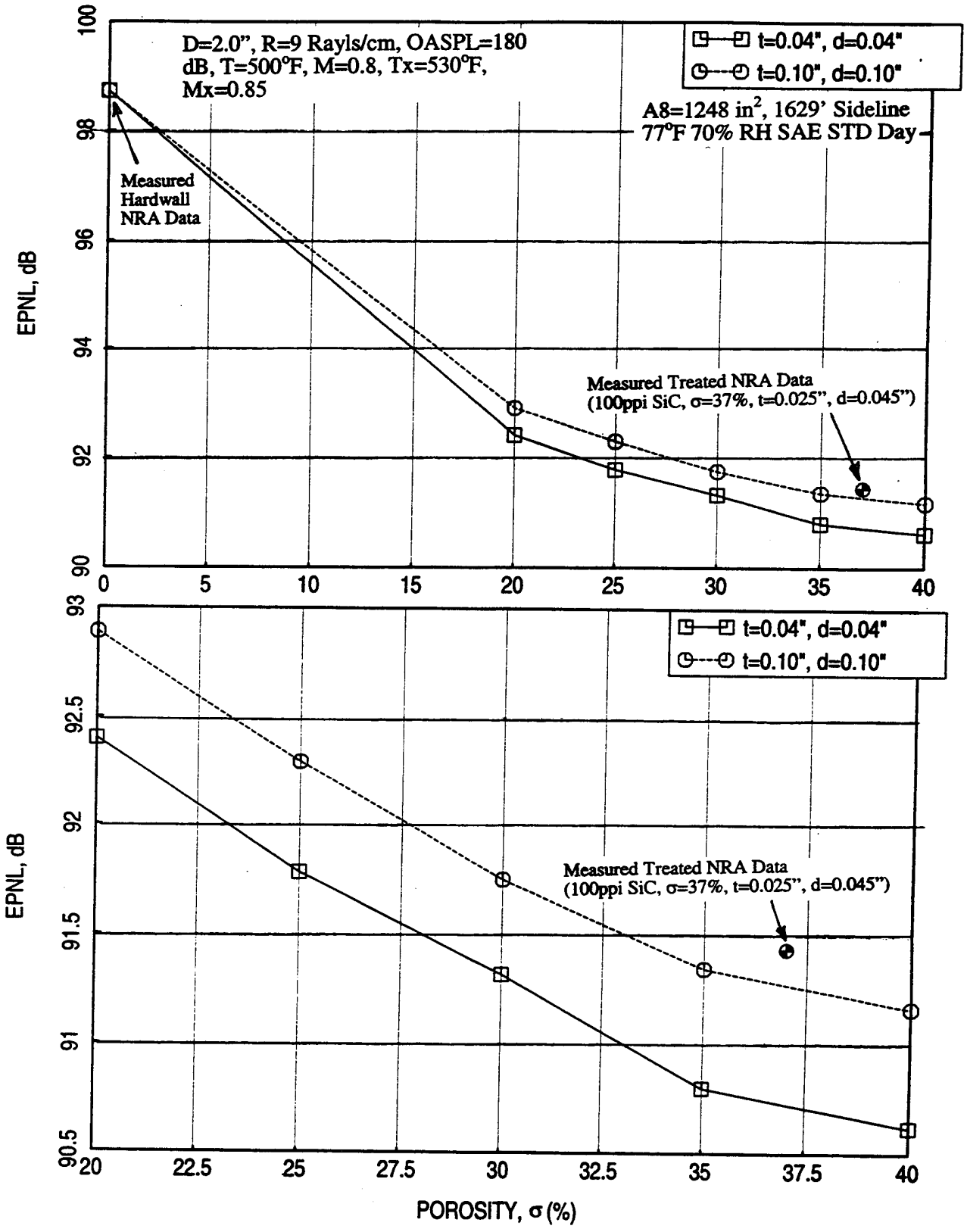

Figure 73. Effect of facesheet porosity (σ) on predicted internal component of EPNL for full-scale scale mixer-ejector liner designs, NPR=3.43, T8=1551°R, V_j=2359 ft/sec, M=0.32 {takeoff}.

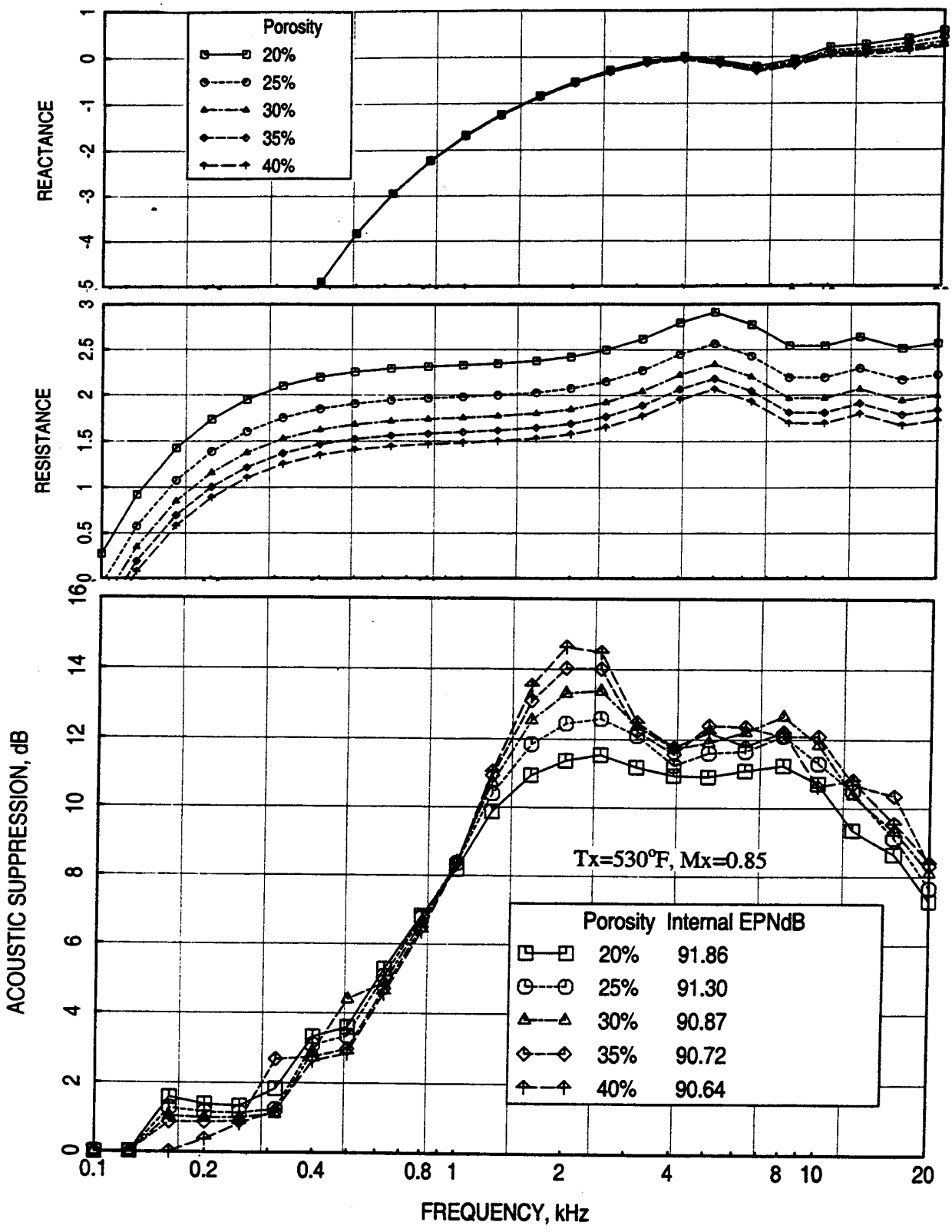

Figure 74. Effect of facesheet porosity (σ) on predicted normal impedance and acoustic suppression spectra for an LSM mixer-ejector liner design, D=1.2", t=0.02", d=0.025", R=20 Rayls/cm, T=500°F, M=0.8, OASPL=177.5 dB (takeoff).

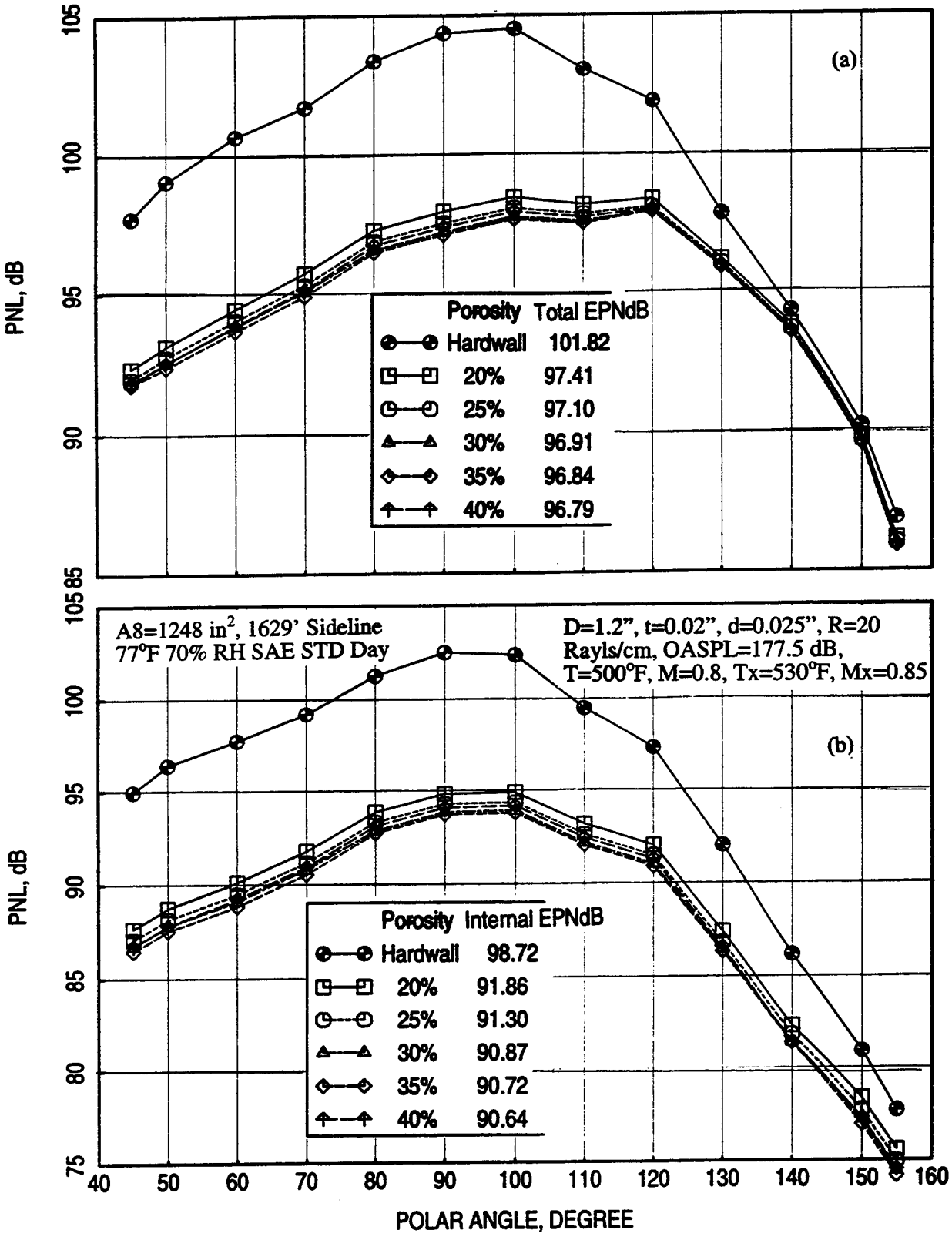

Figure 75. Effect of facesheet porosity (σ) on predicted (a) total and (b) internal component of PNL directivities for an LSM mixer-ejector liner design, NPR=3.43, T8=1551°R, V_j=2359 ft/sec, M=0.32 {takeoff}.

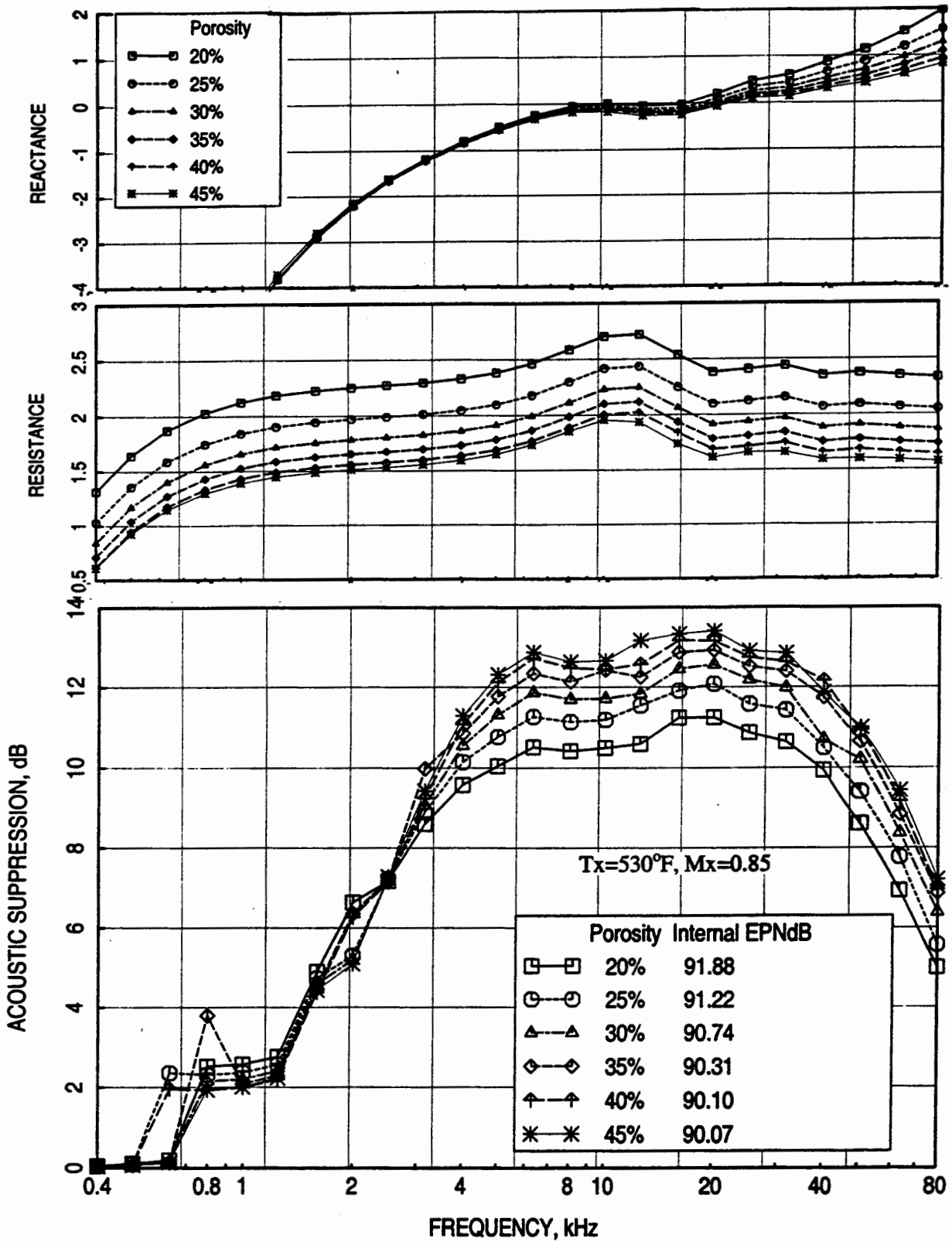

Figure 76. Effect of facesheet porosity (σ) on predicted normal impedance and acoustic suppression spectra for a liner design for NRA model with mixer 8, D=0.485" t=0.015", d=0.02", R=60 Rayls/cm, T=500°F, M=0.8, OASPL=171.5 dB (takeoff).

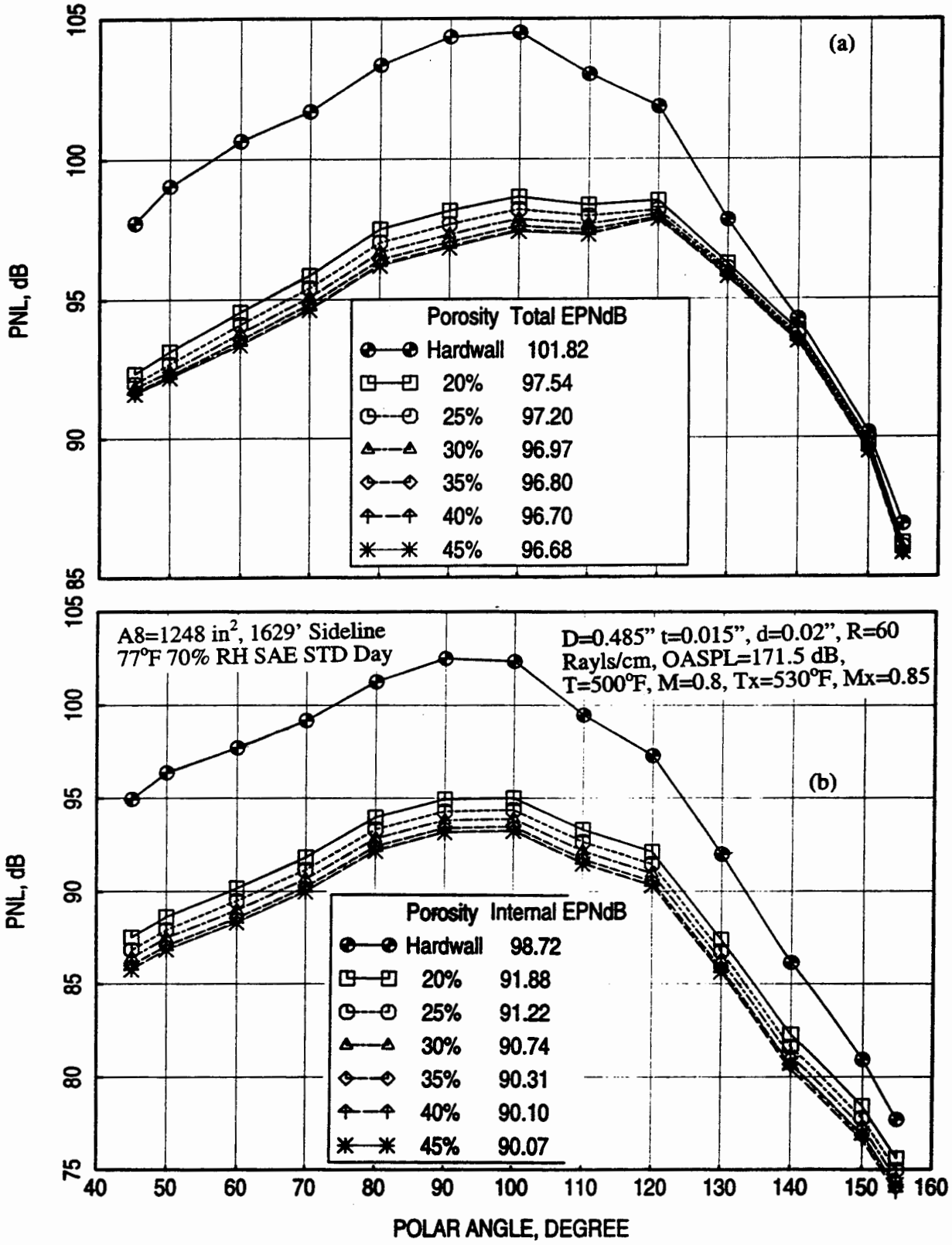

Figure 77. Effect of facesheet porosity (σ) on predicted (a) total and (b) internal component of PNL directivities for a liner design for NRA model with mixer 8, NPR=3.43, T8=1551°R, V_j=2359 ft/sec, M=0.32 {takeoff}.

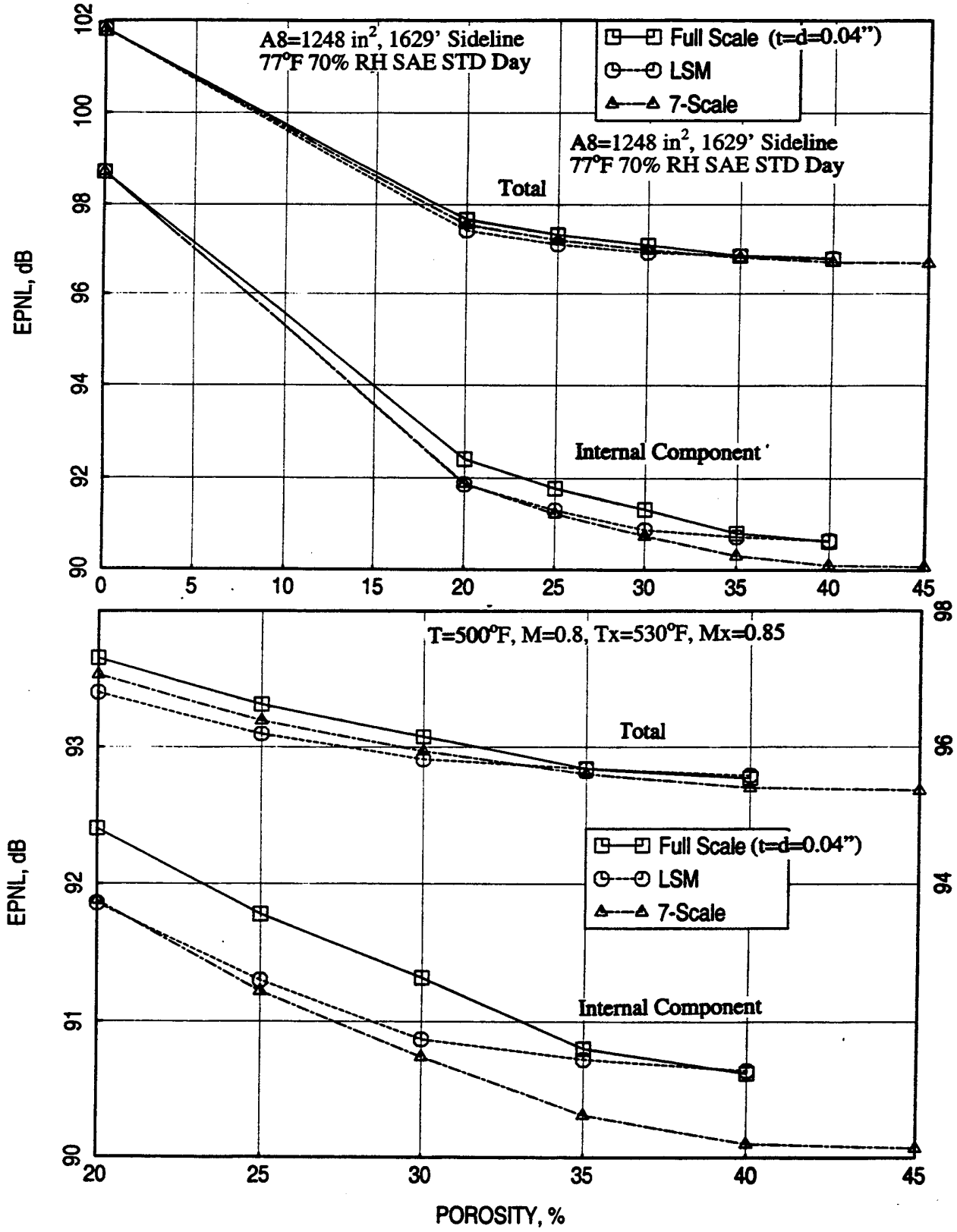

Figure 78. Effect of facesheet porosity (σ) on predicted total and internal component of EPNL for three different scale mixer-ejector liner designs, NPR=3.43, T8=1551°R, V_j=2359 ft/sec, M=0.32 {takeoff}.

However, some variation is applied in this design from practical considerations. For a lower scale liner very thin facesheet is most desirable to control the liner reactance at higher frequencies. However, very thin facesheets are difficult to manufacture and are structurally undesirable. Thus, porosities of 45%, 40%, and 40% are set for 1/7-scale, LSM, and full-scale mixer-ejectors, respectively.

6.4 Facesheet Thickness: Keeping the optimum liner depths, bulk resistivity, and facesheet porosity and hole diameter the same, the facesheet thickness is varied for each of the three mixer-ejector cases. Figure 79 shows predicted normal impedance and acoustic suppression for a full-scale mixer-ejector liner with different facesheet thickness. Reactance increases with increasing thickness, especially at higher frequencies. The impact of thickness seems to be small on acoustic suppression as well as on EPNL for full-scale liners. In general, EPNL decreases first with increasing facesheet thickness and then increases with further thickness increase as listed in the PNL directivity plots (see Figure 80). Similar results for facesheets with larger hole diameter (d=0.1") are also evaluated and presented in Figures 81 and 82. The acoustic characteristics are similar to what is observed for facesheets with smaller hole diameter. The EPNL for these two sets of facesheets is plotted with respect to facesheet thickness in Figure 83. EPNL for both the sets of facesheets decreases first and then increases with increasing facesheet thickness. However, the levels for the facesheets with larger hole diameter are higher compared to the facesheets with smaller hole diameter. This is due to the increased resistance for facesheets with higher hole diameters.

Similar results for LSM and 1/7-scale designs are shown in Figures 84 through 87. Reactance increases with increasing thickness, especially at higher frequencies. The impact of thickness seems to be higher for lower scale mixer-ejectors. For LSM the acoustic suppression increases first and then decreases with increasing facesheet thickness. However, for 1/7-scale liners the acoustic suppression decreases with increasing facesheet thickness. Finally, the EPNL is plotted with respect to facesheet thickness as well as with respect to the ratio of facesheet thickness and linear scale factors for all three mixer-ejector designs in Figure 88. Clearly, the minimum EPNL for all three scale designs decreases first and then increases with increasing facesheet thickness. The minimum EPNL for all three cases come closer when plotted with respect to the ratio of facesheet thickness and linear scale factor. Facesheet thicknesses of 0.015", 0.04", and 0.04 give the minimum EPNL for 1/7-scale, LSM, and full-scale mixer-ejectors, respectively, in the current exercise. However, the optimum facesheet thickness on the basis of normal impedance, manufacturability, and durability are chosen to be 0.015", 0.02", and 0.04" for 1/7-scale, LSM, and full-scale mixer-ejectors, respectively.

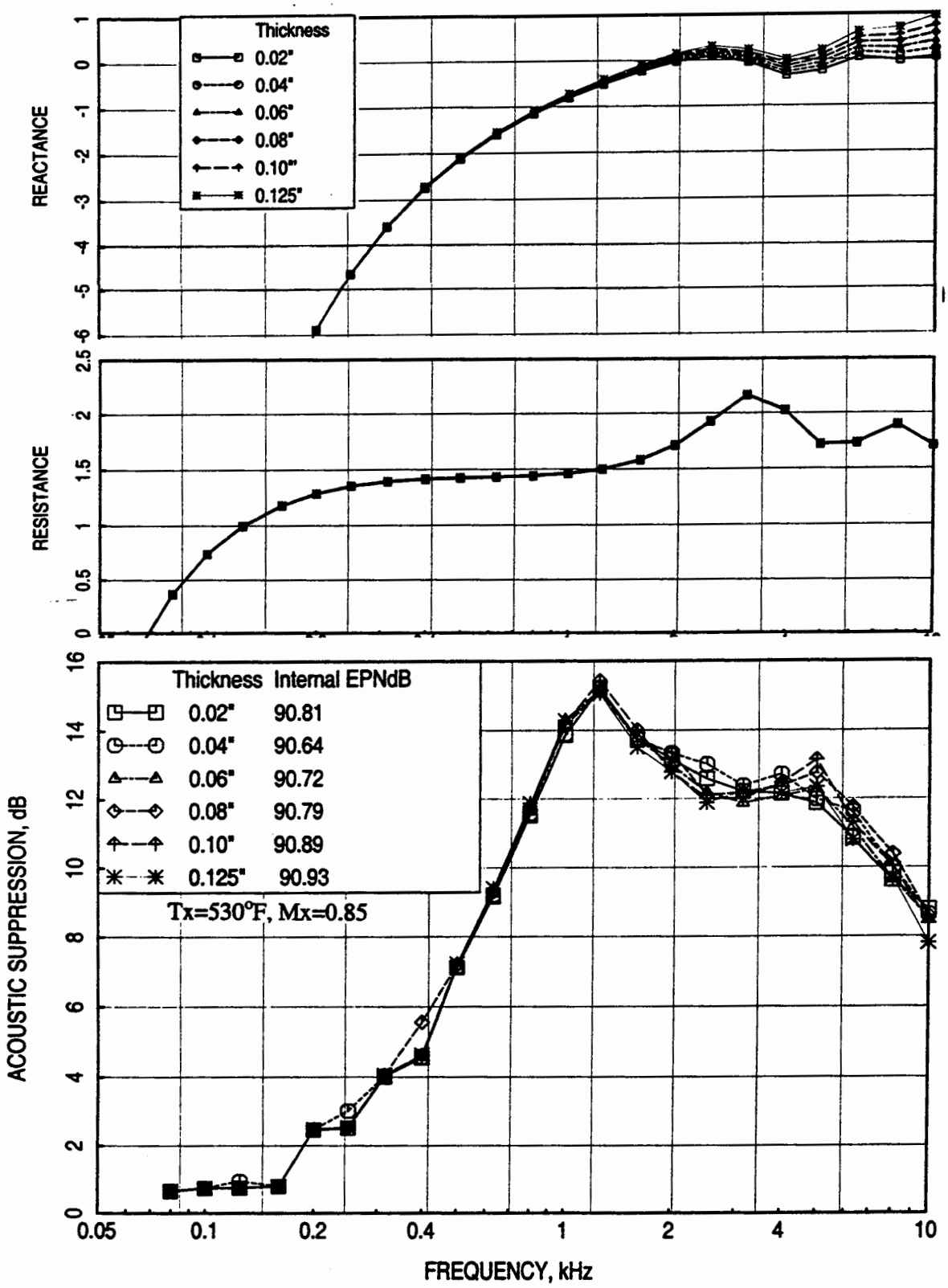

Figure 79. Effect of facesheet thickness (t) on predicted normal impedance and acoustic suppression spectra for a full-scale mixer-ejector liner design, D=2.0", σ=40%, d=0.04", R=9 Rayls/cm, T=500°F, M=0.8, OASPL=180 dB (takeoff).

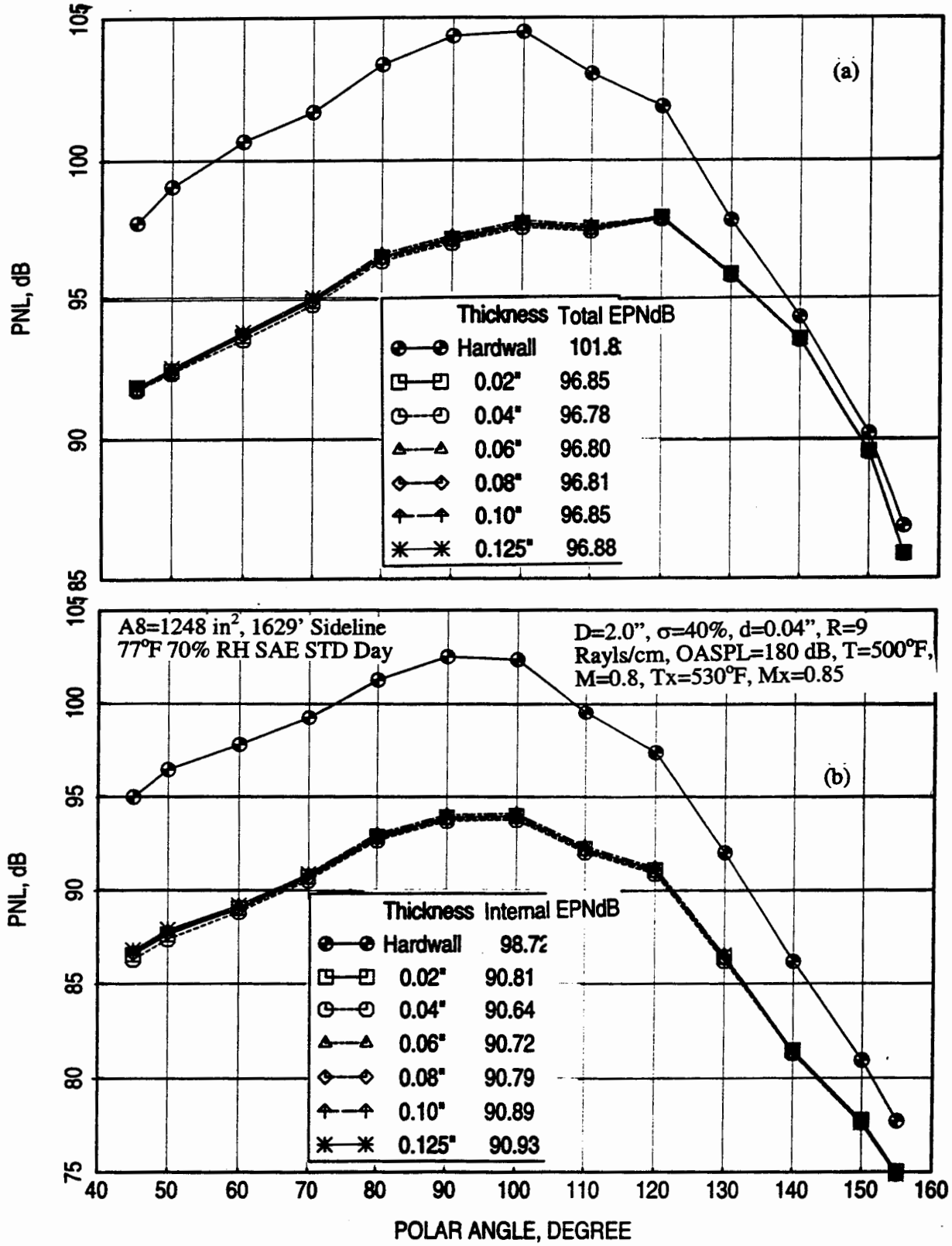

Figure 80. Effect of facesheet thickness (t) on predicted (a) total and (b) internal component of PNL directivities for a full scale mixer-ejector liner design, NPR=3.43, T8=1551°R, V_j=2359 ft/sec, M=0.32 {takeoff}.

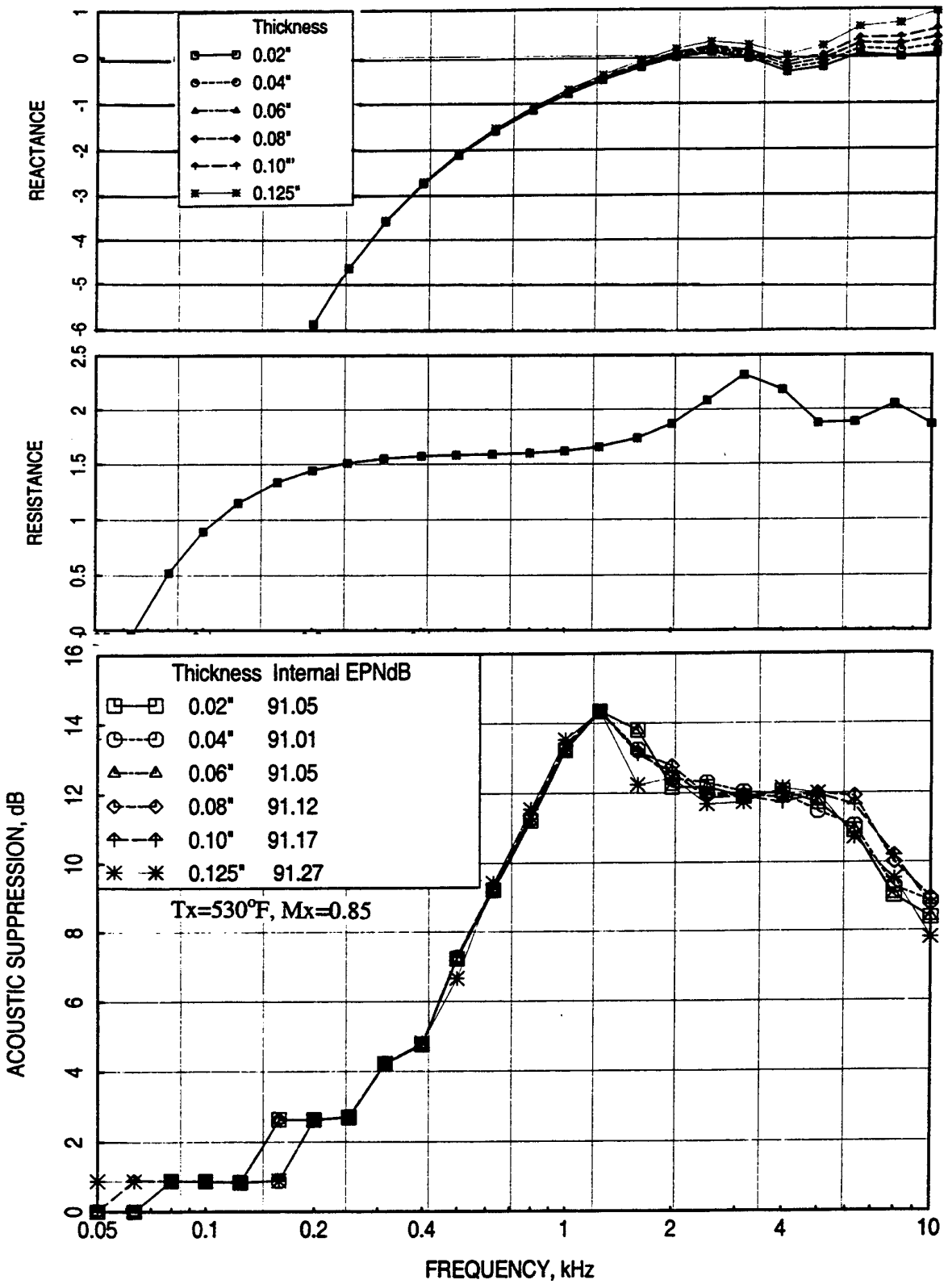

Figure 81. Effect of facesheet thickness (t) on predicted normal impedance and acoustic suppression spectra for a full-scale mixer-ejector liner design, D=2.0", σ=40%, d=0.10", R=9 Rayls/cm, T=500°F, M=0.8, OASPL=180 dB (takeoff).

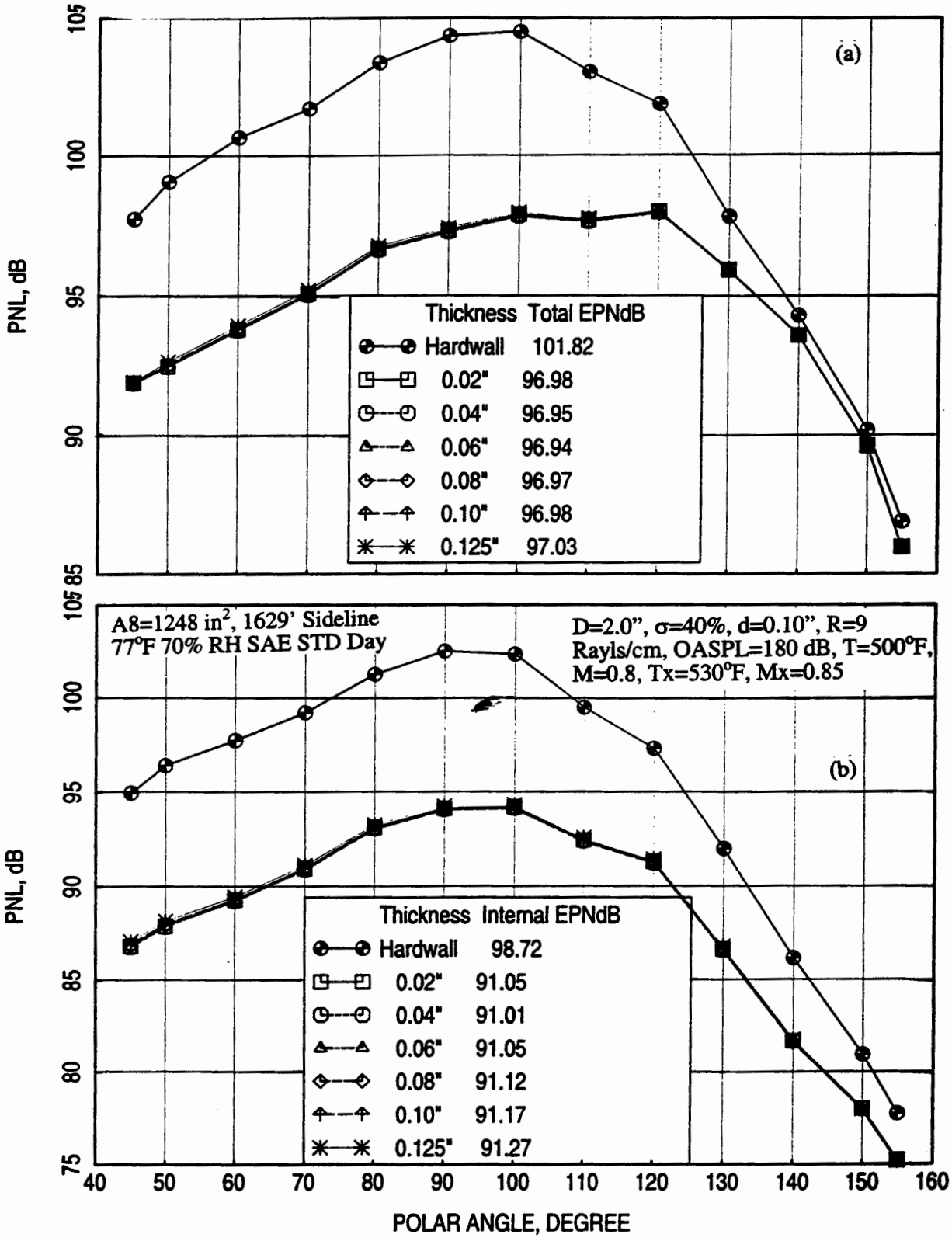

Figure 82. Effect of facesheet thickness (t) on predicted (a) total and (b) internal component of PNL directivities for a full-scale mixer-ejector liner design, NPR=3.43, T8=1551°R, V_j=2359 ft/sec, M=0.32 {takeoff}.

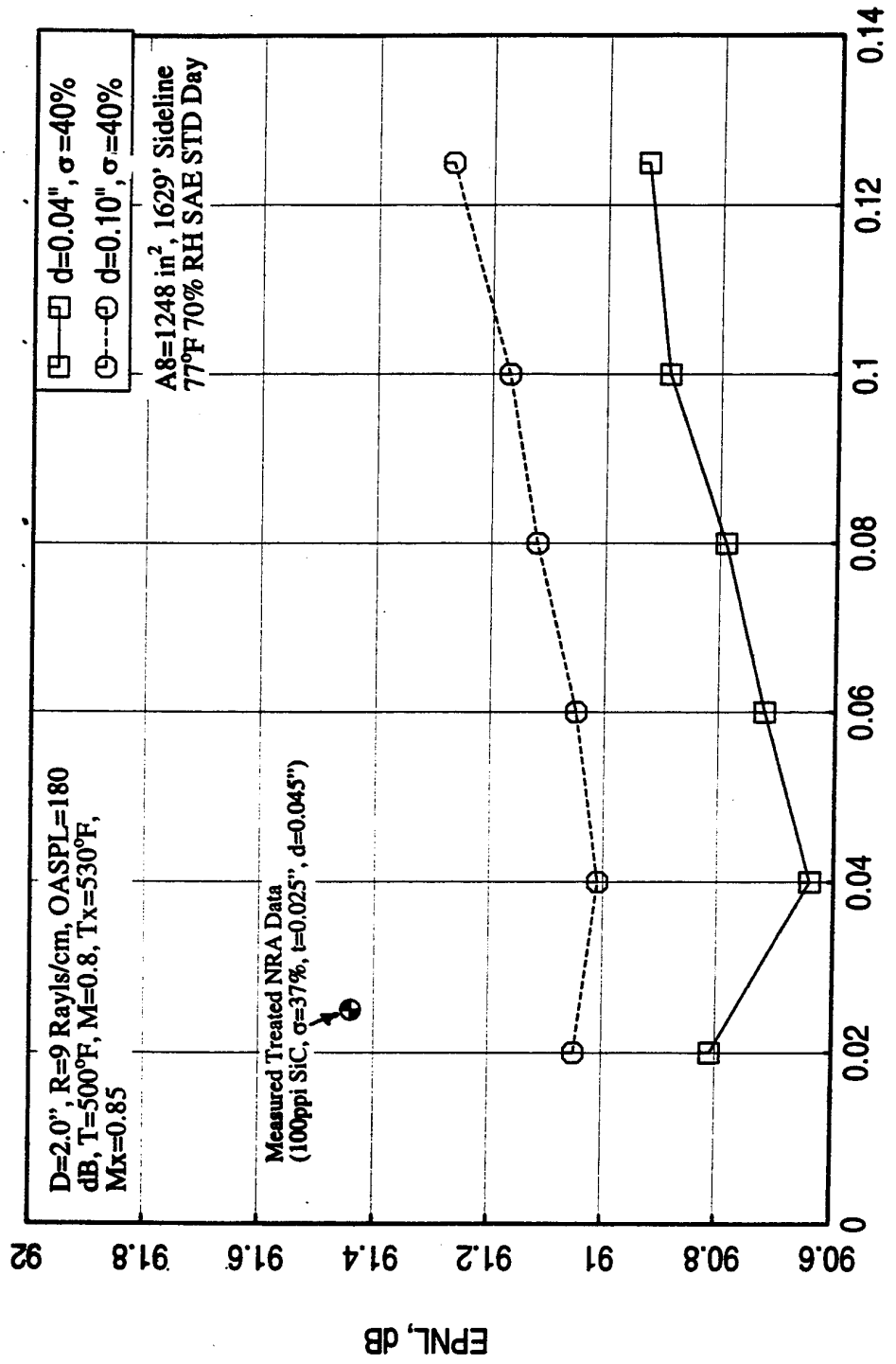

Figure 83. Effect of facesheet thickness (t) on predicted total and internal component of EPNL for full-scale scale mixer-ejector liner designs, NPR=3.43, T8=1551°R, V_j=2359 ft/sec, M=0.32 {takeoff}.

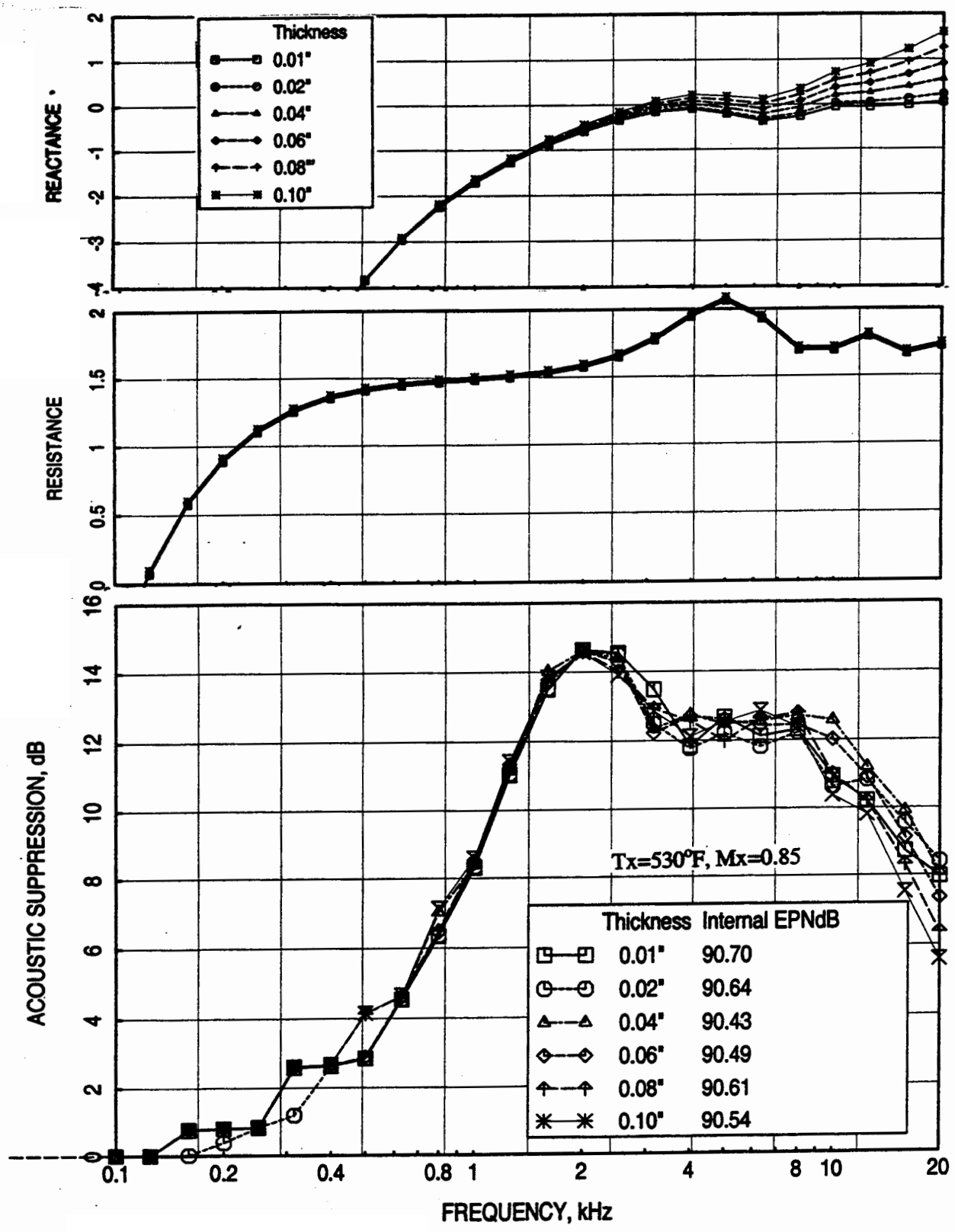

Figure 84. Effect of facesheet thickness (t) on predicted normal impedance and acoustic suppression spectra for an LSM mixer-ejector liner design, D=1.2", σ=40%, d=0.025", R=20 Rayls/cm, T=500°F, M=0.8, OASPL=177.5 dB (takeoff)..

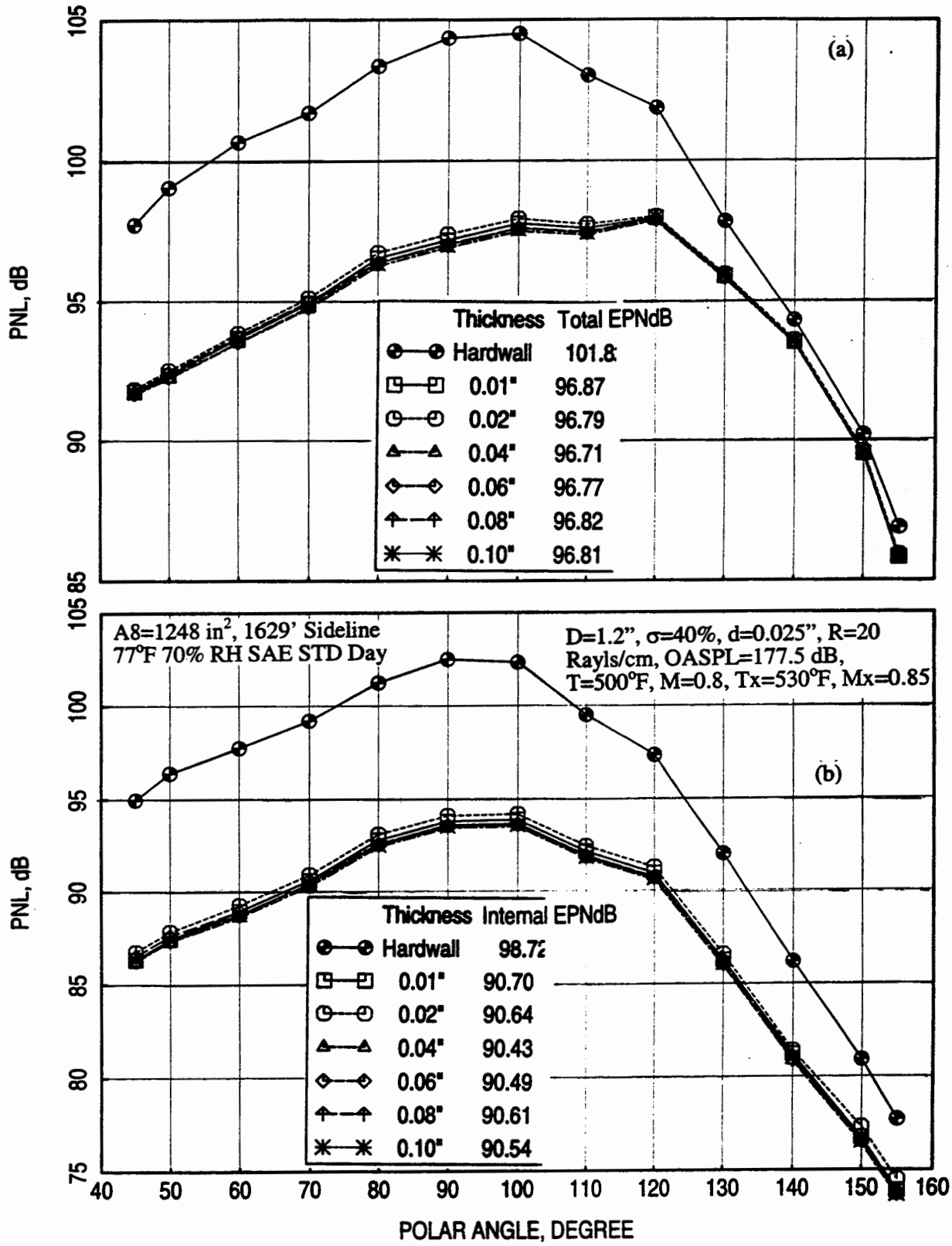

Figure 85. Effect of facesheet thickness (t) on predicted (a) total and (b) internal component of PNL directivities for an LSM mixer-ejector liner design, NPR=3.43, T8=1551°R, V_j=2359 ft/sec, M=0.32 {takeoff}.

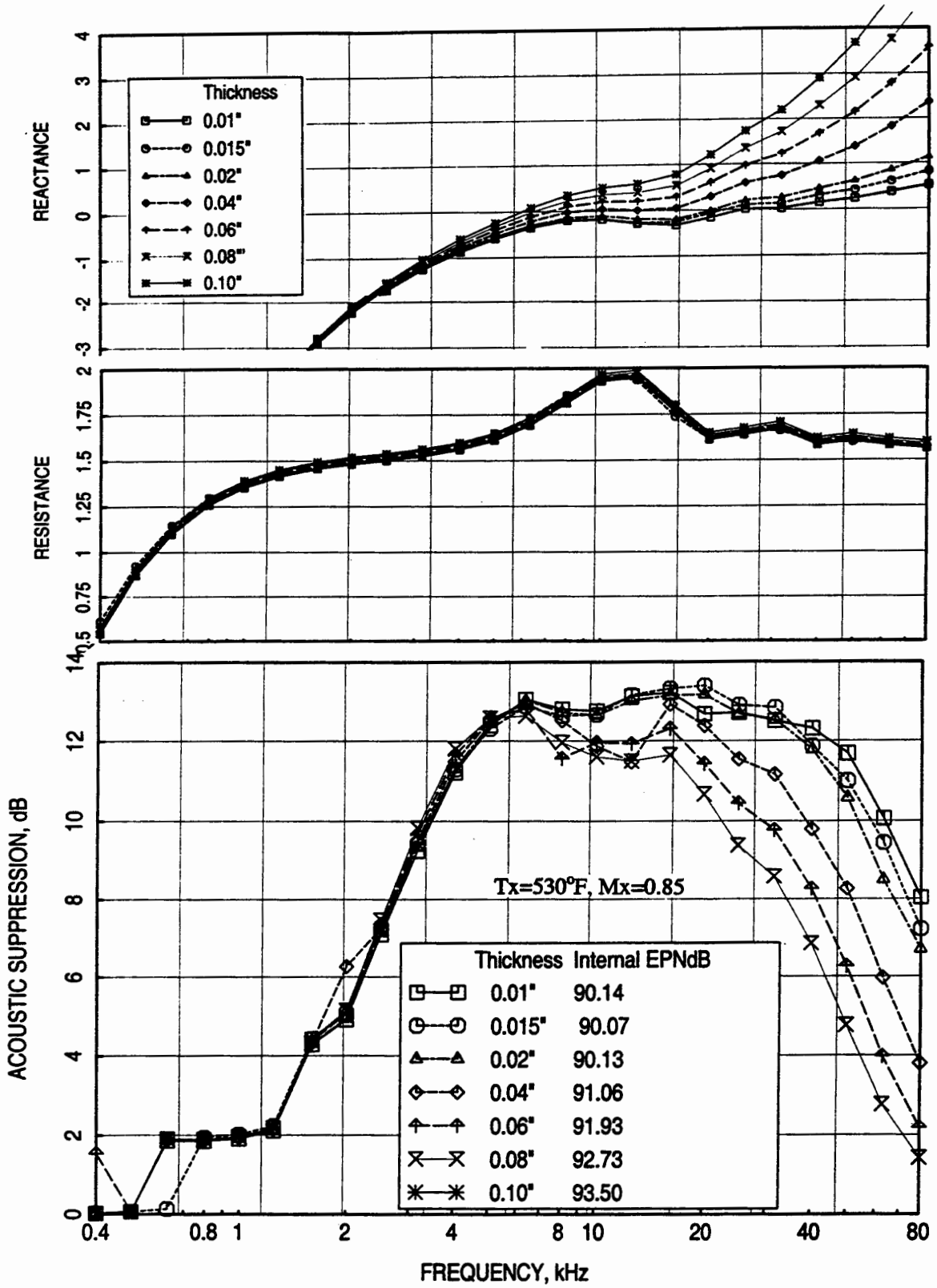

Figure 86. Effect of facesheet thickness (t) on predicted normal impedance and acoustic suppression spectra for a liner design for NRA model with mixer 8, D=0.485" σ=45%, d=0.02", R=60 Rayls/cm, T=500°F, M=0.8, OASPL=171.5 dB (takeoff).

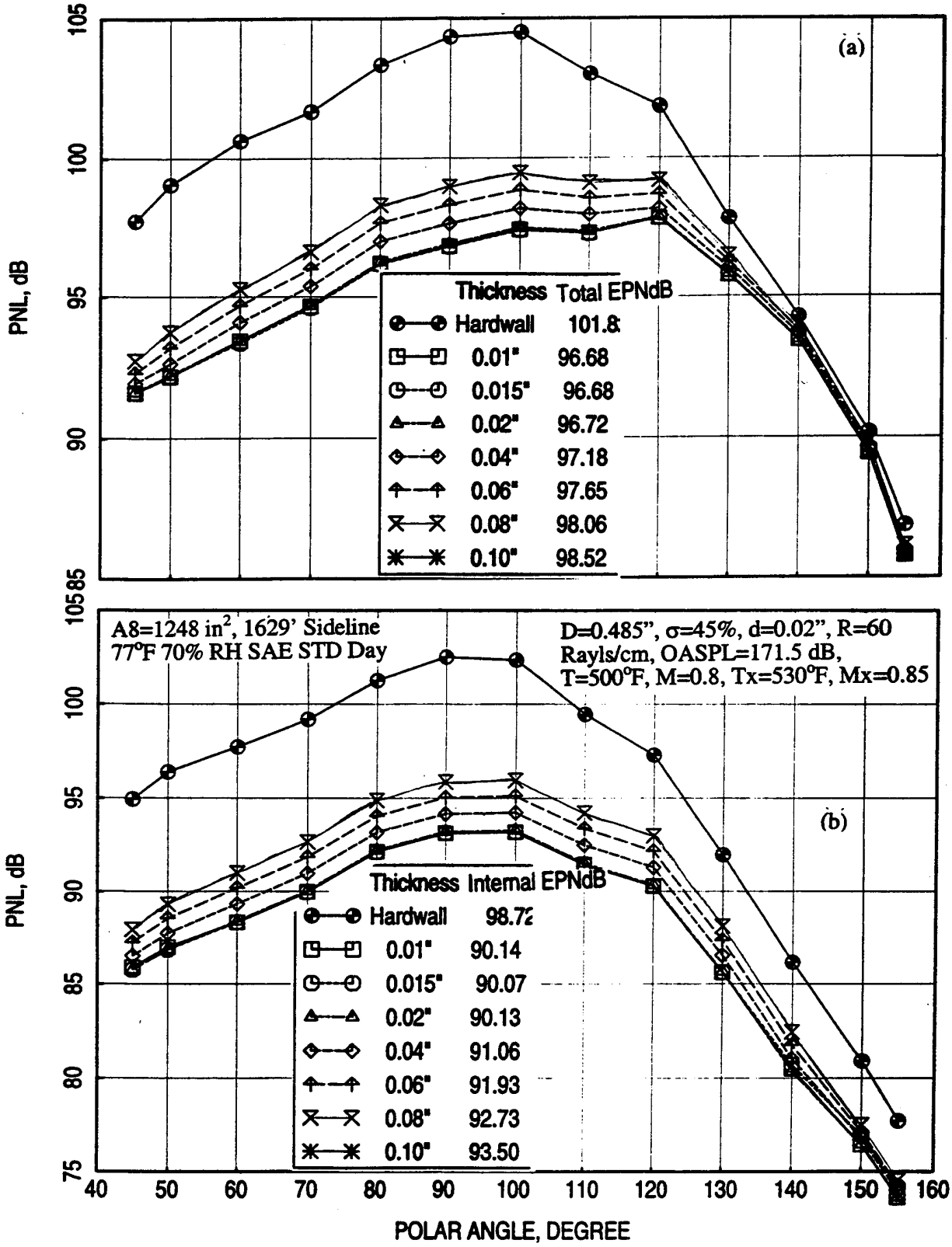

Figure 87. Effect of facesheet thickness (t) on predicted (a) total and (b) internal component of PNL directivities for a liner design for NRA model with mixer 8, NPR=3.43, T8=1551°R, V_j=2359 ft/sec, M=0.32 {takeoff}.

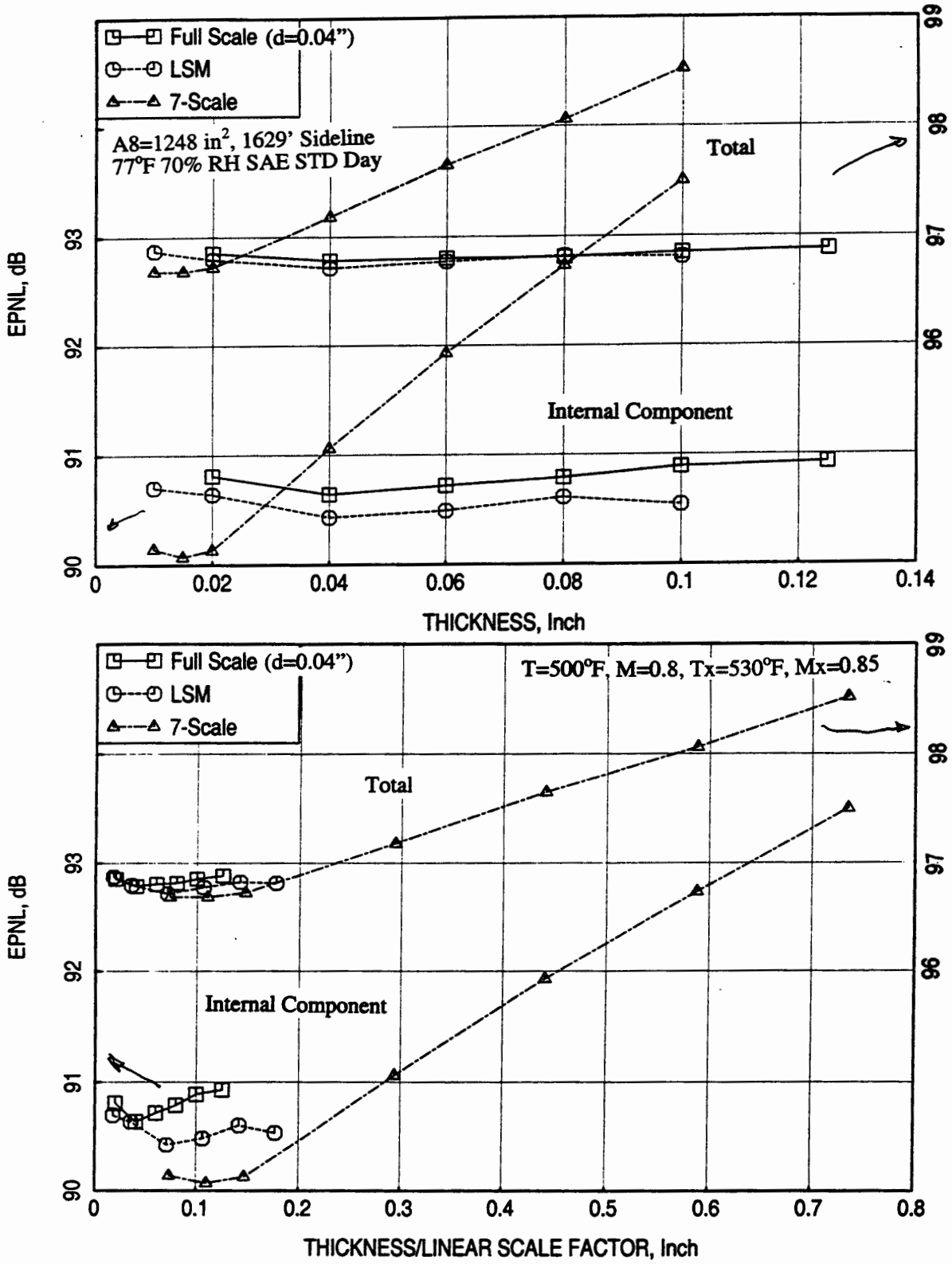

Figure 88. Effect of facesheet thickness (t) on predicted total and internal component of EPNL for three different scale mixer-ejector liner designs, NPR=3.43, T8=1551°R, V_j=2359 ft/sec, M=0.32 {takeoff}.

6.5 Facesheet Hole Diameter: Keeping the optimum liner depths, bulk resistivity, and facesheet porosity and thickness the same, the facesheet hole diameter is varied for each of the three mixer-ejector cases. Figure 89 shows predicted normal impedance and acoustic suppression for a full-scale mixer-ejector liner with different facesheet hole diameters. Resistance increases with increasing facesheet hole diameter at all frequencies. The impact of hole diameter seems to be small on acoustic suppression as well as on EPNL for full-scale liners. In general, EPNL increases first with increasing facesheet hole diameter as listed in the PNL directivity plots (see Figure 90). Similar results for thicker facesheets (t=0.1") are also evaluated and presented in Figures 91 and 92. The acoustic characteristics are similar to what is observed for facesheets of thickness 0.04". The EPNL for these two sets of facesheets is plotted with respect to facesheet hole diameter in Figure 93. EPNL for both the sets of facesheets decreases slightly and then increases with increasing facesheet hole diameter. However, the levels for the thicker facesheets are higher compared to the thinner facesheets. This is due to the increased reactance for thicker facesheets at higher frequencies.

Similar results for LSM and 1/7-scale designs are shown in Figures 94 through 97. Resistance increases with increasing facesheet hole diameter at all frequencies. The impact of hole diameter seems to be higher for lower scale mixer-ejectors. For LSM the impact of facesheet hole diameter is relatively small on acoustic suppression. However, for 1/7-scale liners the acoustic suppression decreases with increasing facesheet hole diameter. Finally, the EPNL is plotted with respect to facesheet hole diameter for all three mixer-ejector designs in Figure 98. Clearly, the EPNL for all three scale designs decreases slightly at the beginning and then increases with increasing facesheet hole diameter, except for 1/7-scale. Apparently, the impact of hole diameter on EPNL is independent of linear scale factor. Facesheet hole diameters of 0.01", 0.04", and 0.04 give the minimum EPNL for 1/7-scale, LSM, and full-scale mixer-ejectors, respectively, in the current exercise. However, the optimum facesheet hole diameters on the basis of normal impedance are chosen to be 0.02", 0.025", 0.04" for 1/7-scale, LSM, and full-scale mixer-ejectors, respectively. For LSM d=0.04" is used for subsequent designs, since this yields a minimum EPNL and more suitable for manufacturing.

Based on the parametric results presented in this section some of the liner parameters depend on the linear scale factor of the mixer-ejector. While the depth of the liner is directly proportional to the mixer-ejector linear scale factor the bulk resistivity is inversely proportional to this factor. A very weak dependency exists between the facesheet thickness and linear scale factor, that the thickness directly varies with this factor. Parameters like facesheet porosity and hole diameters are independent of linear scale factor.

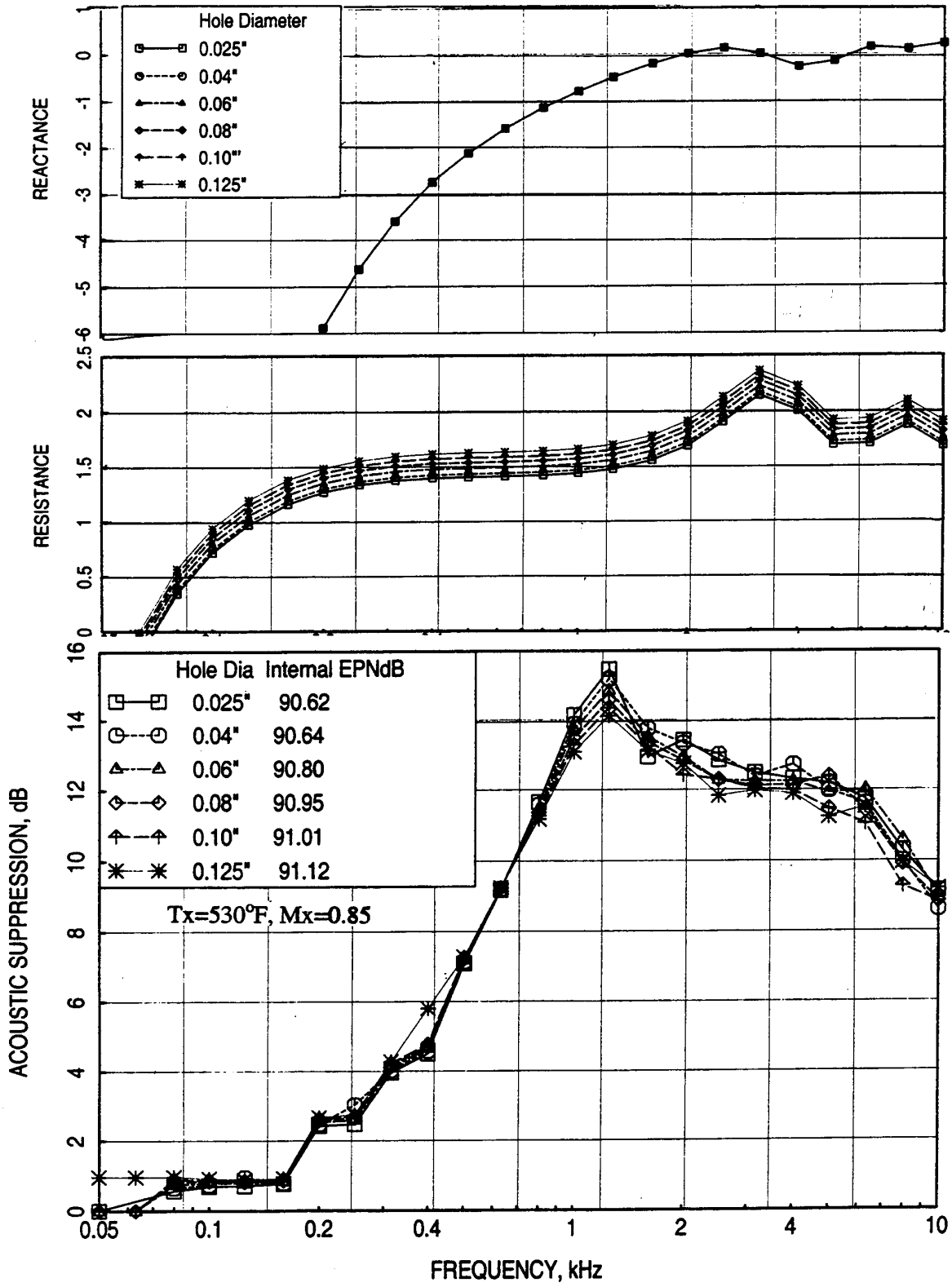

Figure 89. Effect of facesheet hole diameter (d) on predicted normal impedance and acoustic suppression spectra for a full-scale mixer-ejector liner design, D=2.0", σ=40%, t=0.04", R=9 Rayls/cm, T=500°F, M=0.8, OASPL=180 dB (takeoff).

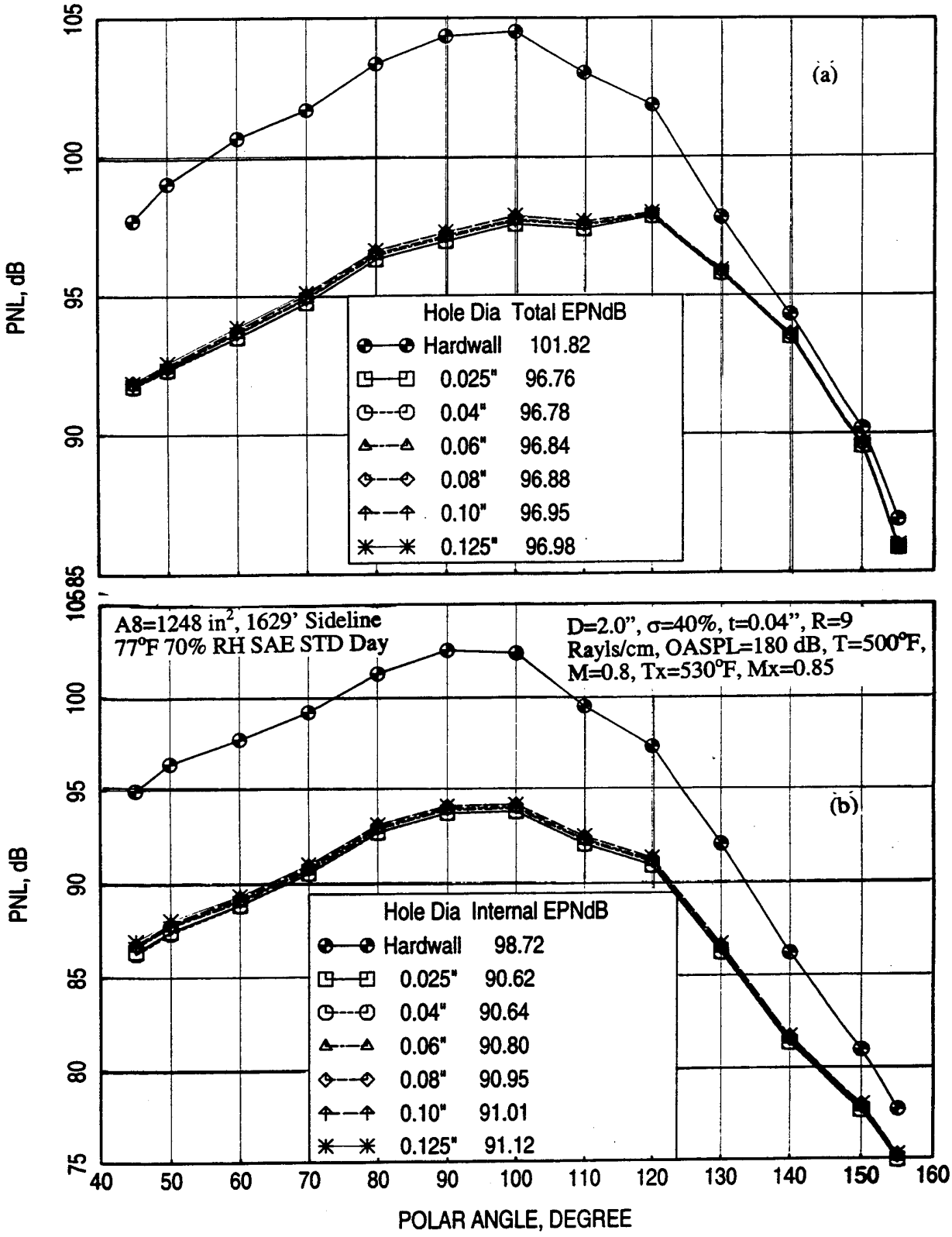

Figure 90. Effect of facesheet hole diameter (d) on predicted (a) total and (b) internal component of PNL directivities for a full-scale mixer-ejector liner design, NPR=3.43, T8=1551°R, V_j=2359 ft/sec, M=0.32 {takeoff}.

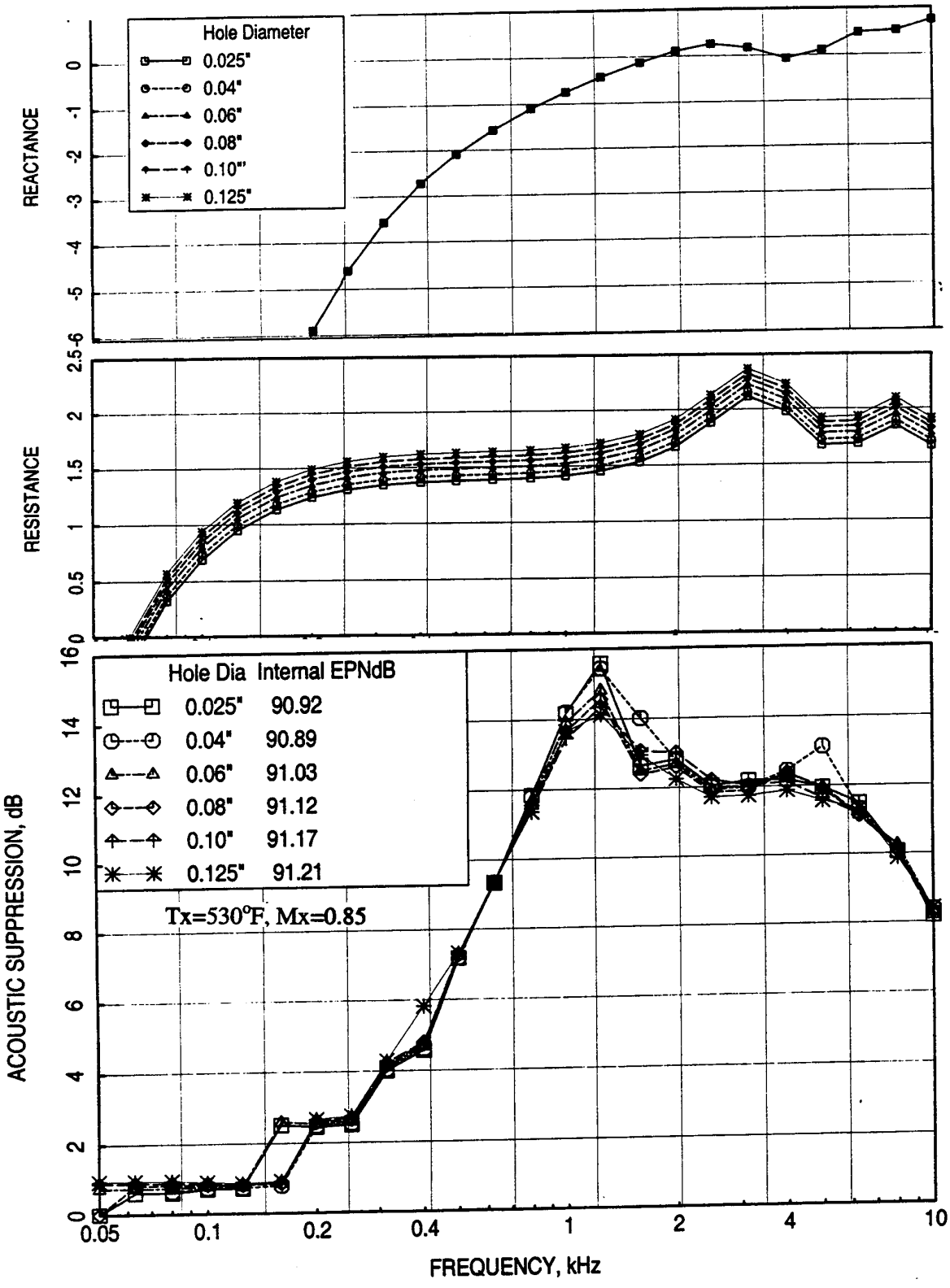

Figure 91. Effect of facesheet hole diameter (d) on predicted normal impedance and acoustic suppression spectra for a full-scale mixer-ejector liner design, D=2.0", σ=40%, t=0.10", R=9 Rayls/cm, T=500°F, M=0.8, OASPL=180 dB (takeoff).

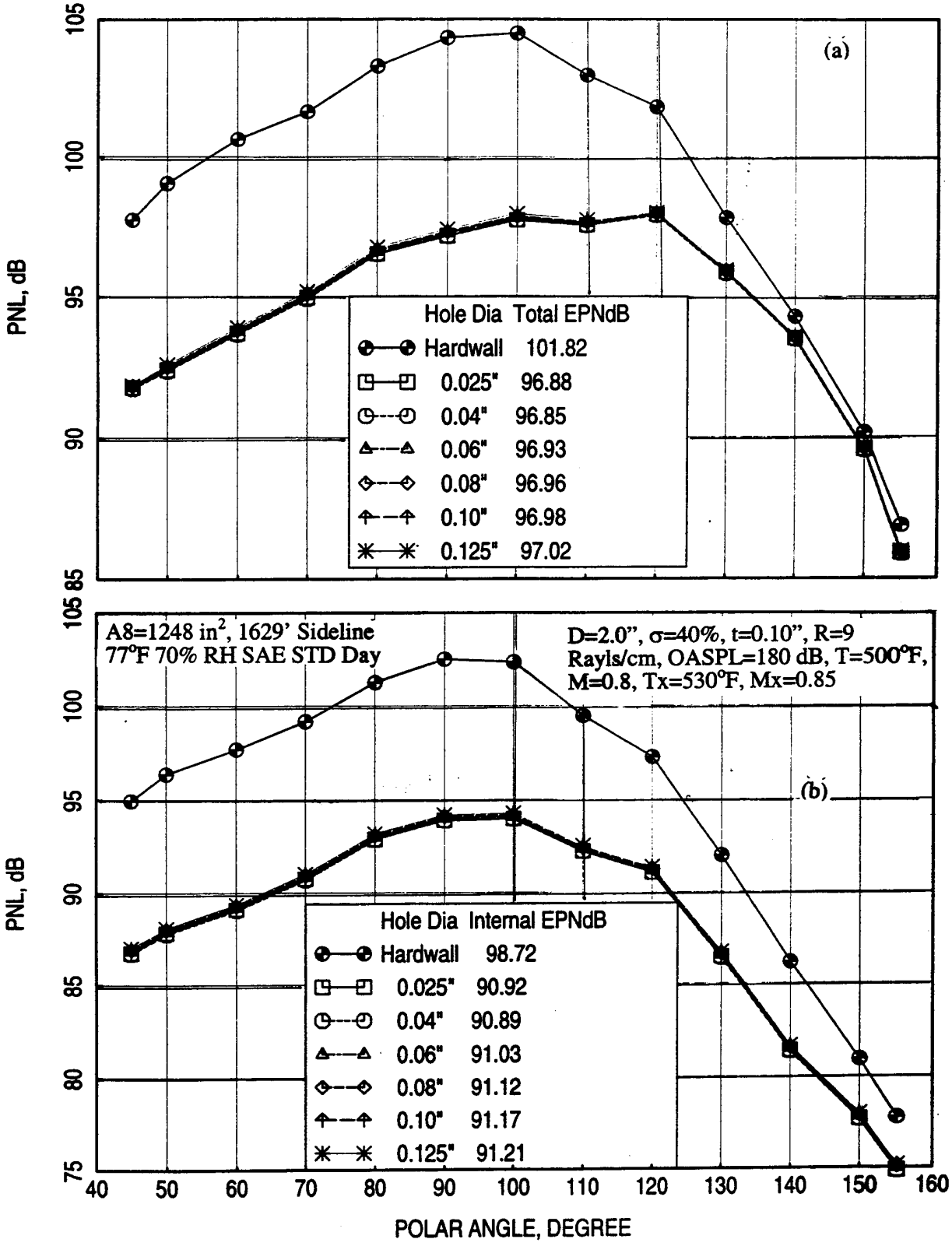

Figure 92. Effect of facesheet hole diameter (d) on predicted (a) total and (b) internal component of PNL directivities for a full-scale mixer-ejector liner design, NPR=3.43, T8=1551°R, V_j=2359 ft/sec, M=0.32 {takeoff}.

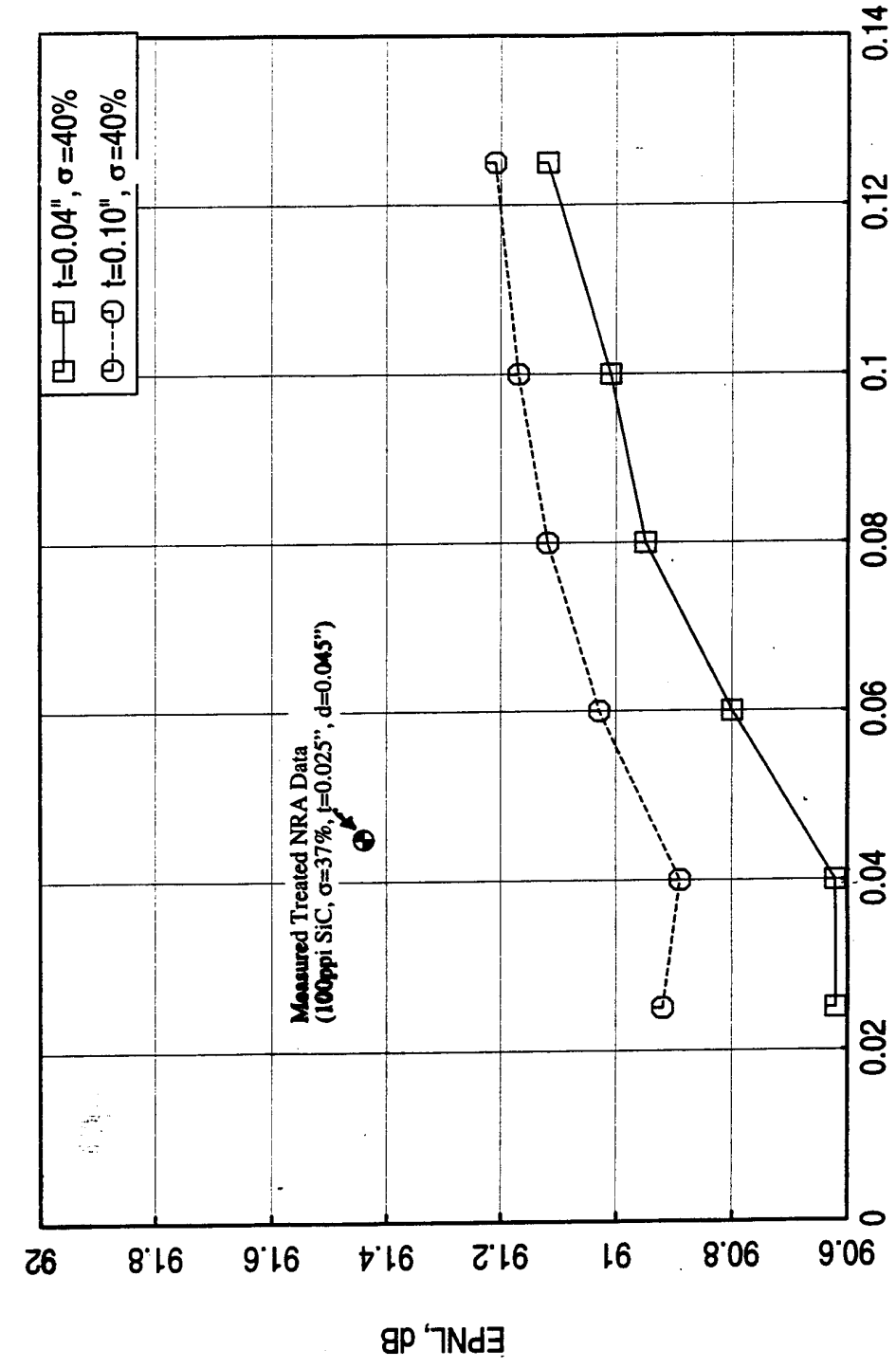

Figure 93. Effect of facesheet hole diameter (d) on predicted total and internal component of EPNL for full-scale scale mixer-ejector liner designs, NPR=3.43, T8=1551°R, V_j=2359 ft/sec, M=0.32 {takeoff}.

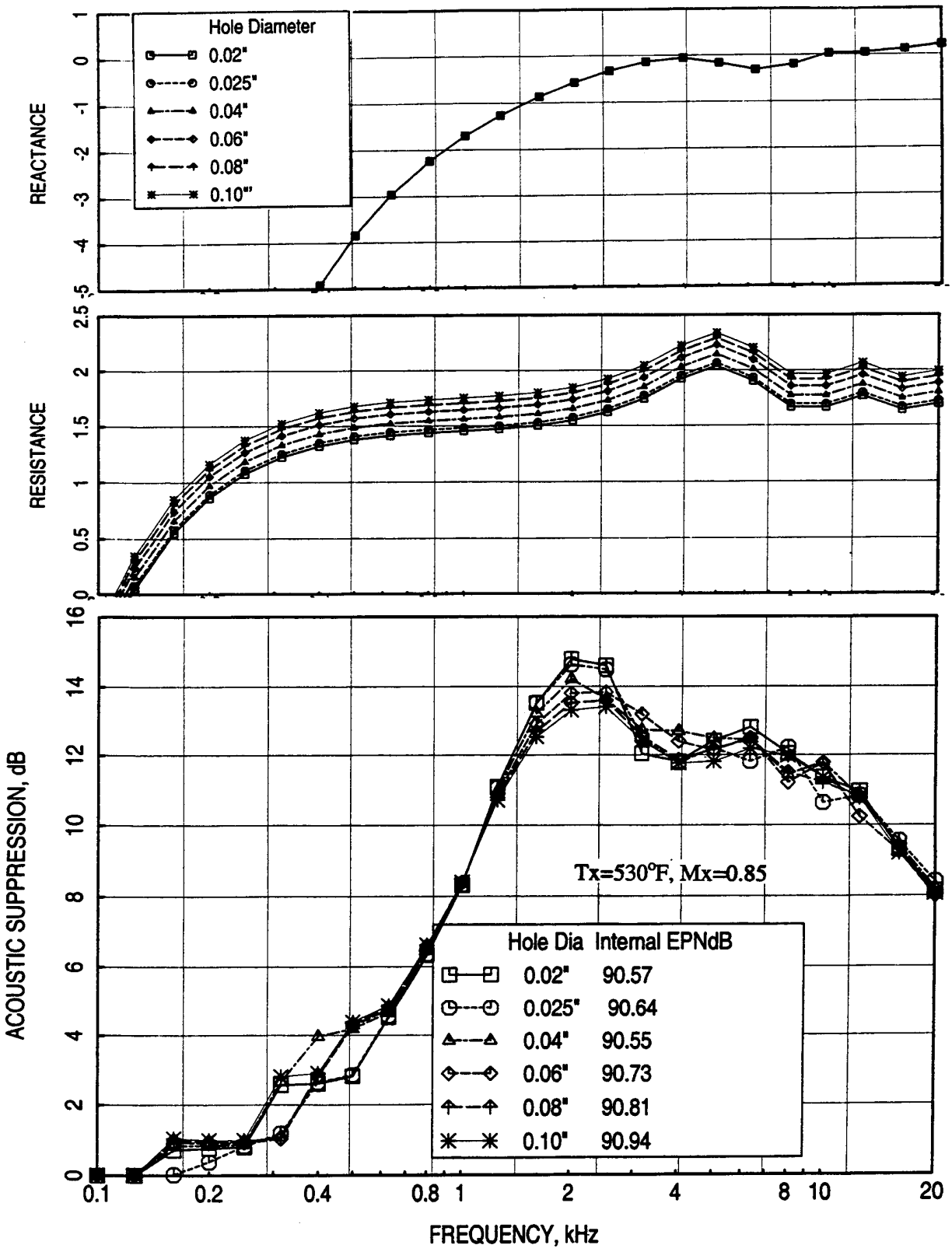

Figure 94. Effect of facesheet hole diameter (d) on predicted normal impedance and acoustic suppression spectra for an LSM mixer-ejector liner design, D=1.2", σ=40%, t=0.02", R=20 Rayls/cm, T=500°F, M=0.8, OASPL=177.5 dB (takeoff).

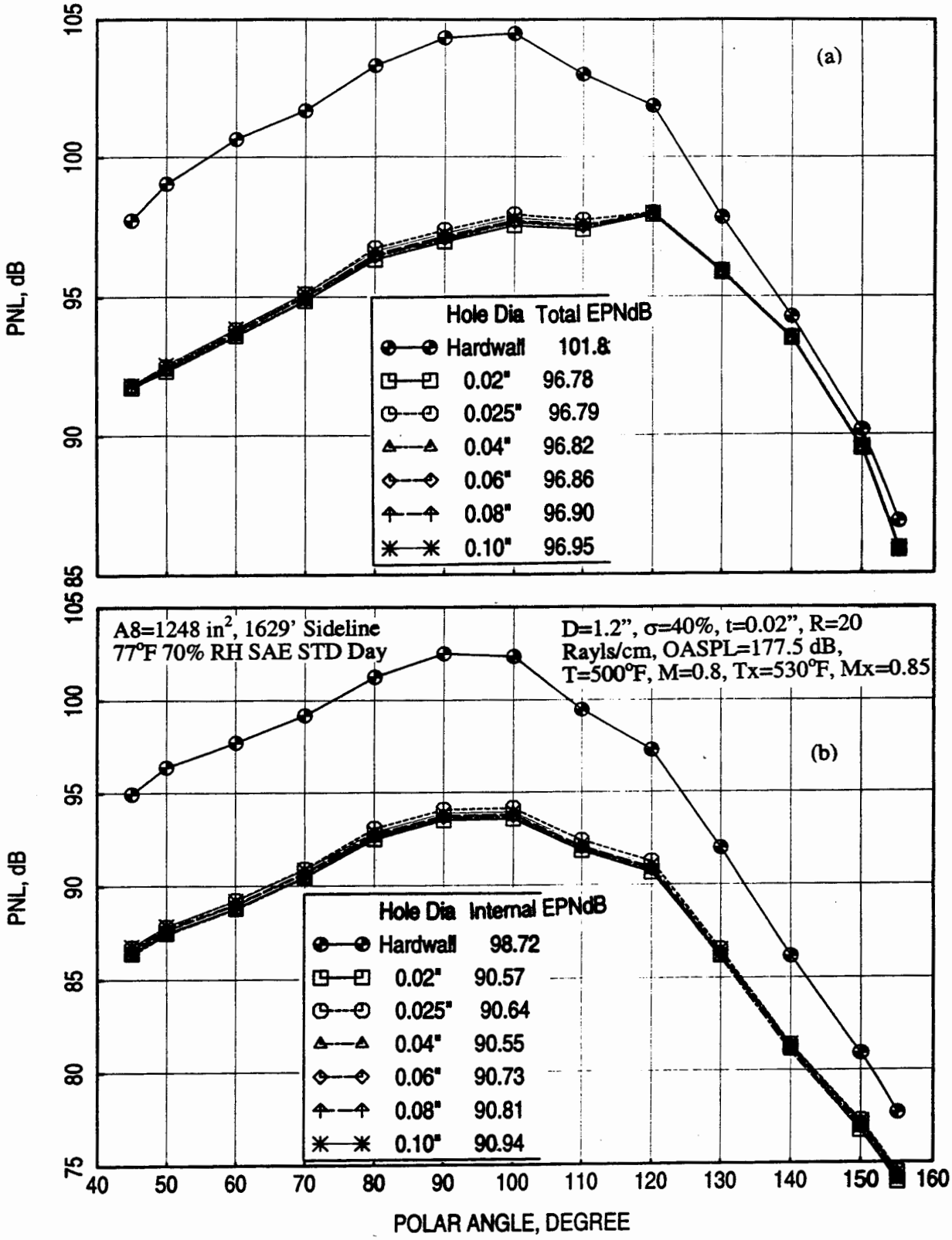

Figure 95. Effect of facesheet hole diameter (d) on predicted (a) total and (b) internal component of PNL directivities for an LSM mixer-ejector liner design, NPR=3.43, T8=1551°R, V_j=2359 ft/sec, M=0.32 {takeoff}.

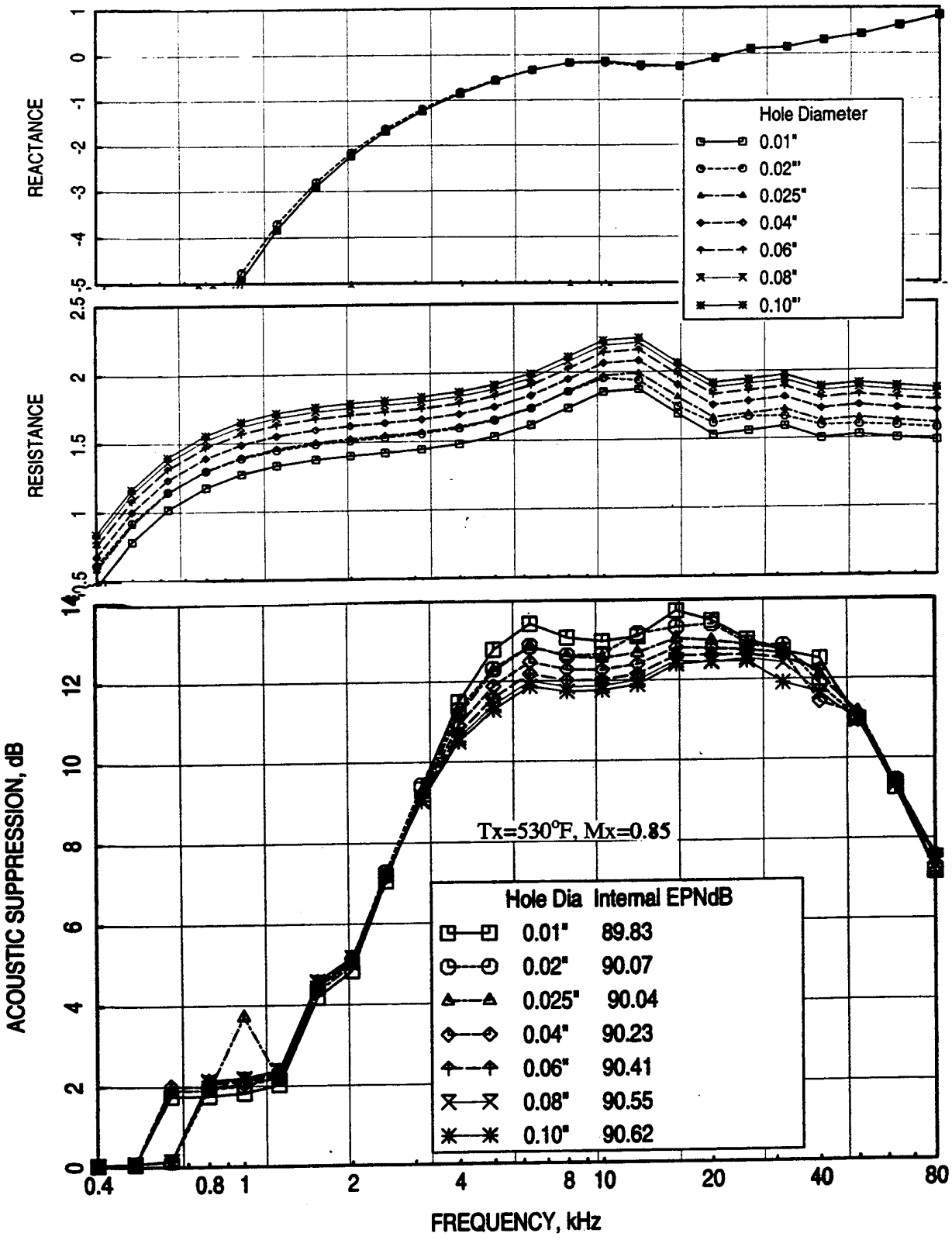

Figure 96. Effect of facesheet hole diameter (d) on predicted normal impedance and acoustic suppression spectra for a liner design for NRA model with mixer 8, D=0.485" σ=45%, t=0.015", R=60 Rayls/cm, T=500°F, M=0.8, OASPL=171.5 dB (takeoff).

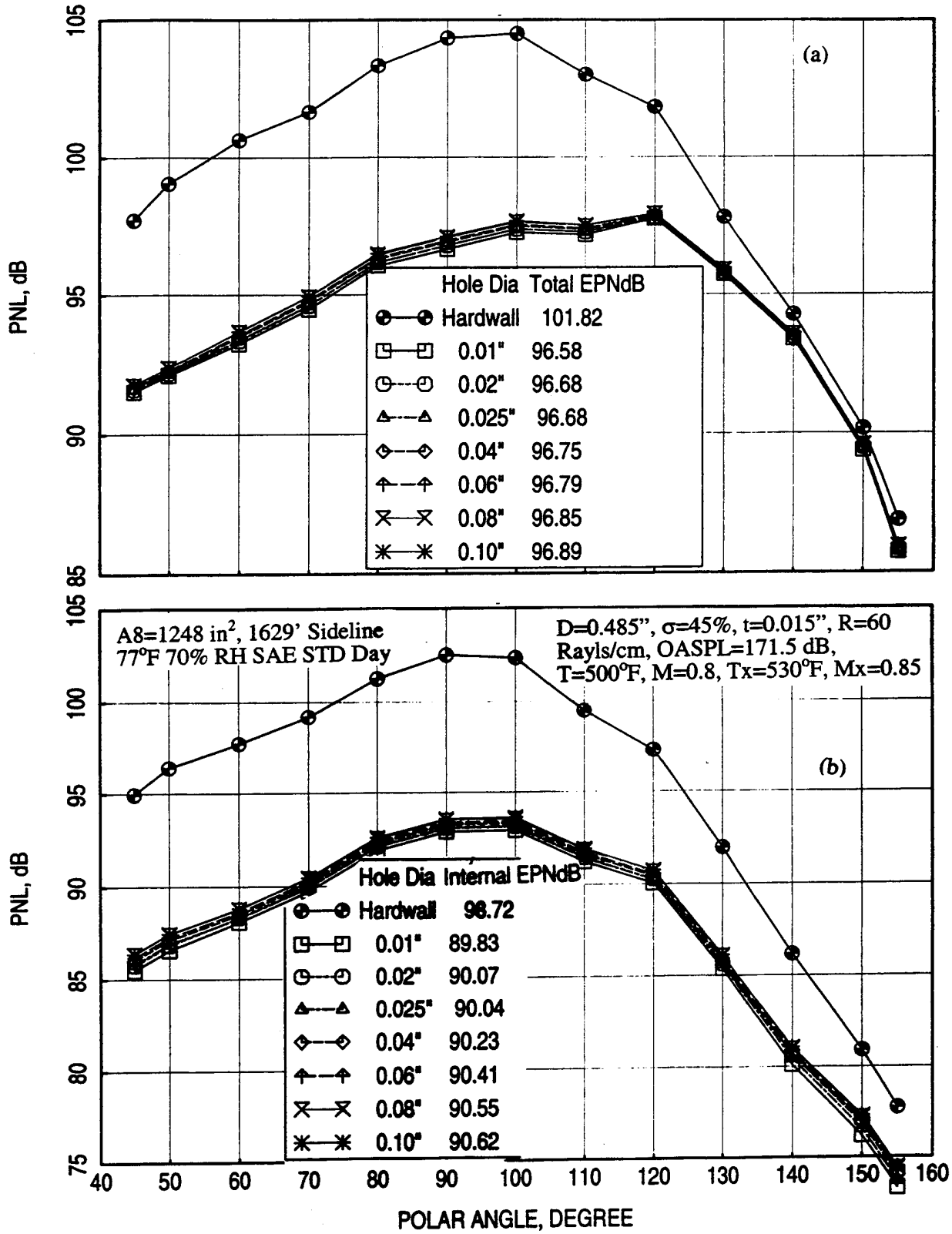

Figure 97. Effect of facesheet hole diameter (d) on predicted (a) total and (b) internal component of PNL directivities for a liner design for NRA model with mixer 8, NPR=3.43, T8=1551°R, V_j=2359 ft/sec, M=0.32 {takeoff}.

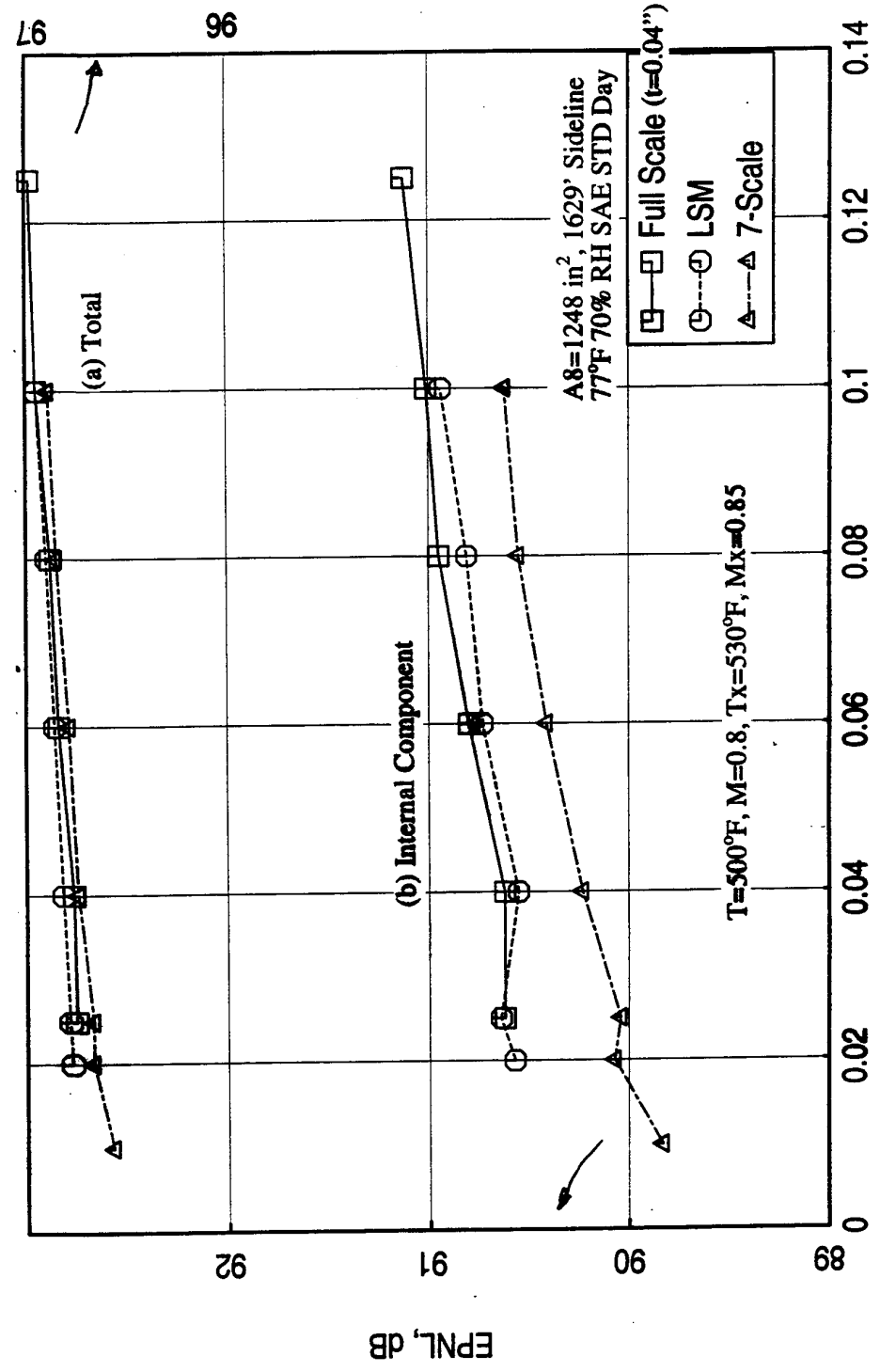

Figure 98. Effect of facesheet hole diameter (d) on predicted total and internal component of EPNL for three different scale mixer-ejector liner designs, NPR=3.43, T8=1551°R, V_j=2359 ft/sec, M=0.32 {takeoff}.

6.6 Sensitivity Studies: In this section the effect of grazing and mean flow parameters, and acoustic intensity of the ejector on the farfield noise is evaluated. In each case, the same physical design of a full-scale liner is used and the ejector flow and acoustic parameters are varied, one at a time, by keeping the other environmental parameters the same. The objective of this study is to evaluate the degree of inaccuracies incurred in the predicted noise field due to any possible error or approximation made for the flow and acoustic input parameters.

Grazing Flow Mach Number (M): Effect of grazing flow Mach number on predicted normal impedance and acoustic suppression spectra are shown in Figure 99. Resistance increases with increasing grazing flow Mach number. However the impact of M on acoustic suppression seems to be small. Grazing flow Mach number impact on PNL directivities and the corresponding EPNL, shown in Figure 100, seems to be insignificant. However, the effect is significant for liners of smaller scale factors. It is expected to be important for the liners with relatively higher resistance levels at critical frequencies, even for full-scale. For these cases, the EPNL would increase significantly with increasing grazing flow Mach number.

Grazing Flow Temperature (T): In this study the bulk resistivity used for normal impedance prediction is varied corresponding to the grazing flow temperature, since the bulk resistivity increases with temperature ($R=R_{amb}\{\mu_{amb}/\mu\}$, μ being the coefficient of viscosity). Effect of grazing flow temperature on predicted normal impedance and acoustic suppression spectra are shown in Figure 101. Resistance increases and reactance decreases with increasing grazing flow temperature. Acoustic suppression decreases with increasing temperature at lower frequencies. The effect is insignificant at higher frequencies. Grazing flow temperature impact on PNL directivities and the corresponding EPNL is shown in Figure 102. EPNL increases with increasing grazing flow temperature.

Acoustic Intensity (OASPL): Effect of acoustic intensity in terms of OASPL on predicted normal impedance and acoustic suppression spectra are shown in Figure 103. Resistance increases with increasing acoustic intensity. Acoustic suppression decreases with increasing OASPL at frequencies above 600 Hz. Acoustic intensity impact on PNL directivities and the corresponding EPNL is shown in Figure 104. EPNL increases with increasing acoustic intensity (OASPL).

Boundary Layer Displacement Thickness (δ^*): Effect of boundary layer displacement thickness (δ^*) on predicted normal impedance and acoustic suppression spectra are shown in Figure 105. Resistance increases and then decreases with increasing δ^*. Acoustic suppression

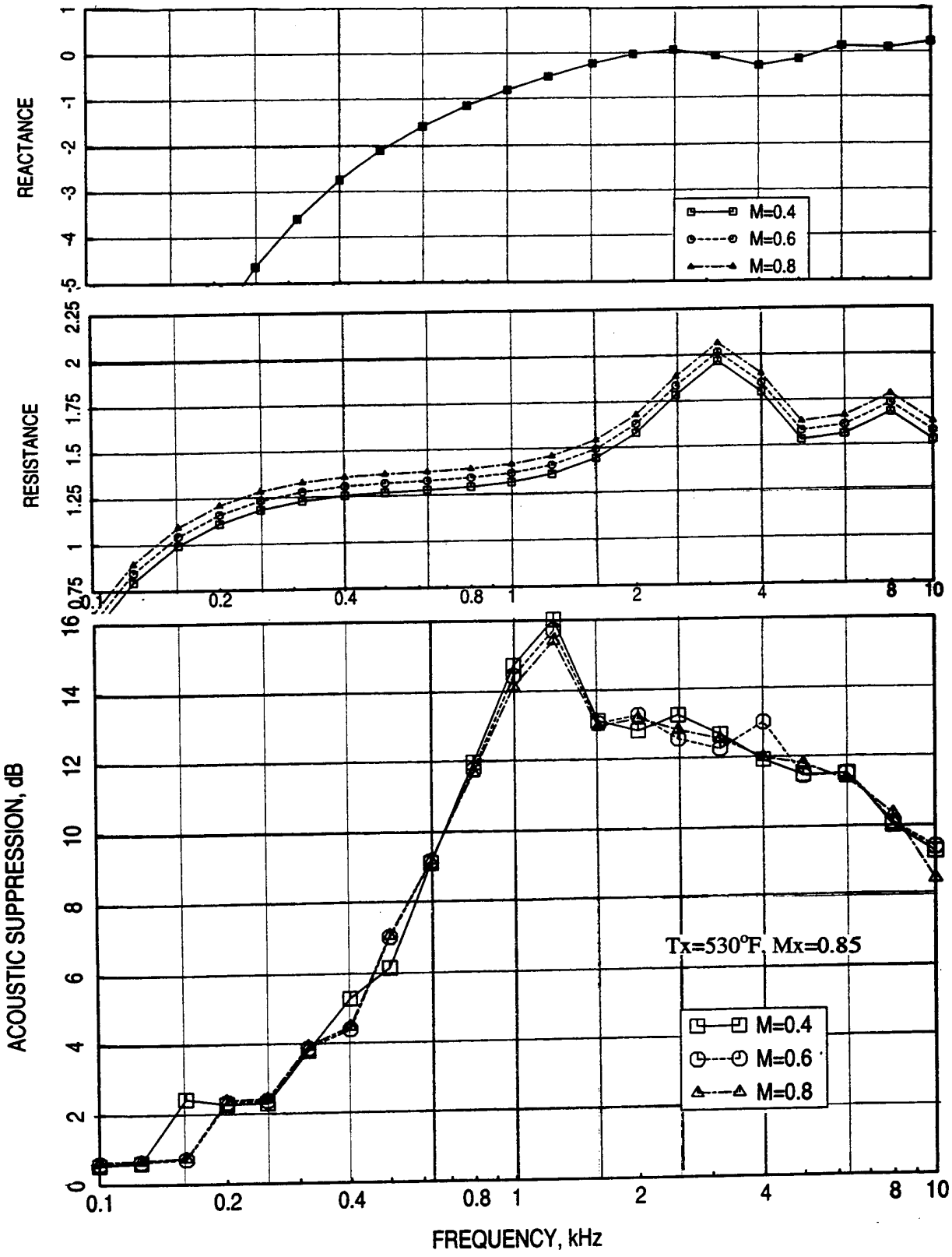

Figure 99. Effect of grazing flow Mach number (M) on predicted normal impedance and acoustic suppression spectra for a full-scale mixer-ejector liner design, D=2.0", σ=40%, t=d=0.04", R=10 Rayls/cm, T=500°F, OASPL=177.4 dB, δ*=0.2".

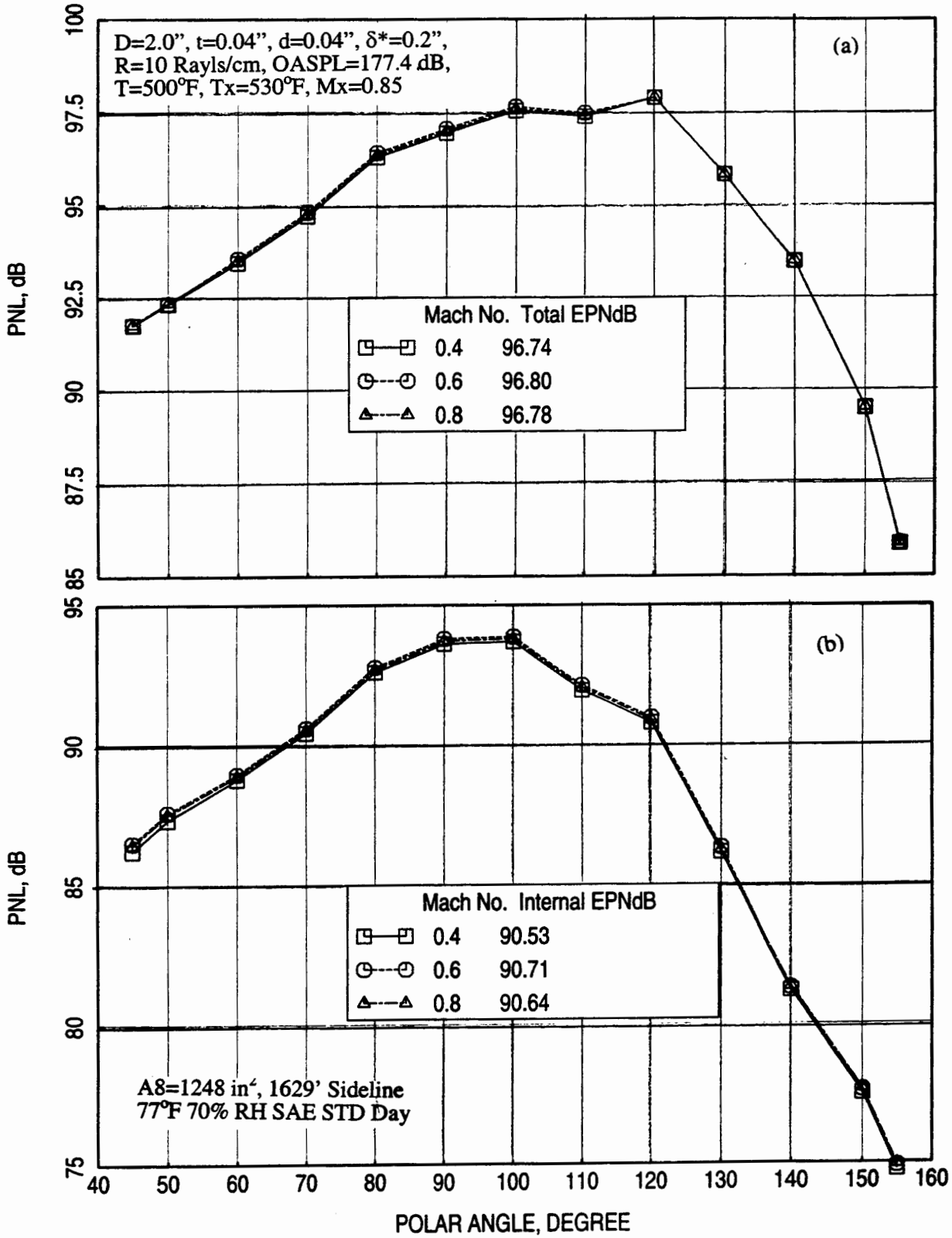

Figure 100. Effect of grazing flow Mach number (M) on predicted (a) total and (b) internal component of PNL directivities for a full-scale mixer-ejector liner design, NPR=3.43, T8=1551°R, V_j=2359 ft/sec, M=0.32 {takeoff}.

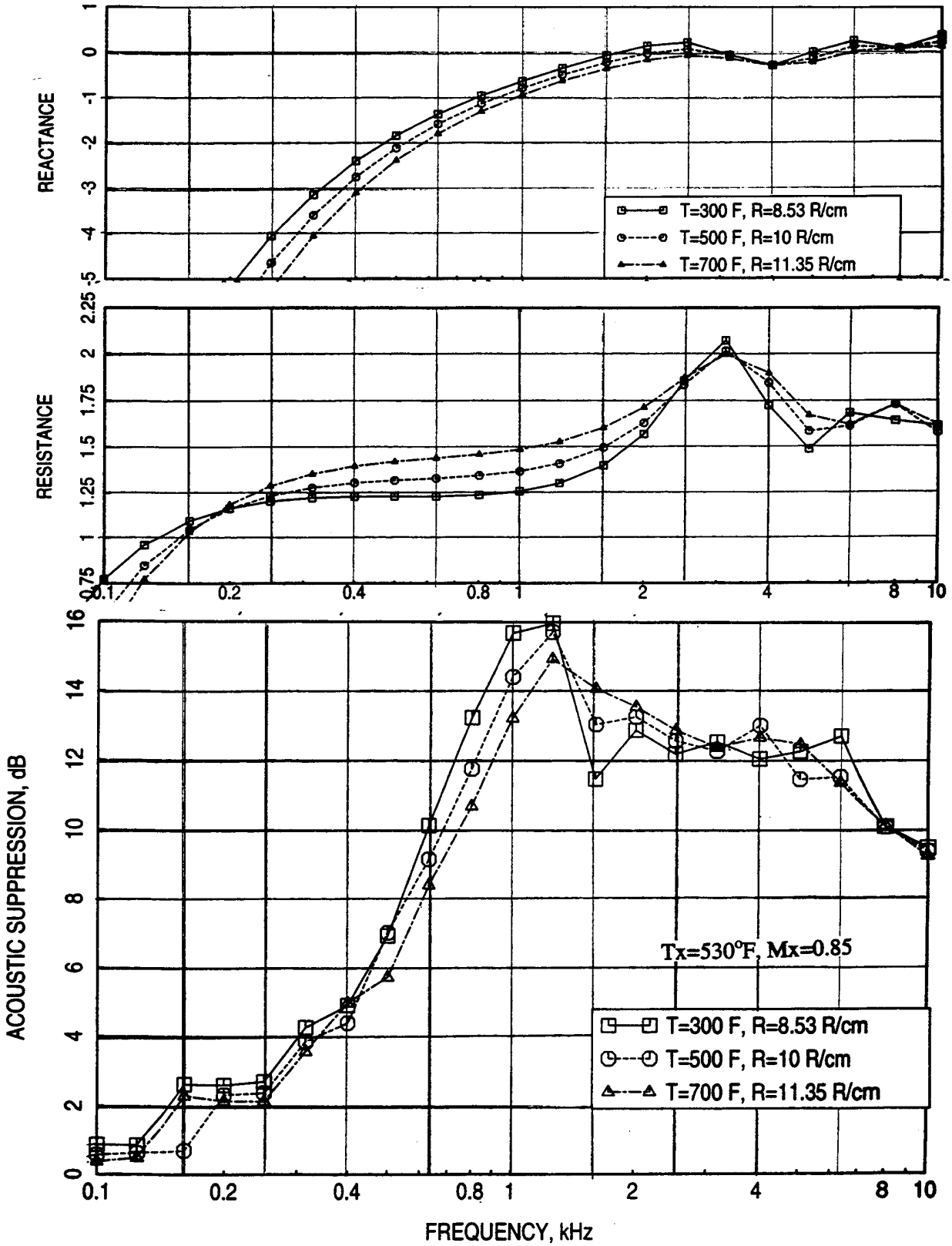

Figure 101. Effect of grazing flow temperature (T) on predicted normal impedance and acoustic suppression spectra for a full-scale mixer-ejector liner design, D=2.0", σ=40%, t=d=0.04", R=10 Rayls/cm, M=0.6, OASPL=177.4 dB, δ*=0.2".

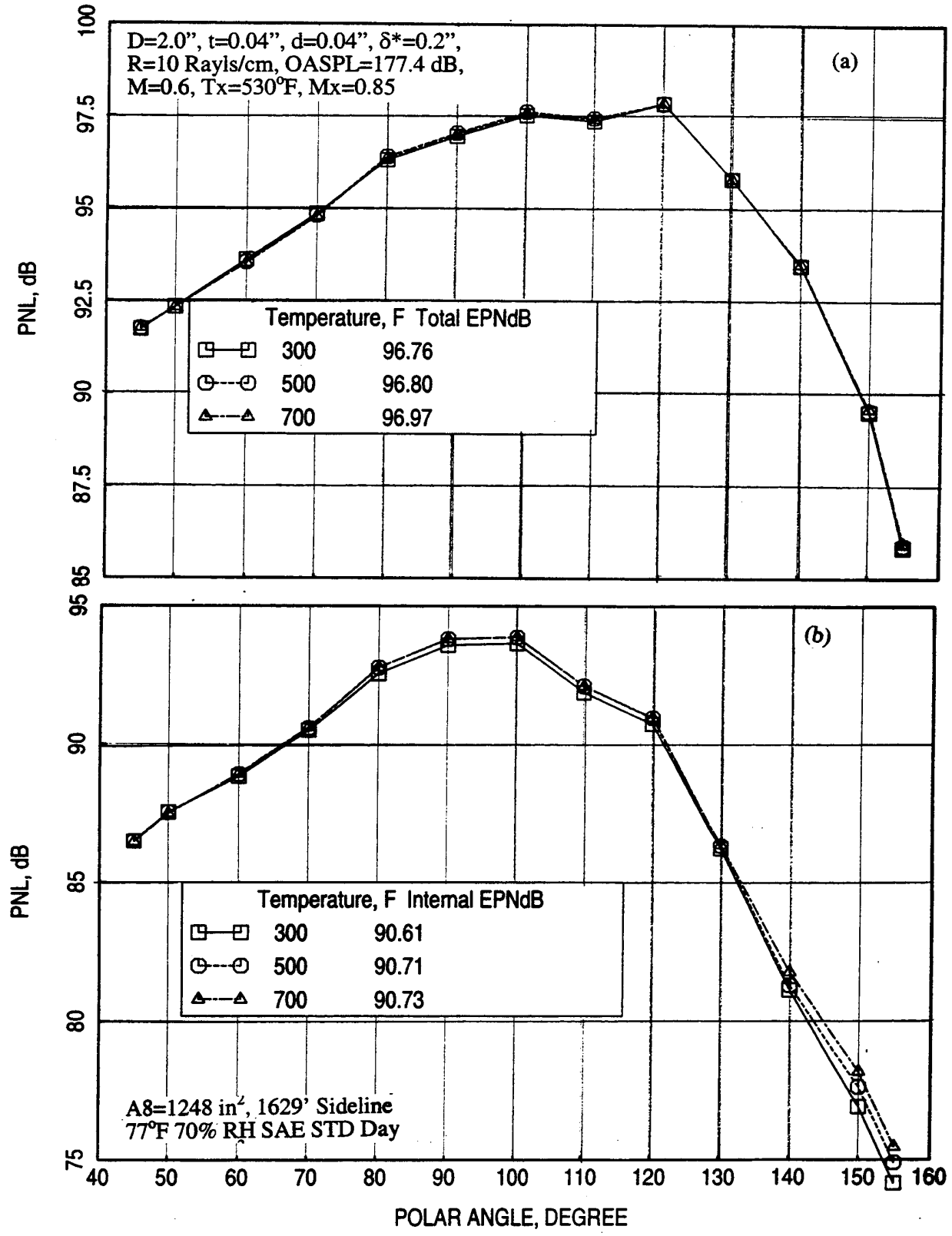

Figure 102. Effect of grazing flow temperature (T) on predicted (a) total and (b) internal component of PNL directivities for a full-scale mixer-ejector liner design, NPR=3.43, T8=1551°R, V_j=2359 ft/sec, M=0.32 {takeoff}.

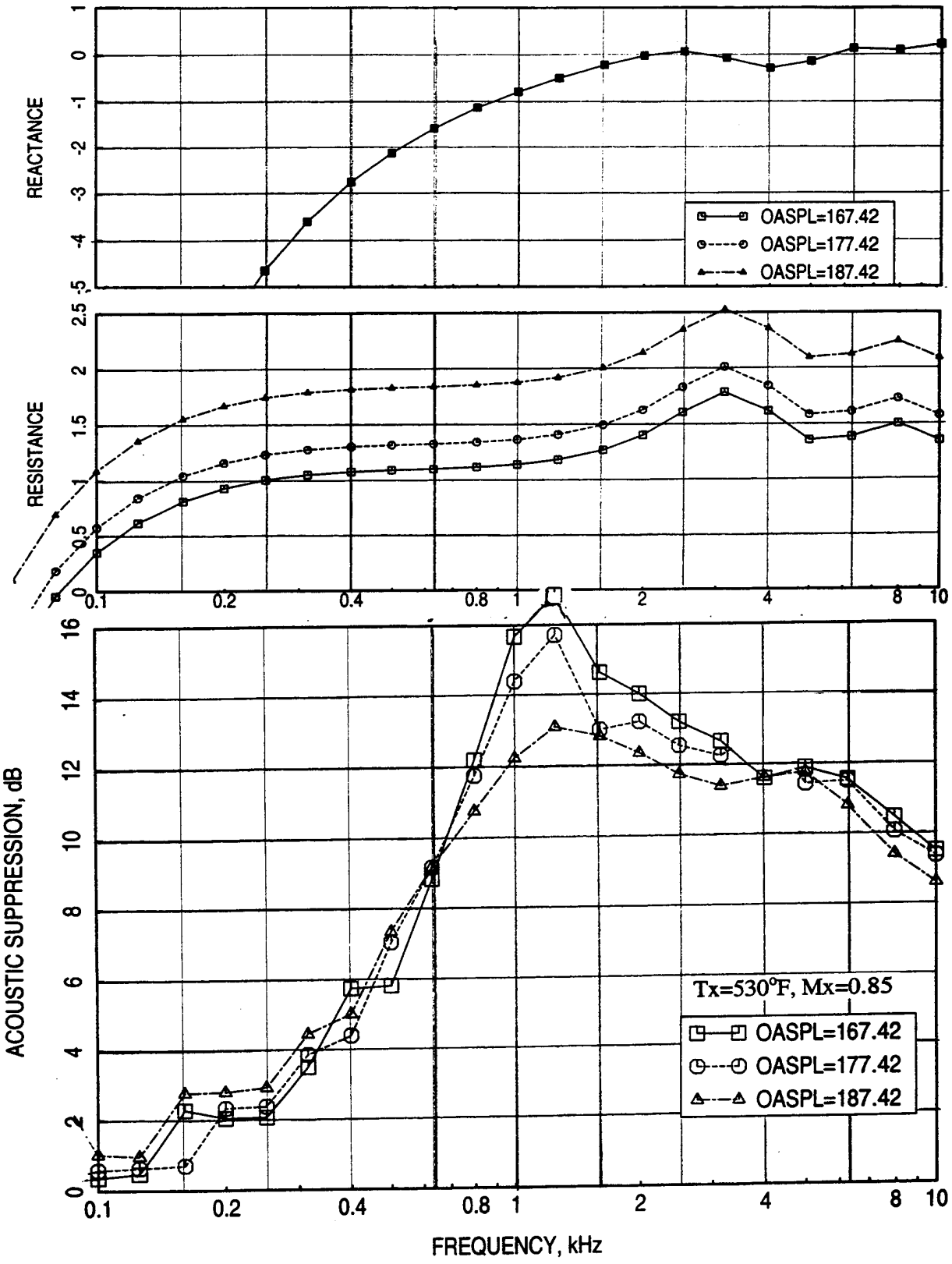

Figure 103. Effect of OASPL on predicted normal impedance and acoustic suppression spectra for a full-scale mixer-ejector liner design, D=2.0", σ=40%, t=d=0.04", R=10 Rayls/cm, M=0.6, T=500°F, δ*=0.2".

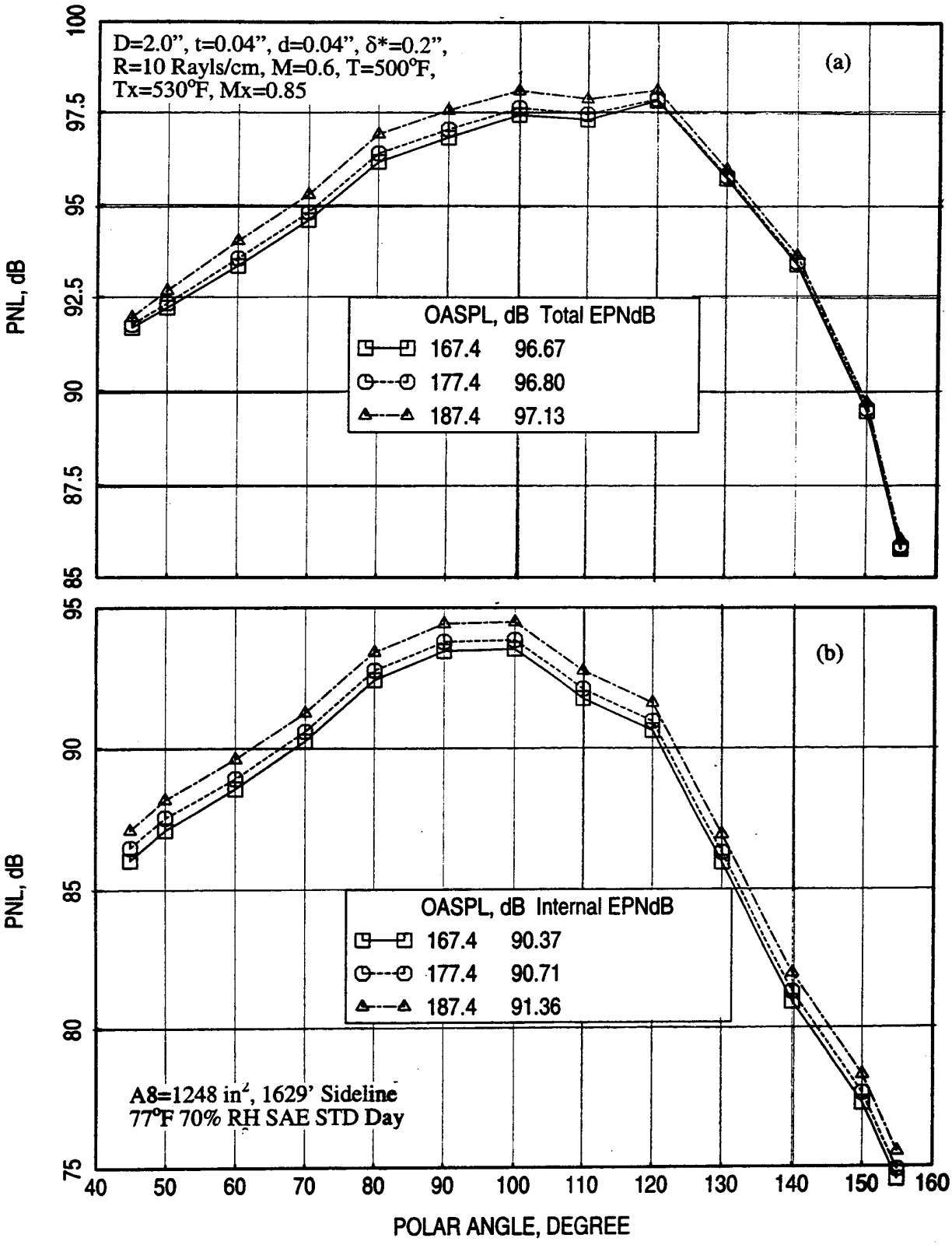

Figure 104. Effect of OASPL on predicted (a) total and (b) internal component of PNL directivities for a full-scale mixer-ejector liner design, NPR=3.43, T8=1551°R, V_j=2359 ft/sec, M=0.32 {takeoff}.

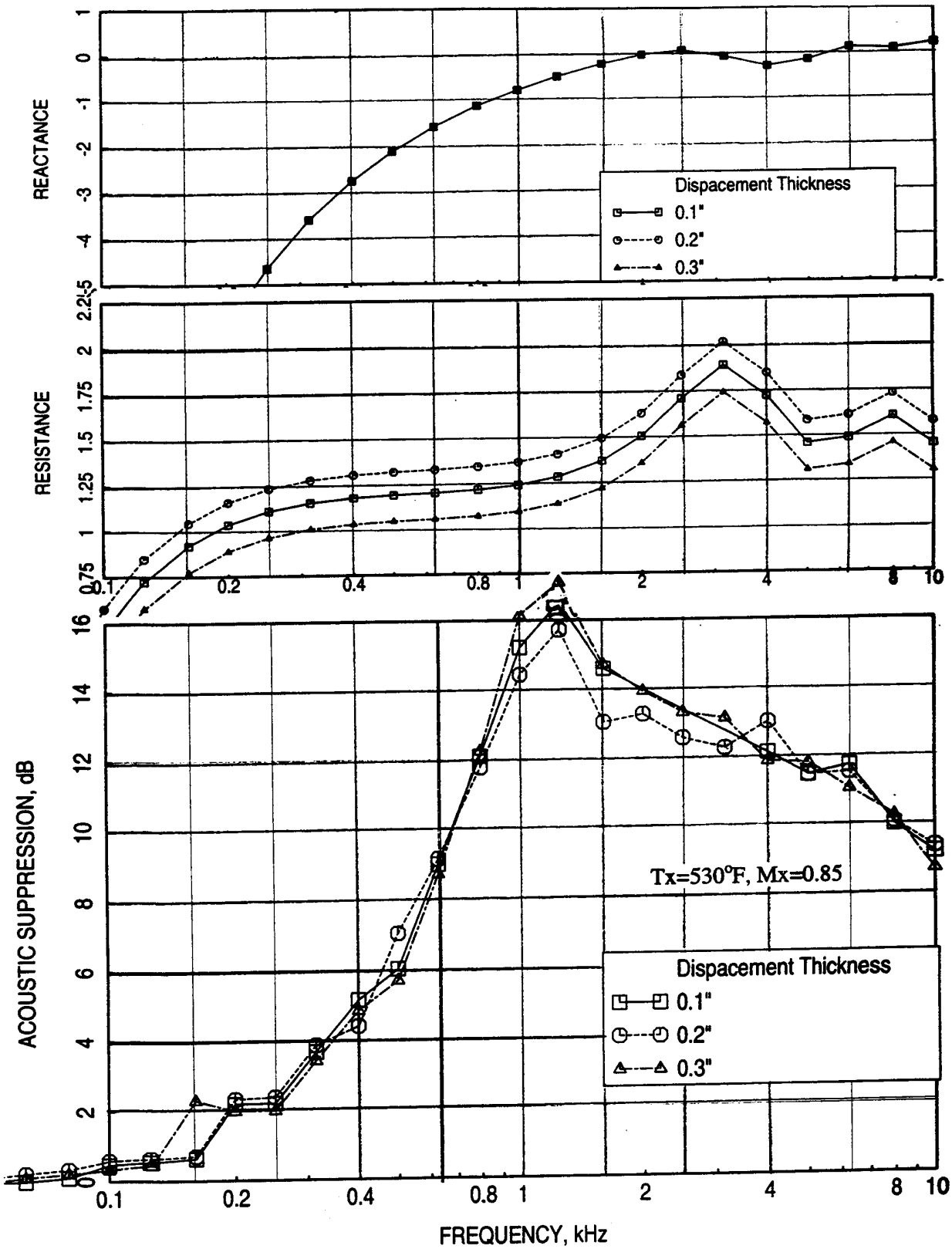

Figure 105. Effect of displacement thickness (δ*) on predicted normal impedance and acoustic suppression spectra for a full-scale mixer-ejector liner design, D=2.0", σ=40%, t=d=0.04", R=10 Rayls/cm, M=0.6, T=500°F, OASPL=177.4 dB.

decreases and then increases with increasing δ^* at mid frequencies. Acoustic intensity impact on PNL directivities and the corresponding EPNL is small as indicated in Figure 106.

Mean Flow Mach Number (Mx): Effect of mean flow Mach number on predicted acoustic suppression spectra and PNL directivities are shown in Figure 107. Acoustic suppression increases and the corresponding EPNL decreases with increasing mean flow Mach number.

Mean Flow Temperature (Tx): Effect of mean flow temperature on predicted acoustic suppression spectra and corresponding PNL directivities are shown in Figure 108. The impact of Tx is insignificant on acoustic suppression and the corresponding EPNL.

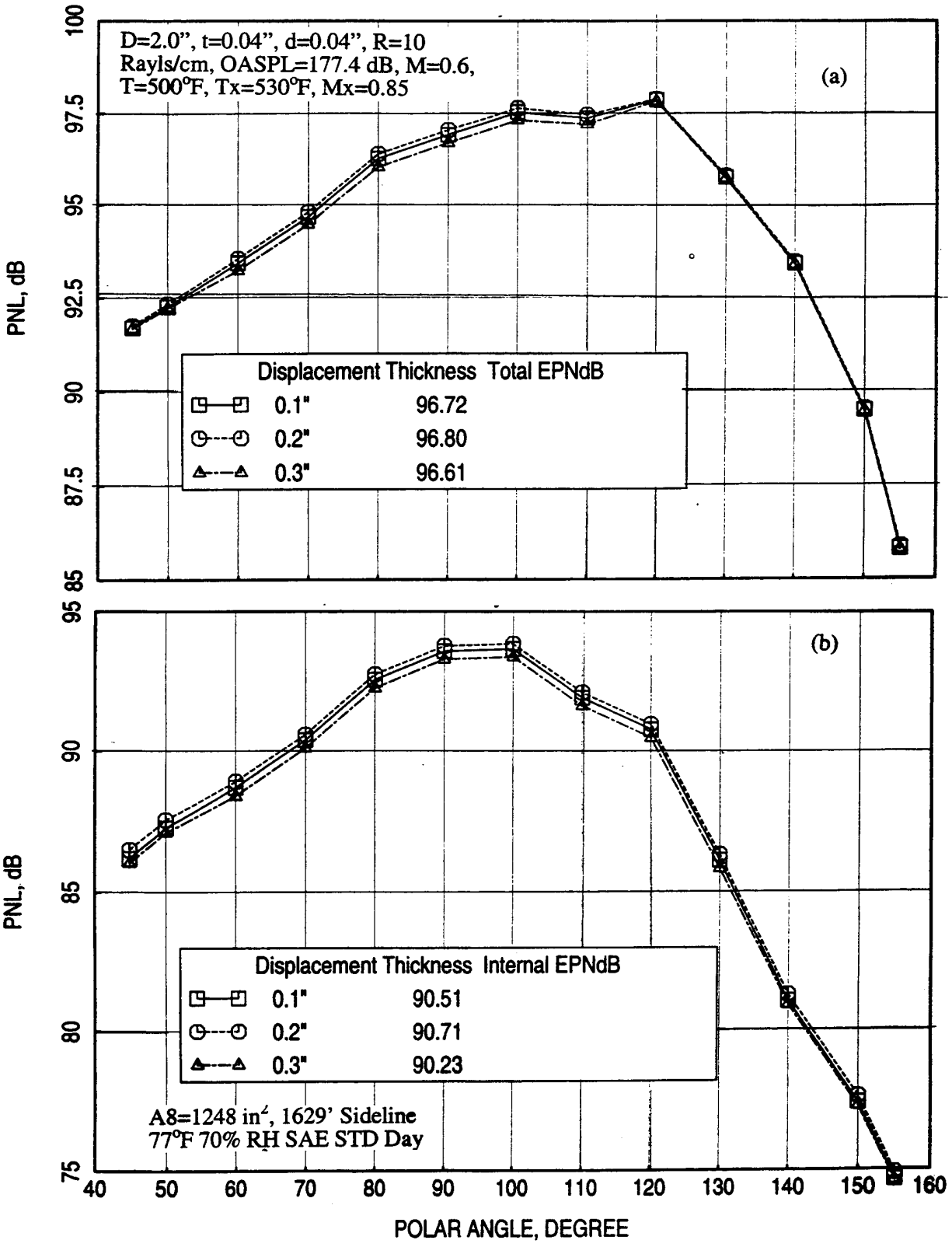

Figure 106. Effect of displacement thickness (δ*) on predicted (a) total and (b) internal component of PNL directivities for a full-scale mixer-ejector liner design, NPR=3.43, T8=1551°R, V_j=2359 ft/sec, M=0.32 {takeoff}.

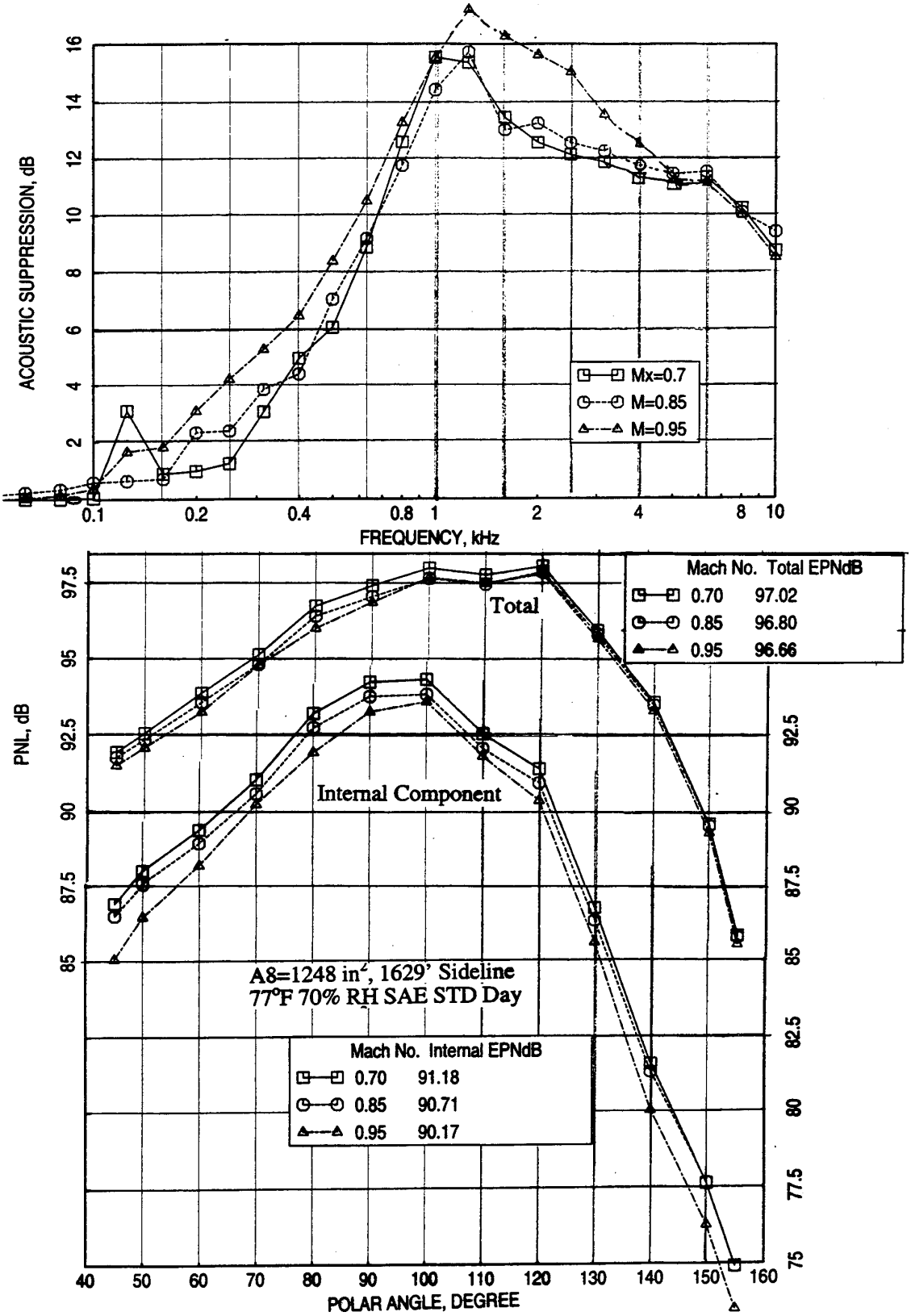

Figure 107. Effect of mean flow Mach number (Mx) on predicted acoustic suppression spectrum and PNL directivities for a full-scale mixer-ejector liner design, D=2.0", σ=40%, t=d=0.04", R=10 Rayls/cm, M=0.6, Tx=530°F, T=500°F, OASPL=177.4 dB, δ*=0.2".

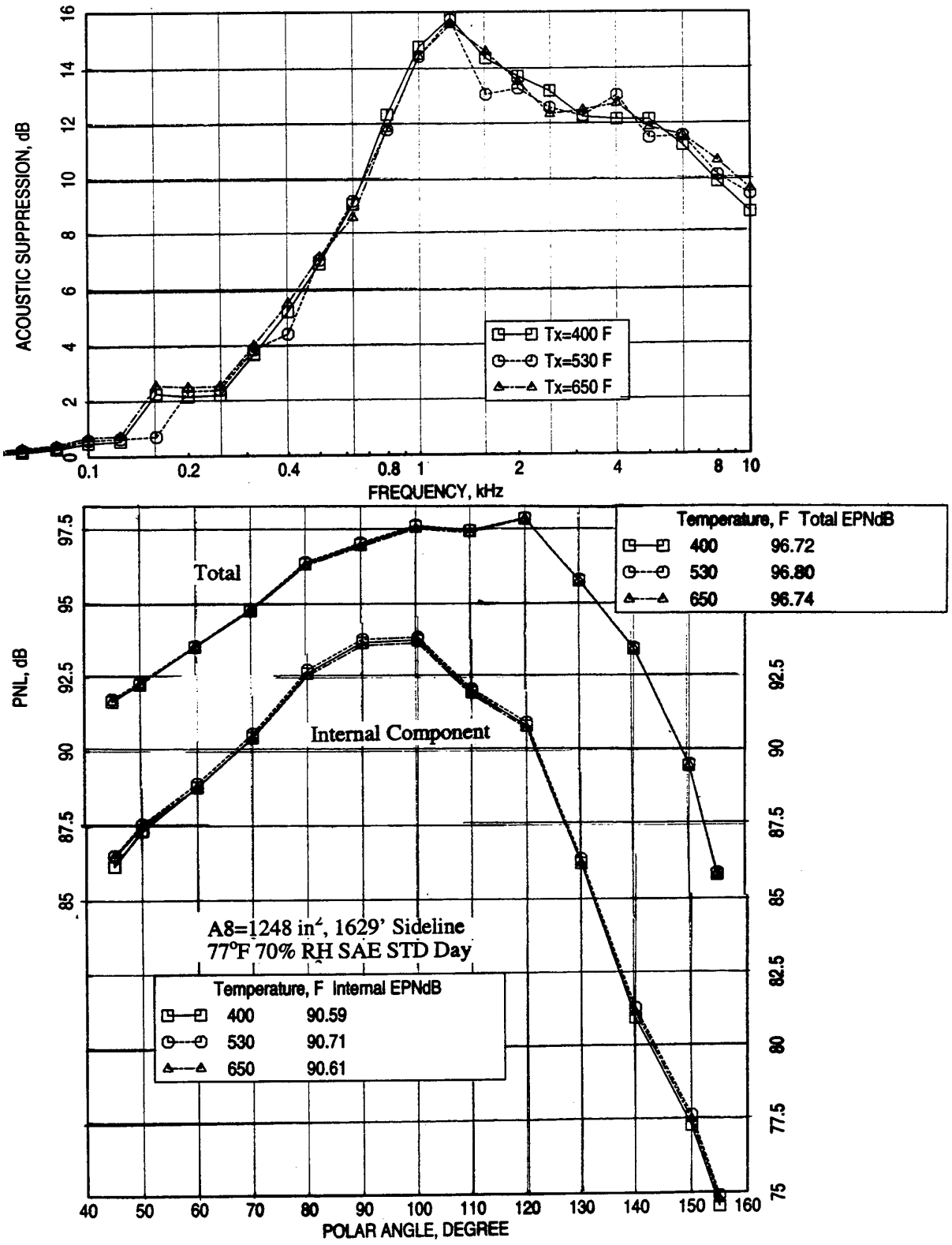

Figure 108. Effect of mean flow temperature (Tx) on predicted acoustic suppression spectrum and PNL directivities for a full-scale mixer-ejector liner design, D=2.0", σ=40%, t=d=0.04", R=10 Rayls/cm, M=0.6, T=500°F, Mx=0.85, OASPL=177.4 dB, δ*=0.2".

7.0 LINER DESIGN AND FARFIELD NOISE PREDICTION

Liners are designed for different realistic materials for each of the full-scale, LSM, and 1/7-scale mixer-ejectors. In addition, an ideal liner is designed for full-scale ejector, for which the impedance levels are chosen to give maximum acoustic suppression. It should be noted that this is a hypothetical design not realistically possible. The nozzle and liner parameters utilized in these designs are listed in section 2. All the liner designs are done for takeoff conditions. However, the acoustic characteristics are also evaluated at cutback conditions for the same liner designs. Predicted normal impedance, acoustic suppression, and farfield noise for the realistic liners, the optimum liner (established in section 6), and the ideal liner are compared for each mixer-ejector scales.

7.1 Normal Impedance and Acoustic Suppression for Ideal Liner: Acoustic suppression spectrum for different fixed impedance values, covering the optimum impedance range (i.e., $R/\rho c$=1.5 to 2.0 and $X/\rho c$=-0.5 to 0.0), are computed for the full-scale mixer-ejector at the takeoff condition. Acoustic suppression results at fixed resistance with varying reactance are shown in Figures 109 and 110. Similar results at fixed reactance with varying resistance are shown in Figures 111 and 112. The effect of reactance on acoustic suppression, as observed from Figures 109 and 110, for a fixed resistance is very small. Whereas, for a fixed reactance the acoustic suppression increases with decreasing resistance up to about 2500 Hz (see Figures 111 and 112). The trend is reversed at higher frequencies. Based on this behavior, for a fixed reactance of -0.5 the resistance values are further decreased beyond the optimum limit and the corresponding acoustic suppression spectra (see Figure 113) are evaluated. Acoustic suppression increases with decreasing resistance at frequencies closer to the peak up to $R/\rho c$ =0.6. The suppression level starts decreasing for entire frequency range with further resistance decrease. Utilizing all the predicted acoustic suppression, ideal impedance spectra, corresponding to maximum possible suppressions, are established.

7.2 Full-Scale Mixer-Ejector: Normal impedance spectra for an optimum design and two other realistic designs, parameters listed below, are predicted at takeoff condition.

	Optimum	Design #1	Design #2
Liner Depth, D	2.0"	2.0"	2.0"
Bulk Resistivity, Rayls/cm	10.0	37.3 (T-Foam)	8.45 (100ppi SiC)
Facesheet Thickness, t	0.04"	0.10"	0.10"
Facesheet Hole Diameter, d	0.04"	0.04"	0.04"
Facesheet Porosity, σ	40%	35%	35%

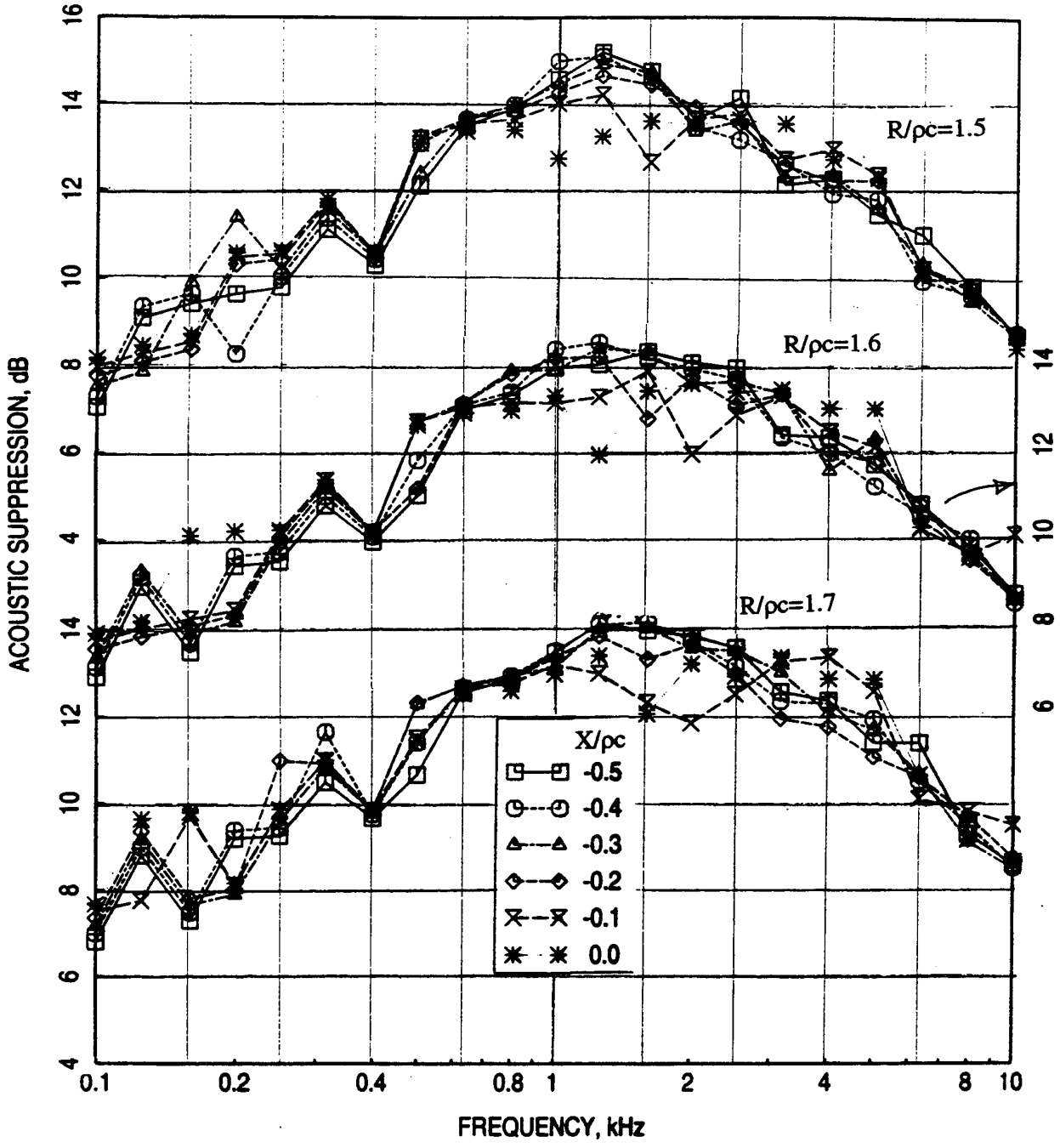

Figure 109. Effect of normal reactance (X/ρc) on acoustic suppression spectra for fixed normal resistance (R/ρc) for full-scale mixer-ejector, Mx=85, Tx=530°F.

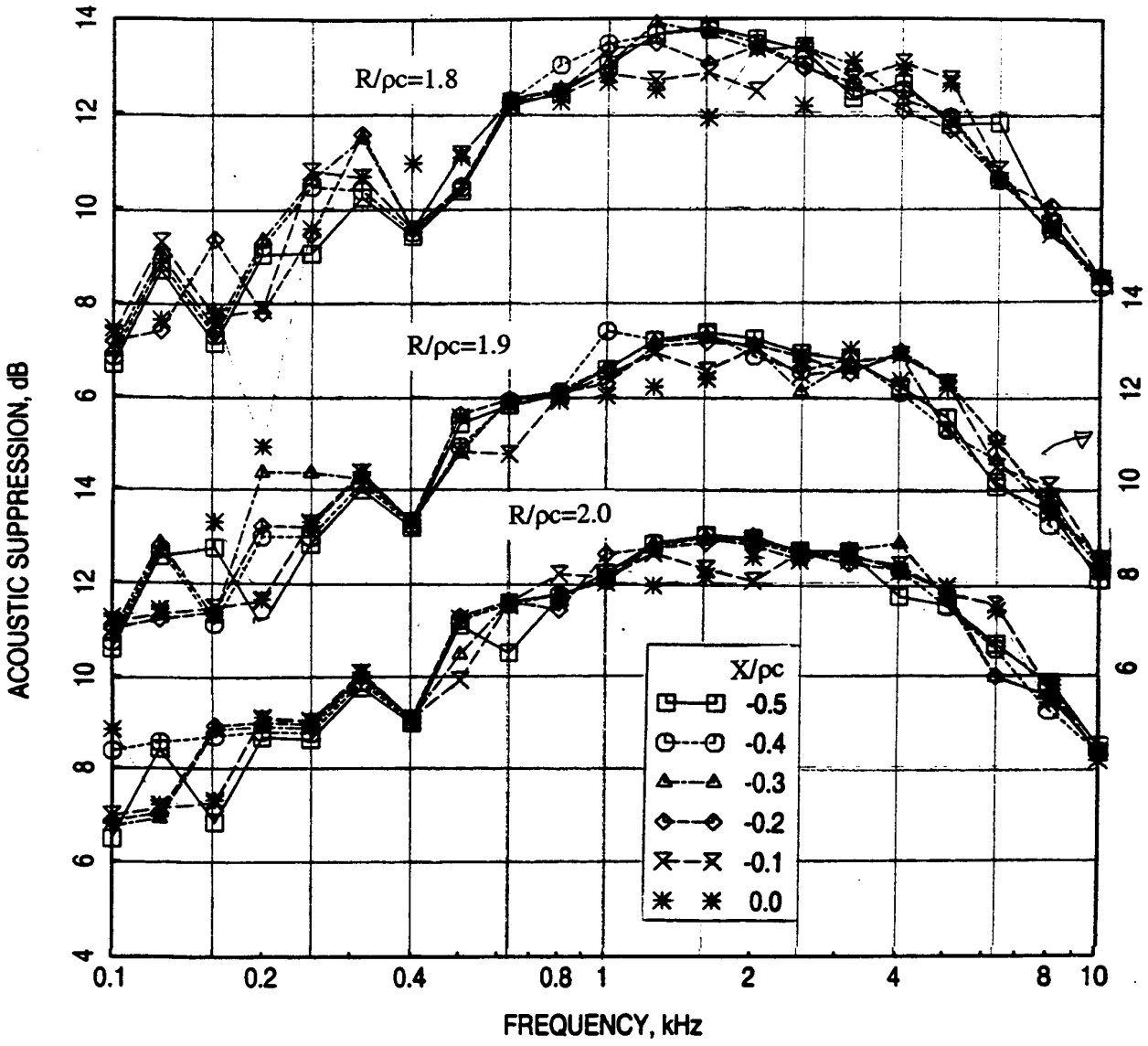

Figure 110. Effect of normal reactance (X/ρc) on acoustic suppression spectra for fixed normal resistance (R/ρc) for full-scale mixer-ejector, Mx=85, Tx=530°F.

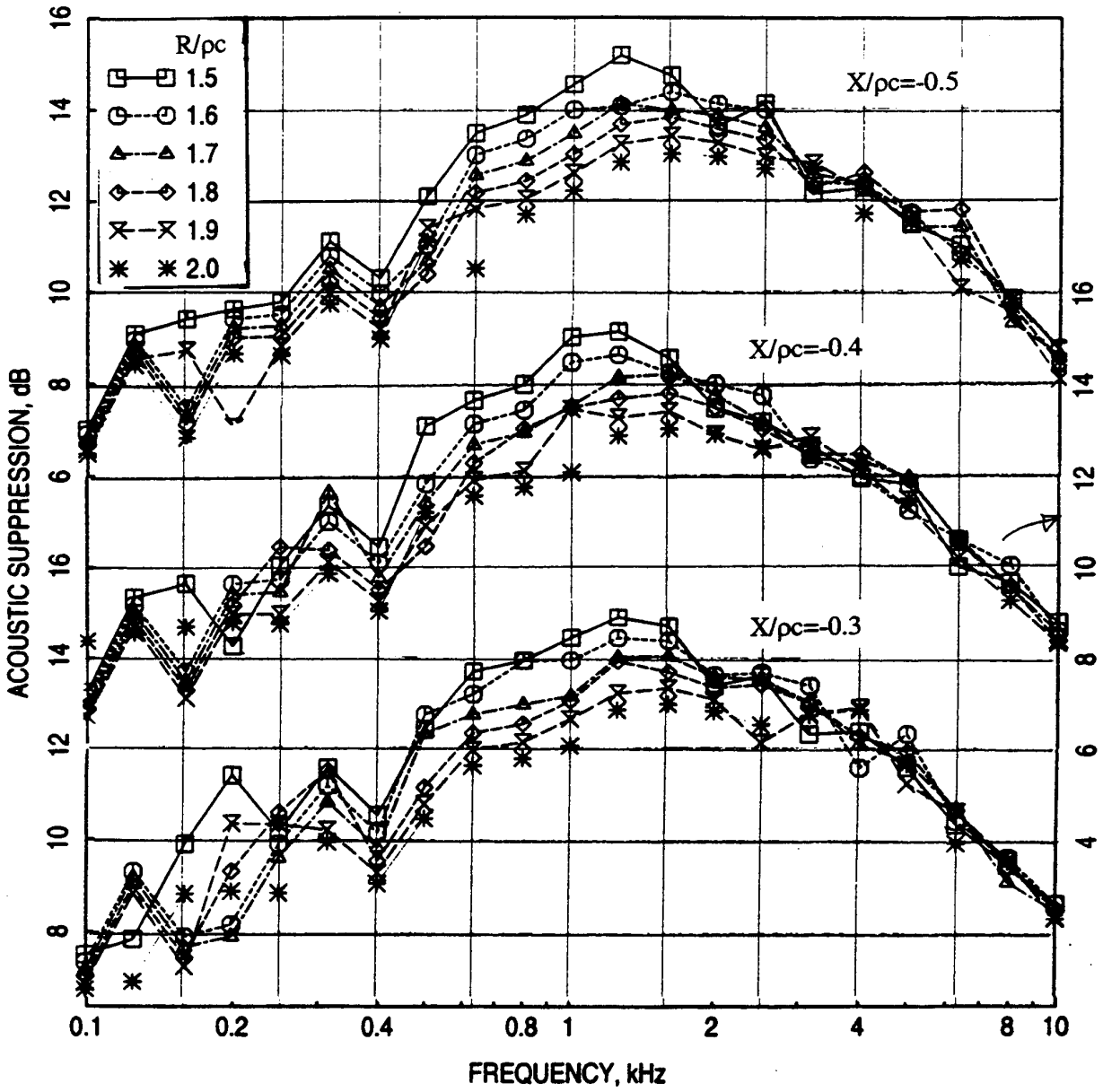

Figure 111. Effect of normal resistance (R/ρc) on acoustic suppression spectra for fixed normal reactance (X/ρc) for full-scale mixer-ejector, Mx=85, Tx=530°F.

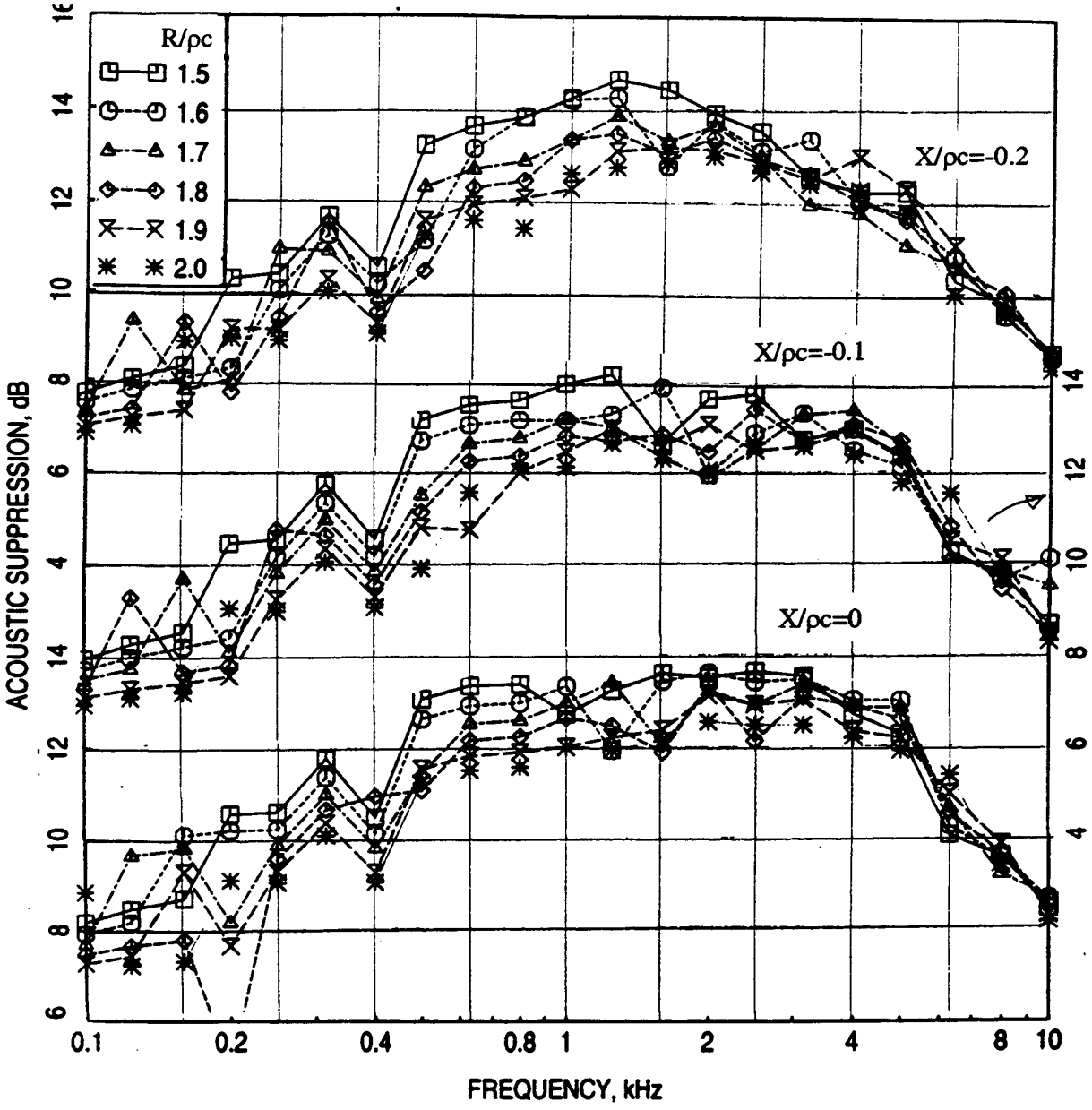

Figure 112. Effect of normal resistance (R/ρc) on acoustic suppression spectra for fixed normal reactance (X/ρc) for full-scale mixer-ejector, Mx=85, Tx=530°F.

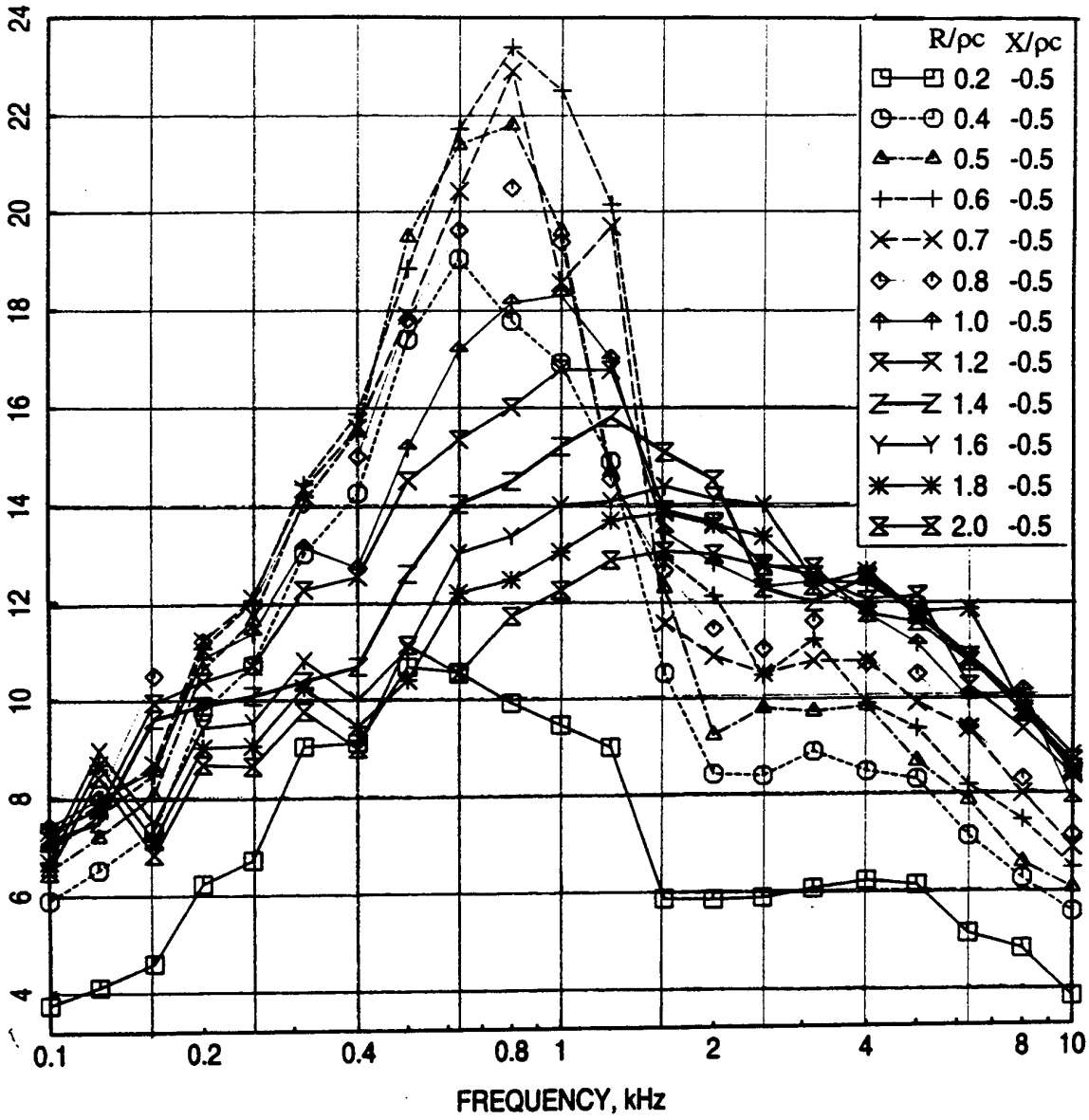

Figure 113. Acoustic suppression spectra for fixed normal impedance for full-scale mixer-ejector, Mx=85, Tx=530°F.

The optimum design is aimed at achieving the optimum impedance at and around the peak noy frequency and thus a minimum EPNL for takeoff could be obtained. The realistic designs are based on the current liner parameters established due to material, manufacturing, and strength considerations. Figure 114 shows the spectral distribution of normal impedance for the ideal, optimum, and the two realistic liner designs. Based on the normal impedance spectra a physical design of the ideal liner is not possible. The design #2 impedance spectra are very close to the optimum design. However, the normal resistance for the design #1 with T-Foam is much higher at frequencies up to about 3 kHz. Acoustic suppression spectrum for each design is predicted for takeoff as well as cutback conditions and is shown in Figures 115 and 116, respectively. The ideal acoustic suppression is much higher compared to the other liner designs at frequencies up to about 4 kHz. The acoustic suppression for the liner design with SiC foam (i.e., Design #2) is very close to the optimum case, where as, the acoustic suppression is much lower for Design #1 at frequencies between 500 to 2500 Hz. The total and internal component of PNL directivities for these liner designs and hardwall configuration are shown in Figure 117. The total and internal component of EPNL is listed in this figure.

The impact of bulk resistivity on EPNL is about 0.4 dB for takeoff and 0.94 dB at cutback, which is very significant. A suitable bulk is, therefore, very important for the successful liner application.

7.3 LSM Mixer-Ejector: The normal impedance spectra for an optimum design and two other realistic designs, parameters listed below, are predicted at takeoff condition.

	Optimum	Design #1	Design #2
Liner Depth, D	1.2"	1.2"	1.2"
Bulk Resistivity, Rayls/cm	20.0	33.8 (T-Foam)	20.0
Facesheet Thickness, t	0.02"	0.04"	0.04"
Facesheet Hole Diameter, d	0.025"	0.054"	0.054"
Facesheet Porosity, σ	40%	37%	37%

Figure 118 shows the spectral distribution of normal impedance for the optimum and the two realistic liner designs. The reactance spectra for all three designs are very close to each other. The design #2 normal resistance spectrum is closer to the optimum design. However, the normal resistance for the design #1 with T-Foam is much higher at frequencies up to about 4 kHz. Design #2 could be achieved by using materials of about 20 Rayls/cm, a SiC foam of about 150ppi. Acoustic suppression spectrum for each design is predicted for takeoff as well as cutback conditions and is shown in Figure 119. Again, the acoustic suppression for the liner design #2 is closer to the optimum case, where as, the acoustic suppression is

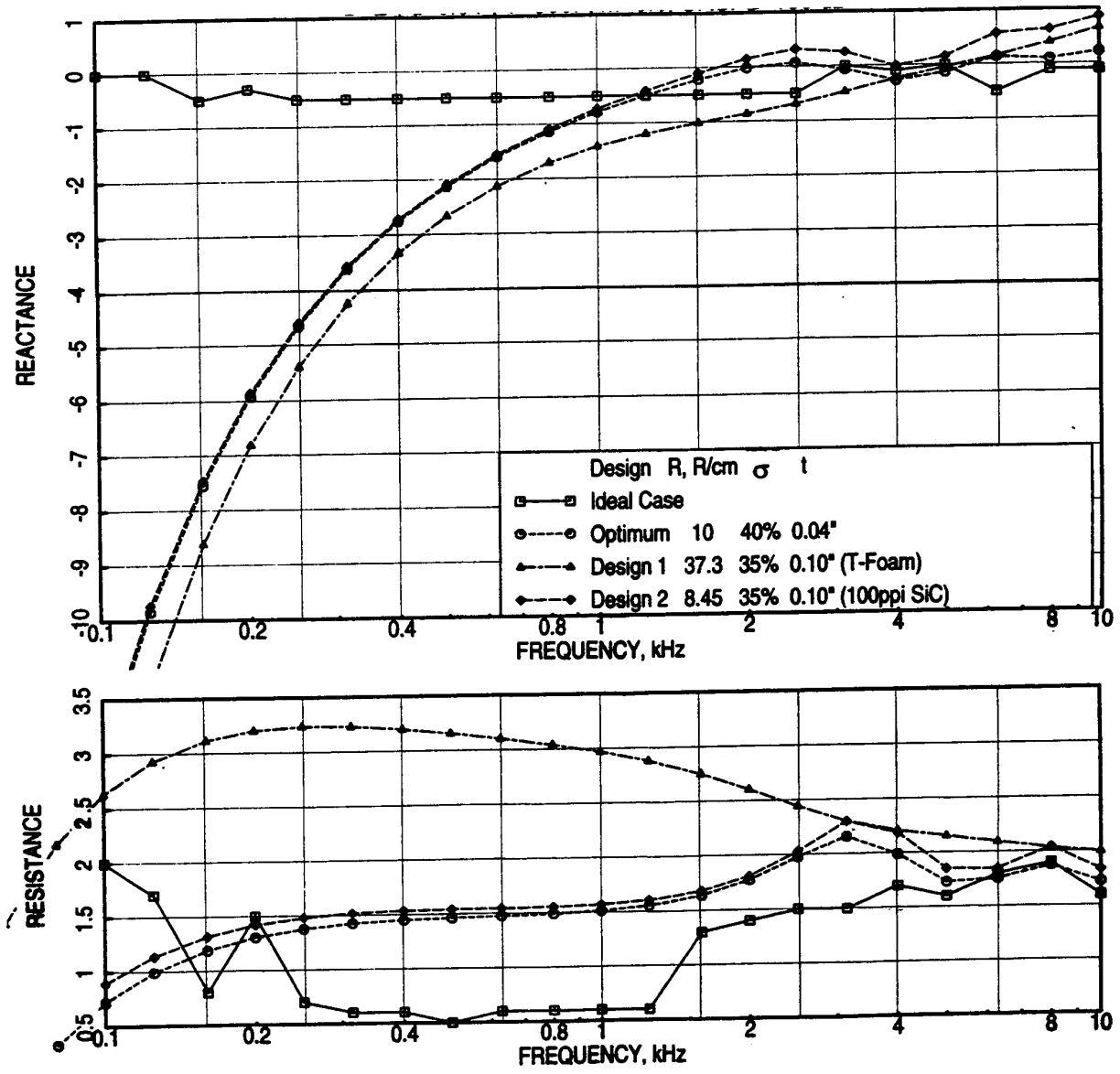

Figure 114. Comparison of predicted normal impedance spectra between ideal, optimum, and two realistic liner designs for full-scale mixer-ejector at takeoff condition, D=2", d=0.04", T=500°F, M=0.8, OASPL=180 dB.

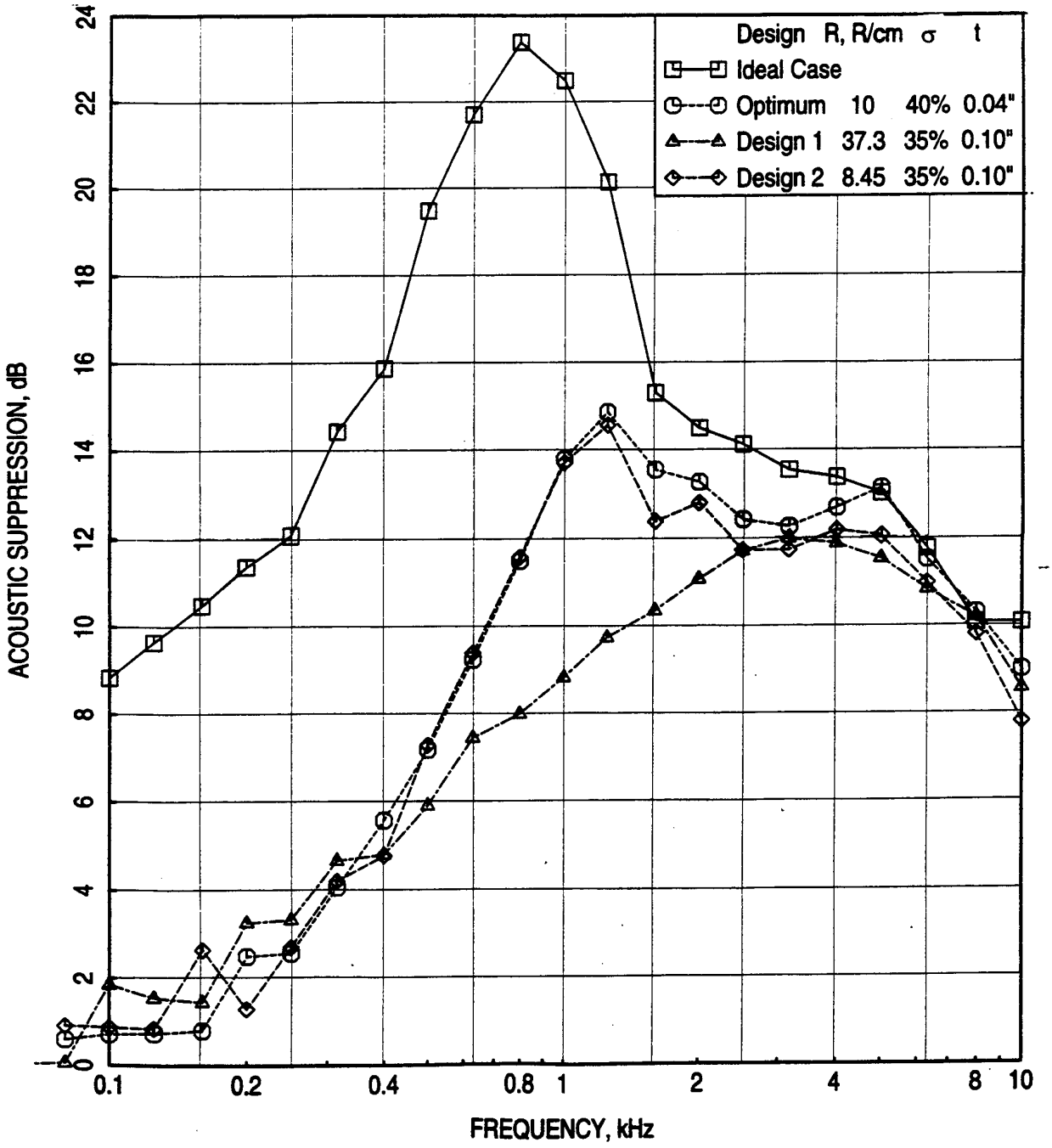

Figure 115. Comparison of predicted acoustic suppression spectra between ideal, optimum, and two realistic liner designs for full-scale mixer-ejector at takeoff condition (Mx=0.85, Tx=530°F), D=2", d=0.04", T=500°F, M=0.8, OASPL=180 dB.

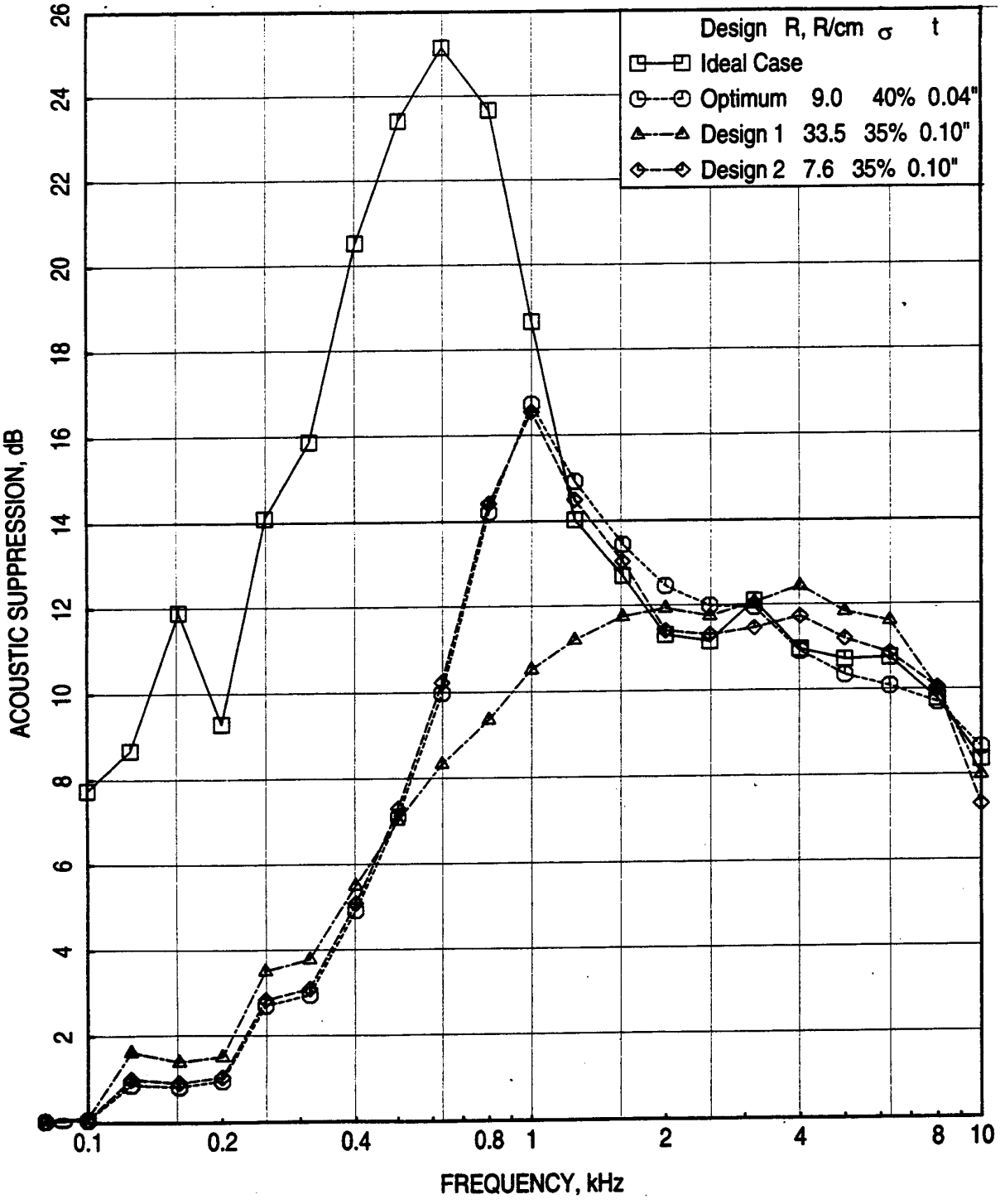

Figure 116. Comparison of predicted acoustic suppression spectra between ideal, optimum, and two realistic liner designs for full-scale mixer-ejector at cutback condition (Mx=0.73, Tx=400°F), D=2", d=0.04", T=360°F, M=0.72, OASPL=174.5 dB.

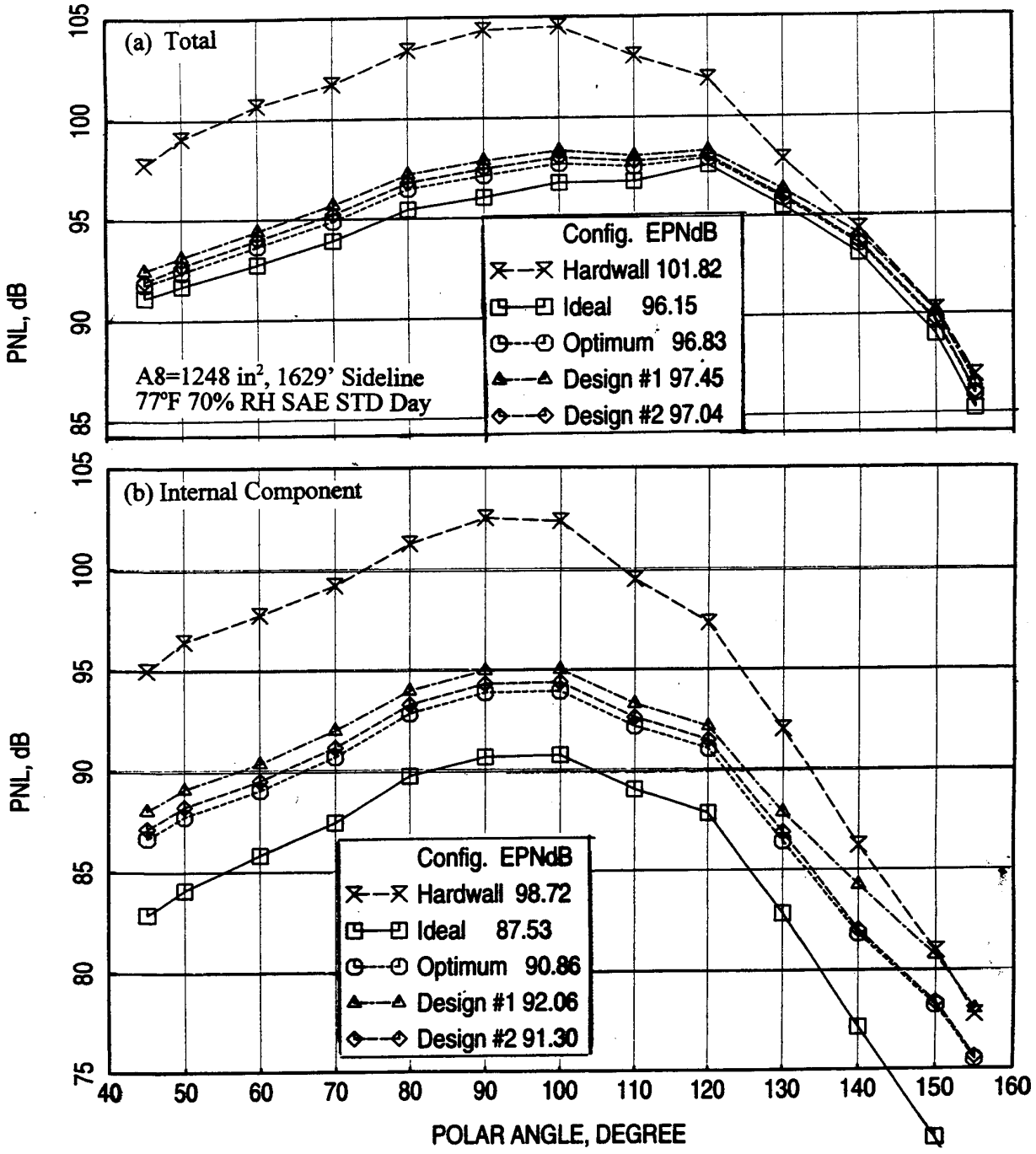

Figure 117. Comparison of predicted (a) total and (b) internal component of PNL directivities between ideal, optimum, and two realistic liner designs for full-scale mixer-ejector at takeoff condition, NPR=3.43, T8=1551°R, V_j=2359 ft/sec, M=0.32.

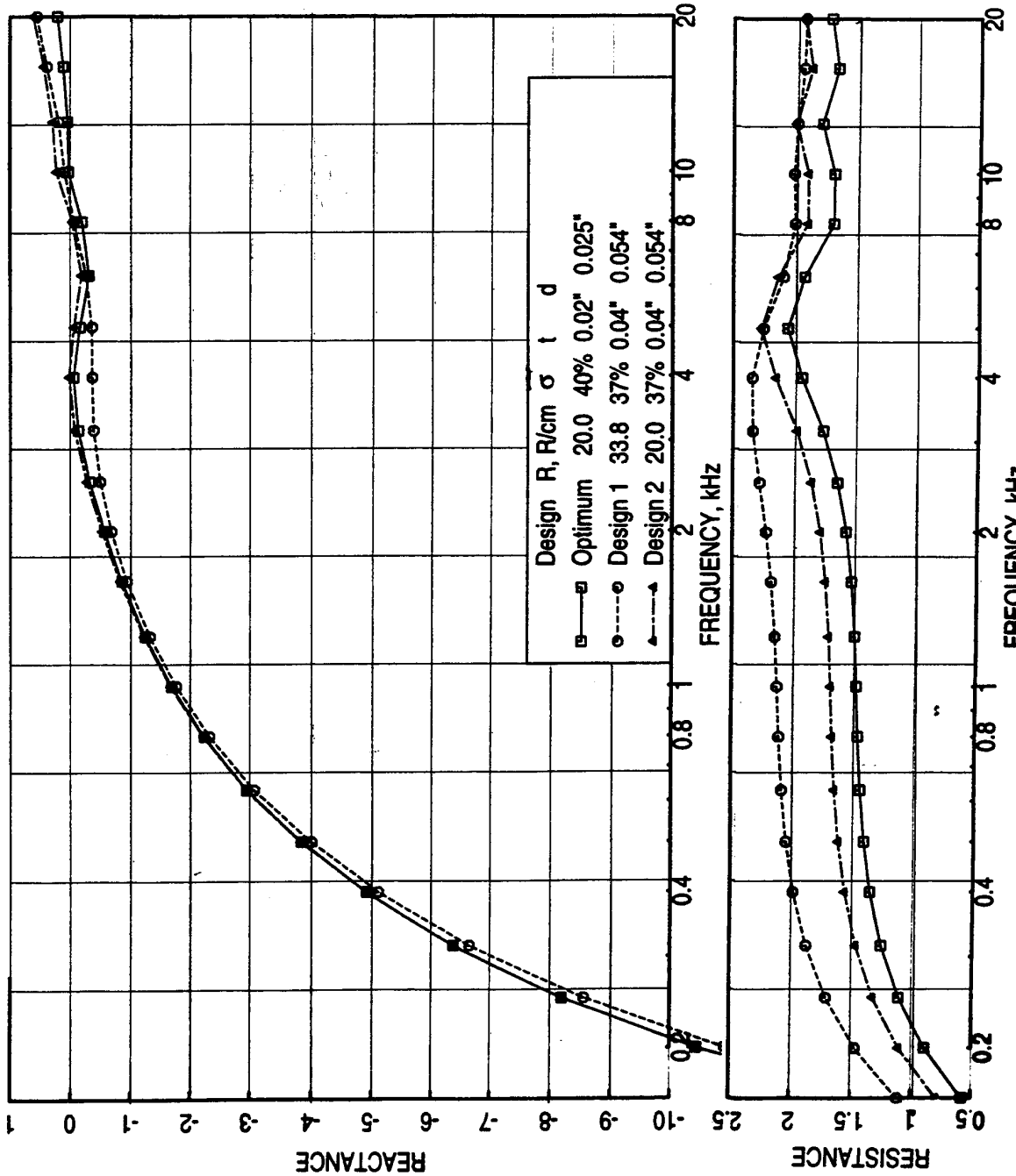

Figure 118. Comparison of predicted normal impedance spectra between optimum and two realistic liner designs for LSM mixer-ejector at takeoff condition, D=1.2", T=500°F, M=0.8, OASPL=177 dB.

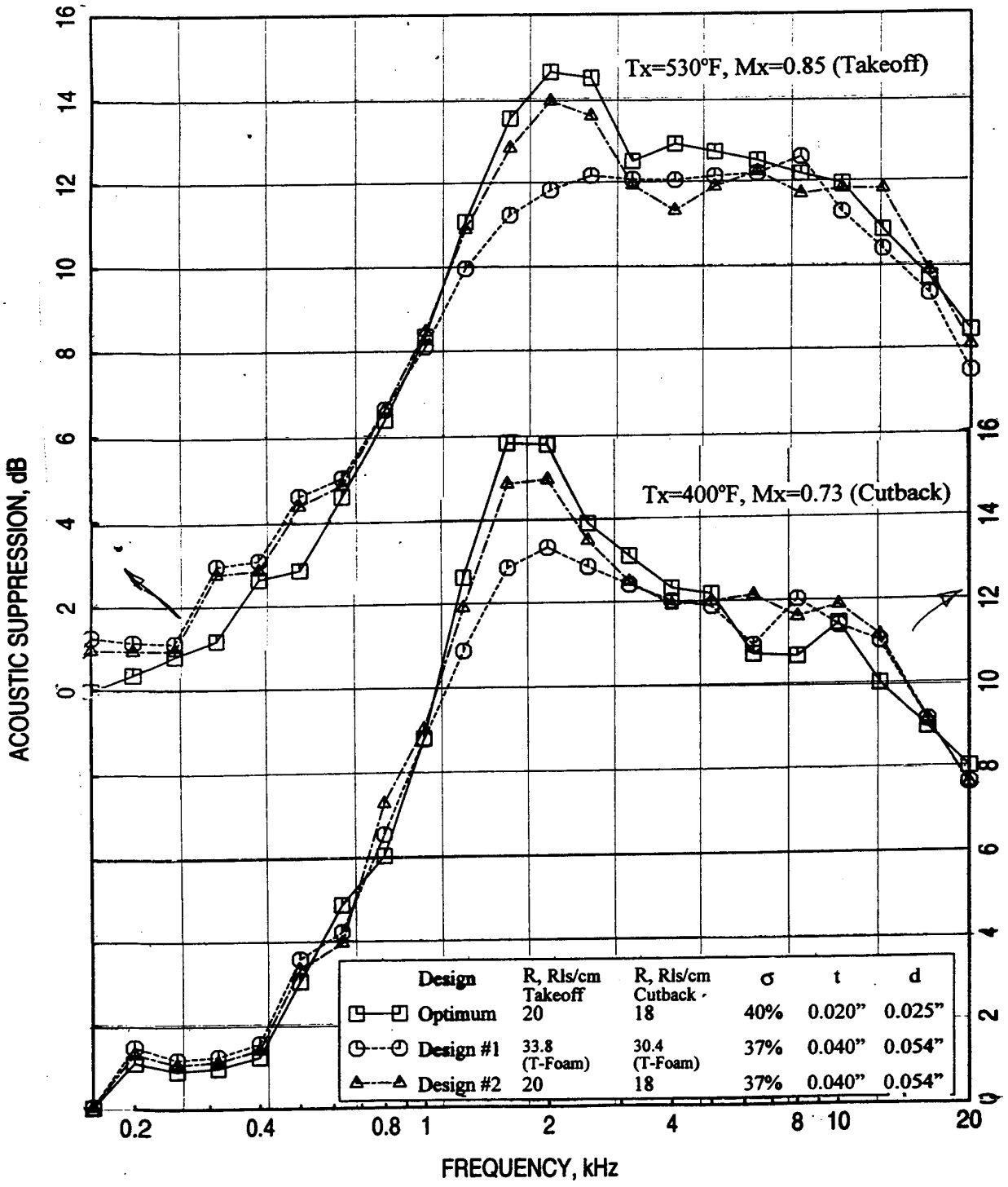

Figure 119. Comparison of predicted acoustic suppression spectra between optimum and two realistic liner designs for LSM mixer-ejector, D=1.2", d=0.04".

significantly lower for Design #1 at frequencies between 1000 to 2500 Hz. The corresponding PNL directivities are plotted in Figure 120. The impact of bulk resistivity on EPNL is small at takeoff. But is significant (i.e., 0.51 dB) at cutback. **Thus, a suitable bulk is necessary to improve the acoustic suppression.**

7.4 1/7-Scale Mixer-Ejector: The optimum bulk liner design for 1/7-scale mixer-ejector was carried out for a grazing flow Mach number M=0.6 with OASPL=177 dB, presented in Coordination Memo GE96-143N (Ref. 8). However, the current design is being performed for a grazing flow Mach number M=0.8 with OASPL=171.5 dB. Thus, the optimum design is repeated by varying the bulk resistivity for the same facesheet parameters in section 6. A resistivity of 60 Rayls/cm is still gives the minimum EPNL with optimum facesheet. However, with the realistic facesheet design a relatively lower bulk resistivity (i.e., about 40 Rayls/cm) is required for minimum EPNL. A liner depth of 0.485" is used for optimum as well as two other designs. However, a liner depth of 0.27" seems to be the required depth if the linear scale factor is applied with respect to full-scale design (i.e., 2.0"). Thus, a third design is made similar to the design #1 with a depth of 0.27" for comparison purpose. The normal impedance spectra for the optimum and the three other realistic designs, parameters listed below, are predicted at takeoff condition.

	Optimum	Design #1	Design #2	Design #3
Liner Depth, D	0.485"	0.485"	0.485"	0.27"
Bulk Resistivity, Rayls/cm	60.0	8.45 (100ppi SiC)	40.0	8.45 (100ppi SiC)
Facesheet Thickness, t	0.015"	0.025"	0.025"	0.025"
Facesheet Hole Diameter, d	0.02"	0.045"	0.045"	0.045"
Facesheet Porosity, S	45%	37%	37%	37%

Figure 121 shows the spectral distribution of normal impedance for the optimum and the three realistic liner designs. The reactance spectra for three designs of same depth are very close to each other, except at frequencies above 10 kHz. However, for D=0.27" (Design #3), the reactance spectrum is considerably different. The design #2 normal resistance spectrum is slightly higher compared to the optimum design. However, the normal resistance for the designs #1 and #3 with 100ppi SiC is much higher at frequencies below 1 kHz and much lower at mid frequency range. Design #2 could be achieved by using materials of about 40 Rayls/cm, a SiC foam of 200ppi (Resistivity 35.3 Rayls/cm) or a SiC foam with slightly higher ppi. The resistivity of 12 lbs/cft T-Foam for 0.5" deep sample is much lower (18 Rayls/cm), even though, the resistivity for 2" deep sample is closer to the optimum (37.3 Rayls/cm). Acoustic suppression spectrum for each design is predicted for takeoff as well as cutback conditions and is shown in Figure 122. Again, the acoustic suppression for the liner design #2 is closer to the optimum case, where as, the acoustic suppression for Design #1 is

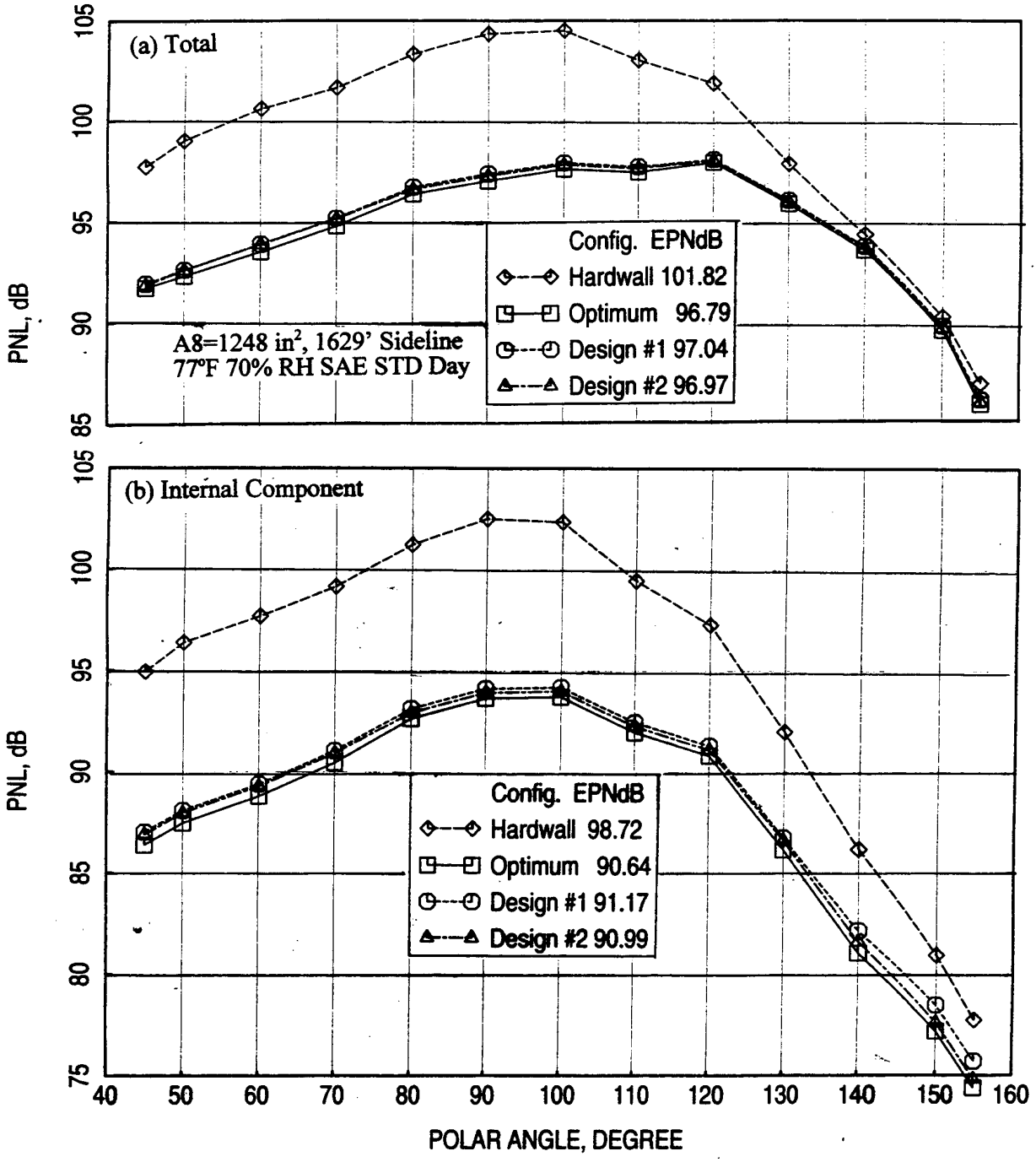

Figure 120. Comparison of predicted (a) total and (b) internal component of PNL directivities between optimum and two realistic liner designs for LSM mixer-ejector at takeoff condition, NPR=3.43, T8=1551°R, V_j=2359 ft/sec, M=0.32.

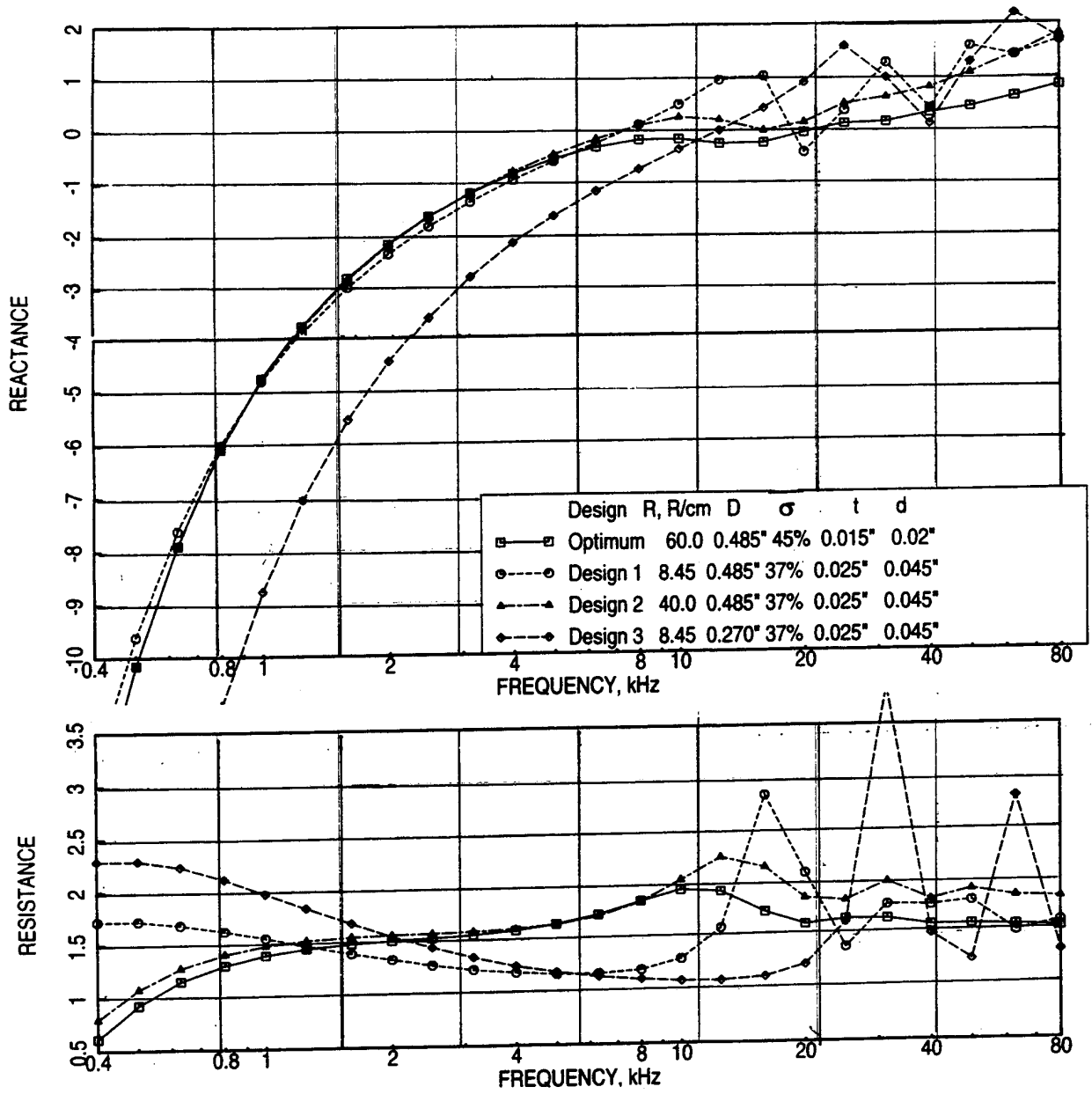

Figure 121. Comparison of predicted normal impedance spectra between optimum and three realistic liner designs for 1/7-scale mixer-ejector at takeoff condition, T=500°F, M=0.8, OASPL=171 dB.

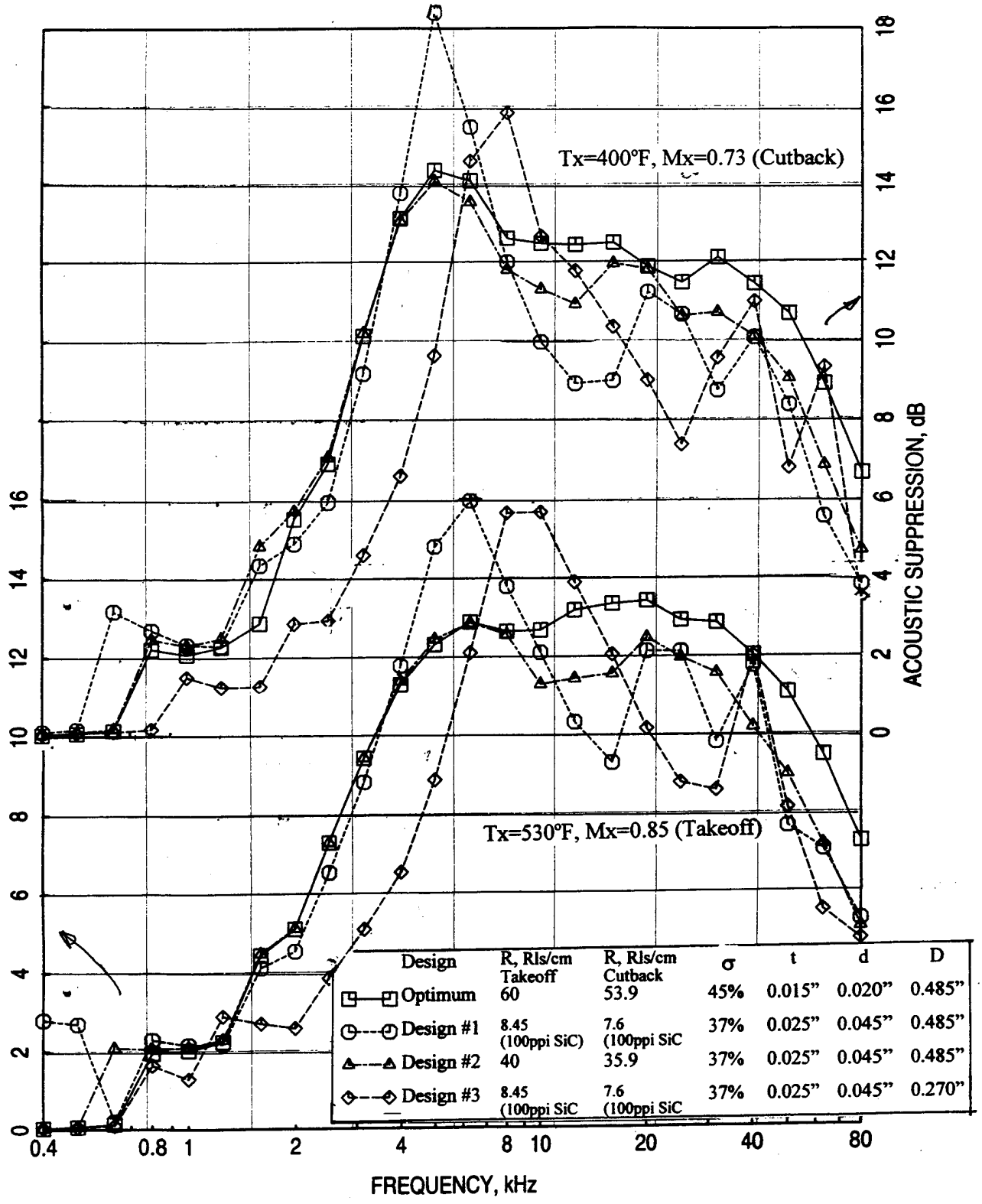

Figure 122. Comparison of predicted acoustic suppression spectra between optimum and three realistic liner designs for 1/7-scale mixer-ejector.

higher at frequencies between 5 and 7 kHz, but significantly lower at a number of higher frequency regions. Acoustic Suppression for design #3 is much lower at frequencies below 6 kHz.

PNL directivities for hardwall and the four liner designs are plotted in Figure 123. The EPNL values are listed in this figure. Acoustic benefit of about 0.7 EPNdB at takeoff (about 0.9 EPNdB at cutback) is shown due to the bulk resistivity. A higher resistive bulk is more noise effective for smaller scale ejector. It should be noted that the reduction of liner depth from 0.485" to 0.27" resulted in an increase of 0.56 EPNdB at takeoff (and 1.36 EPNdB at cutback).

7.5 Comparison of 1/7-Scale, LSM, and Full-Scale Liner Characteristics:

Optimum Liner Designs: Figure 124 shows the normal impedance spectra with respect to the frequency, multiplied with linear scale factor, (i.e., normalized frequency) for the optimum liners of three different scales. In the ideal case the impedance spectra for all three cases would collapse. However, the liner depth and other physical properties are not exactly scaled to the corresponding scale factor. If the depth for LSM and 1/7-scale liners would be set at 1.13" and 0.27" corresponding to their scale factors of 0.565 and 0.136, the impedance peaks would have come together at a fixed normalized frequency. However, the design depth for 1/7-scale liner is chosen to be 0.485", which is much higher compared to 0.27", for better acoustic suppression. The corresponding acoustic suppression spectra for takeoff and cutback conditions are shown in Figure 125. Again, the 1/7-scale acoustic suppression peak is occurring at a lower frequency compared to LSM and full-scale models due to its higher depth.

Design #1 Liners: Figure 126 shows the normal impedance spectra with respect to the frequency, multiplied with linear scale factor, (i.e., normalized frequency) for the full-scale optimum liner and the three different scale liner designs. For 1/7-scale designs 0.27" deep liner results (design #3) are also included. The resistance spectra for LSM and full-scale liners are significantly higher compared to the optimum spectrum. The corresponding acoustic suppression spectra for takeoff and cutback conditions are shown in Figure 127. Again, the acoustic suppression levels for LSM and full-scale liners are much lower compared to the optimum at frequencies closer to the peaks. The suppression peak for 0.27" deep liner coincides with those of other scale results. The corresponding 0.485" deep liner exhibits more low frequency suppression compared to other liners.

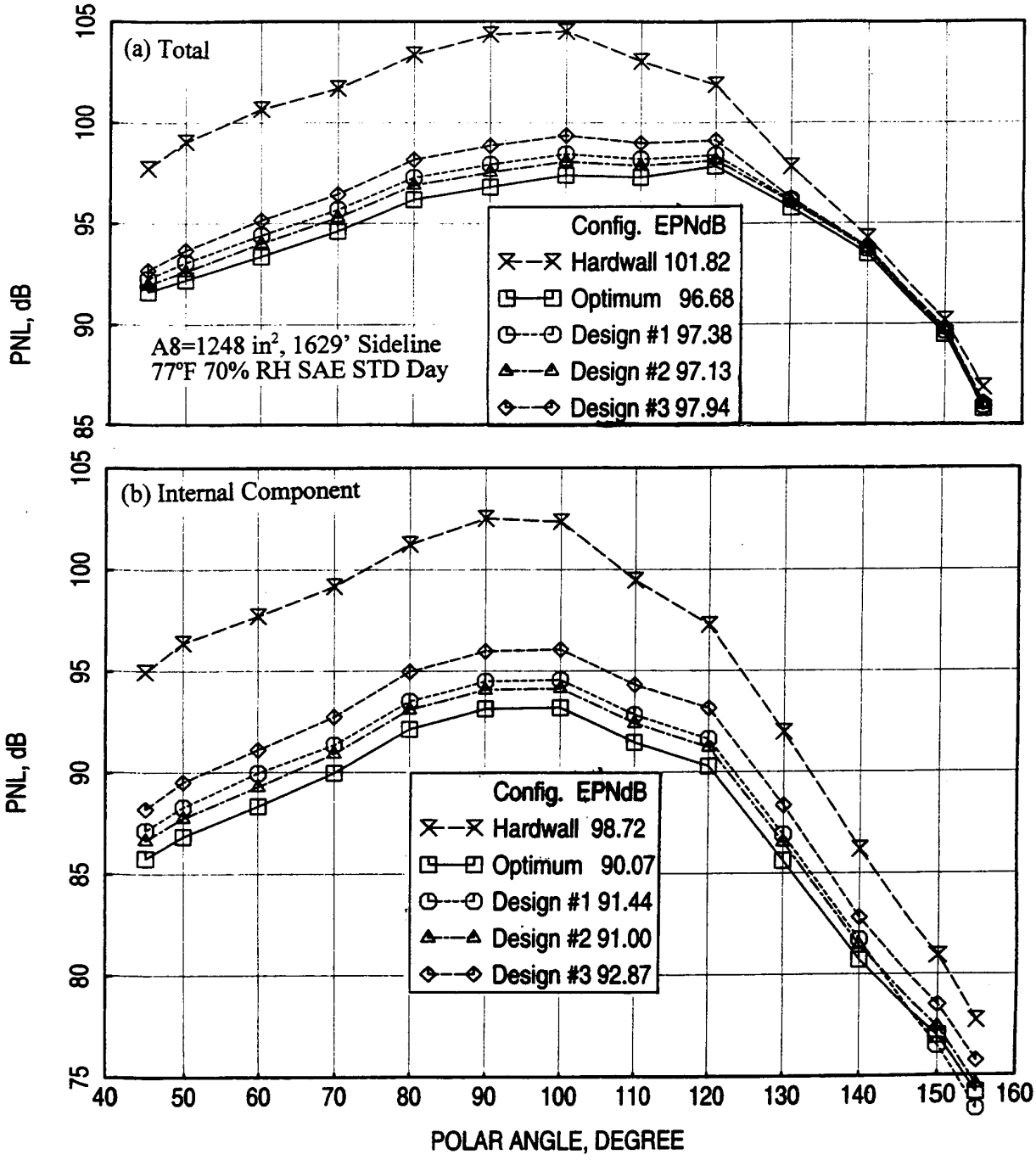

Figure 123. Comparison of predicted (a) total and (b) internal component of PNL directivities between optimum and three realistic liner designs for 1/7-scale mixer-ejector at takeoff condition, NPR=3.43, T8=1551°R, V_j=2359 ft/sec, M=0.32.

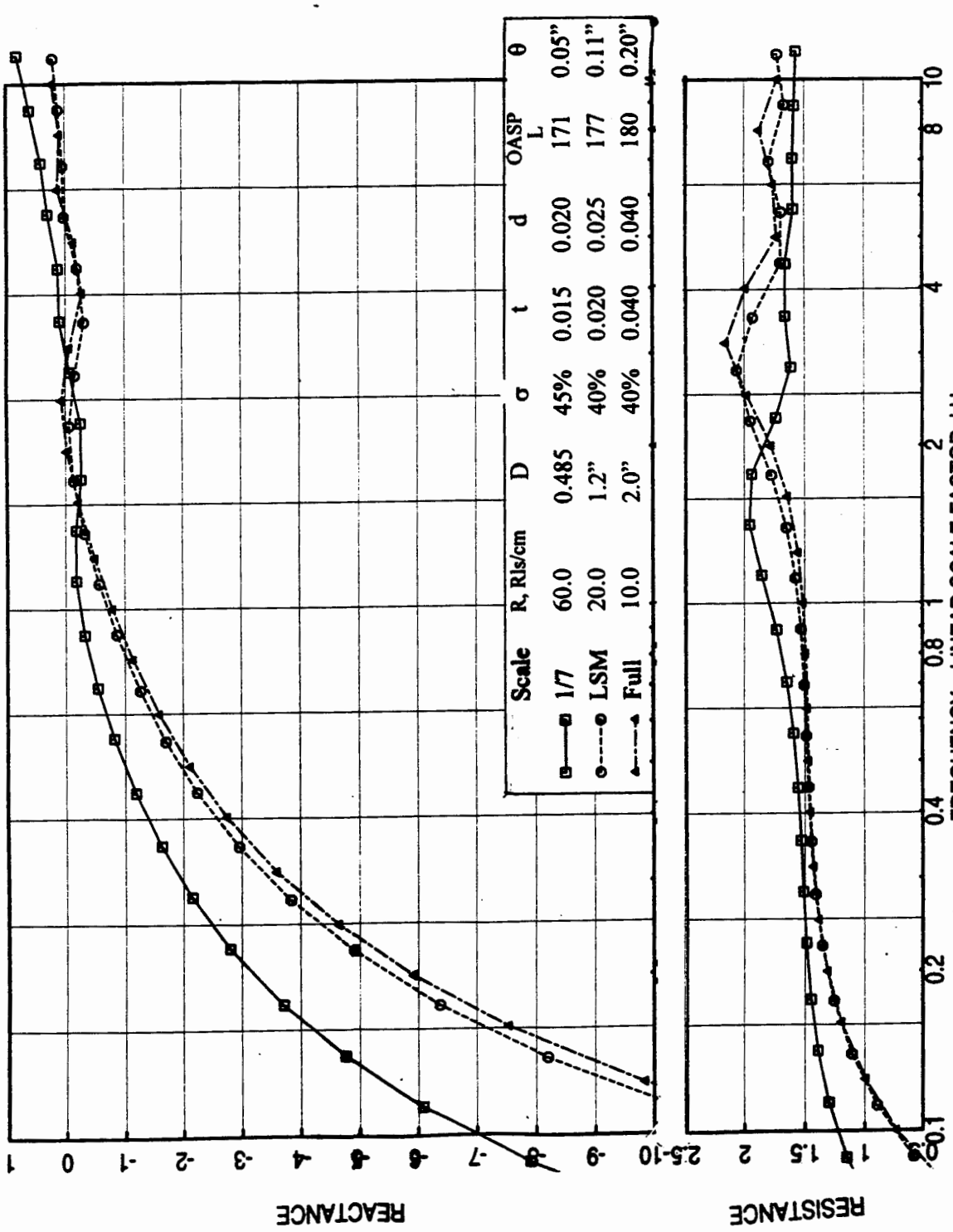

Figure 124. Comparison of predicted normal impedance for optimum liner designs with respect to normalized frequency between 1/7 scale, LSM, and full-scale mixer-ejectors at takeoff condition, T=500°F, M=0.8.

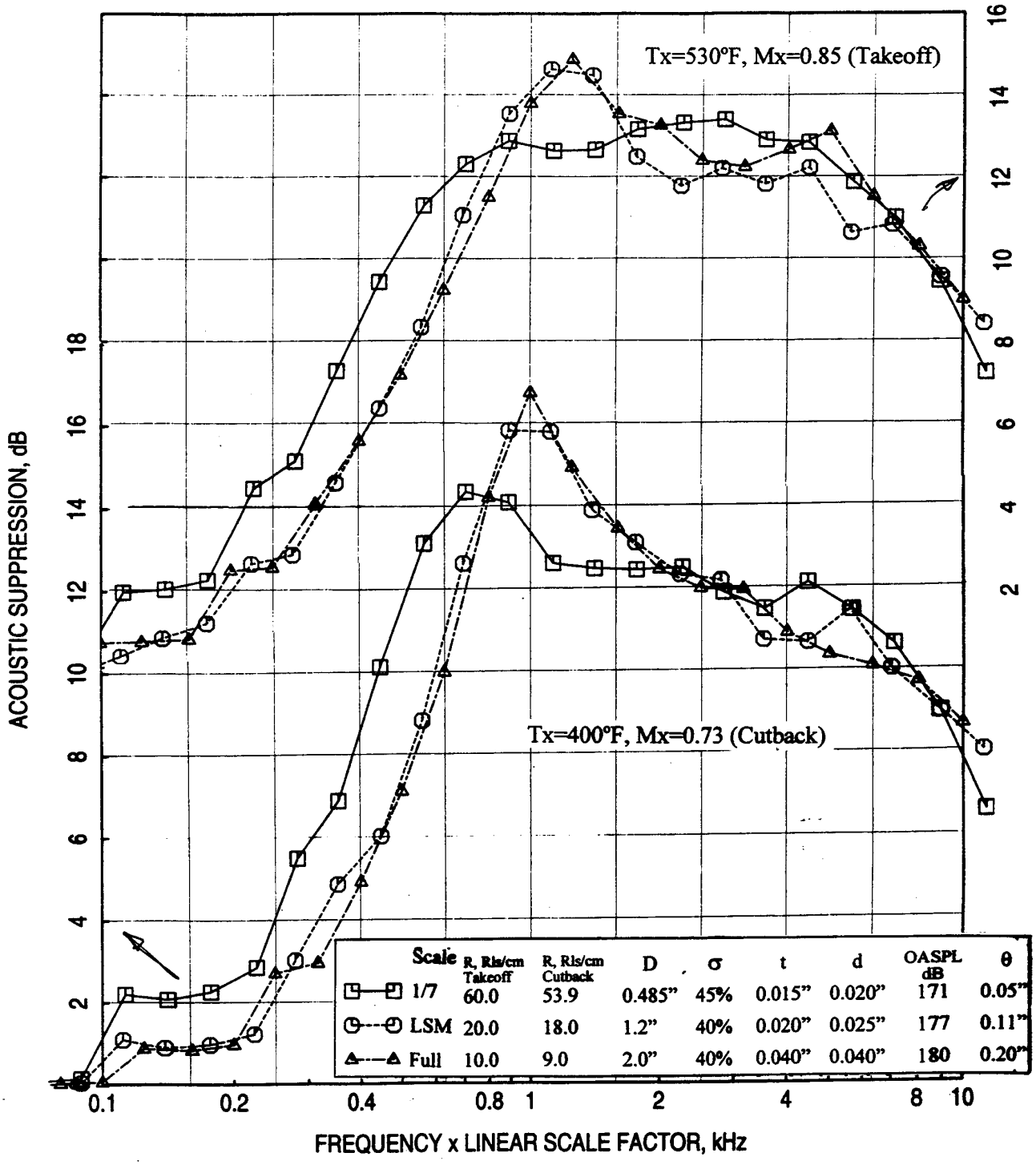

Figure 125. Comparison of predicted acoustic suppression for optimum liner designs with respect to normalized frequency between 1/7 scale, LSM, and full-scale mixer-ejectors.

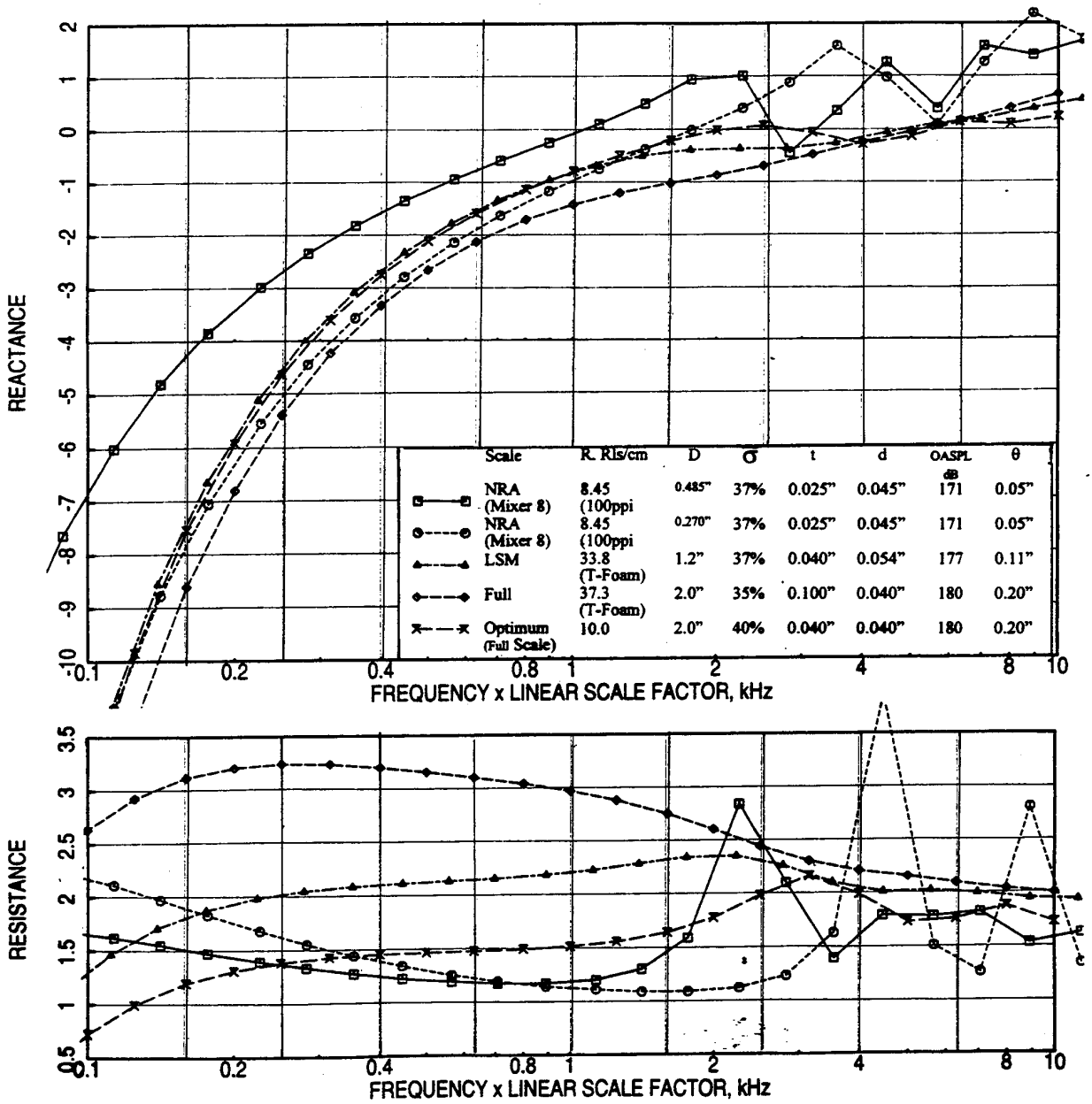

Figure 126. Comparison of predicted normal impedance with respect to normalized frequency between liner designs for 1/7 scale, LSM, and full-scale, and optimum liner design for full-scale mixer-ejectors at takeoff condition, T=500°F, M=0.8.

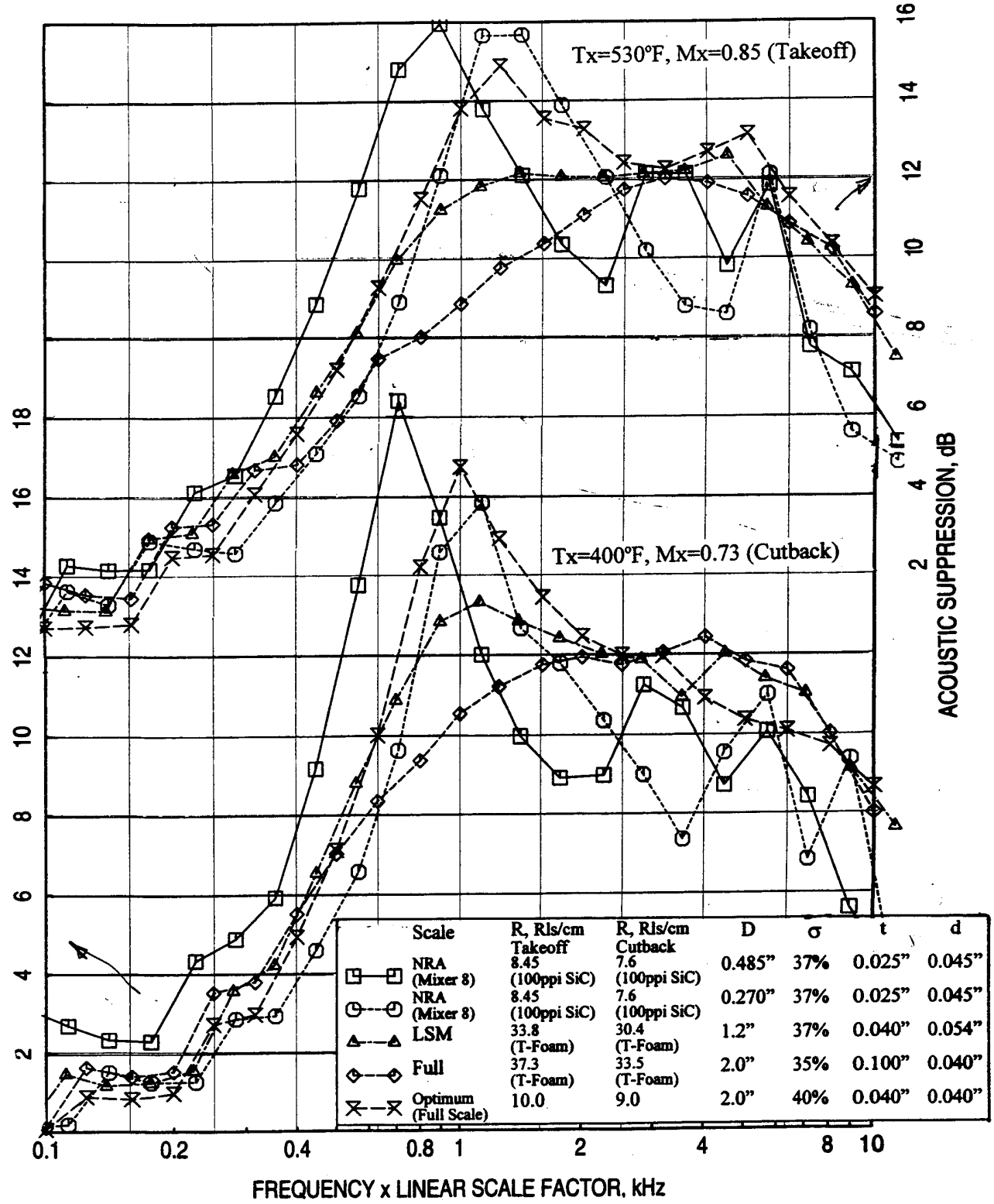

Figure 127. Comparison of predicted acoustic suppression with respect to normalized frequency between liner designs for 1/7 scale, LSM, and full-scale, and optimum liner design for full-scale mixer-ejectors.

Alternate Design #2 Liners: Figure 128 shows the normal impedance spectra for takeoff condition with respect to the frequency, multiplied with linear scale factor, (i.e., normalized frequency) for the full-scale optimum liner and the three alternate different scale liner designs. The resistance spectra for all three liners are very close to the optimum spectrum. The reactance spectrum for LSM and full-scale liners are close to the optimum spectrum. The 1/7-scale (termed as NRA with mixer 8) liner being deeper compared to its scale factor, the reactance spectrum is considerably shifted to the lower frequency compared to the optimum. The corresponding acoustic suppression spectra for takeoff and cutback conditions are shown in Figure 129. The acoustic suppression levels for LSM and full-scale liners are much closer to the optimum. The 1/7-scale acoustic suppression spectrum is shifted to the lower frequency compared to the optimum due to its depth not proportional to its scale factor.

The reasonable agreement of acoustic suppression and EPNL for all three mixer-ejectors with the optimum levels for the alternate liner designs is due to the appropriate bulk resistivity. Thus, it is important to seek suitable bulk materials for efficient liner designs

The predicted EPNL using the process described in section 5 for all the liner designs covering all three scales for takeoff and cutback conditions are listed in Table 1. Compared to the current liner design for 1/7-scale NRA model, tested in Cell 41, acoustic benefits of about 0.6 and 0.9 EPNdB are shown to be achievable at takeoff and cutback conditions for improved liner designs. It should be noted that the 1/7-scale liner depth is not proportional to its linear scale factor. Considering appropriate depth for 1/7-scale liner (i.e., 0.27") acoustic benefits of about 1.2 and 1.9 EPNdB are shown to be achievable at takeoff and cutback conditions.

7.6 Advantages of EPNL Prediction Process: The internal component of noise extraction process is based on Stone's noise prediction model (Ref. 5). This model is developed utilizing measured farfield acoustic data for a number of mixer-ejector configurations with different geometric and aerothermodynamic parameters. Thus, the internal noise component extracted by this method seems to be realistic.

The utilization of acoustic transfer factor to construct ΔPWL from predicted acoustic suppression minimizes uncertainties associated with acoustic suppression prediction, internal noise extraction process, and azimuthal variation of farfield noise. If such a factor is not used, instead the predicted acoustic suppression is assumed to be the ΔPWL for a liner design, the predicted EPNL would be much different from the results shown here and will depend on the number of modes and the assumptions utilized in the acoustic suppression prediction. As

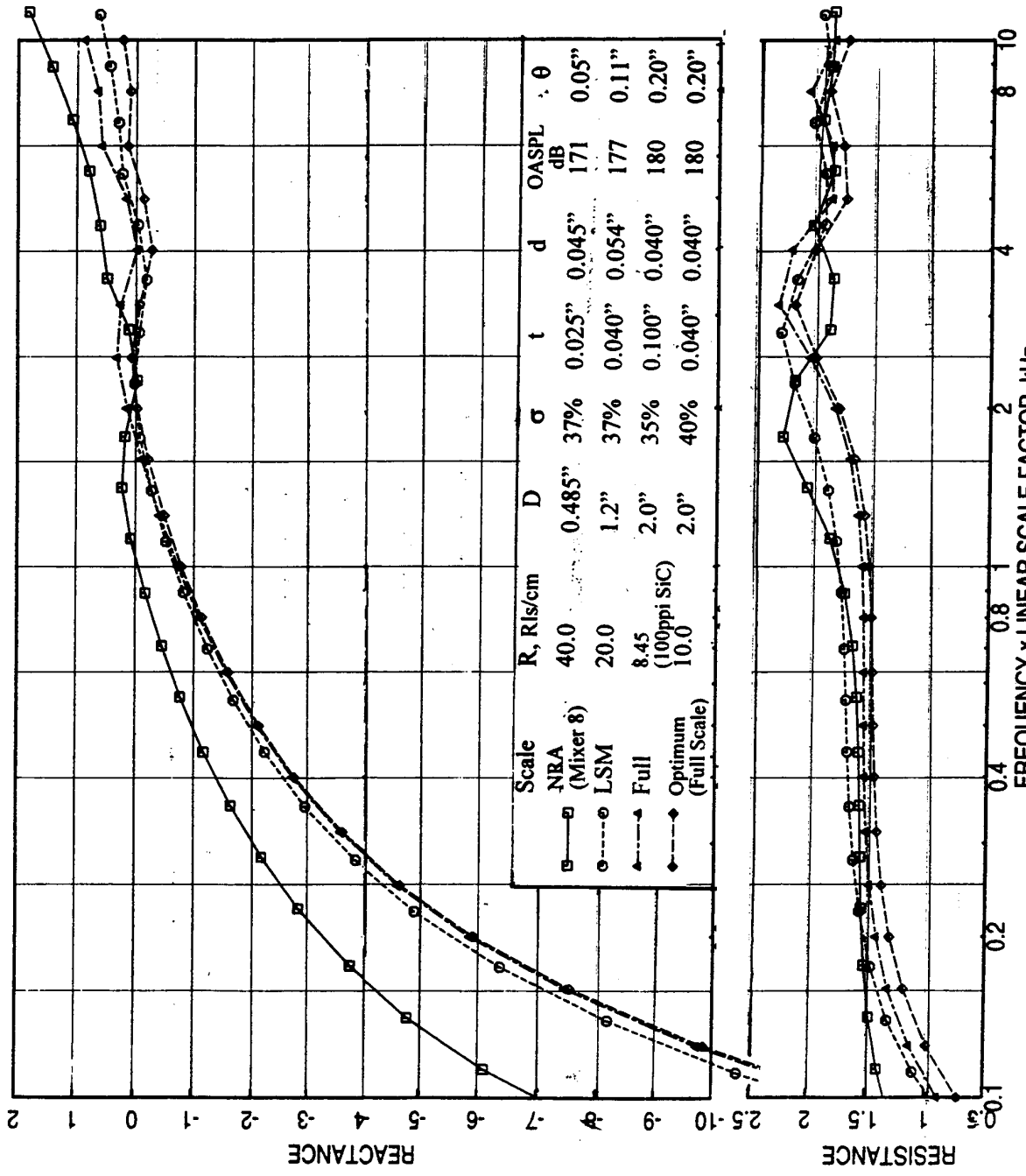

Figure 128. Comparison of predicted normal impedance with respect to normalized frequency between alternate liner designs for 1/7 scale, LSM, and full-scale, and optimum liner design for full-scale mixer-ejectors at takeoff condition, T=500°F, M=0.8.

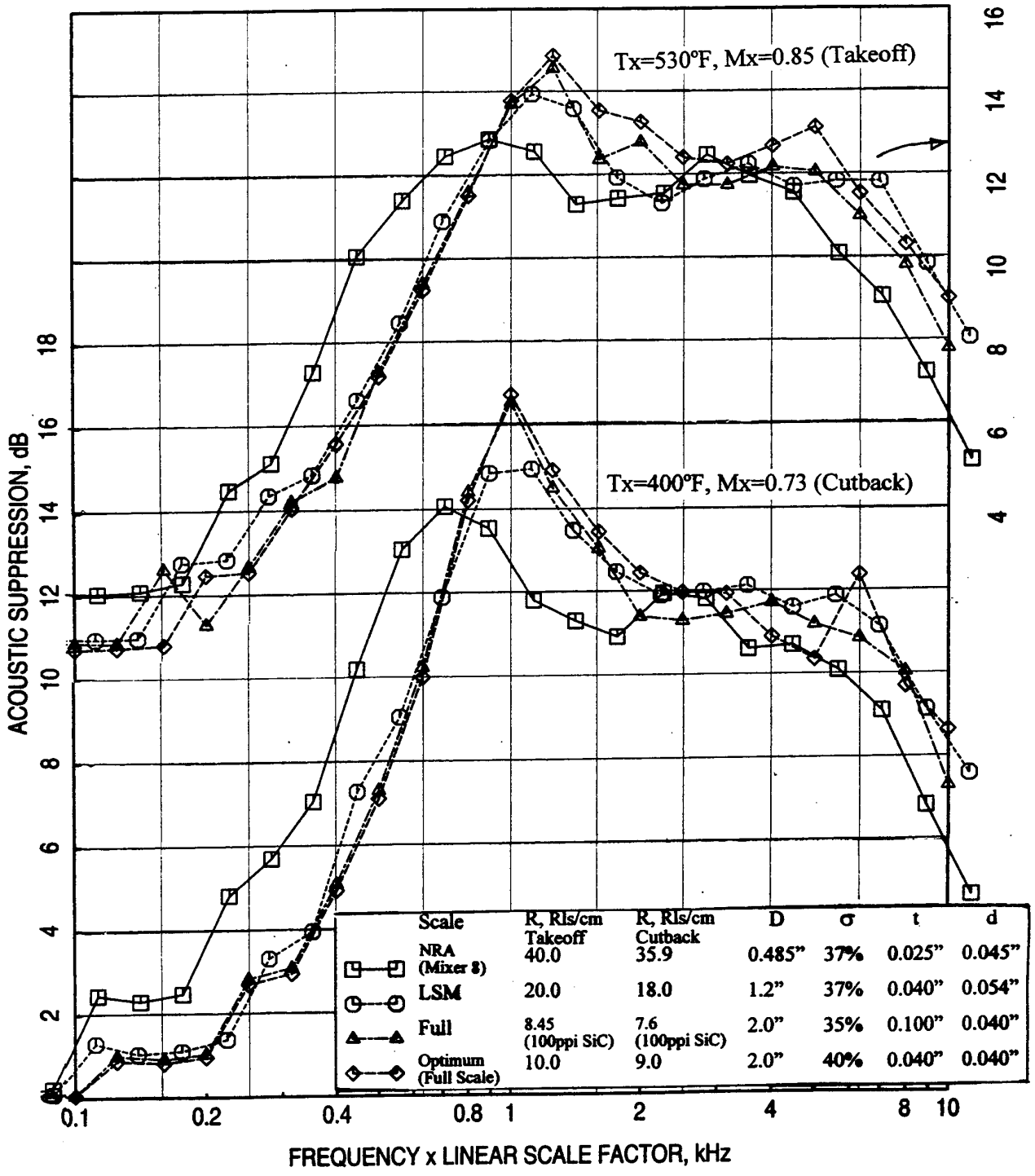

Figure 129. Comparison of predicted acoustic suppression with respect to normalized frequency between alternate liner designs for 1/7 scale, LSM, and full-scale, and optimum liner design for full-scale mixer-ejectors.

Table 1. Measured and predicted HSCT nozzle liner benefits in terms of EPNdB.

	Measured EPNdB for NRA Model with Mixer 8 & 160" Flap, Tested in Cell 41 $A_t/A_m = 8.0$ $A_{teff}/A_m = 6.5$	Projected Liner Attenuation, EPNdB											
Cutback Condition at Flyover at 1629', A8=1248 in^2													
	Hard wall	Treated	NRA with Mixer 8 $A_t/A_m = 8.0$, $A_{teff}/A_m = 6.5$				w/o Internal Noise	Full-Scale $A_t/A_m = 7.4$, $A_{teff}/A_m = 6.7$				LSM $A_t/A_m=7.4$, $A_{teff}/A_m=6.7$		
			Current Design #1 D=0.485"	Optimum Design D=0.485"	Design #2 D=0.485"	Design #3 D=0.27"		Ideal	Optimum Design D=2.0"	Design #1 D=2.0"	Design #2 D=2.0"	Optimum Design D=1.2"	Design #1 D=1.2"	Design #2 D=1.2"
Δ EPNL		-6.49	-6.49	-7.39	-6.83	-4.51	-13.28	-8.14	-6.37	-5.43	-6.37	-6.93	-6.49	-7.00
Total	96.31	89.82	89.82	88.92	89.48	91.18	83.03	88.17	89.94	90.88	89.94	89.38	89.82	89.31
External	84.85	83.03	83.03	83.03	83.03	83.03	83.03	83.03	83.03	83.03	83.03	83.03	83.03	83.03
Internal	94.90	87.27	87.27	86.07	86.75	89.08	0.00	83.83	87.51	88.64	87.51	86.85	87.34	86.68
Takeoff Condition at Sideline at 1629', A8=1248 in^2													
	Hard wall	Treated	NRA with Mixer 8 $A_t/A_m = 8.0$, $A_{teff}/A_m = 6.5$				w/o Internal Noise	Full-Scale $A_t/A_m = 7.4$, $A_{teff}/A_m = 6.7$				LSM $A_t/A_m=7.4$, $A_{teff}/A_m=6.7$		
			Current Design #1 D=0.485"	Optimum Design D=0.485"	Design #2 D=0.485"	Design #3 D=0.27"		Ideal	Optimum Design D=2.0"	Design #1 D=2.0"	Design #2 D=2.0"	Optimum Design D=1.2"	Design #1 D=1.2"	Design #2 D=1.2"
Δ EPNL		-4.44	-4.44	-5.14	-4.69	-3.88	-7.92	-5.67	-4.99	-4.37	-4.78	-5.03	-4.78	-4.85
Total	101.82	97.38	97.38	96.68	97.13	97.94	93.90	96.15	96.83	97.45	97.04	96.79	97.04	96.97
External	94.17	93.90	93.90	93.90	93.90	93.90	93.90	93.90	93.90	93.90	93.90	93.90	93.90	93.90
Internal	98.72	91.44	91.44	90.07	91.00	92.87	0.00	87.53	90.86	92.06	91.30	90.64	91.17	90.99

Note : External noise contains Merged & Premerged components

examples, PNL directivities and corresponding EPNL for three mixer-ejectors of different linear scale factor (i.e., full scale, LSM, and 1/7-scale) with one liner design for each are computed with and without utilizing the acoustic suppression transfer factor and are shown in Figures 130 through 132. For the current study, which utilizes 50 transverse modes with equal energy per mode type assumption, the farfield noise goes down significantly when the transfer factor is not used. Thus, acoustic benefit of about 1 EPNdB is observed for each configuration.

This aspect is further demonstrated with respect to the utilization of different number of modes contributing to the acoustic suppression prediction. Figure 133 shows the acoustic suppression spectra for different number of transverse modes used in the prediction. As expected, more acoustic suppression, especially at higher frequency range, is predicted with more number of modes. The PNL directivities and corresponding EPNL are computed for each of the acoustic suppression spectra of Figure 133 without using the transfer factor. The results are shown in Figures 134 and 135. Clearly, the EPNL reduces with increasing number of modes being used in acoustic suppression prediction. Thus, the use of acoustic suppression transfer factor is a better way to assess relative acoustic benefits of liner designs.

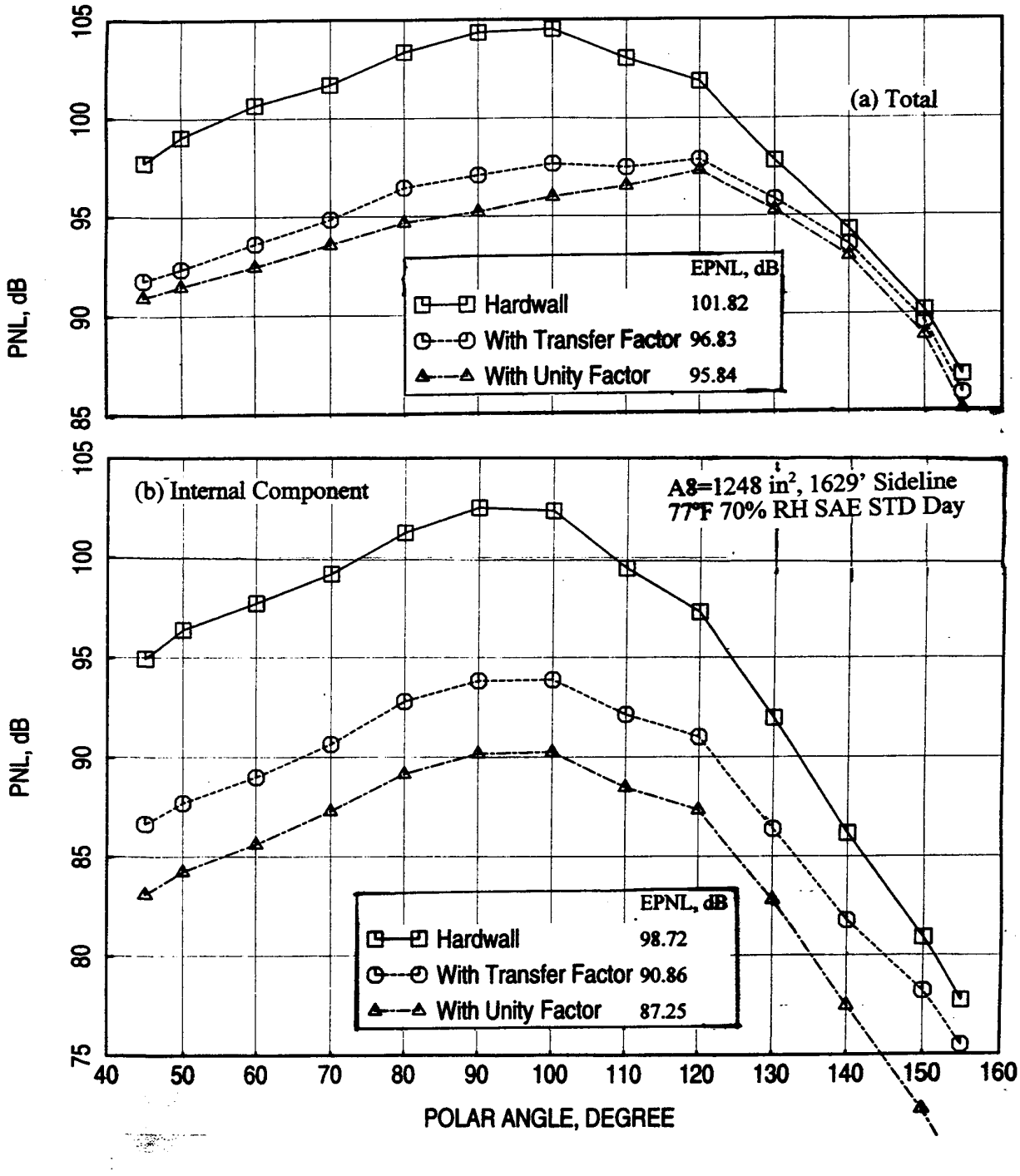

Figure 130. Effect of acoustic suppression transfer factor on predicted (a) total and (b) internal component of PNL directivities for the optimum liner design for full scale mixer-ejector at takeoff condition, NPR=3.43, T8=1551°R, V_j=2359 ft/sec, M=0.32.

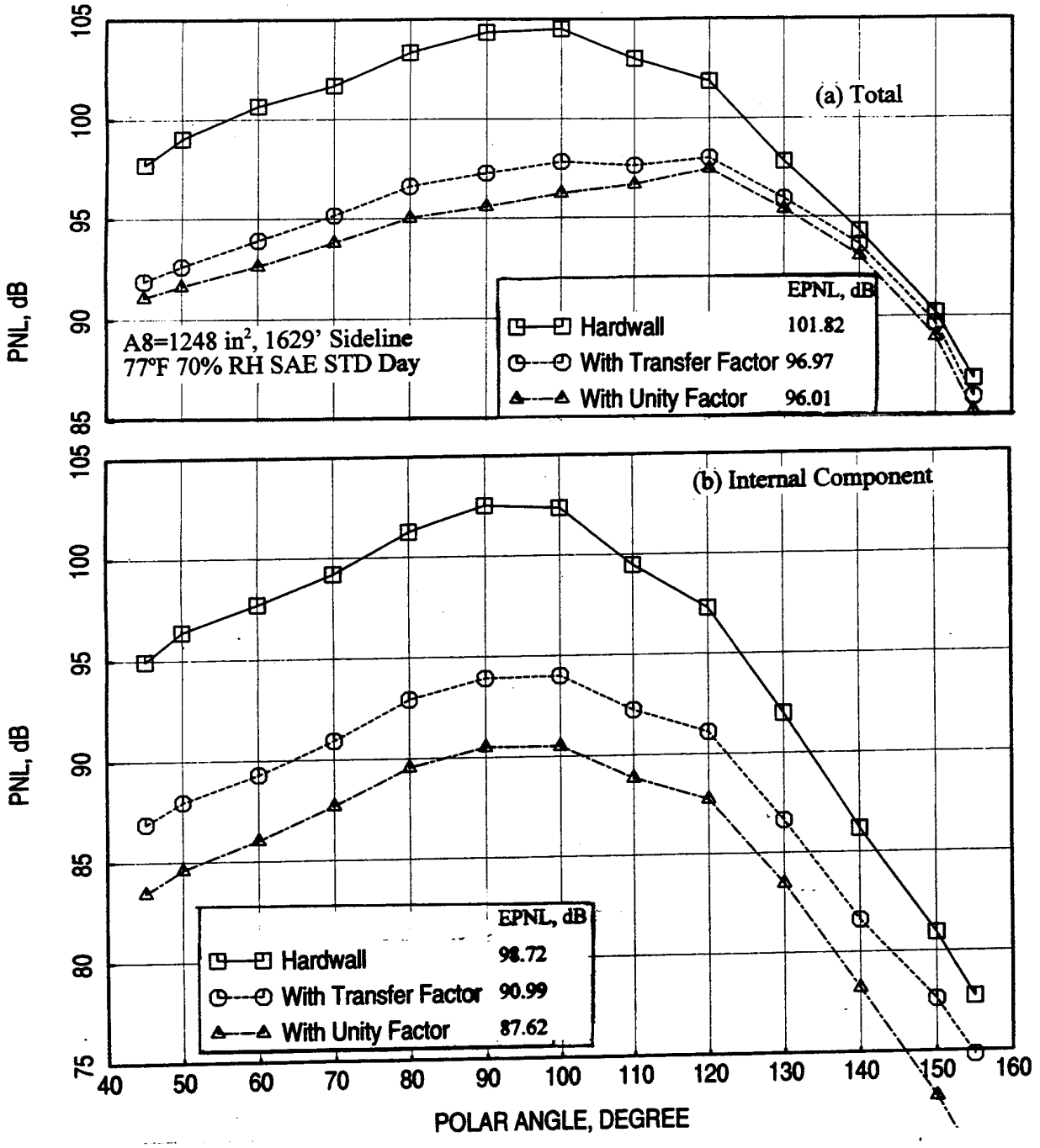

Figure 131. Effect of acoustic suppression transfer factor on predicted (a) total and (b) internal component of PNL directivities for the alternate liner design for LSM mixer-ejector at takeoff condition, NPR=3.43, T8=1551°R, V_j=2359 ft/sec, M=0.32.

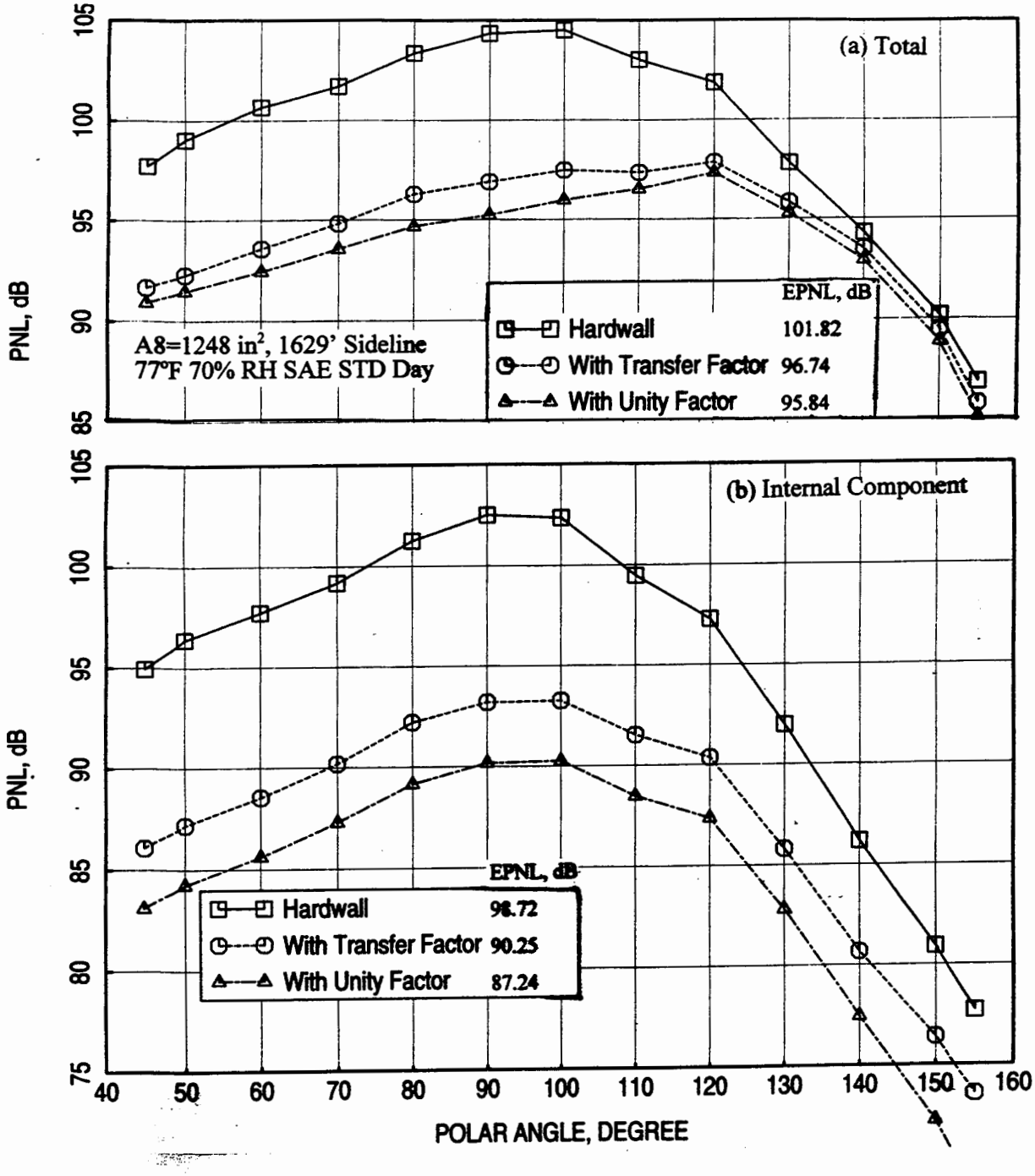

Figure 132. Effect of acoustic suppression transfer factor on predicted (a) total and (b) internal component of PNL directivities for the optimum liner design with bulk resistivity of 40 Rayls/cm for 1/7-scale mixer-ejector at takeoff condition, NPR=3.43, T8=1551°R, V_j=2359 ft/sec, M=0.32.

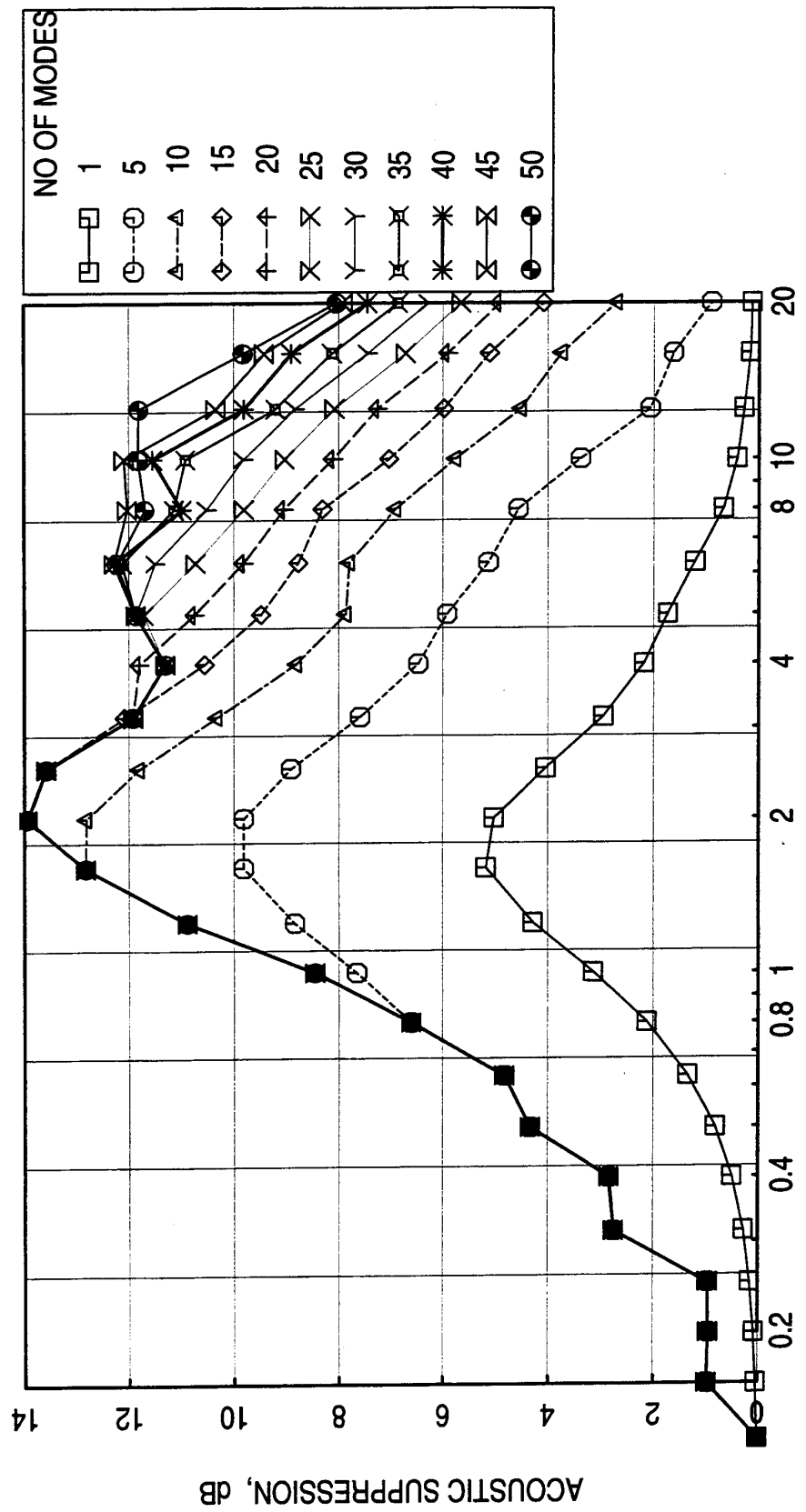

Figure 133. Predicted acoustic suppression spectra due to different number of transverse modes for the alternate LSM mixer-ejector liner design at takeoff condition, D=1.2", R=20 Rayls/cm, σ=37%, t=0.04", d=0.054", Tx=500°F, Mx=0.85, OASPL=177 dB.

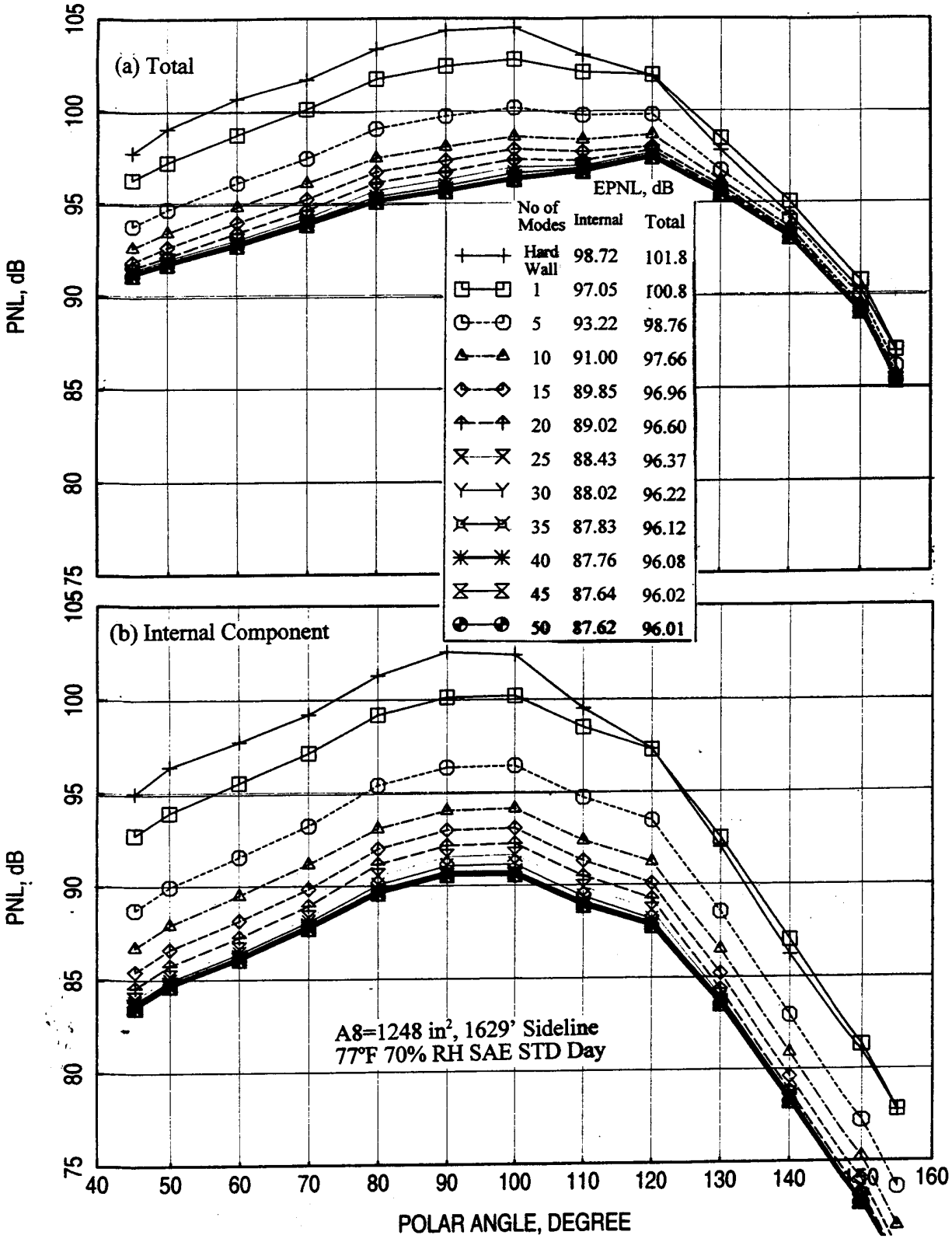

Figure 134. Predicted (a) total and (b) internal component of PNL directivities due to different number of transverse modes for the alternate liner design for LSM mixer-ejector at takeoff condition using unity acoustic suppression transfer factor, NPR=3.43, T8=1551°R, V_j=2359 ft/sec, M=0.32.

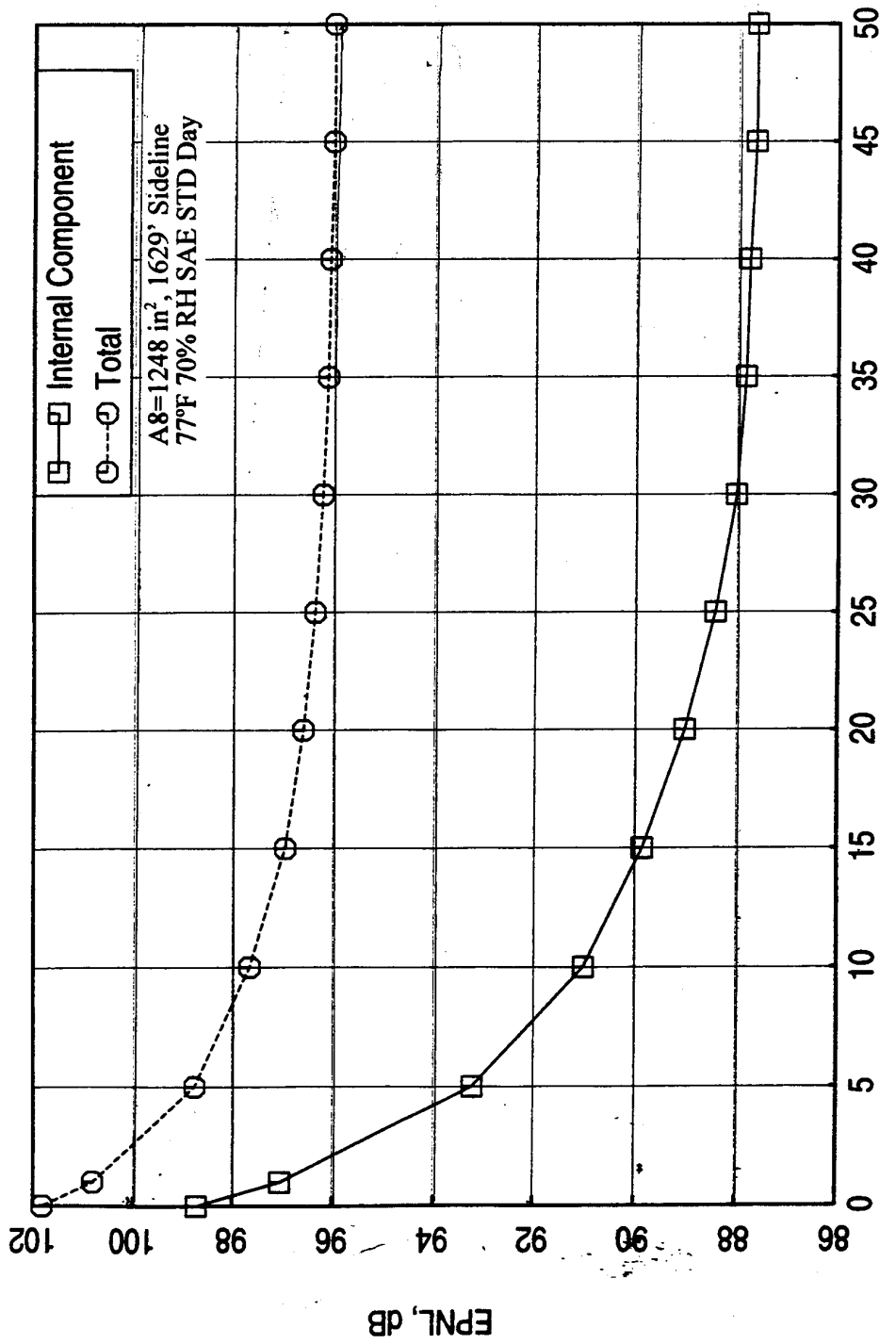

Figure 135. Predicted total and internal component of EPNL with respect to different number of transverse modes for the alternate liner design for LSM mixer-ejector at takeoff condition using unity acoustic suppression transfer factor, NPR=3.43, T8=1551°R, V_j=2359 ft/sec, M=0.32.

8.0 CONCLUDING REMARKS

Possible Inaccuracies and their Remedies: We have developed a process to predict noise field interior to the ejector and in the farfield for any liner design for a mixer-ejector of arbitrary scale factor. However, a number of assumptions, not verified for the current application, utilized in this process, introduce uncertainties in the final result, especially, on a quantitative basis.

The normal impedance model for bulk with perforated facesheet is based on homogeneous foam materials of low resistivity. The impact of flow conditions for HSCT application as well as the impact of perforated facesheet on predicted impedance is not properly accounted. Based on the measured normal impedance for deeper bulk samples (i.e., 2.0") the predicted reactance is much higher compared to the data at frequencies above 2 kHz for T-foam and 200 ppi SiC. The resistance is under predicted at lower frequencies (below 4 kHz) for these samples. Thus, the use of such predicted data in acoustic suppression is likely to introduce inaccuracies. It should be noted that the impedance prediction methods developed recently under liner technology program are not utilized in the studies described in this report due to the program closeout.

Acoustic suppression prediction is based on the uniform flow and temperature conditions in a two-sided treated constant area rectangular duct. In addition, assumptions of equal energy per mode noise field and interaction of all frequencies with the treated surface for the entire ejector length may not be accurate. While, the use of acoustic transfer factor minimizes the inaccuracies associated with the prediction for a known test case, the assumption of the same factor for other liner designs and with different linear scale factor ejectors seems to be very optimistic. As illustrated in appendix D that the predicted noise suppression for LSM-1 is lower compared to the measured data is an indication of the above argument. However, the process seems to be more reliable when used for the same scale models for different liner designs as demonstrated for Gen. 1 mixer-ejectors.

Thus, it is premature to conclude the current results as the final acoustic benefits of the liner designs. These results should be utilized to evaluate relative merits of a design in a qualitative basis. The quantitative evaluation should be made on the basis of more realistic validated prediction models, which are currently being completed under the liner technology program. In addition, LSM-1 test results would have resolved the scaling issues, that, whether the relative EPNL evaluation from 1/7-scale data to LSM or full-scale is appropriate. However, due to a number of discrepancies in LSM-1 tests, not compatible

with the 1/7-scale model tests, prevents resolving the scaling issues. Proposed LSM-2 tests, when conducted, would help to resolve the issues not currently being answered.

Following steps are needed to improve the liner design methodology:

- Normal impedance modeling and correlation between acoustic suppression with normal impedance utilizing measured data, acquired under HSR and CPC programs, need to be utilized in the design methodology process.

- The current modal analysis assumes the interaction of all frequencies with the treated flaps for their entire length. However, an axial source distribution inside the ejector may be a more realistic assumption for acoustic suppression prediction. Interaction of noise field with the length of the treated flaps will be assumed to be longer for higher frequency noise compared to those of lower frequencies.

- The assumption of equivalent flap length to account for the sidewall treatment effect may not be a true representation of the four-sided treated ejectors. Results presented in reference 3 for 1/7-scale model tests with flap only and sidewall only treatments indicate that the above assumption may be realistic.

- Proposed LSM Build-2 needs to be tested to obtain better understanding of the liner scaling. This is a very important aspect for full-scale liner designs

The internal component of EPNL for different liner designs, as listed in Table 1, are significant compared to the external component. In fact, for cutback, the internal component of EPNL is higher compared to the external component. Thus, we have to find ways to reduce the internal noise component substantially to eliminate its impact on total EPNL. The internal noise component for different liner designs can be predicted more accurately using more accurate prediction methods as described above. These predictions may result in a lower level of internal noise component for a liner design compared to the current values. This will be reflected in terms of a lower EPNL. However, we need to redesign the liners with more innovative concepts, if the accurately predicted internal noise levels do not show much acoustic benefits. All these efforts are possible when the HSCT program will begin again in the near future.

APPENDIX A

EPNLPROCESS - LINER DESIGN METHODOLOGY COMPUTER CODE

Liner design methodology consists of a physical design of a liner and prediction of noise in the farfield for a mixer-ejector treated with the liner. Physical design of a liner requires dimensions (depth D, Facesheet Properties: Thickness t, Porosity σ, and Hole Diameter d) and measurable acoustic properties (Resistivity of the bulk, DC flow resistance parameters for linear facesheet) of liner components. Noise prediction includes the prediction of normal impedance, acoustic suppression in the ejector, and farfield noise utilizing the predicted acoustic suppression and extracted farfield noise components from measured hardwall and treated mixer-ejector configurations. In summary following input parameters are required for noise prediction;

- Normal Impedance Prediction
    - Liner Depth
    - Bulk Resistivity
    - Facesheet Parameters
        - Porosity, Thickness, and Hole Diameter for perforated facesheet
        - DC flow resistance for linear facesheet
    - Grazing Flow Mach Number
    - Static Pressure & Temperature
    - Boundary-layer Parameters
    - Dynamic Pressure
- Acoustic Suppression Prediction using Modal Analysis
    - Liner Normal Impedance
    - Ejector Dimensions
        - Equivalent Treatment Length
        - Ejector Width
        - Average Ejector Height
    - Average Ejector Flow Mach Number
    - Average Ejector Pressure & Temperature
    - Boundary-layer Parameters
    - Number of Transverse Modes
- Farfield Noise Prediction
    - Acoustic Suppression
    - Flight Velocity
    - Internal Noise Data for Hardwall Reference Case
    - Internal Noise Data for Treated Reference Case
    - External Noise Data for Treated Reference Case
    - Frequency Factor $\gamma(f)$

A.1 Definition of Input Parameters: Detail steps for each operation is described in various sections of this report. Utilizing these steps a computer code, named EPNLPRCESS is developed. The main program calls various subroutines to predict normal impedance, acoustic suppression, and acoustic parameters, like, PWL, OASPL, PNL, EPNL, etc. The input is fed to the main program using a namelist format file. The definition of the inputs is included in the source program and is listed below;

```
c Main Program Title: EPNLPROCESS
c
c Main Program Purpose:
c
c     CALCULATES NORMAL IMPEDANCE OF LINER
C     COMPUTES ACOUSTIC SUPPRESSION SPECTRUM IN THE EJECTOR
C     CALCULATES INTERNAL, EXTERNAL,AND TOTAL NOISE COMPONENT FOR THE
C     COMPUTED ACOUSTIC SUPPRESSION SPECTRA
c     CALCULATES PNL, PNLT, OASPL, AND EPNL FOR INTERNAL, EXTERNAL, AND
C     TOTAL NOISE COMPONENTS
c
c General Input Description:
c
c     A FILE CONTAINING THE FOLLOWING:
c
c         THE MAIN $EPROC CONTROL NAMELIST PROVIDING RUN OPTIONS,
c         PARAMETERS, AND DATA INPUT & OUTPUT FILENAMES.
c         THIS MUST BE THE FIRST NAMELIST IN THE FILE.
c
c         A NAMELIST TO RUN THE SELECTED IMPEDANCE PREDICTION (IF NOT
C         USING AN IMPEDANCE INPUT FILE). EACH IMPEDANCE PREDICTION
C         ROUTINE HAS A RELATED NAMELIST USED TO PROVIDE DATA AND OPTIONS.
c
c         A $ILOSS NAMELIST TO RUN THE INSERTION LOSS (SUPPRESSION)
C         PREDICTION.
c         THIS MUST BE THE LAST NAMELIST IN THE FILE.
c
c       SEE THE NAMELIST DEFINITIONS IN THE PROGRAM FOR DETAILS.
c
c General Output Description:
c
c     A NEW TREATED CONFIG OUTPUT FILE CONTAINING:
c        INTERNAL SPL & PWL DATA
c        TOTAL SPL & PWL DATA
c        SUMMARY DATA FOR OASPL, PNL, PNLT, & EPNL
c
c       If INDX = 0, A HARDWALL REFERENCE OUTPUT FILE CONTAINING:
c       SUMMARY DATA FOR OASPL, PNL, PNLT, & EPNL
C
C-------------------------------------------------------------------------
C  Namelist $EPROC definitions:
C
C     ITEST       = 0 : TEST CASE,  1 : DESIGN CASE
C     IPRINT      = DIAGNOSTIC OUTPUT FLAG: 0 = N0, 1 = YES
C     NANG        = NUMBER OF ANGLES IN THE INPUT DATA FILES.
```

```
C     NFREQ       = NUMBER OF FREQUENCIES IN THE INPUT DATA FILES -
C                   Starting at 50Hz.
C     DIST        = SIDELINE DISTANCE OF INPUT DATA, FT.
C     FLTVEL      = A/C FLIGHT VELOCITY, FPS. FOR EPNL CALCULATIONS.
C     ICON        = CONFIGURATION IDENTIFIER.
C     HWREFINT    = INTERNAL SPL & PWL FILE FOR REFERENCE HARDWALL CONFIG
C                  (INPUT)
C     TRTREFINT   = INTERNAL SPL & PWL FILE FOR REFERENCE TREATED CONFIG
C                   (INPUT)
C     TRTREFEXT   = EXTERNAL SPL & PWL FILE FOR REFERENCE TREATED CONFIG
C                   (INPUT)
C     REFILSCOEFF = DELTAPWL/ILS COEFFICIENTS FILE FOR REFERENCE CONFIGS
C                   (INPUT)
C     PPANEL      = PANEL TYPE FOR IMPEDANCE PREDICTION:
C
C                       'SDOF_WM' - SDOF WITH WIRE MESH FACE SHEET
C                       'SDOF_PP' - SDIF WITH PERFORATED PLATE FACE SHEET
C                       'BULK   ' - BULK ABSORBER WITHOUT A FACE SHEET
C                       'BULK_WM' - BULK ABSORBER WITH WIRE MESH FACE SHEET
C                       'BULK_PP' - BULK ABSORBER WITH PERFORATED PLATE
C                                   FACE SHEET
C                       'AABULK ' - PREDICT IMPEDANCE USING RICE ROUTINE.
C
C      NOTES:   Each PPANEL type/method uses a namelist with the same name
C              (eg: $SDOF_WM) to provide data and panel options for the
C               selected impedance  prediction.  These namelists are in
C               the same control file (code 20) as the $EPROC namelist.
C
C              You MUST leave PPANEL blank if using a file (IMPDFL) to
C              input the impedance values for the suppression calculation.
C
C
C     TPSFRQ      = TREATMENT PANEL (PPANEL) 1/3 OB STARTING FREQUENCY, Hz
C
C     INDX        = FLAG FOR INPUT OF HARDWALL CONFIGURATION DATA
C                   0 = INPUT HARDWALL DATA
C                   1 = NO HARDWALL DATA
C     FOR BOTH INDX CASES FOLLOWING INPUT FILES ARE NECESSARY
C     HWREFINT    = INTERNAL SPL & PWL FILE FOR REFERENCE HARDWALL
C     TRTREFINT   = INTERNAL SPL & PWL FILE FOR REFERENCE TREATED
C     TRTREFEXT   = EXTERNAL SPL & PWL FILE FOR REFERENCE TREATED
C     REFILSCOEFF = FREQUENCY FACTOR FILE FOR NEW TREATED CONFIGURATION
C                   INPUT IF ITEST=1, OUTPUT IF ITEST=0

C     TRTOUTPUT   = NEW (ITEST=1) OR REFERNCE (ITEST=0) TREATED CONFIG
C                   OUTPUT FILE, contains:
C                     INTERNAL SPL & PWL
C                     TOTAL SPL & PWL
C                     SUMMARY CALCULATIONS OASPL, PNL, PNLT, EPNL
C
C     IF INDX=0 FOLLOWING HARDWALL REFERENCE INFORMATION REQUIRED
C     IRDG        = HARDWALL CONFIGURATION IDENTIFIER
C     HWREFTOTAL  = TOTAL SPL & PWL FILE FOR REFERENCE HARDWALL
C                   CONFIG(INPUT)
C     HWREFEXT    = EXTERNAL SPL & PWL FILE FOR REFERENCE HARDWALL CONFIG
C                   (INPUT)
```

```
C     HWOUTPUT     = TOTAL, INTERNAL, & EXTERNAL SUMMARY FILE FOR HARDWALL
C                    CONFIG (OUTPUT)
C     IMPDFL       = FILE USED TO INPUT TREATMENT PANEL IMPDENCE
C                    (FREQUENCY, RESISTANCE, & REACTANCE)VALUES INSTEAD OF
C                    USING ONE OF THE PREDICTION METHODS DEFINED BY THE
C                    PPANEL INPUT ABOVE.
C                    THE FILE MUST CONTAIN 3 COLUMNS OF DATA WITH NO EADER:
C                    FREQUENCY, RESISTANCE, REACTANCE AND HAVE AT LEAST
C                    'NFREQ' NUMBER OF FREQUENCIES (ROWS) OF DATA.
C                              ~~~~~
C       You can leave IMPDFL blank if using one of the PPANEL predictions.
C
C  Namelist $SDOF_WM definitions:
C
C     R100     =  DC FLOW RESISTANCE AT 100CM/SEC (CGS RAYLS) AT GRAZING
C                 FLOW TEMPERAURE
C     NLF      =  NONLINEAR FACTOR AT 150CM/SEC BY 20CM/SEC
C     XMBYRC   =  MASS REACXTANCE
C     DCV      =  DEPTH OF LINER CAVITY (IN)
C     RHO      =  DENSITY (G/CM^3)
C     TDF      =  TEMPERATURE (DEGREE F)
C     SPL      =  SOUND PRESSURE LEVEL IN EACH FREQUENCY BIN (DB)
C
C  Namelist $SDOF_PP definitions:
C
C     DCV      =  DEPTH OF LINER CAVITY (IN)
C     SIGMA    =  FACESHEET POROSITY
C     THK      =  FACESHEET THICKNESS (IN)
C     DMTR     =  FACESHEET HOLE DIAMETER (IN)
C     CDCH     =  FACESHEET HOLE (ORIFICE) DISCHARGE COEFFICIENT
C     MACH     =  FLOW MACH NUMBER OVER FACESHEET
C     BLT      =  BOUNDARY LAYER DISPLACEMENT THICKNESS (IN)
C     RHO      =  DENSITY (G/CM^3)
C     TDF      =  TEMPERATURE (DEGREE F)
C     SPL      =  SOUND PRESSURE LEVEL IN EACH FREQUENCY BIN (DB)
C
C  Namelist $BULK definitions:
C
C     RSTV     =  BULK B/A RESISTIVITY (CGS RAYLS/CM)AT GRAZING FLOW
C                 TEMPERAURE
C     DCV      =  DEPTH OF LINER CAVITY (IN)
C     RHO      =  DENSITY (G/CM^3)
C     TDF      =  TEMPERATURE (DEGREE F)
C     SPL      =  SOUND PRESSURE LEVEL IN EACH FREQUENCY BIN (DB)
C
C  Namelist $BULK_WM definitions:
C
C     RSTV     =  BULK B/A RESISTIVITY (CGS RAYLS/CM)AT GRAZING FLOW
C                 TEMPERAURE
C     R100     =  DC FLOW RESISTANCE AT 100CM/SEC (CGS RAYLS)
C     NLF      =  NONLINEAR FACTOR AT 150CM/SEC BY 20CM/SEC
C     DCV      =  DEPTH OF LINER CAVITY (IN)
C     RHO      =  DENSITY (G/CM^3)
C     TDF      =  TEMPERATURE (DEGREE F)
C     SPL      =  SOUND PRESSURE LEVEL IN EACH FREQUENCY BIN (DB)

C  Namelist $BULK_PP definitions:
```

```
C
C     RSTV     =  BULK B/A RESISTIVITY (CGS RAYLS/CM)AT GRAZING FLOW
C                 TEMPERAURE
C     DCV      =  DEPTH OF LINER CAVITY (IN)
C     SIGMA    =  FACESHEET POROSITY
C     THK      =  FACESHEET THICKNESS (IN)
C     DMTR     =  FACESHEET HOLE DIAMETER (IN)
C     CDCH     =  FACESHEET HOLE (ORIFICE) DISCHARGE COEFFICIENT
C     MACH     =  FLOW MACH NUMBER OVER FACESHEET
C     BLT      =  BOUNDARY LAYER DISPLACEMENT THICKNESS (IN)
C     RHO      =  DENSITY (G/CM^3)
C     TDF      =  TEMPERATURE (DEGREE F)
C     SPL      =  SOUND PRESSURE LEVEL IN EACH FREQUENCY BIN (DB)
C
C  Namelist $AABULK definitions:
C
C     IBULK    = 1 = SILICON CARBIDE
C                2 = T-FOAM
C                3 = FELTMETAL MATERIAL
C     IFACE    = 0 = NO FACE SHEET
C                1 = PERFORATE FACESHEET
C                2 = LINEAR FACESHEET
C     FMACH    = STEADY GRAZING FLOW MACH NUMBER
C     BLDIS    = BOUNDARY LAYER DISPLACEMENT THICKNESS, INCHES
C     DEPINCH  = DEPTH OF FOAM, INCHES
C     TFARH    = TEMPERATURE, DEGREES FARENHEIT
C     PSIA     = PRESSURE, PSIA
C     OASPL    = OVERALL SOUND PRESSURE LEVEL, DECIBELS
C     RESB0    = STEADY FLOW IMPEDANCE/(RHO*C) FOR LOW INCIDENT VELOCITY,
C                /INCH AT AMBIENT TEMPERATURE
C     RESB100  = STEADY FLOW IMPEDANCE/(RHO*C) AT 100 CM/SEC INCIDENT
C                VELOCITY, /INCH AT AMBIENT TEMPERATURE
C     SIGPERF  = PERFORATED PLATE OPEN AREA RATIO
C     THKPERF  = PERFORATED PLATE THICKNESS, INCHES
C     DIAMPERF = PERFORATED PLATE HOLE DIAMETER, INCHES
C     RESLF0   = LINEAR FACESHEET STEADY FLOW IMPEDANCE/(RHO*C) FOR LOW
C                INCIDENT VELOCITY
C     RESLF100 = LINEAR FACESHEET STEADY FLOW IMPEDANCE/(RHO*C) AT 100
C                CM/SEC INCIDENT VELOCITY
C     POROS    = POROSITY OF BULK MATERIAL
C
C  Namelist $ILOSS definitions:
C
C     XL       =  HEIGHT OF THE RECTANGULAR DUCT (IN)
C     YL       =  WIDTH OF THE RECTANGULAR DUCT (IN)
C     ZL       =  LENGTH OF THE RECTANGULAR DUCT (IN)
C     NDS      =  NUMBER OF INTERPOLATION STEP SIZES
C     DSARRAY  =  NDS NUMBER OF INTERPOLATION STEP SIZES
C     MZU      =  MACH NUMBER IN AXIAL (Z-) DIRECTION OF RECTANGULAR DUCT
C     FTR      =  FLUID TEMPERATURE (DEGREE R)
C     NSIDE    =  NUMBER OF TREATED SIDES:
C                   1 - ONE SIDE LINED
C                   2 - OPPOSITE TWO SIDES LINED
C    IPRTSUMS = DIAGNOSTIC OUTPUT FROM INSLOSS SUBROUTINE: 0 = NO, 1 = YES
```

A.2 Procedure to Predict Liner Performance and Effectiveness: To predict acoustic characteristics of a treated ejector, farfield measured acoustic data for the mixer-ejector with hardwall and with a treated configuration at the desired aerothermodynamic conditions is required. Utilizing the measured farfield sound pressure level (SPL) spectral data for these two configurations the internal and external SPL spectra are evaluated. The internal SPL for hardwall (`HWREFINT.dat`) and internal (`TRTREFINT.dat`) and external (`TRTREFEXT.dat`) SPL for treated configurations are then used as input to the computer code to evaluate the acoustic characteristics of treated ejector with any other arbitrary liner designs. The code is first utilized for the tested treated configuration (ITEST=0) using the above-mentioned SPL spectral data and the liner specifications as input to evaluate the frequency factor $\gamma(f)$ spectrum (`REFILSCOEFF.dat`). Then, the acoustic characteristics of treated ejectors of different liner designs (ITEST=1) for the same aerothermodynamic conditions are evaluated using the above-mentioned three SPL spectra, the evaluated frequency factor $\gamma(f)$ spectrum, and the liner specifications as input. Typical example of both these operations are described below.

Prediction of acoustic suppression undergoes an iterative process utilizing a step size (DSARRAY) for each frequency. Some time the the function does not converge due to numerical instability. This is usually overcome by changing the DSARRAY step size. The current code has the provision to input a maximum of 10 DSARRAY values (NDS). If the function does not converge after using all the prescribed step sizes the suppression for this frequency is evaluated by interpolating the data for the adjacent frequencies. The user can run the program again by selecting different DSARRAY values if not satisfied with the interpolated result.

A.3 Data Contained in HWREFINT = 'HWREFINT.dat'

FLIGHT TRANSFORMED, SCALED, AND EXTRAPOLATED SOUND PRESS
77.0 DEG. F., 70 PERCENT R.H. STD. DAY, SAE 1629.0

IDENTIFICATION - 2683/ 311 goldn1

ANGLES MEASURED FROM INLET, DEGREES

FREQ	45.0	50.0	60.0	70.0	80.0	90.0	100.0	110.0	120.0	130.0	140.0	150.0	155.0	PWL
50.0	45.6	45.9	46.3	46.7	49.0	51.6	52.1	48.3	47.6	44.0	40.6	38.9	37.5	123.1
63.0	47.6	47.9	48.3	48.7	51.0	53.6	54.1	50.3	49.6	46.0	42.6	40.9	39.5	125.1
79.0	49.6	49.9	50.3	50.7	53.0	55.6	56.1	52.3	51.6	48.0	44.6	42.9	41.5	127.2
100.0	51.6	51.9	52.3	52.7	55.0	57.6	58.1	54.3	53.6	50.0	46.6	44.9	43.5	129.3
125.0	53.5	53.8	54.2	54.6	56.9	59.5	60.0	56.2	55.5	51.9	48.5	46.8	45.4	131.3
158.0	55.6	55.9	56.3	56.7	59.0	61.6	62.1	58.3	57.6	54.0	50.6	48.9	47.5	133.4
199.0	57.6	57.9	58.3	58.7	61.0	63.6	64.1	60.3	59.6	56.0	52.6	50.9	49.5	135.6
251.0	59.6	59.9	60.3	60.7	63.0	65.6	66.1	62.3	61.6	58.0	54.6	52.9	51.5	137.7
316.0	61.6	61.9	62.3	62.7	65.0	67.6	68.1	64.3	63.6	60.0	56.6	54.9	53.5	140.0
398.0	63.6	63.9	64.3	64.7	67.0	69.6	70.1	66.3	65.6	62.0	58.6	56.9	55.5	142.2
501.0	65.6	65.9	66.3	66.7	69.0	71.6	72.1	68.3	67.6	64.0	60.6	58.9	57.5	144.6
630.0	67.6	67.9	68.3	68.7	71.0	73.6	74.1	70.3	69.6	66.0	62.6	60.9	59.5	147.0
794.0	69.6	69.9	70.3	70.7	73.0	75.6	76.1	72.3	71.6	68.0	64.6	62.9	61.5	149.6
1000.0	71.5	72.1	71.0	72.8	75.2	77.1	77.8	74.8	73.1	70.4	66.8	63.5	61.4	152.0
1258.0	73.6	73.9	73.5	74.3	78.5	79.3	79.6	76.9	75.8	72.1	67.7	63.0	61.3	155.0
1584.0	75.0	75.9	76.6	77.4	81.6	81.3	81.2	79.0	75.5	70.4	65.4	60.9	58.0	157.9
1995.0	75.9	77.4	78.9	80.1	81.7	82.4	81.4	78.4	76.8	72.2	66.4	60.5	57.4	160.2
2511.0	74.8	76.4	78.3	79.1	80.8	81.9	81.4	78.5	75.9	70.2	64.2	58.8	54.8	161.3
3162.0	71.8	73.8	76.0	77.2	79.4	80.5	80.3	77.4	75.2	69.5	62.6	55.3	49.8	162.1
3981.0	67.4	69.7	72.5	74.8	75.9	77.5	77.7	75.4	73.1	67.1	59.5	50.9	44.7	162.3
5011.0	64.2	66.9	69.8	72.3	74.8	76.1	76.6	74.5	71.4	65.2	57.6	47.8	41.4	162.4
6309.0	60.2	63.1	66.4	68.8	70.5	71.9	72.2	70.0	67.3	60.4	51.6	41.1	31.9	162.7
7943.0	50.1	53.8	58.5	61.7	64.6	66.1	66.6	64.2	61.3	52.9	42.4	29.2	17.6	163.1
10000.0	37.2	41.6	48.2	52.6	56.4	58.7	59.1	56.1	48.1	38.5	25.7	8.6	0.0	163.4

A.4 Data Contained in TRTREFINT = 'TRTREFINT.dat'

FLIGHT TRANSFORMED, SCALED, AND EXTRAPOLATED SOUND PRESS
77.0 DEG. F., 70 PERCENT R.H. STD. DAY, SAE 1629.0

IDENTIFICATION - 2683/ 203 goldn1

ANGLES MEASURED FROM INLET, DEGREES

FREQ	45.0	50.0	60.0	70.0	80.0	90.0	100.0	110.0	120.0	130.0	140.0	150.0	155.0	PWL
50.0	45.3	45.6	46.1	46.5	48.7	51.2	51.7	48.1	47.4	43.9	40.6	38.8	37.4	122.8
63.0	47.2	47.6	48.0	48.5	50.6	53.1	53.6	50.0	49.3	45.8	42.5	40.8	39.3	124.8
79.0	49.2	49.5	49.9	50.4	52.5	55.0	55.4	51.9	51.2	47.8	44.5	42.8	41.3	126.7
100.0	51.0	51.4	51.8	52.3	54.4	56.8	57.2	53.8	53.1	49.7	46.5	44.8	43.2	128.7
125.0	52.8	53.1	53.6	54.1	56.2	58.5	58.9	55.6	54.9	51.6	48.4	46.6	45.1	130.5
158.0	54.7	55.1	55.6	56.1	58.1	60.4	60.7	57.5	56.8	53.6	50.5	48.7	47.1	132.5
199.0	56.5	56.8	57.4	58.0	59.8	62.1	62.4	59.3	58.6	55.5	52.4	50.6	49.0	134.4
251.0	58.2	58.6	59.2	59.8	61.5	63.7	64.0	61.1	60.4	57.4	54.4	52.6	50.9	136.3
316.0	59.8	60.2	60.9	61.5	63.2	65.2	65.4	62.8	62.1	59.2	56.3	54.5	52.7	138.1
398.0	61.3	61.8	62.5	63.2	64.7	66.5	66.7	64.4	63.7	61.0	58.2	56.3	54.5	140.0
501.0	62.8	63.2	64.0	64.9	66.1	67.8	67.8	65.9	65.2	62.7	60.2	58.2	56.2	141.8
630.0	64.0	64.6	65.4	66.4	67.4	68.8	68.7	67.3	66.6	64.4	62.0	60.0	57.9	143.5
794.0	65.1	65.7	66.7	67.8	68.4	69.5	69.3	68.5	67.8	66.0	63.9	61.8	59.5	145.3
1000.0	67.3	67.7	68.9	70.1	70.8	70.9	70.5	69.5	68.0	66.5	64.7	60.8	58.2	147.3
1258.0	67.2	67.5	68.4	70.0	70.6	71.3	70.5	69.5	68.5	66.6	63.9	58.6	56.0	148.1
1584.0	66.3	67.4	68.2	69.5	71.0	71.1	70.5	69.4	68.0	65.6	61.4	56.7	53.8	148.9
1995.0	66.1	67.2	68.4	69.9	71.6	71.8	71.3	70.4	69.0	66.3	60.7	54.4	51.0	150.8
2511.0	65.3	66.4	68.1	69.3	71.3	72.0	71.9	70.4	69.7	64.5	58.5	52.5	48.4	152.3
3162.0	63.1	64.8	67.0	68.2	71.2	72.0	72.1	70.3	69.4	63.4	56.5	49.2	44.0	154.1
3981.0	59.8	61.8	64.6	66.8	68.5	70.1	70.8	69.0	67.3	61.2	53.6	44.9	38.9	155.3
5011.0	56.9	59.4	62.5	65.0	67.7	68.9	69.6	68.1	65.4	59.2	51.5	41.7	35.4	155.5
6309.0	53.1	56.0	59.2	61.7	63.0	64.1	64.6	63.0	60.4	53.8	45.1	34.6	25.5	155.4
7943.0	43.0	46.6	51.3	54.5	56.2	57.2	57.3	55.4	53.0	45.5	35.5	22.3	11.1	154.8
10000.0	30.4	34.3	40.7	44.8	46.0	48.3	48.9	46.5	39.9	31.1	18.9	1.8	0.0	154.5

A.5 Data Contained in TRTREFEXT = 'TRTREFEXT.dat'

JET EJECTOR NOISE SPECTRA
1 ENGINE(S), AT SPECIFIED ANGLES AND RADII (FEET), IN THE PLAN

JETEJ INCLUDES INDIVIDUAL SOURCES (I): 0 0 1 1 1
MIXED EXIT TEMPERATURE AND VELOCITY FROM INPUT
NO INTERNAL SUPPRESSION

	POLAR ANGLE, THETA, DEGREES													
	45.0	50.0	60.0	70.0	80.0	90.0	100.0	110.0	120.0	130.0	140.0	150.0	155.0	PWL
FREQ														
50.0	72.6	72.7	73.7	74.7	76.4	75.7	76.5	79.1	84.3	86.0	87.2	86.7	84.3	159.1
63.0	73.5	73.4	74.4	76.1	77.2	77.5	79.0	81.5	82.9	85.0	86.6	85.7	82.8	158.6
79.0	74.2	74.0	74.9	76.7	75.9	76.4	78.2	80.2	82.9	85.7	87.4	85.5	81.6	158.8
100.0	74.0	74.2	74.7	75.8	75.8	76.4	77.5	79.3	82.6	84.4	85.2	82.5	79.0	157.1
125.0	74.0	74.2	73.8	75.2	76.1	76.4	77.2	79.2	82.4	82.9	82.1	78.0	74.4	155.3
158.0	73.8	73.9	74.1	75.3	76.2	76.8	77.6	79.2	82.3	82.2	80.0	73.9	71.1	154.6
199.0	74.4	74.5	74.8	75.7	77.0	77.2	78.0	79.5	82.5	81.8	78.5	72.1	69.0	154.5
251.0	74.6	74.6	75.8	76.8	77.5	77.8	78.4	79.8	81.9	80.3	76.9	69.7	68.7	154.3
316.0	75.0	74.9	75.8	76.7	76.9	77.2	78.4	79.8	81.0	78.8	74.9	68.1	66.8	153.8
398.0	74.4	74.8	75.4	76.3	76.4	77.0	77.9	79.2	79.6	77.2	72.9	68.4	64.6	153.2
501.0	74.0	74.1	74.3	75.4	75.5	75.6	76.8	78.0	78.1	75.7	71.3	63.5	63.8	152.3
630.0	72.6	72.7	73.3	74.4	74.3	74.5	75.0	76.1	76.6	73.8	68.9	63.2	60.8	151.2
794.0	71.3	71.6	72.2	72.8	73.0	73.0	73.9	74.7	74.9	71.4	66.2	60.2	55.7	150.3
1000.0	68.8	69.5	69.8	70.7	69.7	70.7	72.3	73.1	73.7	69.7	62.4	55.4	50.6	148.9
1258.0	68.1	68.6	68.4	67.7	67.7	67.8	70.1	71.3	71.3	66.0	57.5	49.5	45.8	147.6
1584.0	64.0	63.2	63.6	64.1	65.6	63.5	68.2	69.6	69.6	61.4	52.3	43.4	37.5	145.9
1995.0	57.0	58.1	60.1	59.7	60.1	58.5	63.7	65.4	67.4	56.1	44.4	38.1	30.6	143.3
2511.0	52.0	53.1	54.8	53.0	55.0	55.7	58.6	62.1	62.8	48.2	38.3	26.9	21.5	140.5
3162.0	46.8	48.5	50.7	47.9	47.9	47.6	55.8	58.8	57.9	42.1	29.2	16.8	10.7	138.5
3981.0	35.6	37.6	40.4	40.3	40.3	40.0	45.8	52.7	51.0	33.0	18.8	5.1	-2.0	134.2
5011.0	28.4	30.5	33.5	33.4	33.5	33.1	39.4	47.2	44.1	25.2	10.3	-4.0	-11.7	129.7
6309.0	17.3	19.8	23.3	23.5	23.7	23.3	29.9	37.4	33.8	13.9	-2.0	-18.1	-27.3	124.2
7943.0	2.4	5.6	10.0	10.8	11.3	11.0	17.6	24.7	20.5	-0.3	-17.8	-36.7	-48.2	118.2
10000.0	-16.0	-11.8	-6.1	-4.5	-3.6	-3.8	2.7	9.4	4.4	-17.7	-37.4	-60.2	-74.9	112.2

A.6 Sample Input File for the Program to Evaluate Frequency Factor γ(f) Spectrum (ITEST=0): The input data file is for a 1/7-scale mixer-ejector with mixer 8c (NRA model) for the takeoff conditions (NPR=3.43, T8=1551°R, V_j=2359 ft/sec, M=0.32).

```
$EPROC
  IPRINT       = 0
  NANG         = 13
  NFREQ        = 24
  DIST         = 1629.
  FLTVEL       = 360.
  ICON         = 100
  HWREFINT     = 'HWREFINT.dat'
  TRTREFINT    = 'TRTREFINT.dat'
  TRTREFEXT    = 'TRTREFEXT.dat'
  REFILSCOEFF  = 'REFILSCOEFF.dat'
  TRTOUTPUT    = 'TRTOUTPUTtest0.out'
  INDX         = 1
  PPANEL       = 'BULK_PP'
  TPSFRQ       = 400.
  ITEST        = 0
$END

$BULK_PP
  TDF          = 500
  RSTV         = 8.45
  DCV          = .485
  SIGMA        = .37
  THK          = .025
  DMTR         = .045
  RHO          = .000609
  CDCH         = .76
  MACH         = 0.8
  BLT          = .05
  SPL          = 43.67,144.64,145.64,146.68,147.65,148.62,149.69,150.66,
                 151.63,152.63,153.67,154.64,155.64,156.68,157.65,158.62,
                 159.69,160.66,6*161
$END

$AABULK
  IBULK = 1,
  IFACE = 1,
  FMACH = 0.8,
  BLDIS = 0.078,
  DEPINCH =.485,
  TFARH = 500.0,
  PSIA = 13.24,
  OASPL = 171.5,
  RESB0 = 0.34,
  RESB100 = 0.539,
  SIGPERF = 0.37,
  THKPERF = 0.025,
  DIAMPERF = 0.045,
  RESLF0 = 0.1252,
  RESLF100 = 0.2088,
  POROS = 0.95,
```

```
$END

$ILOSS
  XL          = 6.56
  YL          = 9.64
  ZL          = 21.48
  NDS         = 1
  DSARRAY     = .0001
  MZU         = .85
  FTR         = 990
  NSIDE       = 2
  IPRTSUMS    = 0
$END
```

A.7 Data Contained in Output File 'REFILSCOEFF.dat'

SPECTRAL ENERGY TRANSMISSION LOSS FOR TREATED EJECTOR

EJECTOR DIMENSIONS: XL= 6.56 YL= 9.64 ZL= 21.48 INCHES
MACH NO ALONG Z-DIRECTION= 0.85
TEMPERATURE= 990.00 DEGREE RANKINE
NO OF TRANSVERSE MODES IN X-DIRECTION, NRM = 50
NO OF TRANSVERSE MODES IN Y-DIRECTION, NSM = 1

FREQFS	FREQM	IL	DELPWL	COEFF
50.	400.	0.700	0.400	0.933
63.	500.	0.940	0.500	0.904
79.	630.	1.200	0.600	0.871
100.	800.	1.530	0.800	0.845
125.	1000.	2.150	0.900	0.750
158.	1250.	2.710	1.000	0.675
199.	1600.	3.650	1.300	0.582
251.	2000.	4.530	1.500	0.498
316.	2500.	6.520	2.000	0.353
398.	3150.	8.820	2.300	0.223
501.	4000.	11.770	2.900	0.130
630.	5000.	14.790	3.500	0.074
794.	6300.	15.960	4.300	0.068
1000.	8000.	13.770	4.700	0.124
1258.	10000.	12.090	6.900	0.303
1584.	12500.	10.550	9.000	0.700
1995.	16000.	10.580	9.400	0.762
2511.	20000.	11.120	9.000	0.614
3162.	25000.	11.110	8.000	0.489
3981.	31500.	10.560	7.000	0.441
5011.	40000.	10.000	6.900	0.490
6309.	50000.	8.650	7.300	0.733
7943.	63000.	7.050	8.300	1.334
10000.	80000.	5.270	8.900	2.307

A.8 Data Contained in Output File 'TRTOUTPUTtest0.out'

```
Input parameters for Impedance:

  Bulk Resistivity (rayls/cm) =  8.45
  Facesheet Porosity          =  .37
  Facesheet Hole Dia. (in.)   =  4.500000000000000E-02
  Facesheet Thickness (in.)   =  2.500000000000000E-02
  Axial Mach Number           =  .8
  Temperature (deg. F)        =  500.0
  Panel Depth (in.)           =  .485


Input parameters for Acoustic Suppression:

  Ejector Height (in.) =  6.56
  Ejector Width  (in.) =  9.64
  Ejector Length (in.) =  21.48
  Axial Mach No.       =  .85
  Temperature (deg. R) =  990.0


  Frequency     Resistance    Reactance    Suppression, dB
    400         1.717E+00    -1.206E+01    -3.093E+00
    500         1.722E+00    -9.625E+00    -1.286E-01
    630         1.685E+00    -7.632E+00    -1.982E-01
    800         1.620E+00    -6.011E+00    -2.278E+00
   1000         1.548E+00    -4.809E+00    -2.152E+00
   1250         1.473E+00    -3.840E+00    -2.170E+00
   1600         1.392E+00    -2.977E+00    -4.114E+00
   2000         1.326E+00    -2.343E+00    -4.526E+00
   2500         1.270E+00    -1.815E+00    -6.525E+00
   3150         1.223E+00    -1.352E+00    -8.821E+00
   4000         1.188E+00    -9.391E-01    -1.177E+01
   5000         1.170E+00    -5.930E-01    -1.479E+01
   6300         1.171E+00    -2.541E-01    -1.596E+01
   8000         1.204E+00     1.021E-01    -1.382E+01
  10000         1.300E+00     4.764E-01    -1.209E+01
  12500         1.592E+00     9.397E-01    -1.008E+01
  16000         2.842E+00     1.009E+00    -9.364E+00
  20000         2.102E+00    -4.498E-01    -1.212E+01
  25000         1.388E+00     3.544E-01    -1.231E+01
  31500         1.794E+00     1.264E+00    -9.800E+00
  40000         1.783E+00     3.907E-01    -1.183E+01
  50000         1.819E+00     1.579E+00    -7.815E+00
  63000         1.533E+00     1.398E+00    -7.027E+00
  80000         1.619E+00     1.680E+00    -5.257E+00
```

Flight Transformed, Scaled, and Extrapolated Sound Pressure Levels
77.0 Deg. F., 70 % R.H., SAE Std. Day., Dist = 1629.0

IDENTIFICATION - Treated Configuration = 100

Internal noise spectra:

angle	45.	50.	60.	70.	80.	90.	100.	110.	120.	130.	140.	150.	155.	
freq														pwl
50.	45.3	45.6	46.1	46.5	48.7	51.2	51.7	48.1	47.4	43.9	40.6	38.8	37.4	122.8
63.	47.2	47.6	48.0	48.5	50.6	53.1	53.6	50.0	49.3	45.8	42.5	40.8	39.3	124.8
79.	49.2	49.5	49.9	50.4	52.5	55.0	55.4	51.9	51.2	47.8	44.5	42.8	41.3	126.7
100.	51.0	51.4	51.8	52.3	54.4	56.8	57.2	53.8	53.1	49.7	46.5	44.8	43.2	128.6
125.	52.8	53.1	53.6	54.1	56.2	58.5	58.9	55.6	54.9	51.6	48.4	46.6	45.1	130.5
158.	54.7	55.1	55.6	56.1	58.1	60.4	60.7	57.5	56.8	53.6	50.5	48.7	47.1	132.5
199.	56.5	56.8	57.4	58.0	59.8	62.1	62.4	59.3	58.6	55.5	52.4	50.6	49.0	134.4
251.	58.2	58.6	59.2	59.8	61.5	63.7	64.0	61.1	60.4	57.4	54.4	52.6	50.9	136.3
316.	59.8	60.2	60.9	61.5	63.2	65.2	65.4	62.8	62.1	59.2	56.3	54.5	52.7	138.2
398.	61.3	61.8	62.5	63.2	64.7	66.5	66.7	64.4	63.7	61.0	58.2	56.3	54.5	140.0
501.	62.8	63.2	64.0	64.9	66.1	67.8	67.8	65.9	65.2	62.7	60.2	58.2	56.2	141.8
630.	64.0	64.6	65.4	66.4	67.4	68.8	68.7	67.3	66.6	64.4	62.0	60.0	57.9	143.5
794.	65.1	65.7	66.7	67.8	68.4	69.5	69.3	68.5	67.8	66.0	63.9	61.8	59.5	145.3
1000.	67.3	67.7	68.9	70.1	70.8	70.9	70.5	69.5	68.0	66.5	64.7	60.8	58.2	147.3
1258.	67.2	67.5	68.4	70.0	70.6	71.3	70.5	69.5	68.5	66.6	63.9	58.6	56.0	148.1
1584.	66.3	67.4	68.2	69.5	71.0	71.1	70.5	69.4	68.0	65.6	61.4	56.7	53.8	148.9
1995.	66.1	67.2	68.4	69.9	71.6	71.8	71.3	70.4	69.0	66.3	60.7	54.4	51.0	150.8
2511.	65.3	66.4	68.1	69.3	71.3	72.0	71.9	70.4	69.7	64.5	58.5	52.5	48.4	152.3
3162.	63.1	64.8	67.0	68.2	71.2	72.0	72.1	70.3	69.4	63.4	56.5	49.2	44.0	154.1
3981.	59.8	61.8	64.6	66.8	68.5	70.1	70.8	69.0	67.3	61.2	53.6	44.9	38.9	155.3
5011.	56.9	59.4	62.5	65.0	67.7	68.9	69.6	68.1	65.4	59.2	51.5	41.7	35.4	155.5
6309.	53.1	56.0	59.2	61.7	63.0	64.1	64.6	63.0	60.4	53.8	45.1	34.6	25.5	155.4
7943.	43.0	46.6	51.3	54.5	56.2	57.2	57.3	55.4	53.0	45.5	35.5	22.3	11.1	154.8
10000.	30.4	34.3	40.7	44.8	46.0	48.3	48.9	46.5	39.9	31.1	18.9	1.8	.0	154.5

Flight Transformed, Scaled, and Extrapolated Sound Pressure Levels
77.0 Deg. F., 70 % R.H., SAE Std. Day., Dist = 1629.0

IDENTIFICATION - Treated Configuration = 100

Total noise spectra:

angle	45.	50.	60.	70.	80.	90.	100.	110.	120.	130.	140.	150.	155.	
freq														pwl
50.	72.6	72.7	73.7	74.7	76.4	75.7	76.5	79.1	84.3	86.0	87.2	86.7	84.3	159.1
63.	73.5	73.4	74.4	76.1	77.2	77.5	79.0	81.5	82.9	85.0	86.6	85.7	82.8	158.6
79.	74.2	74.0	74.9	76.7	75.9	76.4	78.2	80.2	82.9	85.7	87.4	85.5	81.6	158.8
100.	74.0	74.2	74.7	75.8	75.8	76.4	77.5	79.3	82.6	84.4	85.2	82.5	79.0	157.1
125.	74.0	74.2	73.8	75.2	76.1	76.5	77.3	79.2	82.4	82.9	82.1	78.0	74.4	155.3
158.	73.9	74.0	74.2	75.4	76.3	76.9	77.7	79.2	82.3	82.2	80.0	73.9	71.1	154.6
199.	74.5	74.6	74.9	75.8	77.1	77.3	78.1	79.5	82.5	81.8	78.5	72.1	69.0	154.6
251.	74.7	74.7	75.9	76.9	77.6	78.0	78.6	79.9	81.9	80.3	76.9	69.8	68.8	154.4
316.	75.1	75.0	75.9	76.8	77.1	77.5	78.6	79.9	81.1	78.8	75.0	68.3	67.0	153.9
398.	74.6	75.0	75.6	76.5	76.7	77.4	78.2	79.3	79.7	77.3	73.0	68.7	65.0	153.5
501.	74.3	74.4	74.7	75.8	76.0	76.3	77.3	78.3	78.3	75.9	71.6	64.6	64.5	152.7
630.	73.2	73.3	74.0	75.0	75.1	75.5	75.9	76.6	77.0	74.3	69.7	64.9	62.6	151.9
794.	72.2	72.6	73.3	74.0	74.3	74.6	75.2	75.6	75.7	72.5	68.2	64.1	61.0	151.5
1000.	71.1	71.7	72.4	73.4	73.3	73.8	74.5	74.7	74.7	71.4	66.7	61.9	58.9	151.2
1258.	70.7	71.1	71.4	72.0	72.4	72.9	73.3	73.5	73.1	69.3	64.8	59.1	56.4	150.8
1584.	68.3	68.8	69.5	70.6	72.1	71.8	72.5	72.5	71.9	67.0	61.9	56.9	53.9	150.6
1995.	66.6	67.7	69.0	70.3	71.9	72.0	72.0	71.6	71.3	66.7	60.8	54.5	51.0	151.5
2511.	65.5	66.6	68.3	69.4	71.4	72.1	72.1	71.0	70.5	64.6	58.5	52.5	48.4	152.6
3162.	63.2	64.9	67.1	68.2	71.2	72.0	72.2	70.6	69.7	63.4	56.5	49.2	44.0	154.2
3981.	59.8	61.8	64.6	66.8	68.5	70.1	70.8	69.1	67.4	61.2	53.6	44.9	38.9	155.3
5011.	56.9	59.4	62.5	65.0	67.7	68.9	69.6	68.1	65.4	59.2	51.5	41.7	35.4	155.5
6309.	53.1	56.0	59.2	61.7	63.0	64.1	64.6	63.0	60.4	53.8	45.1	34.6	25.5	155.4
7943.	43.0	46.6	51.3	54.5	56.2	57.2	57.3	55.4	53.0	45.5	35.5	22.3	11.1	154.8
10000.	30.4	34.3	40.7	44.8	46.0	48.3	48.9	46.5	39.9	31.1	18.9	1.8	.0	154.5

Summary data for treated configuration = 100

total noise			external component			internal component		
oapwl	epnl	epnlt	oapwl	epnl	epnlt	oapwl	epnl	epnlt
168.77	97.38	97.49	167.05	93.90	94.09	163.93	91.45	91.57

ang	oaspl	pnl	pnlt	oaspl	pnl	pnlt	oaspl	pnl	pnlt
45.	85.67	92.25	92.45	85.19	89.06	89.39	75.79	87.16	87.36
50.	85.85	93.07	93.23	85.30	89.38	89.78	76.61	88.31	88.48
60.	86.52	94.40	94.41	85.88	90.07	90.45	77.88	89.98	89.99
70.	87.65	95.69	95.69	86.98	90.84	90.84	79.21	91.37	91.37
80.	88.30	97.27	97.27	87.46	91.17	91.17	80.73	93.52	93.52
90.	88.67	97.92	97.92	87.73	91.44	91.62	81.58	94.50	94.50
100.	89.55	98.44	98.44	88.81	93.05	93.65	81.49	94.58	94.58
110.	90.88	98.19	98.19	90.51	94.80	94.80	80.03	92.85	92.85
120.	93.02	98.38	98.51	92.86	95.99	95.99	78.85	91.66	91.79
130.	93.49	96.16	96.33	93.42	93.73	93.73	75.63	86.93	87.11
140.	93.69	93.73	94.01	93.66	91.59	91.59	72.16	81.74	82.02
150.	91.79	89.66	90.07	91.77	87.68	88.05	68.66	76.50	76.92
155.	88.78	85.98	86.40	88.76	83.95	83.95	66.29	73.38	73.80

It should be noted that the output SPL data are the same as those used as input, since the same test case is being evaluated.

A.9 Sample Input File for the Program to Evaluate Acoustic Characteristics of Treated Ejector of an Arbitrary Liner Design (ITEST=1): The input data file is for a full-scale mixer-ejector with mixer 8c for the takeoff conditions (NPR=3.43, T8=1551°R, V_j=2359 ft/sec, M=0.32).

```
$EPROC
  IPRINT      = 0
  NANG        = 13
  NFREQ       = 24
  DIST        = 1629.
  FLTVEL      = 360.
  ICON        = 113
  HWREFINT    = 'HWREFINT.dat'
  TRTREFINT   = 'TRTREFINT.dat'
  TRTREFEXT   = 'TRTREFEXT.dat'
  REFILSCOEFF = 'REFILSCOEFF.dat'
  TRTOUTPUT   = 'TRTOUTPUTtest1.out'
  INDX        = 1
  PPANEL      = 'BULK_PP'
  TPSFRQ      = 50.
  ITEST       = 1
$END

$BULK_PP
  TDF         = 500
  RSTV        = 10
  DCV         = 2
  SIGMA       = .4
  THK         = .04
  DMTR        = .04
  RHO         = .000609
  CDCH        = .76
  MACH        = 0.8
  BLT         = .2
  SPL         = 151,152,153,154,155,156,157,158,159,160,161,162,163,
                164,165,166,167,168.4,169.4,170.4,170.4,170.5,171.3,171.5
$END

$AABULK
  IBULK = 1,
  IFACE = 1,
  FMACH = 0.8,
  BLDIS=0.078,
  DEPINCH = 2.0,
  TFARH = 500.0,
  PSIA = 14.5,
  OASPL = 180,
  RESB0 = 0.34,
  RESB100 = 0.539,
  SIGPERF = 0.40,
  THKPERF = 0.04,
  DIAMPERF = 0.04,
  RESLF0 = 0.1252,
  RESLF100 = 0.2088,
  POROS = 0.95,
$END
```

```
$ILOSS
  XL          = 48.69
  YL          = 71.17
  ZL          = 166.8
  NDS         = 8
  DSARRAY     = .0001,.00001,.000001,.001,.002,.0002,.00002,.000002
  MZU         = .85
  FTR         = 990
  NSIDE       = 2
  IPRTSUMS    = 0
$END
```

A.10 Data Contained in Output File 'TRTOUTPUTtest1.out'

```
Input parameters for Impedance:

  Bulk Resistivity (rayls/cm) =  10.0
  Facesheet Porosity          =  .4
  Facesheet Hole Dia. (in.)   =  4.000000000000000E-02
  Facesheet Thickness (in.)   =  4.000000000000000E-02
  Axial Mach Number           =  .8
  Temperature (deg. F)        =  500.0
  Panel Depth (in.)           =  2.0


Input parameters for Acoustic Suppression:

  Ejector Height (in.) =  48.69
  Ejector Width  (in.) =  71.17
  Ejector Length (in.) =  166.8
  Axial Mach No.       =  .85
  Temperature (deg. R) =  990.0


  Frequency     Resistance    Reactance    Suppression, dB
     50        -1.091E+00    -2.649E+01      .000E+00
     63        -2.666E-01    -2.064E+01      .000E+00
     80         3.317E-01    -1.595E+01    -5.896E-01
    100         7.209E-01    -1.253E+01    -7.143E-01
    125         9.908E-01    -9.852E+00    -7.311E-01
    160         1.190E+00    -7.547E+00    -7.935E-01
    200         1.305E+00    -5.927E+00    -2.475E+00
    250         1.378E+00    -4.648E+00    -2.538E+00
    315         1.424E+00    -3.602E+00    -4.049E+00
    400         1.450E+00    -2.752E+00    -5.574E+00
    500         1.464E+00    -2.119E+00    -7.165E+00
    630         1.475E+00    -1.589E+00    -9.228E+00
    800         1.489E+00    -1.143E+00    -1.150E+01
   1000         1.513E+00    -7.958E-01    -1.378E+01
   1250         1.555E+00    -4.995E-01    -1.487E+01
   1600         1.640E+00    -2.209E-01    -1.354E+01
   2000         1.775E+00    -2.293E-02    -1.266E+01
   2500         1.979E+00     6.885E-02    -1.240E+01
   3150         2.159E+00    -6.635E-02    -1.223E+01
   4000         1.990E+00    -2.820E-01    -1.224E+01
   5000         1.728E+00    -1.380E-01    -1.157E+01
   6300         1.757E+00     1.374E-01    -1.152E+01
   8000         1.875E+00     9.568E-02    -1.004E+01
  10000         1.722E+00     2.254E-01    -8.846E+00
```

Flight Transformed, Scaled, and Extrapolated Sound Pressure Levels
77.0 Deg. F., 70 % R.H., SAE Std. Day., Dist = 1629.0

IDENTIFICATION - Treated Configuration = 113

Internal noise spectra:

angle freq	45.	50.	60.	70.	80.	90.	100.	110.	120.	130.	140.	150.	155.	pwl
50.	45.9	46.2	46.7	47.1	49.3	51.8	52.3	48.7	48.0	44.5	41.2	39.4	38.0	123.4
63.	47.9	48.3	48.7	49.2	51.3	53.8	54.3	50.7	50.0	46.5	43.2	41.5	40.0	125.5
79.	49.7	50.0	50.4	50.9	53.0	55.5	55.9	52.4	51.7	48.3	45.0	43.3	41.8	127.2
100.	51.6	52.0	52.4	52.9	55.0	57.4	57.8	54.4	53.7	50.3	47.1	45.4	43.8	129.3
125.	54.1	54.4	54.9	55.4	57.5	59.8	60.2	56.9	56.2	52.9	49.7	47.9	46.4	131.8
158.	56.5	56.9	57.4	57.9	59.9	62.2	62.5	59.3	58.6	55.4	52.3	50.5	48.9	134.3
199.	57.6	57.9	58.5	59.1	60.9	63.2	63.5	60.4	59.7	56.6	53.5	51.7	50.1	135.5
251.	60.1	60.5	61.1	61.7	63.4	65.6	65.9	63.0	62.3	59.3	56.3	54.5	52.8	138.2
316.	62.2	62.6	63.3	63.9	65.6	67.6	67.8	65.2	64.5	61.6	58.7	56.9	55.1	140.5
398.	64.4	64.9	65.6	66.3	67.8	69.6	69.8	67.5	66.8	64.1	61.3	59.4	57.6	143.1
501.	67.3	67.7	68.5	69.4	70.6	72.3	72.3	70.4	69.7	67.2	64.7	62.7	60.7	146.3
630.	69.6	70.2	71.0	72.0	73.0	74.4	74.3	72.9	72.2	70.0	67.6	65.6	63.5	149.1
794.	69.6	70.2	71.2	72.3	72.9	74.0	73.8	73.0	72.3	70.5	68.4	66.3	64.0	149.8
1000.	67.3	67.7	68.9	70.1	70.8	70.9	70.5	69.5	68.0	66.5	64.7	60.8	58.2	147.3
1258.	64.4	64.7	65.6	67.2	67.8	68.5	67.7	66.7	65.7	63.8	61.1	55.8	53.2	145.3
1584.	63.3	64.4	65.2	66.5	68.0	68.1	67.5	66.4	65.0	62.6	58.4	53.7	50.8	145.9
1995.	64.0	65.1	66.3	67.8	69.5	69.7	69.2	68.3	66.9	64.2	58.6	52.3	48.9	148.7
2511.	64.0	65.1	66.8	68.0	70.0	70.7	70.6	69.1	68.4	63.2	57.2	51.2	47.1	151.0
3162.	62.0	63.7	65.9	67.1	70.1	70.9	71.0	69.2	68.3	62.3	55.4	48.1	42.9	153.0
3981.	58.1	60.1	62.9	65.1	66.8	68.4	69.1	67.3	65.6	59.5	51.9	43.2	37.2	153.6
5011.	55.3	57.8	60.9	63.4	66.1	67.3	68.0	66.5	63.8	57.6	49.9	40.1	33.8	154.0
6309.	50.2	53.1	56.3	58.8	60.1	61.2	61.7	60.1	57.5	50.9	42.2	31.7	22.6	152.6
7943.	40.0	43.6	48.3	51.5	53.2	54.2	54.3	52.4	50.0	42.5	32.5	19.3	8.1	151.9
10000.	26.8	30.7	37.1	41.2	42.4	44.7	45.3	42.9	36.3	27.5	15.3	-1.8	-3.6	150.9

FlightTransformed, Scaled, and Extrapolated Sound Pressure Levels
77.0 Deg. F., 70 % R.H., SAE Std. Day., Dist = 1629.0

IDENTIFICATION - Treated Configuration = 113

Total noise spectra:

angle	45.	50.	60.	70.	80.	90.	100.	110.	120.	130.	140.	150.	155.	
freq														pwl
50.	72.6	72.7	73.7	74.7	76.4	75.7	76.5	79.1	84.3	86.0	87.2	86.7	84.3	159.1
63.	73.5	73.4	74.4	76.1	77.2	77.5	79.0	81.5	82.9	85.0	86.6	85.7	82.8	158.6
79.	74.2	74.0	74.9	76.7	75.9	76.4	78.2	80.2	82.9	85.7	87.4	85.5	81.6	158.8
100.	74.0	74.2	74.7	75.8	75.8	76.5	77.5	79.3	82.6	84.4	85.2	82.5	79.0	157.1
125.	74.0	74.2	73.9	75.2	76.2	76.5	77.3	79.2	82.4	82.9	82.1	78.0	74.4	155.3
158.	73.9	74.0	74.2	75.4	76.3	76.9	77.7	79.2	82.3	82.2	80.0	73.9	71.1	154.6
199.	74.5	74.6	74.9	75.8	77.1	77.4	78.2	79.6	82.5	81.8	78.5	72.1	69.1	154.6
251.	74.8	74.8	75.9	76.9	77.7	78.1	78.6	79.9	81.9	80.3	76.9	69.8	68.8	154.4
316.	75.2	75.1	76.0	76.9	77.2	77.6	78.8	79.9	81.1	78.9	75.0	68.4	67.1	154.0
398.	74.8	75.2	75.8	76.7	77.0	77.7	78.5	79.5	79.8	77.4	73.2	68.9	65.4	153.7
501.	74.8	75.0	75.3	76.4	76.7	77.3	78.1	78.7	78.7	76.3	72.2	66.1	65.5	153.3
630.	74.4	74.6	75.3	76.4	76.7	77.5	77.7	77.8	77.9	75.3	71.3	67.6	65.4	153.3
794.	73.5	74.0	74.7	75.6	75.9	76.5	76.8	76.9	76.8	74.0	70.4	67.2	64.6	153.0
1000.	71.1	71.7	72.4	73.4	73.3	73.8	74.5	74.7	74.7	71.4	66.7	61.9	58.9	151.2
1258.	69.6	70.1	70.2	70.5	70.8	71.2	72.1	72.6	72.4	68.1	62.7	56.7	53.9	149.6
1584.	66.7	66.9	67.5	68.5	70.0	69.4	70.9	71.3	70.9	65.1	59.4	54.1	51.0	148.9
1995.	64.8	65.9	67.3	68.4	70.0	70.0	70.3	70.1	70.2	64.8	58.8	52.5	49.0	149.8
2511.	64.3	65.4	67.1	68.2	70.2	70.9	70.9	69.9	69.5	63.4	57.3	51.2	47.1	151.4
3162.	62.1	63.8	66.0	67.1	70.1	70.9	71.1	69.6	68.7	62.3	55.4	48.1	42.9	153.1
3981.	58.1	60.1	62.9	65.1	66.8	68.4	69.1	67.5	65.8	59.5	51.9	43.2	37.2	153.7
5011.	55.3	57.8	60.9	63.4	66.1	67.3	68.0	66.6	63.9	57.6	49.9	40.1	33.8	154.0
6309.	50.2	53.1	56.3	58.8	60.1	61.2	61.7	60.2	57.6	50.9	42.2	31.7	22.6	152.6
7943.	40.0	43.6	48.3	51.5	53.2	54.2	54.3	52.4	50.0	42.5	32.5	19.3	8.1	151.9
10000.	26.8	30.7	37.1	41.2	42.4	44.7	45.3	42.9	36.3	27.5	15.3	-1.8	-3.6	150.9

Summary data for treated configuration = 113

total noise			external component			internal component		
oapwl	epnl	epnlt	oapwl	epnl	epnlt	oapwl	epnl	epnlt
168.32	96.90	97.08	167.05	93.90	94.09	162.38	90.98	91.12
ang	oaspl	pnl	pnlt	oaspl	pnl	pnlt	oaspl	pnl	pnlt
45.	85.79	91.81	91.88	85.19	89.06	89.39	76.86	86.70	86.77
50.	85.97	92.41	92.44	85.30	89.38	89.78	77.54	87.80	87.84
60.	86.63	93.70	93.70	85.88	90.07	90.45	78.64	89.43	89.43
70.	87.74	94.93	94.93	86.98	90.84	90.84	79.81	90.77	90.77
80.	88.37	96.53	96.71	87.46	91.17	91.17	81.13	92.92	93.10
90.	88.81	97.18	97.30	87.73	91.44	91.62	82.23	93.94	94.06
100.	89.67	97.75	97.91	88.81	93.05	93.65	82.18	94.01	94.17
110.	90.94	97.57	97.80	90.51	94.80	94.80	80.66	92.27	92.51
120.	93.06	97.96	98.14	92.86	95.99	95.99	79.69	91.13	91.31
130.	93.52	95.89	96.12	93.42	93.73	93.73	76.92	86.50	86.73
140.	93.71	93.56	93.89	93.66	91.59	91.59	74.06	81.87	82.20
150.	91.81	89.63	89.81	91.77	87.68	88.05	71.45	78.25	79.28
155.	88.81	85.98	86.72	88.76	83.95	83.95	69.25	75.49	76.54

APPENDIX B

LINER SUPPRESSION IN EPNdB FOR FULL SCALE MIXER-EJECTOR AT APPROACH CONDITIONS

Acoustic suppression in terms of EPNL for full-scale mixer-ejector nozzles at takeoff and cutback conditions are predicted using the measured data for the NRA model with mixer 8c tested in Cell 41. However, there is no test data available for the NRA model at approach condition. Thus, the current predictions are made using the measured data for LSMS model tested at LSAF of Boeing. The approach condition requirements for the 3770.60 engine are as follows:

Altitude = 394'
Airspeed = 270'/sec (i.e., M=0.24)
NPR=1.466
Primary velocity =1051'/sec
Primary temperature = 937oR
Primary flow rate=358 lbm/sec
Primary area = 8.555 sq ft
Secondary velocity = 392 ft/sec
Secondary temperature = 541.5oR
Secondary flow rate = 373 lbm/sec
Secondary area = 13.448 sq ft
Mixing length = 10.764 ft
Ejector diameter = 5.228 ft
Ejector lining length = 7.689 ft
Throat area = 7.544 sq ft
MAR = 0.98

The test conditions for the data used for the current prediction are closely matched with the above parameters. However, the MAR for the configuration is 0.9 instead of 0.98, since there was no data for this MAR at a flight Mach number of 0.24. The flow and temperature conditions at the liner surface and mean flow conditions are obtained by extrapolating the data used for takeoff and cutback conditions and are listed below;

Temperature at liner surface=225°F
Mach number at liner surface = 0.63
Mean flow temperature=250°F
Mean flow Mach number=0.65
OASPL = 157.5 dB

The measured data exhibits some anomaly at angles greater than 90°, especially for the treated conditions (see Figure B1). The source separation using these data resulted in

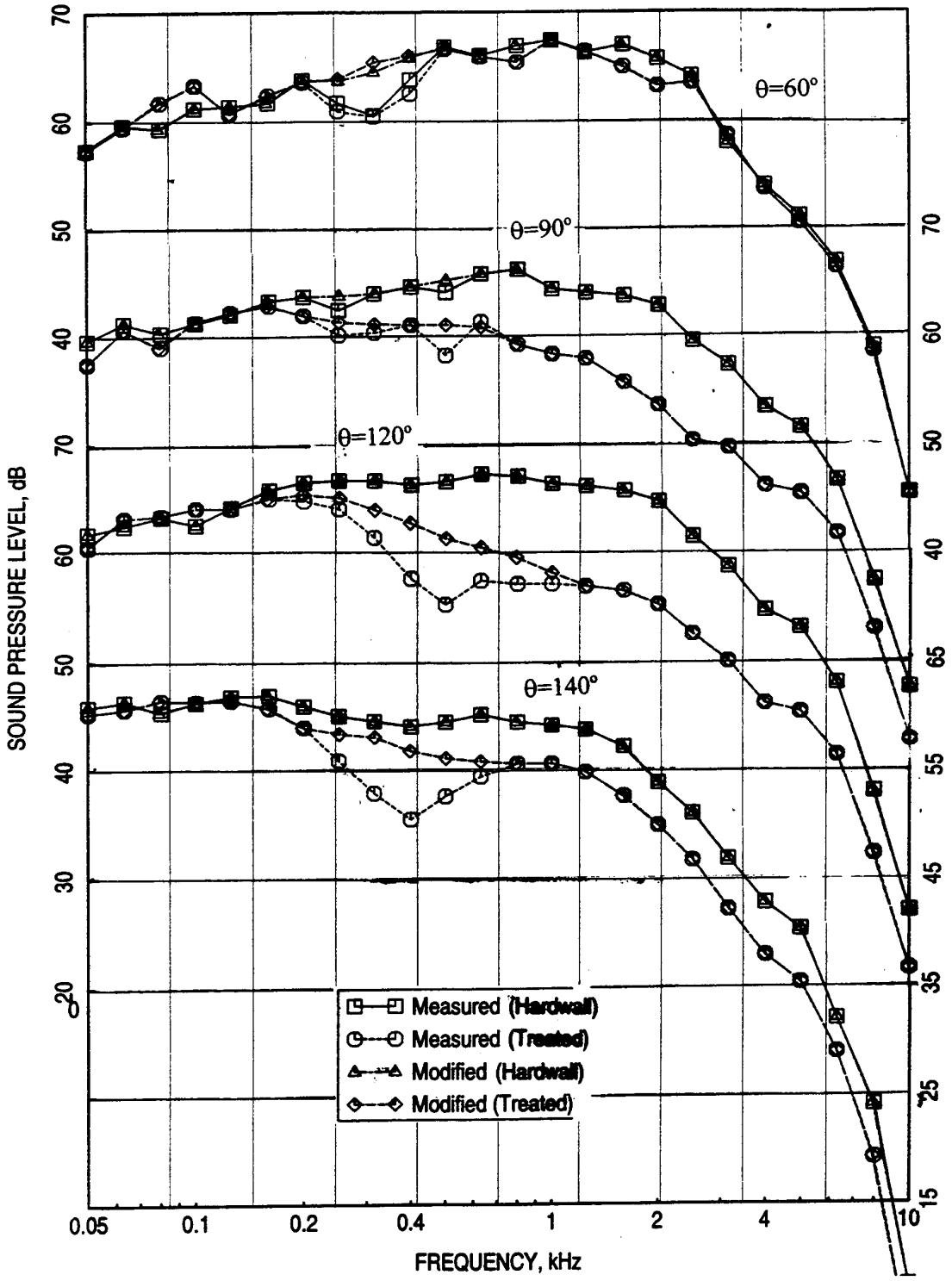

Figure B1. Measured and modified SPL spectra for hardwalled and fully treated 160" long ejector for LSMS model; NPR=1.5, T8=965°R, V_j=1050 ft/sec, M=0.24 {approach}.

unrealistic spectral shapes for the components. Thus, the data is modified, as shown in Figure B1, for the current exercise. The modified data is used to extract various spectral noise components for hardwall and fully treated configurations. Extracted spectral results at typical angles are shown in Figures B2 and B3. The impedance spectra for the test conditions are constructed using the measured normal impedance of the liner configuration at ambient condition and the predicted impact of flow temperature and sound intensity on the impedance levels for approach conditions (see Figure B4). The internal acoustic suppression spectrum is thus predicted using the constructed normal impedance for the LSMS mixer-ejector. Utilizing the predicted internal acoustic suppression and the extracted internal component of PWL and SPL spectra all the relevant correction factor spectra are derived.

Normal impedance spectra at approach for four different liner designs made for full-scale mixer-ejector is evaluated. The four liner designs include an optimum design with a bulk of 8 Rayls/cm, design #1 with 12 lbf/cft T-Foam, design #2 with 8 lbf/cft T-Foam, and design #3 with 100 ppi SiC. For these designs a 40% porous 0.04" thick facesheet with 0.04" diameter holes is utilized. While the normal impedance for the optimum liner is predicted the normal impedance for the other three designs is constructed using the measured ambient impedance data. Figure B5 shows the construction process for these liner designs at approach conditions (T=225°F and M=0.63). Utilizing these impedance spectra for the full-scale liner configurations the corresponding acoustic suppressions are predicted. The normal impedance and the corresponding acoustic suppression spectra for these liners are shown in Figure B6. The results for the LSMS test case are also plotted in this figure. For the sake of compatibility multiplying the linear scale factor of the designs normalizes the frequency for these plots. Utilizing the predicted acoustic suppression and the evaluated correction factor spectra the farfield noise for each of the four liner designs are computed. Figure B7 shows the PNL directivities compared with the hardwall data. The predicted EPNL for various liner configurations are listed in Figure B7 and Table B1. **Suppressions of about 2.5 and 3.3 EPNdB are noticed for the total and internal noise components, respectively.**

It is important to examine the data at forward arc, especially at angles 50° to 80°, that the internal components are not accurately extracted. Figure B2 for 50° case indicates that the internal noise for hardwall and treated cases are very significant and are the same in magnitude. This is physically not possible. Internal noise radiation is relatively small at these angles. Even if we assume that the internal noise is radiated to these angles as extracted for hardwall the corresponding levels for treated case should have been lower, since significant internal noise suppression is observed at higher angles. Therefore, the strong internal noise

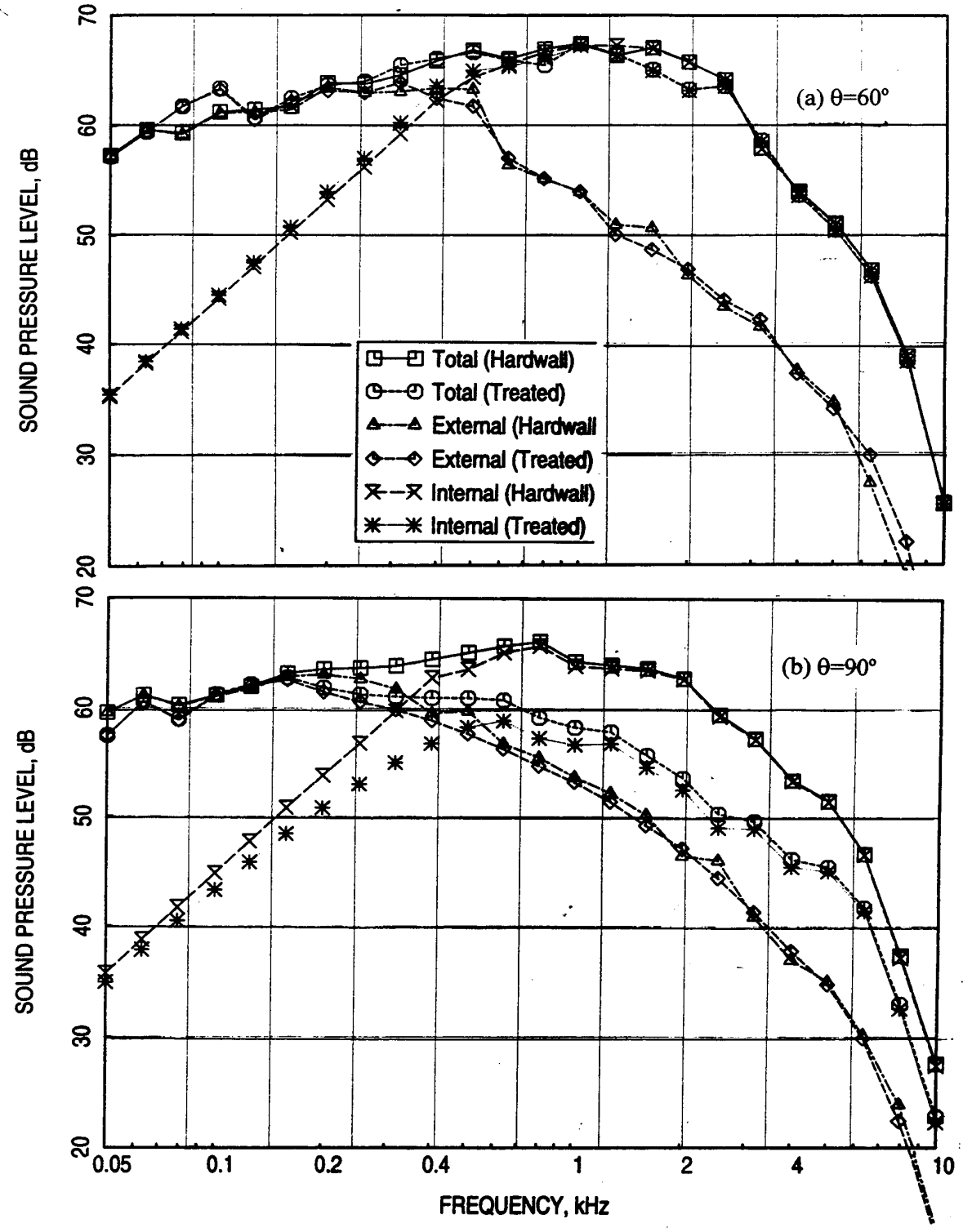

Figure B2. Measured SPL spectra compared with the modified predicted external components (i.e., merged and premerged) and extracted internal components for hardwalled and fully treated 160" long ejector for LSMS model; NPR=1.5, T8=965°R, V_j=1050 ft/sec, M=0.24 {approach}.

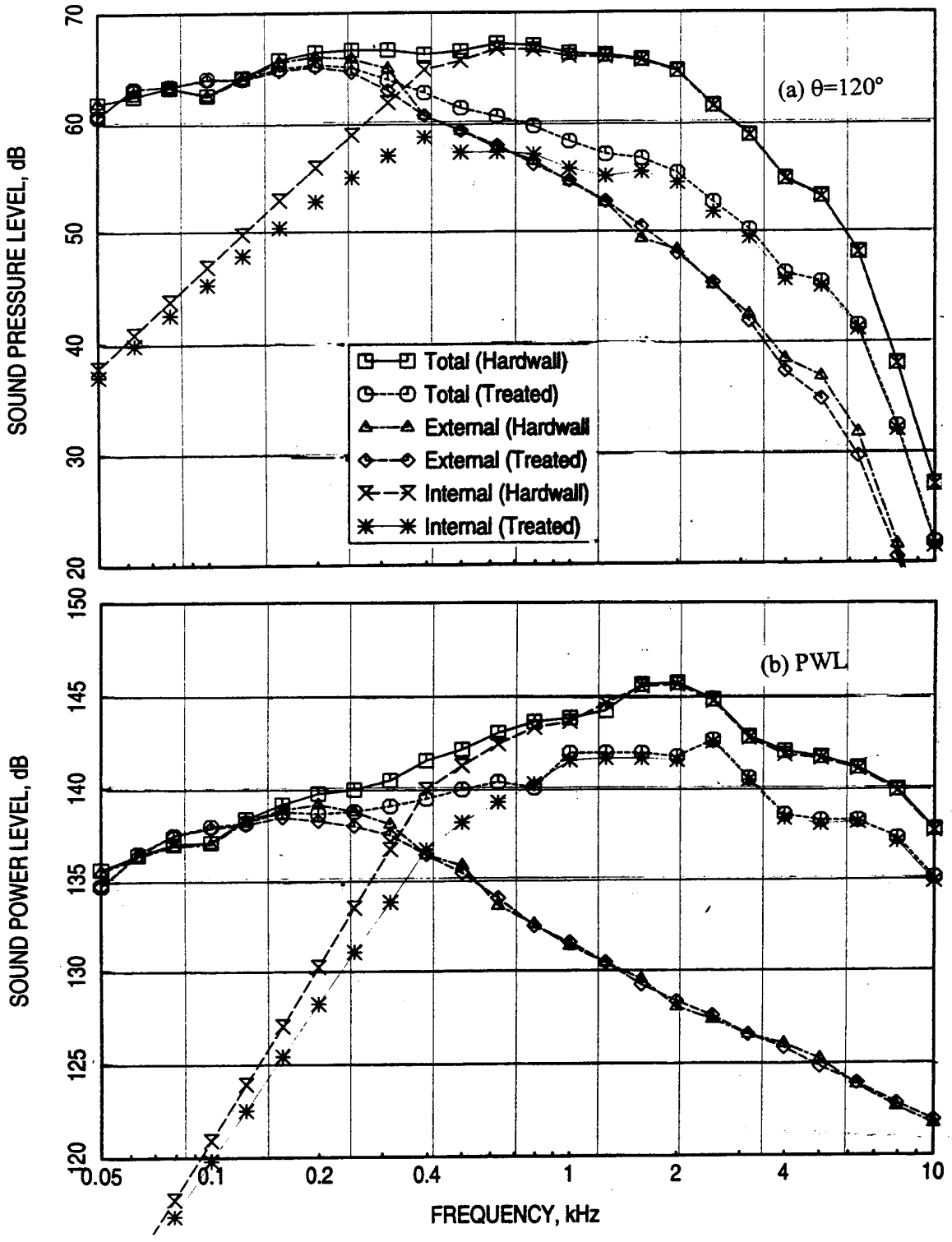

Figure B3. Measured SPL and PWL spectra compared with the modified predicted external components (i.e., merged and premerged) and extracted internal components for hardwalled and fully treated 22.12" long ejector for LSMS model; NPR=1.5, T8=965°R, V_j=1050 ft/sec, M=0.24 {approach}.

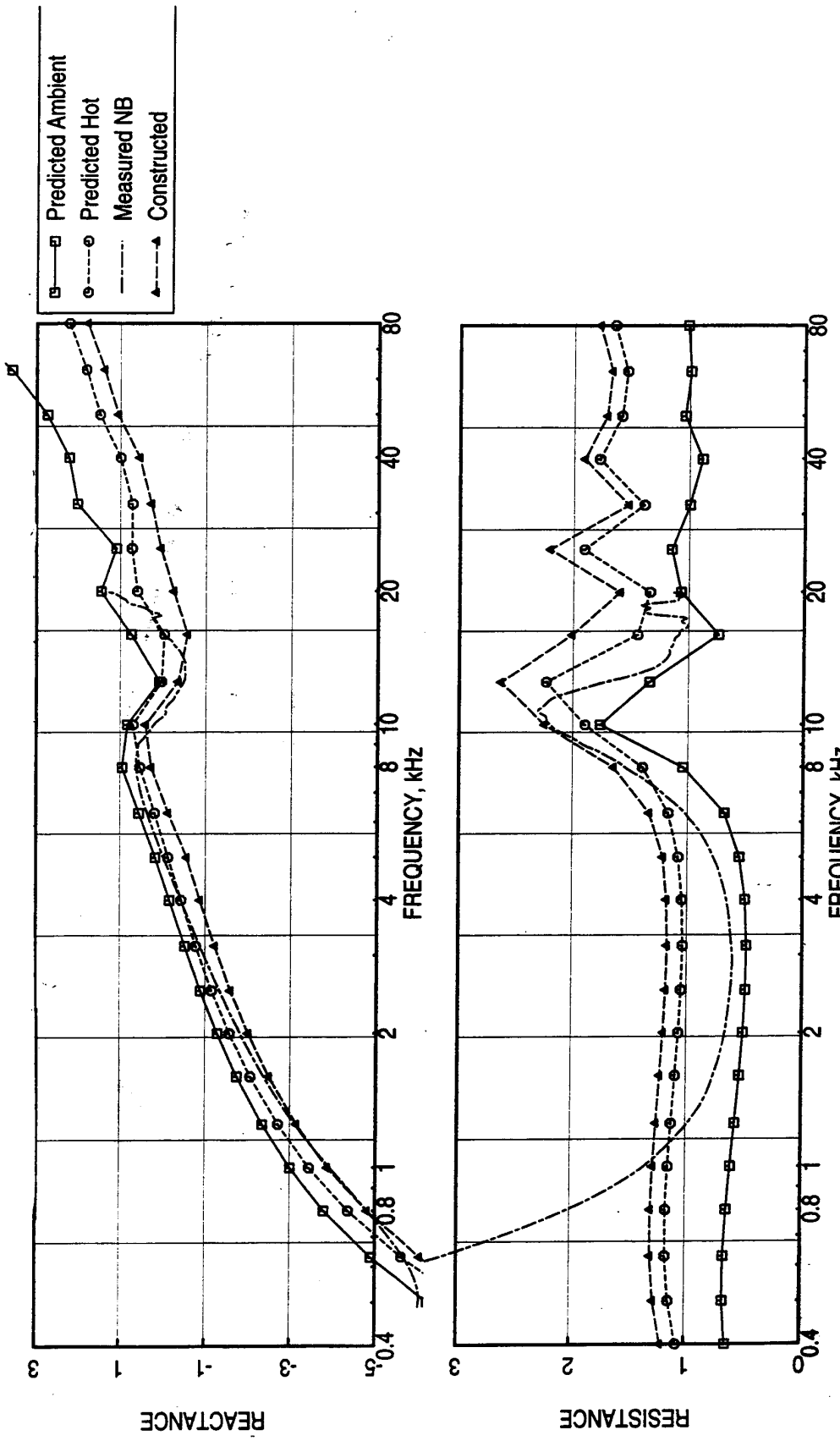

Figure B4. Constructed normal impedance for 0.5"-deep 12 lbf/cft T-Foam bulk absorber utilizing measured ambient data at approach condition, M_F=.0.24, facesheet parameters: porosity=37%, thickness= 0.025", hole diameter = 0.045"; liner surface condition: T=225°F, M=0.063.

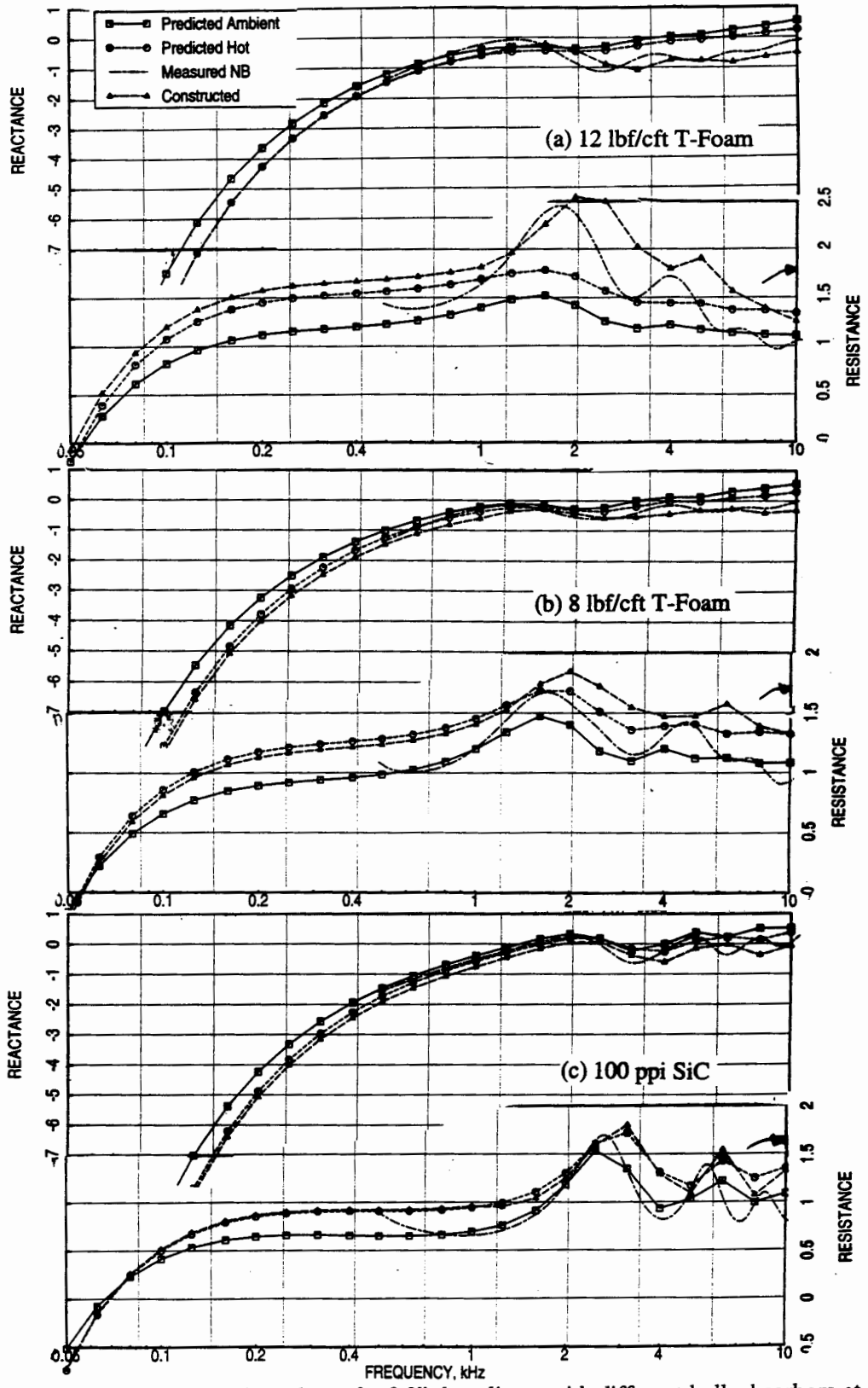

Figure B5. Constructed normal impedance for 2.0"-deep liners with different bulk absorbers at approach condition, M_F=0.24, facesheet parameters: porosity=40%, thickness= 0.04", hole diameter = 0.04"; liner surface condition: T=225°F, M=0.063, 157.5 dB.

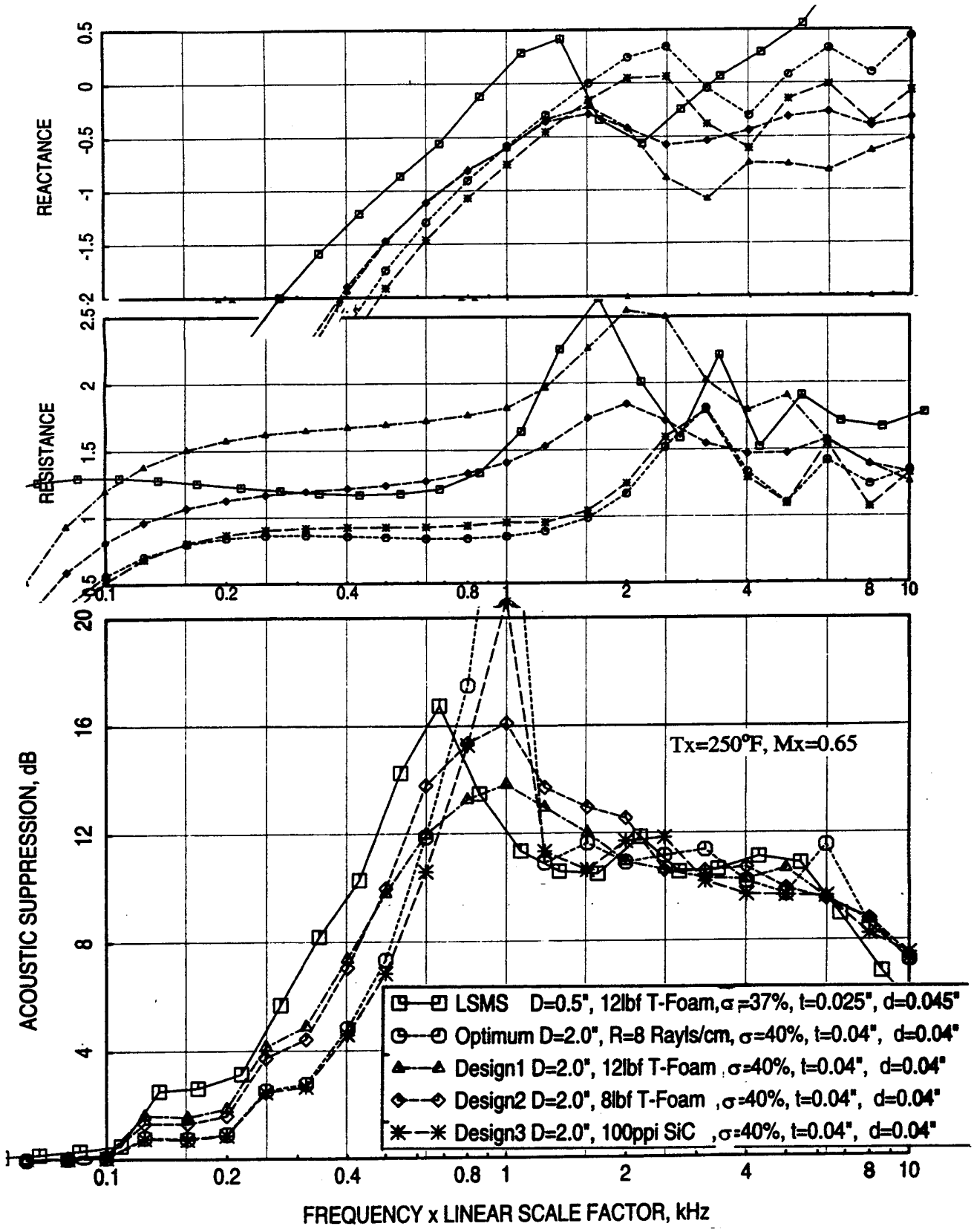

Figure B6. Effect of liner design on predicted normal impedance and acoustic suppression spectra, T=225°F, M=0.63, OASPL=157.5 dB (approach).

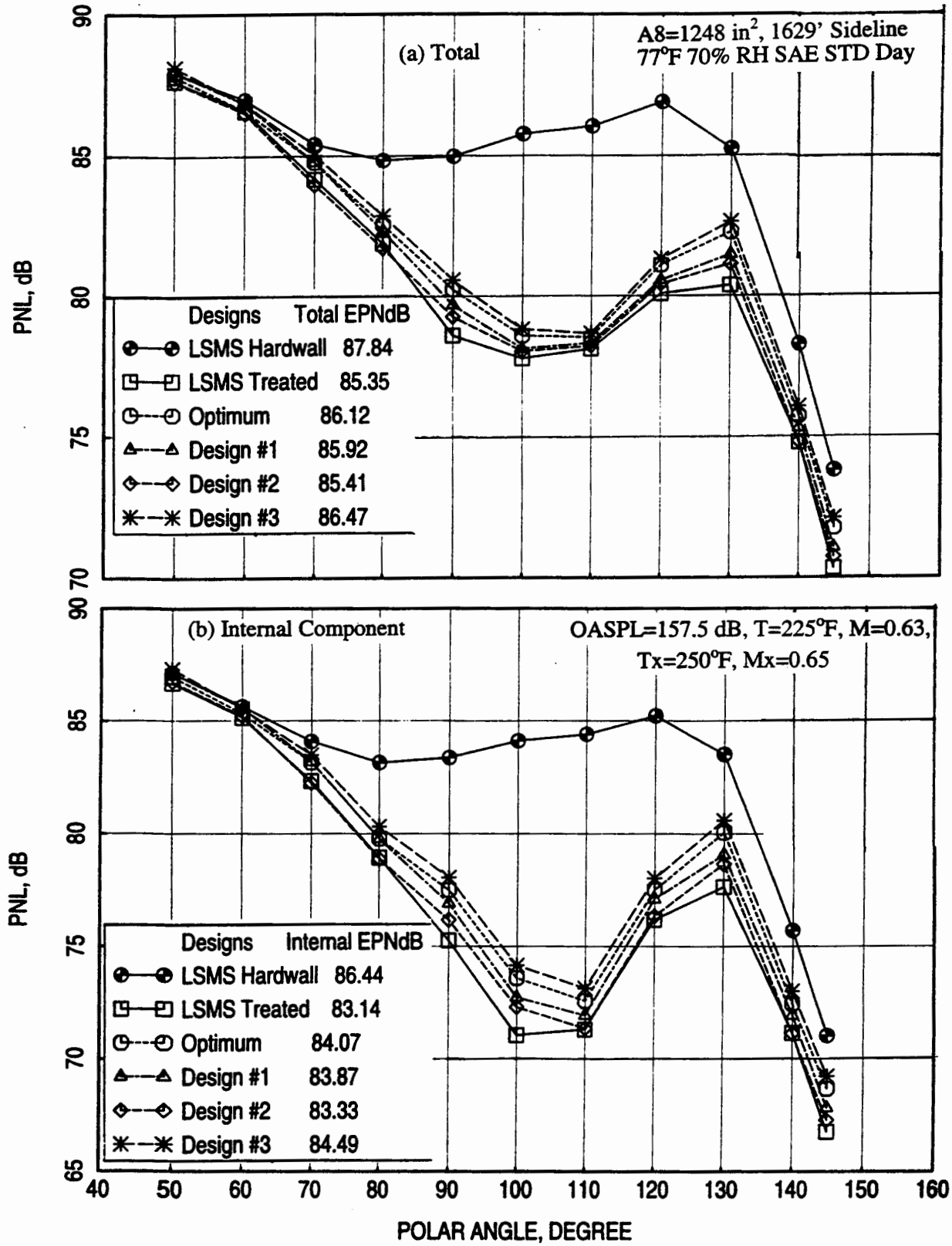

Figure B7. Effect of liner design on predicted (a) total and (b) internal component of PNL directivities for a full-scale mixer-ejector liner design, NPR=1.5, T8=965°R, V_{mix}=670 ft/sec, M=0.24 {approach}.

components obtained at these angles are not real. Most likely, noise radiated from the ejector inlet might have contributed to this effect. Thus, with hypothetically strong internal noise components at angles 50° to 80° the PNL directivity becomes unreal. Therefore, the predicted internal noise suppression is not accurate. If the internal noise spectra at these angles are appropriately corrected then the internal noise suppression will be much higher than the numbers shown in the table. The total suppression levels may not change significantly but their trends with respect to different liner configurations may be different.

It should be noted that the optimum liner is not optimum for this condition, since the optimization is carried out for takeoff condition.

Table B1. Measured and predicted liner benefits in terms of EPNdB for full-scale HSCT nozzle at approach condition (NPR=1.5, T8=965°R, V_{mix}=670 ft/sec) at Flyover distance of 1629', A8=1248 in^2, MAR=0.9, Flight M_F=0.24.

	Measured EPNdB for LSMS Model with 160" Flap, Tested in LSAF, A_t/A_m=8, A_{teff}/A_m=7.4, 12pcf T-Foam 0.5"-Deep bulk liner with perforated Facesheet: Porosity = 37%, Thickness = 0.025", Hole Diameter= 0.045"			Projected EPNdB for Full Scale Model for Different Liners, 160" Treated Flap, A_t/A_m=7.4, A_{teff}/A_m=6.7, 2"-Deep Bulk Liners with Perforated Facesheet: Porosity = 40%, Thickness=0.04", Hole Diameter = 0.04"							
				Optimum Liner		T-Foam 12 lb/cft Standard		T-Foam 8 lb/cft, 3 Paper Layer		100 ppi SiC, 12 lb/cft	
	EPNL Hard Wall	EPNL Treated	Δ EPNL	EPNL,	Δ EPNL	EPNL	Δ EPNL	EPNL	Δ EPNL	EPNL	Δ EPNL
Total	87.84	85.35	-2.49	86.12	-1.72	85.92	-1.92	85.41	-2.43	86.47	-1.37
External	77.93	77.93	0	77.93	0	77.93	0	77.93	0	77.93	0
Internal	86.44	83.14	-3.30	84.07	-2.37	83.87	-2.57	83.33	-3.11	84.49	-1.95

Note: External noise contains Merged & Premerged components. Internal noise components at angles 50° through 80° seem to be unrealistic. The data at these angles might have been contaminated by the noise propagated through the inlet. Thus, the predicted noise suppression may not be accurate.

APPENDIX C

ACOUSTIC SUPPRESSION DUE TO SDOF TYPE LINER DESIGNS FOR LSM MIXER-EJECTOR NOZZLES

C.1 Introduction: Bulk absorber type liners are the primary candidates for mixer-ejector treatment in HSCT application. SDOF type liner designs are being pursued for HSCT application as backup to bulk absorber type liner designs. The objective of the current study of SDOF liner design with constant depth is to implement this liner in the LSM mixer-ejector and to demonstrate experimentally the acoustic suppression capability of this design.

Based on the measured and CFD data for DSM models for a typical takeoff condition (i.e., NPR=3.43, T8=1551°R) the liner designs are carried out for a grazing flow Mach number M of 0.8, liner static temperature T of 500°F, and a static pressure P of 13.24 psi. The cutback conditions (i.e., NPR=2.48, T8=1291°R) are relatively less severe compared to takeoff. The boundary layer displacement thickness for the full-scale ejector is assumed to be 0.20". Thus, the approximate displacement thickness for LSM (~ 56% scale) is about 0.11".

Utilizing the temperature, pressure, and grazing flow conditions for takeoff and using boundary layer displacement thickness for LSM, the liner depth and facesheet properties are varied to arrive at optimum liner designs (i.e., the optimum normal impedance values are attained at critical frequencies, especially at and around the peak Noy frequencies). The optimization of liner design is based on the availability of liner materials and the manufacturing constraints. The current acoustic suppression prediction for the treated ejector assumes rectangular duct with acoustic treatment on two opposite surfaces. The remaining two surfaces are considered to be untreated. Hence, an equivalent treatment length is calculated for the treated ejector, assuming that, the entire treatment is on the two opposing flap surfaces. The equivalent length is utilized in acoustic suppression prediction. Various model-scale mixer-ejector tests have indicated that the treatment on sidewalls is as effective as on flaps. Hence, this procedure is presumed to be reasonable. The acoustic suppression predictions are made assuming uniform flow of Mach number Mx=0.85 and uniform static temperature Tx=530°F. The nozzle parameters for LSM Liner design, considered in the current effort, are listed below:

Nozzle Parameters:

A8 - Square Inches	391
Linear Scale Factor	0.565
Average Sidewall Height - Inches	27.47
Flap Width - Inches	40.20
A_T/A_m	6.7
Equivalent Treatment Length - Inches	94.25

The detail design procedure to establish parameters for a liner to achieve maximum acoustic suppression is described later in section C.2. Based on those results, a **segmented liner** consisting of 3 sections of constant depth but with different facesheet porosity is designed for LSM application. The liner design parameters for LSM mixer-ejector are listed below:

Liner Parameters:

Peak Noy Frequency - Hz.	5600
Maximum Frequency - Hz.	17900
Facesheet Porosity σ, %	20 (L_1), 16 (L_2), & 13 (L_3) - see Figure C1
Facesheet Thickness t, inches	0.018
Facesheet Hole Diameter d, inches	0.03"
Liner Depth D- Inches	0.7"
Expected Total EPNL, dB	97.476
Expected EPNL for Internal Noise, dB	92.137
Linear Scale Factor	0.565
OASPL , dB- Takeoff	176.6 - 167.2 dB
OASPL , dB- Cutback	170.0 - 161.0 dB
Displacement Thickness, θ - Inches	0.11

Liners of depth ranging from 0.6" to 0.8 can be used for efficient acoustic suppression, even though the optimum liner depth on the basis of predicted average EPNL is 0.7". Based on the treatment layout for LSM ejector, the appropriate liner segments of facesheet porosities 20%, 16%, and 13% would begin from the mixer exit and would cover ejector lengths of L_1, L_2, and L_3, respectively, covering the flaps and sidewalls (see Figure C1). The selection of porosities for the three axial segments is based on axial variation of dynamic pressure on liners and associated nonlinear effects on impedance. In the current design constant grazing flow Mach number of 0.8 and static temperature of 500°F are utilized. The optimization may be improved by utilizing appropriate grazing flow Mach numbers and static temperatures for individual liner segment designs. Finally, a comparison of acoustic suppression spectra between SDOF liner design and corresponding bulk absorber type liner designs is shown in Figure C2. The SDOF design results in a predicted EPNL of about 0.4 dB and 0.45 dB higher compared to the current bulk absorber liner Design #1 and optimum design, respectively.

In summary, an axially segmented SDOF type liner is described for LSM which yields about 0.4 EPNdB less noise suppression than the current bulk absorber design and 0.45 EPNdB less than the optimum bulk absorber design. However, further studies in optimizing SDOF liners are worth pursuing as a backup for bulk absorber designs, for the reason of risk reduction. A 0.6" deep segmented SDOF liner with 0.018"-thick facesheet of 0.044" hole diameter was planned to be tested in LSM Build #1. However, this test was never materialized. The fact remains that, such a test for LSM and/or full-scale mixer-ejector to quantify the relative noise suppression capability of an SDOF liner is worth pursuing.

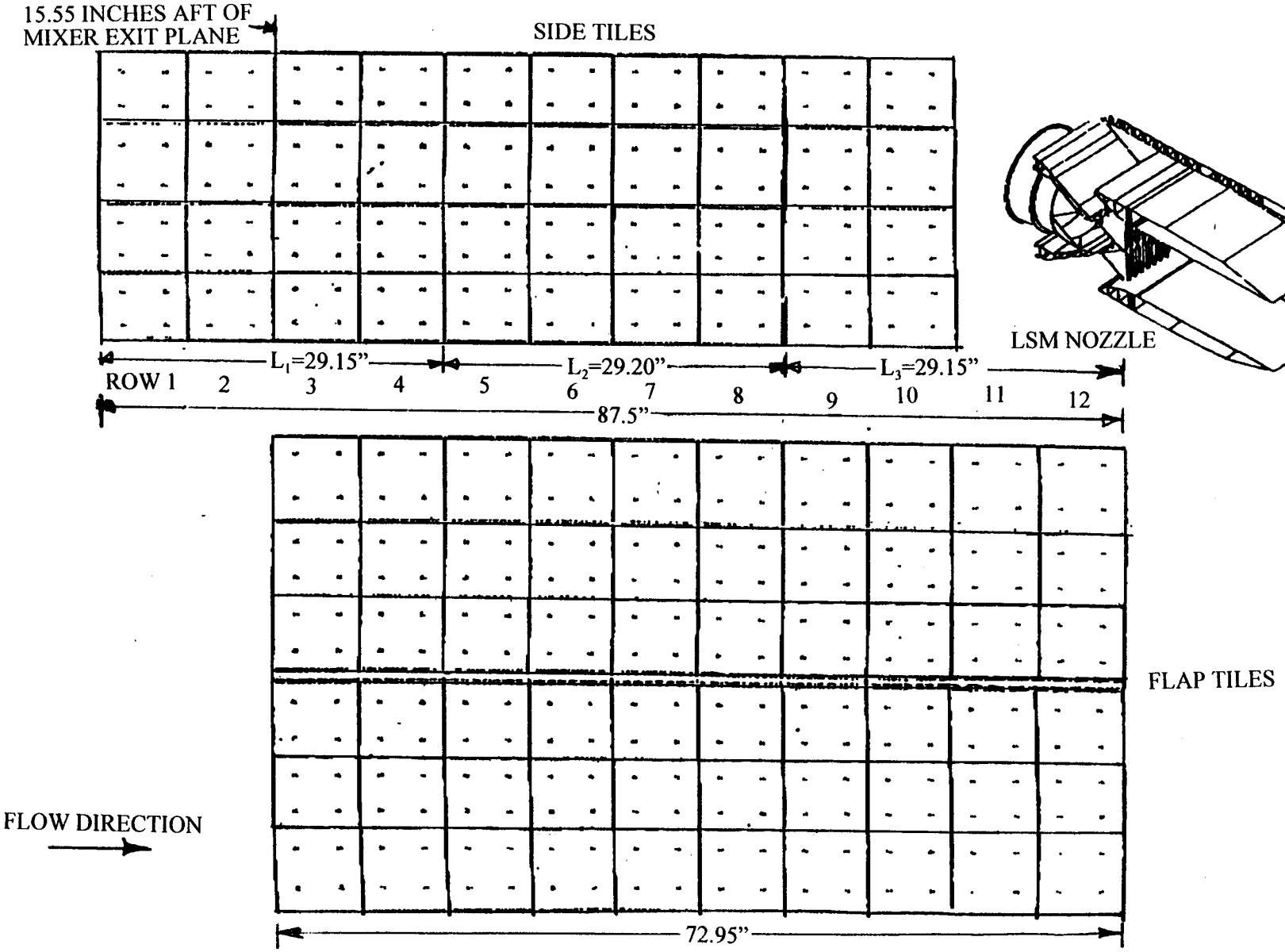

Figure C1. Acoustic treatment layout on flaps and sidewalls for LSM mixer-ejector nozzle.

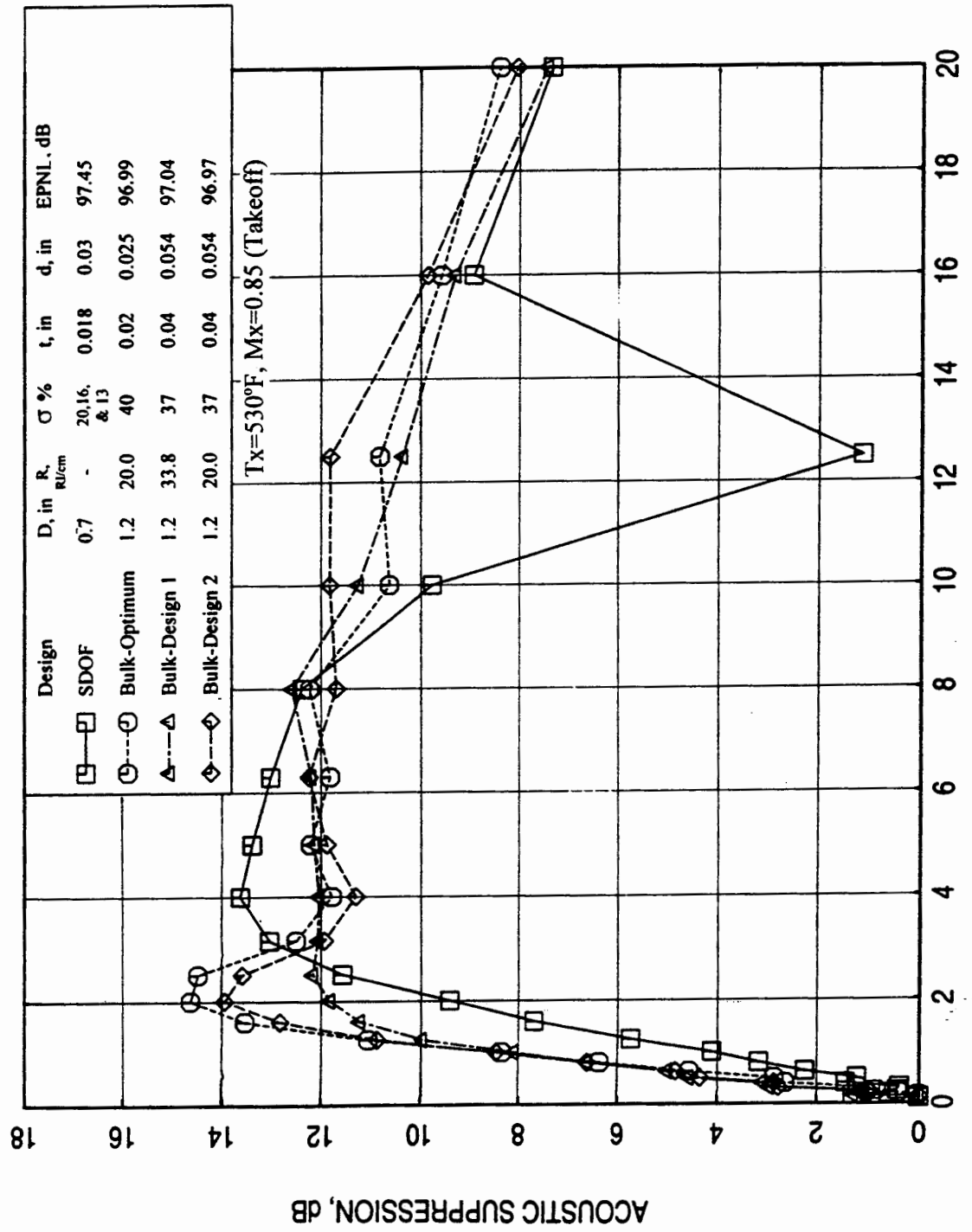

Figure C2. Comparison of predicted acoustic suppression spectra between SDOF type and bulk absorber type liner designs for LSM mixer-ejector, T=500°F, M=0.8.

C.2 Optimization of SDOF Type Liner Design: Parametric study for the SDOF type liners, namely, facesheet properties (i.e., thickness t, hole diameter d, and porosity σ), liner depth D, and dynamic pressure level, are carried out to design an optimum liner. Based on the internal dynamic pressure data for Gen 2 mixer-ejector nozzles, presented in Coordination Memo No. GE95-078-N (Ref. 9), the dynamic pressure levels vary along the length of the ejector. The level seems to be higher closer to the mixer exit and gradually decreases along the ejector length. The impact of dynamic pressure level is expected to influence the SDOF type liner design, for which facesheets of relatively lower porosities are used, compared to the facesheets for bulk absorber liners (nonlinear effect). The ejector is divided into three segments of approximately equal lengths to establish respective average dynamic pressure levels in these segments. These different OASPL levels for the ejector are 176.6 dB, 171.6 dB, and 167.2 dB.

A liner depth of 0.6" (D) with a dynamic OASPL of 176.6 dB is utilized to study the effect of facesheet thickness and hole diameter on acoustic suppression and thereby on EPNdB. To obtain the optimum normal impedance levels at the desired frequency range (4 to 8 kHz for LSM) at takeoff condition a facesheet porosity of 20% (σ) is selected. Figure C-3 shows the predicted normal impedance and acoustic suppression spectra for three different facesheet thicknesses. The effect of facesheet thickness in the range of 0.01" to 0.04" seems to be negligible on acoustic suppression spectra as observed in Figure C-3 in both sets of predictions (i.e., by P&W and GEAE), since, the impedance levels for the facesheet thicknesses considered in this case lie within the optimum range of values. EPNL values calculated using GEAE's predicted acoustic suppression gives a minimum value of 97.49 dB for t=0.018".

Acoustic suppression levels predicted by P&W are lower compared to GEAE's prediction. While, both the predictions are based on modal analysis method, the number of modes utilized by P&W is relatively lower (40 modes) compared to GEAE (50 modes), which may be the cause of the observed difference. However, the liner design is based on relative suppression levels rather than the absolute.

Figure C-4 shows the predicted impedance and acoustic suppression spectra for different facesheet hole diameters for a 0.6" deep liner. The effect of hole diameter is negligible on the acoustic suppression, since, the impedance levels for the facesheet diameters considered in this case lie within the optimum range of values. A hole diameter of 0.03" seems to be slightly favorable on the basis of EPNdB.

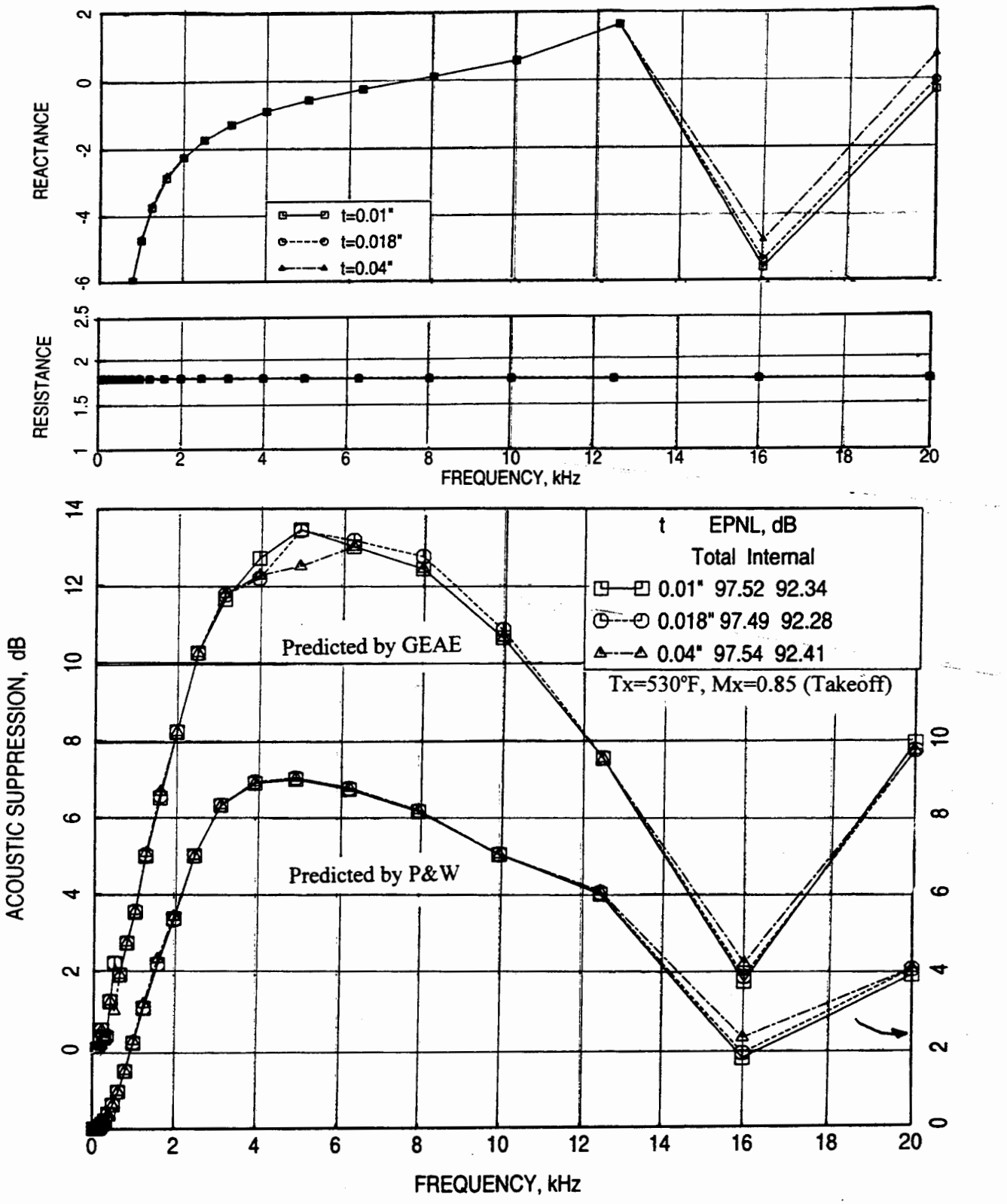

Figure C3. Effect of facesheet thickness t on predicted normal impedance and acoustic suppression spectra for SDOF type liner design for LSM mixer-ejector, D=0.6", σ=20%, d=0.044", OASPL=176.6 dB, T=500°F, M=0.8.

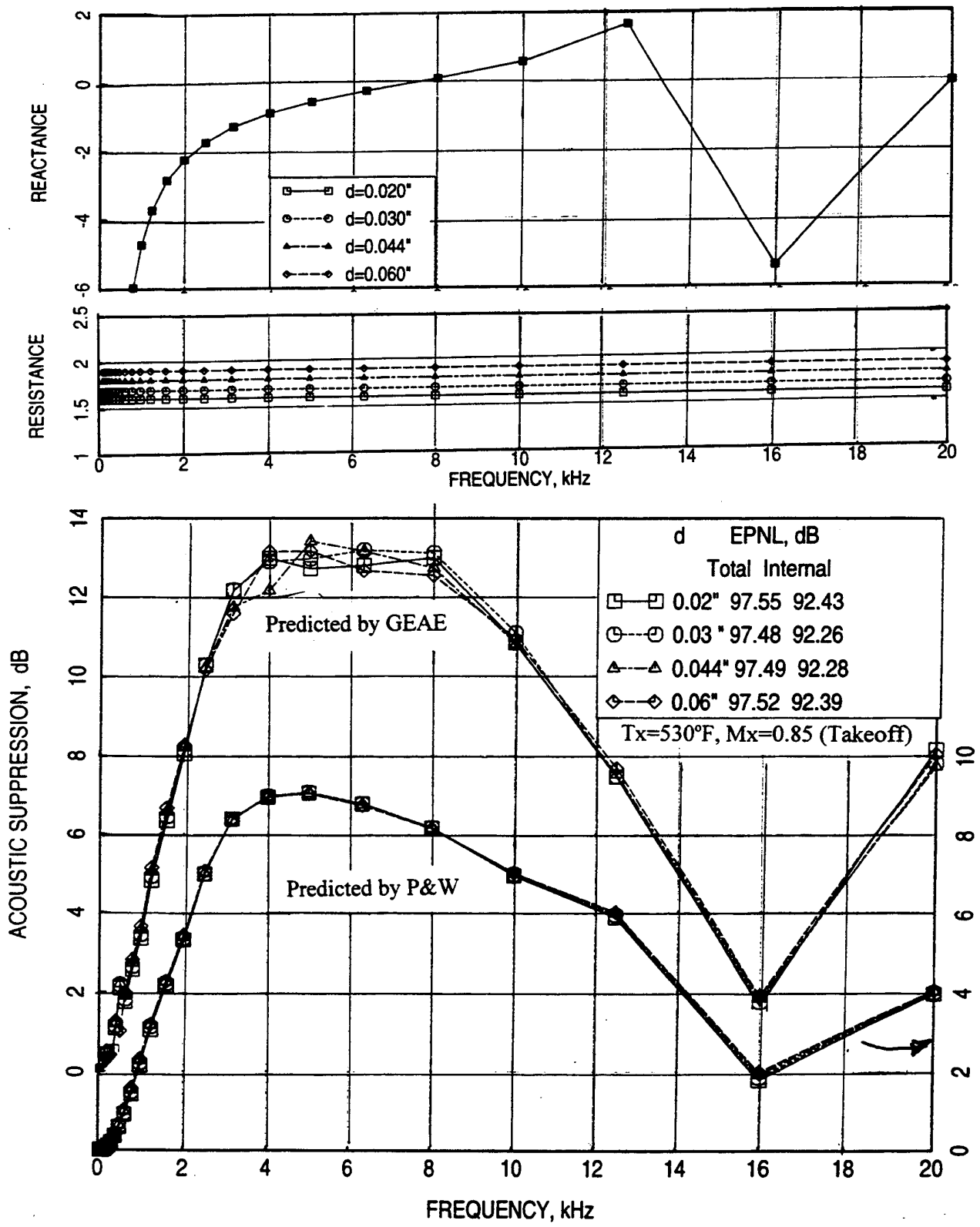

Figure C4. Effect of facesheet hole diameter d on predicted normal impedance and acoustic suppression spectra for SDOF type liner design for LSM mixer-ejector, D=0.6" σ=20%, t=0.018", OASPL=176.6 dB, T=500°F, M=0.8.

Effect of facesheet porosity on acoustic suppression is studied at three OASPLs for a 0.6" deep liner with a 0.018" thick facesheet. Figure C-5 shows the predicted normal impedance and acoustic suppression spectra for an OASPL of 176.6 dB. The acoustic suppression is highest for a 20% porous facesheet. The suppression is lower for other designs of different facesheet porosities, especially, for facesheets with lower porosities for which the resistance levels are much higher compared to the optimum. Similar results for 171.6 dB and 167.2 dB are shown in Figures C-6 and C-7, respectively. The optimum porosity of the facesheets for these cases is 16% and 13%, respectively. These results are summarized in Figure C-8 by plotting EPNL with respect to the facesheet porosity at different dynamic pressure conditions.

Effect of dynamic pressure level on acoustic suppression is further studied for a 0.6" deep liner with 0.018" thick facesheet. Figure C-9 shows the predicted normal impedance and acoustic suppression spectra for a 12% porous facesheet at OASPLs of 167.2 dB and 176.6 dB. For this facesheet, as expected from the earlier results, a higher acoustic suppression is obtained for 167.2 dB OASPL case. Similar result for a 20% porous facesheet is shown in Figure C-10 and is found more efficient in suppressing acoustic energy at an OASPL of 176.6 dB.

Efficient acoustic suppression at dynamic pressure levels of 176.6 dB, 171.6 dB, and 167.2 dB is, therefore, achievable for an SDOF type liner with facesheet porosities of 20%, 16%, and 13%, respectively. Thus, a segmented liner with constant depth but facesheets of different porosities seems to be the solution for efficient acoustic suppression.

With the segmented liner design the optimum liner depth evaluation is carried out for each of the three dynamic level and facesheet porosity combinations. Figure C-11 shows the predicted normal impedance and acoustic suppression spectra for liners of different depths with a 20% porous facesheet at OASPL of 176.6 dB. A 0.6" or 0.7" deep liner seems to be the optimum for this case. Similar results for a 16% porous facesheet at 171.6 dB OASPL and 13% porous facesheet at 167.2 dB OASPL are shown in Figures C-12 and C-13, respectively. Optimum depths for these cases are 0.7" and 0.6" to 0.7", respectively. The EPNL values are plotted with respect to liner depth in Figure C-14.

Finally, the segmented liner results at different liner depths are presented in Figures C-15 through C-17. Figure C-15 shows the predicted normal impedance and acoustic suppression for 0.6"-deep liners of different facesheet porosities along with the corresponding optimum dynamic pressure levels. As expected, the impedance as well as acoustic suppression results are very close to each other for the three cases. Acoustic suppression results for similar liners

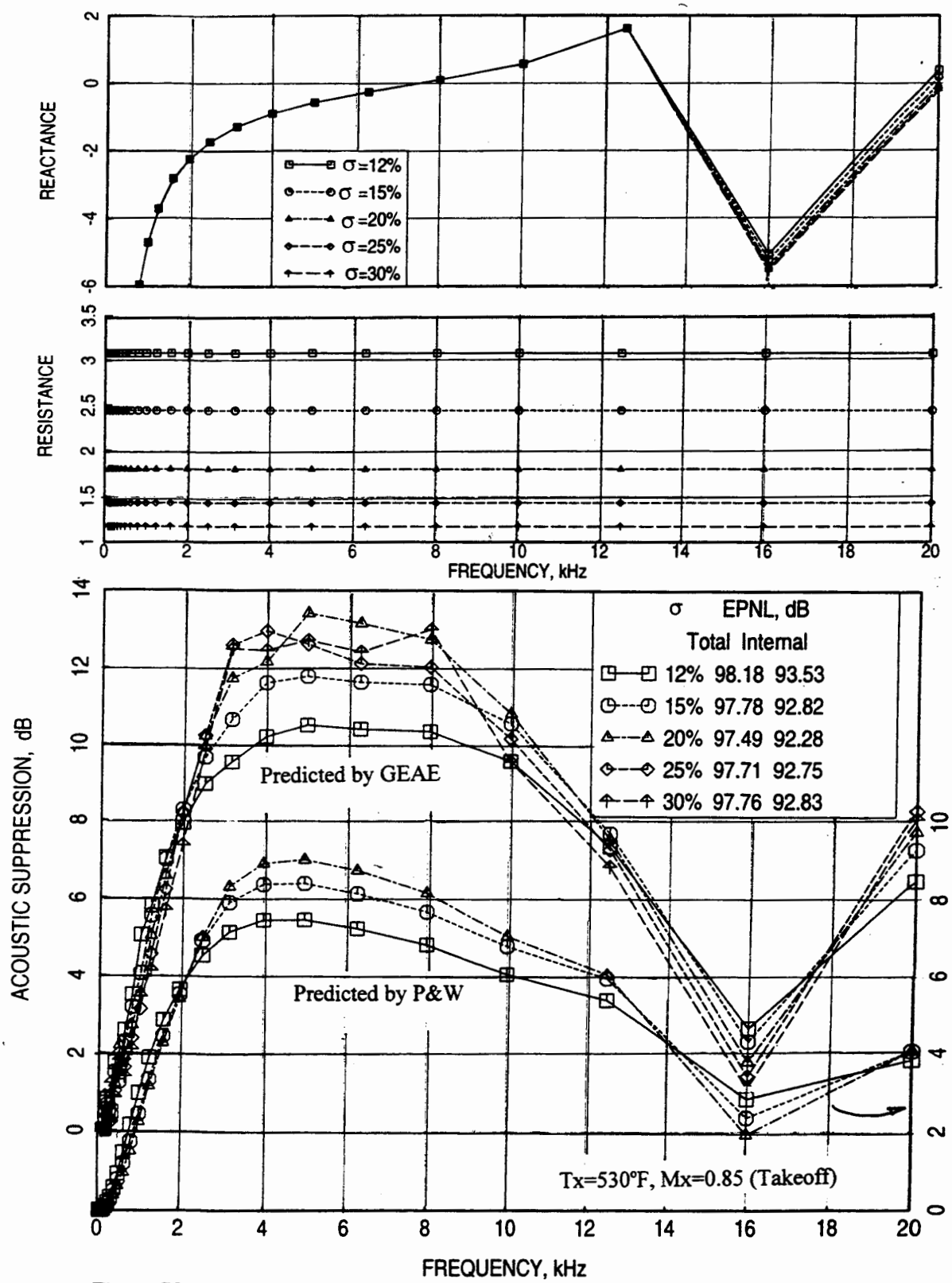

Figure C5. Effect of facesheet porosity σ on predicted normal impedance and acoustic suppression spectra for SDOF type liner design for LSM mixer-ejector, D=0.6", d=0.044", t=0.018", OASPL=176.6 dB, T=500°F, M=0.8.

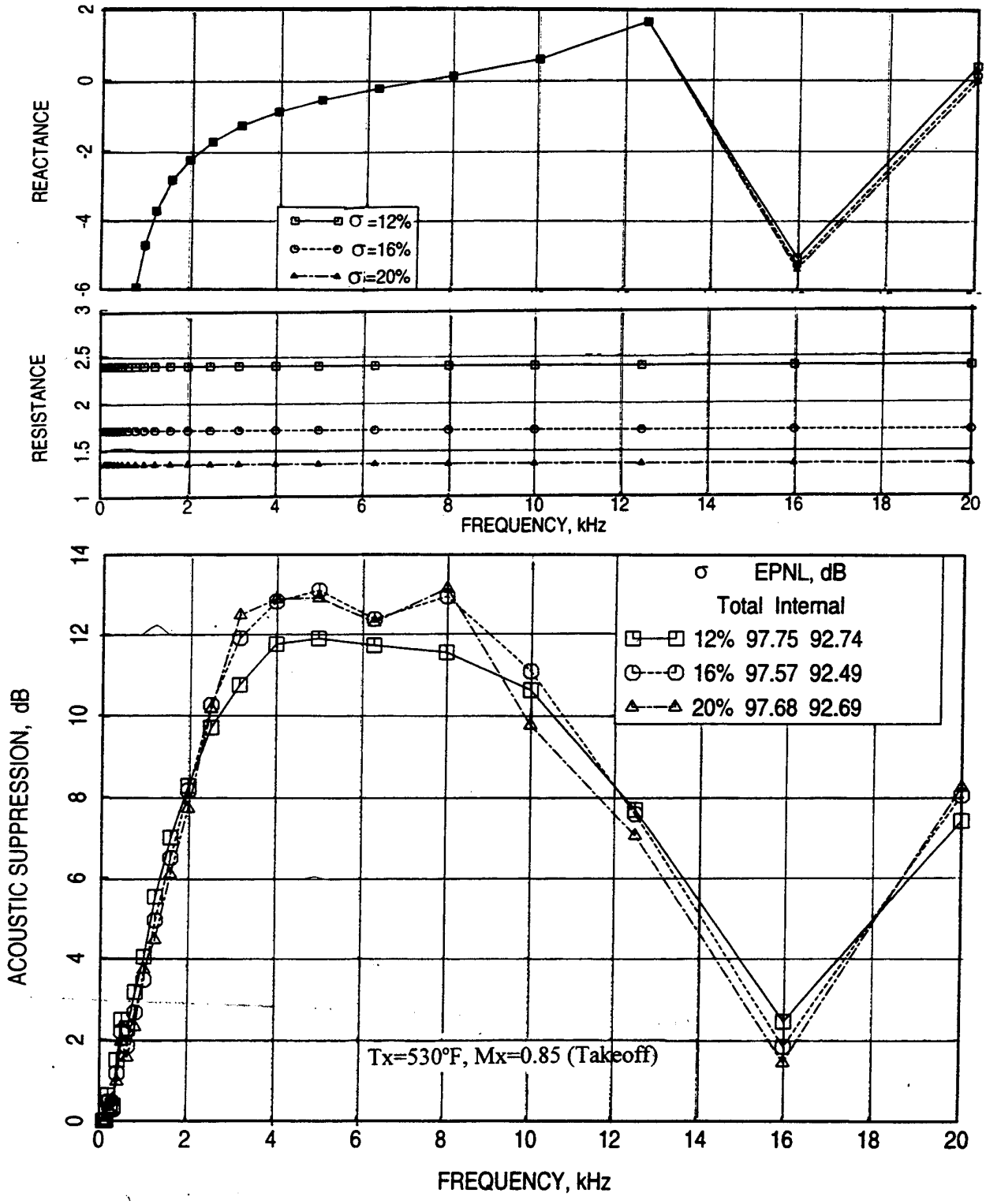

Figure C6. Effect of facesheet porosity σ on predicted normal impedance and acoustic suppression spectra for SDOF type liner design for LSM mixer-ejector, D=0.6", d=0.03", t=0.018", OASPL=171.6 dB, T=500°F, M=0.8.

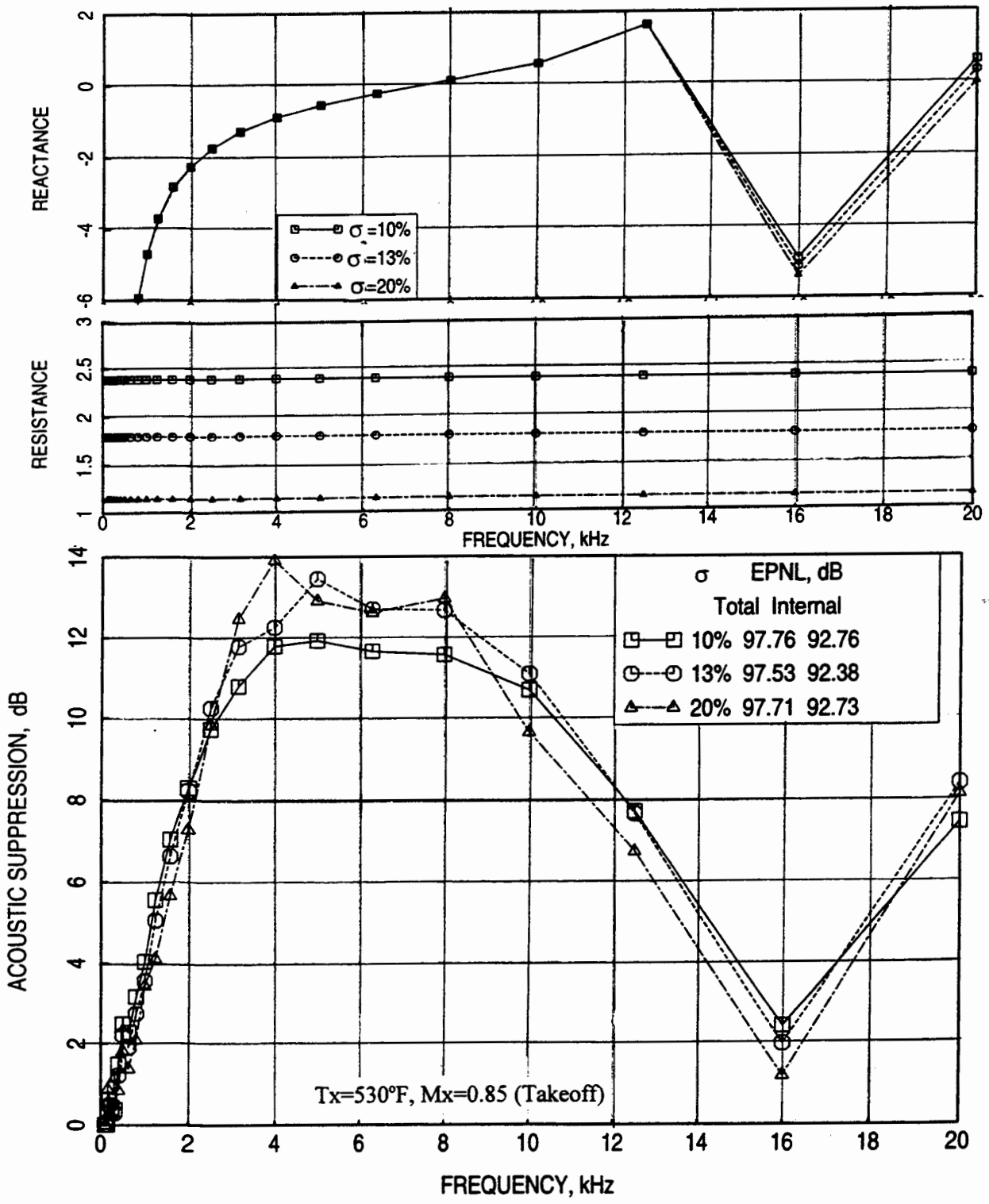

Figure C7. Effect of facesheet porosity σ on predicted normal impedance and acoustic suppression spectra for SDOF type liner design for LSM mixer-ejector, D=0.6", d=0.03", t=0.018", OASPL=167.2 dB, T=500°F, M=0.8.

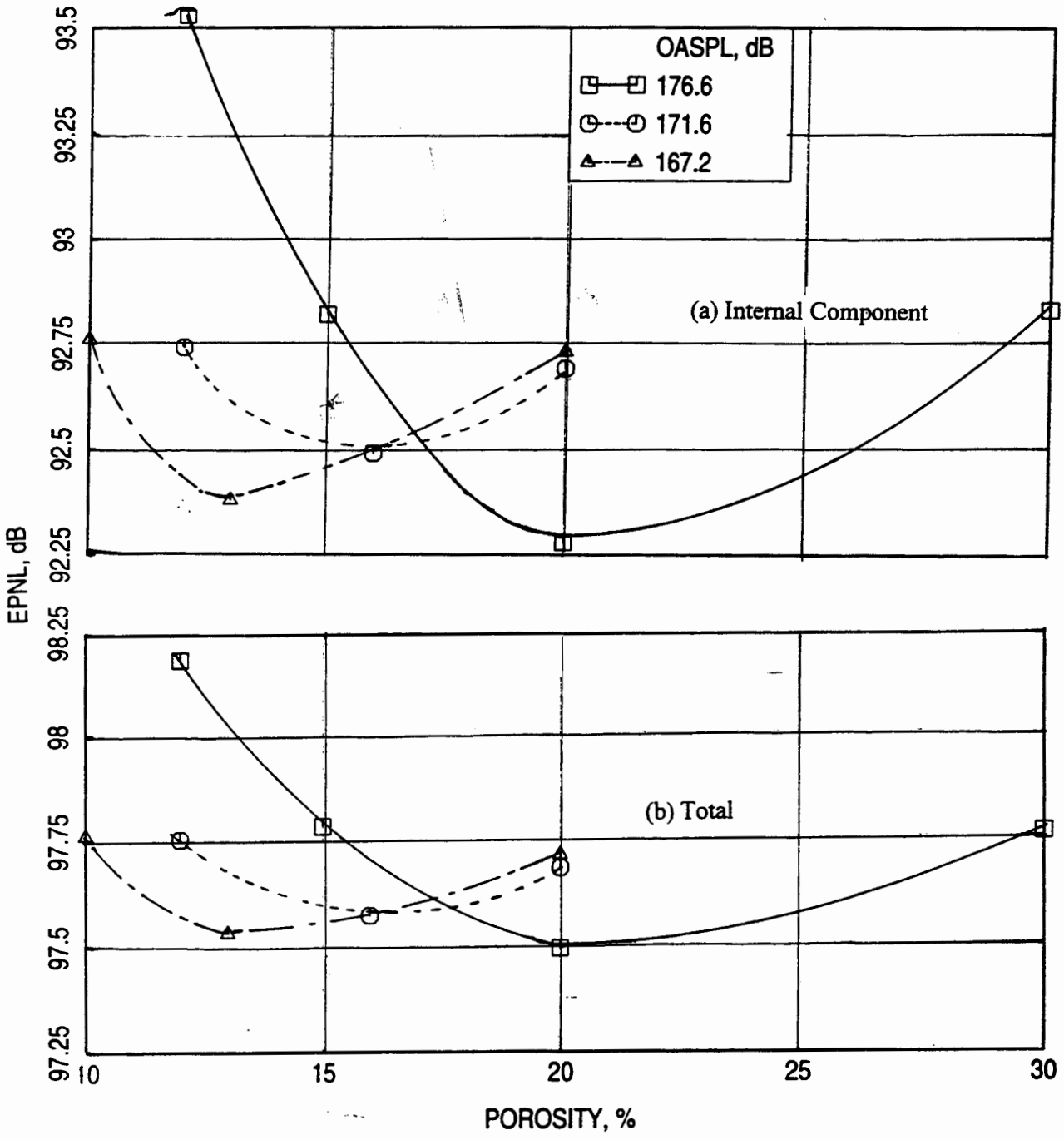

Figure C8. Effect of facesheet porosity S on predicted EPNL for takeoff condition (Tx=530°F, Mx=0.85) at different OASPL for SDOF type liner design for LSM mixer-ejector, D=0.6", d=0.03", t=0.018", T=500°F, M=0.8.

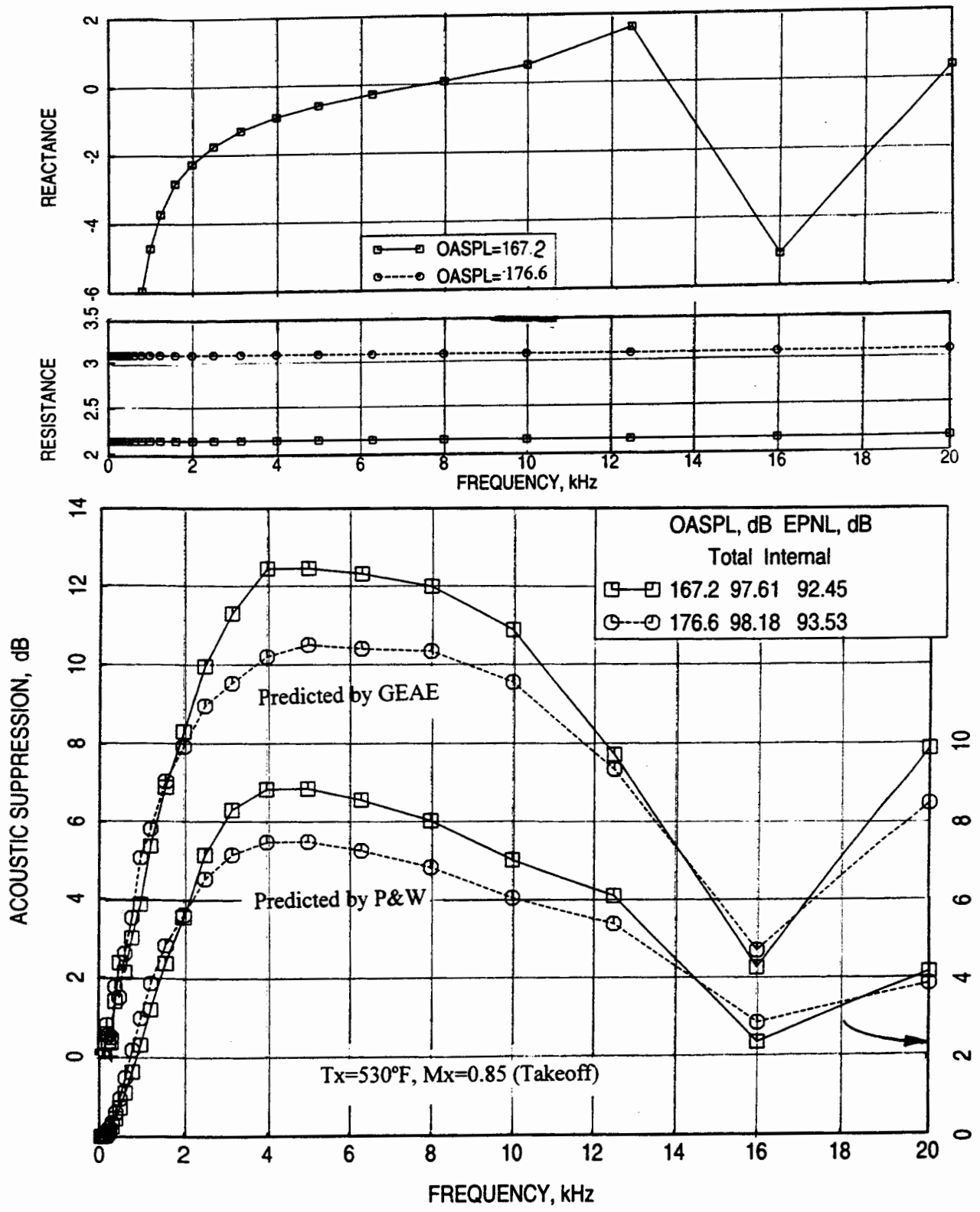

Figure C9. Effect of OASPL on predicted normal impedance and acoustic suppression spectra for SDOF type liner design for LSM mixer-ejector, D=0.6", σ=12%, d=0.044", t=0.018", T=500°F, M=0.8.

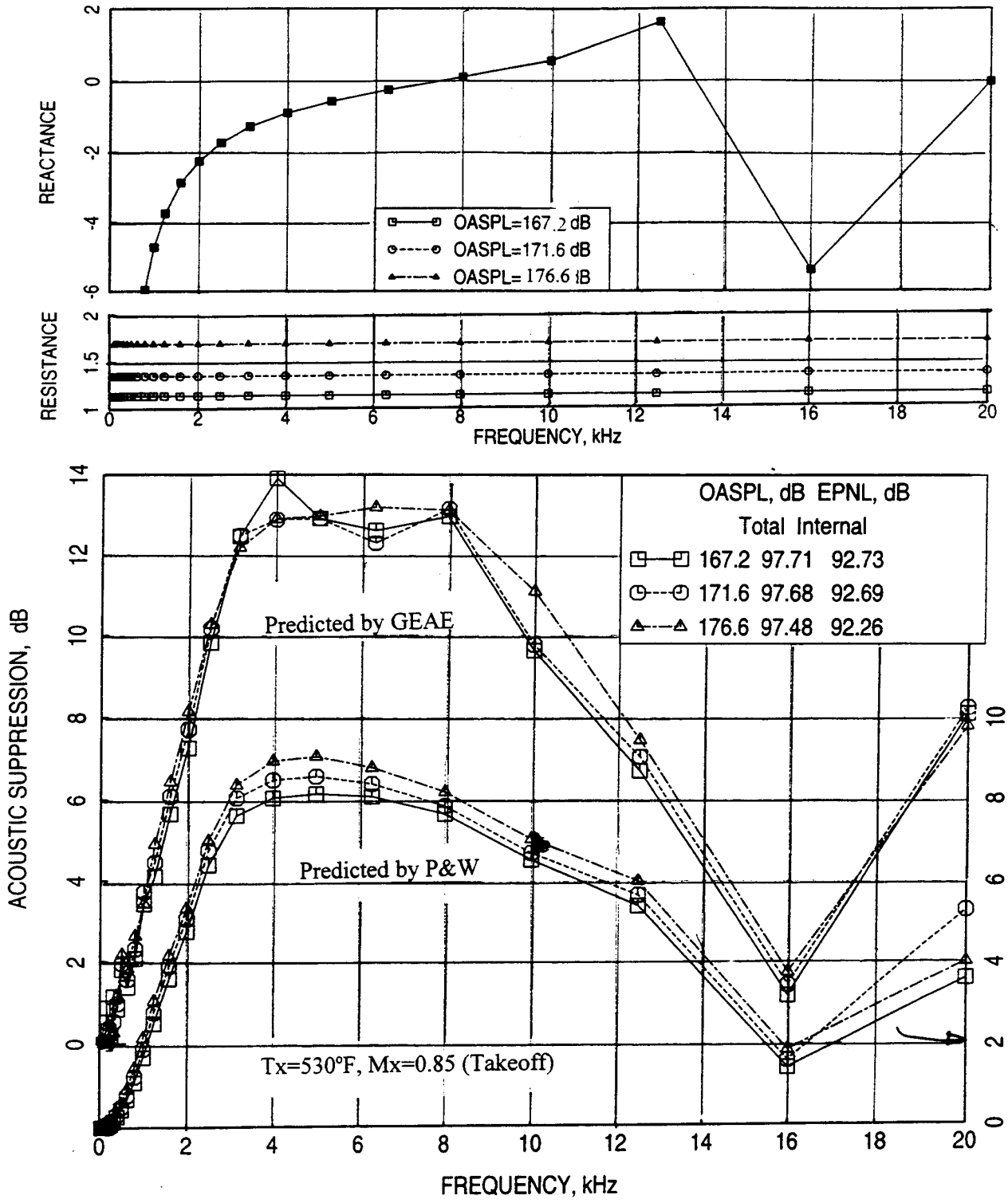

Figure C10. Effect of OASPL on predicted normal impedance and acoustic suppression spectra for SDOF type liner design for LSM mixer-ejector, D=0.6", σ =20%, d=0.03", t=0.018", T=500°F, M=0.8.

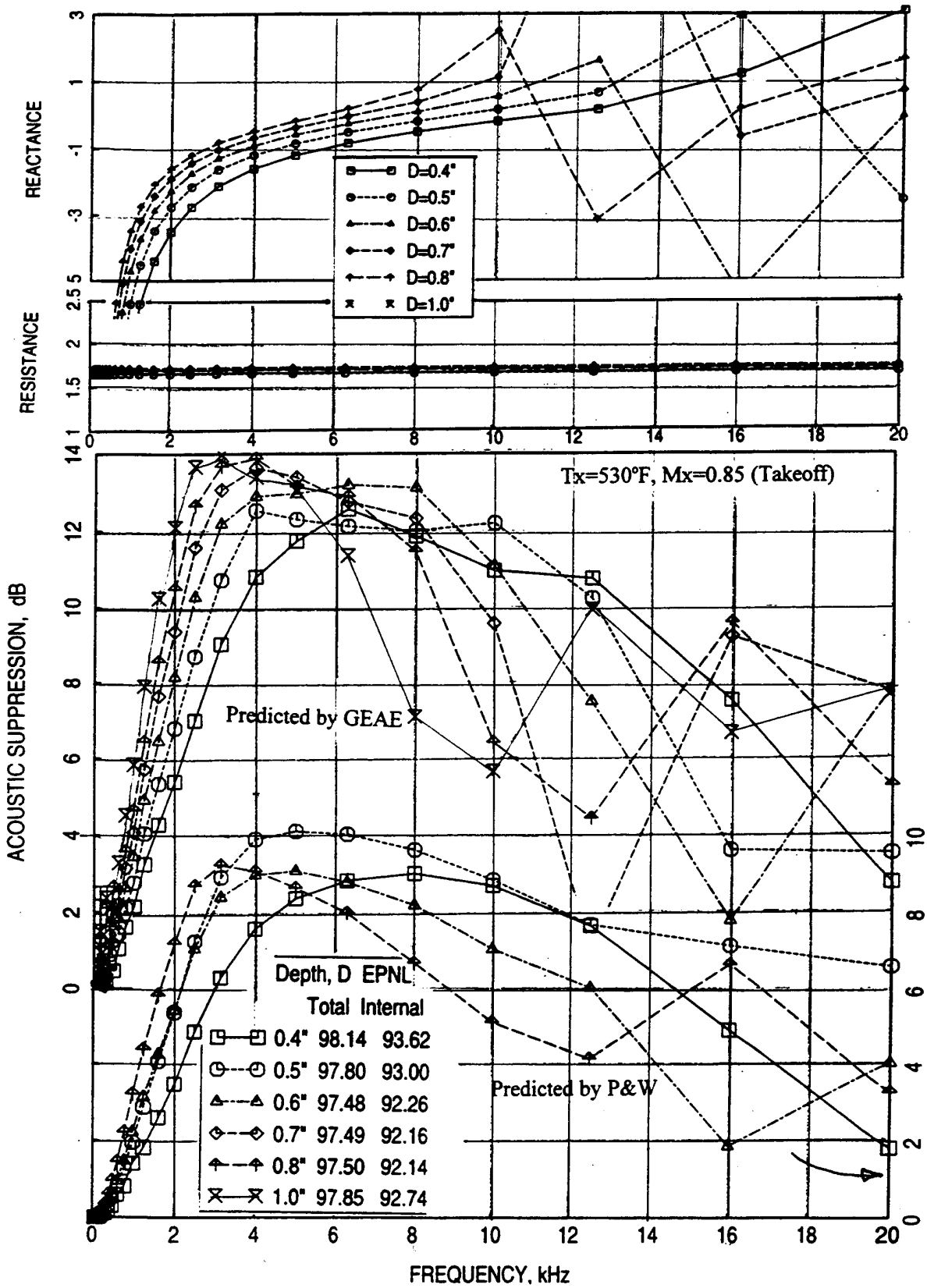

Figure C11. Effect of liner depth D on predicted normal impedance and acoustic suppression spectra for SDOF type liner design for LSM mixer-ejector, S=20%, d=0.03", t=0.018", OASPL=176.6 dB, T=500°F, M=0.8.

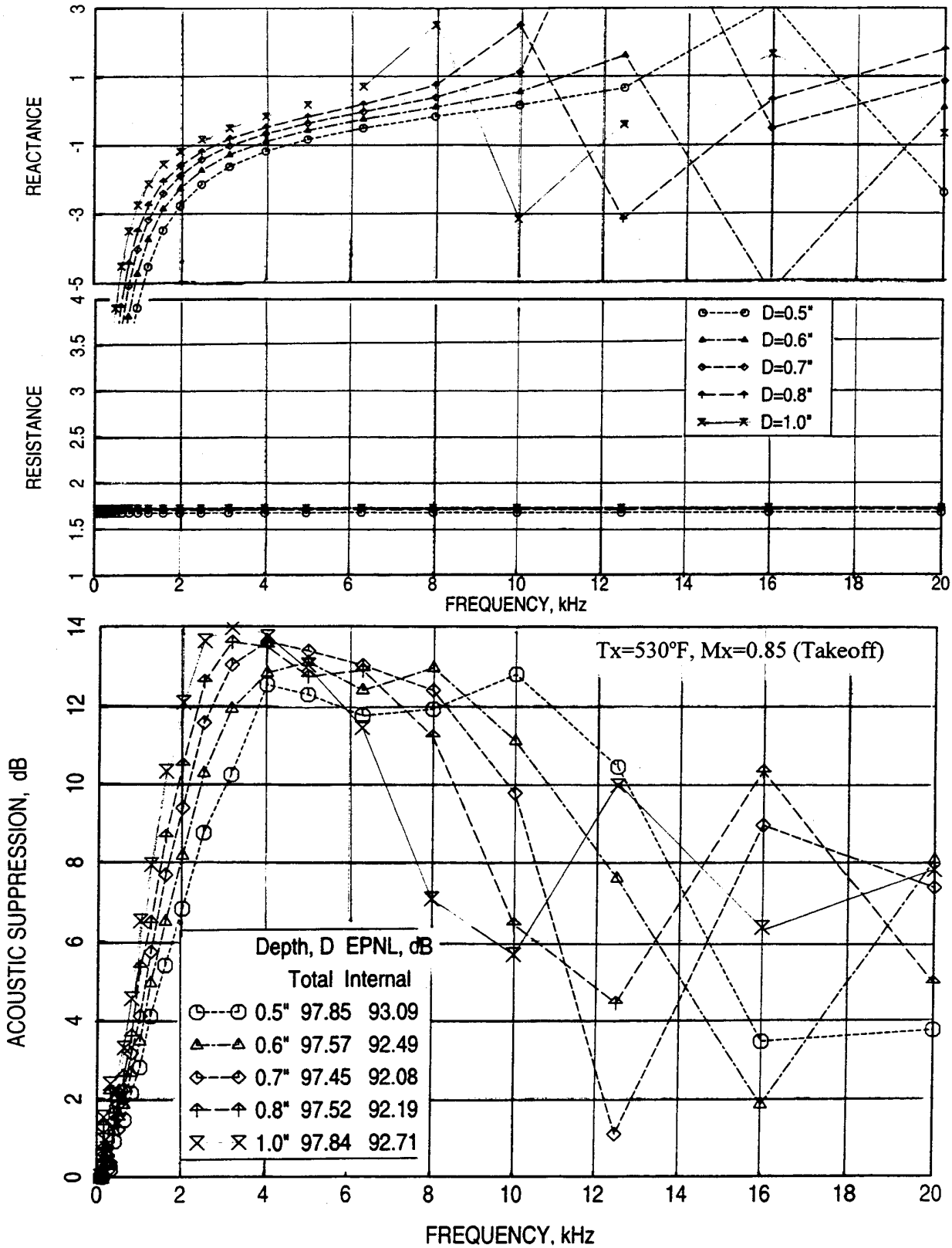

Figure C12. Effect of liner depth D on predicted normal impedance and acoustic suppression spectra for SDOF type liner design for LSM mixer-ejector, S=16%, d=0.03", t=0.018", OASPL=171.6 dB, T=500°F, M=0.8.

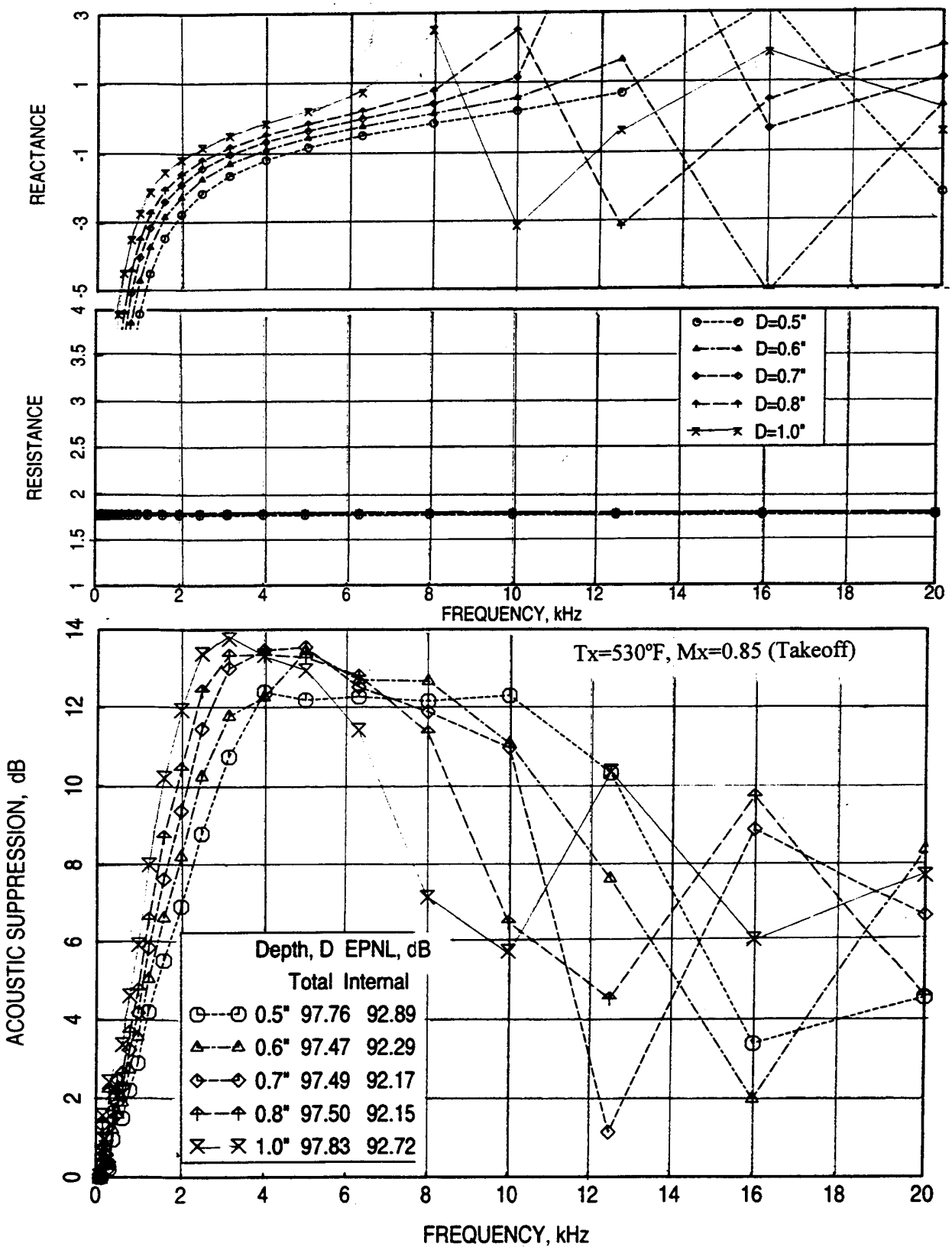

Figure C13. Effect of liner depth D on predicted normal impedance and acoustic suppression spectra for SDOF type liner design for LSM mixer-ejector, S=13%, d=0.03", t=0.018", OASPL=167.2 dB, T=500°F, M=0.8.

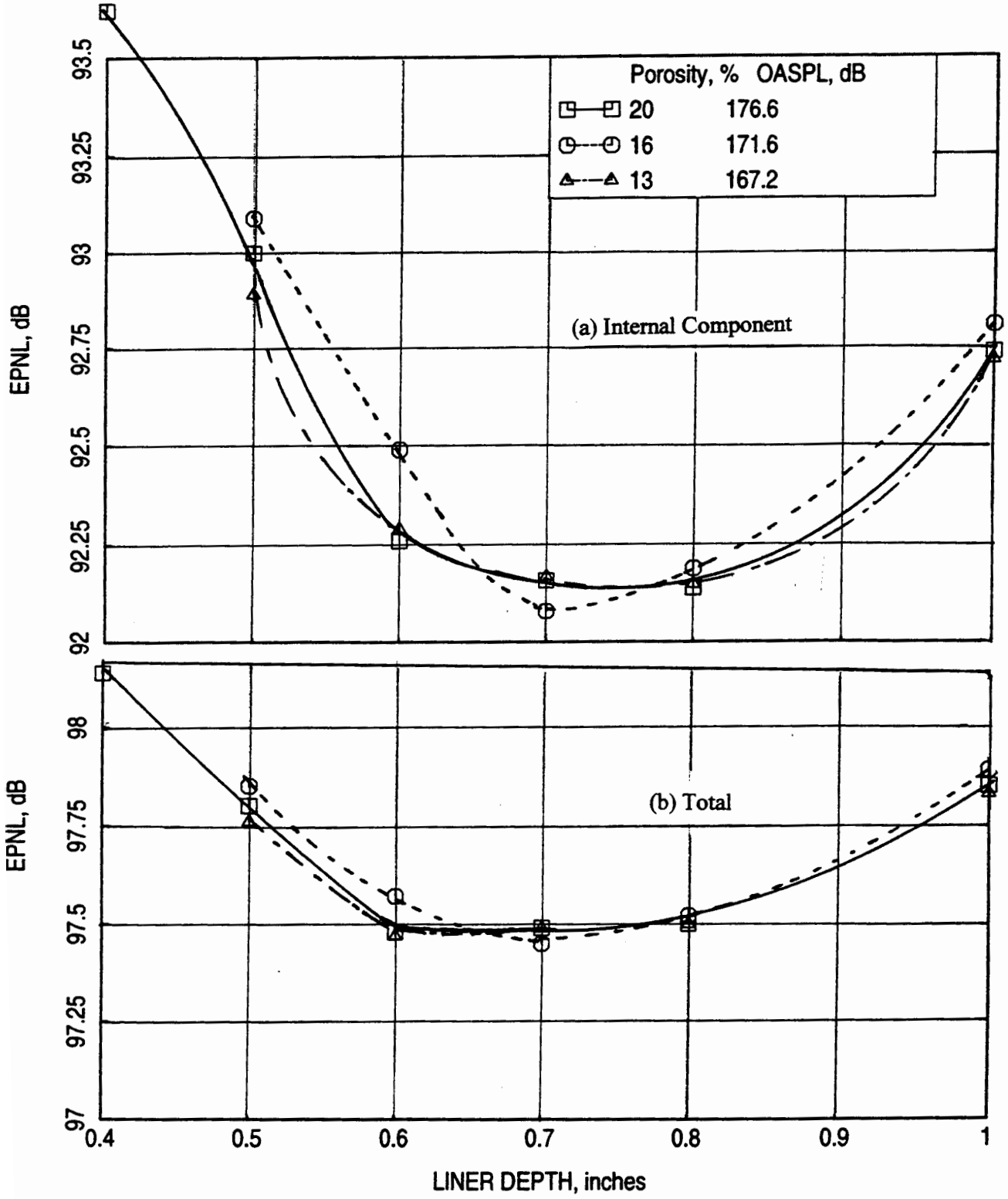

Figure C14. Effect of Liner depth D on predicted EPNL for takeoff condition (Tx=530°F, Mx=0.85) at different facesheet porosity S with varying OASPL for SDOF type liner design for LSM mixer-ejector, d=0.03", t=0.018", T=500°F, M=0.8.

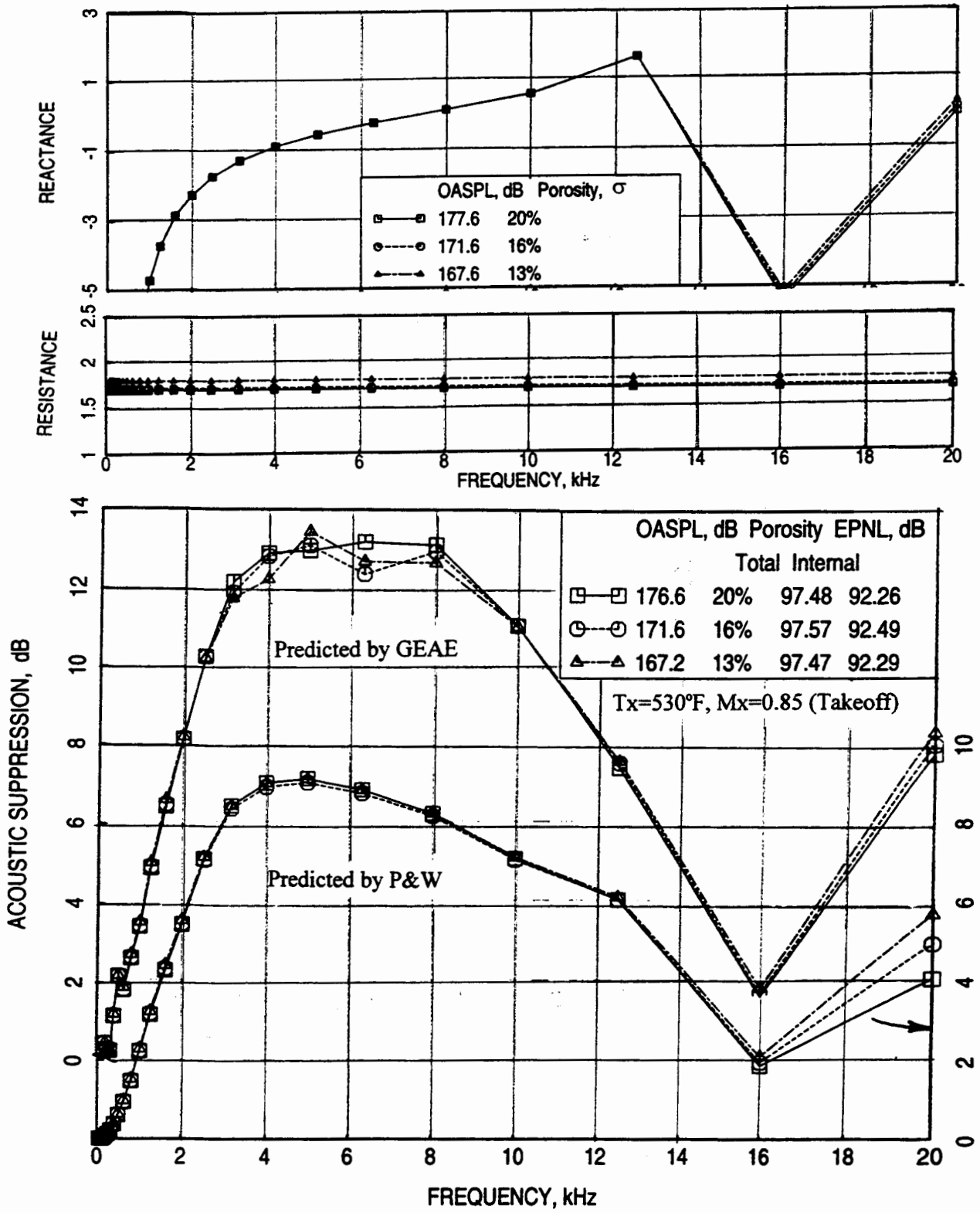

Figure C15. Effect of facesheet porosity S with varying OASPL on predicted normal impedance and acoustic suppression spectra for SDOF type liner design for LSM mixer-ejector, D=0.6", d=0.03", t=0.018", T=500°F, M=0.8.

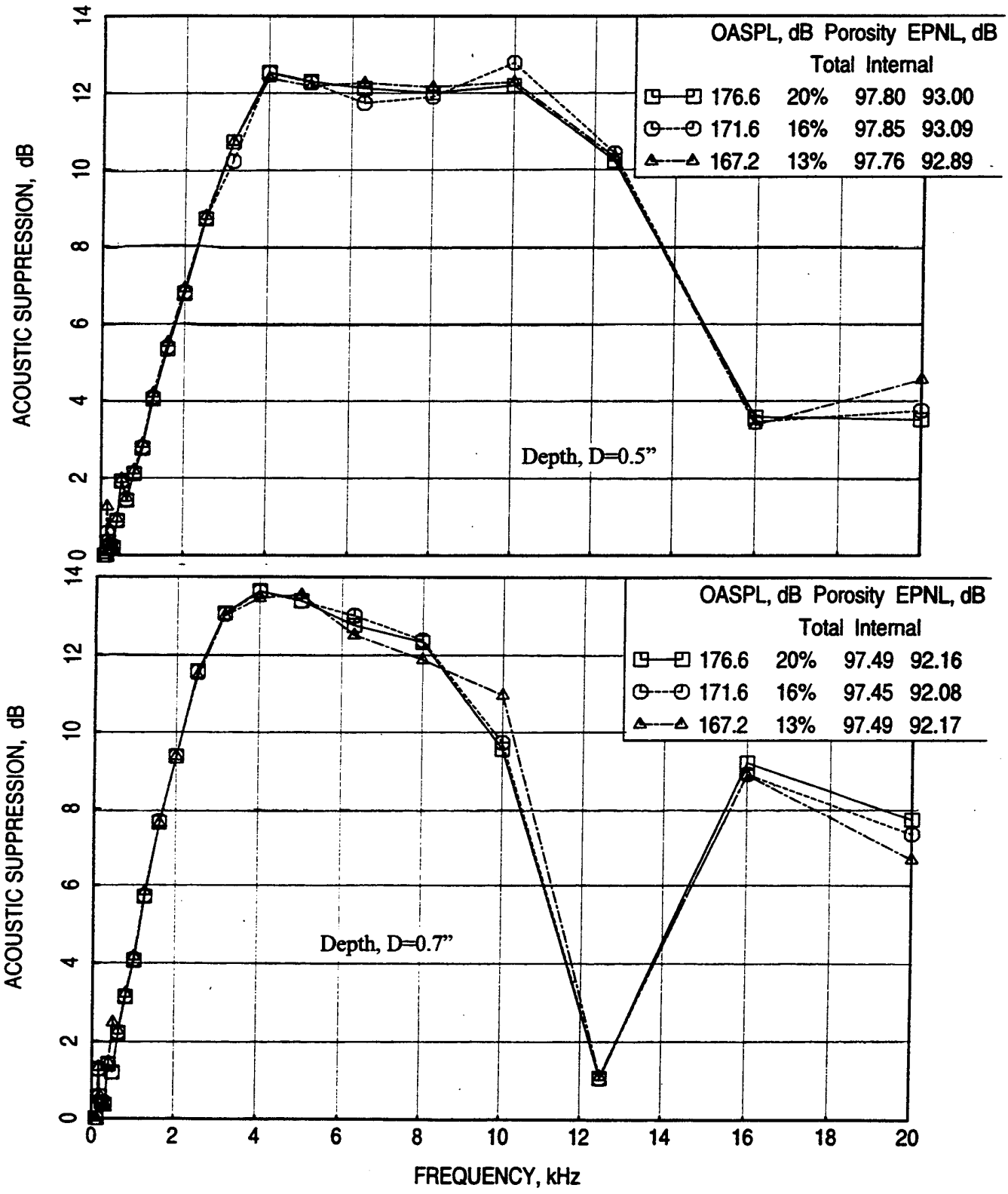

Figure C16. Effect of facesheet porosity S with varying OASPL on predicted acoustic suppression spectra for SDOF type liner design for LSM mixer-ejector, d=0.03", t=0.018", T=500°F, M=0.8.

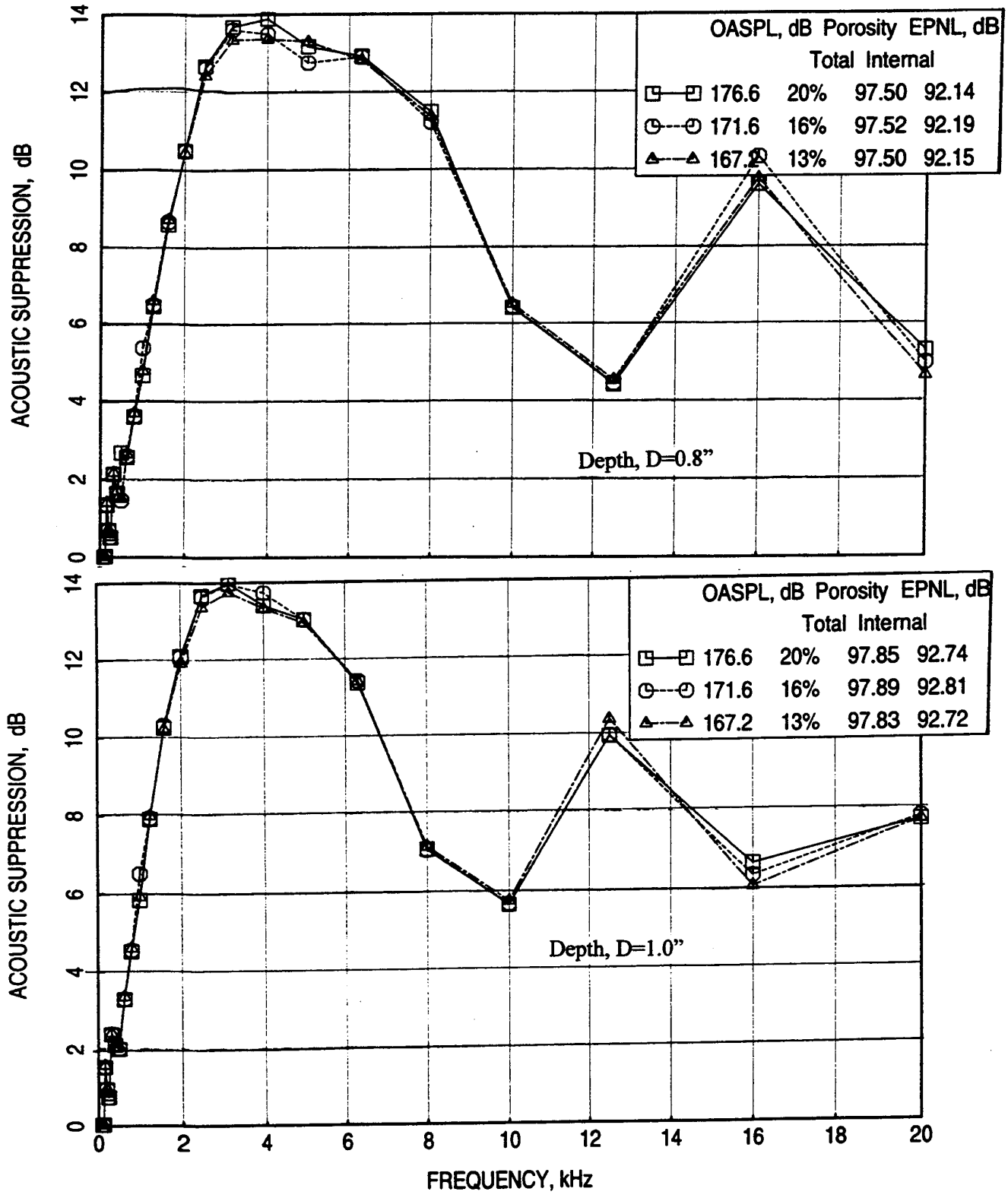

Figure C17. Effect of facesheet porosity S with varying OASPL on predicted acoustic suppression spectra for SDOF type liner design for LSM mixer-ejector, d=0.03", t=0.018", T=500°F, M=0.8.

of depths 0.5", 0.7", 0.8", and 1.0" are shown in Figures C-16 and C-17. Again, at each depth the acoustic suppression levels match for all three porosity/dynamic level combinations. The table below lists the average EPNL with respect to liner depth, assuming that each liner segment is of equal acoustic suppression contributor:

Liner Depth D, Inches	Total Average EPNL, dB	Average EPNL for Internal Noise Components, dB
0.5	97.803	92.993
0.6	97.506	92.346
0.7	97.476	92.137
0.8	97.507	92.160
1.0	97.857	92.757

APPENDIX D

LSM BUILD-1 MIXER-EJECTOR TEST RESULTS AND COMPARISON WITH PREDICTION

The large-scale model of build-1(LSM-1) mixer-ejector was tested in a static stand. Bulk absorber liner with 1.2"-deep 12 lbf standard T-Foam and perforated facesheet (σ=37%, t=0.04", d=0.054") were used for the construction of liner trays. The treatment layout for this configuration is shown in Figure C1. All the earlier farfield noise predictions for LSM model, presented in this report, were made for a flight Mach number of 0.32. Since the actual test was done at static condition it is important to predict the farfield noise at static condition, not only for the LSM-1 but also for 1/7-scale model. Comparison of data between 1/7-scale and LSM-1 and data with prediction for LSM-1 would provide useful insight for liner scaling. Thus, farfield noise for LSM-1 nozzle is predicted utilizing the measured 1/7-scale data at static condition. The procedure is similar to that of flight case, described in this report. In addition, LSM-1 and 1/7-scale model (NRA) measured data at static condition is analyzed.

D.1 Total, External, and Internal Noise Components: Tests were conducted at a number of aerothermodynamic conditions and the data on the ground was measured at sideline and community locations (i.e., φ of 25° and 90°,respectively). Due to the flow and temperature constraints of the test facility the takeoff condition was not reached. Thus, the data for the highest pressure and temperature (i.e., NPR=3.25 and T8=1580°R), which is reasonably closer to the takeoff condition, is analyzed and used for takeoff comparison. Figures D1 and D2 show the total, internal and external noise components in terms of SPL and PWL spectra for hardwall and fully treated LSM-1 configurations at this condition.

Similar analyses are made for NRA nozzle (with mixer 8c and 160" full-scale flap) data at takeoff condition (i.e., NPR=3.43 and T8=1551°R). Bulk absorber liner with 0.485"-deep 100 ppi Silicon carbide with perforated facesheet (σ=37%, t=0.025", d=0.045") was used for ejector treatment. SPL spectra at different polar angles and PWL spectra for total, external, and internal noise components are compared between LSM-1 and NRA nozzles in Figures D3 through D6 for hardwall and fully treated configurations. The external noise components for hardwall as well as treated configurations are reasonably the same between NRA and LSM-1 nozzles. However, the total and internal components for LSM-1 are higher compared to NRA nozzle. Similar comparisons are made with respect to PNL directivities in Figure D7. The EPNL values are listed in this figure. Total and internal noise data for LSM-1 is higher compared to NRA configuration. In terms of EPNL the LSM-1 is about 0.2 and 2.8 EPNdB noisier in total noise and in internal noise, receptively, compared to treated NRA data.

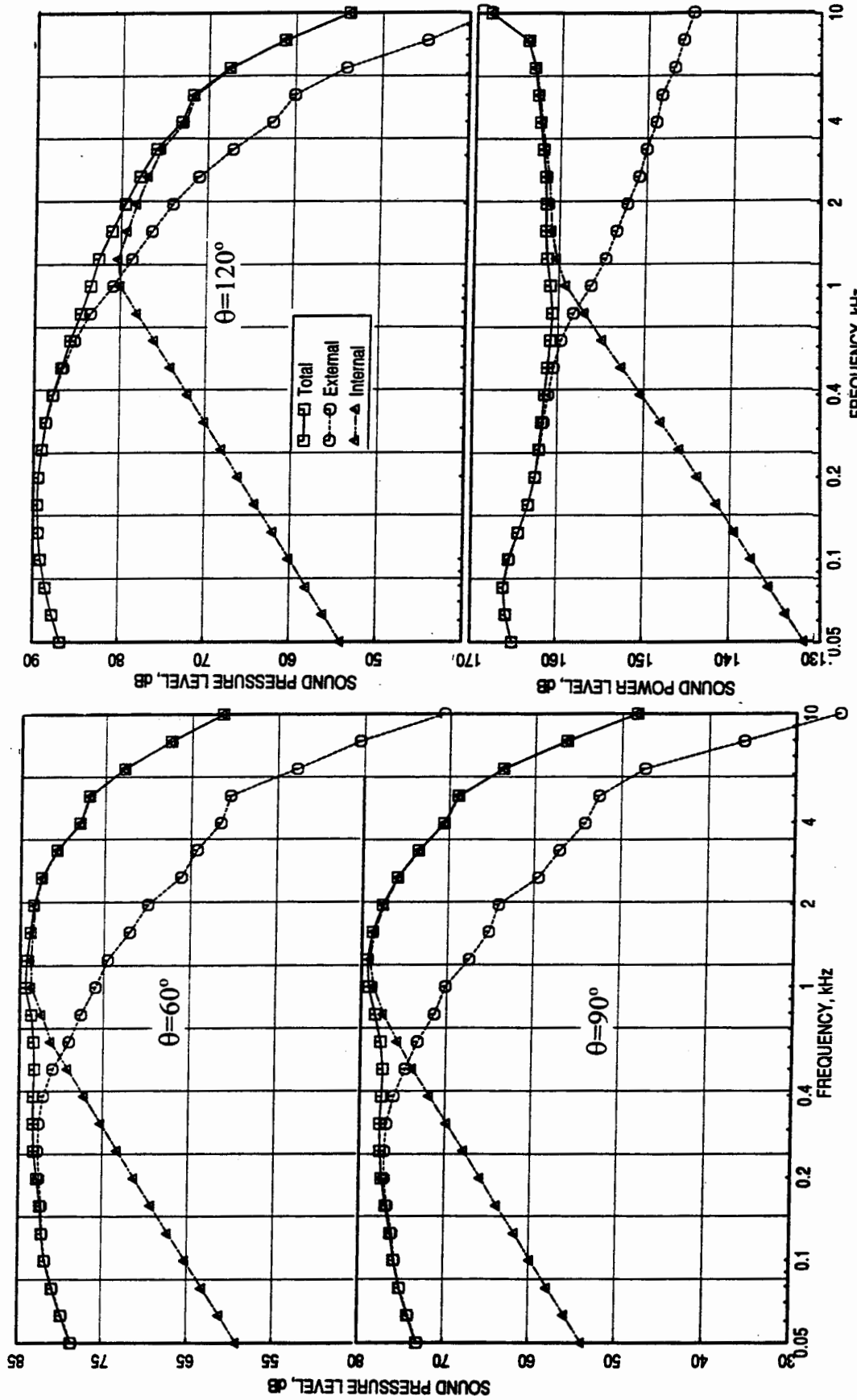

Figure D1. Noise components for hardwall LSM-1 at takeoff conditions (NPR=3.25, T8=1579°R, V_{mix}=1435 ft/sec) at sideline distance of 1629', A8=1248 in2, M_f=0.0.

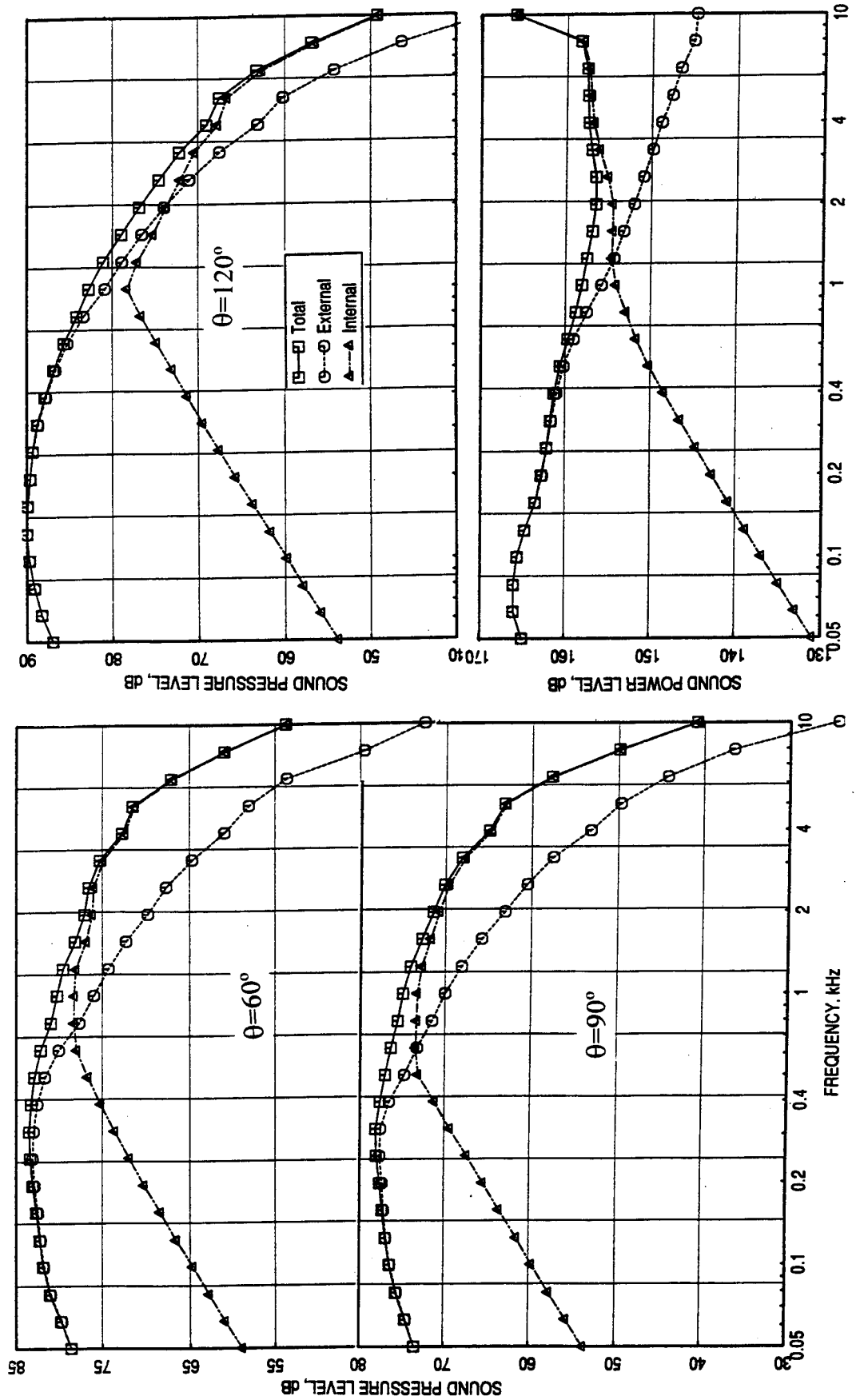

Figure D2. Noise components for fully treated LSM-1 at takeoff conditions (NPR=3.25, T8=1579°R, V_{mix}=1435 ft/sec) at sideline distance of 1629', A8=1248 in2, M_F=0.0.

	NPR	T8, °R	Pumping	V_{mix}, ft/sec
LSM:	3.25	1580	0.62	1435
NRA:	3.43	1551	0.63	1450

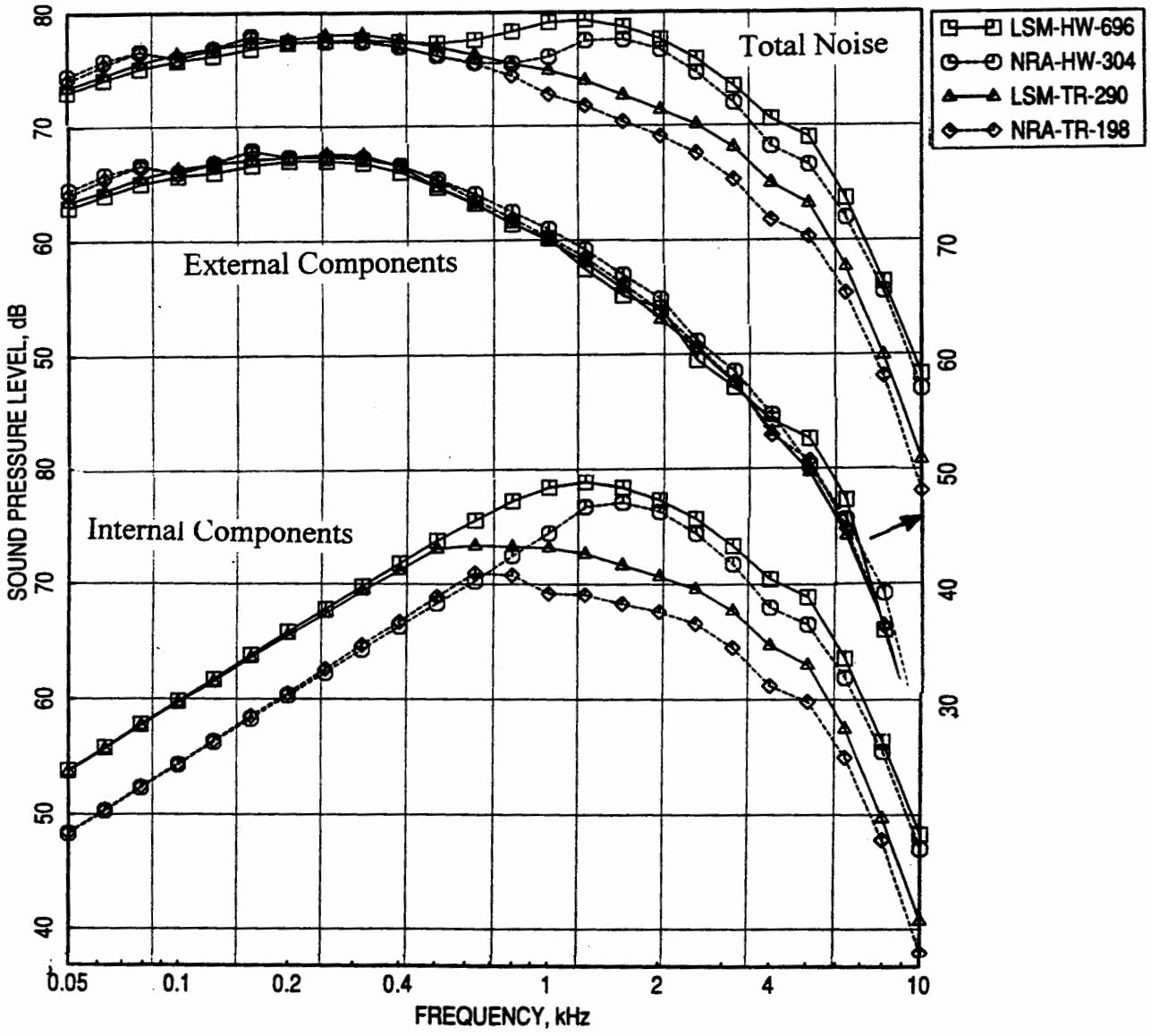

Figure D3. Comparison of SPL spectra at θ=60° between LSM-1 and 1/7-scale NRA (mixer 8c) nozzles at takeoff conditions at sideline distance of 1629', A8=1248 in2, M_P=0.0.

	NPR	T8, °R	Pumping	V_{mix}, ft/sec
LSM:	3.25	1580	0.62	1435
NRA:	3.43	1551	0.63	1450

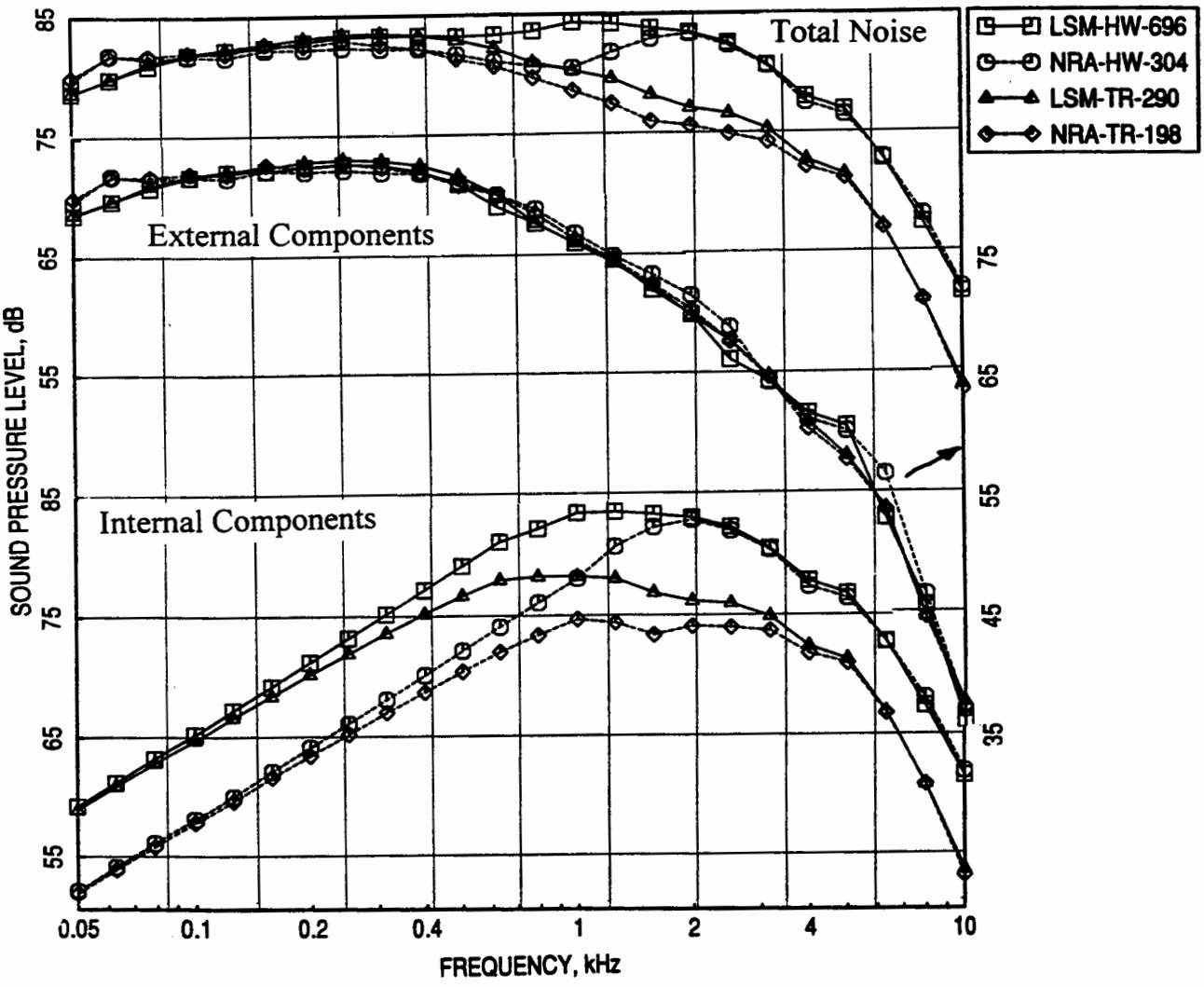

Figure D4. Comparison of SPL spectra at θ=90° between LSM-1 and 1/7-scale NRA (mixer 8c) nozzles at takeoff conditions at sideline distance of 1629', A8=1248 in2, M_F=0.0.

	NPR	T8, °R	Pumping	V_{mix}, ft/sec
LSM:	3.25	1580	0.62	1435
NRA:	3.43	1551	0.63	1450

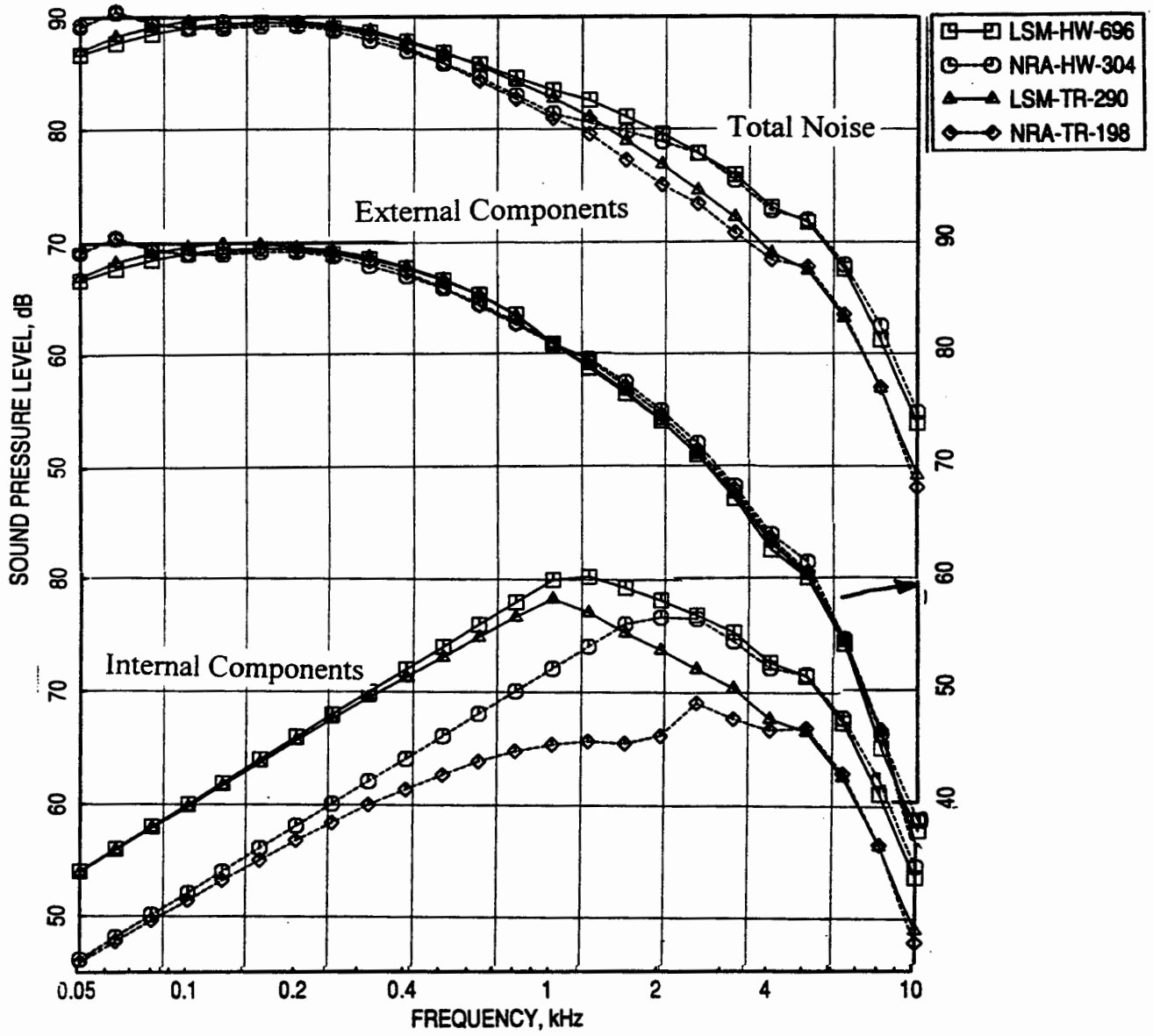

Figure D5. Comparison of SPL spectra at θ=120° between LSM-1 and 1/7-scale NRA (mixer 8c) nozzles at takeoff conditions at sideline distance of 1629', A8=1248 in2, M_F=0.0.

	NPR	T8, °R	Pumping V_{mix}, ft/sec	
LSM:	3.25	1580	0.62	1435
NRA:	3.43	1551	0.63	1450

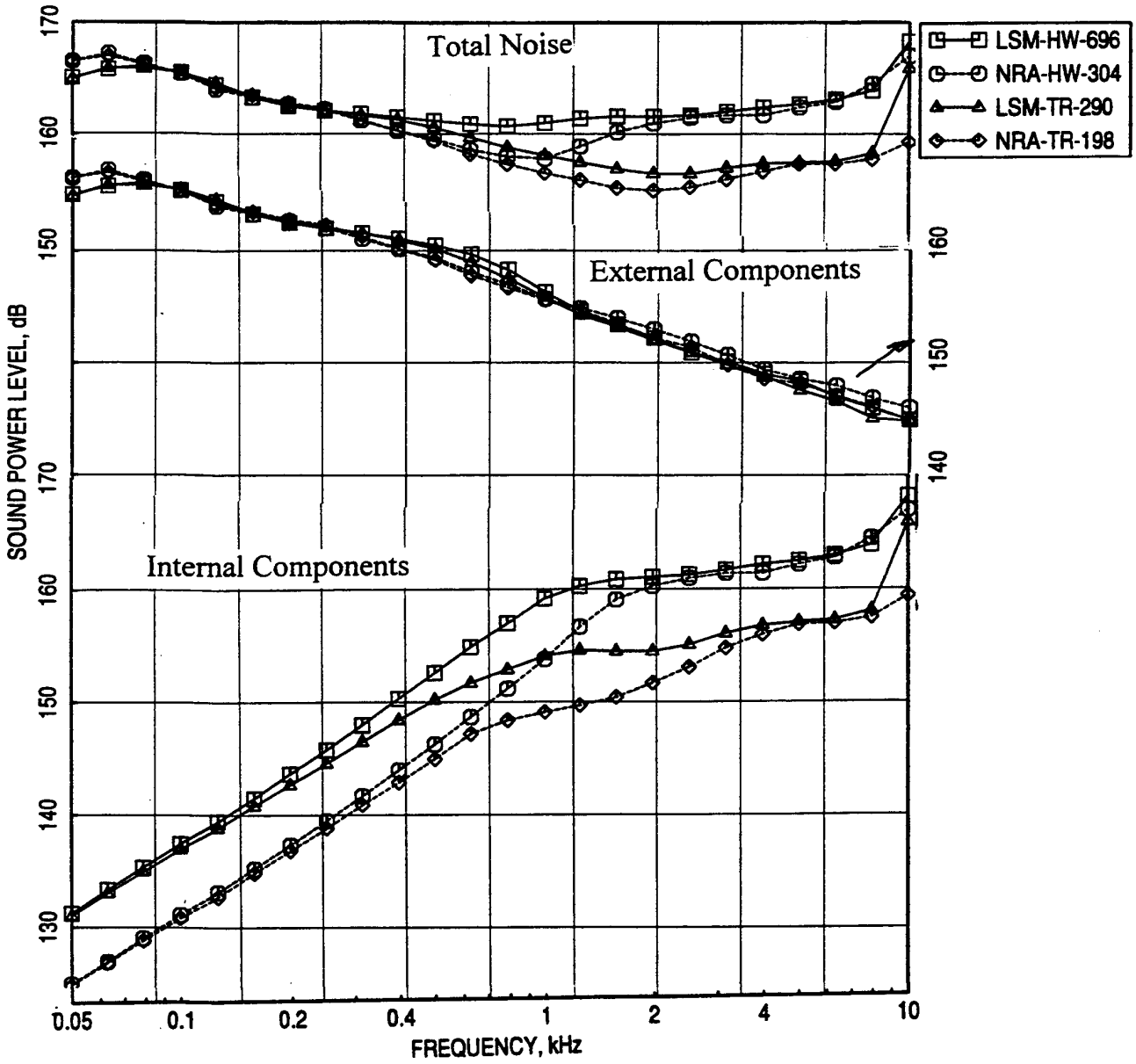

Figure D6. Comparison of PWL spectra between LSM-1 and 1/7-scale NRA (mixer 8c) nozzles at takeoff conditions at sideline distance of 1629', A8=1248 in2, M_F=0.0.

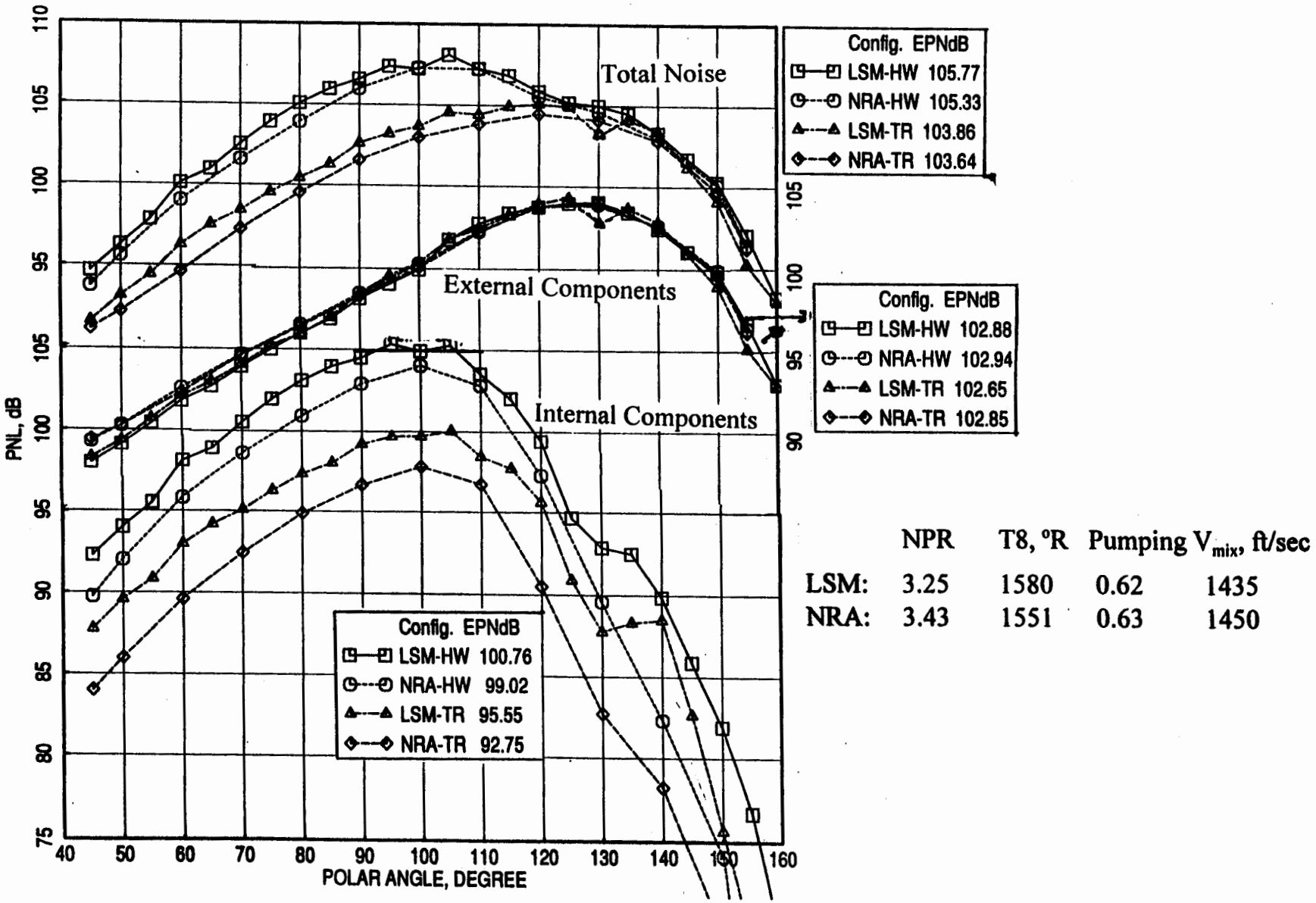

Figure D7. Comparison of PNL directivities between LSM-1 and 1/7-scale NRA (mixer 8c) nozzles at takeoff conditions at sideline distance of 1629', A8=1248 in2, M_F=0.0.

LSM-1 and NRA data for cutback condition is also analyzed. Again, the test conditions are slightly different between these configurations. Test condition for LSM-1 (NPR=2.5 and T8=1370°R) is higher compared to NRA model (NPR=2.37 and T8=1238°R). Figures D8 and D9 show the total, internal and external noise components in terms of SPL and PWL spectra for hardwall and fully treated LSM-1 configurations. SPL spectra at different polar angles and PWL spectra for total, external, and internal noise components are compared between LSM-1 and NRA nozzles in Figures D10 through D13 for hardwall and fully treated configurations. All three noise components, total, external and internal, for LSM-1 are significantly higher compared to NRA nozzle. Similar comparisons are made with respect to PNL directivities in Figure D14. The EPNL values, listed in this figure, indicate higher levels for LSM-1 compared to NRA for each noise components.

D.2 Comparison between Measured and Predicted EPNL: In section 7 three different liner designs are considered for LSM mixer-ejector treatment. The Design #1 was used for LSM nozzle tests at static condition. The farfield noise for LSM-1 nozzle with all three liners is predicted in section 7 for a flight Mach number of 0.32. Following the same procedure the farfield noise at static condition is estimated in this section. Similar results are also derived for NRA model at static condition. Predicted normal impedance and the corresponding acoustic suppression are plotted in Figures D15 and D16, respectively. Table D1 summarizes the predicted and measured EPNL values for LSM-1 and NRA models for static as well as simulated flight conditions.

Based on the performance of the liner (i.e., suppression capability for internal noise component) the predicted levels of 6.42 and 8.48 EPNdB for takeoff and cutback conditions are about 1.2 to 1.3 dB higher compared to the measured data. Since the predictions are based on the 1/7-scale model data, these discrepancies could be attributed to several differences between LSM-1 and NRA models and their aerothermodynamic conditions. Possible reasons for such differences are listed in Table D2.

D.3 Effect of Incremental Treatment on Noise Suppression: Tests were conducted for LSM-1 nozzle at cutback condition by increasing the ejector treatment in increments. Figure D17 illustrates the incremental arrangement of ejector treatment. The measured data is used to extract the internal noise component for different amount of treatment configurations. Figure D18 shows the spectral variation of internal noise component due to treatment variation. SPL levels decrease significantly at the beginning when the treatment area is increased. However, approaching full treatment the effect of treatment area variation is small

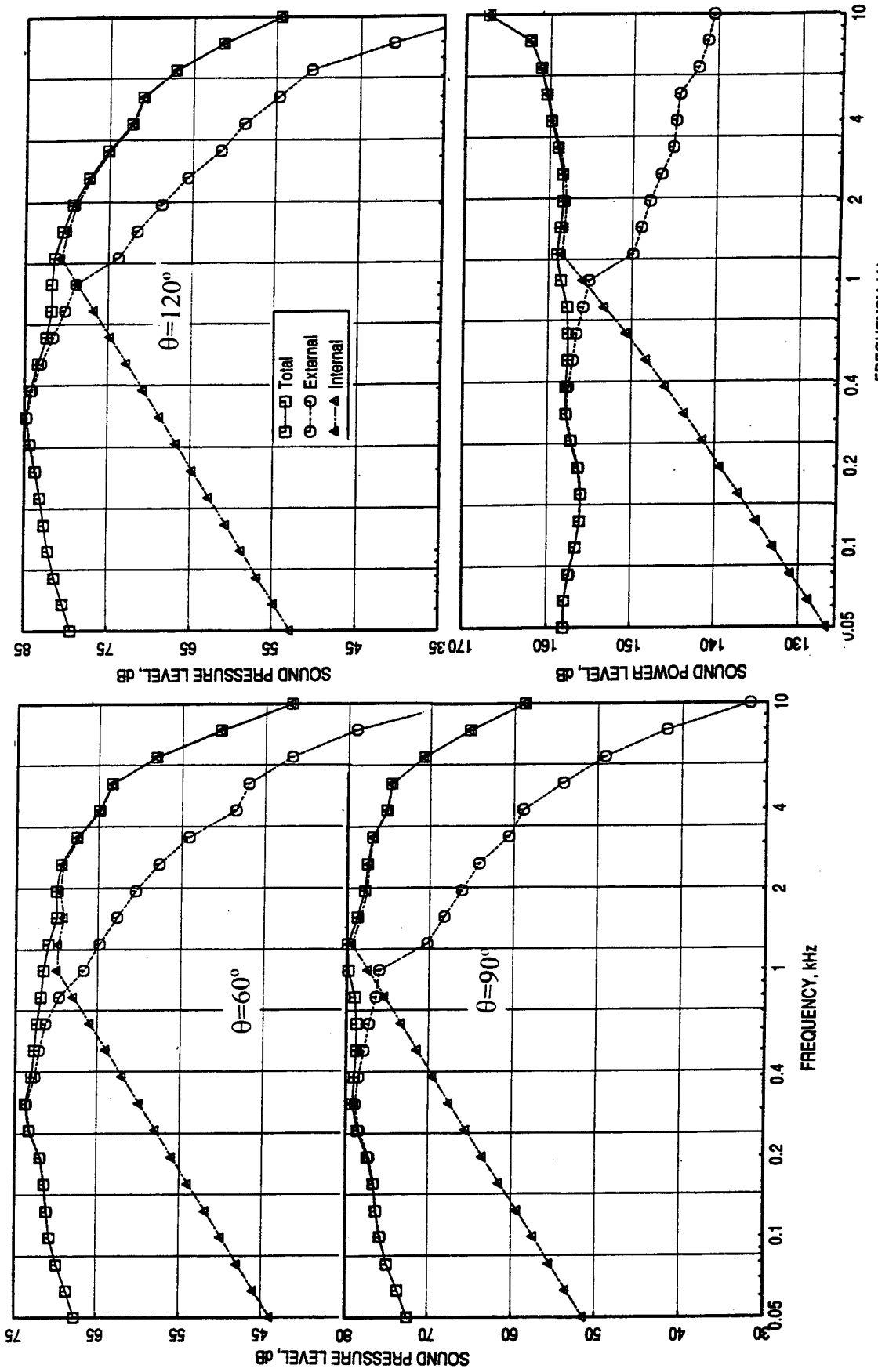

Figure D8. Noise components for hardwall LSM-1 at cutback conditions (NPR=2.5, T8=1370°R, V_{mix}=1135 ft/sec) at flyover distance of 1629', A8=1248 in2, M_F=0.0.

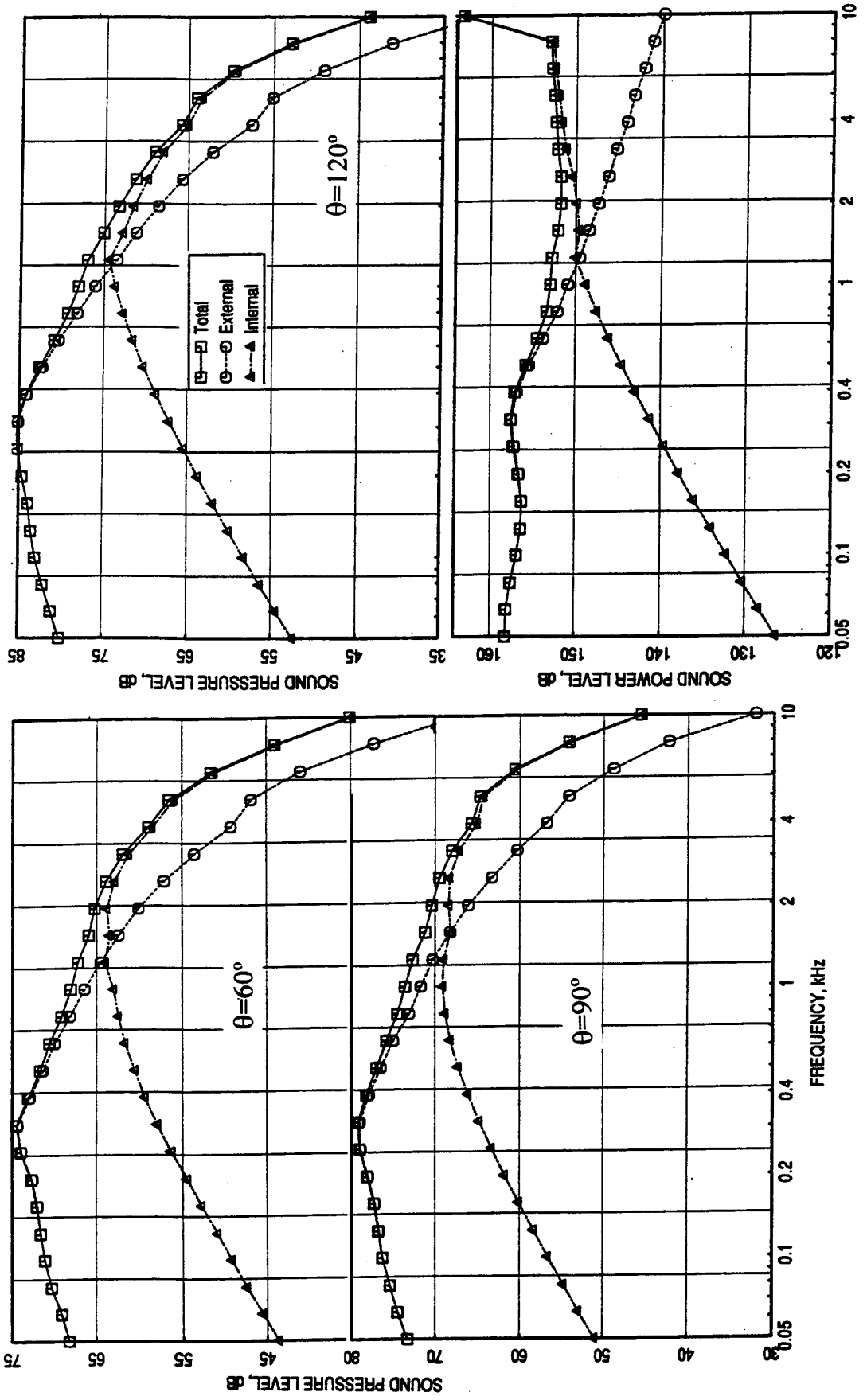

Figure D9. Noise components for fully treated LSM-1 at cutback conditions (NPR=2.5, T8=1370°R, V_{mix}=1135 ft/sec) at flyover distance of 1629', A8=1248 in2, M_F=0.0.

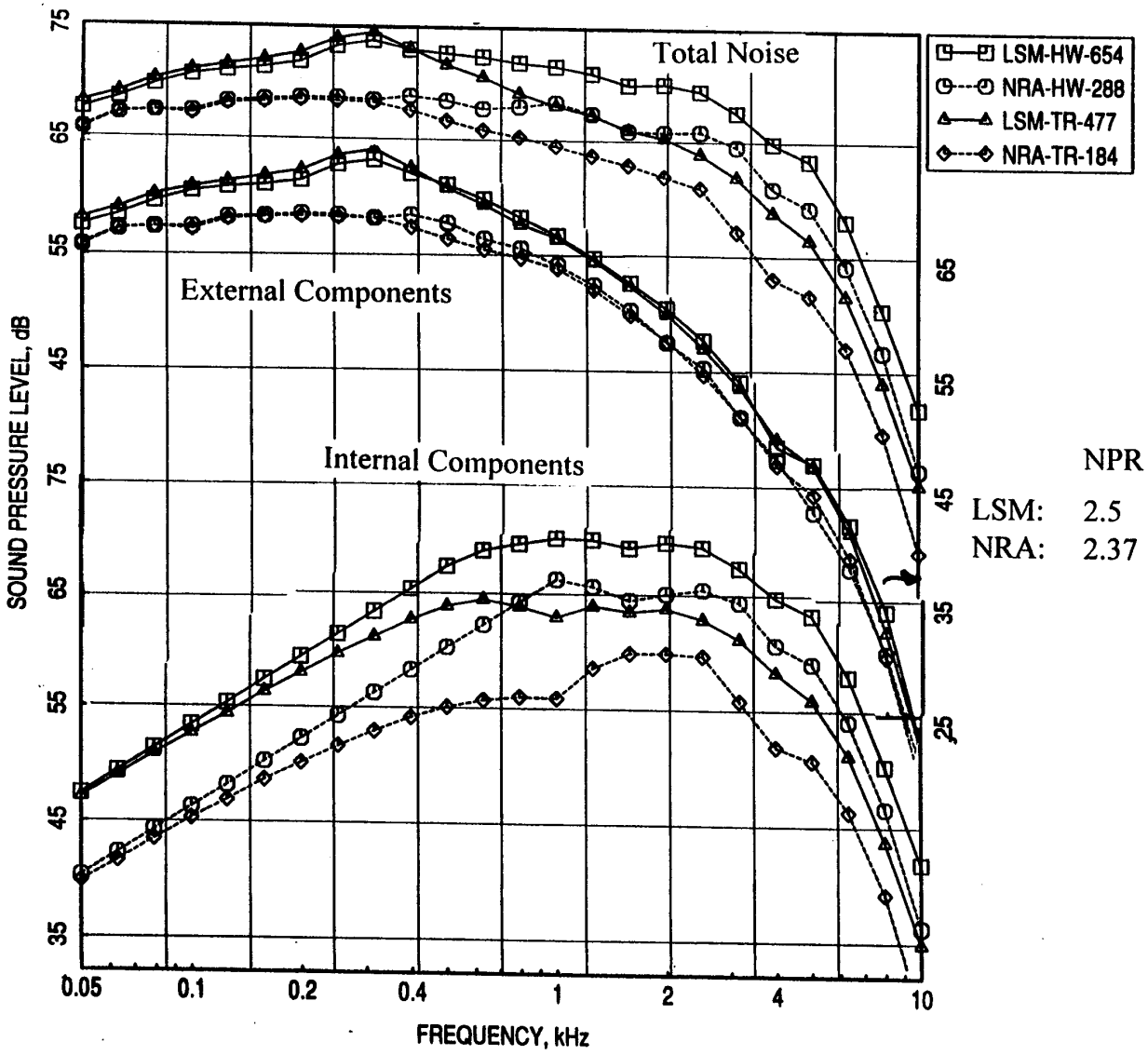

	NPR	T8, °R	Pumping V_{mix}, ft/sec	
LSM:	2.5	1370	0.72	1135
NRA:	2.37	1238	0.84	1040

Figure D10. Comparison of SPL spectra at θ=60° between LSM-1 and 1/7-scale NRA (mixer 8c) nozzles at cutback conditions at flyover distance of 1629', A8=1248 in2, M_F=0.0.

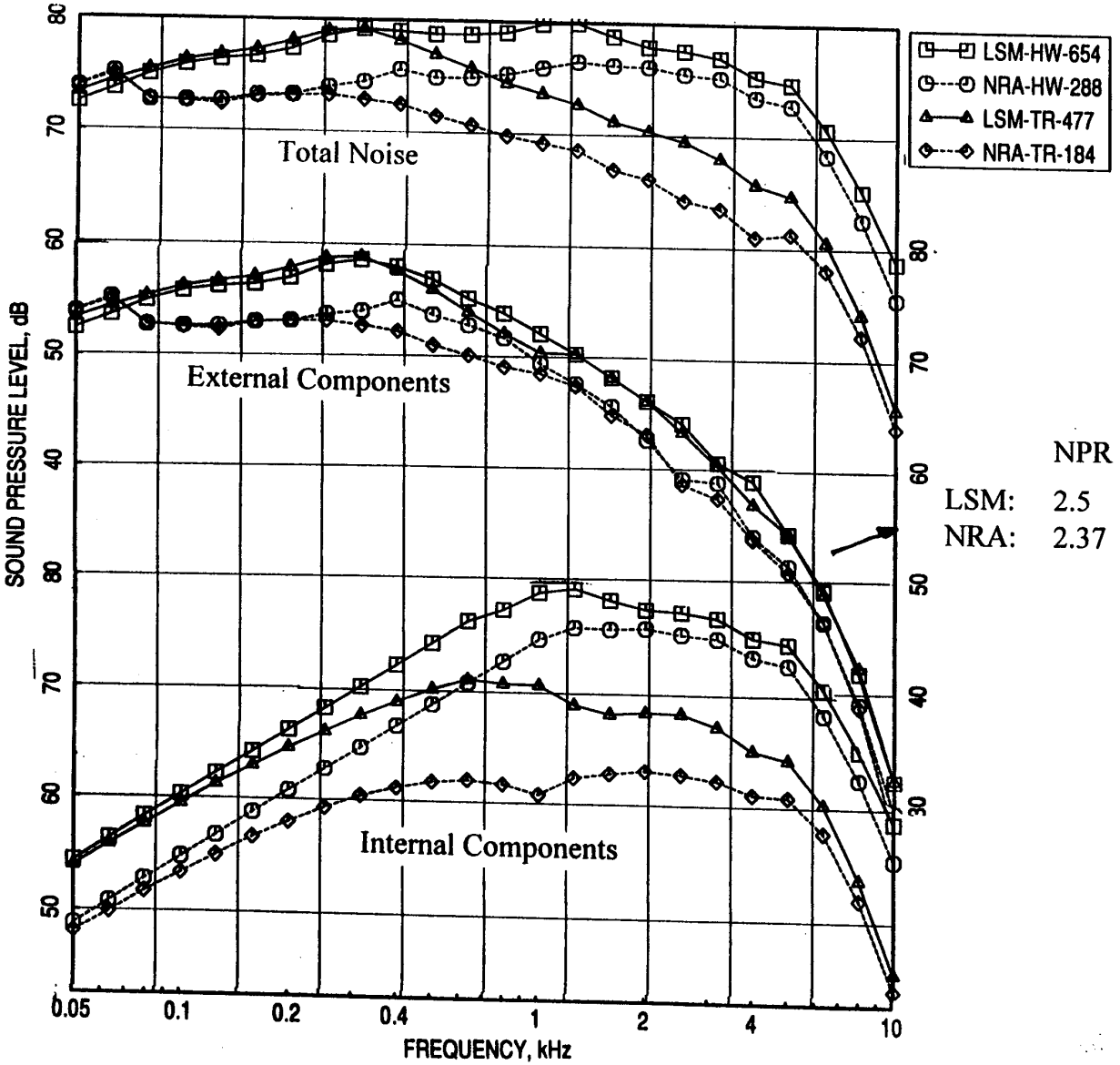

	NPR	T8, °R	Pumping	V_{mix}, ft/sec
LSM:	2.5	1370	0.72	1135
NRA:	2.37	1238	0.84	1040

Figure D11. Comparison of SPL spectra at θ=90° between LSM-1 and 1/7-scale NRA (mixer 8c) nozzles at cutback conditions at flyover distance of 1629', A8=1248 in2, M_F=0.0.

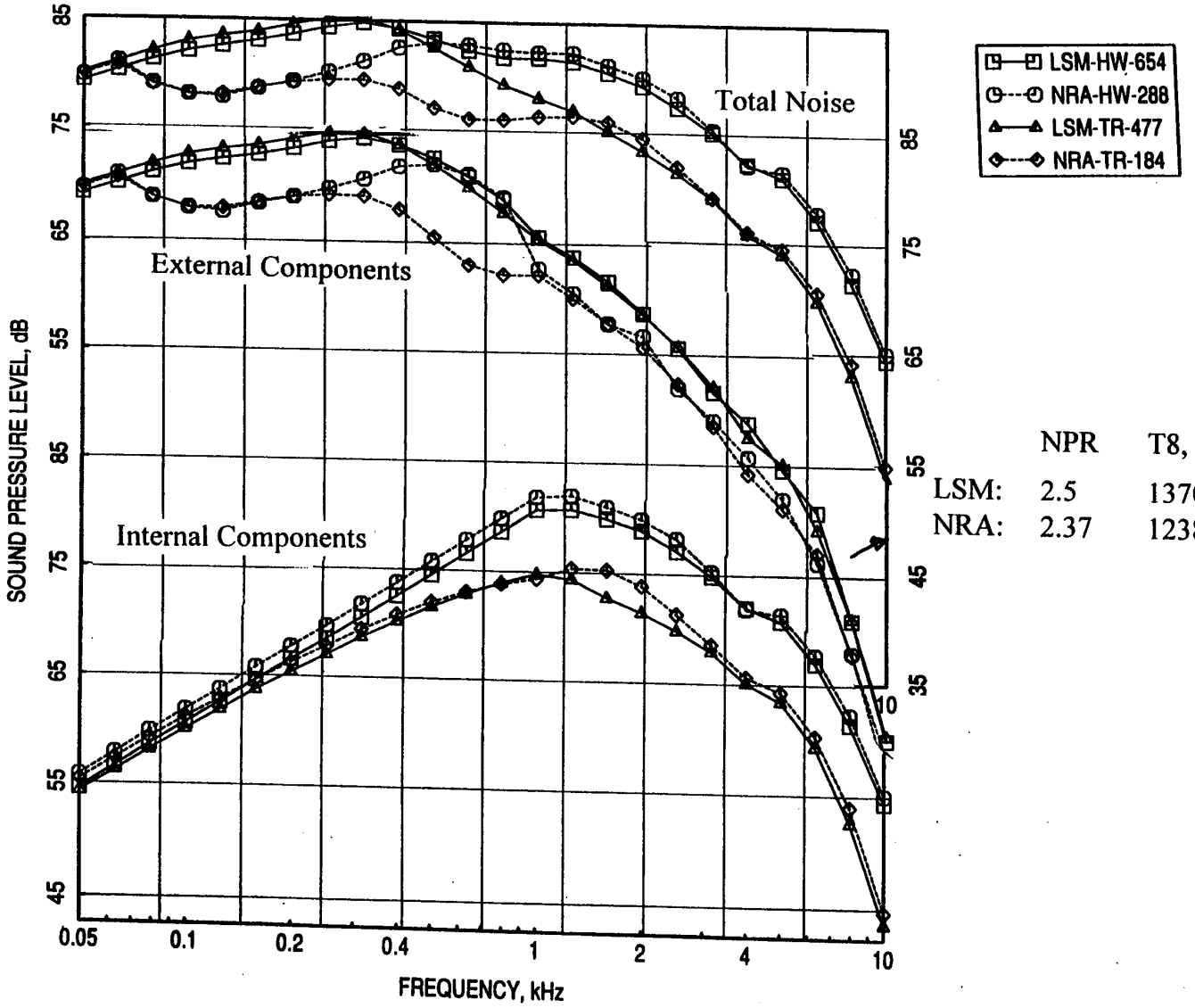

	NPR	T8, °R	Pumping	V_{mix}, ft/sec
LSM:	2.5	1370	0.72	1135
NRA:	2.37	1238	0.84	1040

Figure D12. Comparison of SPL spectra at θ=120° between LSM-1 and 1/7-scale NRA (mixer 8c) nozzles at cutback conditions at flyover distance of 1629', A8=1248 in2, M_F=0.0.

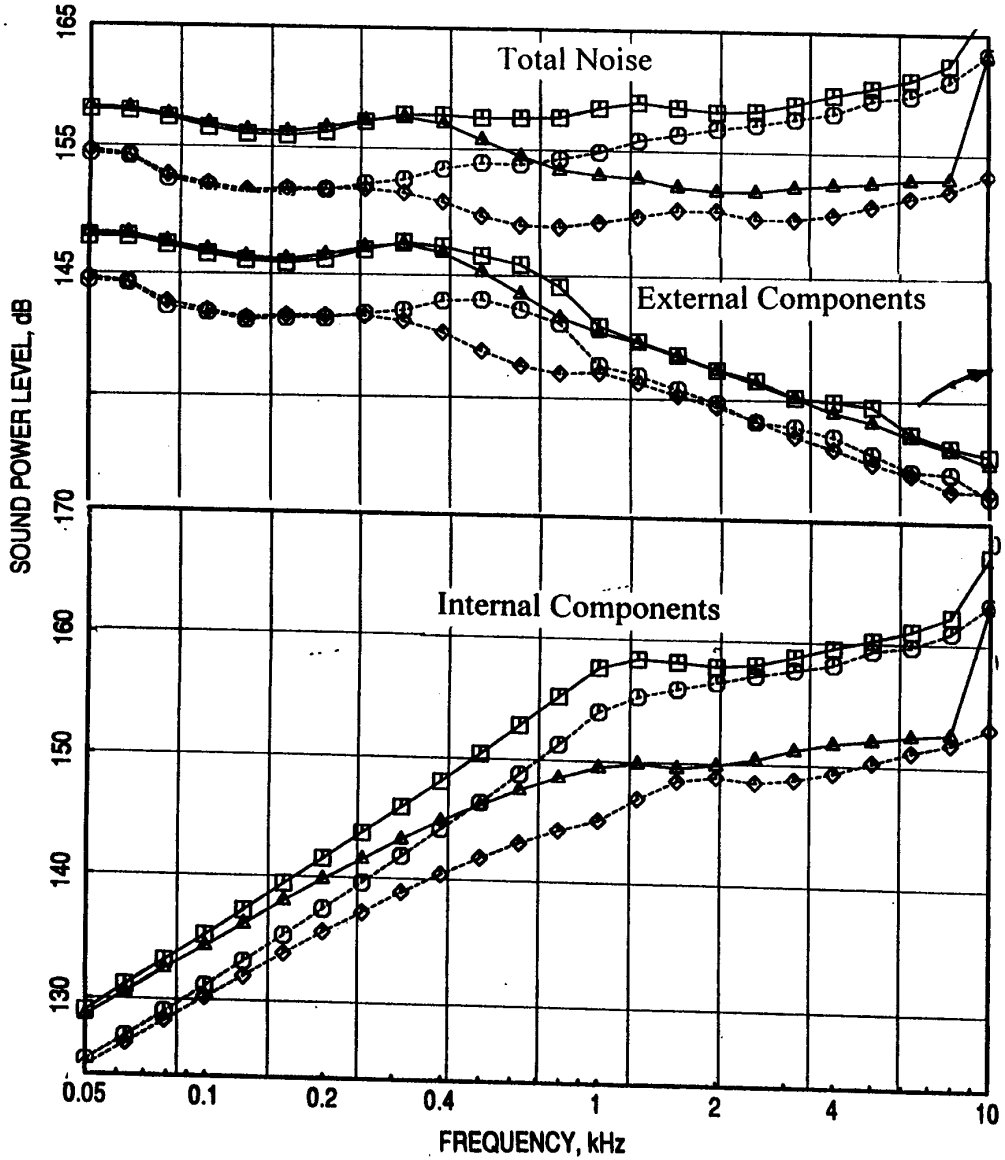

	NPR	T8, °R	Pumping	V_{mix}, ft/sec
LSM:	2.5	1370	0.72	1135
NRA:	2.37	1238	0.84	1040

Figure D13. Comparison of PWL spectra between LSM-1 and 1/7-scale NRA (mixer 8c) nozzles at cutback conditions at flyover distance of 1629', A8=1248 in2, M_F=0.0.

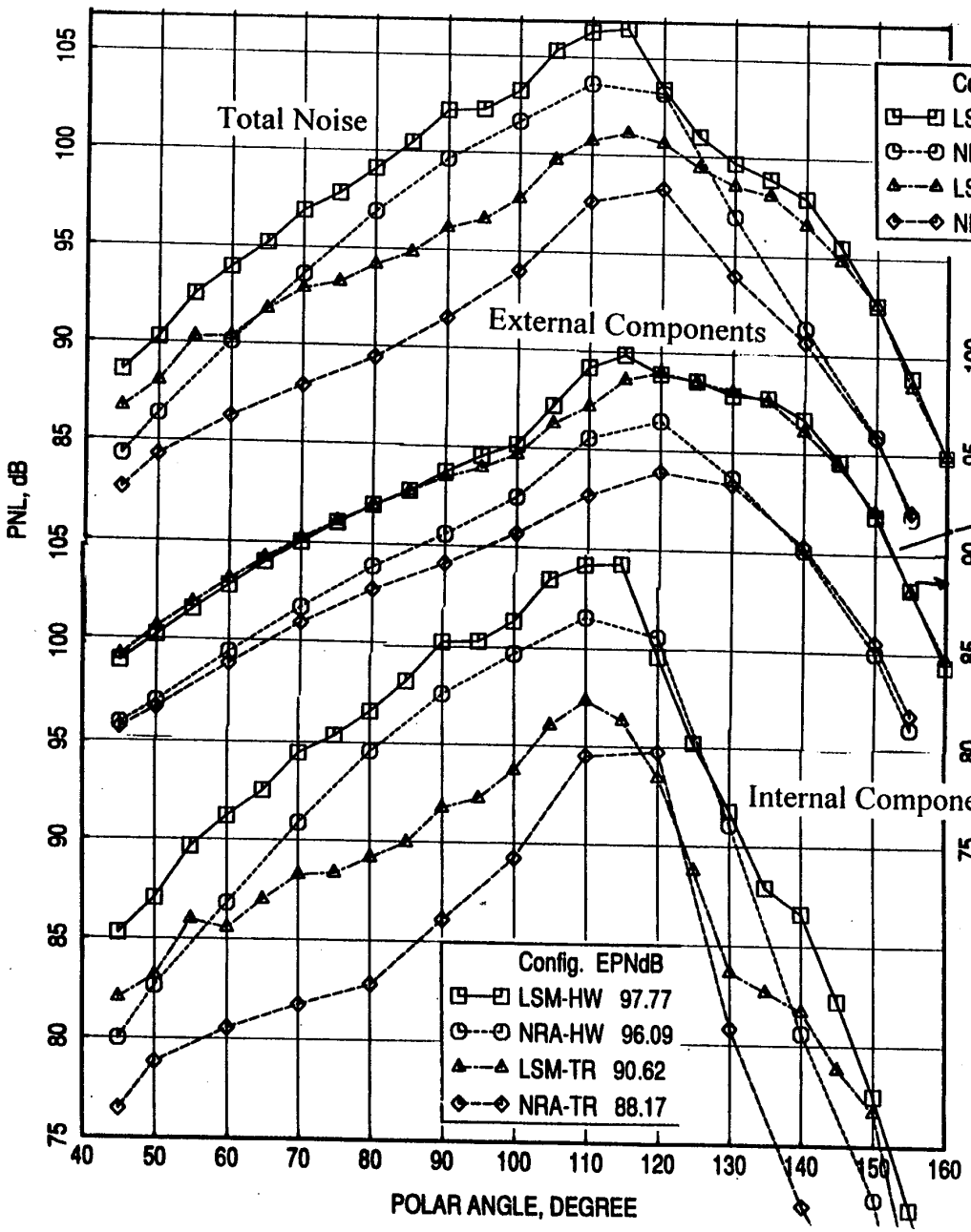

	NPR	T8, °R	Pumping	V_{mix}, ft/sec
LSM:	2.5	1370	0.72	1135
NRA:	2.37	1238	0.84	1040

Figure D14. Comparison of PNL directivities between LSM-1 and 1/7-scale NRA (mixer 8c) nozzles at cutback conditions at flyover distance of 1629', A8=1248 in2, M_F=0.0.

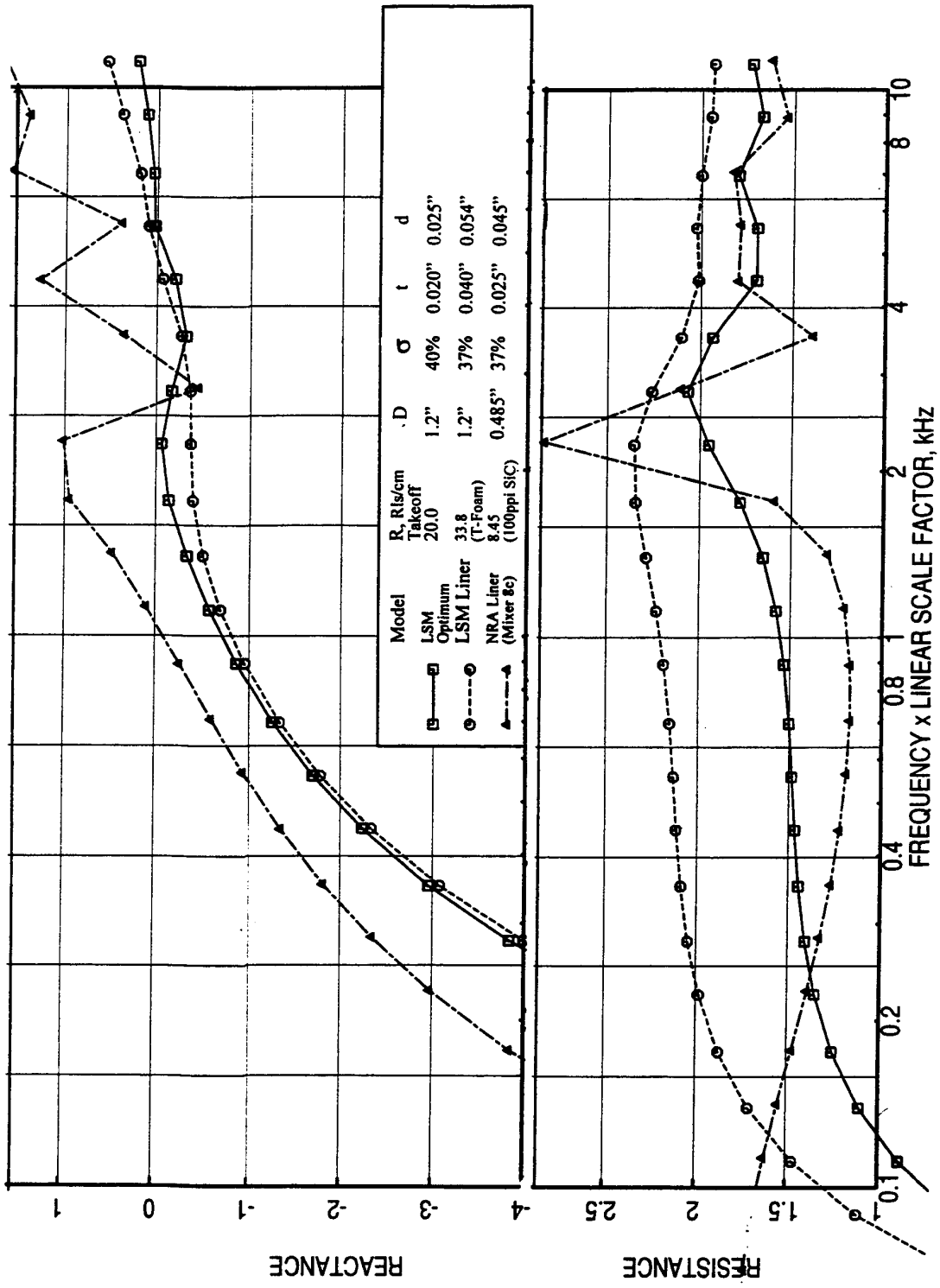

Figure D15. Predicted normal impedance spectra for various liner designs at takeoff condition, Ejector liner surface: static temperature = 500°F, grazing flow Mach number = 0.8, OASL = 177 dB.

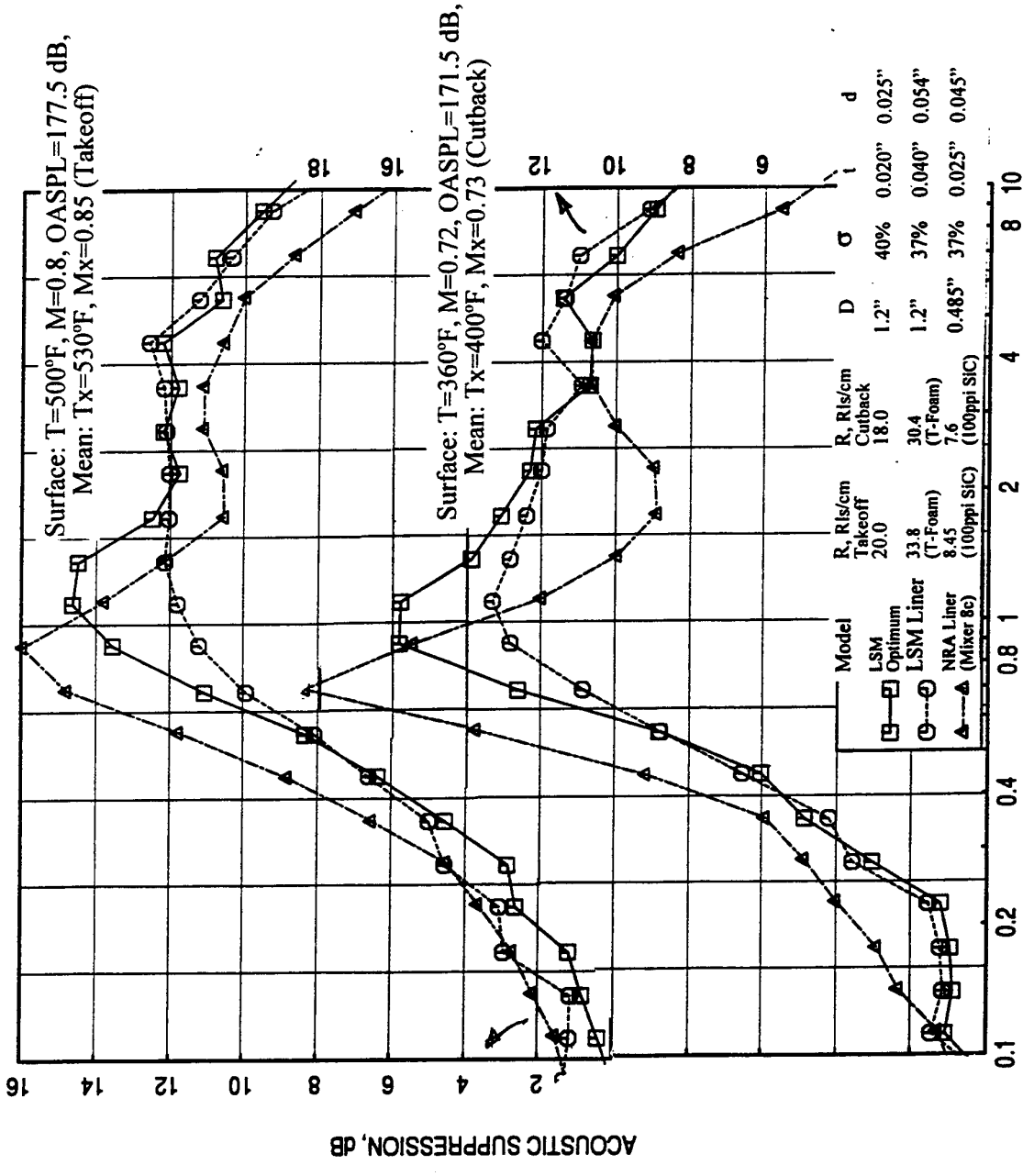

Figure D16. Predicted acoustic suppression due to various liner designs for the ejector at takeoff and cutback conditions.

Table D1. Measured and predicted HSCT Nozzle Liner Benefits in terms of EPNdB .

	Measured EPNdB for NRA Model with Mixer 8c & 160" Flap, Tested in Cell 41, A_t/A_m=8, A_{teff}/A_m=6.5			Projected EPNdB for LSM-1 Model for Different Liners, A_t/A_m=7.4, A_{teff}/A_m=6.7						Measured EPNdB for LSM-1 Model, A_t/A_m=7.4, A_{teff}/A_m=6.7		
				Optimum Design		Liner used in LSM-1		Alternate Design				
	Hard Wall	Treated	Δ EPNL	Treated	Δ EPNL	Treated	Δ EPNL	Treated	Δ EPNL	Hard Wall	Treated	Δ EPNL
	MAR=0.95, NPR=2.37, T8=1238°R, V_{mix}=1040 ft/sec									MAR=0.9, NPR=2.5, T8=1370°R, V_{mix}=1135 ft/sec		
Cutback Condition at Flyover at 1629', A8=1248 in^2, Static												
Total	99.02	93.90	-5.12	93.46	-5.56	93.54	-5.48	93.38	-5.64	101.60	98.30	-3.30
External	92.99	91.61	-1.38	91.63	-1.11	91.60	-1.14	91.60	-1.14	97.47	96.97	-0.50
Internal	96.09	88.17	-7.92	87.50	-8.86	87.88	-8.48	87.24	-9.12	97.77	90.62	-7.15
Cutback Condition at Flyover at 1629', A8=1248 in^2, Flight M_F=0.32												
Total	96.31	89.82	-6.49	89.38	-6.93	89.82	-6.49	89.31	-7.00			
External	84.85	83.03	-1.82	83.03	-1.82	83.03	-1.82	83.03	-1.82			
Internal	94.90	87.27	-7.63	86.85	-8.05	87.34	-7.56	86.68	-8.22			
	MAR=0.95, NPR=3.43, T8=1551°R, V_{mix}=1450 ft/sec									MAR=0.9, NPR=3.25, T8=1580°R, V_{mix}=1435 ft/sec		
Takeoff Condition at Sideline at 1629', A8=1248 in^2, Static												
Total	105.33	103.64	-1.69	103.45	-1.88	103.53	-1.80	103.50	-1.83	105.77	103.86	-1.91
External	103.12	102.85	-0.27	103.56	0.44	102.85	-0.27	102.85	-0.27	102.88	102.65	-0.23
Internal	99.02	92.75	-6.27	92.07	-6.95	92.60	-6.42	92.37	-6.65	100.76	95.55	-5.21
Takeoff Condition at Sideline at 1629', A8=1248 in^2, Flight M_F=0.32												
Total	101.82	97.38	-4.44	96.79	-5.03	97.04	-4.78	96.97	-4.85			
External	94.17	93.90	-0.27	93.90	-0.27	93.90	-0.27	93.90	-0.27			
Internal	98.72	91.44	-7.28	90.64	-8.08	91.17	-7.55	90.99	-7.73			

Note : External noise contains Merged & Premerged components

Table D2. Impact of Various Parameters on Noise Suppression due to Acoustic Liner

	LSM-1	NRA with Mixer 8c	Effect due to the Difference
Takeoff Conditions	NPR=3.25, T8=1580°R, V_{mix}=1435 ft/sec, Ws/Wp=0.61~0.63	NPR=3.43, T8=1551°R, V_{mix}=1450 ft/sec, Ws/Wp=0.63~0.68	Noise level may be slightly higher for NRA due to higher NPR. But higher temperature for LSM-1 may also generate more noise.
Cutback Conditions	NPR=2.5, T8=1370°R, V_{mix}=1135 ft/sec, Ws/Wp=0.71~0.74	NPR=2.37, T8=1238°R, V_{mix}=1040 ft/sec, Ws/Wp=0.79~0.84	Noise Level, External & Internal, should be higher for LSM-1 due to significantly higher NPR
MAR	0.90	0.95	Noise level may be slightly higher for LSM-1 due to lower MAR (Mixing Area Ratio)
Sidewall Condition	Hot	Cold	May not be any measurable effect for the 160" flap length used
Liner Impedance (see Figure D15)	Higher than optimum at critical frequencies	Closer to optimum for critical frequencies	Less noise Suppression for LSM-1 (Higher EPNdB)
Acoustic Suppression (see Figure D16)	Lower than optimum at critical frequencies	Much higher at lower frequencies due to proportionally higher liner depth	Lower noise suppression compared to optimum liner. The low frequency benefit included in the process of using 1/7-scale model data is not achievable due to relatively smaller liner depth for larger scale models
External & Internal Noise Components @ Takeoff	External: 103 dB Internal :101 dB HW 95.5 dB TR	External: 103 dB Internal: 99 dB HW 93 dB TR	No impact of internal noise difference, since external is same and higher than internal for both.
External & Internal Noise Components @ Cutback	External: 97 dB Internal :98.4 dB HW 91 dB TR	External: 92 dB Internal: 96.4 dB HW 88.3 dB TR	External is higher for LSM-1. Thus the total is higher irrespective of significant internal noise reduction

Some amount of external noise increase for LSM-1 nozzle is possibly due to the higher aerothermodynamic conditions (i.e., NPR & T8). Other factors, like non-uniform temperature and thick boundary layer in the ejector, noise contamination due to inlet noise, etc. might have contributed to the farfield noise increase for LSM-1 nozzle.

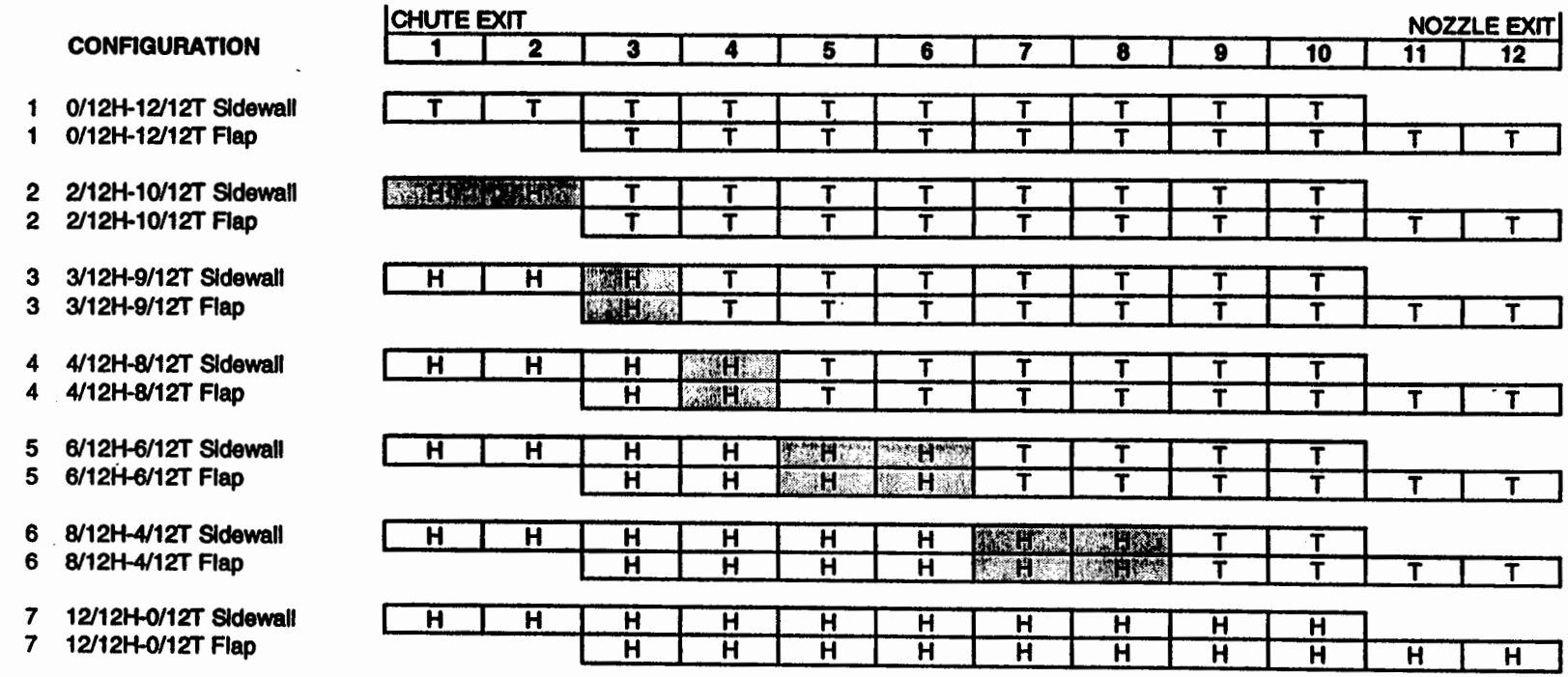

Figure D17. Incremental treatment area for LSM-1 mixer-ejector nozzle.

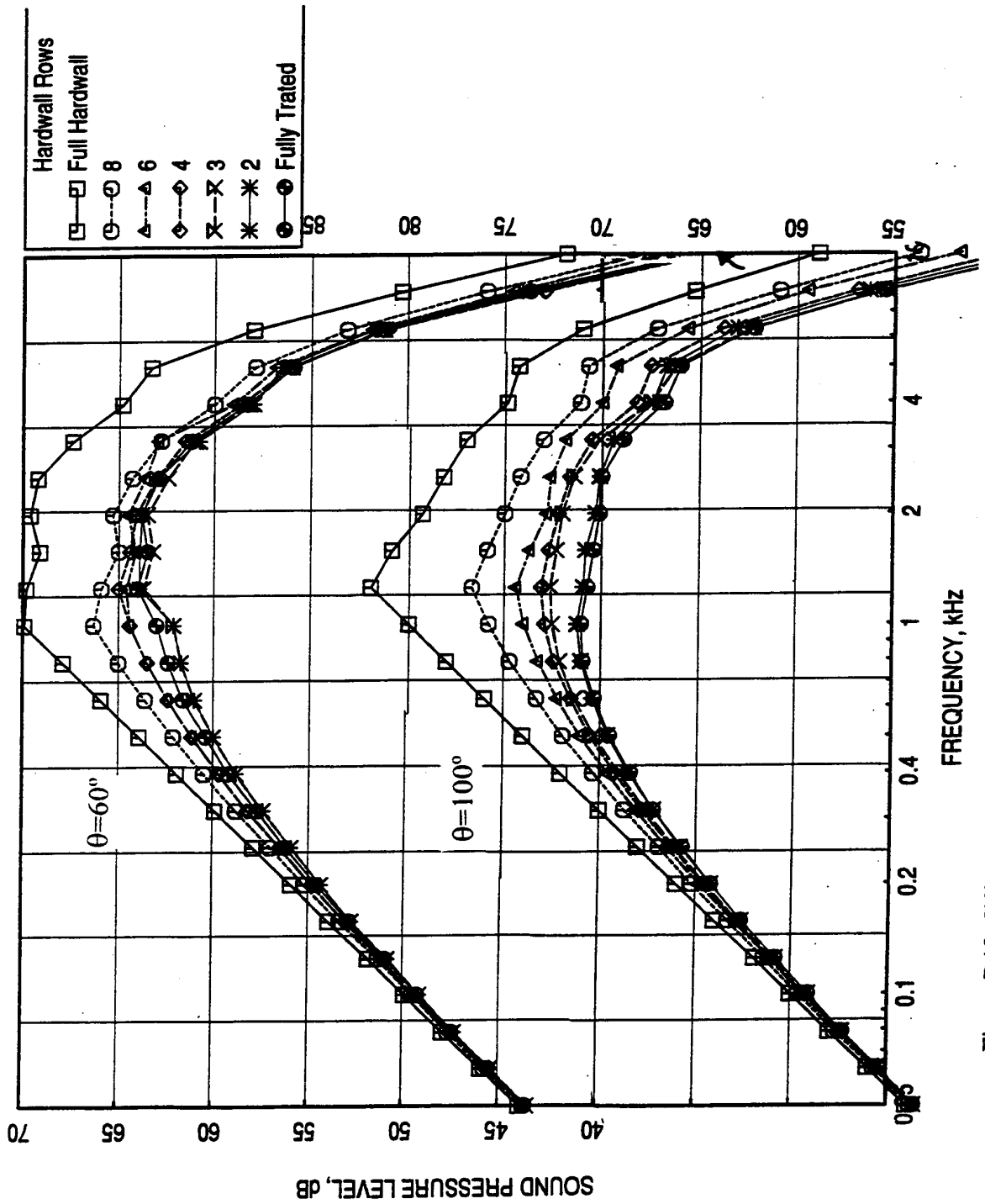

Figure D18. Effect of incremental treatment on SPL spectra for LSM-1 nozzle at cutback conditions (NPR=2.5, T8=1370°R, V_{mix}=1135 ft/sec) at flyover distance of 1629', A8=1248 in2, M_f=0.0.

on noise reduction. This is further demonstrated in terms of PWL spectra and PNL directivities for total and internal noise components in Figures D19 and D20. Finally, the noise levels in terms of EPNdB are plotted against the treatment rows (i.e., area) in Figure D21. Again, the performance as well as the effectiveness of the liner is less sensitive to treatment area increase towards the final steps to attain full treatment.

This exercise was conducted by increasing the treatment starting from the ejector exit and increasing towards the mixer exit. Based on the observation it may be concluded that the treatment closer to mixer exit is not very effective in noise suppression. However, this is not conclusive on the basis of the way this study was conducted. The approach to verify the observation is to begin treatment from mixer exit and to march towards the ejector exit.

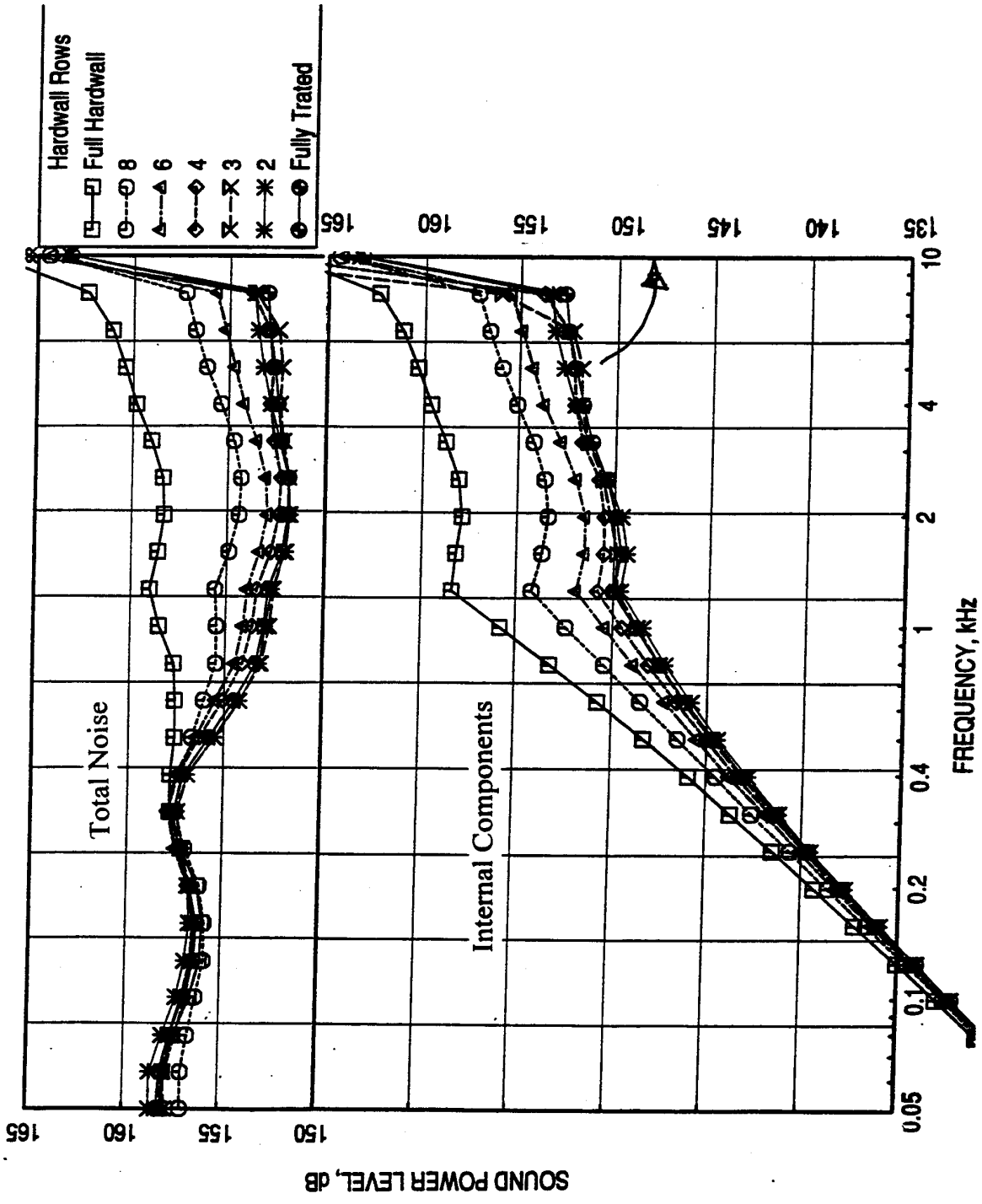

Figure D19. Effect of incremental treatment on PWL spectra for LSM-1 nozzle at cutback conditions (NPR=2.5, T8=1370°R, V_{mix}=1135 ft/sec) at flyover distance of 1629', A8=1248 in2, M_f=0.0.

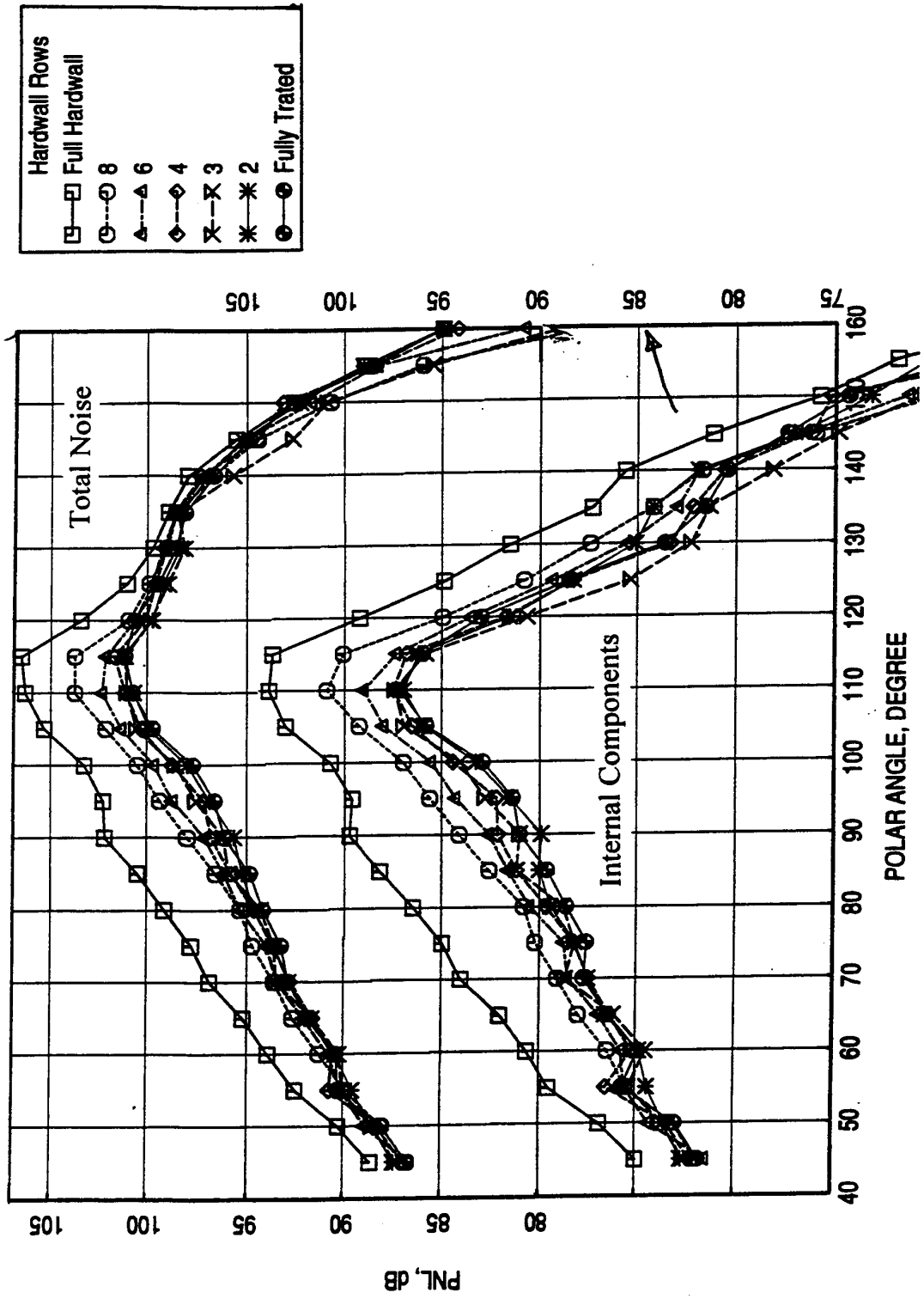

Figure D20. Effect of incremental treatment on PNL directivities for LSM-1 nozzle at cutback conditions (NPR=2.5, T8=1370°R, V_{mix}=1135 ft/sec) at flyover distance of 1629', A8=1248 in2, M_F=0.0.

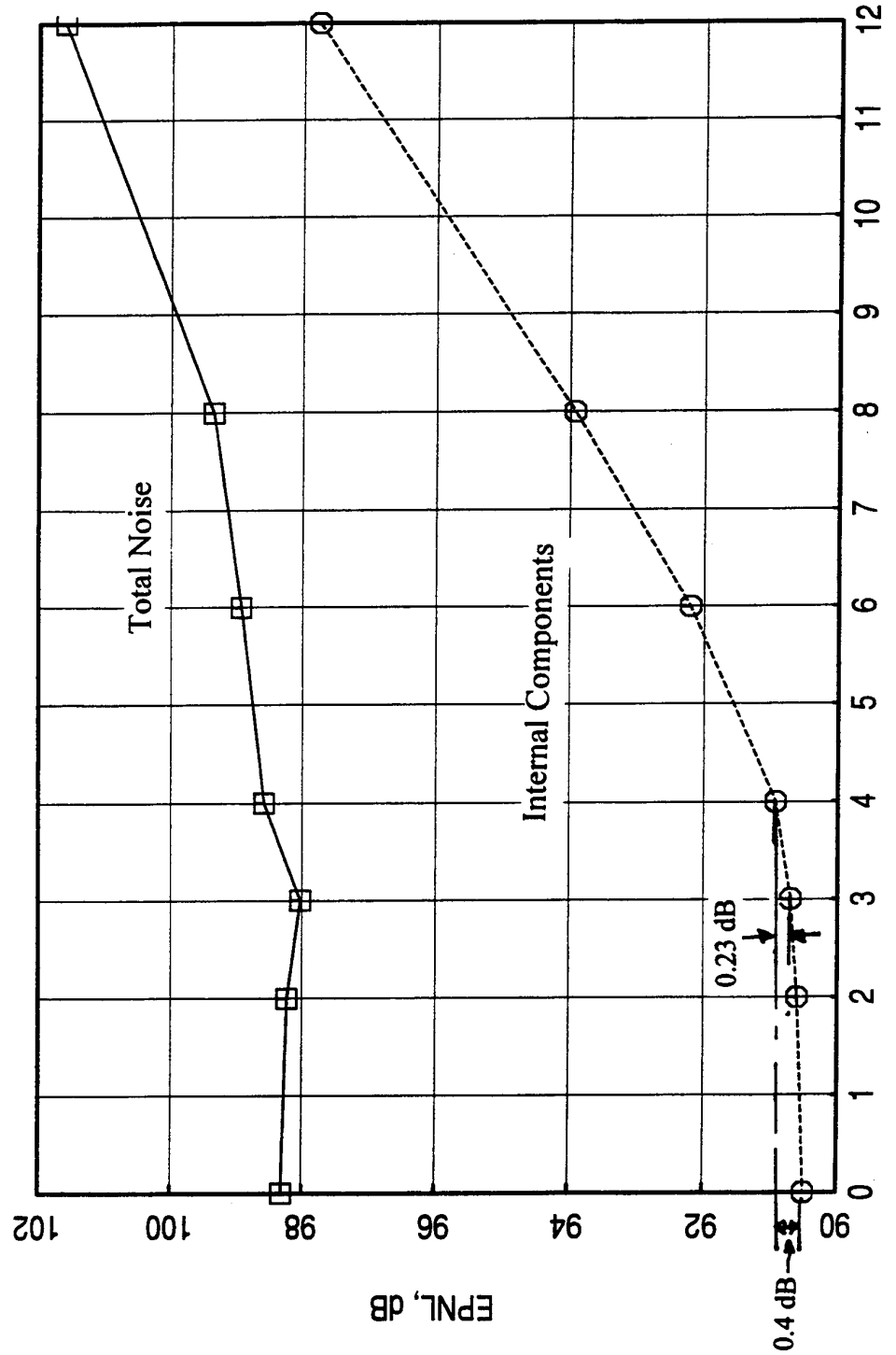

Figure D21. Effect of incremental treatment on EPNL for LSM-1 nozzle at cutback conditions (NPR=2.5, T8=1370°R, V_{mix}=1135 ft/sec) at flyover distance of 1629', A8=1248 in2, M_F=0.0.

APPENDIX E

LINER DESIGN AND FARFIELD NOISE PREDICTION FOR PROPOSED LSM BUILD-2 (LSM-2) MIXER-EJECTOR

LSM build-1 (LSM-1) test results indicated an increase of about 2.5 EPNdB for hardwall configuration at cutback for static condition compared to the prediction made utilizing 1/7-scale test results. For treated configuration the increase is about 4.7 EPNdB. For takeoff the differences between measured and predicted levels are small. However, the LSM-1 results, projected for flight Mach number of 0.32, are significantly higher than the target EPNL values set for FAA requirements. A number of reasons are attributed for the noise increase. One of the reasons is the bulk absorber material for the ejector treatment, which was not an optimum bulk. A second LSM (LSM-2) test was then proposed to address all the issues possibly responsible for noise increase. Various T-Foam bulk materials of different construction processes are studied (Ref. 3) to reduce the internal noise component.

E.1 Optimization of Facesheet Parameters: Utilizing the measured normal impedance data for standard 12 lb/cft 1.2"-deep T-Foam sample with facesheets of varying porosity, thickness, and hole diameter, the EPNLs are computed for LSM model at static condition. Similar results are also derived for an optimum bulk of about 20 Rayls/cm at 500°F. Such a bulk is expected from currently processed T-Foam and/or Silicon Carbide of about 150 ppi. Since the LSM designs are based on static condition, the sensitivity of various liner parameters is reduced in terms of total EPNdB due to the higher level of external noise component. To reflect the effect of various liner parameters on the acoustic suppression, the EPNdB of the internal noise component is presented here.

Figure E1 shows the effect of facesheet porosity on predicted normal impedance for the optimum bulk (a resistivity of 20 Rayls/cm at 500°F), the thickness and hole diameter of the facesheet being 0.02" and 0.04", respectively. The reactance and resistance for 40% porous facesheet lie within the optimum impedance goal for the critical frequency range of 2 to 6 kHz. Figure E2 shows the similar results for a 12 lb/cft T-Foam of standard construction with facesheet thickness of 0.1" and hole diameter of 0.07". These results are based on the measured normal impedance at room temperature conditions. For the entire frequency range the resistance values are higher compared to the optimum goal, even for 40% porous facesheet. For a limited frequency range of 2 to 4 kHz the reactance levels meet the optimum goal. The acoustic suppression for these liners is expected to be poor.

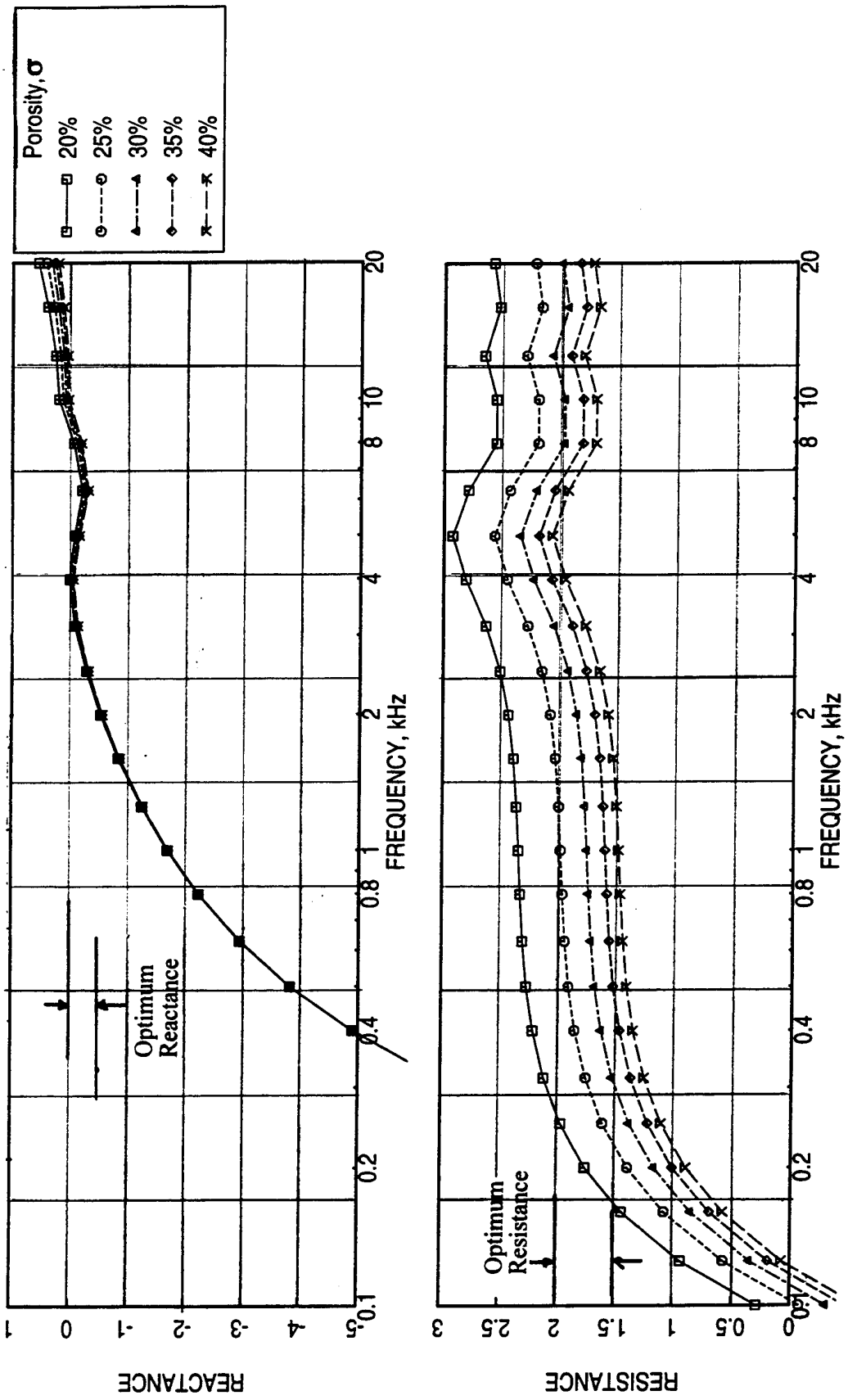

Figure E1. Effect of facesheet porosity σ on predicted normal impedance spectra for various LSM-2 scale liners at takeoff condition, Optimum bulk of resistivity 20 Rayls/cm, depth=1.2", thickness = 0.02", hole diameter = 0.04", static temperature = 500°F, grazing flow Mach number = 0.8, OASL = 177 dB.

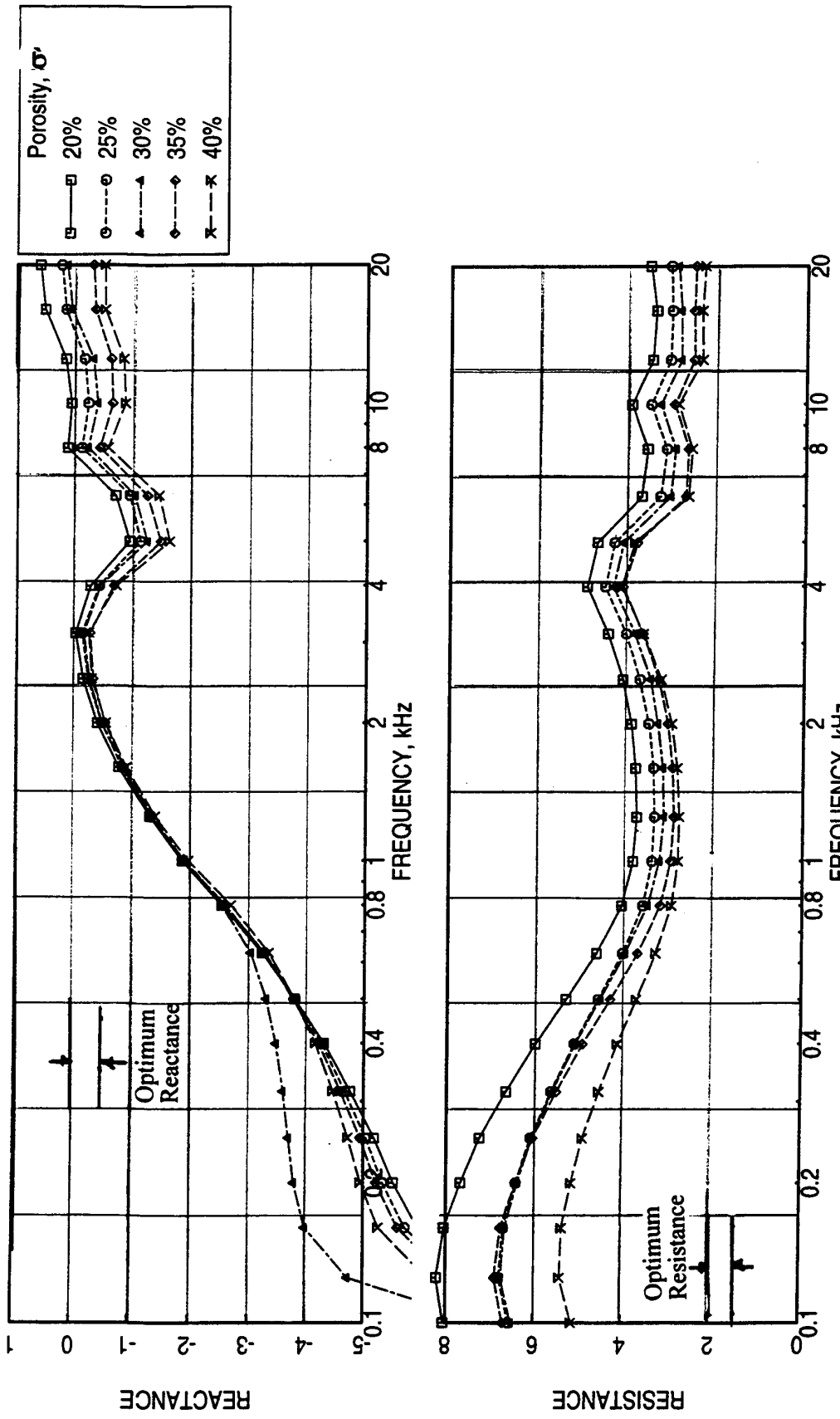

Figure E2. Effect of facesheet porosity σ on constructed normal impedance spectra for various LSM-2 scale liners at takeoff condition, 12 lbf T-Foam, depth=1.2", thickness = 0.10", hole diameter = 0.07", static temperature = 500°F, grazing flow Mach number = 0.8, OASL = 177 dB.

Figure E3 shows the impedance for four liner designs with 35% porous facesheet. The configurations for optimum bulk resulted in more acceptable impedance compared to the 12 lb/cft T-Foam configuration. The impedance level shifts, due to thicker facesheet with larger hole diameter, are relatively small compared to the shifts caused due to the change of bulk from optimum to 12 lb/cft T-Foam. Thus, a significant suppression loss is expected for 12 lb/cft T-Foam configuration.

Figure E4 shows the effect of facesheet porosity on internal EPNdB noise component for three different liner configurations. A significant 2 EPNdB difference is experienced between the optimum bulk and 12 lb/cft T-Foam configurations. The use of thicker facesheets with larger hole diameters on optimum bulk show significant suppression loss. A small amount of EPNdB increase is observed by increasing the hole diameter from 0.07" to 0.1" with the same 0.1" thick facesheet. The impact of facesheet parameters is small and their trends are not clear for the T-Foam configurations. This aspect is discussed later. Figure E5 is the same as Figure E4, except the EPNL for hardwall configuration is shown in this plot.

Figure E6 shows the effect of facesheet thickness on internal EPNdB noise component for four different liner configurations. Again, a significant 2 EPNdB difference is experienced between the optimum bulk and 12 lb/cft T-Foam configurations. For optimum bulk the EPNL decreases first and then increases with increasing facesheet thickness; resulting in an optimum thickness of about 0.04". Similar trend is also observed with T-Foam configuration, with d=0.04" and σ=40%. Even with T-Foam configurations, the EPNL is lower for 40% porous with d=0.04" compared to 35% porous with larger hole diameters.

Figure E7 shows the effect of facesheet hole diameter on internal EPNdB noise component for four different liner configurations. In general, EPNL increases with increasing hole diameter. This is more systematic for optimum bulk configurations. The effect of facesheet thickness increase from 0.02" to 0.1" is clearly observed for optimum bulk. Clear trends are not observed for T-Foam configurations due to their non-optimum impedance characteristics. For these cases the change of facesheet parameters brings the impedance levels closer to optimum goals at some frequencies and makes them worse at other frequencies. The sum total effect on acoustic suppression is, therefore, becomes arbitrary rather than systematic.

The impact of each of the facesheet parameters is not linear in nature. For example the impact of hole diameter at a given porosity and thickness will be different at a different porosity and thickness. One may arrive at a wrong conclusion if the EPNL is interpolated using the data shown in Figures E4 through E7. For example an EPNL of 93.6 dB can be

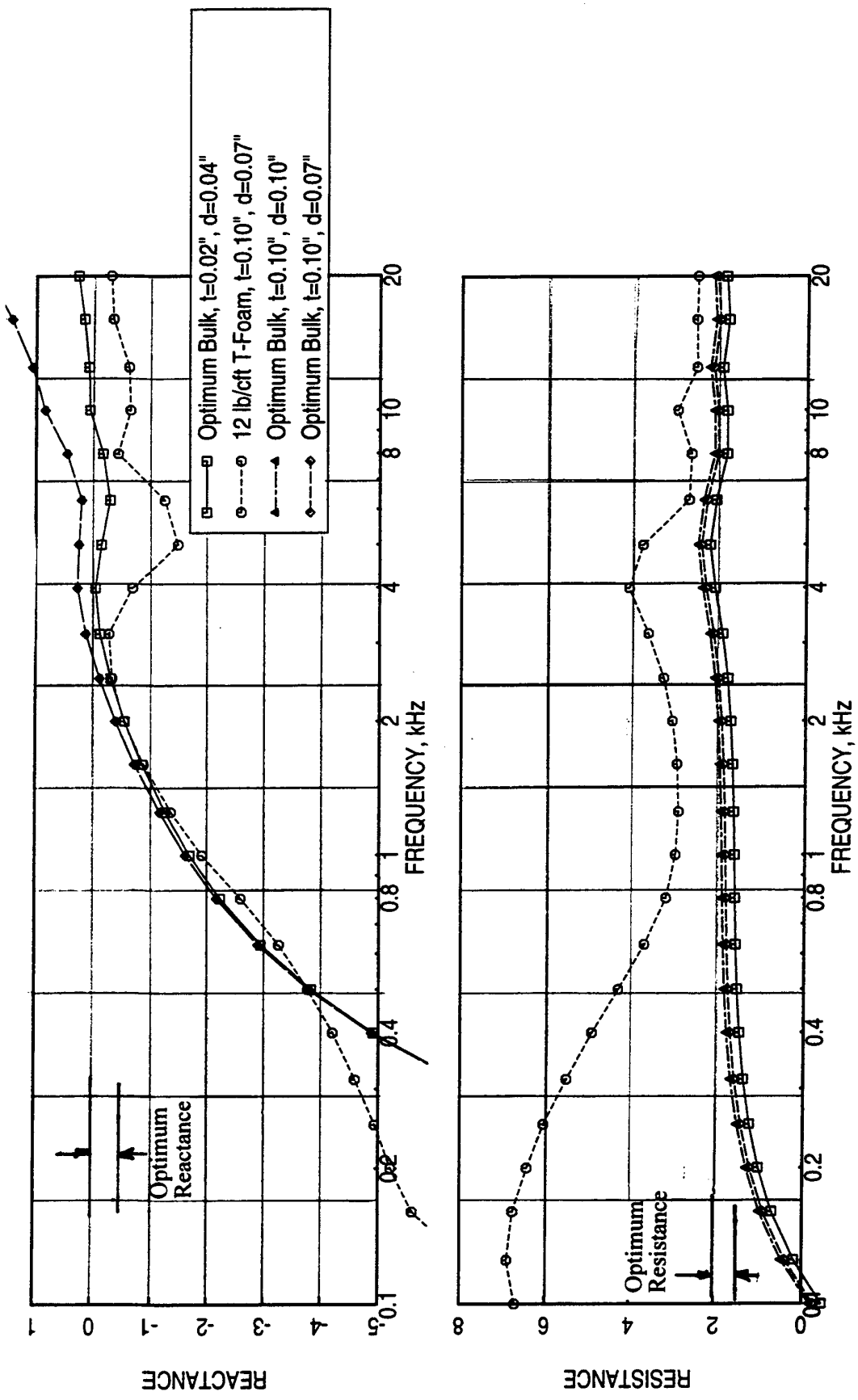

Figure E3. Effect of design parameters on normal impedance spectra for various LSM-2 scale liners at takeoff condition, depth=1.2", Facesheet porosity=35%, static temperature = 500°F, grazing flow Mach number = 0.8, OASL = 177 dB.

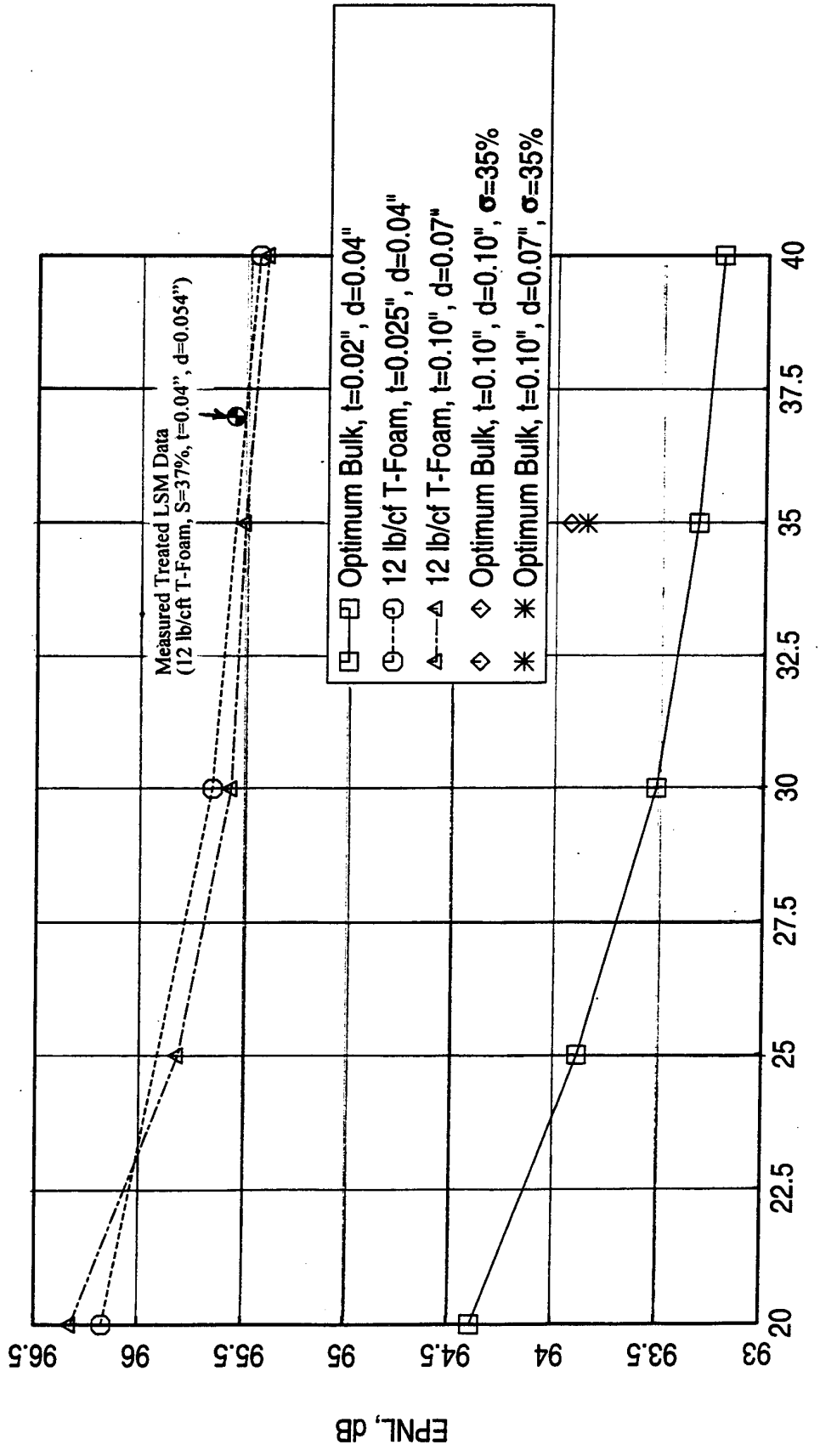

Figure E4. Effect of facesheet porosity σ on predicted internal EPNdB for various LSM-2 scale liners for fully treated (full-scale 160" ejector) ejector at takeoff condition (NPR=3.25, T8=1579°R, V_{mix}=1430 ft/sec, M_P=0.0), mean flow temperature = 530°F, mean flow Mach number = 0.85, Liner conditions: depth=1.2", static temperature = 500°F, grazing flow Mach number = 0.8, OASL = 177 dB.

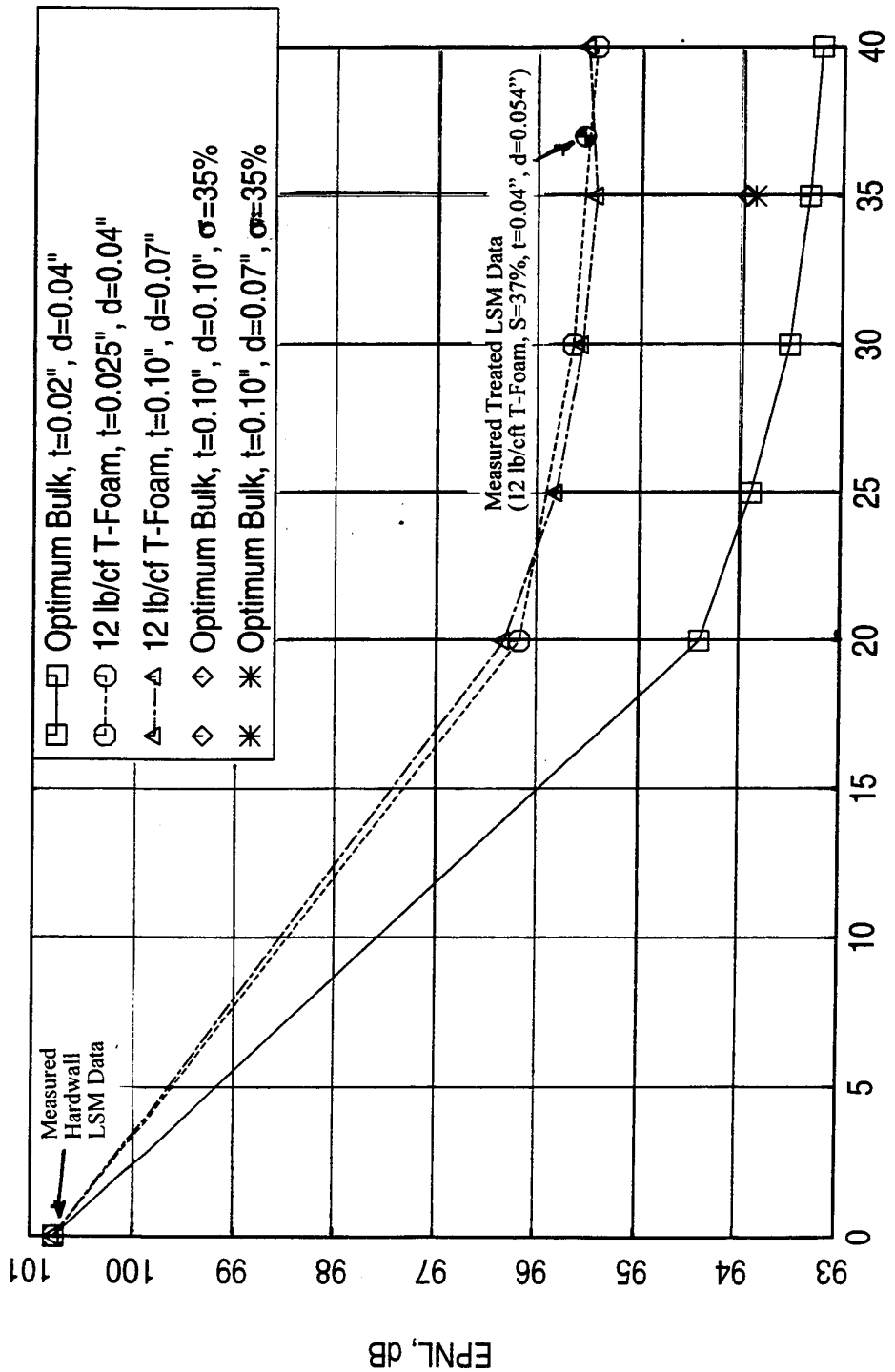

Figure E5. Effect of facesheet porosity σ on predicted internal EPNdB for various LSM-2 scale liners for fully treated (full-scale 160" ejector) ejector at takeoff condition (NPR=3.25, T8=1580°R, V_{mix}=1435 ft/sec, M_F=0.0), mean flow temperature = 530°F, mean flow Mach number = 0.85, Liner conditions: depth=1.2", static temperature = 500°F, grazing flow Mach number = 0.8, OASL = 177 dB.

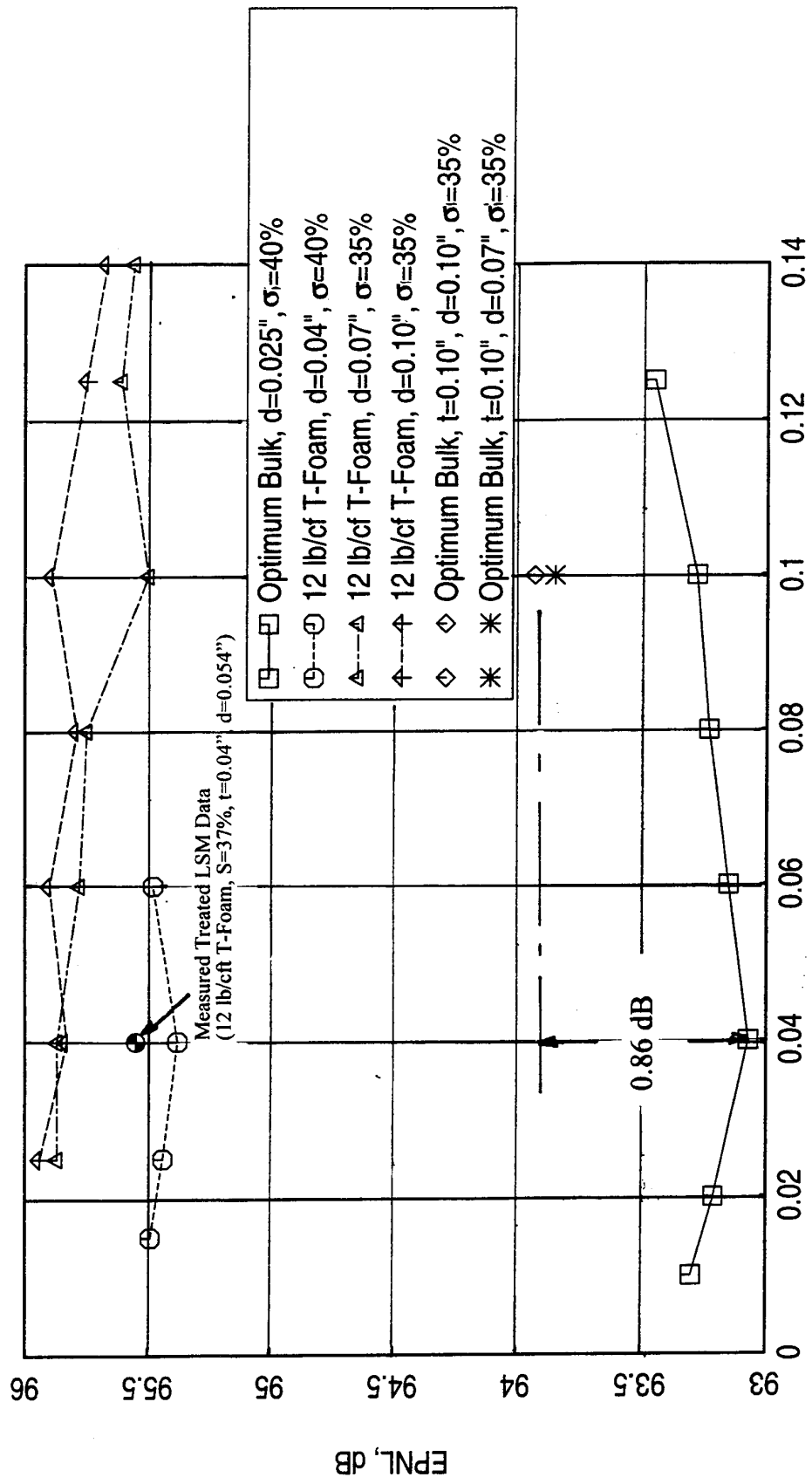

Figure E6. Effect of facesheet thickness t on predicted internal EPNdB for various LSM-2 scale liners for fully treated (full-scale 160" ejector) ejector at takeoff condition (NPR=3.25, T8=1580°R, V_{mix}=1435 ft/sec, M_F=0.0), mean flow temperature = 530°F, mean flow Mach number = 0.85, Liner conditions: depth=1.2", static temperature = 500°F, grazing flow Mach number = 0.8, OASL = 177 dB.

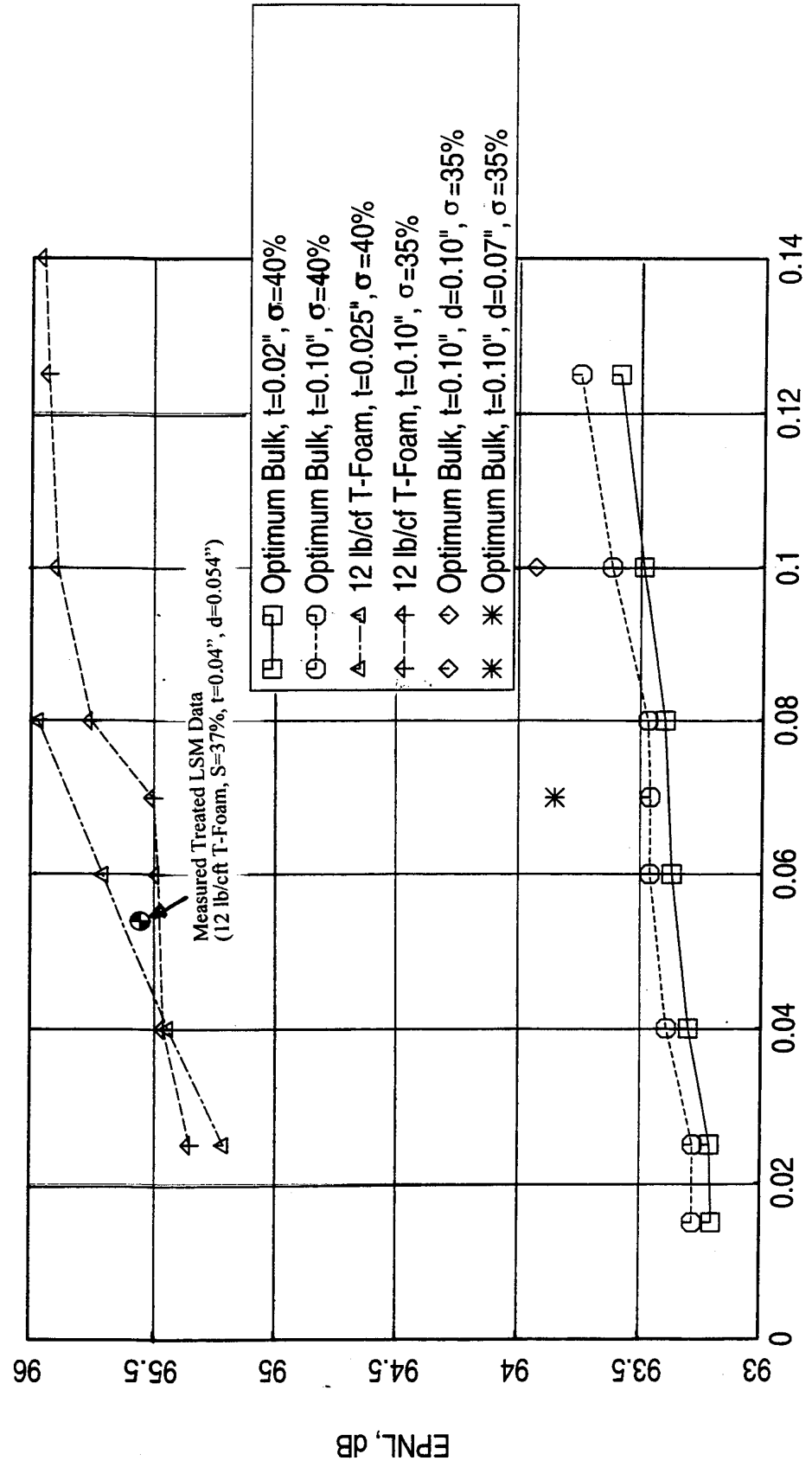

Figure E7. Effect of facesheet hole diameter d on predicted internal EPNdB for various LSM-2 scale liners for fully treated (full-scale 160" ejector) ejector at takeoff condition (NPR=3.25, T8=1580°R, V_{mix}=1435 ft/sec, M_p=0.0), mean flow temperature = 530°F, mean flow Mach number = 0.85, Liner conditions: depth=1.2", static temperature = 500°F, grazing flow Mach number = 0.8, OASL = 177 dB.

deduced for a 35% porous, t=0.1", d=0.08" facesheet from two sets of data, predicted for (1) 40% porous facesheets of hole diameter d=0.025" with varying thickness and (2) 40% porous facesheets of thickness t=0.1" with varying hole diameter. To illustrate that the deduced EPNL is not the same if it is directly predicted for the 35% porous facesheet with t=0.1" and d=0.08", EPNL for the internal noise component are predicted for 35% porous facesheets of thickness t=0.1" with varying hole diameter (see Figure E8). Thus, one can obtain the impact of hole diameter directly for 0.1"-thick 35% porous facesheets. As can be seen that the predicted EPNL for 0.1"-thick 35% porous facesheet with 0.08" hole diameter is 93.86 dB compared to the previously deduced level of 93.6 dB.

Based on the results presented in this appendix it is evident that the selection of an appropriate bulk material is very important. The facesheet optimization is effective when an optimum bulk is used. As indicated in the past and apparent from the current results, a highly porous facesheet with smaller hole diameter is more effective in acoustic suppression. An optimum thickness of about 0.04" is acoustically desirable for LSM size liners. Based on the optimum bulk the EPNL increases by **0.86** dB when the optimum facesheet (i.e., S=40%, t=0.04", and d=0.025) is replaced by a 0.1" thick 35% porous facesheet with d=0.1". An EPNL increase of **0.78** dB is experienced by altering the optimum facesheet to a 0.1" thick 35% porous facesheet with d=0.07". Simply increasing the hole diameter from 0.07" to 0.1" for the 0.1"-thick 35% porous facesheet the EPNL increase is about 0.1 dB (exactly 0.08 dB for the current exercise).

E.2 Acoustic Suppression Characteristics of LSM-2 Liner Designs with Different T-Foam Bulk Absorbers: It clearly evident that the standard T-Foam bulk material is not suitable for optimum acoustic suppression for LSM scale. Thus, attempts are made to improve the construction process for T-Foam bulks (Ref. 3). In this process a number of different T-Foam bulk materials are obtained. One specific construction, in which, several woven paper layers are imbedded in to the T-Foam at various depths, shows significant improvement towards noise suppression. Several such bulk materials are considered for LSM-2 liners by predicting farfield noise for the absorbers.

Figure E9 shows the normal impedance spectra up to 6 kHz. at ambient conditions for three different 1.2"-deep T-Foam bulk absorber samples of 1.25" diameter. The standard 12 lb/cft T-Foam exhibits much higher resistance (between 2.5 to 5 kHz) and reactance (between 1.5 to 4 kHz) compared to the other two samples of special construction. Similar results up to 20 kHz, measured using 0.6" diameter samples, are shown in Figure E10. Similar results up to 20 kHz. are obtained with a number of facesheets of varying porosity, thickness, and hole

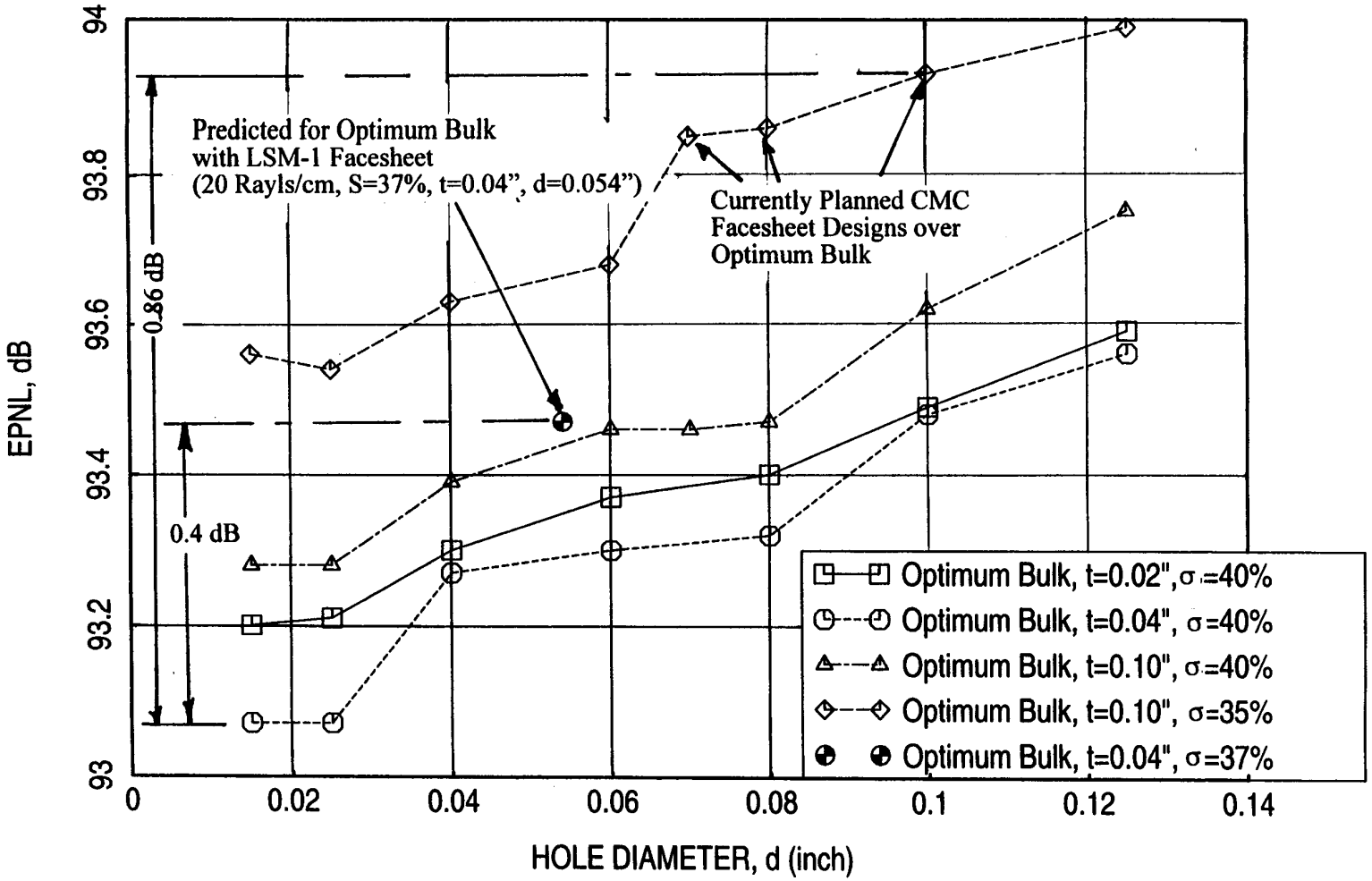

Figure E8. Effect of facesheet hole diameter d on predicted internal EPNdB for various LSM-2 scale liners for fully treated (full-scale 160" ejector) ejector at takeoff condition (NPR=3.25, T8=1580°R, V_{mix}=1435 ft/sec, M_F=0.0), mean flow temperature = 530°F, mean flow Mach number = 0.85, Liner conditions: depth=1.2", static temperature = 500°F, grazing flow Mach number = 0.8, OASL = 177 dB.

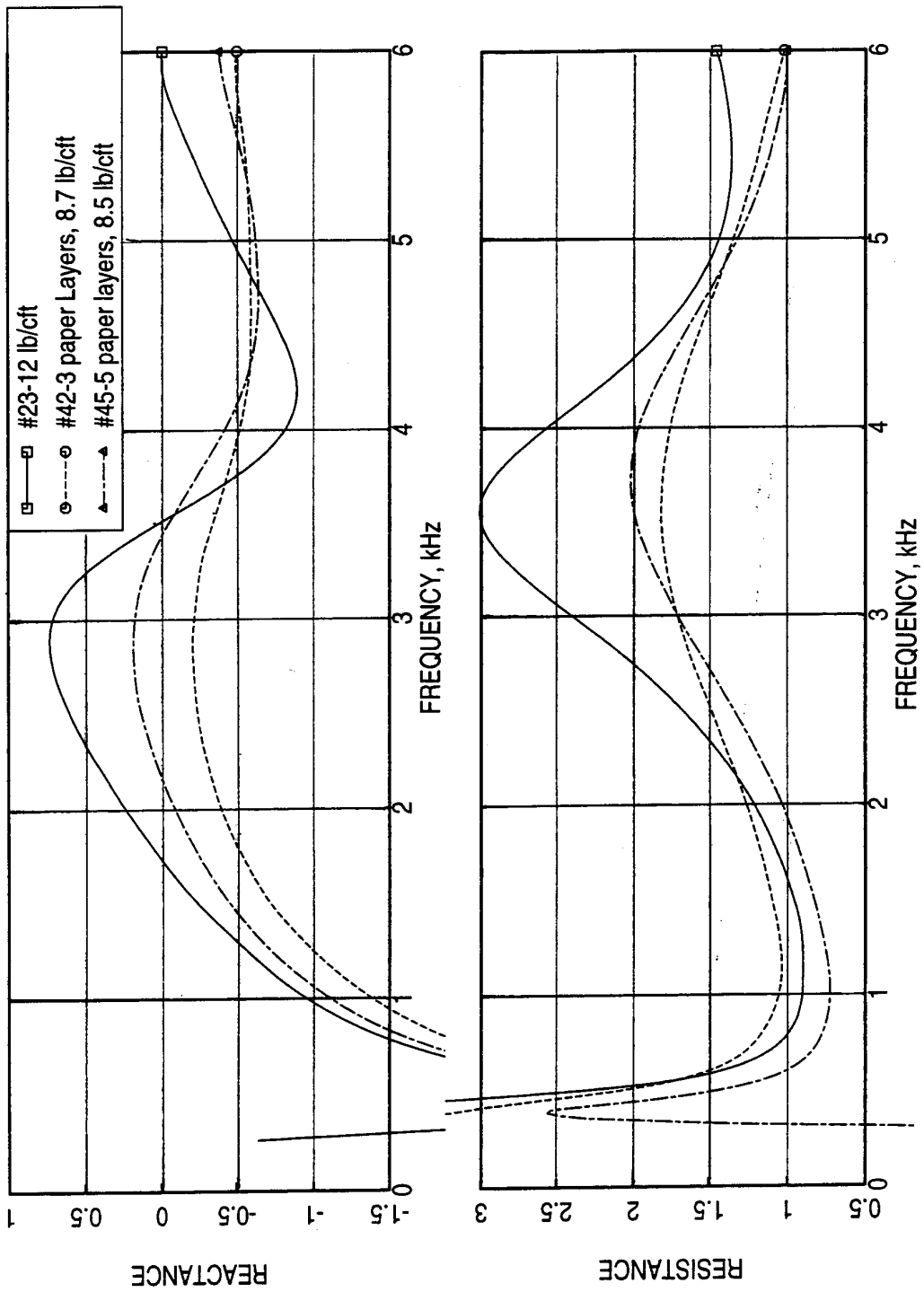

Figure E9. Measured normal impedance spectra up to 6 kHz for various LSM scale T-Foam samples (1.25" diameter) at ambient condition, depth=1.2", OASL = 150 dB.

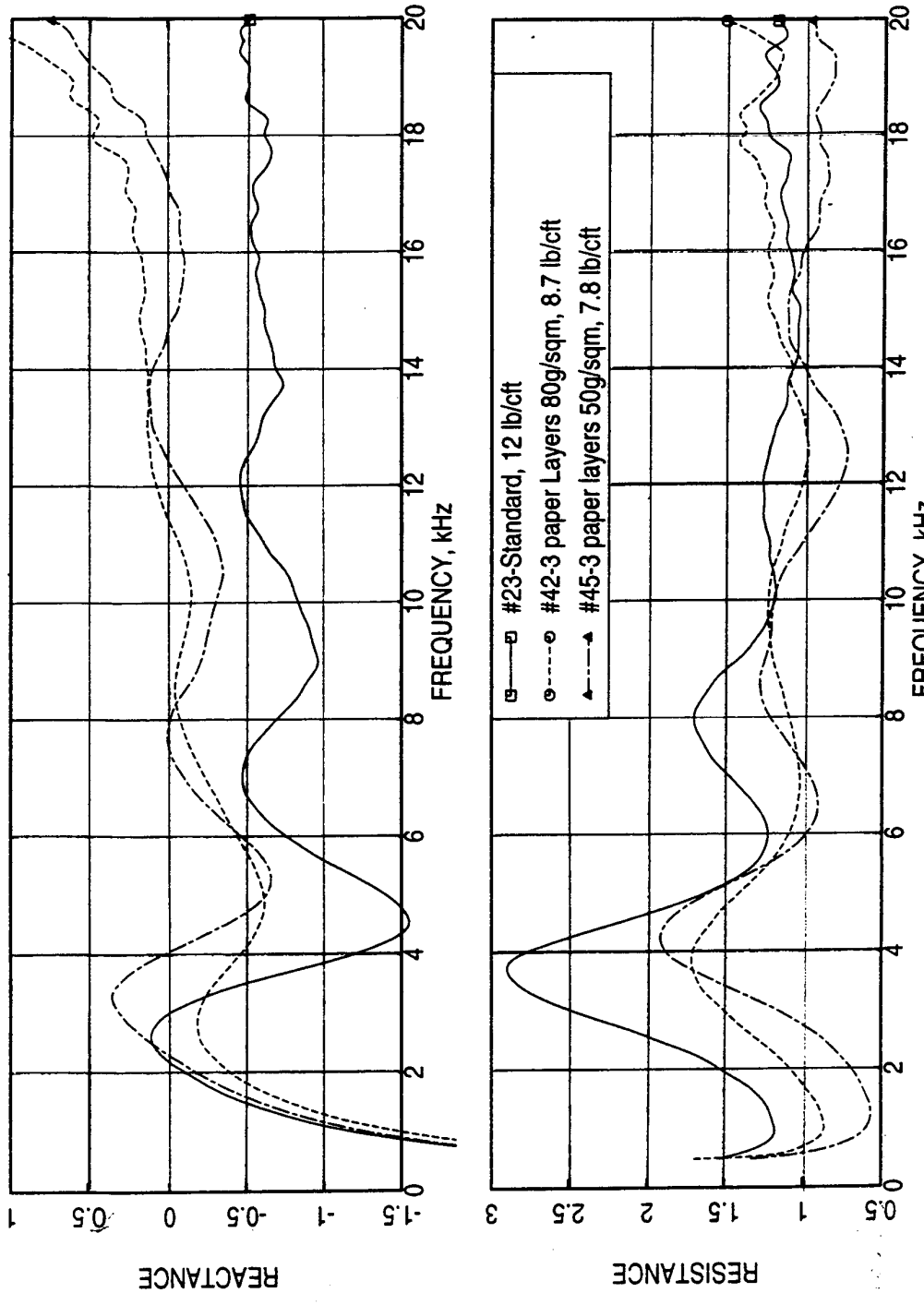

Figure E10. Measured normal impedance spectra up to 20 kHz for various LSM scale T-Foam samples (0.6" diameter) at ambient condition, depth=1.2", OASL = 150 dB.

diameter (not shown here). The measured ambient impedance results are corrected for the ejector flow, temperature, and acoustic intensity environment. These corrections are based on the existing prediction methods. Figure E11 shows the normal impedance spectra for various bulk absorbers with a 0.04"-thick and 40% porous facesheet with 0.04" diameter holes for a typical ejector environment. Similar results, predicted for an optimum bulk of about 20 Rayls/cm at 500°F, are also included in this figure. The constructed normal impedance spectra for the standard 12 lb/cft T-Foam lies outside the optimum impedance levels (i.e., **specific resistance of 1.5 to 2 and specific reactance of -0.5 to 0.0**) for most frequencies. In contrast, the optimum bulk normal impedance lies within the optimum limits for most frequencies. The impedance spectra for the T-Foam with 3 paper layers of $80g/m^2$ are much closer to the optimum bulk results. It should be noted that the 3 paper layer T-Foam and even the optimum bulk impedance levels lie slightly outside the optimum impedance limits for some frequencies, especially, between 3 to 6 kHz.

Thus, the objective is to improve the bulk absorber to meet the impedance requirements to able to maximize the acoustic suppression. The impedance spectral characteristics must be better than the so-called optimum bulk.

Utilizing the constructed impedance spectra for various liner configurations the EPNLs for internal noise component at the takeoff condition are computed for LSM-2 model. Some of the results are listed in Table E1. As listed in the table, the lowest EPNLs are achieved for 0.04"-thick 40% porous facesheets with 0.04" diameter holes. As a typical example, the effect of facesheet porosity on internal EPNL for various bulk absorbers is shown in Figure E12. As expected, the EPNL decreases with increasing porosity. The most important massage is that the 3 paper layer T-Foam configurations are much better absorbers compared to the standard 12 lb/cft type T-Foam configurations. **We are about 0.5 internal EPNdB higher compared to the optimum bulk configurations. Thus, the 3-paper layer construction needs to be improved further to exceed the optimum bulk results.**

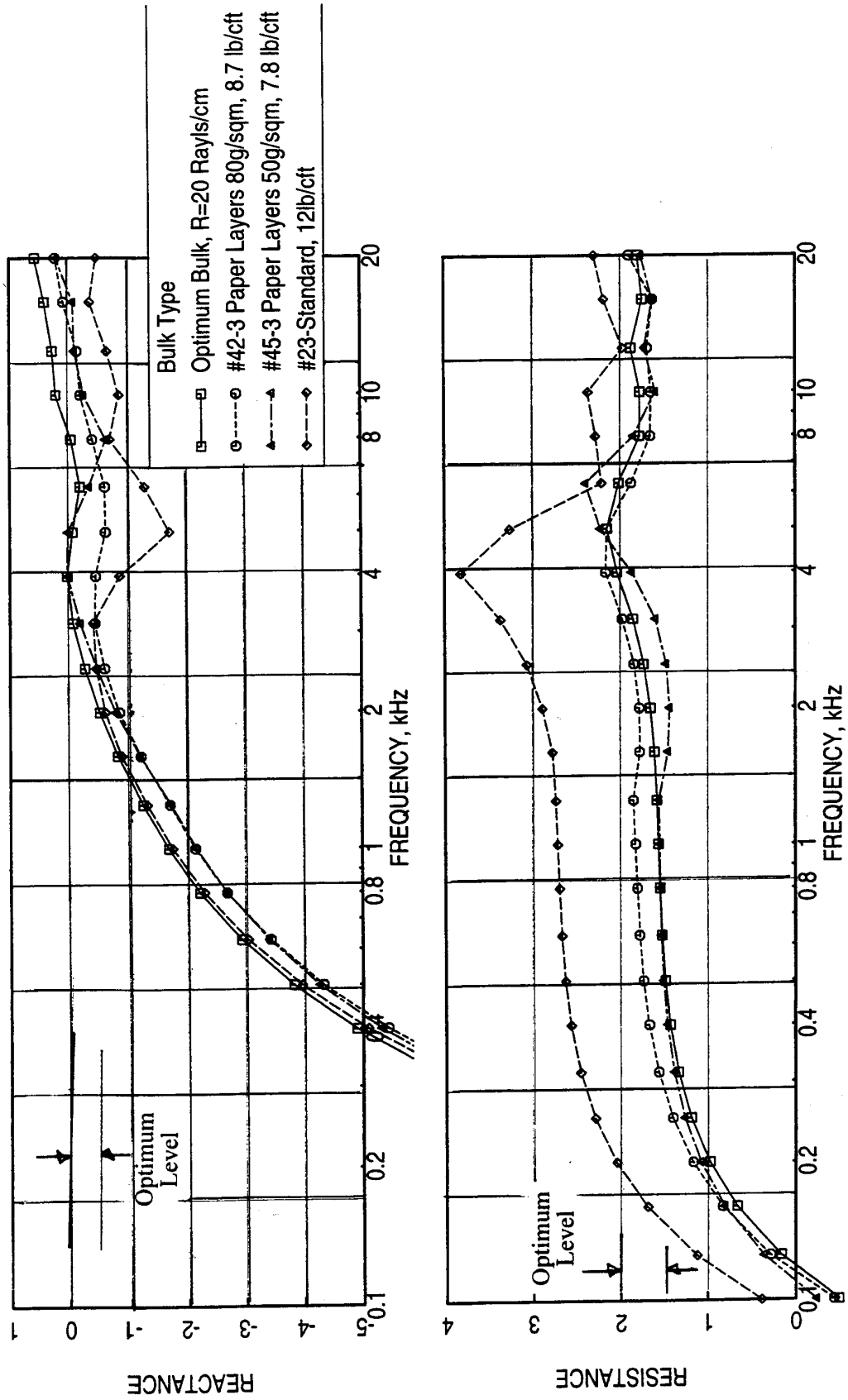

Figure E11. Predicted normal impedance spectra for various LSM-2 scale liners at takeoff condition, depth=1.2", facesheet: porosity = 40%, thickness = 0.04", hole diameter = 0.04", static temperature = 500°F, grazing flow Mach number = 0.8, OASL = 177 dB.

Table E1. Predicted EPNL (dB) for Internal Noise component for LSM Liner Configurations with T-Foam as the Bulk Absorber

Facesheet Parameters: σ (%), t (in), d (in) → Bulk Specifications ↓	LSM-1 Facesheet σ=37% t=0.04" d=0.054"	σ=20% t=0.025" d=0.04"	σ=30% t=0.025" d=0.04"	σ=40% t=0.025" d=0.04"	**σ=40% t=0.04" d=0.04"**	σ=35% t=0.1" d=0.08"	σ=40% t=0.1" d=0.08"
Optimum Bulk, R=20 R/cm	93.47	94.58	93.62	93.41	**93.27**	93.86	93.47
#42 T-Foam with 3 Layers Paper 80g/m2, 8.7 lb/cft	93.78	95.02	94.12	93.76	**93.56**	93.98	93.71
#45 T-Foam with 3 Layers Paper 50g/m2, 7.8 lb/cft	94.10	95.22	94.32	93.83	**93.51**	94.35	94.16
#23 Standard T-Foam 12 lb/cft	95.54	96.13	95.65	95.46	**95.12**	95.74	95.50

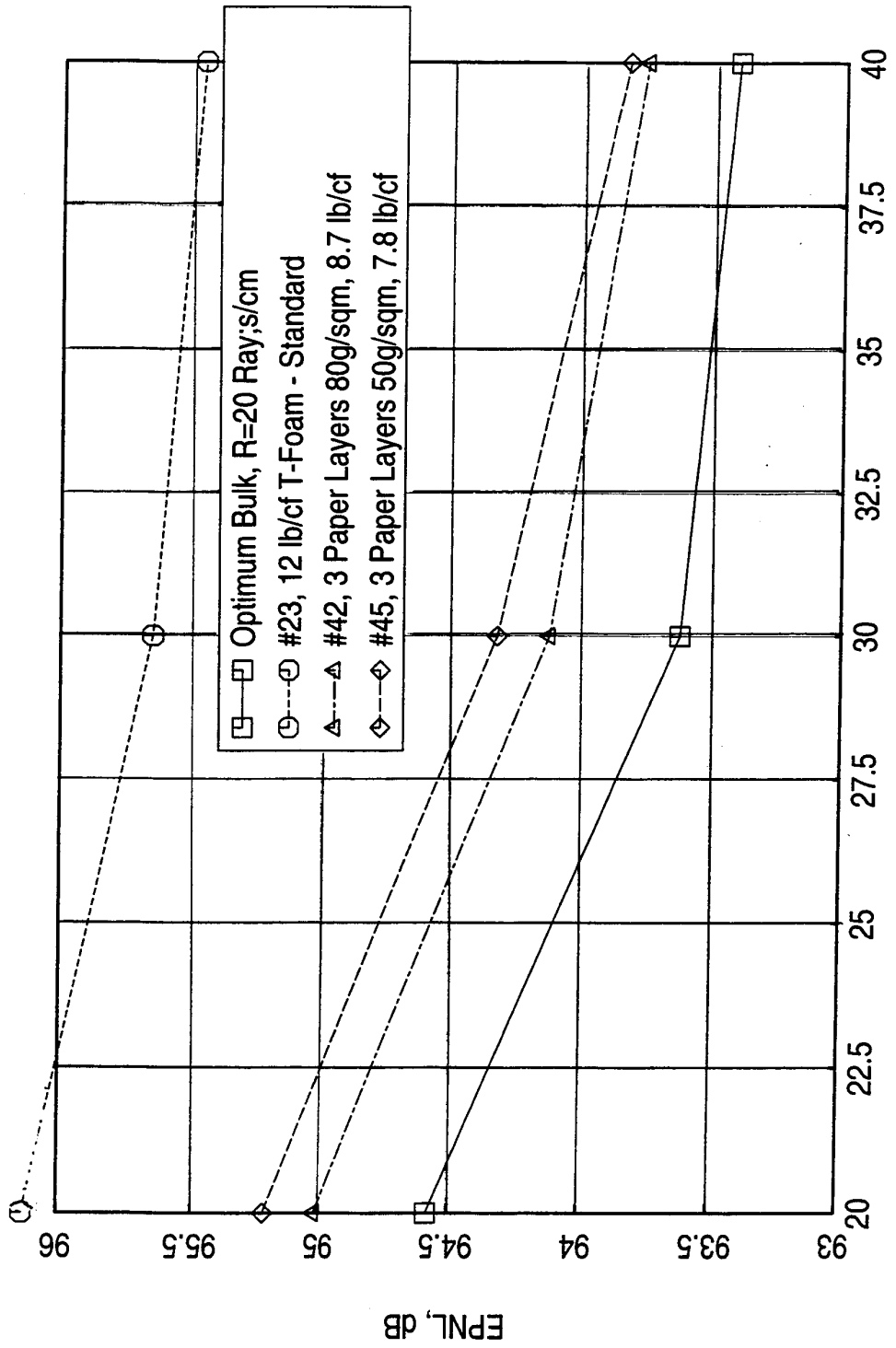

Figure E12. Effect of facesheet porosity σ on predicted internal EPNL for various LSM-2 scale liners for fully treated (full-scale 160" ejector) ejector at takeoff condition (NPR=3.25, T8=1580°R, V_{mix}=1435 ft/sec, M_p=0.0), mean flow temperature = 530°F, mean flow Mach number = 0.85, Liner conditions: depth=1.2", t=0.025", d=0.04", static temperature = 500°F, grazing flow Mach number = 0.8OASL = 177 dB.

REFERENCES

1. Salikuddin, M., "Acoustic Characteristics of Various Treatment Panel Designs for HSCT Ejector Liner Acoustic Technology Development Program". 1999, HSR/CPC Coordination Memo No: GE99-025-N.

2. Rice, E. J. and Salikuddin M., "Semi-Empirical Correlation between Liner Insertion Loss and Normal Impedance – HSR Related Duct and Mixer-Ejector." 1999, HSR/CPC Program Coordination Memo No: GE99-008-N, NAS3-27235.

3. Salikuddin, M., "Acoustic Characteristics of Various Treatment Panel Designs Specific to HSCT Mixer-Ejector Application". 1999, HSR/CPC Coordination Memo No: GE99-030-N.

4. Rice, E. J. and Salikuddin M., "Models for Acoustically Treated Mixer-Ejector Suppressors and the Related Acoustic Impedance Models for Bulk Absorbers with Heated grazing flow". 1999, HSR/CPC Coordination Memo No: GE99-033-N.

5. Stone, J. R., Clark, B. J., and Krejsa, E. A., "2-D Mixer-Ejector Nozzle Noise Analysis and Prediction Code Development." 1999, HSR/CPC Coordination Memo No: GE99-034-N.

6. Motsinger, R. E., and Kraft, R. E., "Design and Performance of Duct Acoustic Treatment", in "Aeroacoustics of Flight Vehicles : Theory and Practice - Volume 2: Noise Control" NASA reference Publication 1258, Vol 2, WRDC TR 90-3052.

7. Delany, M. E. and Bazley, E. N., "Acoustical Properties of Fibrous Absorbent Materials." Applied Acoustics, 3 (2), pp. 105-116, 1970.

8. Salikuddin, M., "Bulk Absorber Liner Designs For Full-Scale, LSM, and 1/7-Scale Mixer-Ejector Nozzles.." 1996, HSR/CPC Program Coordination Memo No: GE96-143-N, NAS3-27235.

9. Salikuddin, M., "Dynamic Pressure Field Internal to the Ejector for 2D Mixer-Ejector Nozzles." 1995, HSR/CPC Program Coordination Memo No: GE95-078-N, NAS3-27235.

REPORT DOCUMENTATION PAGE

Form Approved
OMB No. 0704-0188

1. AGENCY USE ONLY (*Leave blank*)	2. REPORT DATE	3. REPORT TYPE AND DATES COVERED
	September 2006	Final Contractor Report

4. TITLE AND SUBTITLE

Development of a Liner Design Methodology and Relevant Results of Acoustic Suppression in the Farfield for Mixer-Ejector Nozzles

5. FUNDING NUMBERS

WBS 984754.02.07.03.04.01
NAS3–26617 and NAS3–27235

6. AUTHOR(S)

M. Salikuddin

7. PERFORMING ORGANIZATION NAME(S) AND ADDRESS(ES)

General Electric Aircraft Engines
One Neumann Way
Cincinnati, Ohio 45215

8. PERFORMING ORGANIZATION REPORT NUMBER

E–15679

9. SPONSORING/MONITORING AGENCY NAME(S) AND ADDRESS(ES)

National Aeronautics and Space Administration
Washington, DC 20546–0001

10. SPONSORING/MONITORING AGENCY REPORT NUMBER

NASA CR—2006-214400
GE99–030–N

11. SUPPLEMENTARY NOTES

This research was originally published internally as GE99–030–N in December 1999. Project Manager, Clayton L. Meyers. Responsible person, Diane Chapman, Ultra-Efficient Engine Technology Program Office NASA Glenn Research Center, organization code PA, 216–433–2309.

12a. DISTRIBUTION/AVAILABILITY STATEMENT

Unclassified - Unlimited
Subject Category: 07

Available electronically at http://gltrs.grc.nasa.gov

This publication is available from the NASA Center for AeroSpace Information, 301–621–0390.

12b. DISTRIBUTION CODE

13. ABSTRACT ***(Maximum 200 words)***

We have developed a process to predict noise field interior to the ejector and in the farfield for any liner design for a mixer-ejector of arbitrary scale factor. However, a number of assumptions, not verified for the current application, utilized in this process, introduce uncertainties in the final result, especially, on a quantitative basis. The normal impedance model for bulk with perforated facesheet is based on homogeneous foam materials of low resistivity. The impact of flow conditions for HSCT application as well as the impact of perforated facesheet on predicted impedance is not properly accounted. Based on the measured normal impedance for deeper bulk samples (i.e., 2.0 in.) the predicted reactance is much higher compared to the data at frequencies above 2 kHz for T-foam and 200 ppi SiC. The resistance is under predicted at lower frequencies (below 4 kHz) for these samples. Thus, the use of such predicted data in acoustic suppression is likely to introduce inaccuracies. It should be noted that the impedance prediction methods developed recently under liner technology program are not utilized in the studies described in this report due to the program closeout. Acoustic suppression prediction is based on the uniform flow and temperature conditions in a two-sided treated constant area rectangular duct. In addition, assumptions of equal energy per mode noise field and interaction of all frequencies with the treated surface for the entire ejector length may not be accurate. While, the use of acoustic transfer factor minimizes the inaccuracies associated with the prediction for a known test case, the assumption of the same factor for other liner designs and with different linear scale factor ejectors seems to be very optimistic. As illustrated in appendix D that the predicted noise suppression for LSM-1 is lower compared to the measured data is an indication of the above argument. However, the process seems to be more reliable when used for the same scale models for different liner designs as demonstrated for Gen. 1 mixer-ejectors.

14. SUBJECT TERMS	15. NUMBER OF PAGES
Propulsion systems (aircraft)	282
	16. PRICE CODE

17. SECURITY CLASSIFICATION OF REPORT	18. SECURITY CLASSIFICATION OF THIS PAGE	19. SECURITY CLASSIFICATION OF ABSTRACT	20. LIMITATION OF ABSTRACT
Unclassified	Unclassified	Unclassified	